BMR JOURNAL
OF AUSTRALIAN GEOLOGY & GEOPHYSICS

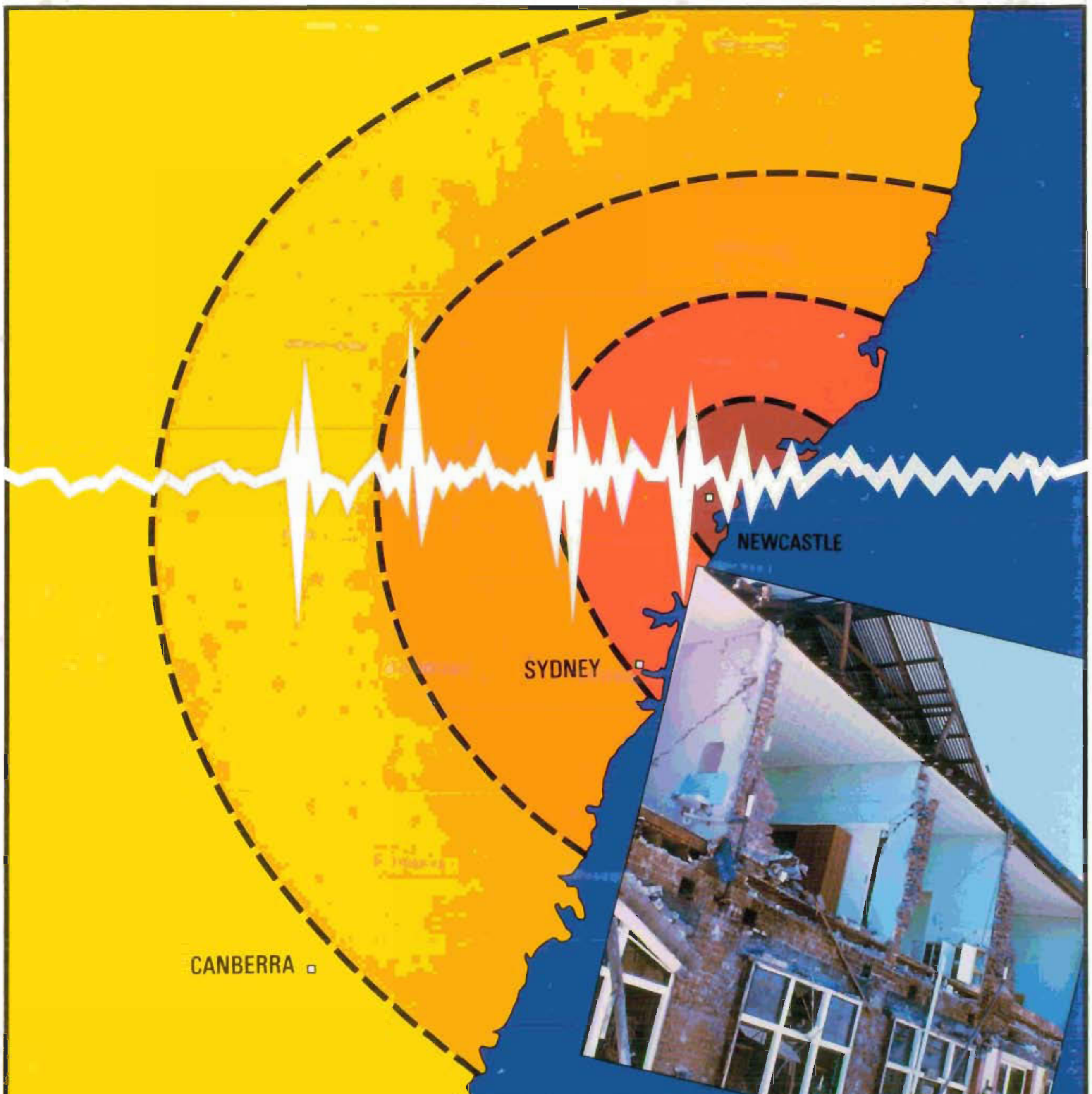

BMR Journal of Australian Geology & Geophysics Volume 11 (4)

VOLUME 11 NUMBER 4

BMR JOURNAL

OF AUSTRALIAN GEOLOGY & GEOPHYSICS

VOLUME 11 NUMBER 4

CONTENTS

Front cover: The Newcastle earthquake, 28 December 1989, is discussed in this issue in a paper by Kevin McCue, Vaughan Wesson & Gary Gibson. Cover design by Leanne McMahon.

AUSTRALIAN GOVERNMENT PUBLISHING SERVICE CANBERRA 1990

ISSN 0312-9608

Month of issue: September

Subscriptions to the BMR Journal are managed by the Australian Government Publishing Service (Mail Order Sales, GPO Box 84, Canberra, ACT 2601; telephone (06) 295 4485), to which enquiries should be directed.

Other matters concerning the Journal should be sent to the Director, marked for the attention of the Editor, BMR Journal.

Department of Primary Industries and Energy

Minister for Resources: The Hon. Alan Griffiths, MP

Secretary: Geoff Miller

Bureau of Mineral Resources, Geology and Geophysics

Director: R.W.R. Rutland, A.O.

Editor, BMR Journal: Bernadette Hince

Printed in Australia by Alken Press Pty. Ltd. — Smithfield

BMR Journal of Australian Geology & Geophysics, 11, 397-414

A new lithostratigraphic framework for the Early Jurassic units in the Bundamba Group, Clarence-Moreton Basin, Queensland and New South Wales.

A.T.Wells[1], P.E. O'Brien[1], I.L. Willis[2] & L.C. Cranfield[3]

Recent detailed studies of key transects throughout the Clarence-Moreton Basin have shown that a revision of nomenclature is required for units in the Late Triassic to Early Jurassic Bundamba Group. Revision of the stratigraphic nomenclature and elimination of the existing confusion in names of units in the basin was considered an essential first step in understanding basin evolution and assessing petroleum potential. We redefine the Marburg Formation as the Marburg Subgroup of the Bundamba Group and divide the Subgroup into two distinct lithostratigraphic units, the uniform sandstone of the Gatton Sandstone and the mixed sandstone and mudrocks of the younger Koukandowie Formation. The formations are upgraded existing members. The Gatton Sandstone contains locally developed members along the western basin margin. The Koreelah Conglomerate Member forms the base of the Gatton Sandstone where it overlaps basement rocks, and the Calamia Member of mixed shale, mudrocks and sandstone is a basal unit in the Gatton Sandstone in more basinward sections. The Heifer Creek Sandstone Member is a prominent quartzose sandstone unit in the Koukandowie Formation along the western margin and central parts of the basin. The older mixed mudrocks and sandstone of the Ma Ma Creek Member of the Koukandowie Formation are mainly known from the northwest. This new nomenclature preserves the integrity of existing stratigraphic names and is applicable basin-wide. One new stratigraphic name, the Koreelah Conglomerate Member, is introduced.

Introduction

Recent studies of the Clarence-Moreton Basin in Queensland and New South Wales (Fig. 1) have revealed inconsistencies in stratigraphic nomenclature, with a plethora of names mostly applied only to local areas. In addition, several units designated as members were observed to have basin-wide extent. This has severely hampered the systematic study of the basin, and indicated the need for a basin-wide consistent stratigraphic scheme, the abandonment of many published and unpublished names, and the change in status of several existing names. One new stratigraphic name is proposed to account for a locally developed conglomerate present at the base of the Early Jurassic sediments where they overlap the older sedimentary sequence and rest on Palaeozoic basement rocks. The integrity of widely used and accepted names has otherwise been preserved.

History of stratigraphic nomenclature

The principal references on the evolution and formulation of stratigraphic nomenclature of the Bundamba Group in the Clarence-Moreton Basin (Fig. 2) are Cameron (1907), Whitehouse (1955), McElroy (1963), McTaggart (1963), Staines (1964), Cranfield & Schwarzbock (1972), Day & others (1974), Cranfield, Schwarzbock & Day (1976), and Etheridge & others (1985). These papers are not discussed in detail; they are mentioned briefly in reference to the suggested upgrading of the nomenclature and the choice of existing stratigraphic names[4].

The Early Jurassic sedimentary sequence under discussion constitutes part of the 'Bundamba Beds' (now known as Bundamba Group) of Cameron (1907). He applied the term to the unproductive sandstones between the Ipswich Coal Measures and the Walloon Coal Measures in the Ipswich area. This definition is accepted here (Figs 2, 3). The upper Early Jurassic part of this sequence has been referred to as the 'Marburg Stage' (Reid, 1921), 'Marburg Sandstone' (Swindon, 1956, 1960) and 'Marburg Formation' (Whitehouse, 1955; McElroy, 1963; McTaggart, 1963). McElroy (1963) defined two members of the 'Marburg Formation', the 'Blaxland Fossil Wood Conglomerate Member' and the younger 'Koukandowie Sandstone Member' in the New South Wales part of the basin. In the northern Clarence-Moreton Basin, McTaggart (1963) subsequently divided the strata between the Esk Trough sequence and the Walloon Coal Measures (i.e. the Bundamba Group) in the Laidley Valley area into Helidon Sandstone and the overlying 'Marburg Formation' (a redefinition of 'Marburg Sandstone' of Swindon, 1956, 1960). McTaggart (1963) recognised four members within the 'Marburg Formation' — the 'Heifer Creek Sandstone Member', 'Ma Ma Creek Sandstone Member', 'Tenthill (or 'Winwill') Conglomerate Member' (Cranfield & others (1976) referred to this unit as the Winwill Conglomerate Member) and 'Gatton Sandstone Member' (Fig. 2). We restrict the name Helidon to the building stone unique to the Helidon area, and use instead Woogaroo Subgroup, or its constituent formations where appropriate, in areas where the name Helidon Sandstone has been used previously. This usage of the nomenclature conforms with that outlined by Cranfield & Schwarzbock (1972) (see below).

Staines (1964) defined three formations — Ripley Road Sandstone, Raceview Formation and Aberdare Conglomerate — below the 'Marburg Formation' in the Ipswich area (Fig. 2).

The Aberdare Conglomerate was redefined from a term originally used by Reid & Moreton (1922). These three new units were included in the Woogaroo Subgroup by Cranfield & Schwarzbock (1972), who suggested discarding the name Helidon Sandstone which they considered to include time and rock equivalents of the three lower formations of the Bundamba Group. These authors therefore recognised a subdivision of the Bundamba Group into the 'Marburg Formation' and the underlying Woogaroo Subgroup. The distinction between the subdivisions relies basically on sandstone composition. The Woogaroo Subgroup contains dominantly quartzose sandstone whereas the 'Marburg Formation' contains silty, quartz-lithic and feldspathic sandstone. The two divisions also approximate the subdivisions of McElroy (1963) in New South Wales — the 'Marburg Formation' and his 'Bundamba Group' (sic) (Fig. 2). In a review of the whole Clarence-Moreton Basin, Day & others (1974) broadly correlated the Mesozoic units in the coastal basins, mainly on the presence of an oolite marker bed, but no attempt was made to correlate the members of the 'Marburg Formation'.

The results of the Geological Survey of Queensland stratigraphic drilling in the northern Clarence-Moreton Basin

[1] Onshore Sedimentary & Petroleum Geology Program, Bureau of Mineral Resources, GPO Box 378, Canberra ACT 2601

[2] Formerly Geological Survey of New South Wales; present address: Exploration Division, Aberfoyle Resources Ltd, 119-121 Chloride St, Broken Hill, NSW 2880

[3] Geological Survey of Queensland, GPO Box 194, Brisbane, Queensland 4001

[4] Stratigraphic names modified or abandoned in this revision are enclosed in single inverted commas throughout this paper.

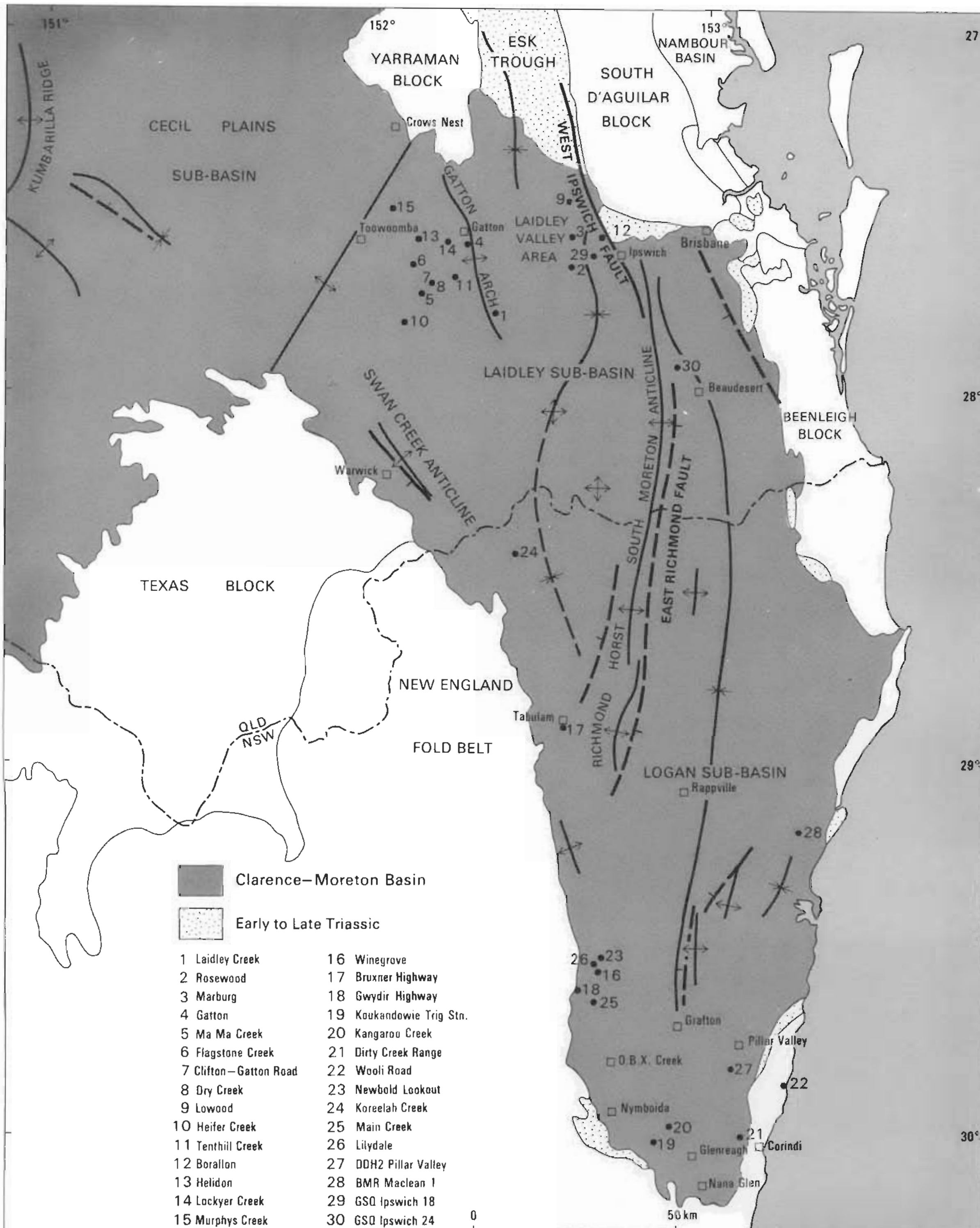

Figure 1. Locality map.

were synthesised by Gray (1975). He identified and correlated the members of the Marburg Formation, named by McTaggart (1963), across the northern part of the basin. The geology of the Ipswich and Brisbane 1:250 000 sheet areas was documented by Cranfield & others (1976), who gave a comprehensive account of the history of nomenclature for each stratigraphic unit of the Clarence-Moreton Basin.

Pillar Valley DDH 2 (Etheridge & others, 1985), a continuously cored drill hole in the southeast of the basin (Fig. 1), added considerable stratigraphic information to a poorly known part of the basin sequence. The Calamia Member, a new member at the base of the 'Marburg Formation', was identified and defined in this drill hole. The rest of the sequence was correlated with some of the members of the 'Marburg Formation' and formations of the Woogaroo Subgroup defined in the Queensland part of the basin (Figs 2, 3).

The results of BMR drilling in the Evans Head and Mallanganee areas (BMR Maclean No.1: Wells & O'Brien,

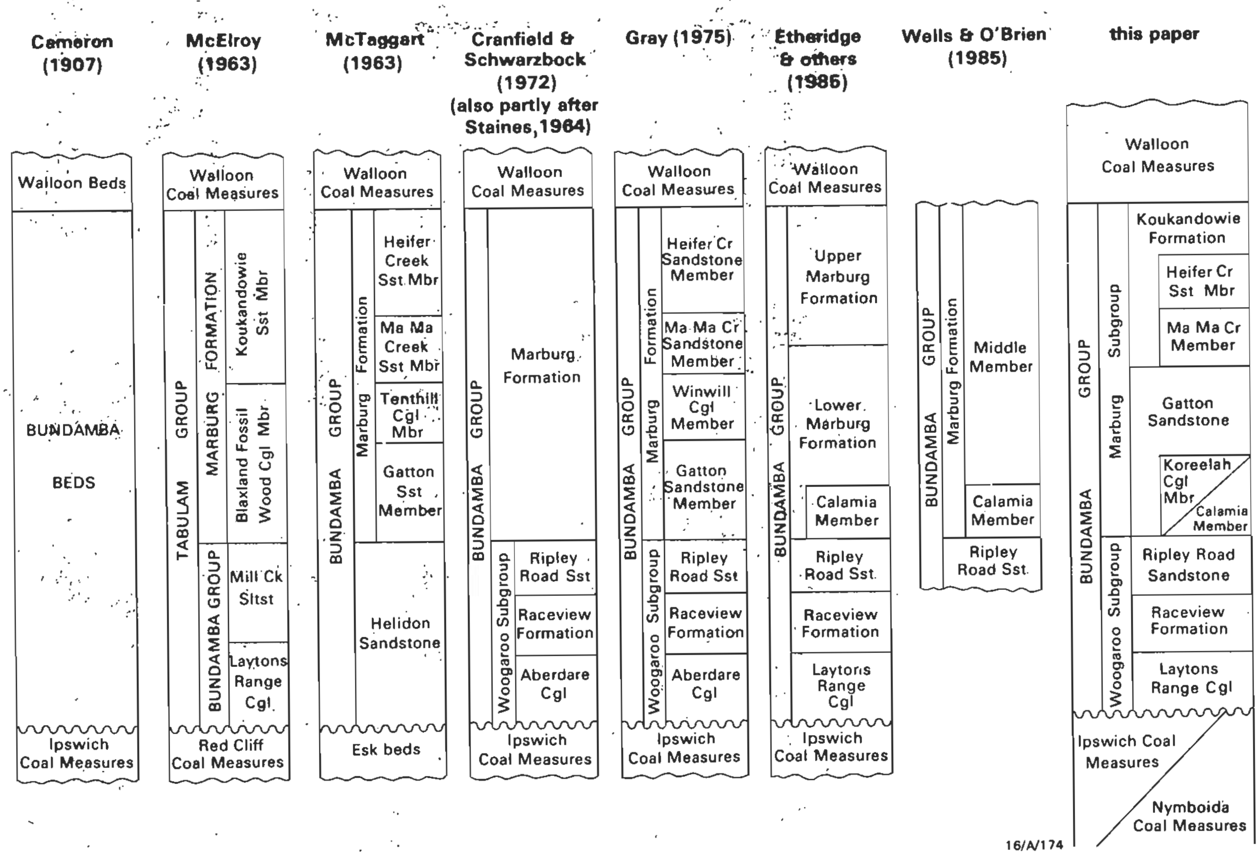

Figure 2. Evolution of stratigraphic nomenclature in the Bundamba Group and Marburg Subgroup.

1985; BMR Warwick 6 & 7: Wells, O'Brien, Willis & McMinn, 1990) extended most of the formations and members identified in the Pillar Valley area, and confirmed their continuity from Queensland into New South Wales.

Review of stratigraphic units

This review documents the origins and general concepts of the existing stratigraphic names as well as summarising the basin-wide characteristics of each unit, based on recent field research[5], logging of stratigraphic drill holes, interpretation of wireline logs and seismic record sections. The revised nomenclature of each unit is then presented.

'Marburg Formation' — 'Heifer Creek Sandstone Member'

The name 'Heifer Creek Sandstone Member' of the 'Marburg Formation' was applied by McTaggart (1963, p. 100) to '600–800 feet [180–240 m] of coarse, ferruginous siliceous sandstones, with minor shale and flaggy sandstone beds that can be traced between Toowoomba and Laidley Creek'.

McTaggart (1963) described the base of the 'Heifer Creek Sandstone Member' as a resistant sandstone at 800 feet [240 m] elevation that can be traced south of Helidon to Laidley Creek. This unit is a coarse-grained conglomeratic and lithic sandstone bed exposed in a very steep cutting where the Clifden–Gatton Road crosses Ma Ma Creek (Fig. 5, in the interval from 636 m to ~660 m). The composition of this sandstone is quite unlike any in the 'Ma Ma Creek Sandstone Member' below or any of the sandstones in the rest of the 'Marburg Formation' above. It is much siltier and more poorly sorted and contains more lithic clasts, mainly concentrated at the base of channel sands. This unit has also been recognised in cuttings on the railway line between Toowoomba and Murphys Creek, where it occurs in a similar stratigraphic position. McTaggart (1963) included intervals of interbedded mudrock, shale and some coal beds above this sandstone and below the predominantly quartz sandstone at the top of the sequence. He also included a two foot [~0.6 m] coal bed 100 feet [~30 m] above the base of the member in the valley of Flagstone Creek.

The new nomenclature distinguishes this intervening interval of mudrock, shale and some coal between the distinctive sandstones, one at the top of the 'Marburg Formation' and the sandstone in the Ma Ma Creek cutting on the Clifden–Gatton Road. This is necessary to rationalise the section and distinguish clear lithostratigraphic units. We consider that the sandstone shown in the interval 636–~660 m (Fig. 5) and the underlying siltstone from ~660 m to 710 m should not be included in the Heifer Creek Sandstone Member, but should be part of the undifferentiated formation.

McTaggart (1963) stated that the member is less discernible in the east where it plunges beneath the Walloon Coal Measures around Rosewood, although he considered it identifiable in the Marburg area. The member was differentiated in part on a sketch map of McTaggart (1963, text-fig. 1) and on the Ipswich 1:100 000 sheet area (Cranfield & others, 1981).

In the northwest Clarence–Moreton Basin, in the Gatton–Toowoomba area, the 'Heifer Creek Sandstone Member' occupies the interval (approximately 140 m) from the base of the Walloon Coal Measures to the top of the undivided 'Marburg Formation'.

[5] A key to all symbols used in graphic sections is shown in Fig. 4.

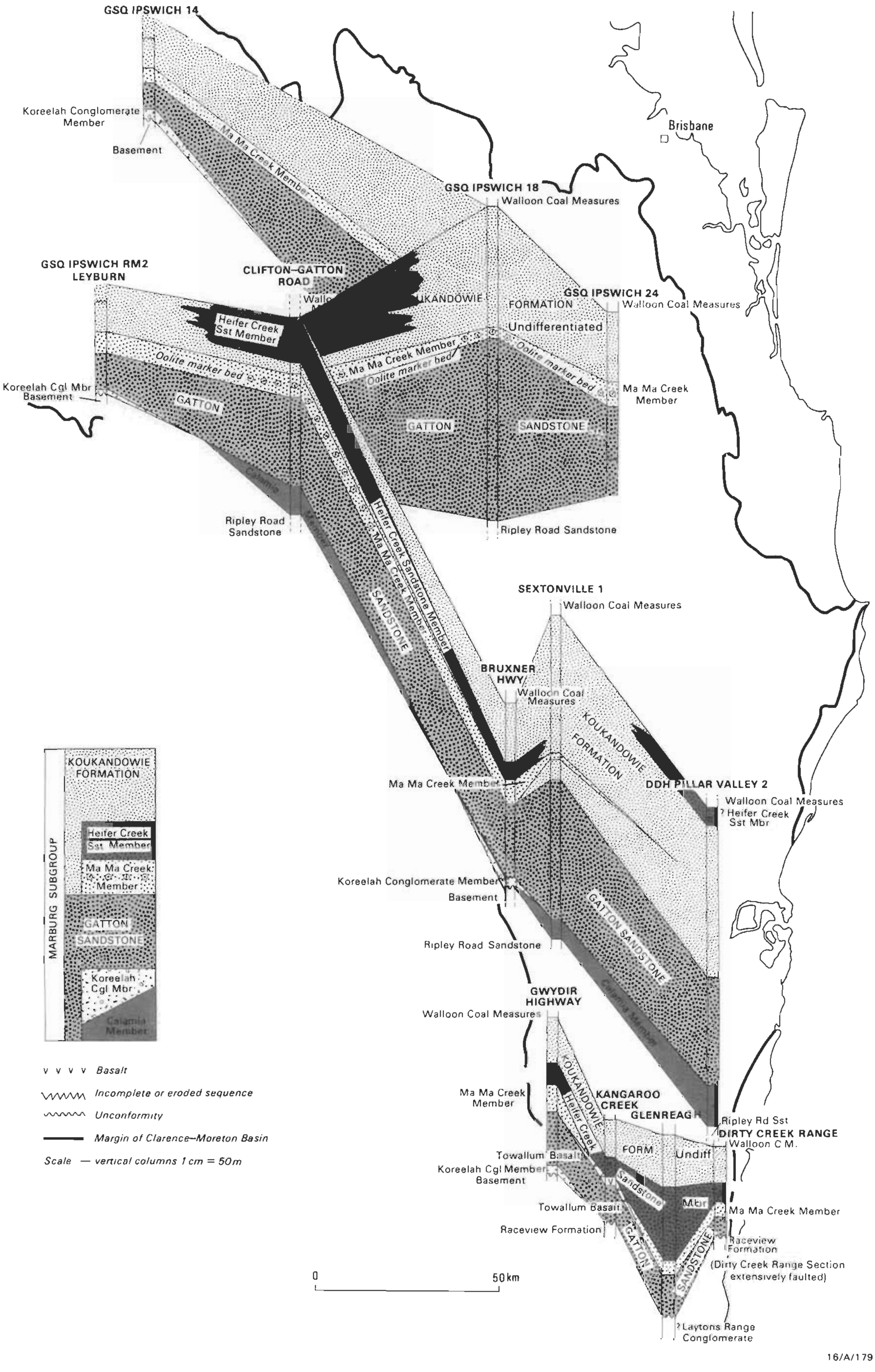

Figure 3. Marburg Subgroup distribution and correlations in the Clarence-Moreton Basin.

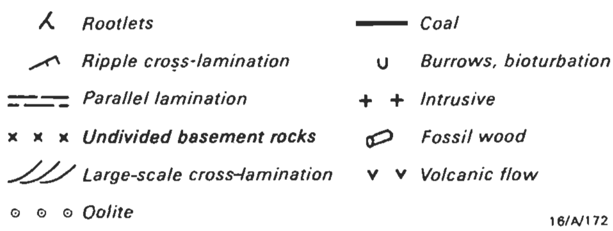

Figure 4. Explanation of symbols used on graphic logs.

The equivalent interval on the flanks of the South Moreton Anticline is much reduced in thickness and the rest of the 'Marburg Formation' below the 'Heifer Creek Sandstone Member' is undivided, indicating that the 'Ma Ma Creek Sandstone Member' is not identifiable in this region. This undivided sequence is identified on the Ipswich 1:100 000 sheet area and is most likely all 'Gatton Sandstone Member'.

The significance of the absence of the 'Ma Ma' Creek Sandstone Member' in this sequence is discussed later under this member.

Gray (1975) nominated sections in the interval 62–876 m in drill hole GSQ Ipswich 18 as new lithological reference sections for McTaggart's (1963) members.

In GSQ Ipswich 18 the reference section of the 'Heifer Creek Sandstone Member' of Gray (1975) occupies the interval from 62 m to 315 m, which includes thick (up to 15 m) intervals of shale. The member has an aggregate thickness of 60 m (or about 25%) of shale and mudstone in this drill hole. More significantly, thin beds of oolite occur at 74 m and 177 m. Oolite beds also occur lower in the sequence at 378 m and 381 m, in the 'Ma Ma Creek Sandstone Member' which occupies the interval 315 m to 417 m. Oolite has been used as a stratigraphic marker in Early Jurassic sequences in southeastern Queensland, mainly for correlation of the 'Ma Ma Creek Sandstone Member'. Day & others (1974, p. 338) stated that 'an essentially isochronous oolitic ironstone containing the acritarch-bearing horizons, has been traced from the Surat and Mulgildie Basins through the Moreton and Nambour Basins to the Maryborough Basin'.

The presence of oolite near the top of the 'Marburg Formation'[6] in GSQ Ipswich 18 indicates a brief reversal to shallow water, probably lacustrine, conditions that are normally recorded near the middle of the unit. It also casts some doubt on the stratigraphic uniqueness of the oolite horizon, and indicates that some care is required if it is to be used for correlation.

A comparison of the reference section and the outcrop on the Clifden–Gatton road shows that the 'Heifer Creek Sandstone Member' changes in lithology from east to west across the northern part of the basin. This change is interpreted as an indicator of major differences in depositional environments and distance from the provenance. In the sequence penetrated in GSQ Ipswich 24 (nominated as a reference section in this paper: see Appendix 1), the member comprises mainly overbank deposits, including bioturbated shale and mudstone and crevasse splay sandstone. By contrast the section further west at Heifer Creek contains a much higher percentage of quartzose and lithic sandstone. The sandstone occurs in fining up sequences that are terminated in places by shale; this indicates a high energy–low sinuosity stream environment of deposition.

[6] An alternative interpretation offered by one of the authors (LCC) is that the oolite could be in the base of the Walloon Coal Measures.

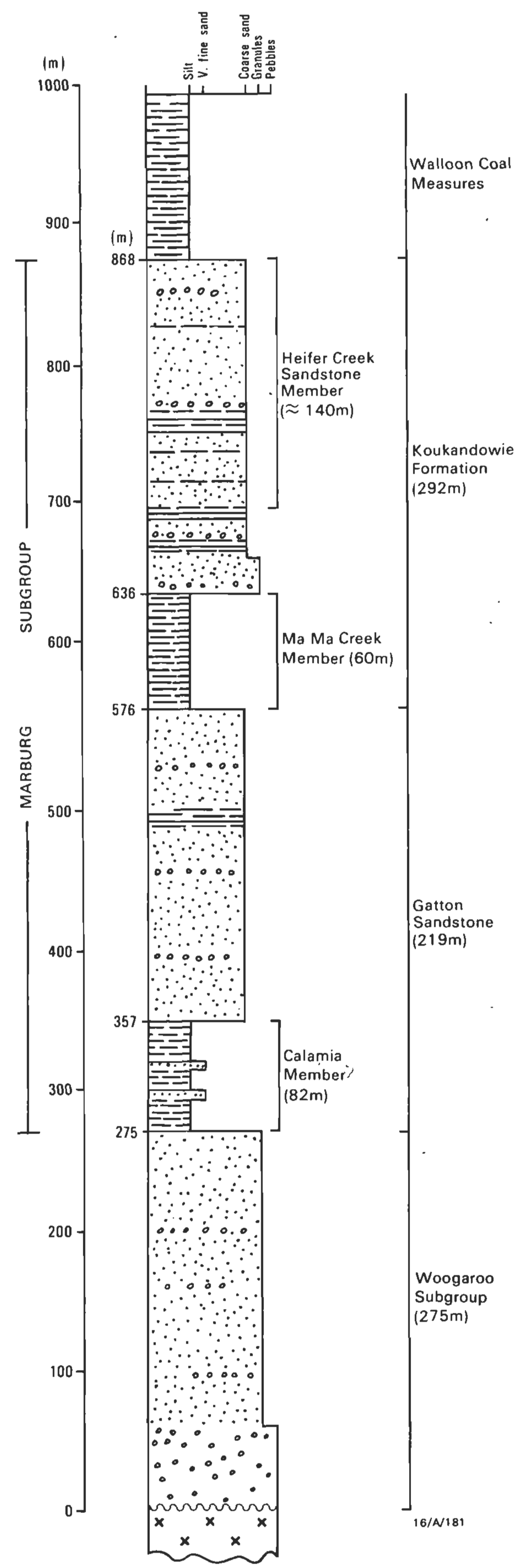

Figure 5. Graphic log, Clifden–Gatton Road.

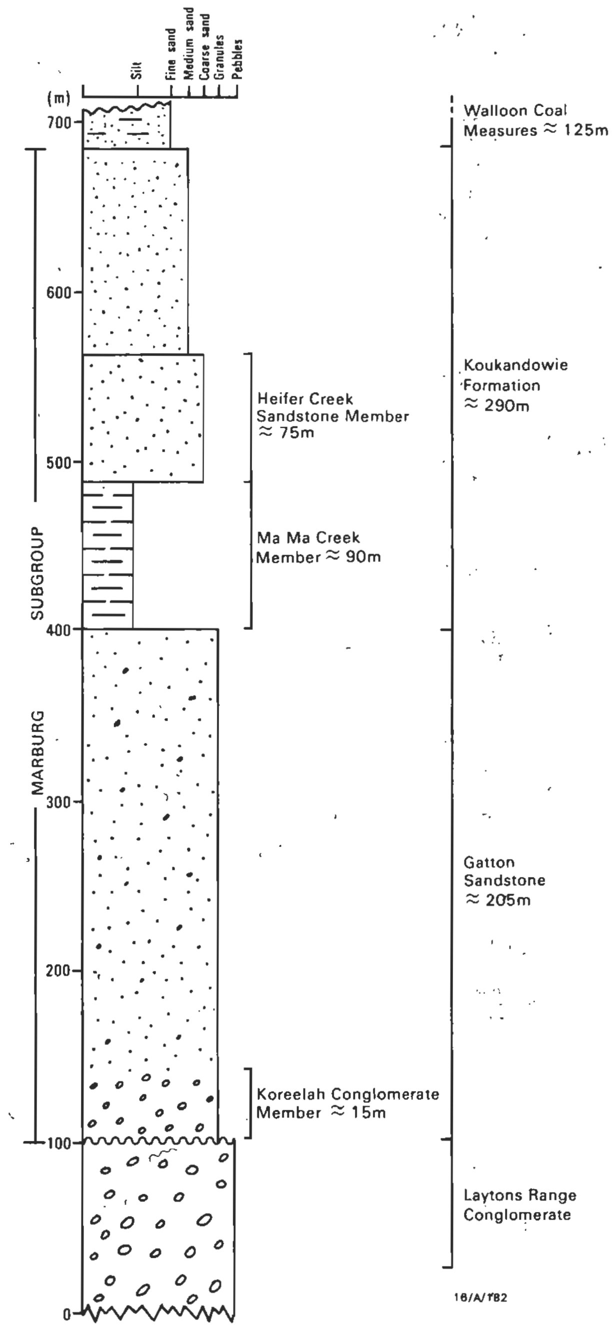

Figure 6. Graphic log, Bruxner Highway.

The sedimentary structures and fluvial architecture of the member exposed in road cuttings at Marburg indicate a contribution of high sinuosity, low energy stream deposition, as well as thicker stacked channel sand deposits. Marburg lies in an intermediate position between Heifer Creek and the reference section.

An east to west lithological transition similar to that found in the northern Clarence–Moreton Basin is apparent in the New South Wales part of the basin. A highly quartzose sandstone unit included in McElroy's (1963) 'Koukandowie Sandstone Member' is present in the west and south (Figs 5–10), and finer and siltier rocks are present in the east. The significance of the occurrence of quartzose beds in the 'Koukandowie Sandstone Member' to the new nomenclature is considered in further detail below in the section 'Koukandowie Sandstone Member', where McElroy's (1963) nomenclature is discussed. Therefore the regional facies trend in the 'Heifer Creek Sandstone Member' across the Clarence–Moreton Basin is a change in composition with an increase eastwards in the proportion of silts and muddy matrix, mudrock interbeds and lithic fragments in the sandstone.

The composition of the sandstone in the 'Heifer Creek Sandstone Member' is distinct from that in the lower part of the 'Marburg Formation'. This is used to distinguish and define the two formations (see 'Gatton Sandstone Member' section, and Appendix 1).

A new name is required for the younger of the two major units of the 'Marburg Formation' for the following reasons:

i) it is composed of distinct lithological assemblages;
ii) it incorporates areas where members are readily discernible;
iii) it incorporates areas where members are not developed and the whole unit cannot be subdivided.

It is proposed that the name Koukandowie Formation be retained for this unit. The name is derived from McElroy's (1963) 'Koukandowie Sandstone Member', the younger of the two major subdivisions of the 'Marburg Formation'.

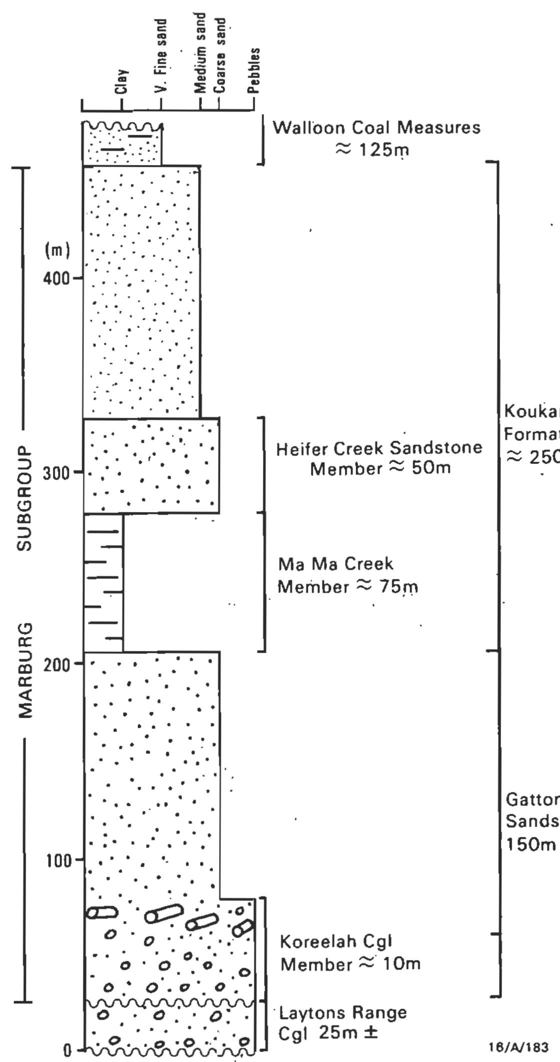

Figure 7. Graphic log, Gwydir Highway.

'Ma Ma Creek Sandstone Member'

The *'Ma Ma Creek Sandstone Member'* was defined by McTaggart (1963, p. 99) as '250 feet [76 m] of flaggy lithic sandstones, shales, and siltstones with minor fossil wood conglomerate bands. It shows good exposures around the lower reaches of Ma Ma Creek; Flagstone Creek derives its name from the strata'. McTaggart (1963) stated that the boundary with his 'Tenthill Conglomerate Member' is not sharply defined; no type section was nominated.

Gray (1975) nominated the interval 315 m to 417 m in GSQ Ipswich 18 as the lithological reference section for the member. Here the unit is predominantly shale and mudstone in the lower half, and a mixture of mostly medium and some fine to coarse grained, parallel and cross-laminated sandstone and subordinate mudstone in the upper part.

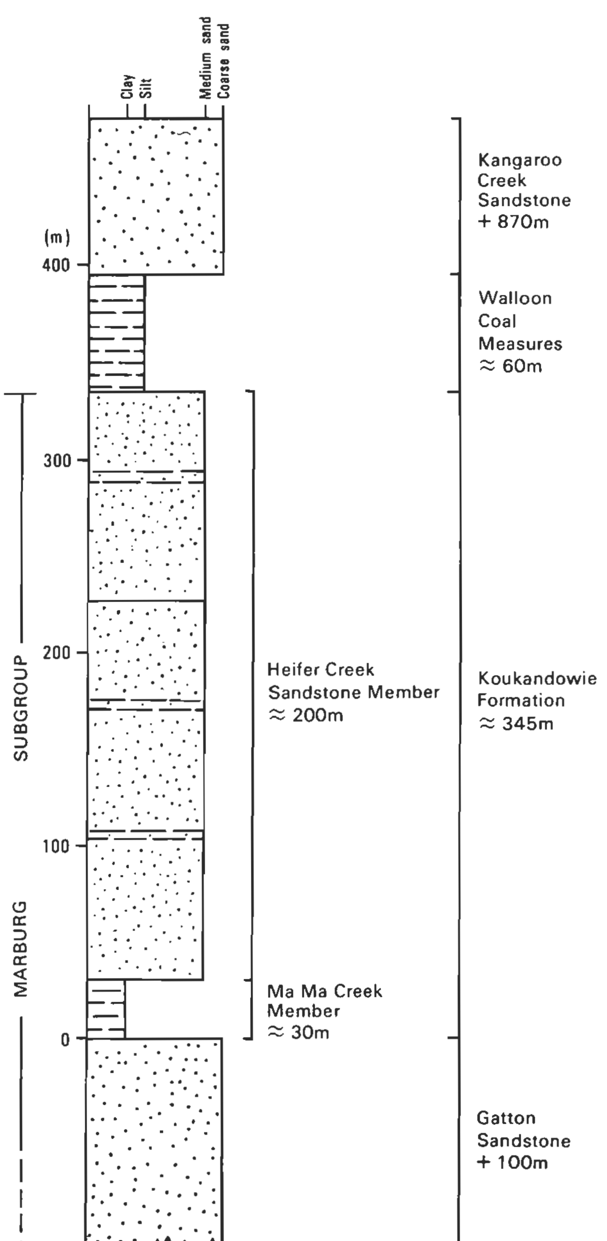

Figure 8. Graphic log, Waihou Trig, Glenreagh.

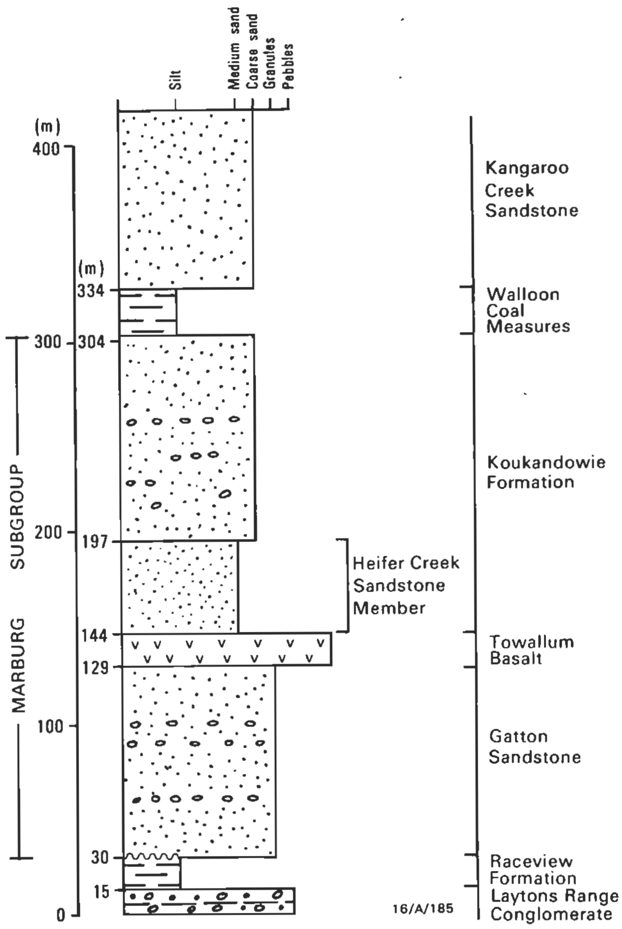

Figure 9. Graphic log, Kangaroo Creek.

The most characteristic rock type in exposures of the member is the finer grained, probably lacustrine, shale such as that exposed at Dry Creek on the Clifden–Gatton road and at Lowood. The characteristic marker oolite bed has been found only at two localities in outcrop, one a few kilometres north of Beaudesert, and the second on the Clifden–Gatton road section at 9342-153.357 on the Helidon 1:100 000 sheet area.

The 'Ma Ma Creek Sandstone Member' is not present in either BMR Maclean No.1 or the DM Pillar Valley DDH No.2 core holes but has been identified in BMR Warwick 7 (Wells & others, 1990).

In the rest of the New South Wales part of the Clarence–Moreton Basin the 'Ma Ma Creek Sandstone Member' is difficult to identify and probably does not exist in most sections. An added complication is that shaly intervals occur in the sequence above and below the prominent quartzose sandstone within McElroy's (1963) 'Koukandowie Sandstone Member'. The member occupies a stratigraphic position in the upper part of the 'Marburg Formation' and may be diachronous from north to south. Shale intervals occur in the sequences above the 'Gatton Sandstone Member' on the western flanks of the basin and the 'Ma Ma Creek Sandstone Member' has been identified on stratigraphic, lithological and palynological evidence in a stratigraphic drill hole on the basin's western flank (Wells & others, 1990). The only additional recorded occurrence of the member in the southern part of the basin includes an interval about 60 m thick in Sextonville 1 well.

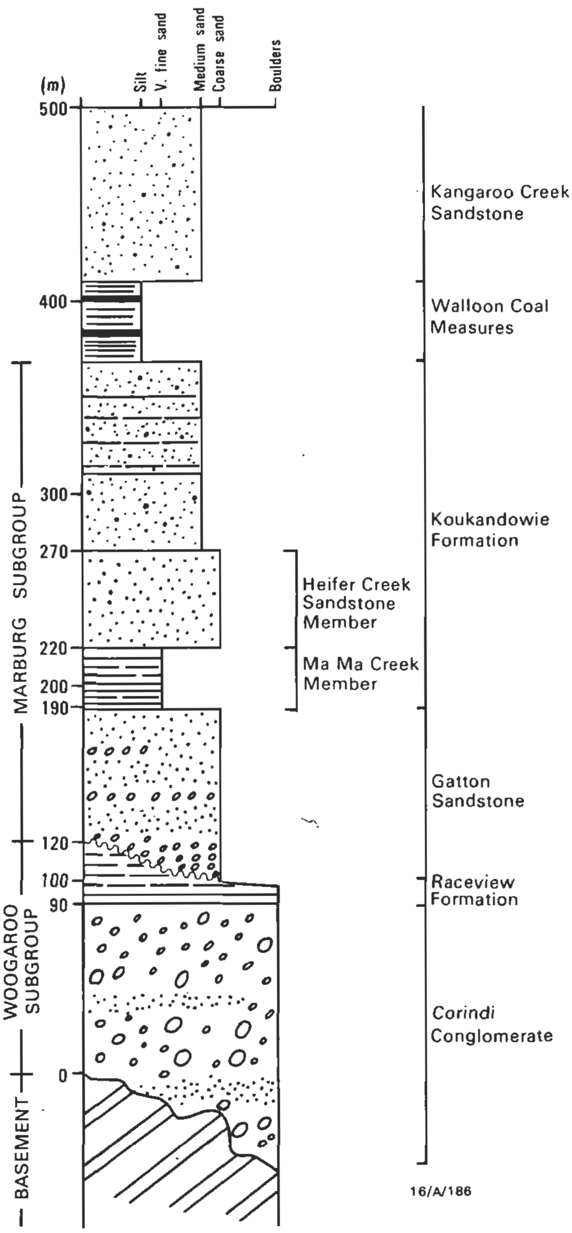

Figure 10. Graphic log, Pacific Highway.

The 'Ma Ma Creek Sandstone Member' is retained in the new nomenclature, except that the term sandstone is deleted from the name. The member has been shown to contain roughly equal proportions of sandstone and shale.

The type section (Fig. 11; Appendix 1) is composed of 54% shale and siltstone, and the rest is mostly fine-grained sandstone and rare thin coal interbeds.

'Tenthill Conglomerate Member'

The 'Tenthill Conglomerate Member' (subsequently termed the 'Winwill Conglomerate Member') of the Marburg Formation was defined by McTaggart (1963, p. 99) as '100–150 feet [30–46 m] of white flaggy sandstone with fossil-wood conglomerates that typically crop out along the lower reaches of Tenthill and Ma Ma Creeks'. It was described as having limited area, extending as far west as Crows Nest and as far east as Borallon. 'The Member is more resistant to erosion than its immediate neighbours and forms low cliffs and abrupt changes of slope' (McTaggart, 1963, p. 99).

Recent investigations in the Laidley Valley have indicated that conglomerate occurs at many levels in the 'Marburg Formation'. They have not substantiated the presence of a mappable unit of conglomerate at a unique level. Conglomerate occurs mainly as channel lag deposits, and its presence is dependent on the formation of thick channel sands. Because the 'Marburg Formation' has a fluvial architecture made up of multistorey channel sands, conglomerate can be expected to occur at several stratigraphic levels.

All the sections documented in the 'Marburg Formation' indicate that conglomerate units are not reliable stratigraphic markers, as it cannot be demonstrated that they have formed at a unique stratigraphic level. The names applied to these conglomerates are therefore abandoned.

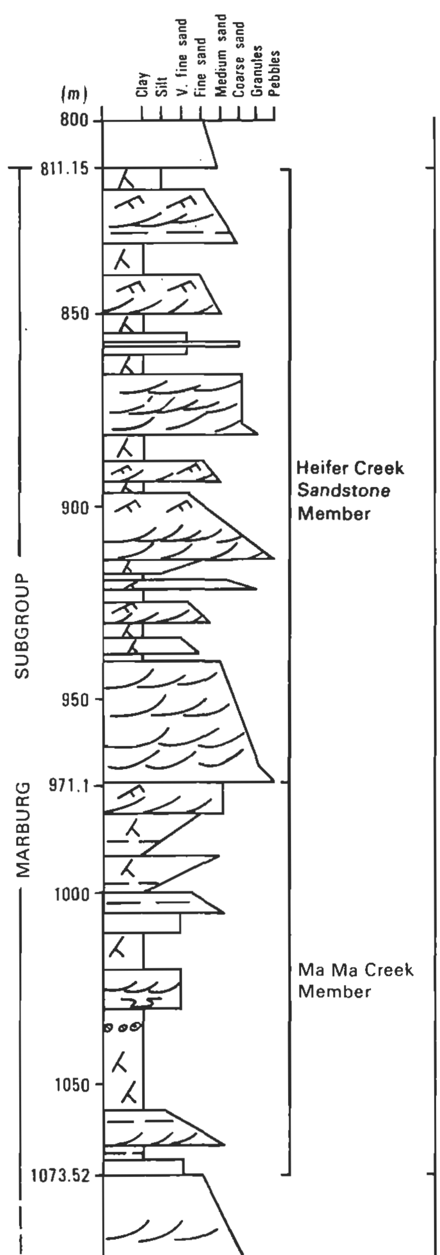

Figure 11. Generalised graphic log of the Koukandowie Formation in GSQ Ipswich 24.

'Gatton Sandstone Member'

The lowermost member defined in the Marburg Formation by McTaggart (1963) is the *'Gatton Sandstone Member'*.

> The Gatton Sandstone Member comprises 100–200 feet [30–61 m] of caliche lithic sandstone that conformably overlies the Helidon Sandstone. It shows good exposure in the bed of Lockyer Creek between Helidon and Gatton. The sandstone is quite massive and devoid of cross-bedding. Lithologically it is composed of grains of quartz and some lithic fragments set in an argillaceous matrix rich in carbonates of sodium, calcium, and magnesium. The member is an aquifer with artesian head around Helidon Spa and the above information was obtained from water bore analyses (McTaggart, 1963, p. 99).

The friable easily eroded sandstone of the Gatton Sandstone Member forms the bed of Lockyer Creek along most of its course. The member is well exposed in cuttings at the lower end of the Murphys Creek road and on the Warrego Highway near Gatton.

The 'Gatton Sandstone Member' has been identified throughout the southern part of the Clarence–Moreton Basin by its lithology, well log character and superposition. It occurs in outcrop around the margins of the basin, in stratigraphic drill holes at Evans Head, BMR Maclean No.1 and DM Pillar Valley DDH No.2, and has been identified in most of the deep petroleum exploration wells.

The composition of the 'Gatton Sandstone Member' is distinct from the 'Heifer Creek Sandstone Member'. The 'Gatton Sandstone Member' contains a high proportion of clay and silt matrix, and lithic grains. In places it is extremely poorly sorted. It commonly occurs in well defined channel sand bodies. The sedimentary structures indicate predominantly high energy, low sinuosity channel deposits, with preservation of predominantly multistorey channel sand bodies and minor overbank and splay deposits. Both planar and trough cross-bedding indicating cross-channel bars and dunes are well preserved. The composition of the 'Gatton Sandstone Member' varies only marginally throughout the basin except along the western edge, where it overlaps older units and rests unconformably on Palaeozoic basement rocks. Towards this region the unit becomes progressively more coarse-grained and grades laterally into and overlies the Koreelah Conglomerate Member.

These significant differences in composition of the two major sandstone bodies allow an easily recognisable basin-wide twofold subdivision of the 'Marburg Formation', and it is therefore proposed that the 'Gatton Sandstone Member' be elevated to formation status.

A twofold division of the 'Marburg Formation' was recognised by McElroy (1963) in the southern part of the Clarence–Moreton Basin. The name 'Koukandowie Sandstone Member' was applied to the upper part and the name 'Blaxland Fossil Wood Conglomerate Member' to the lower part. The 'Blaxland Fossil Wood Conglomerate Member' therefore approximates the 'Gatton Sandstone Member' of McTaggart (1963) and the 'Koukandowie Sandstone Member' approximates the remainder of the 'Marburg Formation' above the 'Gatton Sandstone Member'.

'Koukandowie Sandstone Member'

McElroy (1963) described a dominantly sandstone sequence of the upper part of the 'Marburg Formation' in the southern Clarence–Moreton Basin which conformably overlies the 'Blaxland Fossil Wood Conglomerate Member' in the Nymboida-Kangaroo Creek area. The name *'Koukandowie Sandstone Member'* was given to this upper unit.

> This member is well exposed 2 miles (3 km) west of Koukandowie T.S. on the east side of Kangaroo Creek, and crops out on the Grafton–Nymboida road 3.5 miles [5.6 km] northeast of Nymboida Power Station (McElroy, 1963). The maximum observed thickness is stated by McElroy as 400 feet [120 m] 2.5 miles [4 km] northeast of Nymboida Colliery, although no complete section was measured and no type section was nominated. It is conformably overlain by the Towallum Basalt where this unit is developed, and elsewhere by the Walloon Coal Measures (McElroy, 1963). Recent field research in the Kangaroo Creek–Nymboida area has shown that the Towallum Basalt consistently occurs at the boundary between McElroy's (1963) 'Koukandowie Sandstone Member' and the 'Gatton Sandstone Member' (Fig. 9). This revision has meant better concordance between the isotopic dating of the Towallum Basalt and the palynological age obtained for the sediments (see Appendix 1).

The name Koukandowie is retained for the upper of the two units in the 'Marburg Formation', and is elevated to formation status.

A relatively clean quartzose sandstone within McElroy's (1963) 'Koukandowie Sandstone Member' forms a prominent sandstone bench and cliff-forming interval in the upper half of the 'Marburg Formation'. This prominent quartz sandstone member has been identified in several sections in over 500 km along the western and southern margins of the basin (Figs 5–10) and is an important marker unit. It has not so far been differentiated on the eastern basin margin such as the Pillar Valley section of the Wooli Road, or in the Pillar Valley DDH No.2, although quartzose sandstone intervals have been described from the upper part of the 'Marburg Formation' in the drill hole. West of Kangaroo Creek it has been identified on the Grafton–Nymboida Road, OBX Creek and north to the Gwydir Highway, near Newbold Lookout, in a quarry south of Tabulam on the Rappville road, in the Bruxner Highway sections, in the Koreelah Creek area and in railway cuttings and small scarps on hillslopes on the northwestern outskirts of Warwick. In the Warwick area the quartz sandstone member occupies the same stratigraphic position as the quartzose sandstone in the upper part of the Clifden–Gatton road section at Heifer Creek, i.e. in the upper part of the 'Marburg Formation' just below the Walloon Coal Measures. Hence the quartz sandstone unit is undoubtedly equivalent to the Heifer Creek Sandstone Member of McTaggart (1963).

The quartz sandstone marker bed occurs at various stratigraphic levels in the Marburg Formation, as follows:

- Pacific Highway/Dirty Creek Range — above the ?Ma Ma Creek Member (Fig. 10);
- Glenreagh — in the basal part of the Koukandowie Formation overlying possible Ma Ma Creek Member (Fig. 8);
- Kangaroo Creek — above the Towallum Basalt at the base of the Koukandowie Formation (Fig. 9);
- Gwydir Highway/Newbold Lookout — in the basal half of the Koukandowie Formation (Fig. 7);
- Bruxner Highway — in the basal part of the Koukandowie Formation (Fig. 6);
- Warwick/Clifden-Gatton Road — occupies the upper part of the Marburg Subgroup and is equated with the 'Heifer Creek Sandstone Member' of McTaggart (1963) (Fig. 5).

The name Heifer Creek Sandstone Member is therefore extended to the southern parts of the basin to describe this important quartz sandstone marker bed within the Koukandowie Formation.

'Blaxland Fossil Wood Conglomerate Member'

The base of the 'Marburg Formation' in New South Wales was defined by McElroy (1963) as the stratigraphic interval containing 'a remarkable accumulation' of fossil wood in a coarse-grained conglomeratic sandstone, granule conglomerate and minor cobble and pebble conglomerate.

The name *'Blaxland Fossil Wood Conglomerate Member'* was used for the unit. McElroy (1963) used the 'Blaxland Fossil Wood Conglomerate Member' to differentiate the Marburg Formation from his 'Bundamba Group' (sic) (equivalent to the Woogaroo Subgroup in Queensland). The member is the older of the two units constituting the 'Marburg Formation' in the southern, New South Wales part of the Clarence-Moreton Basin.

The term 'Blaxland Fossil Wood Conglomerate Member' is abandoned and the name Gatton Sandstone is retained for this unit. The principal reasons for this change are detailed in Appendix 1. The term Gatton Sandstone has been more widely accepted than the term 'Blaxland Fossil Wood Conglomerate Member'. The position and identification of the latter has commonly been misinterpreted in the Early Jurassic sequence in New South Wales. Although the Gatton Sandstone commonly contains abundant fossil wood and conglomerate in discrete intervals, the beds seem to occur at different stratigraphic levels, and their position is probably controlled by the preservation of a fluvial sedimentation cycle.

The maximum thickness quoted for the 'Member' by McElroy (1963) is 150 feet [45 m], and logs of fossil wood up to 60 feet [18 m] long and up to 2 feet [0.6 m] in diameter are reported. The host rock is medium to coarse grained quartz-lithic sandstone and quartz sandstone, fine quartz sandstone to fine quartz-pebble and granule conglomerate. White quartz pebbles are common to most outcrops of the member. The wood is mostly replaced by hematite and limonite, and rarely by silica. Although no type section was nominated, an excellent continuous exposure is cited by McElroy (1963) 2.5 miles [4 km] northeast of Nana Glen, which is the maximum known thickness.

Revised stratigraphic framework

The recent research in the Clarence-Moreton Basin has highlighted major inconsistencies of the previous stratigraphic nomenclature and duplication of names for the same unit. This has been especially noticeable when attempting correlation of formations across the border from New South Wales into Queensland, and has severely hampered basin-wide studies.

The principal reasons for this unsatisfactory nomenclature have been the lack of data and the lack of a basin-wide perspective of regional facies relationships. Many of the stratigraphic schemes proposed were based on sequences established at the basin margins where local facies are developed. Workers studying local areas invented new local names which were isolated from the concept of a basin-wide stratigraphic scheme. Reconciliation of these sequences with those in central basin areas is possible only with a new stratigraphic scheme.

The new scheme presented here is based on a study of selected sections throughout the basin, re-interpretation of all deep well sections, new seismic sections, and the results from fully cored stratigraphic drill holes. This synthesis has largely overcome the major difficulties of regional facies correlation. From the discussion in the review of stratigraphic units it is apparent that several lithofacies in the Marburg sequence have a basin-wide distribution, whilst others are comparatively locally developed. A revised nomenclature is therefore necessary. The suggested scheme for the rationalisation of the previous nomenclature, to account for the distribution of these lithological associations, is outlined below and shown in Figures 3 and 12.

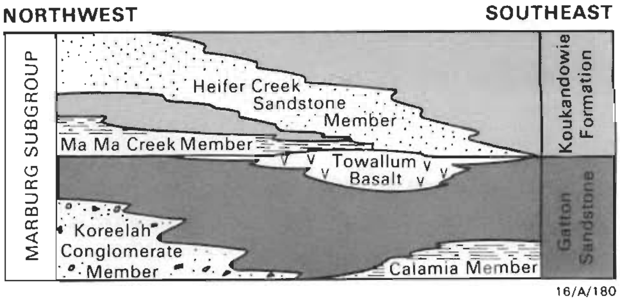

Figure 12. Rock relationship diagram.

All the criteria necessary for redefining and revising the existing and new stratigraphic units discussed are detailed in Appendix I.

Marburg Subgroup

The Marburg Subgroup is upgraded from the 'Marburg Formation'. The precise limits of the Marburg interval have not been adequately described and the boundaries nominated in various publications are unsatisfactory.

We define the limits of the Marburg Subgroup primarily on sandstone composition; the quartz-feldspar-lithic arenites of the Marburg Subgroup are overlain by the Walloon Coal Measures which contain volcanic litharenites; the lower boundary is marked by a change to clean quartz sandstone in the Ripley Road Sandstone of the Woogaroo Subgroup.

Gatton Sandstone

Field sections, well logs, and seismic reflection sections (Fig. 13) all support the basic twofold division of the Marburg Subgroup. The lower uniform quartz-feldspathic and lithic arenite comprises the Gatton Sandstone. The name Gatton Sandstone is derived from McTaggart's (1963) 'Gatton Sandstone Member' but is redefined to include the conglomerates formerly called either the Tenthill or Winwill Conglomerate Members, lithostratigraphic terms that are now discarded.

Calamia Member

The Calamia Member (Etheridge & others, 1985) of mixed sandstone, shale and mudrock is a basal unit in the Gatton Sandstone in basinward sections.

Koukandowie Formation

The upper lithologically more variable sequence is composed of quartzose and quartz-feldspathic-lithic sandstone, siltstone, mudrock and some coal of the Koukandowie Formation. The name is derived from McElroy's (1963)

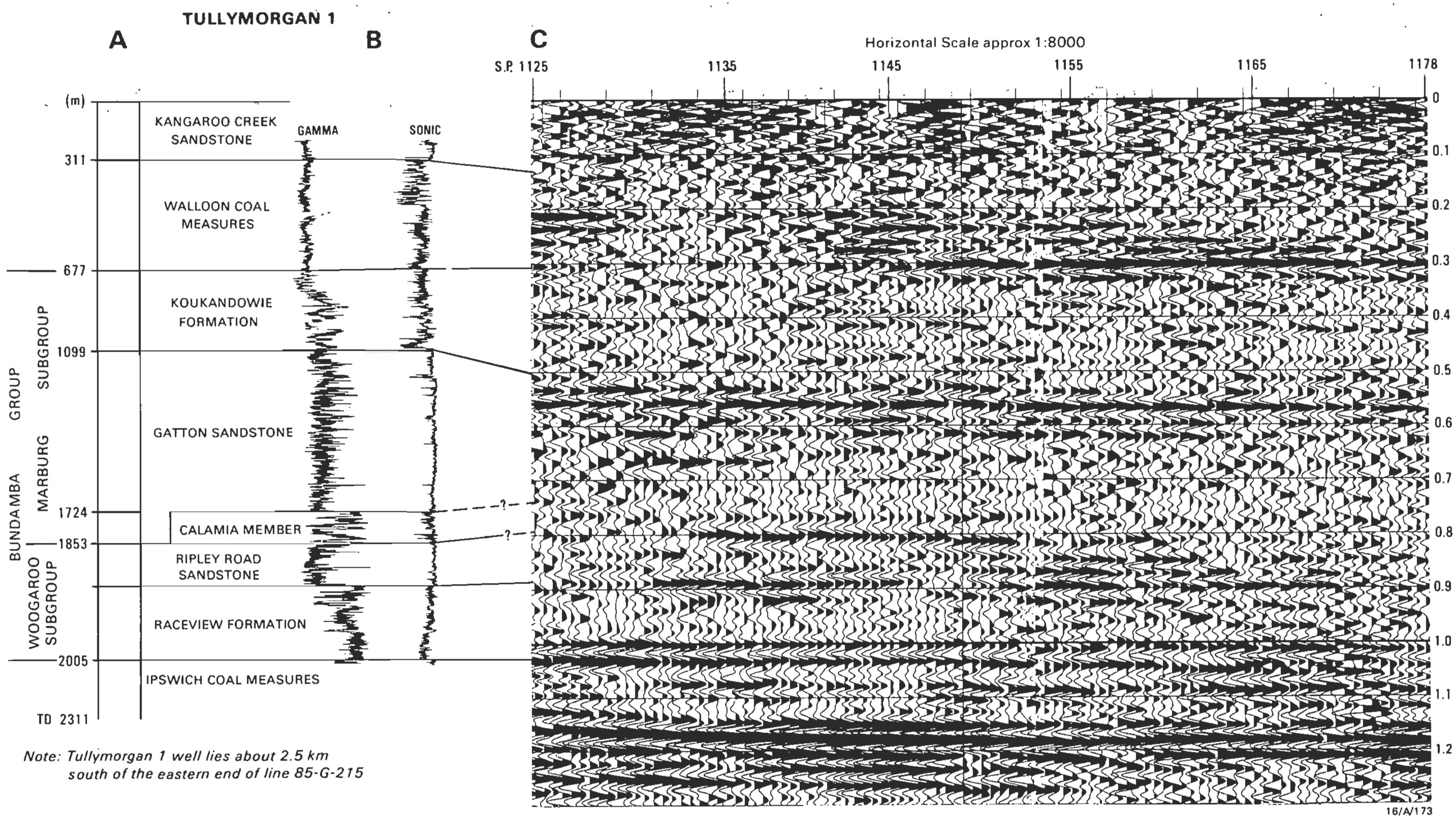

Figure 13. Seismic character of Bundamba Group.
A, Well sequence in Tullymorgan No.1 (Boisvert & Williams, 1965); B, Gamma and sonic logs of Tullymorgan No.1; C, Segment of data from Grafton seismic survey, Line 85-G-215 (Hartogen Energy Ltd).

'Koukandowie Sandstone Member' and includes all the sequence in the Marburg Subgroup above the Gatton Sandstone.

These contrasting sequences in the two formations are similarly well defined on seismic record sections (Fig. 13), and the upper boundaries of the two units are readily distinguished. However, the base of the Gatton Sandstone is mostly not easily identified on these records, because it has a similar seismic acoustic response to the underlying Ripley Road Sandstone.

The term 'Blaxland Fossil Wood Member' of McElroy (1963) is discarded in favour of Gatton Sandstone, a more widely used and accepted term for the older of the two formations in the Marburg Subgroup.

Ma Ma Creek and Heifer Creek Sandstone Members

Two members are defined in the Koukandowie Formation — a siltstone, shale, sandstone sequence of the Ma Ma Creek Member, and the prominent bench-forming quartz sandstone unit, the Heifer Creek Sandstone Member. The name 'Ma Ma Creek Member' is redefined from McTaggart's (1963) Ma Ma Creek Sandstone Member because in most sections it is a unit of mixed lithology and in some sections mudrock predominates. The name Heifer Creek Sandstone Member is derived from McTaggart's (1963) unit of the same name. It is redefined and restricted to the prominent resistant bench and cliff forming quartzose planar cross-bedded sandstone that occurs at various stratigraphic levels in the Koukandowie Formation.

Koreelah Conglomerate Member

The Koreelah Conglomerate Member is a new name proposed for a conglomerate locally developed at the base of the Gatton Sandstone. The member is present on the basin's western margin, and possibly also in the south, where the Gatton sandstone overlaps older sediments and rests either on older basin formations or basement rocks.

In the light of this new nomenclature it is worth noting that the generalised stratigraphy in the New South Wales part of the Clarence-Moreton Basin proposed by Ties & others (1985; Figs 4-6) recognised the basic subdivisions of the Bundamba Group but assigned incorrect names to the units. Their sequence, from the base of the Bundamba Group, is Raceview Formation/Laytons Range Conglomerate, 'Pillar Valley Formation' (informal unit), Ripley Road Sandstone, and Marburg Formation. Regional correlation of well logs and seismic lines shows that the correct sequence of units should be Raceview Formation/Laytons Range Conglomerate, Ripley Road Sandstone, Gatton Sandstone, and Koukandowie Formation. No evidence has been found for a regional unconformity in the Marburg Subgroup as suggested by Ties & others (1985).

Conclusions

Recent field studies and a re-interpretation of well logs and seismic reflection sections in the Clarence-Moreton Basin have indicated that major changes in stratigraphic nomenclature are required.

A revised stratigraphic framework for the Early Jurassic sequences of the Clarence-Moreton Basin has been developed that clarifies the sedimentary history of the basin and the distribution of porous and permeable units. The new scheme, which involves mainly a change of status of units, recognises the distribution and continuity of lithologic entities and their depositional environments. It should assist systematic basin-wide study.

Acknowledgements

The manuscript benefited immeasurably from the comments of Dr C.T. McElroy, who contributed data from his own knowledge of the area, as well as a critical review of the paper. The refereeing of Drs J.F. Lindsay and M.R. Walter is acknowledged. Published with the permission of the Director, Geological Survey of New South Wales, Sydney, and the Chief Government Geologist, Geological Survey of Queensland, Brisbane.

References

Boisvert, T.H., & Williams, R.S., 1965 — Tullymorgan No.1 Well completion report, Australia-Cities Service Inc.

Cameron, J.B., 1970 — The Rosewood-Walloon coalfield. *Geological Survey of Queensland, Publication* 344.

Cameron, W.E., 1907 — Second report on the West Moreton (Ipswich) coalfield. *Geological Survey of Queensland, Publication* 204, 1-37.

Cranfield, L.C., 1981 — Stratigraphic drilling report — GSQ Ipswich 24 and 25. *Queensland Government Mining Journal,* 82, 468-477.

Cranfield, L.C., Hutton, L.J., & Green, P.M., 1981 — Ipswich, Queensland, 1:100 000 geological series, sheet 9442. *Department of Mines, Geological Survey of Queensland, Brisbane.*

Cranfield, L.C., & Schwarzbock, H., 1972 — Nomenclature of some Mesozoic rocks in the Brisbane and Ipswich areas, Queensland. *Queensland Government Mining Journal,* 73, 414-416.

Cranfield, L.C., Schwarzbock, H., & Day, R.W., 1976 — Geology of the Ipswich and Brisbane 1:250 000 sheet areas. *Geological Survey of Queensland, Report* 95.

Day, R.W., Cranfield, L.C., & Schwarzbock, H., 1974 — Stratigraphy and structural setting of Mesozoic basins in southeastern Queensland and northeastern New South Wales. *In* Denmead, A.K., Tweedale, G.W., & Wilson, A.F., (editors), 1974 — The Tasman Geosyncline, a symposium. *Geological Society of Australia, Queensland Division,* 319-362.

De Jersey, N.J., 1971 — Palynological evidence for a facies change in the Moreton Basin. *Queensland Government Mining Journal,* 72, 464-472.

De Jersey, N.J., 1976 — Palynology and time relationships in the Lower Bundamba Group (Moreton Basin). *Queensland Government Mining Journal,* 77, 460-465.

Etheridge, L.T., Hamilton, D.S., McDonald, I., McMinn, A., & Smythe, M., 1985 — Clarence-Moreton Basin stratigraphic drill hole. *Geological Survey of New South Wales, Quarterly Notes* 60, 5-21.

Evans, P.R., 1966 — Mesozoic stratigraphic palynology in Australia. *Australasian Oil and Gas Journal* 12(6), 58-63.

Flint, J.C.E., Lancaster, C.G., Gould, R.E., & Hensel, H.D., 1976 — Some new stratigraphic data from the southern Clarence-Moreton Basin. *Queensland Government Mining Journal,* 77, 397-401.

Gray, A.R.G., 1975 — Bundamba Group stratigraphic relationships and petroleum prospects. *Queensland Government Mining Journal,* 76, 311-323.

Helby, R.J., Morgan, R., & Partridge, A.D., 1987 — A palynological zonation of the Australian Mesozoic. *Association of Australasian Palaeontologists, Memoir* 4, 1-85.

McElroy, C.T., 1963 — The geology of the Clarence-Moreton Basin. *Memoirs of the Geological Survey of New South Wales, Geology* 9.

McKellar, J.L., 1974 — Jurassic miospores from the upper Evergreen Formation, Hutton Sandstone, and basal Injune Creek Group, northeastern Surat Basin. *Geological Survey of Queensland, Publication* 361. *Palaeontological Paper* 35.

McKellar, J.L., 1981 — Palynostratigraphy of samples from the Lockyer Valley, Moreton Basin. *Queensland Government Mining Journal,* 82, 540-544.

Reid, J.H., 1921 — Geology of the Walloon-Rosewood coalfield. *Queensland Government Mining Journal,* 22, 223-227, 264-270, 310-316, 357-359.

Reid, J.H., & Morton, C.C., 1922 — Contributions to the geology of Ipswich. *Queensland Government Mining Journal*, 23, 355–358, 390–392.

Staines, H.R.E., 1964 — Stratigraphic nomenclature of the Bundamba Group in the Ipswich area. *Queensland Government Mining Journal*, 65, 33–35.

Swindon, V.G., 1956 — The geology of the Rosewood-Wivenhoe area, with particular reference to the sandstones. *B.Sc.(Hons) thesis, Department of Geology, University of Queensland.*

Ties, P., Shaw, R.D., & Geary, G.C., 1985 — The petroleum prospectivity of the Clarence-Moreton Basin in New South Wales. *The APEA Journal*, 25, 15–33.

Wells, A.T., & O'Brien, P.E., 1985 — BMR Maclean No.1 stratigraphic drill hole, Clarence-Moreton Basin. *Bureau of Mineral Resources, Record* 1985/86.

Wells, A.T., O'Brien, P.E., McMinn, A., & Willis I.L., 1990 — New data on Mesozoic sedimentary sequences from BMR Warwick 6 and 7 stratigraphic drill holes, Clarence-Moreton Basin, New South Wales. *Bureau of Mineral Resources, Record* 1990/8.

Whitehouse, F.W., 1955 — Appendix G. The geology of the Queensland portion of the Great Artesian Basin. *In* Artesian water supplies in Queensland. *Department of the Co-Ordinator General, Public Works, Queensland Parliamentary Paper A*, 56-1955.

Appendix 1. Definition and redefinition of stratigraphic units.

Name and rank: Marburg Subgroup, Bundamba Group

Derivation. The name is from the town of Marburg in the Ipswich 1:250 000 sheet area, Queensland.

Synonymy. The unit is redefined from Marburg Formation and upgraded to the Marburg Subgroup. The name was originally used by Reid (1921) as Marburg Stage of the Walloon Coal Measures. The term Marburg Formation was first published by Whitehouse (1955) and this name was formally defined by McTaggart in 1963 (see Cranfield, Schwarzbock & Day, 1976).

Distribution. Throughout the Clarence-Moreton Basin.

Geomorphic expression. See description of constituent formations and members. The cleaner quartzose conglomeratic sandstone intervals form prominent benches and cliffs. The lithic and silty sandstones form rounded hills and slopes, and the siltstone and mudrocks weather recessively.

Reference section. Outcrops of most units are incomplete and deeply weathered. A reference section was nominated by Gray (1975) in GSQ Ipswich 18 stratigraphic drill hole over the interval 203'5" [620 m] to 2874' [876 m].

Type section. The type section of the Marburg Subgroup is described under the two constituent formations — the Koukandowie Formation (GSQ Ipswich 24). and the Gatton Sandstone (GSQ Ipswich 18; Figs 11, 14).

GSQ Ipswich 24 and Ipswich 18 were originally logged and described by officers of the Geological Survey of Queensland (Gray, 1975; Cranfield, 1981) and subsequently relogged by A.T. Wells and P.E. O'Brien of the Bureau of Mineral Resources, Canberra.

Description at type section. The Marburg Subgroup comprises the Koukandowie Formation and the underlying Gatton Sandstone and their respective component members, and as such is described under each of the members. The Marburg Subgroup is conformably overlain by the Walloon Coal Measures in GSQ Ipswich 18 and 24, and conformably overlies the Woogaroo Subgroup in GSQ Ipswich 18. The base of the Subgroup was not reached in GSQ Ipswich 24.

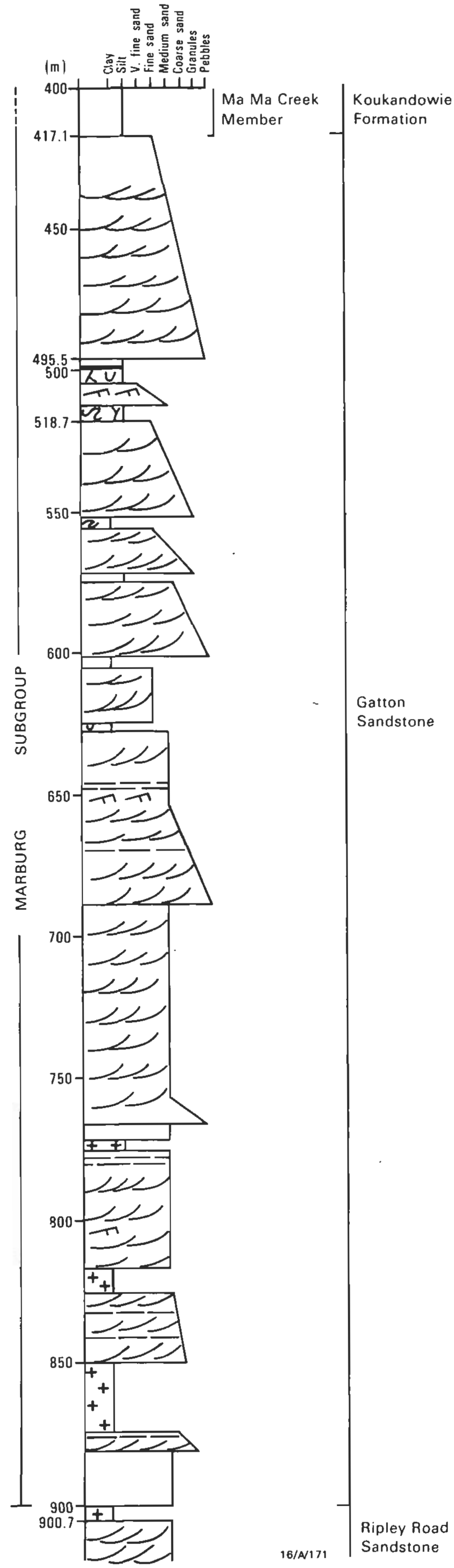

Figure 14. Generalised graphic log of the Gatton Sandstone in GSQ Ipswich 18.

The Ma Ma Creek Member of the Koukandowie Formation is differentiated in GSQ Ipswich 18 and 24, but no members of the Gatton Sandstone are apparent in either well section.

Regional aspects. The Marburg Subgroup occurs throughout the Clarence–Moreton Basin. In all outcrops where the upper contact is visible (there are very few) it is conformably overlain by the Walloon Coal Measures. The lower contact is an unconformity over wide areas, particularly on the western margin of the basin where the Subgroup overlaps Late Triassic sediments and Palaeozoic basement rocks. In the southern part of the Clarence–Moreton Basin (notably in the Coast Range, Glenreagh and Nymboida areas), an angular unconformity occurs at the contact with the underlying Woogaroo Subgroup. Elsewhere the Marburg and Woogaroo Subgroups are apparently conformable.

McElroy (1963) used the base of the lowest fossil wood horizon as the base of his Marburg 'Formation'. The top was taken as the first pebble band below the Walloon Coal Measures or alternatively at the base of the coal-bearing sequence of dark shales, claystones and friable sandstone of the Walloon Coal Measures.

These boundary criteria have proved to be unsatisfactory. Sandstone composition is proposed as the most reliable method of distinguishing the Marburg Subgroup from bounding sequences. The Marburg Subgroup contains labile quartzose-lithic and feldspathic sandstones, whereas the underlying Ripley Road Sandstone is predominantly clean quartzose sandstone that is very resistant to weathering. The sandstones in the overlying Walloon Coal Measures are volcanolithic and very friable.

Constituent units. The basic subdivisions of the Marburg Subgroup are the Koukandowie Formation and the underlying Gatton Sandstone and their respective members. The names Koukandowie and Gatton were formerly applied to members, but as it has been demonstrated that they extend over the basin as mappable units, they are redefined as formations. The Marburg 'Formation', of which they were a part, is therefore upgraded to Marburg Subgroup.

Age and evidence. Palynofloral assemblages in the Marburg Subgroup indicate an Early Jurassic age (Rhaetian to possibly basal Bajocian) (Cranfield & others, 1976; McKellar, 1981). Details of the ages of each formation and member of the subgroup are described later in this report.

References. Reid (1921), McTaggart (1963).

Name and rank: Koukandowie Formation, Marburg Subgroup

Derivation. From Koukandowie Mountain (Trig Station), (MM874.824, Grafton 1:100 000 sheet area 9438) at the southern margin of the Clarence–Moreton Basin.

Synonymy. The unit name is derived from the Koukandowie 'Sandstone Member' of the 'Marburg Formation' as published by McElroy (1963). The formation is the younger of the two units of the Marburg Subgroup defined in this paper.

Distribution. The formation has been identified throughout the Clarence–Moreton Basin, wherever the Marburg Subgroup is identified.

Reference section. No type section was given for the Koukandowie Sandstone Member by McElroy. Gray (1975) subsequently nominated the interval in GSQ Ipswich 18 from 203′5″ [62.0 m] to 1368′4″ [417.07 m] as the reference section for the interval equivalent to the Koukandowie Formation.

Type section. The interval from 811.15 m to 1073.52 m in GSQ Ipswich 24 (Fig. 11) is here nominated as the type section, as it is considered that the reference section in GSQ Ipswich 18 is atypical and the boundaries with adjacent units are not readily defined.

Description at type section. In the type section in GSQ Ipswich 24 the total Koukandowie Formation contains about 67% sandstone. The Ma Ma Creek Member contains 54% shale and siltstone whereas the overlying remainder of the undifferentiated Koukandowie Formation contains 80% sandstone.

The sandstone in the undifferentiated upper part of the Koukandowie Formation is fine to coarse grained, commonly in stacked multistorey fining-up sequences about 10 m thick in the upper part of the formation and up to 40 m thick in the lower part. The sandstone is mostly cross-laminated and rippled. Thin pebble conglomerates occur at the base of channel sands. Interbedded mudstone intervals are 10–12 m thick with fine-grained sandstone laminae, cross-laminae and rootlets. In places the mudstone exhibits brecciated soil textures.

Fossils. The formation contains plant fossils, fossil wood and palynomorphs.

Depositional environments. The upper part of the Koukandowie Formation in GSQ Ipswich 24 was laid down as predominantly channel deposits, with floodplain siltstone interspersed with probable fining-up crevasse splay sandstones. The lower part of the formation — the Ma Ma Creek Member — is mainly claystone and shale with chamositic oolite, deposited in lacustrine conditions.

Relationships and boundary criteria. The boundaries of the formation with other units are conformable.

The upper boundary of the Koukandowie Formation corresponds to the change of sandstone composition described under the Marburg Subgroup.

The lower boundary of the formation is defined as the change from predominantly mudrocks of the Ma Ma Creek Member to the multistory medium to very coarse grained, quartz-lithic to lithic sandstone bodies of the Gatton Sandstone.

Where the Ma Ma Creek Member is not recognisable, the boundary is the change from the variable sandstone/siltstone/shale sequence of the Koukandowie Formation to the uniform quartz–feldspathic–lithic sandstone and subordinate conglomerate of the Gatton Sandstone.

In the southern part of the Clarence–Moreton Basin the Koukandowie Formation disconformably overlies the Towallum Basalt which in turn overlies the Gatton Sandstone.

Distinguishing features. The sandstone composition, lithological assemblages and associations, and stratigraphic position are the main methods for distinguishing the formation. The characteristics and sequences in the constituent members, where they are identifiable, can also be used to distinguish the formation.

Most of the attributes of the formation are shown on the graphic log of GSQ Ipswich 24 (Fig. 11).

The sandstone of the Koukandowie Formation is quartzose to quartz-lithic, with silty and clayey matrix and varying amounts of channel-base conglomerate and overbank shale. The lithological sequence penetrated in GSQ Ipswich 24 is characteristic of the formation.

Regional aspects. The Koukandowie Formation is widely distributed and identified throughout the Clarence-Moreton Basin in the Marburg Subgroup.

The Koukandowie Formation has been identified in most deep well sections; in the southern Clarence–Moreton Basin it has been continuously cored in Pillar Valley DDH No.2 stratigraphic drill hole and corresponds to the 'Upper Marburg Formation' of Etheridge & others (1985).

Constituent units. Two members, the Heifer Creek Sandstone Member and the Ma Ma Creek Member, occur within the Koukandowie Formation. In many areas the members cannot be identified, and under the revised stratigraphic scheme the sequence is referred to as undivided Koukandowie Formation.

Correlation. The Koukandowie Formation is broadly correlated with the Hutton Sandstone and upper part of the Evergreen Formation of the Surat Basin sequence.

Age and evidence. The formation contains plant fossils, fossil wood, spores, pollen grains and sporadic acritarchs.

The Koukandowie Formation contains palynofloras similar to those formed in the lower Eurombah Formation, Hutton Sandstone and the post-oolite ironstone section of the upper Evergreen Formation of the Surat Basin. The age of the palynoflora is late Toarcian to early Bajocian, interpreted principally from McKellar (1974, 1981). The Towallum Basalt, which underlies the Koukandowie Formation, is dated isotopically at 187±5 Ma (Flint & others, 1976; corrected) and agrees well with the ages assigned to the palynofloras (193–181 Ma; D. Burger, BMR, personal communication, 1989).

Reference. The name 'Koukandowie Sandstone Member' was first proposed by McElroy (1963).

Name and rank: Heifer Creek Sandstone Member, Koukandowie Formation

Derivation. The name is derived from Heifer Creek in the southern Laidley Valley area in southeast Queensland.

Synonymy. The term was first published by McTaggart (1963), but no type section was nominated and its full extent was not adequately described.

The unit as redefined corresponds to the upper predominantly quartzose sandstone of McTaggart's (1963) Heifer Creek Sandstone Member, described chiefly from the southern part of the Laidley Valley and in southeast Queensland.

Distribution. The Heifer Creek Sandstone Member is present mainly along the western and southern flanks and central parts of the Clarence–Moreton Basin.

Geomorphic expression. The Heifer Creek Sandstone Member is resistant to erosion and commonly forms low but steep cliff faces, benches, and abrupt changes in hill slopes.

Reference section. No type section was given for the Heifer Creek Sandstone Member by McTaggart (1963). Gray (1975) nominated the interval 62 m to 315 m in GSQ Ipswich 18 as the lithological reference section for the member. This section is considered to be lithologically atypical of the member, and the boundaries with adjacent units are not readily defined. It is therefore not suitable for a type section. We nominate the section from 841.15 m to 971.1 m in GSQ Ipswich 24 as a more representative reference section (Fig. 11).

Type section. The section exposed on the Clifden-Gatton road between grid references 110.265 and 116.316 on the Helidon 1:100 000 sheet area (9342) is here defined as the type section (Fig. 5).

Description at type section. The Heifer Creek Sandstone Member is predominantly quartz rich and some quartz-lithic, medium to very coarse grained sandstone in thick to very thick beds, with steep planar cross-beds. The sandstone occurs mostly in thick fining-up sequences with thin beds of granule conglomerate at the base, and grading through fine sandstone to siltstone beds at the top of the sequence.

The Heifer Creek Sandstone Member is about 125 m thick in the Clifden–Gatton road section, but is about half this thickness in the southern and western parts of the basin.

Fossils. Plant microfossils, including spores, pollen grains and sporadic acritarchs; non-diagnostic plant impressions and fossil wood.

Depositional environment. The depositional environment is low sinuosity, fluvial, stacked channel-sand deposits.

Relationships and boundary criteria. Boundaries with other units are conformable. A contact with extrusives is present in the south where the Heifer Creek Sandstone Member overlies the Towallum Basalt.

The stratigraphic position of the Heifer Creek Sandstone Member varies within the Koukandowie Formation (Fig. 4). It may underlie either undifferentiated Koukandowie Formation or the Walloon Coal Measures, and overlie the Gatton Sandstone, undifferentiated Koukandowie Formation or the Towallum Basalt. Some well intersections indicate an interdigitating relationship of the member with the Koukandowie Formation.

The upper boundary of the member is taken as the change from predominantly light coloured, medium to coarse and very coarse grained quartzose sandstone to silty, finer grained, khaki weathered quartz-lithic sandstone of the Koukandowie Formation, or in places by the contact with dark grey to black shale, carbonaceous shale, and volcaniclastic, quartz-poor, fine-grained sandstone of the Walloon Coal Measures.

The lower boundary is taken as the change from predominantly medium to very coarse grained quartzose sandstone to quartz-lithic, yellow brown and khaki weathered sandstone and shale of the Koukandowie Formation, or in places, quartz and quartz-lithic sandstone and grey shale and siltstone of the Ma Ma Creek Member of the Koukandowie Formation.

Distinguishing features. The quartzose lithology, coarse grain size, pebble beds, thick to very thick beds, prominent steep planar cross-beds and scarp-forming habit of the member are the main distinguishing features.

Regional aspects. The member extends almost continuously from Murphys Creek in the north, to the upper reaches of Heifer Creek, to Warwick, Koreelah Creek, Bruxner Highway, Gwydir Highway, OBX Creek, Georges Knob, Kangaroo Creek, Glenreagh and probably as far southeast as the Dirty Creek and Coast Ranges.

The member has not so far been distinguished in well sections from the central part of the Clarence–Moreton Basin.

The member occurs at a progressively lower stratigraphic level in the Heifer Creek Formation from north to south. In the Clifden–Gatton road section the member occurs at the top of the Marburg Subgroup; on the Bruxner Highway near Tabulam it occurs near the middle of the subgroup above the upper boundary of the Gatton Sandstone; at Blaxlands Flat it immediately overlies the Gatton Sandstone, and at Kangaroo Creek it is in contact with the Towallum Basalt which in turn overlies the Gatton Sandstone.

Correlation. The Heifer Creek Sandstone Member is lithologically similar to the Hutton Sandstone of the Surat Basin sequence.

Age. The age is late Early Jurassic on the evidence of spores and pollen grains from the member in the northern part of the basin chiefly in the Ipswich 1:250 000 sheet area. The member here ranges in age from Toarcian to Bajocian, and contains palynofloras similar to those of the post-oolitic ironstone section of the upper Evergreen Formation, Hutton Sandstone and lower Eurombah Formation of the Surat Basin (De Jersey, 1971; McKellar, 1981).

Because the Heifer Creek Sandstone Member occurs at different stratigraphic levels within the Koukandowie Formation, it may be time transgressive.

Reference. McTaggart (1963).

Name and rank: Ma Ma Creek Member, Koukandowie Formation

Derivation. The name comes from Ma Ma Creek in the Laidley Valley, southeast Queensland.

Synonymy. The name of the unit was first proposed by McTaggart (1963) and published as Ma Ma Creek 'Sandstone' Member.

Distribution. The member is recognised chiefly in the Laidley Valley area. Identification of the member elsewhere is difficult, although it is possibly present in parts of the southern Clarence–Moreton Basin. It is absent at many localities and in many well sections.

Geomorphic expression. Not characteristic; mostly weathers recessively, and generally obscured by alluvium,.

Reference section. McTaggart (1963) did not nominate a type section. Gray (1975) designated the interval 1030′3″ [314.02 m] to 1368′4″ [417.07 m] in GSQ Ipswich 18 as a reference section.

Type section. The type section for the Ma Ma Creek Member is nominated as the interval 971.1 m to 1073.52 m in GSQ Ipswich 24 (Fig. 11).

Description at type section. The graphic log of GSQ Ipswich 24 (Fig. 11) shows the lithological sequence in the member. The depositional environment is considered to be lacustrine. The member is characterised by the presence of a chamositic oolite in the siltstone.

Fossils. Plant and wood fossils and spores, pollen grains and sporadic acritarchs.

Depositional environment. The most characteristic rock type is a fine-grained, grey shale/siltstone sequence which in drill core commonly contains 2–10 cm beds of chamositic oolite. The depositional environment is considered to be lacustrine.

Relationships and boundary criteria. The base is generally taken as a sharp boundary between dark grey siltstone and shale of the Ma Ma Creek Member with quartzose, lithic and feldspathic, cross-bedded sandstone, fine to coarse and very coarse grained sandstone of the underlying Gatton Sandstone.

The upper boundary is less well defined because many sections of the Ma Ma Creek Member, such as those present in GSQ Ipswich 18 and 24, show a high proportion of sandstone in the upper part of the member. The upper boundary is therefore taken as the first appearance of coarse to very coarse grained sandstone, the base of which is commonly marked by a thin granule and pebble conglomerate. This boundary is interpreted as the base of the first stacked multistorey, fining-up channel sand.

The underlying, upper part of the Ma Ma Creek Member is commonly cross-laminated to ripple cross-laminated, uniform, fine and medium grained sandstone with interbedded mudstone intervals. This sandstone commonly forms 2–5 m cliff faces in the creeks around the Lockyer Valley.

Regional aspects. Identified outcrops of the Ma Ma Creek Member are confined to the northern part of the basin, and the finer grained shale and siltstone are poorly exposed and difficult to identify. Poor outcrops doubtfully referred to as the Ma Ma Creek Member are found as far south as sections on the western flank of the basin where they are cut by the Bruxner and Gwydir Highways.

Correlation. The Ma Ma Creek Member is broadly correlated with the upper part of the Evergreen Formation in the Surat Basin sequence.

Age. The member is late Early Jurassic and contains the upper limit of palynological assemblage D (De Jersey, 1971, 1976; McKellar, 1981) which lies in the interval 1035.29–1034.19 m of GSQ Ipswich 18. It is also associated with the succeeding interval J2 (Toarcian) in JM Urbenville 1.

The palynofloras are equivalent to those recovered from beds next to the oolitic ironstone sequence in the upper Evergreen Formation and the basal Hutton Sandstone of the Surat Basin. The age is Toarcian, according to McKellar (1974, 1981).

Reference. McTaggart (1963).

Name and rank: Gatton Sandstone, Marburg Subgroup

Derivation. The name comes from the township of Gatton in the Laidley Valley, Ipswich 1:250 000 sheet area, Queensland.

Synonymy. The unit was originally named Gatton Sandstone Member by McTaggart (1963). Although the 'Blaxland Fossil Wood Conglomerate Member' of McElroy (1963) was never adequately defined, it is evident that it is equivalent to the Gatton Sandstone. Although McElroy's (1963) unit name has equal priority, we prefer to use Gatton Sandstone because:

1. it has gained wide acceptance and is entrenched in the literature, particularly in Queensland where the Marburg Subgroup is well documented;
2. the term 'Blaxland Fossil Wood Conglomerate Member' has not been widely used or accepted, and is commonly used in a variety of ways. We prefer to avoid further confusion by redefining the formation, and retaining the name Gatton Sandstone.

Distribution. The formation is basin-wide in the Marburg Subgroup.

Geomorphic expression. Mostly rounded hillslopes of low relief. No characteristic topographic features.

Type section. McTaggart (1963) did not give a type section for the Gatton Sandstone Member. Gray (1975) nominated GSQ Ipswich 18 over the interval 1368.1′ [417.07 m] to 2955.0′ [900.7 m] as the reference section; this is here designated the type section (Fig. 14).

Description at type section. The lithological succession and thickness in the type section are shown in GSQ Ipswich 18 drill log (Fig. 14).

The principal rock types in the type section are:

sandstone	quartz-lithic to lithic, cross-bedded, medium to very coarse grained in multistorey fining-up sequences, interspersed clasts, in white silty matrix; carbonaceous laminae, pebbly at channel bases, mostly poorly sorted and bedded, subangular, in part feldspathic, occasional volcanic clasts and coal spars, clay pellets, in part finely micaceous, parallel-laminated, cross-laminated and ripple cross-laminated, common fossil wood fragments.
conglomerate	pebble and cobble, mostly at base of channel sands, clasts of jasper, quartzites, volcanic metasediments; very coarse grained quartzose/quartz-lithic/feldspathic matrix;
siltstone/shale	dark grey to black, wavy irregular bedding, possible relict soil intervals, thin interlaminae of siltstone, in part bioturbated, occasional load casts;
coal	very thin laminae in siltstone.

Fossils. Fossils include wood fragments, plant remains and spores, pollen grains, and sporadic acritarchs.

Relationships and boundary criteria. Minor diastems and hiatuses are present in the Gatton Sandstone but no major depositional breaks are recorded. Upper and lower contacts are apparently conformable, except where the formation overlaps Palaeozoic basement, in which case the lower boundary is an angular unconformity. A regional unconformity separates the Gatton Sandstone from the Raceview Formation of the Woogaroo Subgroup in the southeast at the Coast and Dirty Creek Ranges.

Distinguishing features. The stratigraphic position and lithology of the sequence are the main distinguishing features. The sandstone in the formation is predominantly very coarse grained, poorly sorted, quartz-lithic and lithic sandstone in channel sand bodies and minor overbank deposits. The formation commonly contains fossil wood.

Depositional environment. Predominantly low sinuosity fluvial deposits in high energy environments.

Regional aspects. The lithology of the formation varies little throughout the basin, except where it overlaps the Palaeozoic basement rocks in the west. Here the formation is much coarser grained, contains beds of conglomerate and grades downwards into thick conglomerate. The conglomerate is formally defined in this paper as the Koreelah Conglomerate Member of the Gatton Sandstone.

The upper boundary of the Gatton Sandstone is marked by the change from uniform quartz-lithic and lithic sandstone to a variable sequence of quartzose and quartz-lithic sandstone, siltstone, shale and some coal of the overlying Koukandowie Formation.

The lower boundary is delineated mostly by a change in sandstone composition to clean quartz sandstone of the Ripley Road Sandstone. In places the base of locally developed members forms the lower boundary of the Gatton Sandstone. The Koreelah Conglomerate Member of the Gatton Sandstone unconformably overlies basement rocks, and in more basinward areas the interbedded siltstone, shale, and fine and medium grained sandstone of the Calamia Member form the base of the Formation.

Constituent units. The Calamia Member is a thin unit at the base of the Gatton Sandstone and the Koreelah Conglomerate Member forms the base of the Gatton Sandstone where the formation overlaps basement rocks.

A prominent thin unit near the base of the Gatton Sandstone is characterised by the abundance of large fossil wood fragments (commonly ferruginised) in a coarse-grained, conglomeratic sandstone matrix.

The beds occur in outcrop along the western and southern flanks of the basin and are best exposed in road cuttings on the Gwydir Highway, Bruxner Highway and Copmanhurst–Jackadgery road (grid reference MN 697.317, Grafton 1:100 000 sheet area). The thickness of this unit is an estimated 5–10 m. It contains blocks and logs of fossil wood up to 20 m long and nearly 1 m in diameter.

Further study of these beds may show that they constitute an important marker bed near the base of the Gatton Sandstone and deserve formal status. Definition and naming of this unit should wait until it can be shown that it is a continuous member in the formation.

Correlation. The Gatton Sandstone is correlated with the lower part of the Evergreen Formation of the Surat Basin.

Age and evidence. The formation is basal Early Jurassic and includes elements of palynostratigraphic assemblages C and D (De Jersey, 1976; McKellar, 1981) and unit J1 of Evans (1966).

Palynofloras of assemblage D from the upper part of the formation indicate a Toarcian age (McKellar, 1974; Helby & others, 1987) equivalent to assemblages from the immediate pre-oolitic ironstone sequence of the Ma Ma Creek Member (McKellar, 1981).

Reference. McTaggart (1963).

Definition of new stratigraphic unit

Name and rank: Koreelah Conglomerate Member, Gatton Sandstone

Derivation. The name comes from the small settlement of old Koreelah in northeastern New South Wales (grid reference MP 435.585, Warwick 1:100 000 sheet area).

Synonymy. The Koreelah Conglomerate Member has not been recognised previously either as a facies equivalent of part of the Gatton Sandstone or as a discrete mappable unit. On existing geological maps, many of the outcrops previously mapped as Laytons Range Conglomerate and Marburg 'Formation' have been shown to be a conglomerate developed as a western marginal facies of the Gatton Sandstone (principally the basal Gatton Sandstone).

Distribution. The member is preserved chiefly in narrow discontinuous strips along the western and parts of the southern margin of the Clarence–Moreton Basin. The strips are oriented parallel to the basin margins. The conglomerate was probably deposited in alluvial fans and stream channels emanating from them. The discontinuous outcrops suggest that they may represent parts of preserved fans and deposits along palaeo-stream axes.

Geomorphic expression. Mostly poorly exposed in low mounds or in road cuttings.

Type section. The type section lies about 10 km southwest of Warwick along the New England Highway, at grid reference LP 978.702 on the Allora 1:100 000 sheet area.

There are no continuous complete sections of the Koreeelah Conglomerate Member. The best outcrops are those along road cuttings on the New England and Bruxner Highways. The base of the member in the type section is present in outliers and at the basin margin east and southeast of the Leslie Hall Dam, such as outcrops at LP 963.784 and outcrops on the Cunningham Highway 15–17 km west of Warwick.

The top of the member grades into the Gatton Sandstone between the exposures on the New England Highway and a quarry in the Gatton Sandstone at MP 002.708.

Description of type area. The member consists of conglomerate, sandstone, siltstone and shale. Pebble to cobble conglomerate is the dominant lithology in most outcrops but the relative proportion of rock types varies considerably from one outcrop to another.

The predominantly clast-supported conglomerate is polymict with subrounded and a few angular and rounded clasts mostly 3–5 cm (and a maximum of 16 cm) across. The conglomerate is predominantly mudstone metasediments, with subordinate black chert, felsic volcanics, fine-grained sandstone, slatey metasediments and reef quartz in a matrix of coarse-grained sandstone containing fresh angular feldspar grains.

The conglomerate is both matrix and clast supported and has poorly defined bedding, including trough cross-beds. In a few places the clasts show a slight imbrication.

Fine and coarse grained lithic and feldspathic sandstone occurs as interbeds of variable thickness.

Red and grey siltstone is interbedded in some of the conglomerate exposures. In places the mudstone encloses lenses of conglomerate and coarse-grained sandstone up to 3 m thick.

Thickness. Only incomplete sections are present in outcrop. The maximum known exposed thickness is ~20–30 m on the Bruxner Highway (grid reference 470.030, Drake 1:100 000 sheet area)

About 5 m of conglomerate penetrated by GSQ Ipswich RM2 at Leyburn probably equates with the Koreelah Conglomerate Member.

Fossils. The member has no internal evidence for depositional age. Superimposition and lateral relationships indicate that the member is approximately the same age as the Early Jurassic Gatton Sandstone of the Marburg Subgroup.

Diastems and hiatuses. There is evidence for minor hiatuses and diastems.

Depositional environment. The member was probably deposited as a series of alluvial fans and braided stream deposits along the western and southern margins of the Clarence–Moreton Basin.

Relationships and boundary criteria. The member unconformably overlies Palaeozoic and Early Triassic basement rocks, and is inferred to overlie Late Triassic sediments of the Bundamba Group.

The member occurs at the local base of the Marburg Subgroup. It is interpreted to grade laterally into the Gatton Sandstone, and doubtfully into the Heifer Creek Sandstone of the Marburg Subgroup. Precise boundaries are not readily defined, because of lateral and vertical facies transitions. Lateral and vertical boundaries may be defined by the last significant beds of pebble conglomerate in the unit. Contacts are rarely observed and are typically gradational.

Distinguishing features. The combination of pebble–cobble conglomerate and coarse-grained arenitic assemblages in the member distinguishes it from the bulk of the basin sequence. The Late Triassic basal conglomerates of the basin (Laytons Range, Corindi and Aberdare Conglomerates) are superficially similar to the Koreelah Conglomerate Member, but there is usually a higher proportion of sandstone interbedded in the Koreelah Conglomerate Member, and it is distinguished in many places by the abundance of fossil wood. The sandstone interbeds are lithologically similar to those of the Gatton Sandstone.

It is not always easy to distinguish the basal Late Triassic conglomerates from those in the Early Jurassic, and in some instances a demonstration of lateral transition to the Marburg Subgroup is the surest way of distinguishing the two.

Structural attitude. The Koreelah Conglomerate Member generally dips at low angles into the basin.

Regional aspects. The Koreelah Conglomerate Member is distributed along the western and southern margins of the basin on the Cunningham and New England Highways, west and south of Warwick, on the Bruxner Highway west of Tabulam, Gwydir Highway west of Main Creek and probably also on the Pacific Highway at the Dirty Creek Range.

The proportion of conglomerate, sandstone, and fine-grained rocks varies from locality to locality. In places shales and fine sandstones are present in the sequence. Ferruginised and siliceous fossil wood, logs and fragments are common.

The formation typically occurs as a pebble-cobble conglomerate, with abundant coarse sandstone interbeds and a similar sandy matrix. The lithology of the clasts in the conglomerate is controlled largely by the composition of the underlying basement.

The known maximum exposed thickness is ~20-30 m in the area west of Tabulam on the Bruxner Highway. The true thickness is probably much greater, but exposure is discontinuous.

Correlation. There are no units that can be correlated both lithologically and temporally with the Koreelah Conglomerate Member.

The Koreelah Conglomerate Member is laterally continuous with the Gatton Sandstone of the Marburg Subgroup.

Its relationship to the Calamia Member, a basal member of the Gatton Sandstone further east, is not known.

Discussion. The evidence for the existence of the younger conglomerate and the reasons for proposing a new member name may be summarised as follows:

1. The conglomerate occurs in the exposed base of the Marburg Subgroup along the western and southern margins of the basin. In this area the subgroup overlaps the older formations in the basin and unconformably overlies Palaeozoic and Early Triassic basement rocks.
2. The Marburg Subgroup shows evidence of general coarsening towards the basin margin, and the proportion and thickness of conglomerate interbeds increase towards the margin.
3. The clast composition is noticeably different in some local areas from that found in the Laytons Range, Aberdare, and Corindi Conglomerates. Fossil wood commonly constitutes a large percentage of these clasts.
4. The sandstone interbeds in the conglomerate are similar in composition to those found in the Marburg Subgroup.
5. The basal conglomerate member is apparently continuous with the Marburg Subgroup. No unconformity is apparent between the Marburg Subgroup and the conglomerate member which would be expected if an overlapping relationship existed.
6. The suggested identification of the conglomerate present locally at the base of the Marburg Subgroup in contact with the Raceview Formation in the southeast provides additional evidence for the age and stratigraphic position of the member.

Data on other units

Name and rank: Calamia Member, Gatton Sandstone

Derivation. From Calamia Parish in the Pillar Valley area, southeast of Grafton, New South Wales.

Synonymy. First published by Etheridge & others (1985).

Distribution. The member was first identified in the DM Pillar Valley DDH No.2 drill hole and was thereafter extended to neighbouring well sections.

Geomorphic expression. The member weathers recessively and outcrop is fragmentary. A few poor exposures are present in the Coast Range, the best being in a quarry on the Grafton-Wooli Road, grid reference NN 171.047 on the Bare Point 1:100 000 sheet area. Shale of the Calamia Member crops out here beneath bluffs of the Gatton Sandstone.

Type section. The type section nominated by Etheridge & others (1985) is the interval 92 m thick [926-1018 m] in the DM Pillar Valley DDH No.2, based principally on the gamma ray log response. An alternative interpretation of the boundaries based solely on the lithological log is a sequence 108 m thick in the interval 881-989 m.

Description. The detailed sequence in the member is given in the Department of Mines descriptive log of Pillar Valley DDH No.2, and on a graphic log re-compiled by two of the authors (ATW & PO'B) from this description.

The member is composed of siltstone and mudrocks, and fine to medium grained sandstone. It is 137 m thick in Pillar Valley DDH No.2. No palynomorphs were recovered from one sample collected from the member. There is no record of diastems or hiatuses.

Depositional environment. Predominantly overbank and minor channel depositional facies of a fluvial environment.

Relationships. The member is apparently conformable with bounding units. It separates the Gatton Sandstone of the Marburg Subgroup from the Ripley Road Sandstone.

Boundary criteria. The member is lithologically similar to the Gatton Sandstone but contains a higher proportion of siltstone and claystone units. The channel sandstones are finer grained, quartzose and have a siliceous matrix.

Distinguishing features. The lithology of the member and its gamma ray log response distinguish it from neighbouring units.

Regional aspects. The member is widespread in the subsurface but does not outcrop well and has been observed only in fragmentary exposures in the Coast Range. A correlatable unit with a similar stratigraphic position, gamma ray response and lithology has been identified in Tullymorgan No.1 and Sextonville No.1 wells, and as far north as the Laidley Sub-basin (Ipswich 19-22R and Beef City Water Bore).

The interval in Ipswich 19-22R falls within Assemblage D.

Correlation. Etheridge & others (1985) consider that it may represent a distal facies of the lower Evergreen Formation from the Surat Basin.

Age. The member contains no internal evidence of age. The Marburg Subgroup is Early Jurassic. The basal parts of the subgroup, probably including strata equivalent to the Calamia Member, contain the upper limit of the basal Early Jurassic *Polycingulatisporites crenulatus* zone. The Ripley Road Sandstone beneath is Upper Triassic in NS 272 Ipswich, and in GSQ Ipswich 1 the uppermost part of the sandstone is in the lower part of Assemblage C, and thus is probably latest Triassic.

Reference. Etheridge & others (1985).

BMR Journal of Australian Geology & Geophysics, 11, 415–420

The earthquake near Nhill, western Victoria, on 22 December 1987 and the seismicity of eastern Australia

Kevin McCue[1], Gary Gibson[2] & Vaughan Wesson[2]

On 22 December 1987 a shallow magnitude 4.9 earthquake occurred in western Victoria where there is no record of previous seismic activity. It was felt over a remarkably wide area of Victoria and South Australia and caused minor damage in the epicentral area. There were no foreshocks and only ten aftershocks were recorded on the nearest seismograph, near Willalooka in South Australia. All ten occurred within five days of the mainshock. The earthquake occurred in a seismic zone that extends over a 500 km wide belt along the entire eastern coast of Australia linking the Southeast Seismic Zone of South Australia with the Eastern Highlands Zone through Queensland, New South Wales, Victoria and Tasmania. Its focal mechanism, a thrust with a principal stress directed east-west, is typical of earthquakes in the Lachlan Fold Belt.

Introduction

Sometimes earthquakes occur where they are least expected, and one such earthquake was that of 22 December 1987 Universal Coordinated Time (UTC), near Nhill, western Victoria, in southeastern Australia (Fig. 1). This earthquake at 2.06 am Eastern Standard Summer Time on the 23rd shook a wide area of the State (Fig. 2) and caused minor damage as far as 80 km from the epicentre. A search of earthquake data files at the Bureau of Mineral Resources and Seismology Research Centre for the period 1 January 1900 to 22 December 1987 revealed only four small earthquakes within 100 km, and none within 75 km, of the epicentre. Its Richter or local magnitude was estimated to be ML 4.9. Earthquakes of a similar size have occurred during the last 100 years along the continental shelves of both Victoria and adjacent South Australia to the southwest and south, in Victoria to the east and in southwestern New South Wales to the northeast (Fig. 3). Few aftershocks were observed after the Nhill earthquake and few followed the 1982 Wonnangatta earthquake

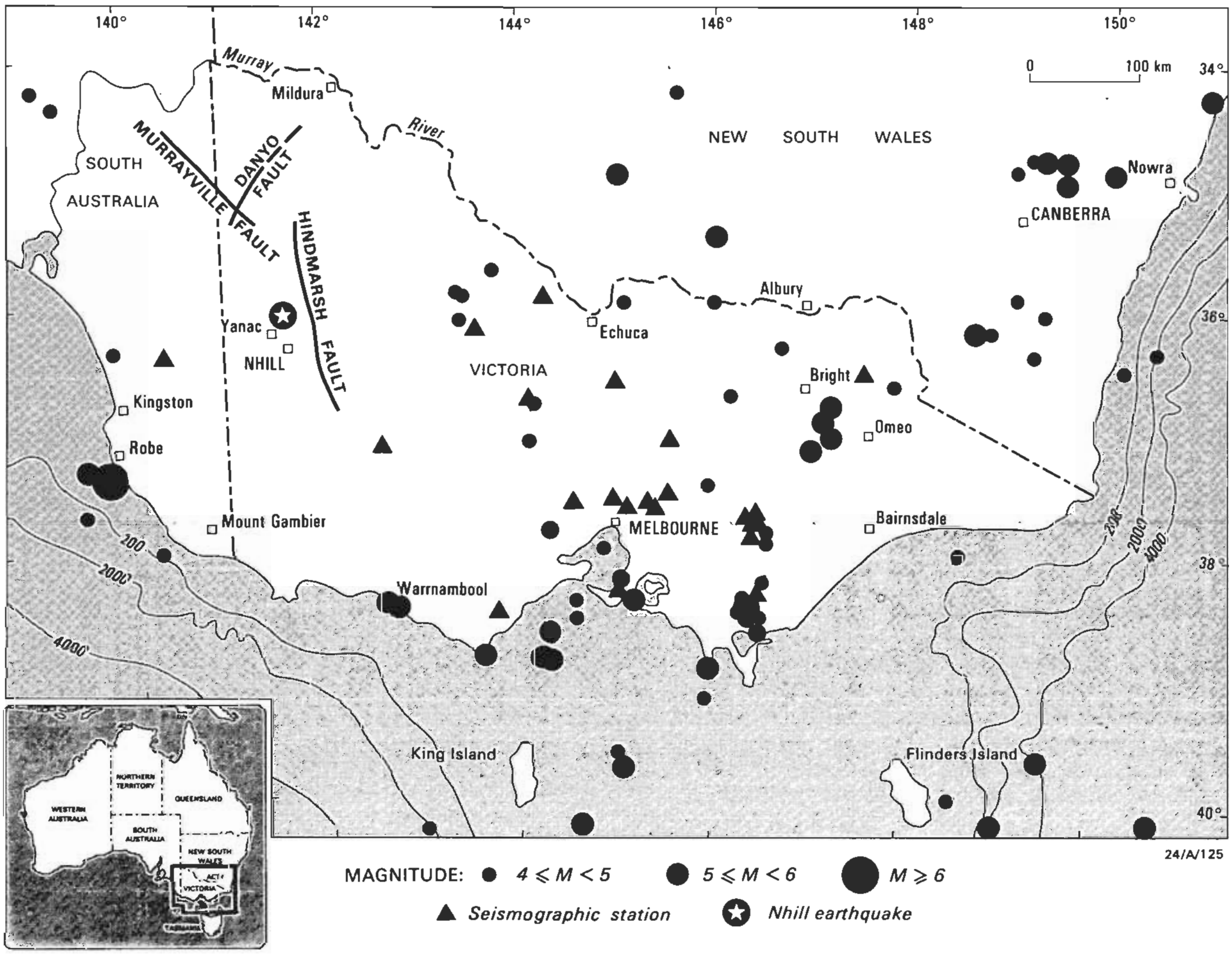

Figure 1. Southeast Australian earthquakes of magnitude >3.9, 1897–1987.
Circles are epicentres, 1897–1987, ML >3.9; the star is the Nhill earthquake epicentre. Seismograph stations are plotted as triangles. Tertiary faults close to the epicentre are also shown.

[1] Australian Seismological Centre, Bureau of Mineral Resources, GPO Box 378, Canberra, ACT 2601
[2] Seismology Research Centre, Phillip Institute of Technology, Bundoora, Victoria 3083

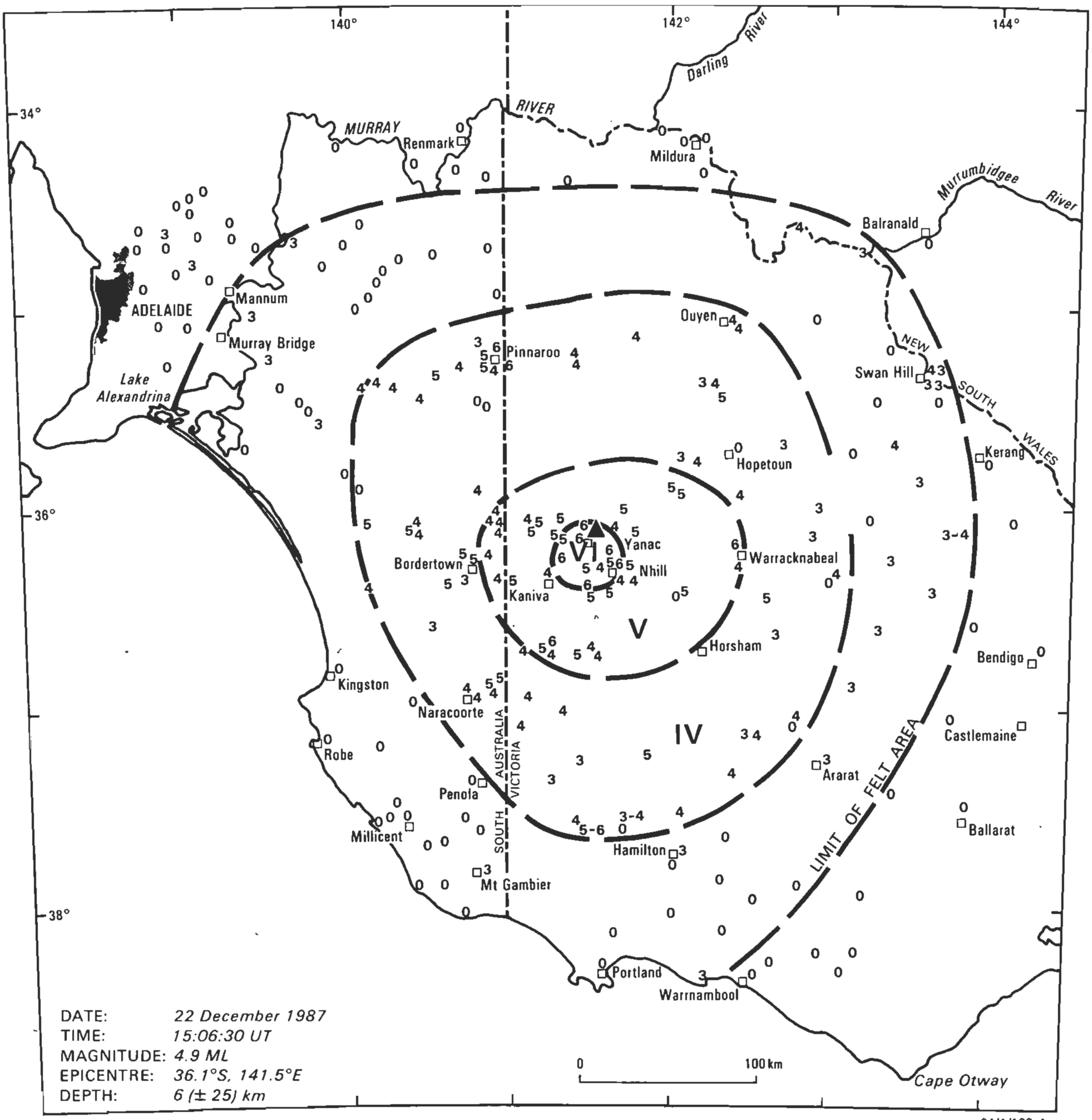

Figure 2. Isoseismal map of the Nhill earthquake, western Victoria, 22 December 1987.

(Denham & others, 1985). The small number of aftershocks may be a characteristic feature of Victorian earthquakes. For comparison, the smaller ML 4.3 earthquake near Dalton, New South Wales, on 9 August 1984 was followed by more than one hundred aftershocks of magnitude 2.0 or more (Bureau of Mineral Resources, 1985).

A study of the focal mechanism of the mainshock has demonstrated that the direction of the principal stress in the crust is similar to that throughout southeastern Australia, but different from that in central and South Australia (Denham & others, 1985).

The earthquake sequence

No earthquakes larger than ML 0 preceded the mainshock at 1506 UTC, and only ten aftershocks were recorded on the closest seismographic station at Willalooka, 115 km away in South Australia. Seismology Research Centre seismologists at Phillip Institute of Technology set up three portable recorders in the epicentral region and staff at the Sutton Institute in the South Australian Mines Department installed an additional recorder at Pinnaroo, but not in time to record the last widely felt aftershock at 0543 UTC on 23 December. The few detected aftershocks were very small and essentially all the seismic energy was released during the mainshock.

The Willalooka (WKA), Bellfield Victoria (BFD), Toolangi Victoria (TOO) and Adelaide South Australia (ADE) seismographs were saturated during the early part of the P wave of the mainshock, so neither shear wave arrival times nor amplitude data were available from these critical, close in seismographs for the location and magnitude evaluation. As a result, the focal depth is poorly constrained. Some control is provided by the difference in time between the direct (Pg) and refracted (Pn) P wave phases at Cobar (CMS) and Bundoora (PIT), but the computed focal depth of 7 km

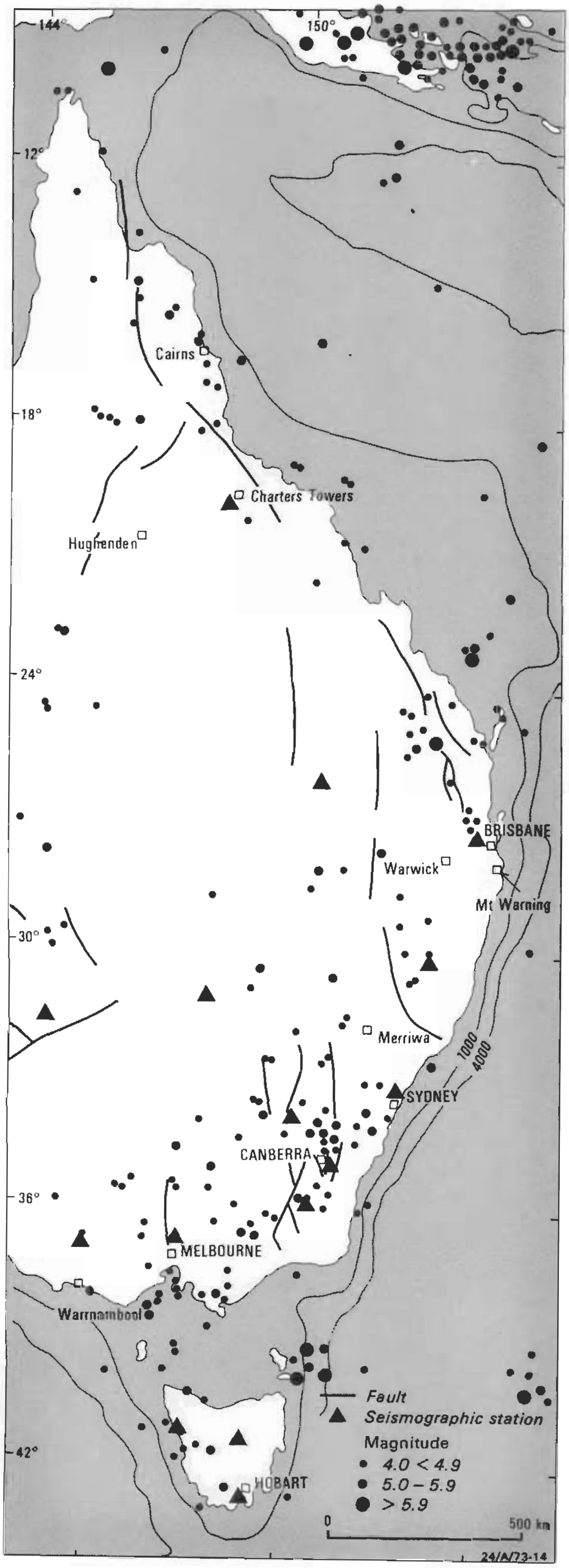

Figure 3. Epicentres of all earthquakes of magnitude 4 or greater in eastern Australia from 1900 to 1987.
The symbol diameter is proportional to the earthquake magnitude.

is very dependent on the crustal model used. Secondary phases of the ML 3.1 aftershock at 0543 on 23 December were well recorded and the better controlled focal depth was 10 km using the Victorian crustal model VIC5A (Gibson & Wesson, 1985), whilst, with a New South Wales model DAL1 (based on the model of Finlayson & McCracken, 1981), the computed focal depth was negative. The epicentral distance of the closest seismograph was still approximately ten times our preferred depth of 10±3 km.

Only two of the three temporary PIT stations recorded the last small aftershock, so its focal depth was indeterminate; if it was constrained to have the same epicentre as the mainshock, then its focal depth was 15 km. Details of the origin times and magnitudes for the eleven earthquakes of the sequence are listed in Table 1. All but two aftershocks were recorded on insufficient seismographs for the epicentre to be located, so the truncated mainshock coordinates are listed.

Table 1. Epicentre parameters and magnitudes.

Date (1987)	*Time (UTC)*	*Location*[1] °*S*	°*E*	*Duration (s)*	*Magnitude*[2] *(ML)*
22 December					
	1506 30.7	36.11	141.54	750	4.9
	1700 18.8	36.1	141.5	70	(0.8)
	1746 26.5	36.1	141.5	40	(0.0)
	1825 42.3	36.14	141.45	300	(0.1)
	1901 55.0	36.1	141.5	45	(0.1)
	2130 00.5	36.1	141.5	40	(0.0)
23 December					
	0225 53.0	36.1	141.5	110	1.6
	0543 53.6	36.17	141.44	210	3.1
24 December					
	1036 08.9	36.1	141.5	46	(0.1)
25 December					
	1408 34.7	36.1	141.5	31	(–0.3)
26 December					
	1655 16.3	36.10	141.5	105	(1.4)

[1] Coordinates with single decimal point are truncated mainshock locations.
[2] Magnitudes in parentheses, as (0.1), are imputed from the coda duration on WKA seismograms.

Richter or local magnitudes were measured from seismograms recorded at Canberra (CNB), Cobar (CMS), Armidale (COO) and Riverview (RIV), and these averaged ML 4.9 for the mainshock, similar to the coda-duration magnitude value of 4.8 from BMR stations. The South Australian network estimate of duration magnitude was only 3.8 while the surface-wave magnitude measured from the Alice Springs seismogram was Ms 3.7, corresponding to a Richter magnitude of 4.4. The magnitude imputed from the radius of perceptibility (Rp), defined to be the radius of a circle equal in area to the area of the Modified Mercalli III isoseismal (McCue, 1980), is 5.5. This is a surprisingly high value compared with the measured value of ML 4.9, especially for a time of day when MMIII was difficult to assess, since most people were asleep and Rp likely to be underestimated.

Seven of the aftershocks were recorded only on WKA. Their magnitudes were derived by plotting the Richter magnitudes (ML) of the four larger earthquakes against their coda duration (τ) on the WKA seismographs, measured in seconds from the P wave arrival time to the time at which the amplitude returned to background-noise levels (Fig. 4), and interpolating for the smaller events. The equation relating ML to the duration (τ) is:

$$ML = 3.8(\pm 0.4)\log(\tau) - 6.0\ (\pm 1.0)$$

where the errors in brackets are standard deviations.

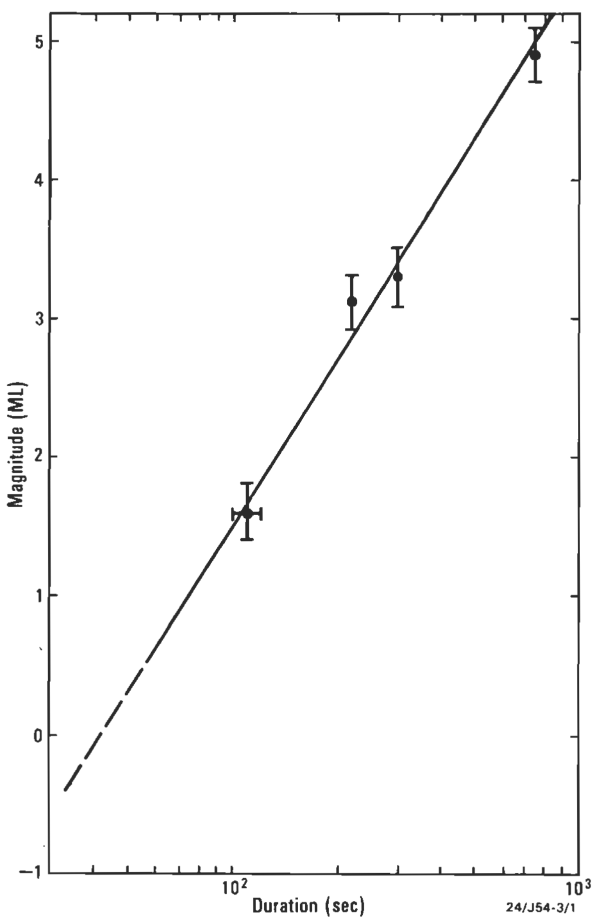

Figure 4. Magnitude vs coda duration on the Willalooka seismograms.

Geology

The earthquake sequence occurred beneath the Tertiary sediments of the Murray Basin, which are approximately 200 m thick in the vicinity of the epicentre and covered with a thin veneer of Quaternary sediments (Lawrence & Abele, 1976). Basement in the epicentral region consists of Cambrian or older volcanics which have a strong total magnetic intensity and Bouguer gravity signature, and which are exposed north of the Murray Basin (Brown & others, 1988). Several north-south-trending faults, which were active through the Tertiary to at least the early Miocene, have been mapped in the basin, but the closest (the Hindmarsh Fault) is about 40 km east of the epicentres. The Danyo and Murrayville faults, north of the epicentre (Fig. 1), strike northeast and northwest respectively. A thorough search of the epicentral region by one of us (G. Gibson) within a few days of the earthquake failed to find any evidence of surface faulting.

Isoseismal map

An excellent response was received to the intensity questionnaires distributed to residents of Victoria, southeastern South Australia and southwestern New South Wales. These were used to compile the isoseismal map of Figure 2 using the Modified Mercalli intensity scale. Minor damage occurred in brick and mud-brick houses in the closest towns, Yanac and Nhill, and reports of damage were also received from towns further afield as far as Bordertown in South Australia, 80 km from the epicentre. The earthquake was felt over an area of 145 000 km^2 which is large for an earthquake of this size. In fact, the felt area was similar to that of the considerably larger Wonnangatta earthquake of November 1982 (Denham & others, 1985). The Nhill earthquake was one of the most widely felt in Victoria this century.

Fault plane solution

The focal mechanism shown in Figure 5 is based on polarities of first ground motions recorded on short period seismographs. It indicates that faulting had about equal components of strike-slip and dip-slip motion on either a near-vertical plane striking at N133°E or a plane with a dip of 50° to the southeast and striking at N50°E. Uncertainties in these strike directions are no more than ±7°.

Both the Bouguer gravity anomaly and magnetic pixel maps (Brown & others, 1988) outline a basement structure in the epicentral region, the Stavely Belt, 40 km wide and 400 km long, which strikes SSE and which the authors have interpreted to be Cambrian or older volcanics. The nodal planes parallel the Danyo and Murrayville Faults 80 km to the north rather than the closer Hindmarsh Fault which strikes north-south (Fig. 1). The principal stress direction, N264°E, is close to the east-west orientation typical of other earthquake mechanisms in southeastern Australia, as opposed to the NE to NNE direction from central and South Australian earthquakes (Denham & others, 1985).

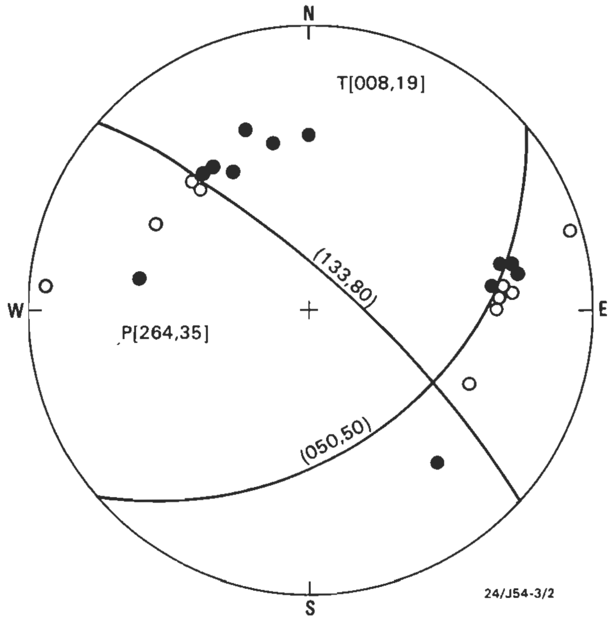

Figure 5. Focal mechanism solution (lower hemisphere Wulff projection).
Solid circles are compressions on short period seismograms; open circles are dilations on short period seismograms.

Discussion

Underwood (1972, p. 27) repeated the assertion of Jaeger and Browne (1958) that 'the very scarcity of shocks (in Victoria) can be an advantage because it allows the pattern of seismicity to be observed rather clearly'. Gregory (1903) compiled a list of felt earthquakes for the period 1884–1901 and observed that earthquakes were prevalent along the coastline, particularly in Bass Strait, off Gabo Island, under Port Phillip Bay, and in the Victorian Alps between Bright and Omeo. After short-period seismographs were installed in 1959, most of the recorded activity to 1966 was in the east of Victoria (Underwood, 1972) whilst epicentres between 1976 and 1980 were predominantly in central Victoria (Gibson & others, 1981). In the later period, the authors considered that a contributing factor to the apparent geographic distribution of epicentres was the non-uniform distribution of seismograph stations, rather than a genuine change in the spatial distribution, and this is undoubtedly true of the earlier period for the smaller events.

When viewed over a broader region and with earthquakes in a limited magnitude range, ML 4 or greater (Fig. 3), the Victorian epicentres form part of a 500 km wide belt of seismicity extending west from the eastern seaboard of Australia, as discussed by Denham & others (1975). The belt is apparently continuous and parallel to the coast, extending from about 44° S off the continental slope south of Tasmania to the northeast tip of the continent at about 10° S.

What was not obvious previously but has now been demonstrated by the earthquake near Nhill is that the seismic zone of southeastern South Australia (Sutton & others, 1977) is also linked with the entire Eastern Highlands Seismic Zone including Tasmania. Both the epicentre pattern and similarity of principal stress directions support this view. With time the apparent pattern of seismicity has been clarified, and a relatively large number of discrete seismic zones throughout eastern Australia have coalesced into a broad zone covering the eastern seaboard.

The seismicity generally coincides with both the Eastern Highlands and outcropping Cainozoic volcanic rocks, the latest of which were erupted about 5000 years B.P. in southeastern South Australia and Queensland. The general coincidence of the volcanics and seismicity can be seen by comparing Figures 3 and 6. The earthquakes and focal mechanisms demonstrate that uplift of the Eastern Highlands is continuing by horizontal compression of the crust rather than by isostatic forces, but whether or how this relates to the volcanics is unclear.

The seismicity is not uniformly distributed in time or space and there are several small clusters of prolonged, above-average seismicity such as the Dalton–Gunning seismic zone in New South Wales (McCue & others, 1989). There, four earthquakes have exceeded magnitude 5.0 in the last century (the largest of them was of magnitude ML 5.6 in 1934), and the computed return period for a magnitude ML 6.0 earthquake is 120 years. Large earthquakes (with a magnitude of 6.0 or more) have occurred in the seismic zone during the last century, off northeast Tasmania in 1884 (ML 6.4), 1885 (ML 6.8) and 1892 (ML 6.9; Michael-Leiba, 1989), off Kingston, South Australia in 1897 (ML 6.5; Sutton & others, 1977) and near Bundaberg, Queensland in 1918 (ML 6.0; Rynn, in press). In recent time but before the arrival of European settlers, large earthquakes occurred near Echuca on the New South Wales/Victorian border where the Murray River has been offset by a 45 km long, 1 m high scarp leaving sag ponds and swamps and the former river course now high and dry (Hills, 1975).

There is, as yet, no explanation for the occurrence of intraplate earthquakes such as those along the eastern coast of Australia, and no reason why large earthquakes, 5 of which are known to have occurred within this Eastern Highlands seismic zone, could not occur anywhere within it. The apparent average return period for a magnitude 6 or greater earthquake in eastern Australia is about 20 years, although they are strongly clustered in time. The last earthquake of this size was offshore between Bundaberg and Rockhampton, Queensland, in 1918.

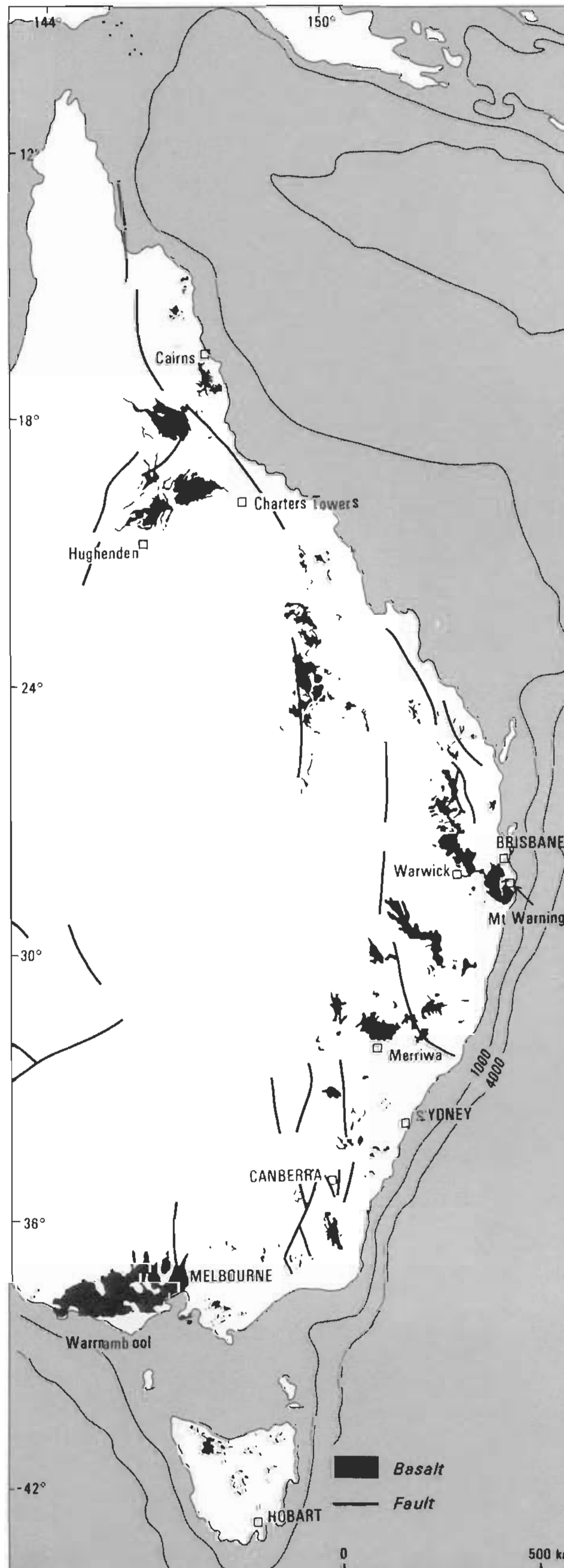

Figure 6. Cainozoic volcanics of eastern Australia (courtesy R.W. Johnson, BMR).

Acknowledgements

Trevor Jones, Jerry Vahala, Spiro Spiliopoulos and James Lewis at the Australian Seismological Centre, Canberra, and David Love at the Sutton Institute, Adelaide, distributed questionnaires after the earthquake. Seismograms were read by Mary Douch (BMR), Janet Weekes and Clementine Krayshek (ANU), and Alison McArdle and Jeanette Brown (Sutton Institute).

References

Brown, C.M., Tucker, D.H., & Anfiloff, V., 1988 — An interpretation of the tectonostratigraphic framework of the Murray Basin region of Southeastern Australia, based on an examination of airborne magnetic patterns. *Tectonophysics*, 154, 309-333.

Bureau of Mineral Resources, 1985 — Oolong earthquake series, August-December 1984. *BMR Research Newsletter* 2, 10.

Denham, D., Gibson, G., Smith, R., & Underwood, R., 1985 — Source mechanisms and strong ground motion from the 1982 Wonnangatta and the 1966 Mount Hotham earthquakes. *Australian Journal of Earth Sciences*, 32, 37-46.

Denham, D., Small, G.R., Cleary, J.R., Gregson, P.J., Sutton, D.J., & Underwood, R., 1975 — Australian earthquakes (1897-1972). *Search*, 6 (1-2), 34-37.

Finlayson, D.M., & McCracken, H.M., 1981 — Crustal structure under the Sydney Basin and Lachlan Fold Belt, determined from explosion seismic studies. *Journal of the Geological Society of Australia*, 28, 177-190.

Gibson, G., & Wesson, V., 1985 — A tectonic model of Victoria based on earthquake data. *In* VandenBerg, A.H.M., (editor), The Victorian lithosphere — a symposium. *Geological Society of Australia & Australian Society of Exploration Geophysics, Melbourne*, 16-18.

Gibson, G., Wesson, V., & Cuthbertson, R., 1981 — Seismicity of Victoria to 1980. *Journal of the Geological Society of Australia*, 28, 341-356.

Gregory, J.W., 1903 — The geography of Victoria. *Whitcombe & Tombs, Melbourne*, 163-179.

Hills, E.S., 1975 — The physiography of Victoria. *Whitcombe & Tombs, Melbourne*, 373 pp.

Jaeger, J.C., & Browne, W.R., 1958 — Earth tremors in Australia and their geological importance. *Australian Journal of Science*, 20, 225-228.

Lawrence, C.R., & Abele, C., 1976 — Murray Basin. *In* Douglas, J.G., & Ferguson, J.A., (editors), Geology of Victoria, *Geological Society of Australia Special Publication* No. 5, 191-198.

McCue, K.F., 1980 — Magnitude of some early earthquakes in Southeastern Australia. *Search*, 11(3), 78-80.

McCue, K.F., Kennett, B., Gaull, B., Michael-Leiba, M., Weekes, J., & Krayshek, C., 1989 — A century of earthquakes in the Dalton-Gunning region of New South Wales. *BMR Journal of Australian Geology & Geophysics*, 11(1), 1-9.

Michael-Leiba, M., 1989 — Macroseismic effects, locations and magnitudes of some early Tasmanian earthquakes. *BMR Journal of Australian Geology & Geophysics*, 11(1), 89-99.

Rynn, J., in press — A reappraisal of Queensland's largest known earthquake — the 'Queensland' earthquake of 6 June 1918, magnitude ML 6.3. *University of Queensland, Department of Geology Papers.*

Sutton, D.J., McCue, K.F., & Bugeja, A., 1977 — Seismicity of the southeast of South Australia. *Journal of the Geological Society of Australia*, 25(6), 357-364.

Underwood, R., 1972 — Studies of Victorian seismicity. *Proceedings of the Royal Society of Victoria*, 85, 27-48.

Young, R.W., 1985 — Introduction and evidence from southern NSW (Abstract). *In* The evolution of the Eastern Highlands — a workshop. *Geological Society of Australia, Research School of Earth Sciences, Australian National University, 9 August 1985*, 1.

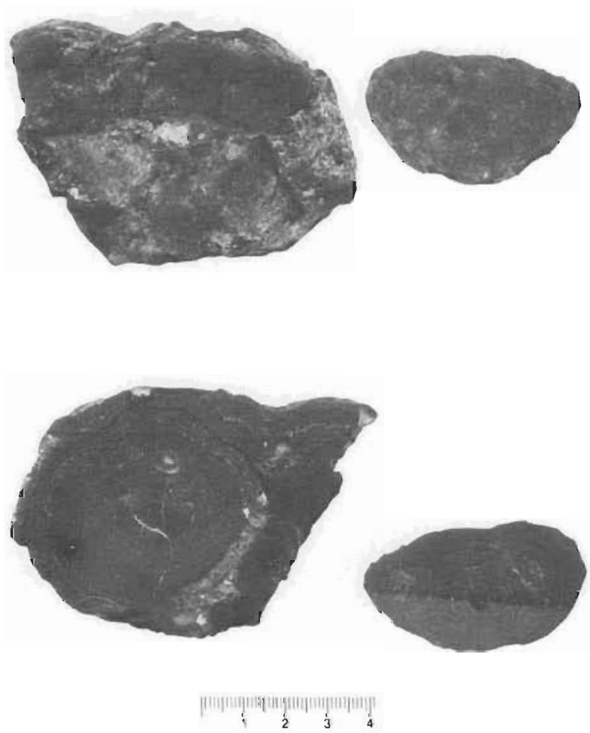

A

Regional setting and descriptions of samples

Two dredge and five core stations were occupied by R.V. *Sonne*, and ferromanganese nodules and crusts were recovered at both dredge stations and in one core (Roeser & others, 1985). Station 57, a dredge (Fig. 1), was sited on a scarp on the western side of Dampier Ridge, on BMR seismic profile 15/058. The dredge returned small fragments of granite, gabbro, microdiorite and feldspathic sandstone, and abundant ferromanganese nodules and crusts up to 20 cm thick, from water 2600–2400 m deep. There was a full range from round mononucleate nodules with small volcanic nuclei, to polynucleate nodules, to nodules bound together as crusts, and to laminated crusts (Fig. 2). One particularly spectacular crust (Fig. 2B) consisted of a lower 5 cm of layered crust (assumed to have formed on basement rocks) and an upper 10 cm of nodules bound together. The ferromanganese layers varied from relatively hard and very dark, with a metallic lustre on newly cut surfaces, to yellowish brown and highly porous. Some deposits contained thin layers of clayey volcaniclastic debris.

One other *Sonne* dredge station (63) recovered ferromanganese from an embayment within the eastern Lord Howe Rise marking the western end of the Vening-Meinesz Fracture Zone, in a position where seismic profiles suggest basement is at the surface. The dredge returned a large block of calcareous limestone, thickly encrusted with ferromanganese, and numerous nodules with cores of sandstone, quartzite, limestone, phyllite and granite. Roeser & others (1985, p. 162)

B

Figure 2.

A. External and internal features of nodules from station 57 (36-57KD5.1 and 36-57KD5.3). Scale is in centimetres.

B. Layered ferromanganese crust at bottom and bound nodules at top. Scale below sample identification is 22 cm long.

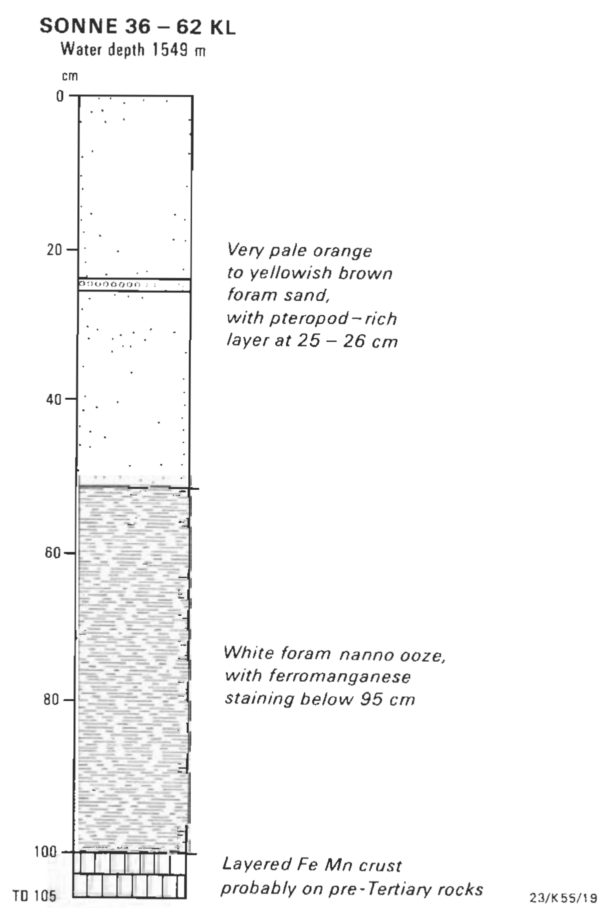

Figure 3. Log of *Sonne* core 36-62KL, which recovered ferromanganese deposits from the eastern flank of Lord Howe Rise. Sediments overlying ferromanganese deposits are of Pleistocene and Holocene age.

BMR Journal of Australian Geology & Geophysics, 11, 421-427

Thick ferromanganese deposits from the Dampier Ridge and the Lord Howe Rise off eastern Australia

B.R. Bolton[1], N.F. Exon[2] & J. Ostwald[3]

Chemical and mineralogical data are presented for four ferromanganese samples (two nodules and two crusts) from two stations of the West German vessel *Sonne*. Three samples came from a dredge on the flanks of the Dampier Ridge in water 2400–2700 m deep. One came from a core on the Lord Howe Rise in water 1549 m deep. Thick ferromanganese deposits overlie a variety of substrates including granite, gabbro and feldspathic sandstone. The ferromanganese deposits, which are up to 20 cm thick, range from round mononucleate nodules with small volcanic nuclei, to polynucleate nodules, to nodules bound together as crusts, and to laminated crusts. Both nodules and crusts are hydrogenetic in origin and have low contents of Ni, Cu and Co, and low Mn:Fe ratios of 0.48–0.91. A comparison of these results with those from three deeper water stations of *Galathea* and *Tangaroa* indicates that Mn:Fe ratios, Ni% and Cu% increase markedly in deeper water, where Mn:Fe ratios exceed 2.5, and Ni+Cu+Co values exceed 1.25%. Any future search for nodules of economic significance should be concentrated in the even deeper water areas (>5000 m) east and southeast of Gascoyne Seamount.

Introduction

In this paper we present geochemical and mineralogical data for four ferromanganese samples (nodules and crusts) collected from two stations on the flanks of the Dampier Ridge and the Lord Howe Rise in the Tasman Sea during the 1985 cruise of the R.V. *Sonne*, involving scientists from the Bundesanstalt fuer Geowissenschaften und Rohstoffe (BGR) and the Australian Bureau of Mineral Resources (SO-36C; Roeser & others, 1985) (Fig. 1). We also discuss the origin of the ferromanganese deposits and compare them with similar deposits from elsewhere.

Bulk compositions of samples were determined using X-ray fluorescence or atomic absorption techniques and quoted as elemental values. Mineralogies were determined using X-ray diffraction or an electron microprobe; compositions derived from microprobe analyses are quoted as oxides.

Little is known of the nature, distribution and abundance of ferromanganese deposits in the Tasman Sea region (Jones, 1980; Glasby, 1986). Manganese nodules from three sites in the Tasman Sea southeast of Sydney, New South Wales, have been described by Exon, Moreton & Hicks (one site, 1980) and Glasby & others (two sites, 1986). Manganese nodules, often forming extensive pavements, have also previously been described from the South Tasman Sea and parts of the South Tasman Rise by Goodell, Meylan & Grant (1971), Watkins & Kennett (1971, 1972, 1977), Conolly & Payne (1972), Payne & Conolly (1972) and Glasby (1973).

The ferromanganese crusts and nodules described here were taken from two deep-water stations from offshore continental blocks: the Lord Howe Rise and Dampier Ridge (Fig. 1; Roeser & others, 1985). The Lord Howe Rise is a very large feature in water 1000–2500 m deep, which extends about 2000 km from the Coral Sea region to the Challenger Plateau off New Zealand; it averages 400 km in width. The general structure of the rise (Fig. 1) has been described in detail by Willcox & others (1980) and Roeser & others (1985). The eastern part of the rise has continental basement rocks relatively close to outcrop, but there is a series of basins, apparently containing 3000 m and more of Mesozoic and Cainozoic rocks, on the western flank.

The Dampier Ridge is a much smaller feature in water 2000–3000 m deep, and lies between Australia and the Lord Howe Rise (Fig. 1). Dredging of granite and gabbro by the R.V. *Sonne* showed that the ridge is a continental sliver (Roeser & others, 1985; Symonds, Willcox & Kudrass, 1988).

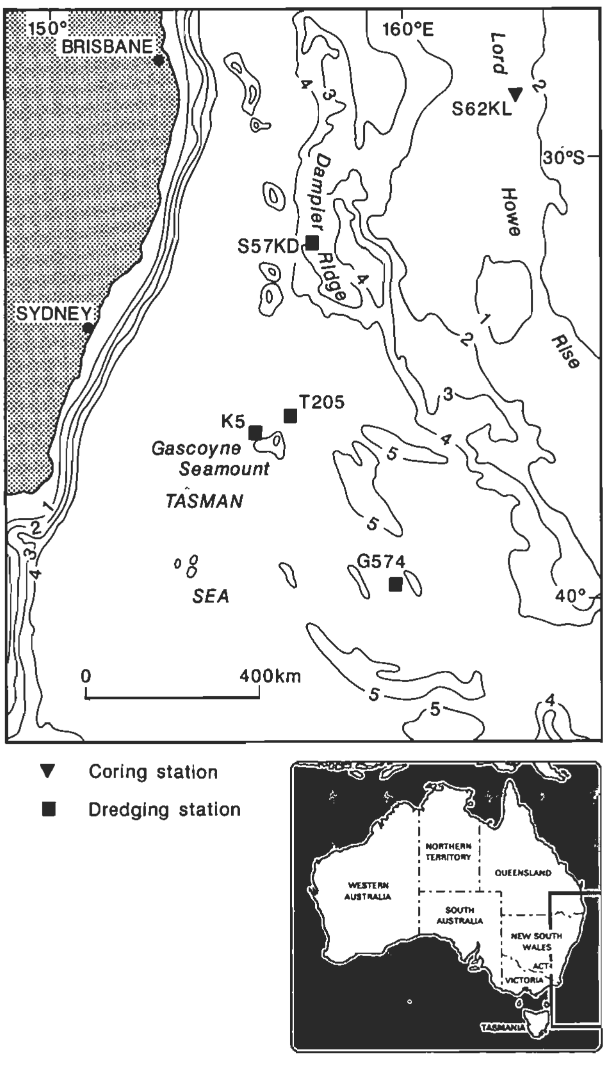

Figure 1. Location map showing sampling stations and major bathymetric features.
S, T, K and G denote *Sonne, Tangaroa, Kimbla* and *Galathea* stations, respectively.

[1] Department of Geology and Geophysics, University of Adelaide, PO Box 498, Adelaide, SA 5001
[2] Marine Geosciences and Petroleum Geology Program, Bureau of Mineral Resources, GPO Box 378, Canberra City, ACT 2601
[3] Central Research Laboratories, Broken Hill Proprietary Co. Ltd, PO Box 188, Wallsend, NSW 2287

stated that 'the presence of intercalated ore mineral layers within an unusually complex stratigraphy of dark and dense Mn/Fe crusts at this locality suggests that past hydrothermal activity associated with the Vening-Meinesz Fracture Zone at least partly influences the growth of these crusts'. This deposit is the subject of a separate publication currently in preparation and is not dealt with further in this paper.

At station 62, a core taken near station 63 on the Lord Howe Rise penetrated a metre of Pleistocene and Holocene foram-nanno ooze and foram sand before striking virtually impenetrable ferromanganese crust, of which 5 cm was recovered (Fig. 3). It is likely that the black, laminated crust formed on a pre-Tertiary unconformity. Four other *Sonne* cores were taken towards the centre of the Lord Howe Rise about 220 km northwest, in areas of thick sediments, and recovered Pleistocene–Recent nanno-foram and foram-nanno oozes with no associated ferromanganese (Roeser & others, 1985).

Composition of ferromanganese deposits

Mineralogy

The ferromanganese crusts and nodules were analysed by X-ray diffraction, and the results are summarised in Table 1. The dominant mineral in the samples (crusts and nodules) was ferruginous vernadite with broad peaks at 2.45 and 1.42 angstroms. Todorokite was present in one of the four samples examined and here was subordinate to vernadite. Birnessite was not identified in any of the samples. Other common minerals included, quartz and feldspar, while calcite was identified in core 62 in minor quantities. Non-manganiferous phases occurred mostly as entrapped detrital grains and as nuclei (Fig. 2).

Polished sections of nodules from station 57 indicated the existence of finely-laminated ferruginous vernadite, recognised by its low reflectance in optical images (reflectance of about 9% for 500–650 nm, Ostwald, 1984) and low electron backscatter in polished sections under the scanning electron microscope, owing to its high hydration (Fig. 4). Laminae of todorokite occur rarely in the polished specimens examined, as 0.01 mm layers of higher optical reflectance and higher electron backscatter (lower hydration) than the vernadite. Microanalyses of both phases are given in Tables 2 & 3. It will be seen that the todorokite contains 6.6% to 1.2% NiO, but very low to zero Cu and Co. Vernadite contains very little Ni, Cu and Co.

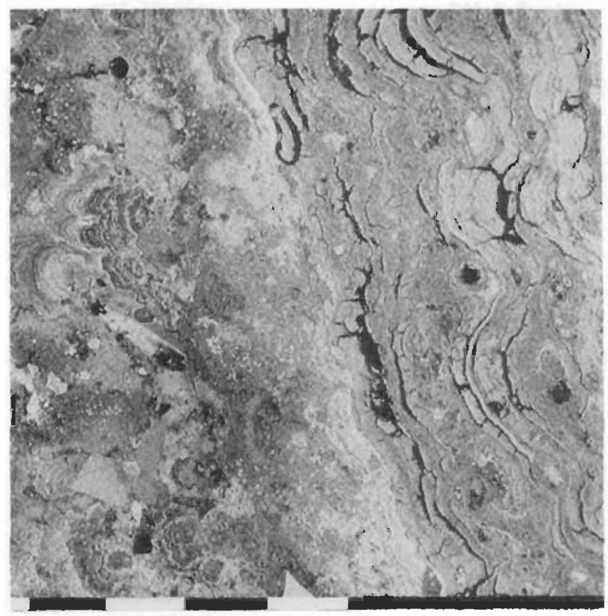

Figure 4. Scanning electron microscope (SEM) micrograph of polished section of Dampier Ridge ferromanganese oxides (Station 57), showing complex layering of ferruginous vernadite (dark) containing thin layers of todorokite (light).
White scale bar is 0.1 mm.

Table 1. Location, physical characteristics and mineralogy of ferromanganese deposits.

Sample number	*Latitude & longitude*	*Location*	*Water depth (m)*	*Substrate lithology*	*Deposit type*[1]	*Deposit thickness or diameter (cm)*
Dredged surface deposits						
57KD 5.1	31°51.8'S 157°22.6'E	Upper part, west-facing slope of Dampier Ridge	2370–2530	metamorphosed granite and microdiorite	N[P]	13.0
57KD 5.2	31°51.8'S 157°22.6'E	Upper part, west-facing slope of Dampier Ridge	2370–2530	metamorphosed granite and microdiorite	C	8.0
57KD 5.3	31°51.8'S 157°22.6'E	Upper part, west-facing slope of Dampier Ridge	2370–2530	metamorphosed granite and microdiorite	N[P]	5.0
Cored sub-surface deposits						
62KL 8.2 100–105 cm	28°35.8'S 163°05.4'E	Upper part, west-facing slope of Lord Howe Rise	1549	not known	C	5.0

Sample number	*Physical characteristics* *Surface texture*	*Internal structure*	*Mineralogy*[2]
Dredged surface deposits			
57KD 5.1	smooth	fine concentric lamination; minor radial cracks; nodule fragment comprises small nucleus	A: vernadite C: quartz
57KD 5.2	smooth, dense, gently undulating	fine wavy lamination	A: vernadite C: quartz, plagioclase
57KD 5.3	smooth, slightly gritty in places	fine concentric lamination, vertical growth structures in thicker laminae	A: vernadite, todorokite C: quartz
Cored subsurface deposits			
62KL 8.2 100–105 cm	not known	black, massive, porous	A: vernadite M: quartz, calcite

[1] C crust, N nodule, [P] polynucleate
[2] A abundant, C common, M minor

In one section the laminated manganese oxides contained rare grains of silver (Fig. 5) which was identified by its X-ray energy spectrum. Irregular particles up to 0.01 mm were detected. These are morphologically similar to silver grains reported by Bolton, Ostwald & Monzier (1986) from the South Rennell Trough–Loyalty Islands zone of the southwest Pacific, although the latter were typically situated in clays associated with ferromanganese crusts, rather than in the manganese oxides. A genetic relationship between the silver in the Dampier Ridge ferromanganese oxides and the previously reported silver occurrence appears likely.

Polished sections of the sub-surface manganese crust (core 62) showed it to be a dense mass of ferruginous vernadite columns (Fig. 6) containing disseminated quartz and carbonate debris.

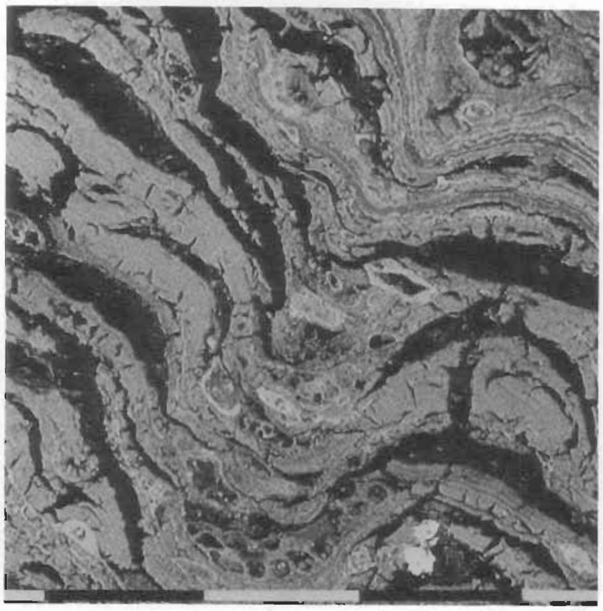

Figure 5. SEM micrograph of polished section of Dampier Ridge layered ferruginous vernadite (Station 57), showing desiccation fracturing and silver grains (white) near base of micrograph.
White scale bar is 0.1 mm.

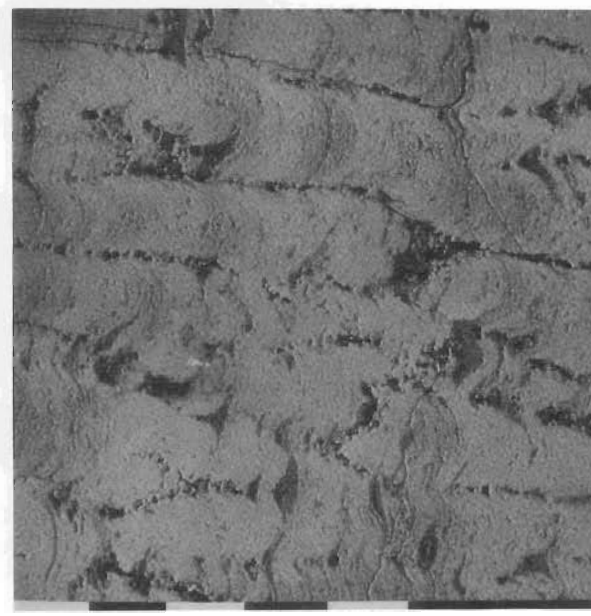

Figure 6. SEM micrograph of polished section of subsurface ferruginous vernadite crust (Station 62), Lord Howe Rise.
White scale bar is 0.1 mm.

Table 2. Microanalysis of ferruginous vernadite from the Dampier Ridge and Lord Howe Rise (weight per cent).

	1	*2*	*3*	*4*	*5*	*6*	*7*	*8*	*9*	*10*	*11*	*12*
MnO_2	16.3	17.6	16.9	20.9	17.8	18.4	32.0	28.5	37.9	31.5	39.2	36.6
Fe_2O_3	39.1	35.0	34.6	38.4	29.2	38.6	34.3	26.7	27.8	27.5	28.4	26.3
CaO	1.3	1.5	1.3	1.0	1.7	1.6	2.6	2.9	2.9	2.6	2.4	3.3
MgO	1.3	1.6	1.4	4.4	2.4	1.6	1.7	1.5	1.9	1.8	1.3	2.2
Na_2O	2.2	2.2	1.2	2.0	4.0	nd	1.8	1.9	2.2	1.5	1.0	2.5
K_2O	0.5	0.4	0.2	0.3	0.5	0.2	0.3	0.4	0.4	0.3	0.3	0.4
P_2O_5	1.3	1.4	1.2	1.7	1.9	1.5	1.6	1.4	1.6	1.5	1.5	1.7
Al_2O_3	2.2	2.3	2.2	5.1	3.4	2.8	1.3	1.1	1.5	1.5	1.3	1.4
SiO_2	8.0	7.9	7.9	7.4	9.1	10.6	6.6	5.3	5.7	5.2	5.5	5.5
NiO	0.3	0.1	nd	0.7	nd	0.3	0.4	0.2	0.3	0.2	0.4	0.6
CuO	nd	nd	nd	nd	nd	nd	nd	nd	nd	nd	nd	nd
CoO	nd	nd	nd	nd	0.1	nd	0.2	nd	0.3	0.5	0.4	0.5
Total	72.5	70.0	66.9	81.9	70.1	75.6	82.8	79.9	82.5	74.1	81.7	81.0

Analysis 1–6, Dampier Ridge, Station 57 (dredge); 7–12, Lord Howe Rise, Station 62 (core)
nd not detected

Table 3. Microanalysis of todorokite from Station 57 on Dampier Ridge (weight per cent).

	1	*2*	*3*	*4*	*5*	*6*	*7*	*8*
MnO_2	52.4	56.1	57.6	53.2	58.5	56.3	57.4	58.2
Fe_2O_3	1.7	4.8	6.6	2.4	2.8	2.1	7.1	4.2
CaO	0.5	0.7	1.2	0.7	0.8	0.4	1.3	0.6
MgO	10.9	8.8	8.3	9.2	9.9	8.8	7.2	9.8
Na_2O	nd	nd	nd	0.1	0.1	nd	nd	nd
K_2O	0.2	0.3	0.2	0.3	0.3	0.2	0.2	0.4
P_2O_5	0.6	0.6	nd	nd	nd	nd	0.1	nd
Al_2O_3	9.1	5.7	4.7	6.3	8.7	7.9	8.3	7.7
SiO_2	3.6	3.1	1.4	1.7	2.3	2.1	1.7	2.3
NiO	6.6	4.8	4.7	3.2	2.1	1.4	1.6	1.2
CuO	nd	0.1	0.6	0.1	0.2	nd	nd	nd
CoO	0.2	nd	0.2	0.1	0.1	nd	nd	nd
Total	85.8	85.0	85.5	77.3	85.8	79.2	84.9	84.0

nd not detected

Microanalyses on the vernadite (Table 2) indicate a maximum of 0.5% CoO and 0.6% NiO. Todorokite was not detected in the Lord Howe Rise material.

The Mn:Fe ratio of the ferruginous vernadite appears to be much higher in the Lord Howe Rise crust than in the Dampier Ridge specimens, a fact indicated by bulk analyses. This may be due to decreasing amounts of terrigenous ferruginous material available for co-precipitation with manganese in the offshore direction.

Bulk chemical composition

Major and minor element concentrations in all samples were determined by X-ray fluorescence and atomic absorption spectroscopy, and the results are summarised in Table 4. Summary statistics for selected metals and elemental ratios are compared in Table 5 with results from nodules recovered at *Kimbla* Station 5 (36° 15'S, 155°35'E), with results from nodules recovered at *Galathea* Station 547, with results from 9 nodules recovered from the Tasman Sea, with average values for ferromanganese deposits from the southwest Pacific, and with average values for south Pacific nodules.

The most significant feature of the data shown in Table 4 is the generally marked difference in metal values between the two sites sampled. Samples from station 57 are generally depleted in Mn (Mn:Fe ratio of 0.59) compared with those from station 62 (Mn:Fe ratio of 0.91), and slightly depleted in combined content of the metals Ni, Cu and Co (0.75, compared with 0.81 from station 62).

Discussion and origin of deposits

Our samples (Table 5) are broadly similar in composition to the nodules from the *Kimbla* station, southwest of the study area and in water 4300 m deep, and to the crusts and nodules from the southwest Pacific as a whole. In particular, they are comparable in having low values of Mn, a low Mn:Fe ratio, and low values of Ni, Cu and Co. They are markedly different from abundant nodules recovered east of the *Kimbla* station by R.V. *Tangaroa* at two stations (Glasby & others, 1986). Station U205 was at 36°48.6'S, 156°31.8'E in water 4548–4714 m deep, and U206 was at 35°33.3'S, 155°40.4'E in water 4408–4418 m deep. U205 had an Mn:Fe ratio of about 2.5, and combined Ni+Cu+Co content of about 1.30% (Ni 0.85%, Cu 0.40%, Co 0.05%). Our values are also in marked contrast to the analyses from the thin crusts on a whale's earbone and on pumice recovered by *Galathea* at 39°45'S, 159°39'E in a greater water depth of 4800 m (Ahrens, Willis & Oosthuizen, 1967). These had Mn:Fe ratios of about 3.4, and combined Ni+Cu+Co content of about 2.05% (Ni 1.27%, Cu 0.60%, Co 0.18%).

The reasons for the differences between the metal values in the *Sonne* and *Kimbla* samples (low Mn:Fe, and low Ni and Cu) and the *Galathea* and *Tangaroa* samples (high Mn:Fe, and moderately high Ni and Cu) are no doubt

Table 4. Bulk chemistry of ferromanganese deposits from the Dampier Ridge and Lord Howe Rise (weight per cent; dried at 110°C).

Sample number	*Deposit type*[1]	*Mn*	*Fe*	*Ni*	*Cu*	*Co*	*Zn*	*Pb*	*%Ni+Cu+Co*	*Mn:Fe*
Surface deposits from Dampier Ridge										
57KD-5.1	Ns	11.37	23.91	0.46	0.12	0.19	0.11	0.11	0.77	0.48
57KD-5.2	Cs	12.02	20.03	0.21	0.09	0.19	0.07	0.11	0.49	0.60
57KD-5.3	Ns	13.98	20.44	0.57	0.14	0.28	0.09	0.13	0.99	0.68
Subsurface deposits from Lord Howe Rise										
62KL (100–105 cm)	C	21.28	23.28	0.32	0.06	0.43	0.10	0.20	0.81	0.91
Surface deposits from Dampier Ridge										
		Si	*Al*	*Ti*	*Mg*	*Ca*	*Na*	*K*	*P*	*L.O.I.*
57KD-5.1	Ns	12.72	4.94	0.34	1.45	1.01	0.3	0.47	0.36	11.63
57KD-5.2	Cs	14.7	5.81	0.54	1.67	1.44	0.38	0.43	0.38	11.59
57KD-5.3	Ns	12.37	5.94	0.52	1.70	1.13	0.45	0.51	0.34	12.01
Subsurface deposits from Lord Howe Rise										
62KL (100–105 cm)	C	3.12	2.65	0.71	1.20	3.39	0.24	0.30	0.58	16.2

[1] C crust, N nodule, r rough, s smooth

Note: All samples were dried at 110°C. Loss on ignition (L.O.I.) was measured at 960°C. Mn, Fe, Ni, Cu, Zn, Pb and Na were measured by atomic absorption spectrography. All other elements were measured using X-ray fluorescence spectrography.

Table 5. Average metal contents and Mn:Fe ratios for ferromanganese deposits from the Dampier Ridge, the Lord Howe Rise, and elsewhere in the South Pacific. All data are in weight per cent.

	This study	*Kimbla Stn 5 Exon & others (1980)*	*Galathea 574 Ahrens & others (1967)*	*Tasman Sea Glasby & others (1986)*	*Southwest Pacific*	*S Pacific nodules Cronan (1972)*
Number of analyses	4	2	2	9	70	ng
Element						
Mn	14.66	5.9	26.8	19.89	14.2	16.6
Fe	21.92	15.8	7.76	8.13	16	13.9
Ni	0.39	0.26	1.28	0.85	0.22	0.43
Cu	0.31	0.18	0.60	0.40	0.08	0.19
Co	0.27	0.06	0.19	0.06	0.27	0.6
Zn	0.14	ng	ng	0.14	0.05	ng
Pb	0.14	ng	ng	0.22	n.g.	0.07
%Ni+Cu+Co	0.92	0.49	2.06	1.31	0.57	1.22
Mn:Fe	0.66	0.37	3.46	2.45	0.9	1.19

ng not given

complex. However, it does appear that Mn:Fe ratio increases and Ni and Cu percentages increase with increasing water depth in the Tasman Sea, the normal situation in the world ocean. The depression containing the *Galathea* and *Tangaroa* samples is more than 4400 m deep; it is far from land, accessible to Antarctic deep water and below the carbonate compensation depth, so sedimentation rates are low and oxidising conditions prevail. Such conditions are favourable to the development of nodule fields and of high grade nodules. Any future search for nodules of economic significance should probably be concentrated in waters more than 5000 m deep southeast and east of Gascoyne Seamount (Fig. 1), although four Kimbla grabs in that area (Exon, 1979) did not recover nodules.

The ferromanganese deposits examined in this study were formed predominantly by slow precipitation of ferromanganese phases (mainly vernadite) directly from near-bottom seawater (i.e. hydrogenetically) which contains Mn and Fe mainly in colloidal solutions (Halbach & Ozkara, 1979; Cronan, 1984). They all fall within the area of hydrogenous deposits (Fig. 7) as defined by Bonatti, Kraemer & Rydell (1972). There is no evidence either of direct hydrothermal contribution, or of significant accumulation of metals following diagenetic remobilisation from underlying substrates. The variations of composition observed in our samples are interpreted as reflecting different degrees of dilution by aluminosilicates and biogenic detritus, rather than two different sources of metals or environments of growth. The close similarity in mineralogy, chemistry and physical appearance of our samples to typical, deep-water, hydrogenetic ferromanganese deposits described elsewhere appears to support this interpretation (Halbach & Ozkara, 1979; Cronan, 1980; Usui, 1983).

Acknowledgements

We are grateful to BGR Chief Scientist K. Hinz and geologists H.R. Kudrass and M. Wiedicke, who acquired the material on the 1985 *Sonne* cruise in which Exon also participated. Geoff O'Brien of BMR is thanked for reviewing the manuscript.

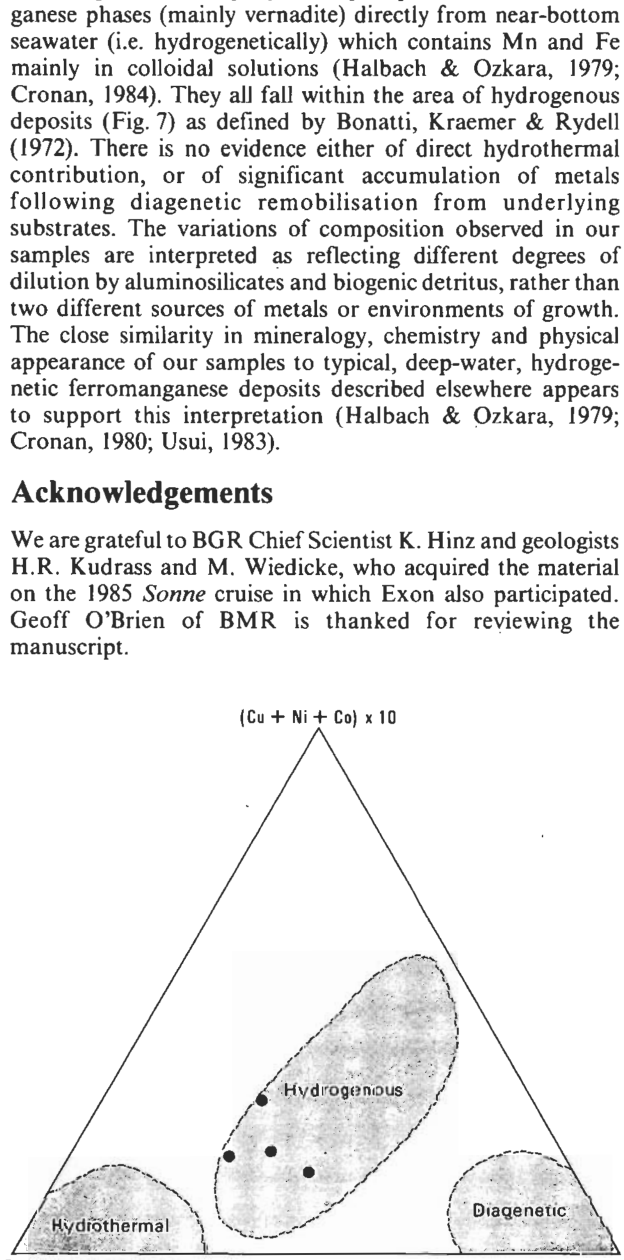

Figure 7. Ternary diagram of Mn/Fe/Cu+Ni+Co concentrations for samples from this study, compared with deep-sea ferromanganese nodules of hydrogenous, hydrothermal, and diagenetic origin.
Outlines of fields from Bonatti & others (1972).

References

Ahrens, L.H., Willis, J.P., & Oosthuizen, C.O., 1967 — Further observations on the composition of manganese nodules with particular reference to some of the rarer elements. *Geochemica et Cosmochimica Acta*, 31, 2169–2180.

Bolton, B.R., Ostwald, J., & Monzier, M., 1986 — Precious metals in ferromanganese crusts from the south-west Pacific. *Nature*, 320, 518–520.

Bonatti, E., Kraemer, T., & Rydell, H., 1972 — Classification and genesis of submarine iron-manganese deposits. *In* Horn, D.R., (editor), Conference on ferromanganese deposits on the ocean floor. *Office of the International Decade of Ocean Exploration, National Science Foundation, Washington DC*, 149–166.

Conolly, J.R., & Payne, R.R., 1972 — Sedimentary patterns within a continent-mid-oceanic ridge-continent profile: Indian Ocean south of Australia. *In* Hayes, D.E., (editor), Antarctic Oceanology II: The Australian-New Zealand sector. *Antarctic Research Series*, 19, *American Geophysical Union, Washington DC*, 295–315.

Cronan, D.S., 1972 — Regional geochemistry of ferromanganese nodules in the world ocean. *In* Horn, D.R., (editor), Conference on ferromanganese deposits on the ocean floor. *Office of the International Decade of Ocean Exploration, National Science Foundation, Washington, DC*, 19–29.

Cronan, D.S., 1980 — Underwater minerals. *Academic Press, London*, 362 pp.

Cronan, D.S., 1984 — Criteria for the recognition of areas of potentially economic manganese nodules and encrustations in the CCOP/SOPAC region of the central and southwestern tropical Pacific. *South Pacific Marine Geological Notes*, 3, 1–17.

Exon, N.F., 1979 — Deepsea sediments and manganese nodules from the southern Tasman Sea. *Bureau of Mineral Resources, Australia, Record* 1979/62.

Exon, N.F., Moreton, D., & Hicks, G., 1980 — Manganese nodules from the Tasman Sea off Sydney. *BMR Journal of Australian Geology & Geophysics*, 5, 67–68.

Glasby, G.P., 1973 — Manganese deposits in the southwest Pacific. *In* Inter-university program of research on ferromanganese deposits of the ocean floor, Phase I. Report sponsored by Seabed Assessment Program, International Decade of Ocean Exploration, *National Science Foundation, Washington DC*, 137–169.

Glasby, G.P., 1986 — Hiatuses in manganese nodule growth: relation to bottom current activity? *Geo-marine Letters*, 5, 247–252.

Glasby, G.P., Stoffers, P., Grapes, R.H., Pluger, W.L., McKnight, D.G., & Main, W.deL., 1986 — Manganese nodule occurrence in the Tasman Sea. *New Zealand Journal of Marine and Freshwater Research*, 20, 489–494.

Goodell, H.G., Meylan, M.A., & Grant, B., 1971 — Ferromanganese deposits of the South Pacific Ocean, Drake Passage, and Scotia Sea. *In* Reid, J.L., (editor), Antarctic Oceanology, I. *Antarctic Research Series*, 15, 27–92.

Halbach, P., & Ozkara, M., 1979 — Morphological and geochemical classification of deep-sea ferromanganese nodules and its genetical interpretation. *In* Lalou, C., (editor), Colloques Internationaux du C.N.R.S. No. 289, La genese des nodules de manganese. *C.N.R.S., Paris*, 77–88.

Jones, H.A., 1980 — Deepsea manganese nodules in the Australian region — a review. *Australian Mineral Industry Quarterly*, 33(1), 1–14.

Ostwald, J., 1984 — Vernadite — a possible hybrid structured mineral. *Australian Mineralogist*, July, 269–271.

Payne, R.R., & Conolly, J.R., 1972 — Pleistocene manganese pavement production: its relationships to the origin of manganese in the Tasman Sea. *In* Horn, D.R., Delach, M., & Horn, B., (editors), Conference on ferromanganese deposits on the ocean floor. *Office of International Decade of Ocean Exploration, Washington DC*, 81–92.

Roeser, H.A., & others, 1985 — Geophysical, geological and geochemical investigations on the Lord Howe Rise. Final Report on the R/V 'Sonne' Cruise, SO-36, Part 2, *Bundesanstalt fuer Geowissenschaften und Rohstoffe Cruise Report*, 193 pp.

Symonds, P.A., Willcox, J.B., & Kudrass, H.R., 1988 — Dampier Ridge in the Tasman Sea — a continental fragment. *9th Australian Geological Convention, Geological Society of Australia, Abstract Volume* 21, 393–394.

Usui, A., 1983 — Regional variation of manganese nodule facies on the Wake-Tahiti transect: Morphological, chemical and mineralogical study. *Marine Geology*, 54, 27–51.

Watkins, N.D., & Kennett, J.P., 1971 — Antarctic bottom water: major change in velocity during the late Cenozoic between Australia and Antarctica. *Science*, 173, 813–818.

Watkins, N.D., & Kennett, J.P., 1972 — Regional sedimentary disconformities and Upper Cenozoic changes in bottom water velocities between Australasia and Antarctica. *In* Hayes, D.E., (editor), Antarctic Oceanology II: The Australian-New Zealand sector. *Antarctic Research Series*, 19, *American Geophysical Union, Washington DC*, 273–293.

Watkins, N.D., & Kennett, J.P., 1977 — Erosion of deep-sea sediments in the Southern Ocean between longitudes 70° E and 190° E and contrasts in manganese nodule development. *Marine Geology*, 23, 103–111.

Willcox, J.B., Symonds, P.A., Hinz, K., & Bennett, D., 1980 — Lord Howe Rise, Tasman Sea — preliminary geophysical results and petroleum prospects. *BMR Journal of Australian Geology & Geophysics*, 5, 225–236.

BMR Journal of Australian Geology & Geophysics, 11, 429-447

A belemnite biozonation for the Jurassic-Cretaceous of Papua New Guinea and a faunal comparison with eastern Indonesia

A.B. Challinor[1]

Middle and Late Jurassic and some Early Cretaceous Belemnitida collected mostly within the region covered by the Ok Tedi and Mianmin 1:250 000 sheets in the central highlands of Papua New Guinea are identical with those of eastern Indonesia. *Conodicoelites kalepuensis* confirms that part of the Maril Formation is Bathonian in age. Members of the *Belemnopsis moluccana-B. galoi-B. stolleyi* lineage which spans the Late Jurassic of Indonesia confirm that the Imburu Mudstone and Upper Maril Formation are Oxfordian-Late Tithonian in age. *Hibolithes australis* n. sp. spans the Late Tithonian-earliest Berriasian interval; *Belemnopsis jonkeri* and *Hibolithes gamtaensis* n. sp. range from Berriasian to Valanginian confirming these ages for the Toro Sandstone, basal Ieru Formation and basal Tubu unit. *Hibolithes taylori* n. sp. (Aptian-Albian), *Parahibolites feraminensis* n. sp. (Albian) and *Dimitobelus macgregori* (Albian-Cenomanian) are present in the Upper Ieru Formation and Chim Formation. The presence of *Hibolithes taylori* in outcrops previously mapped as Toro Formation suggests that the Aptian-Albian Omati Unit has been wrongly identified as Toro Formation in some instances.

Introduction

This paper erects a belemnite biozonation for the Late Jurassic and Early Cretaceous of Papua New Guinea. It establishes the approximate stratigraphic ranges of nine belemnite species including two new taxa not known from other regions. It uses macrofossil and dinoflagellate data to provisionally correlate and date the taxa, and compares the Papua New Guinea belemnite succession with that of eastern Indonesia.

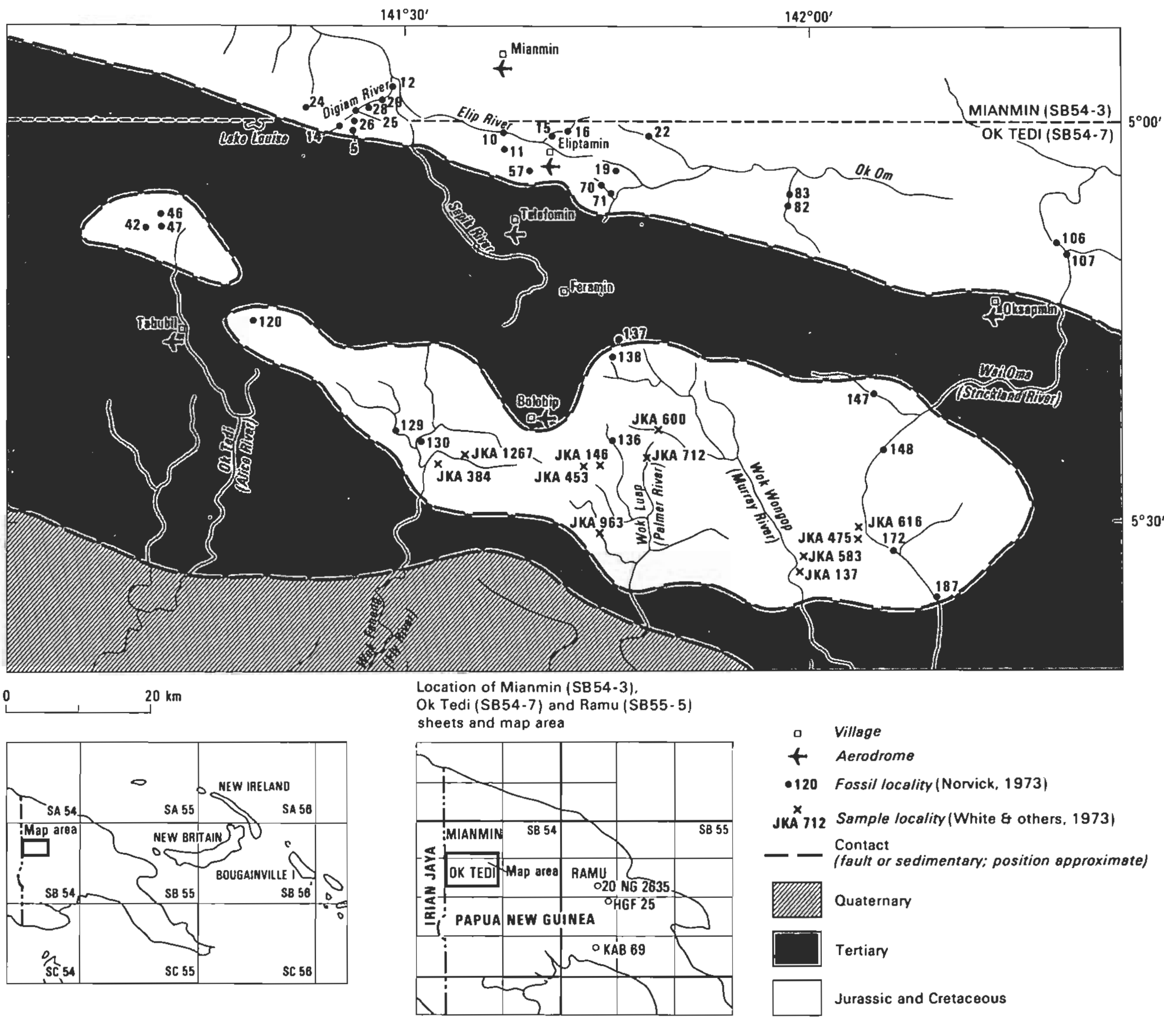

Figure 1. Geological sketch map (igneous and metamorphic rocks omitted) of Ok Tedi sheet and southern part of Mianmin sheet, illustrating location of material studied.
Approximate location of samples from outside map area shown on index diagrams.

[1] 25 Bailey Avenue, Hamilton, New Zealand

The region from which the fossils were collected is mountainous and mostly covered by rainforest, and its geology is complex (Davies & Norvick, 1974). A proximal to distal sedimentary sequence fining northwards with lateral facies changes and deformed by folding and numerous faults (normal, thrust, and possible strike slip) has led to many stratigraphic problems. The recognition of individual units in some instances is difficult and the position of fossil localities relative to formation boundaries is poorly known, particularly in the more distal beds of the northerly part of the region.

Most of the belemnites discussed were collected within the area covered by the Ok Tedi (formerly Blucher Range) and Mianmin 1:250 000 sheets (International index SB/54-7, SB/54-3) published by the Bureau of Mineral Resources, Australia (BMR) and Geological Survey of Papua New Guinea (GSPNG). Collections located on the Ok Tedi and Southern Atbalmin 1:100 000 sheet (sheet 7187/7188 published by the GSPNG) and from a number of measured sections in the Telefomin (SB/54-7/2), Palmer River (SB/54-7/5) and Muller Range (SB/54-7/6) sheets plotted on British Petroleum 1:100 000 base maps were also studied. These localities lie within sheets SB/54-7 and SB/54-3 but not all are shown on them. Fossil localities are indicated in Figure 1 and the approximate positions of those outside the Ok Tedi and Mianmin sheets are shown on locality diagrams.

Most of the fossils studied are held at the Bureau of Mineral Resources, Canberra, Australia. Figured specimens with catalogue numbers preceded by CPC are held in the Commonwealth Palaeontological Collection housed at the BMR. Figured specimens with catalogue numbers preceded by IMC are held in the Indonesian Macropaleontology Collection housed at the Geological Research and Development Centre, Bandung, Indonesia.

Lithostratigraphy

The stratigraphy adopted here (Fig. 2) has been developed by G. Francis (GSPNG). Some nomenclature is provisional

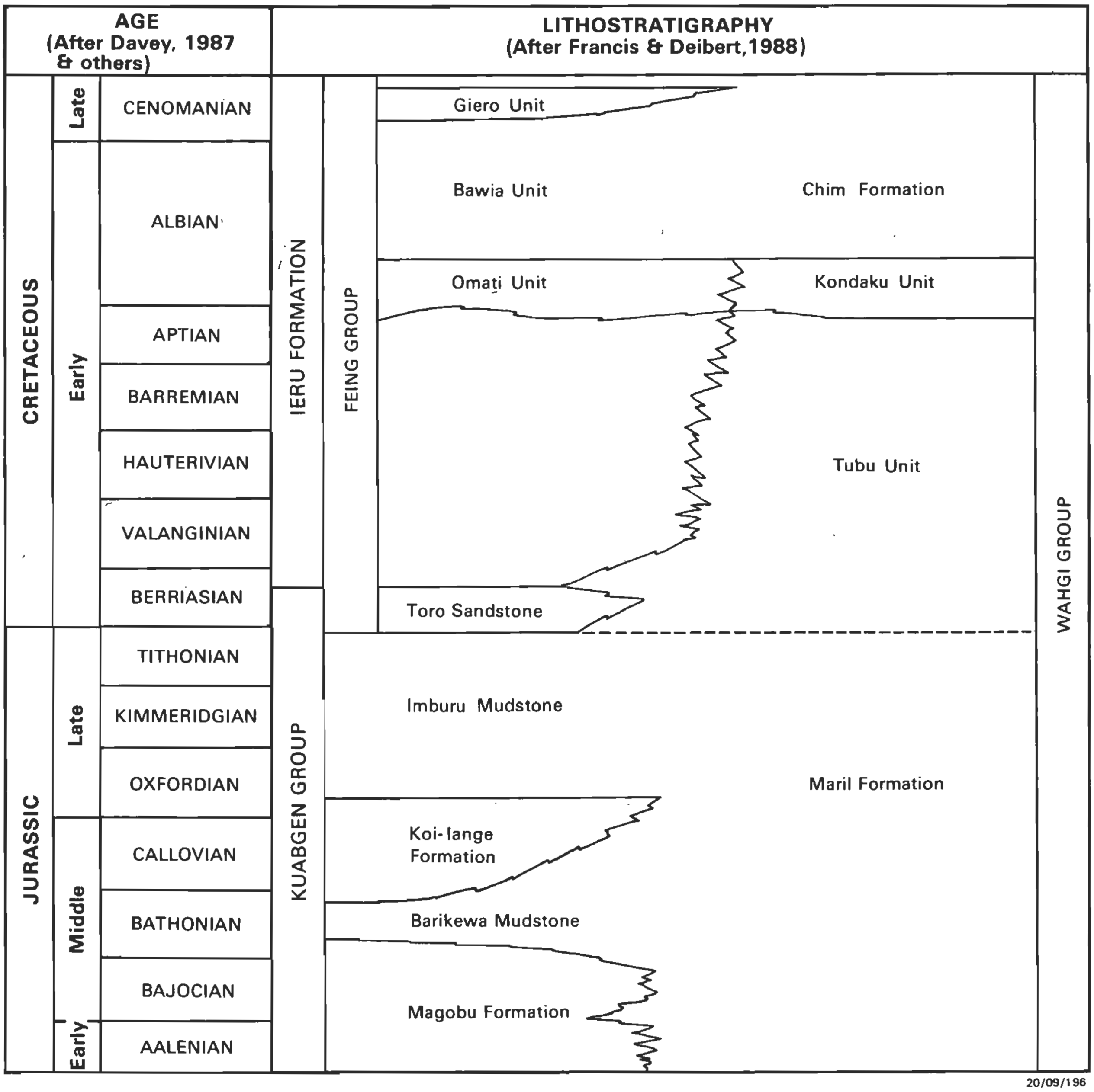

Figure 2. Provisional lithostratigraphy and age correlation of Jurassic-Cretaceous within Ok Tedi and Mianmin sheets (after Francis & Deibert, 1988, with addition of the Feing Group of authors).

with informal units used in subdivision of the Ieru Formation and upper Wahgi Group. Formation ages have been determined largely by palynology (Davey, 1987) and micropalaeontology, and there are some unresolved problems.

The original lithostratigraphic nomenclature (used in BMR fossil collection records) is based on White & others (1973) and Davies & Norvick (1977) but is undergoing revision on more recent data. These include remapping of part of the Mianmin 1:250 000 sheet by GSPNG (Rogerson & others, in press), a review by Francis (1986), a revision of the Wahgi Group in its type area (Haig & others, 1986), more precise dating of the Imburu Mudstone, Toro Sandstone and lower Ieru Formation (Davey, 1987) and a reassessment of correlations of the Toro Sandstone and lower Ieru Formation (Francis, 1988). Major problems are the lack of precision in definition and a proliferation of lithostratigraphic nomenclature with different names used for the same unit in adjacent regions. Synonyms relevant to this paper include:

Chim Formation	Maram Shales and Chimbu Tuffs (Edwards & Glaessner, 1953) Chim Formation and uppermost Kondaku Tuff (Bain & others, 1975) Chim Formation (Haig & others, 1986)
Kondaku Unit	Purari Greywackes, ?in part (Edwards, 1950) middle Kondaku Tuffs (Edwards & Glaessner, 1953) middle Kondaku Tuffs (Bain & others, 1975) Kondaku unit (Francis, 1986) Kondaku unit (Haig & others, 1986)
Wahgi Group	Wahgi Group and Jimi Greywacke (Bain & others, 1975)
Maril Formation	Maril Shale and lower Kondaku Tuff (Edwards & Glaessner, 1953) ?Kompiai Formation, Maril Shale and lower Kondaku Tuff (Dow & Dekker, 1964) Maril Shale and Sitipa Shale (Dow & others, 1972) Maril Shale and lower Kondaku Tuff (Bain & others, 1975) lower Om beds (Davies & Norvick, 1977) Maril Formation (Haig & others, 1986).

Stratigraphic distribution of belemnites

Details of belemnite collections examined are tabled in Appendix 1. The following comments expand that list and present additional data. New taxa discussed here are described or discussed elsewhere, either in Appendix 2 or in Challinor (1989b, in press).

Conodicoelites kalepuensis is known from several localities, all within the Maril Formation. It is present in mid-Bathonian beds in Sula Islands (Challinor & Skwarko, 1982) but, in view of its occurrence at several localities in Papua New Guinea, an unrestricted Bathonian age is suggested here. Ages suggested for ammonites and bivalves associated with *C. kalepuensis* range from Bajocian to Oxfordian (Norvick, 1973).

Belemnopsis moluccana occurs at a number of localities in the Maril Formation and at one locality (sample JKA 600) in the lower Imburu Mudstone. In eastern Indonesia *B. moluccana* ranges through the Oxfordian to early Tithonian (Challinor, 1989b, in press). An Oxfordian–early Tithonian age is suggested for the material studied here but the stratigraphic range of these collections is not known. Specimens in sample P 5014 may be early forms (Challinor, 1989b, in press); if so, they are probably early Oxfordian in age. Ages adopted for associated macrofossils in Papua New Guinea range from late Bajocian to Tithonian (Norvick, 1973; Arnold & others, 1979).

Belemnopsis galoi occurs in the Maril Formation and Imburu Mudstone. In eastern Indonesia the taxon is restricted to the early Tithonian (Challinor, in press). The stratigraphic positions of the Maril occurrences are not known, but on field evidence all occurrences in the Imburu Mudstone (samples JKA 583 (float), JKA 616 and JKA 1267) are close to the base of the formation. According to Francis (1986), the lower Imburu Mudstone is Oxfordian–Kimmeridgian in age and the stated stratigraphic position of the samples cannot be reconciled with the known age range of the taxon. Sample JKA 137 contains early forms of the species and samples JKA 712, JKA 616 and JKA 1267 late forms, so much of the stratigraphic range of the taxon is included within its collection localities. Ages for associated bivalves and ammonites range from late Bajocian to Tithonian (Norvick, 1973; Davies, 1982).

Belemnopsis stolleyi has not been certainly identified (all specimens are poorly preserved) but *B.* cf. *stolleyi* is present in the Maril Formation (locality 71 sheet SB/54-7) where it is associated with *Hibolithes australis, H.* cf. *australis* and *Belemnopsis* cf. *mangolensis. B. stolleyi, H. australis* and *B. mangolensis* are known from the Late Tithonian in eastern Indonesia (Challinor & Skwarko, 1982) and the association of specimens comparable with or identical to each of the three species points to a Late Tithonian age. Associated bivalves at locality 71 have been assigned a Callovian–Tithonian age (Norvick, 1973).

Hibolithes australis or *H.* cf. *australis* occurs in the Maril Formation and Imburu Mudstone and in the Tubu unit of the Wahgi Group (sample KAB 69). It ranges from Late Tithonian to early Berriasian in eastern Indonesia (Challinor, in press) and Papua New Guinea. Ammonites and bivalves associated with *H. australis* at locality 71 suggest a Late Jurassic age (Norvick, 1973).

Hibolithes gamtaensis and *Belemnopsis jonkeri* are present in the basal Toro Sandstone (sample JKA 453 sheet SB/54-7/2) and Ieru Formation (locality 187, sheet SB/54-7). *H. gamtaensis* is probably identical with *Hibolithes* sp. cf. *obtusirostris* of authors, and in Papua New Guinea this species has been recorded throughout the Berriasian and Valanginian. It occurs within the latest Berriasian to earliest Valanginian *Egmontodinium torynum* dinoflagellate zone of Davey (1987) in the Strickland Gorge type section of the lower Ieru Formation (G. Francis, GSPNG, personal communication, 1986). Ammonites and bivalves of Early Cretaceous age are associated with *B. jonkeri* at locality 187 (Norvick, 1973) and the Toro Sandstone has been firmly dated at Latest Tithonian–Berriasian by palynology (Davey, 1987). Both *H. gamtaensis* and *B. jonkeri* occur in the Neocomian of Indonesia (Challinor, in press).

Hibolithes taylori is present at a number of localities originally mapped as Toro Sandstone (samples JKA 146, JKA 384, sheets SB/54-7/2, 7/5; localities 42, 136, sheet SB/54-7) and Maril Formation (localities 26, 29, sheet 7187/7188). These units are apparently misidentified because:

(1) *Hibolithes gamtaensis* and *Belemnopsis jonkeri* are known from the Toro Sandstone and basal Ieru

Formation and in age equivalent strata in Irian Jaya and Misool (Challinor, 1989a, in press) but are nowhere associated with *H. taylori*;

(2) *H. taylori* and *Parahibolites* are associated at two localities (26 and 29, sheet 7187/7188), and *Parahibolites* is restricted to post-Neocomian strata worldwide (Stevens, 1965, 1973).

G. Francis (GSPNG, personal communication, 1986) suggests that the 'Toro Sandstone' at localities JKA 146, JKA 384, 42, 136 is in fact Omati unit, and 'Maril Formation' at localities 26 and 29 is Chim Formation. Microfossil evidence from localities 42 and 136 suggests Late Jurassic–Late Cretaceous ages and 'probably Callovian' bivalves are present (Norvick, 1973). A Kimmeridgian–Tithonian age for localities 26 and 29 was suggested in Arnold & others (1979) but this was based on the belemnites, ages and identifications of which are revised here. An Aptian–Albian age is accepted here for *Hibolithes taylori.*

Parahibolites feraminensis is known from float collections at localities 26 and 29 (sheet 7187/7188) and in poorly localised or apparently mixed collections (sample 919, locality 71; sample 1057, near locality 137; Appendix 1). Most of the latter material was collected by the people of Feramin Village from their gardens near locality 137 on sheet SB/54-7. As stated above, *Parahibolites* has an Aptian–Cenomanian age on the world scene (Stevens, 1973). Glaessner (1945) considered his specimens of *Parahibolites blanfordi* to be Albian in age and Stevens (1965) suggested an Aptian–Albian age for Papua New Guinea *Parahibolites.* Little evidence of age is available from other sources and, as mentioned above, localities 26 and 29 were originally dated as Kimmeridgian–Tithonian on their belemnite content. An Albian age is adopted here for *Parahibolites feraminensis.*

The single specimen of *Dimitobelus macgregori* examined (sample HGF 25) was found within the Chim Formation where it is abundant and associated with latest Albian planktic foraminifera (locality 68, Haig 1981). *D. macgregori* is of ?late Albian–early Cenomanian age in New Zealand (Stevens, 1965) and late Albian–Cenomanian in Papua New Guinea (G. Francis, GSPNG, personal communication, 1988).

Early belemnite records

Belemnites have been recorded from the central highlands by earlier researchers. The record of *Parahibolites* by Glaessner (1945) has been discussed. In the same publication he identified *Belemnopsis gerardi* (Oppel) and *B.* cf. *indica* Kruizinga from the Kuagben Group on the Fly River (Wok Feneng). The specific name *gerardi* is not valid for Indonesian material (Stevens, 1963). The specimens from Indonesia identified as *B. gerardi* by Kruizinga (1920) and Stolley (1929) include early and late *B. galoi*, transitional forms, and *B. stolleyi* (Challinor, 1989b).

Glaessner's figured specimens of *B. gerardi* (1945, Pl. 6, figs 8, 9a,b) appear to be early *B. galoi*. This is supported by their occurrence with *Malayomaorica malayomaorica* (Krumbeck) and *'Inoceramus'. Belemnopsis indica* Kruizinga is a synonym of *B. moluccana* (Boehm) (Challinor, 1989b, in press) and Glaessner's description indicates his *B.* cf. *indica* is without doubt *B. moluccana.*

Banner & others (1961) recorded belemnites from the 'Tubu Shales' in the Kereru Range, later identified by W.J. Arkell as *Hibolithes lagoicus* (Boehm) and *Belemnopsis alfurica* (Boehm). To judge from the Indonesian belemnite succession (Challinor, in press) and the Papua New Guinea collections studied here, the specimens identified by Arkell are probably either *Hibolithes australis* and *Belemnopsis stolleyi* or *Hibolithes gamtaensis* and *Belemnopsis jonkeri.*

Age correlation of assemblages

This section attempts to establish ages for the belemnite assemblages discussed. Because most are known from eastern Indonesia where provisional ages have been assigned, their ages in that region are considered first.

Macrofossil evidence for belemnite ages in Indonesia

Most Jurassic and Early Cretaceous belemnites discussed here are present in eastern Indonesia, particularly Sula Islands and Misool, but the Jurassic–Cretaceous of that region has not been accurately correlated at stage level. Stage boundaries and belemnite time ranges adopted here were established during a study of belemnite distributions, mostly in the Misool Archipelago (Challinor, in press) and the evidence on which they are based is restated briefly here.

Subdivisions adopted are based mostly on macrofossils and differ in some instances from those of palynologists, particularly dinoflagellate workers. Time distributions of the correlating macrofossils have been studied by Helby & others (1988) who examined diverse source material. Their work provides a modern summary of probable distributions but uncertainties remain, and ages based on them cannot be regarded as unequivocal.

Stratigraphic distribution of the belemnites is best known from the Misool Archipelago where they are associated over parts of their ranges with other molluscs of time-diagnostic value. Identifications of the latter have been provided by F. Hasibuan, University of Auckland. Fossil occurrences and stage boundaries adopted for Misool are summarised in Figure 3. Belemnite distributions are essentially continuous throughout the sequence (within the limits imposed by incomplete outcrop) and appear in most exposures. Other molluscs appear at few outcrops separated by intervals apparently devoid of macrofossils other than belemnites. Thus the belemnites are of potentially great value as zone fossils.

Following Stolley (1929, 1935) the base of the Cretaceous system in Misool is placed at the first appearance of the belemnite genus *Duvalia.* This must be regarded as an approximate position (Challinor, in press) but is the only macrofossil evidence available at present. No other macrofossil control is available for the Neocomian. *Belemnopsis jonkeri* and *Hibolithes gamtaensis* (and other Belemnitida not recorded from Papua New Guinea; Fig. 4) are assigned ages on their apparent relative stratigraphic positions.

Only beds included in the Tithonian *sensu* Harland & others (1982) contain a significant range of molluscs other than belemnites (Fig. 3). The base of the stage is placed at a horizon containing diverse early Tithonian bivalves and ammonites. These include taxa which, on present evidence (Helby & others, 1988), are either confined to the Tithonian (*Paraboliceras, Torquatisphinctes, Retroceramus haasti*) or extend into it (*Kossmatia, R. galoi, R. subhaasti, Malayomaorica malayomaorica*).

Beds between basal Tithonian outcrops and those placed in the Oxfordian are assigned an undifferentiated Oxfordian–Kimmeridgian age. Little evidence is available for the age of this sequence.

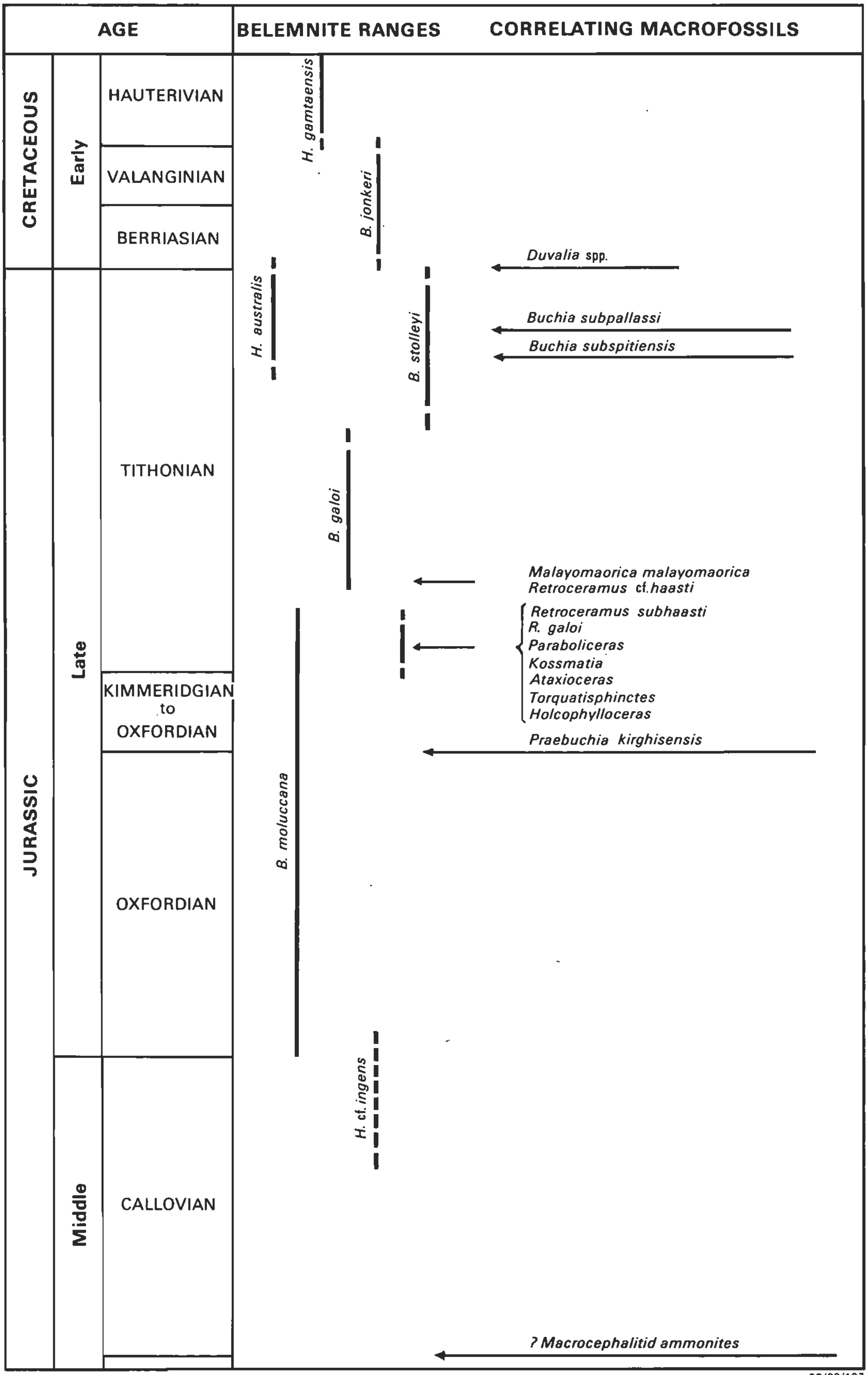

Figure 3. Time distribution of Belemnitida in eastern Indonesia.
Macrofossil evidence for position of stage boundaries in Misool indicated. Relative sedimentary thickness of each stage in Misool Archipelago indicated approximately (after Challinor, in press).

Little macrofossil evidence exists for that part of the sequence included in the Oxfordian apart from the presence of *Praebuchia kirghisensis* Sokolov (Oxfordian: Li & Grant-Mackie, 1988) at its top. No macrofossil evidence is known for basal Oxfordian which is provisionally marked by the first appearance of *Belemnopsis moluccana*, but the presence of early Oxfordian dinoflagellates (Fig. 4) suggests that its position is at least approximately correct.

The base of the Callovian in Misool has been placed at a horizon containing possibly macrocephalitid ammonites, the latter traditionally regarded as indicating early Callovian. Again, this boundary must be regarded as provisional, because recent research on the Macrocephalitinae of Sula Islands and Papua New Guinea (Westermann & Callomon, 1988) indicates they extend into at least the late Bathonian.

Dinoflagellate evidence for belemnite ages in Indonesia

Palynological research in western and northern Australia and in the Papuan basin has enabled Helby & others (1987) to develop a dinoflagellate zonal scheme which appears

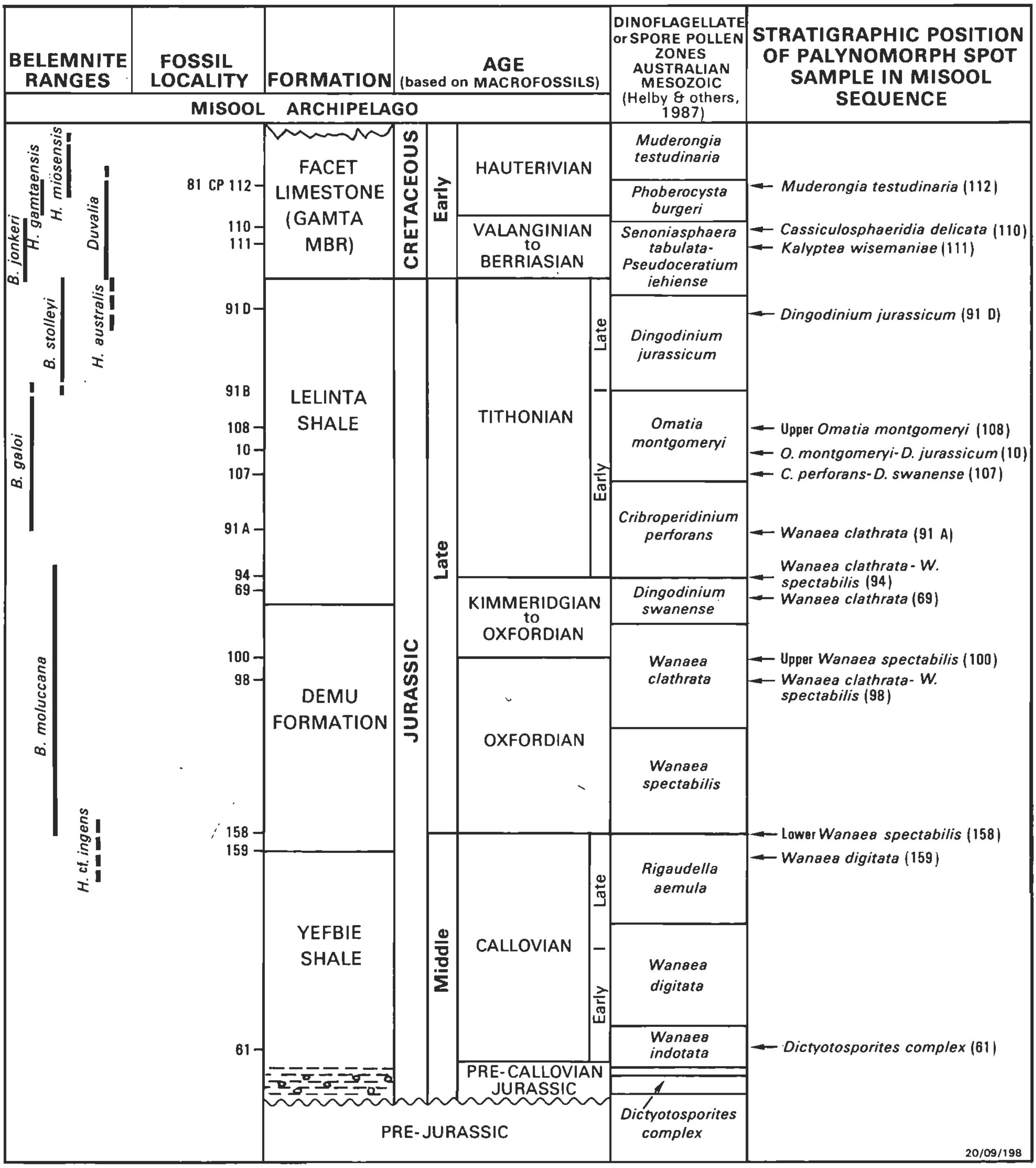

Figure 4. Generalised lithostratigraphy of Jurassic and early Cretaceous of Misool Archipelago (Pigram & others, 1982) with stage boundaries positioned on macrofossil evidence (Challinor, in press).
Dinoflagellate or spore pollen zones of Australian Mesozoic (Helby & others, 1987) for these stages indicated. Arrows indicate position of dinoflagellate spot samples. Note lack of agreement between dinoflagellate zones and position of some spot samples.

applicable to the Misool Sequence. Problems with age control remain, particularly in the Late Jurassic and early Cretaceous where belemnites have been used for correlation (Helby & others, 1987, appendix 3). Most of these identifications (*Belemnopsis tanganensis, Hibolithes* cf. *obtusirostris, Acroteuthis subquadratus, Belemnopsis* cf. *aucklandica*) are almost certainly incorrect (Stevens, 1965; Challinor, in press) and others (*Belemnopsis* cf. *alfurica*) are potentially so (Challinor, 1989b). Therefore the possibility of miscorrelation exists.

Figure 4 relates the dinoflagellate zones of Helby & others (1987) to Misool stages (boundaries located by macrofossil data as discussed above). A number of spot samples from Misool have been examined for dinoflagellates by R.W. Helby (F. Hasibuan, University of Auckland, personal communication, 1988). Sampling was not continuous or closely spaced but many of the zones of Helby & others (1987) are present. The location and dinoflagellate zone of the samples is indicated in Figure 4 and a number of interesting features emerge:

(1) there is no clear evidence for Kimmeridgian strata (cf. Helby & others, 1987, fig. 12), possibly a result of discontinuous sampling;

(2) beds which on macrofossil evidence are basal Tithonian (localities 81CP69, 94) are late Oxfordian by dinoflagellate spot sample;

(3) Beds of Valanginian age on macrofossil evidence (admittedly slight) are early Berriasian by dinoflagellates.

The zones of *Cassiculosphaeridia delicata* and *Kalyptea wisemaniae* (early Berriasian: Helby & others, 1987) occur in the lower part of the division marked *Senoniasphaera tabulata* to *Pseudoceratium iehiense* (Fig. 4) but the spot samples were collected within beds assigned on macrofossil evidence to the uppermost Berriasian–Valanginian.

The ages of Misool belemnites according to their associated macrofossils and dinoflagellates are compared in Table 1.

Table 1. Age correlation of Belemnitida of Misool based on macrofossils and dinoflagellates.

Belemnite	*Age based on macrofossils (Challinor, in press)*	*Age based on dinoflagellate zonation of Helby & others (1987)*
Belemnopsis moluccana	Oxfordian–early Tithonian	Oxfordian
Belemnopsis galoi	early Tithonian	early Tithonian
Belemnopsis stolleyi	late Tithonian	late Tithonian
Hibolithes australis	late Tithonian	late Tithonian
Belemnopsis jonkeri	Berriasian–Valanginian	Berriasian
Hibolithes gamtaensis	Hauterivian	Hauterivian

Agreement on the range of *Belemnopsis moluccana* (Oxfordian-Tithonian by macrofossils; Oxfordian by dinoflagellate spot sample) and *Belemnopsis jonkeri* (Berriasian and Valanginian by macrofossils, Berriasian by dinoflagellate spot sample) is only partial but, as pointed out, macrofossil control in the Neocomian of Misool is poor. The two zonal schemes give similar ages for the remaining belemnites.

Belemnite ages in Papua New Guinea

An alternative dinoflagellate zonation for the Papuan basin has been developed by Davey (1987) based on sections on the Strickland River and tributaries. Many dinoflagellates present are endemic to the Australia-Papua New Guinea region. Correlation with western European type sections and ammonite-dated sequences is by those relatively few taxa common to Papua New Guinea and Europe. However, the ranges of some species and genera differ in the two regions (Davey, 1987, fig. 13). Furthermore, the zones from *Wanaea clathrata* to *Omatia montgomeryi* are regarded as systematically older by Davey (mid-Oxfordian to late Oxfordian–early Kimmeridgian) than by Helby & others (1987, late Oxfordian to mid-Tithonian). Again the possibility of miscorrelation exists.

G. Francis (GSPNG) has plotted the apparent distributions of bivalves and belemnites ('apparent' because few direct associations of macrofossils and dinoflagellates are known; correlation between the two is by stratigraphic and lithologic means) in relation to Davey's dinoflagellate zones (Fig. 5). Using Davey's zonal scheme and the belemnite distributions by Francis, belemnite ages are listed in Table 2.

Table 2. Age correlation of Belemnitida of Papua New Guinea based on macrofossils and dinoflagellates.

Belemnite	*Age in Misool based on macrofossils (Challinor, in press)*	*Age in PNG based on dinoflagellates (after Davey, 1987)*
Belemnopsis moluccana	Oxfordian–early Tithonian	early and mid Oxfordian
Belemnopsis galoi	early Tithonian	mid Oxfordian–late Kimmeridgian
Belemnopsis stolleyi	late Tithonian	
B. cf. *stolleyi*		late Kimmeridgian to mid Tithonian
Hibolithes australis	late Tithonian	early Tithonian–early Berriasian
Belemnopsis jonkeri	Berriasian–Valanginian	Berriasian
Hibolithes gamtaensis	Hauterivian	Berriasian–Valanginian
Hibolithes taylori		Aptian–Albian
Parahibolites feraminensis		Albian
Dimitobelus macgregori		?Albian–Cenomanian

Belemnite ages given here are systematically older than those from macrofossil associations in Misool. In the Oxfordian–Tithonian they are generally older than those determined by the dinoflagellate zonation of Helby & others (1987). As well, the concurrent range zone of *Retroceramus galoi, R. subhaasti* and *Malayomaorica malayomaorica* (Fig. 5) has an apparent mid-Oxfordian age. Macrofossil data in Helby & others (1988) suggest this horizon could be as young as early Tithonian.

The concurrent range zone of *B. moluccana* and *B. galoi* (Fig. 5) presents a further anomaly. There is clear evidence from Misool and Sula Islands (and elsewhere in Indonesia) that *B. galoi* is the descendant of *B. moluccana* (Challinor, 1989b) and no concurrent range zone of the two is known. *B. galoi* invariably succeeds *B. moluccana.* In one known instance the two occur at the same locality (2D, Wai Galo, Sula Islands, Challinor & Skwarko, 1982), but this locality spans some 25 m of beds (Sato & others, 1978) and lies within the transition zone between *B. moluccana* and *B. galoi.* All *B. galoi* present at locality 2D approach *B. moluccana* in morphology (Challinor, 1989b).

Glaessner's (1945) record of *B. moluccana* and *B. galoi* in the Kuabgen Group is mentioned above. *B. galoi* is associated there with *Malayomaorica malayomaorica* and *Retroceramus: B. moluccana* is present some 12 m below. This is the stratigraphic relationship of these taxa in the early Tithonian of Misool (Fig. 3) and in the Sula Islands (Challinor & Skwarko, 1982), but Glaessner's specimens are from the lower Imburu Mudstone (~20 m above base, G. Francis, GSPNG, personal communication, 1988) and are Oxfordian on stratigraphic evidence (Fig. 2).

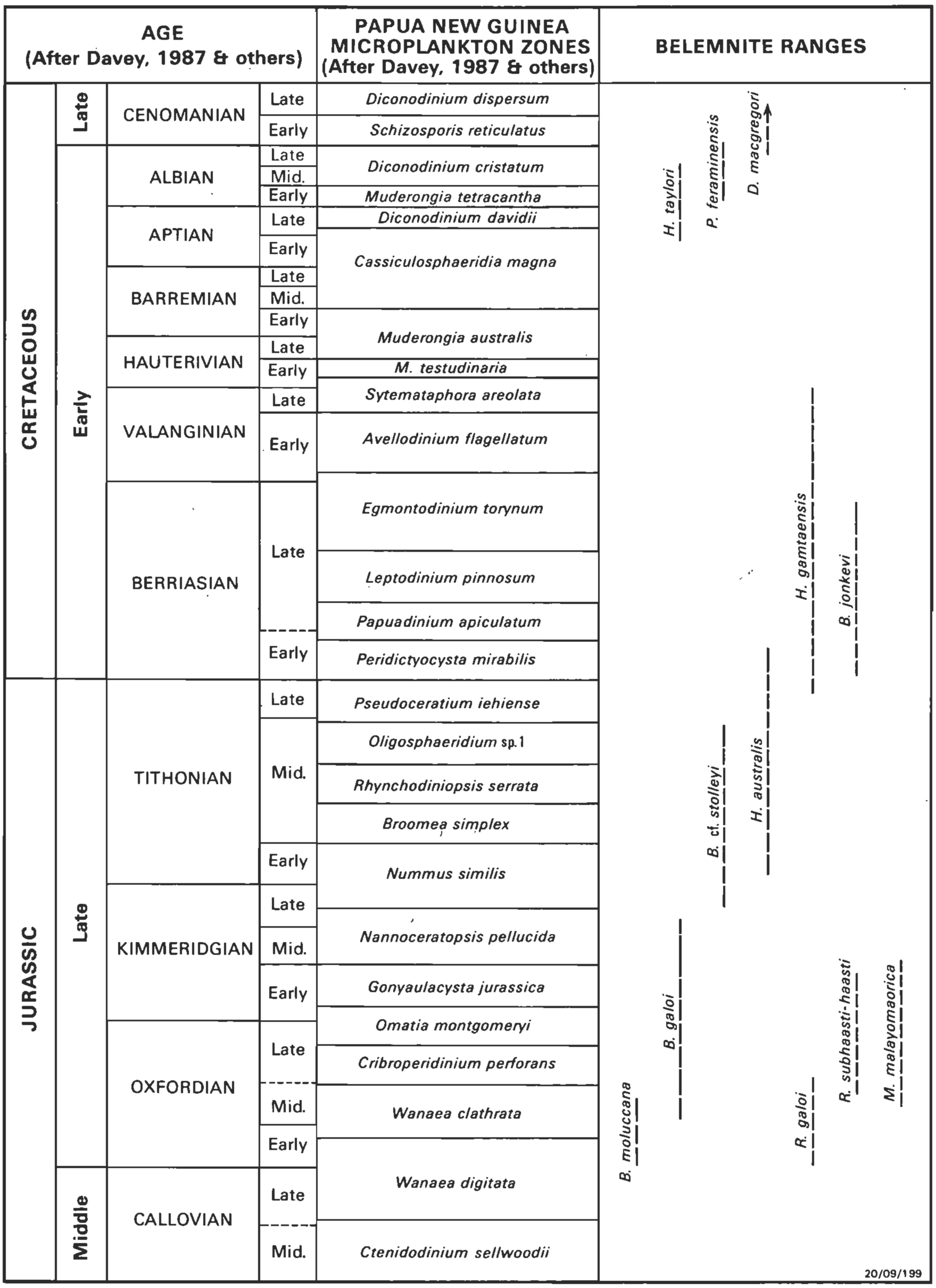

Figure 5. Papua New Guinea dinoflagellate zones of Davey (1987) & others, and apparent distribution of Belemnitida in that region.
Note possible concurrent range zone of *Belemnopsis moluccana* and *B. galoi*, and apparent age of concurrent range zone of *Retroceramus galoi, R. subhaasti-haasti* and *Malayomaorica malayomaorica* (cf. Fig. 3).

The few samples which contain both belemnites and dinoflagellates are: JKA 600, *Belemnopsis moluccana* and dinocysts of the *Wanaea clathrata* zone; JKA 616, *B. galoi* and *W. clathrata* zone; JKA 712 and 1267, *B. galoi* and *Cribroperidinium perforans* zone (dinoflagellate determinations by A. Welsh, BP Australia). Therefore, the transition from *B. moluccana* to *B. galoi* occurs within the *W. clathrata* zone and is early to mid-Oxfordian according to Davey (1987, fig. 3), late Oxfordian to early Kimmeridgian according to Helby & others (1987, fig. 12) and early Tithonian on macrofossil evidence. Note that the dinoflagellate zones of Davey (1987) and Helby & others (1987) are not identical in concept (Davey, 1987, pp. 4, 22).

Until the conflict between the dinoflagellate ages of Helby & others (1987) and Davey (1987) is resolved, and until unequivocal evidence for age of the relevant macrofossils is available, no precise time ranges for the belemnites can be stated. Meanwhile belemnite ages determined on macrofossil evidence are accepted here.

Distribution anomalies

Apart from the apparent concurrent range zone of *Belemnopsis moluccana* and *B. galoi*, other differences are present in the belemnite assemblage of Papua New Guinea when compared with that of eastern Indonesia.

Three species of *Duvalia* (?earliest Berriasian to ?mid-Hauterivian) are present in Misool where they are associated with both *Belemnopsis jonkeri* and *Hibolithes gamtaensis* (Challinor, in press). They are not present in the BMR Papua New Guinea collections, although there are poorly documented records of the genus earlier (de Verteuil & McWhae, 1948; Stevens, 1965). *Hibolithes miosensis* Challinor is also present in the mid-Hauterivian of Misool (Challinor, in press) but is not known from Papua New Guinea. *B. jonkeri, H. gamtaensis* and *H. miosensis* are all present in Irian Jaya (Challinor, in press) although *Duvalia* is apparently missing.

In Misool *B. jonkeri* is thought to range through the Berriasian and Valanginian with *H. gamtaensis* confined to the Hauterivian (Fig. 4). In Papua New Guinea however they both appear in the early Berriasian. *B. jonkeri* is confined to that stage and *H. gamtaensis* extends into the late Valanginian (Fig. 5). This conflict in apparent distributions may result from the different correlations used, but an incorrect assessment of ages and collection of *H. gamtaensis* from only part of its range in Misool are possible factors.

Eight belemnite species (in addition to *B. moluccana* and *Hibolithes* cf. *ingens*) representing five genera occur in the Callovian-Oxfordian of Misool. Most are abundant and all range through half a stage or more (Challinor, in press) but none are known from Papua New Guinea. If beds regarded as Callovian and Oxfordian in Misool and Papua New Guinea are time equivalent it is difficult to explain the absence of so many taxa, particularly when species common to both regions occur in older and younger beds. The Papua New Guinea Callovian–Tithonian belemnite succession resembles that of the Sula Islands where the rich Callovian–Oxfordian fauna of Misool is also apparently missing.

Differing belemnite assemblages may be due to several factors. Provincialism may be significant but geographic proximity argues against this, as does the presence of common taxa. Selective collecting from beds containing conspicuous macrofossil assemblages (e.g. the relatively high frequency of *Belemnopsis galoi* from the *Retroceramus–Malayomaorica* zone) may be important in Papua New Guinea. Several statements of other belemnite occurrence are present in the literature but the fossils are not present in the BMR collections studied, and it is possible they were not collected due to a presumption of no stratigraphic value. Collection failure for one reason or another seems a possibility.

Although belemnites are not thought to be strongly facies controlled elsewhere, this factor may be significant in Papua New Guinea. Belemnite occurrences appear to be more common in transgressive facies such as the lower Imburu Mudstone and Ieru Formation (G.Francis, GSPNG, personal communication, 1988). Regressive facies (Toro Sandstone, Koi-Iange Formation) may have been environmentally less suitable. The Koi-Iange Formation in particular is known to be marginal-marine to non-marine in part (White & others, 1973; Davey, 1987). A follow-up study to examine belemnite collections from Papua New Guinea held by organisations other than BMR is planned, and this may throw some light on what are poorly understood distribution problems.

Acknowledgements

I thank the following people and organisations for assistance during this work: The Executive Director, BMR (for loan of specimens), S.K. Skwarko (for suggesting this study), E. Truswell, H. Davies, M. Dickens and D. Strusz of the BMR, Prof. J. McCraw, Earth Sciences Department, University of Waikato (for laboratory facilities, preparation of photographs); BP Australia Ltd (for biostratigraphic data). I am particularly grateful to Peter Doyle, British Antarctic Survey, for critically reviewing the manuscript, and Geoff Francis, Geological Survey of Papua New Guinea, for reviewing the manuscript, and for continuing assistance throughout the study. One of the referees provided a particularly thoughtful and constructive criticism which greatly improved final presentation.

References

Arnold, G.O., Griffin, T.J., & Hodge, C.C., 1979 — Geology of the Ok Tedi and Southern Atbalmin 1:100 000 sheet. Part 2: Stratigraphy of sedimentary units. *Geological Survey of Papua New Guinea Report* 79/3.

Bain, J.H.C., Mackenzie, D.E., & Ryburn, R.J., 1975 — Geology of the Kubor Anticline, central highlands of Papua New Guinea. *Bureau of Mineral Resources, Australia, Bulletin* 155.

Banner, F.T., & others, 1961 — Geological results of petroleum exploration in Western Papua 1937-1961. *Journal of the Geological Society of Australia*, 8(1), 1-133.

Challinor, A.B., 1989a — Early Cretaceous Belemnites from the Central Birds Head, Irian Jaya, Indonesia. *Geological Research and Development Centre, Indonesia. Paleontology Series* No. 5, 1-21.

Challinor, A.B., 1989b — The succession of *Belemnopsis* in the Late Jurassic of eastern Indonesia. *Palaeontology*, 32(3), 571-596.

Challinor, A.B., in press — Jurassic and Cretaceous Belemnitida of Misool Archipelago, Irian Jaya, Indonesia. *Geological Research and Development Centre, Indonesia, Special Publication Series.*

Challinor, A.B., Doyle, P., Howlett, P.J., Nal'nyaeva, T.I., in press — Belemnitida. *In* Westermann, G.E.G., (editor), Jurassic of the Circum-Pacific. *Cambridge University Press, New York.*

Challinor, A.B., & Skwarko, S.K., 1982 — Jurassic belemnites from Sula Islands, Moluccas, Indonesia. *Geological Research and Development Centre, Indonesia. Paleontology Series* No. 3. 88 pp., 21 pl.

Davey, R.J., 1987 — Palynological zonation of the Callovian to Aptian in the northwestern Papuan Basin, Papua New Guinea. *Geological Survey of Papua New Guinea, Memoir* 13.

Davies, H.L., 1982 — Explanatory notes on the Mianmin Geological Sheet. International Index SB/54-3. *Geological Survey of Papua New Guinea.*

Davies, H.L., & Norvick, M., 1974 — Explanatory notes on the Blucher Range sheet. International Index SB/54-7. *Bureau of Mineral Resources, Australia.*

Davies, H.L., & Norvick, M., 1977 — Blucher Range stratigraphic nomenclature. *Geological Survey of Papua New Guinea, Report* 77/14.

de Verteuil, J.P., & McWhae, R., 1948 — Report on the geology of the southern flank of the Kereru Range. *Australian Petroleum Company Report, Appendix I* (unpublished).

Dow, D.B., & Dekker, F.E., 1964 — Geology of the Bismarck Mountains, New Guinea. *Bureau of Mineral Resources, Australia, Report* 76.

Dow, D.B., Smit, J.A.J., & Ryburn, R.J., 1972 — Geology of the south Sepik region, New Guinea. *Bureau of Mineral Resources, Australia, Bulletin* 133.

Doyle, P., 1985 — 'Indian' belemnites from the Albian (Lower Cretaceous) of James Ross Island, Antarctica. *British Antarctic Survey, Bulletin* 69, 22–34.

Edwards, A.B., 1950 — The petrology of the Cretaceous greywackes of the Purari Valley, Papua. *Proceedings of the Royal Society of Victoria*, 60, 163–71.

Edwards, A.B., & Glaessner, M.F., 1953 — Mesozoic and Tertiary sediments from the Wahgi Valley, New Guinea. *Proceedings of the Royal Society of Victoria*, 64, 93–112.

Francis, G., 1986 — Some current problems of Mesozoic geology in the Papuan Basin. *Geological Survey of Papua New Guinea, Technical Note* TN 4/86.

Francis, G., 1988 — Problems with Toro Sandstone correlations in the Ok Tedi 1:250 000 sheet area. *Geological Survey of Papua New Guinea, Technical Note* TN 14/88.

Francis, G., & Deibert, D.H., 1988 - Petroleum potential of the northern New Guinea Basin and associated infrabasins. *Geological Survey of New Guinea, Report* 88/37.

Glaessner, M.F., 1945 — Mesozoic fossils from the central highlands of New Guinea. *Proceedings of the Royal Society of Victoria*, 56, 151–68.

Haig, D.W., 1981 — Mid Cretaceous foraminiferids from the Wahgi Valley, central highlands of Papua New Guinea. *Micropaleontology* 27(4), 337–351.

Haig, D.W., Humphreys, G.S., Rogerson, R., & Francis, G., 1986 — Field Guide to the Kubor anticline, central highlands. *12th International Sedimentological Congress, 1986, Canberra.*

Harland, W.B., Cox, A.V., Llewellyn, P.G., Pickton, C.A.G., Smith, A.G., & Walters, R., 1982 — A geologic time scale. *Cambridge University Press, Cambridge.*

Helby, R., Morgan, R., & Partridge, A.D., 1987 — A palynological zonation of the Australian Mesozoic. *Memoir of the Association of Australasian Palaeontologists*, 4, 1–94.

Helby, R., Wilson, G.J., & Grant-Mackie, J.A., 1988 — A preliminary biostratigraphic study of Middle to Late Jurassic dinoflagellate assemblages from Kawhia, New Zealand. *Memoir of the Association of Australasian Palaeontologists*, 5, 125–166.

Jeletzky, J.A., 1966 — Comparative morphology, phylogeny and classification of fossil Coleoidea. Mollusca, Article 7. *Paleontological Contributions, University of Kansas*, 162 pp., 25 pl.

Kruizinga, P., 1920 — Dei Belemniten uit de Jurassische afzettingen van de Soela-Eilanden. *Jaarboek van het Mijnwezen in Nederlandsch Oost-Indie* 49(2), 161–89, pl. 6.

Li, Xiaochi, & Grant-Mackie, J.A., 1988 — Upper Jurassic and Lower Cretaceous *Buchia* (Bivalvia) from Southern Tibet and some wider considerations. *Alcheringa* 12, 249–268.

Mutterlose, J., 1986 — Upper Jurassic belemnites from Orville Coast, Western Antarctica, and their paleobiogeographical significance. *British Antarctic Survey, Bulletin* 70, 1–22.

Mutterlose, J., 1988 — Migration and evolution patterns in Upper Jurassic and Lower Cretaceous belemnites. *In* Wiedman, J., & Kullman, J., (editors), Cephalopods — present and past. *Schweizerbart'sche Verlagsbuchhandlung, Stuttgart*, pp. 525–537.

Norvick, M., 1973 — Results of palaeontological work, Blucher Range 1:250 000 sheet area, Papua New Guinea. *Bureau of Mineral Resources, Australia, Record* 1973/101.

Pigram, C.J., Challinor, A.B., Hasibuan, F., Rusmana, E., & Hartono, U., 1982 — Geological results of the 1981 expedition to Misool Archipelago, Irian Jaya. *Geological Research and Development Centre, Indonesia, Bulletin* 6.

Rogerson, R.J., Hilyard, D., Finlayson, E.J., Holland, D.S., Nion, S.J.S., Sumaiang, R.S., Dagaman, J., & Loxton, C., in press — The geology and mineral resources of the Sepik headwaters region, Papua New Guinea. *Geological Survey of Papua New Guinea, Memoir* 12.

Sato, T., Westermann, G.E.G., Skwarko, S.K., & Hasibuan, F., 1978 — Jurassic biostratigraphy of the Sula Islands, Indonesia. *Geological Survey of Indonesia, Bulletin* 4(1), 1–28.

Stevens, G.R., 1963 — The systematic status of Oppel's specimens of *Belemnopsis gerardi*. *Palaeontology* 6(4), 690–698.

Stevens, G.R., 1965 — The Jurassic and Cretaceous belemnites of New Zealand and a review of the Jurassic and Cretaceous belemnites of the Indo-Pacific region. *New Zealand Geological Survey Paleontological Bulletin* 36, 1–283, 25 pl.

Stevens, G.R., 1973 — Cretaceous belemnites. *In* Hallam, A., (editor), Atlas of palaeobiogeography. *Elsevier Scientific Publishing Co., Amsterdam*, pp. 259–274.

Stolley, E., 1929 — Uber Ostindische Jura-Belemniten. *Palaeontology of Timor* 16(29), 91–213, 9 pl.

Stolley, E., 1935 — Zur Kenntnis des Jura und der Unterkreide von Misool. Palaontologischer Teil. *Neues Jahrbuch fur Mineralogie, Geologie und Palaontologie* 73, 42–69.

Westermann, G.E.G., & Callomon, J., 1988 — The Macrocephalitinae and associated Bathonian and Early Callovian (Jurassic) ammonoids of Sula Islands and New Guinea. *Palaeontographica A*, 203, 1–90.

White, M.F., Boxall, A.M., Findlay, A.L., Sweetman, I.A.D., & Visser, B., 1973 — Report on the Fly–Palmer Geological Survey. *Australian Petroleum Company Pty. Ltd, Report* 4/W/15 (unpublished).

Willey, L.E., 1973 — Belemnites from south-eastern Alexander Island. 2: The occurrence of the family Belemnopseidae in the Upper Jurassic and Lower Cretaceous. *British Antarctic Survey, Bulletin* 36, 33–59.

Appendix 1. Collections studied.

Map index	*Locality*	*Sample*	*Taxon*	*Age adopted here*	*Unit*
SB/54-7	5	7152-1355	*Hibolithes gamtaensis* n. sp.		
		1352	*Hibolithes* cf. *gamtaensis*	Berriasian–Valanginian	Feing Group
		4102	*Hibolithes* sp.		
		1055	*Belemnopsis* sp.		
	11	522	*Belemnopsis galoi* (Boehm)	early Tithonian	Maril
		4098	*Belemnopsis galoi*		
	15	4307	*Conodicoelites kalepuensis* Challinor	Bathonian	Maril
	16	603	*Conodicoelites kalepuensis*		
		619	*Conodicoelites kalepuensis*	Bathonian	Maril
		618	*Conodicoelites* cf. *kalepuensis*		
	19	5216	*Belemnopsis galoi*	early Tithonian	Maril
	22	360	*Conodicoelites kalepuensis*	Bathonian	Maril
	42	1220	*Hibolithes taylori* n. sp.		
		1221	*Hibolithes taylori*		
		1223	*Hibolithes taylori*	Aptian–Albian	Omati

Map index	*Locality*	*Sample*	*Taxon*	*Age adopted here*	*Unit*
	42	1230	*Hibolithes taylori*		
		1229	*Hibolithes* cf. *taylori*		
	46	3462	*Hibolithes taylori*		
		3465	*Hibolithes taylori*	Aptian–Albian	Omati
		3471	*Hibolithes taylori*		
	57	657	*Hibolithes taylori*	Aptian–Albian	Ieru
	70	4001	*Belemnopsis galoi*		
		4001	*Belemnopsis* cf. *galoi*		
		4007	*Belemnopsis* cf. *galoi*	early Tithonian	Maril
		4009	*Belemnopsis* cf. *galoi*		
		4001	*Hibolithes* juv.		
		4004	*Hibolithes* juv.		
	71	910	*Belemnopsis* cf. *stolleyi* Stevens		
		912	*Belemnopsis* cf. *stolleyi*		
		914	*Belemnopsis* cf. *stolleyi*		
		918	*Belemnopsis* cf. *stolleyi*		
		919[1]	*Belemnopsis* cf. *stolleyi*		
		2076	*Belemnopsis* cf. *stolleyi*	late Tithonian	Maril
		2082	*Belemnopsis* cf. *stolleyi*		
		2078	*Belemnopsis* cf. *mangolensis* Challinor		
		912	*Hibolithes australis* n. sp.		
		918	*Hibolithes* cf. *australis*		
		2078	*Hibolithes* cf. *australis*		
		914	*Hibolithes* sp.		
SB/54-7	82	7152-129	*Hibolithes taylori*	Aptian–Albian	Ieru
	83	763	*Belemnopsis* cf. *moluccana* (Boehm)	Oxfordian–Kimmeridgian	Ieru
	106	4048	*Conodicoelites kalepuensis*		
		4049	*Conodicoelites kalepuensis*		
		4050	*Conodicoelites kalepuensis*	Bathonian	Maril
		4051	*Conodicoelites kalepuensis*		
	107	491	*Belemnopsis* cf. *galoi*	early Tithonian	Maril
	120	1239	*Hibolithes taylori*	Aptian–Albian	Ieru
	136	1204	*Hibolithes taylori*	Aptian–Albian	Omati
	Near 137	1057[2]	*Parahibolites feraminensis* n. sp.	Albian	Ieru
	147	1283	*Belemnopsis* cf. *jonkeri* Stolley	Berriasian–Valanginian	Ieru
	148	1284	*Hibolithes* sp.		
		4069	*Hibolithes* sp.	?	?
	187	7152-4016	*Hibolithes gamtaensis*		
		4019	*Hibolithes gamtaensis*		
		4020	*Hibolithes gamtaensis*		
		4021	*Hibolithes gamtaensis*	Berriasian–Valanginian	Ieru
		1163	*Hibolithes* sp.		
		4015	*Belemnopsis jonkeri* Stolley		
		4018	*Belemnopsis jonkeri*		
		4017	*Belemnopsis* cf. *jonkeri*		
		4037	*Hibolithes* sp. I		
SB/54-3	12	P 5003	*Belemnopsis galoi*	early Tithonian	Maril
	14	P 5006	*Belemnopsis* cf. *galoi*	early Tithonian	Maril
SB/54-7/5		JKA 137	*Belemnopsis galoi*	early Tithonian	Imburu
			Belemnopsis cf. *galoi*		
			Hibolithes sp.		
		JKA 146	*Hibolithes taylori*	Aptian–Albian	Omati
		JKA 583	*Belemnopsis galoi*	early Tithonian	Imburu
SB/54-7/2		JKA 384	*Hibolithes taylori*	Aptian–Albian	Omati
		JKA 453	*Belemnopsis jonkeri*	Berriasian	Toro
			Hibolithes gamtaensis		
		JKA 600	*Belemnopsis moluccana*	Oxfordian–Kimmeridgian	Imburu
SB/54-7/2		JKA 1267	*Belemnopsis galoi*	early Tithonian	Imburu
SB/54-7/6		JKA 616	*Belemnopsis galoi*	early Tithonian	Imburu
SB/54-7/5		JKA 963	*Belemnopsis galoi*	early Tithonian	Imburu
SB/54-7/2		JKA 712	*Belemnopsis galoi*	early Tithonian	?Imburu
7187/7188	24	P 5014*	*Belemnopsis moluccana*	Oxfordian–Kimmeridgian	Maril
	25	P 5008	*Belemnopsis moluccana*	Oxfordian–Kimmeridgian	Maril
	26	P 5009*	*Hibolithes taylori*	Albian	Chim
			Parahibolites feraminensis		
	29	P 5003*	*Belemnopsis jonkeri*	Berriasian–Valanginian	?

Map index	*Locality*	*Sample*	*Taxon*	*Age adopted here*	*Unit*
	29	P 5002*	*Parahibolites feraminensis* *Hibolithes taylori*	Albian	Chim
	29	P 5004	*Hibolithes taylori*	Albian	Chim
SB/55-5		20NG 2635	cf. *Hibolithes ingens*	?Callovian–early Oxfordian	?Maril
SB/55-13		KAB 69	*Hibolithes australis*	late Tithonian–early Berriasian	Tubu
7885		HGF 25	*Dimitobelus macgregori*	Albian-Cenomanian	Chim

[1] 919 This collection is apparently derived from two distinct stratigraphic horizons indicating late Tithonian and Albian ages. It contains
Parahibolithes feraminensis (Albian)
Belemnopsis cf. *stolleyi* } (late Tithonian)
Hibolithes australis }
The matrix associated with the specimen of *Parahibolites* differs from that of the other specimens and their preservation is different.

[2] 1057 A mixed collection containing
Parahibolites feraminensis (Albian)
Belemnopsis cf. *galoi* (early Tithonian)
Differences in matrix and preservation similar to those of sample 919 are present.

* Float collections.

Appendix 2. Systematic descriptions.

Terminology and study techniques are detailed elsewhere (Challinor & Skwarko, 1982) and broadly follow Stevens (1965). The classification of Belemnitida follows Jeletzky (1966).

Order **Belemnitida** Zittel 1895
Suborder **Belemnopseina** Jeletzky 1965
Family **Belemnopseidae** Naef 1922
Genus ***Conodicoelites*** Stevens 1964

Type species. *Dicoelites keeuwensis* Boehm 1912

Conodicoelites kalepuensis Challinor
Figures 6, 7a–i

1982 *Conodicoelites kalepuensis*; Challinor & Skwarko, Pl. 3, Pl. 4.

Localities and material. Approximately 15 specimens from localities 15, 16, 22, 106 (sheet SB/54-7).
Note: Conodicoelites kalepuensis was described originally from Wai Kalepu, Taliabu, Sula Islands (Challinor & Skwarko, 1982) on limited material. The collections studied here allow a slightly emended description and these comments should be read in conjunction with the earlier description.

Age. Bathonian.

Description. Guard conical, elongate, moderately robust. Estimated maximum total length ~180 mm; observed maximum length 150 mm. Postalveolar length 70–100 mm. Ratio of postalveolar length to maximum diameter 4–4.5 in mature guards; 5–6 in less fully developed specimens.

Outline elongate, conical and symmetrical (Fig. 7a,d,g). Maximum transverse diameter at extreme anterior. Anterior two-thirds of guard weakly conical; sides converge apically at 5–7.5°. Posterior region more obtusely conical; sides converge at about 11–15°. Apex acute. Profile asymmetric, conical (Fig. 7c,f). Dorsal and ventral surfaces converge apically in a similar manner and at a similar rate to flanks. Ventral surface slightly inflated in mid-apical region; apex slightly dorsally placed.

Cross-sections (Figs 6, 7h,i) usually slightly compressed anteriorly, sometimes slightly depressed; either slightly compressed to slightly depressed posteriorly. Median ventral groove narrow, shallow, V-shaped in profile, extends from anterior break almost to guard apex (Fig. 7g). Dorsal groove subequal in development (perhaps slightly narrower and shallower) terminating about 30–40 mm from apex.

Lateral lines are visible on only one fragment; double, poorly defined, situated ventro-laterally at a point about 50 mm from apex. All specimens have damaged surfaces and any weakly defined lateral lines are unlikely to have been preserved. They cannot be seen in transverse sections. Internal features as described in Challinor & Skwarko (1982). Splitting surfaces probably extend further towards apex than illustrated by them, and are visible in transverse section at a point about 50 mm from apex in one specimen.

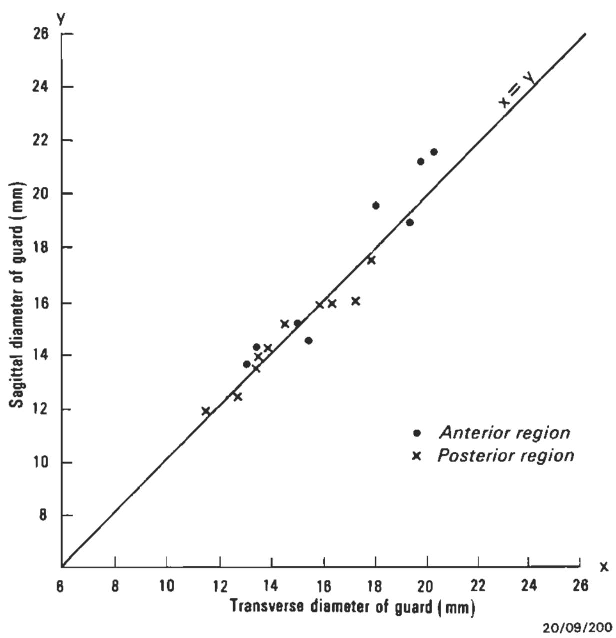

Figure 6. Relationship between guard diameters in *Conodicoelites kalepuensis*.

Figure 7.
Magnification ×1 unless otherwise stated.
a–c, *Conodicoelites kalepuensis* Challinor, CPC 27687, Locality 106, Lagaip River-Ok Om Junction, sheet SB/54-7. a, ventral view; b, dorsal view; c, left lateral view (ventral surface facing left). Specimen partially coated with concretionary matrix. **d–f**, *Conodicoelites kalepuensis* Challinor, CPC 27688, Locality 106, Lagaip River-Ok Om Junction, sheet SB/54-7. d, ventral view; e, dorsal view; f, left lateral view. Specimen partially coated with concretionary matrix; P, approximate position of protoconch. **g**, *Conodicoelites kalepuensis* Challinor, CPC 27689, Locality 22, tributary to Ok Om, sheet SB/54-7. Ventral view. Specimen sheared and metamorphosed, illustrating ventral groove. **h**, *Conodicoelites kalepuensis* Challinor, CPC 27690, ×3, Locality 16, Abum Stream, sheet SB/54-7. Transverse section 60 mm from apex. Dorsal and ventral splitting surfaces visible. Specimen from metamorphic zone of Maril Formation. **i**, *Conodicoelites kalepuensis* Challinor, CPC 27691, ×3, Locality 16, Abum Stream, sheet SB/54-7. Transverse section near apex. **j, k**, *Hibolithes australis* n. sp., CPC 27692, Locality KAB 69, Kereru Range, sheet SB/55-13. j, ventral view; k, right lateral view. Ventro-lateral surface of apical region eroded. P, approximate position of protoconch. **l, m**, *Hibolithes australis* n. sp., IMC 763, Locality 1 D, Wai Kronci, Taliabu, Sula Islands. l, ventral view; m, left lateral view. Immature specimen. P, approximate position of protoconch.

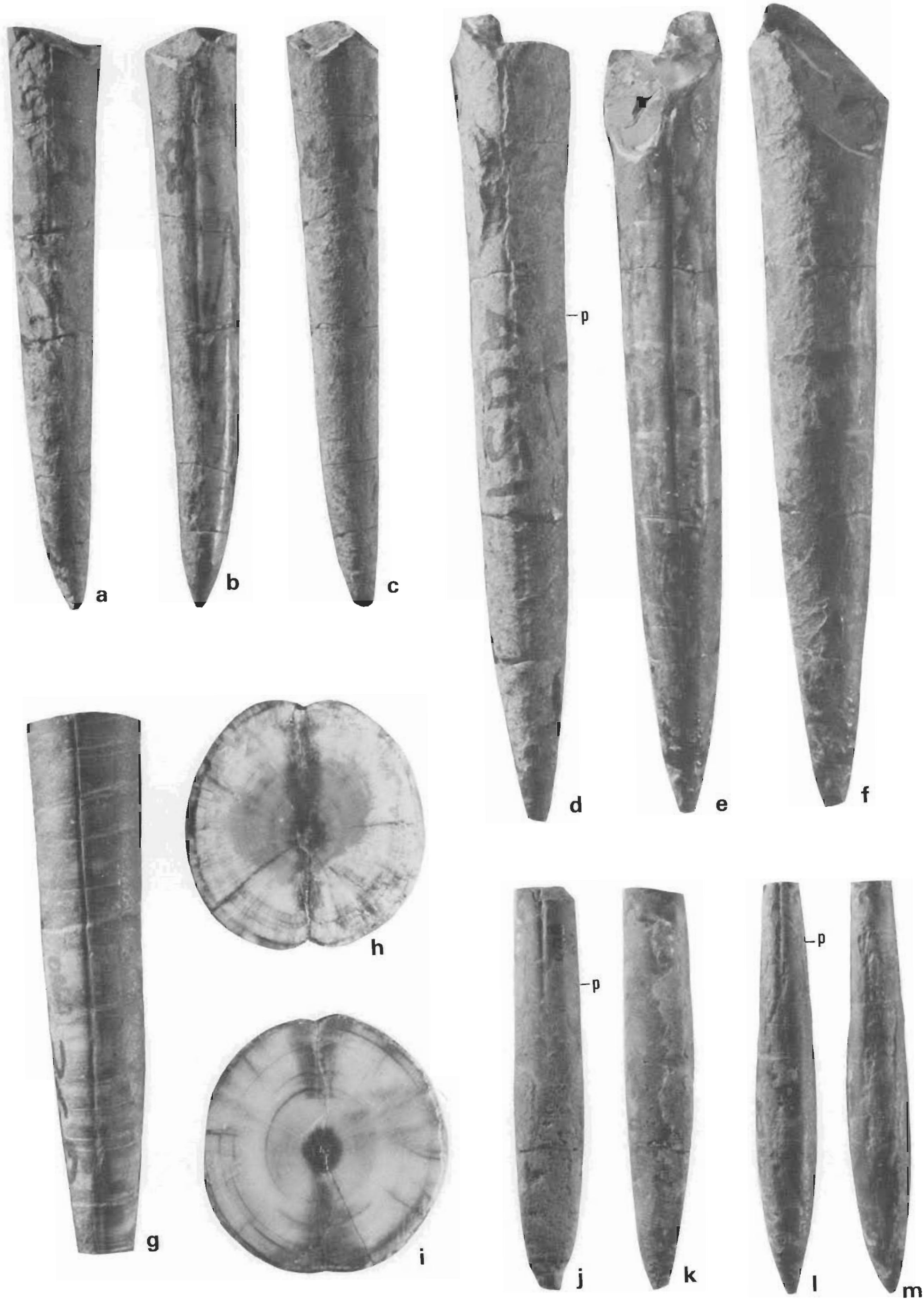
a
b
c
p
d
e
f
g
h
i
p
j
k
p
l
m

Relationship to *Conodicoelites keeuwensis* (Boehm) has not been elucidated (see Challinor & Skwarko, 1982) even though numerous specimens are available for this study. Only one specimen approaches the short conical form of *keeuwensis* but this fragment is barely 33 mm long and is probably the mid-apical region of a very large *kalepuensis*.

The Early Callovian age for *C. kalepuensis* in Sula Islands (Challinor & Skwarko, 1982) has now been revised to mid-Bathonian after re-examination of associated *Macrocephalites* and other ammonites (Westermann & Callomon, 1988). The taxon is not known from beds dated as early Callovian in Misool Archipelago (Challinor, in press) and no pre-Callovian belemnites are known from that region. The Sula Islands record may not represent the first appearance of the taxon and an unrestricted Bathonian age is proposed.

Genus *Hibolithes* Montfort 1808

Type species. *Hibolithes hastatus* Montfort

Hibolithes australis n. sp.
Figures 7j–m, 8, 9a–i

1982 *Hibolithes* sp. A Challinor & Skwarko, Pl. 8, figs 7, 8.
1982 *Hibolithes* sp. B Challinor & Skwarko, Pl. 8, figs 9, 10.

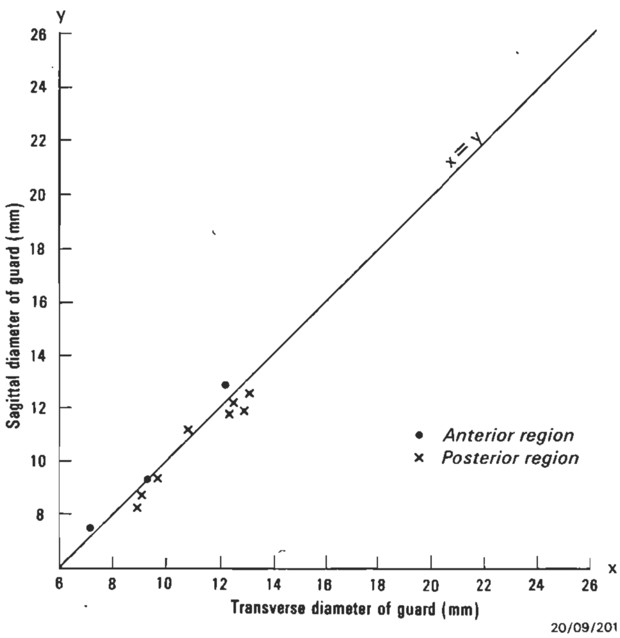

Figure 8. Relationship between guard diameters in *Hibolithes australis* n. sp.

Localities and material. 14 specimens from localities 71 (sheet SB/54-7) Papua New Guinea; KAB 69, Tubu Unit, Kereru Range, Papua New Guinea (sheet SB/55-13): ID, 8G, 81, Sula Islands (Sato & others, 1978); 81CP74, 91C, 93, 81R, 76M, Misool Archipelago (Challinor, in press).

Age and stratigraphic horizon. *Hibolithes australis* occurs in the Tubu Unit and Maril Formation in Papua New Guinea, in an unnamed 'marly claystone with concretions' in Sula Islands (Sato & others, 1978) and in the upper Lelinta Shale and basal Gamta Limestone in Misool Archipelago (Challinor, in press). It is of Late Tithonian-earliest Berriasian age.

Brief description. This description is based mostly on poorly preserved fragments. A few specimens are almost complete but most have surface damage. The largest guards are moderately elongate and slightly hastate (Figs 7j,k, 9c,d). Postalveolar length is about five times maximum diameter; total length estimated at 6–7 times maximum diameter.

Outline symmetrical and slightly hastate. Widest point near midpoint, apex moderately elongate; flanks converge slightly towards anterior (maximum diameter of largest specimen, Fig. 7j,k, 13.1 mm; diameter at anterior break 11.6 mm). Profile asymmetric, less hastate than outline. Ventral surface slightly inflated in apical region, apex slightly dorsally placed.

Cross-sections almost circular, slightly depressed in apical half of guard, very slightly compressed anteriorly (Figs 8, 9e,h,i). Flanks, dorsal and ventral surfaces regularly rounded. Median ventral alveolar groove shallow, moderately narrow, well defined only in alveolar region, extends onto postalveolar guard as a shallow depression; terminates well before midpoint.

Lateral lines not seen in most specimens due to poor preservation; one better preserved guard bears two well defined closely spaced lines near the midline of the apical region; they deflect ventrally at the estimated midpoint.

Apical line centrally or slightly ventrally placed. Growth lines numerous, closely spaced, usually no systematic division into major growth stages although a juvenile stage about half the diameter of the adult is sometimes clearly defined. No information on protoconch, phragmocone or alveolus available.

Ontogeny. Juvenile and immature guard much more hastate than adult (Figs 7 l,m, 9a,b). Widest point located near midguard. In late ontogeny anterior half of the guard apparently increases in diameter more rapidly than posterior half, markedly reducing hastation in the adult.

Discussion. The taxon has been recorded from eastern Indonesia as well as Papua New Guinea but all adult Indonesian specimens are fragments. The single specimen from the Tubu Unit, Papua New Guinea (Fig. 7j,k), although abraded posteriorly, is the most nearly complete adult specimen known.

H. australis may have affinities with *Hibolithes brevis* (Stolley, 1929) but this is uncertain because all Stolley's specimens are poorly preserved fragments (as are all *H. australis* from Misool and Papua New Guinea and most from Sula). Stolley's specimens were collected from Timor (locality details unknown) and their age cannot be more closely defined than Late Jurassic. *Hibolithes* sp. B is a near adult *H. australis* and *Hibolithes* sp. A an immature guard (Challinor & Skwarko, 1982).

Because *Hibolithes australis* has been described from mostly fragmentary specimens from widely separated localities, the possibility that it is a composite taxon cannot be entirely eliminated. However, the morphology of all specimens is consistent with specific identity as is the age information available.

Etymology. *Hibolithes australis* — southern *Hibolithes*.

Figure 9.
Magnification X1 unless otherwise stated.
a, b, *Hibolithes australis* n. sp., IMC 331, Locality 8 G, Minaluli, Mangole, Sula Islands. a, ventral view; b, left lateral view. Immature specimen. **c–e**, *Hibolithes australis* n. sp., IMC 764, Locality 81CP74, Misool Archipelago. c, ventral view; d, left lateral view; e, transverse section just posterior to protoconch, X3. **f–h**, *Hibolithes australis* n. sp., IMC 765, Locality 8 I, Minaluli, Mangole, Sula Islands. f, ventral view; g, left lateral view; h, transverse section at anterior end of specimen, X3. **i**, *Hibolithes australis* n. sp., IMC 766, Locality 81CP74, Misool Archipelago. Transverse section at midguard, X3. **j, k**, *Hibolithes gamtaensis* n. sp., CPC 27693, Locality 187, Strickland River, sheet SB/54-7. j, ventral view; k, left lateral view. P, approximate position of protoconch. **l**, *Hibolithes gamtaensis* n. sp., CPC 27694, Locality 187, Strickland River, sheet SB/54-7. Transverse section in posterior half of guard, X3. **m, n**, *Hibolithes* sp. 1, CPC 27709, Locality 187, Strickland River, sheet SB/54-7. m, ventral view; n, left lateral view. **o**, *Hibolithes taylori* n. sp., CPC 27695, Locality 29, Dagiam River, sheet 7187/7188. Ventral view. P, approximate position of protoconch. **p**, *Hibolithes taylori* n. sp., CPC 27696, Locality 29, Dagiam River, sheet 7187/7188. Ventral view. Juvenile specimen coated with concretionary matrix. *Note*: Scale X1.3, differs from that of other specimens illustrated. **q**, *Hibolithes taylori* n. sp., CPC 27697, Locality 42, Ok Tedi, sheet SB/54-7. Transverse section in apical region, X3. **r, s**, *Hibolithes taylori* n. sp., CPC 27698, Locality 29, Dagiam River, sheet 7187/7188. r, ventral view; s, left lateral view. P, approximate position of protoconch; T, posterior termination of ventral groove. Specimen coated with concretionary matrix.

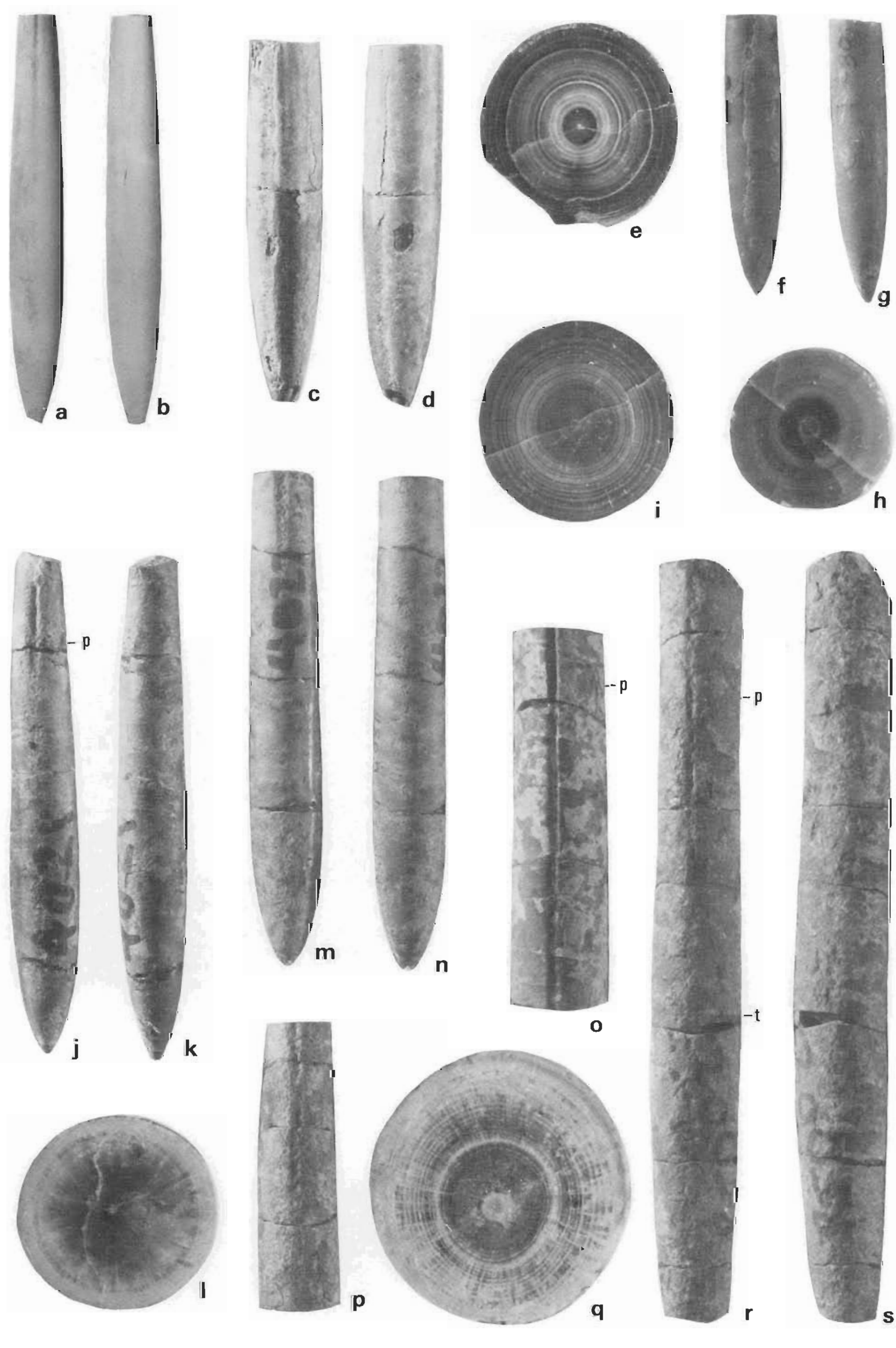
a
b
c
d
e
f
g
i
h
p
j
k
m
n
o
r
s
t
l
q

Hibolithes gamtaensis n. sp.
Figure 9j–l

1935 *Hibolithes subfusiformis* Raspail; Stolley Pl. 5, figs 7, 8: *non* fig. 6.
1989a *Hibolithes miosensis* Challinor *partim*. Pl. 2, figs 13–15, 24, 26 only; Pl. 5, figs 12, 13 only.
in press *Hibolithes gamtaensis* Challinor Pl. 14, figs 1–22.

Localities and material. Approximately 10 specimens from localities 5 and 187 (sheet SB/54-7) and collection JKA 453 (sheet SB/54-7/2).

Age and stratigraphic horizon. *Hibolithes gamtaensis* occurs in the Toro Sandstone and basal Ieru Formation in the central highlands of Papua New Guinea, in the Kembelangen group on the Mios and Ainim Rivers in the central Birds Head of Irian Jaya, and in the lower Facet Limestone (Gamta Member) of the Misool Archipelago. It is Neocomian (provisionally Berriasian–Valanginian) in age in Papua New Guinea.

Note. This brief description is published to validate the taxon for the purposes of this paper. A full description based on abundant material from the Misool Archipelago, Irian Jaya, will be published elsewhere (Challinor, in press).

Brief description. Guard slender and elongate, usually moderately hastate. Total length of a typical adult is ~80–90 mm. Widest point usually situated in posterior half of guard. Guard tapers steadily towards anterior; occasional specimens are only slightly hastate. Profile less hastate than outline. Dorsal surface often slightly more inflated near apex than ventral surface, apex then slightly dorsally placed. Cross-sections usually slightly depressed throughout (A value* 101–108 posteriorly, 99–107 anteriorly). Flanks, dorsal and ventral surfaces regularly rounded.

Median ventral groove narrow, shallow, usually confined to alveolar and immediately postalveolar region, extending a little further adapically in some adults. Double lateral lines present on most well preserved specimens. They are situated at about the guard midline throughout their length, are well defined, narrow, sharply incised and close together in the apical half of the guard, less well defined and a little further apart in the oral half. Apical line approximately centrally placed. Growth lines numerous, closely spaced, major growth stages not regularly defined. A splitting surface is present beneath the ventral groove.

Etymology. *Hibolithes gamtaensis* is named from the Gamta Islands, Misool, Indonesia.

Hibolithes taylori n. sp.
Figures 9 o–s, 10, 11a–e, 12

Localities and material. Approximately 20 specimens from localities 26 and 29 (sheets 7187/7188): 42, 46, 57, 82, 136 (sheet SB54-7) and Samples JKA 384 (sheet SB/54-7/2) and 146 (sheet SB/54-7/5).

Age and stratigraphic horizon. *Hibolithes taylori* occurs in the Ieru and Chim Formations and is of Aptian–Albian age.

$$*A = \frac{\text{Transverse diameter (mm)}}{\text{Sagittal diameter (mm)}} \times 100$$

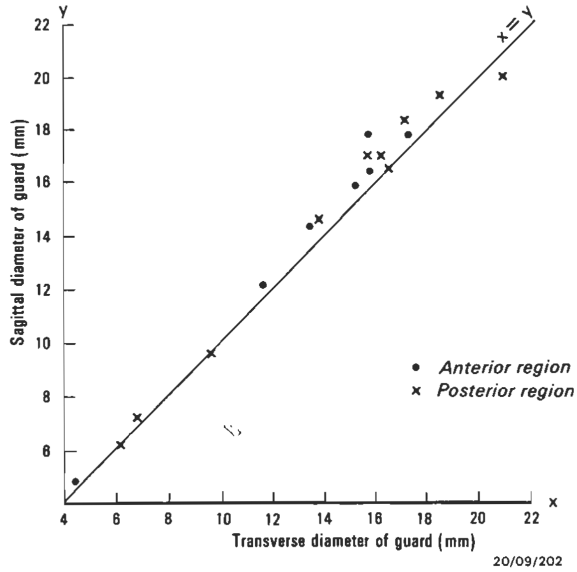

Figure 10. Relationship between guard diameters in *Hibolithes taylori* n. sp.

Diagnosis. Guard large, elongate, relatively slender, hastate, compressed in cross-section, ventral groove extends about midway along guard.

Description. *External features.* Guard large, elongate and relatively slender; length about 8–10 times maximum diameter. Largest almost complete specimen available ~150 mm in length, 16.5 mm in maximum diameter (Fig. 9r,s). Fragments over 20 mm in diameter observed.

Outline symmetrical and hastate (Fig. 9r). Widest point located about midway along guard. Sides at first converge gradually towards apex, more rapidly over terminal 30–40 mm; apical region moderately acute. Sides converge steadily anteriorly to produce moderate transverse hastation; observed differences between maximum and minimum diameters of between 1.6 and 3.0 mm. Profile asymmetrical and hastate. Deepest point located about midway along guard (Figs 9s, 11b). Dorsal surface almost straight, converges gradually towards midline anteriorly, remains almost parallel to midline posteriorly, converges rapidly towards apex over terminal 20–30 mm. Ventral surface inflated near midguard, converges anteriorly to produce moderate sagittal hastation; converges towards apex gradually over terminal 40–60 mm, more rapidly near apex. Ventral inflation and differing position and rates of apical curvature of dorsal and ventral faces produce marked asymmetry of profile.

Cross-sections slightly to moderately compressed (A = ~95), slightly more so anteriorly (Figs 10, 11c,d). A few specimens are approximately equidimensional posteriorly (Fig. 11e). Cross-section regularly oval in posterior regions; widest point situated about midway between dorsal and ventral surfaces; flanks, dorsal and ventral surfaces regularly rounded. Cross-section slightly ovoid anteriorly (Fig. 11c,d), widest point situated nearer a wider rounded dorsal face, ventro-lateral flanks flattened, converging towards a relatively narrow ventral face.

Figure 11.
Magnification ×1 unless otherwise stated.
a, b, *Hibolithes taylori* n. sp., CPC 27699, Locality 26, Dagiam River, sheet 7187/7188. a, ventral view; b, left lateral view. **c**, *Hibolithes taylori* n. sp., CPC 27700, Locality 42, Ok Tedi, sheet SB/54-7. Transverse section near protoconch, ×3. **d**, *Hibolithes taylori* n. sp., CPC 27701, Locality 120, Hindenberg Wall, sheet SB/54-7. Transverse section in anterior region of guard, ×3. **e**. *Hibolithes taylori* n. sp., CPC 27702, Collection JKA 384, sheet SB/54-7/2. Transverse section in apical region ×3. **f, g**. *Parahibolites feraminensis* n. sp., CPC 27703, Locality 29, Dagiam River, sheet 7187/7188. f, ventral view; g, left lateral view. P, approximate position of protoconch. T, posterior termination of ventral groove. **h–j**. *Parahibolites feraminensis* n. sp., CPC 27704, Collection 1057 unlocalised, near Feramin Village, sheet SB/54-7. h, ventral view; i, left lateral view; j, view of alveolar end, ×3. P, approximate position of protoconch; T, termination of ventral groove. **k, l**, *Parahibolites feramensis* n. sp., CPC 27705, Collection 1057 unlocalised, near Feramin Village, sheet SB/54-7. k, ventral view; l, left lateral view. P, approximate position of protoconch. **m–o**. *Parahibolites feraminensis* n. sp., CPC 27706, Collection 1057 unlocalised, near Feramin Village, sheet Sb/54-7. m, left lateral view; n, ventral view; o, transverse section near protoconch, ×3. Note pronounced lateral flattening of growth lines. **p, q**. *Parahibolites feraminensis* n. sp., CPC 27707, Collection 919, locality 71, Anamen Creek, sheet SB/54-7. p, alveolar view; q, transverse section at guard anterior, ×3. Guard fragment is 32 mm long. Note flattened growth lines on q. *Note*: Locality details uncertain (see above). **r**. *Parahibolites feraminensis* n. sp., CPC 27708, Collection 1057, unlocalised, near Feramin Village, sheet SB/54-7. Left lateral view of apical fragment illustrating apical asymmetry.

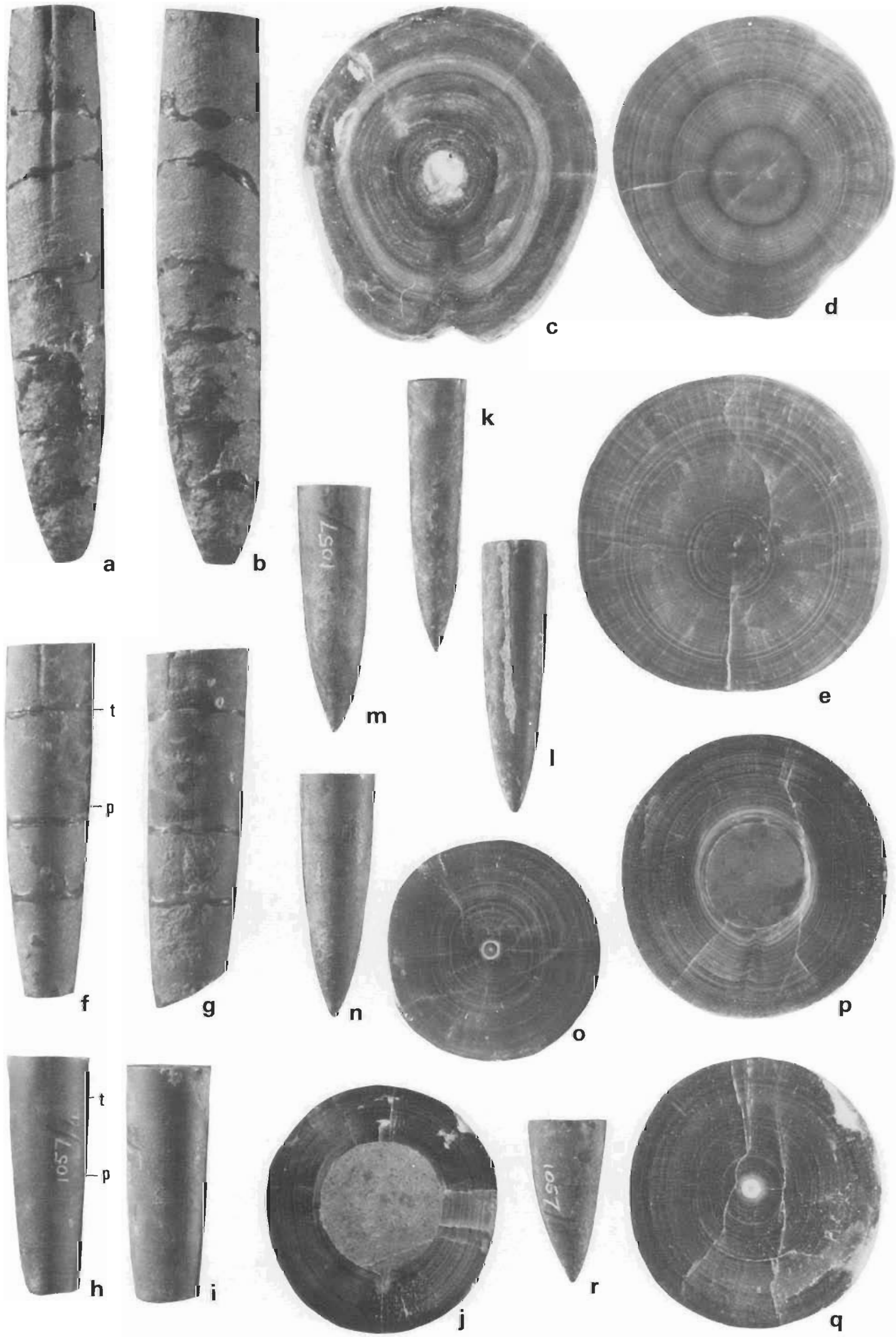
a
b
c
d
k
e
m
l
t
p
f
g
n
o
p
t
p
h
i
j
r
q
1057
1057
1057

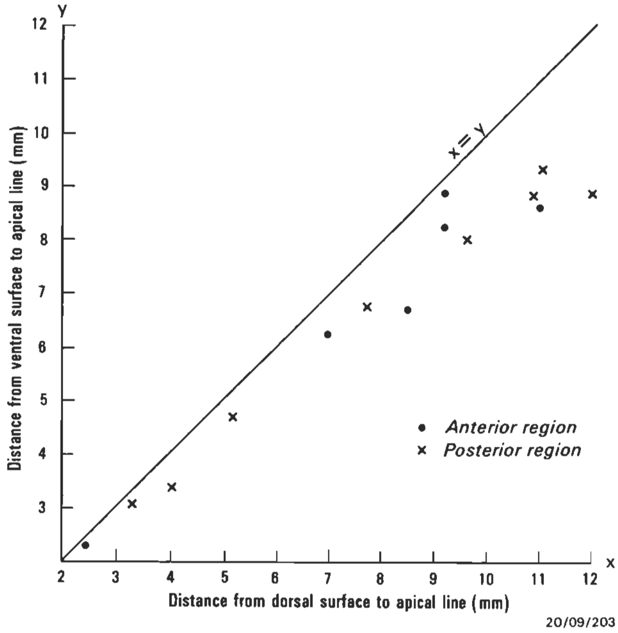

Figure 12. Position of the apical line in *Hibolithes taylori* n. sp.

Median ventral groove commences at alveolar break, terminates between midpoint of the guard and the apex (Figs 9r, 11a). It is well defined, narrow, moderately shallow, V-shaped in section and sharply incised into guard surface in anterior one-third (Fig. 9 o). Over the guard mid to apical region it widens, shallows posteriorly and becomes imperceptible.

Lateral lines are double, situated close together, commencing on the dorso-lateral surface near the apex and passing obliquely towards the ventral surface over the posterior 60–70 mm of the guard. Near mid-guard they are visible as a single wider depression. They are visible in many transverse sections as shallow embayments in the growth lines of mid-guard fragments and their presence anteriorly is probably responsible for the ventro-lateral flattening of the flanks noted above.

Internal features and ontogeny. Alveolus short in relation to guard length. Details of phragmocone and protoconch not known. Apical line usually ventrally placed, strongly so in large specimens (Figs 9q, 11e, 12). A splitting surface underlies the ventral groove and is visible in most transverse sections of the anterior guard. Growth lines are numerous, clearly defined in transverse sections and closely spaced. A prominent line or group of lines outlines a well defined juvenile growth stage in most specimens. This probably marks the transition from early ontogeny when growth is mainly lengthwise, to late ontogeny when growth is largely diametral, a characteristic feature in the growth of belemnopseids.

Discussion. The belemnites of eastern Indonesia are now moderately well known, both stratigraphically and taxonomically (Challinor & Skwarko, 1982; Challinor, 1989a,b, in press). The youngest known *Hibolithes* of the region are early Hauterivian in age (Challinor, 1989a, in press). *Hibolithes taylori* apparently postdates these taxa and therefore has a maximum age of late Hauterivian or Barremian. However, it is associated in collections P 5002 and P 5009 with *Parahibolites*, and this genus is not known earlier than Aptian time (Stevens, 1973). Furthermore, *H. taylori* and *Parahibolites* are associated only in siltstones interpreted as Chim Formation; there is no indication they occur together in the Omati unit. New Guinea *Parahibolites* have been dated by Glaessner (1945) as Late Albian and by Stevens (1965) as Aptian–Albian. Therefore, *Hibolithes taylori* is unlikely to be older than Late Neocomian and may be as young as Late Albian. Although *Hibolithes sensu stricto* was of major importance in the Tethyan fauna from Bajocian to Tithonian time, it declined in the Neocomian and was apparently absent from the Tethys after the Barremian (Stevens, 1973) and after the early Aptian in the Boreal Realm (Mutterlose, 1988). The occurrence of *Hibolithes* in Aptian–Albian beds represents an extension of its known time range.

Hibolithes taylori is quite distinct from all previously described Indonesian and New Guinea Cretaceous *Hibolithes*. Those species from eastern Indonesia which are abundant and stratigraphically useful are depressed in cross-section, smaller, and have short ventral grooves (Challinor, 1989a, in press). A number of poorly known *Hibolithes* of Berriasian–Hauterivian age occur in the Misool Archipelago (Challinor, in press); most are represented by single specimens, are depressed in cross-section and are short grooved, but one or two are either compressed in cross-section or have long ventral grooves. They are much smaller than *Hibolithes taylori* and are quite different in form.

Hibolithes taylori resembles West Antarctic and New Zealand Late Jurassic or Early Cretaceous *Hibolithes* (e.g. *H.* aff. *arkelli*, Mutterlose 1986; *H. arkelli*, Stevens 1965; *H. antarctica*, Willey 1973) in its compressed cross-section and long ventral groove. Evidence is accumulating to suggest that New Zealand and South American Belemnitida are closely related and that New Zealand faunas migrated from the Antarctic Peninsula–southern South America region via West Antarctica (Challinor & others, in press). *Hibolithes taylori* may have followed this route and continued on into New Guinea.

Etymology. *Hibolithes taylori* is named for my late son-in-law, Bruce Alan Taylor.

Hibolithes sp. I
Figure 9m,n

Locality and material. One specimen from locality 187 (sheet SB/54-7).

Age and stratigraphic horizon. *Hibolithes* sp. I is known only from the Ieru Formation where its age is Berriasian–Valanginian.

Brief description. This description is based on a single incomplete specimen which consists of most of the postalveolar guard. It is 88 mm long, 13 mm in maximum diameter and is slightly eroded along one flank.

Guard elongate and moderately slender; postalveolar length estimated at about 7–8 times maximum diameter; total length about 9 times maximum diameter. Outline symmetrical and slightly hastate; widest point situated in posterior one-third of guard; apical regions moderately obtuse. Sides converge gradually towards anterior; maximum transverse diameter estimated at 13.0 mm, transverse diameter at anterior break 11.4 mm. Profile similar to outline; maximum sagittal diameter 13.0 mm, sagittal diameter 11.6 mm anteriorly.

Cross-section approximately equidimensional posteriorly, slightly compressed (A = 98) anteriorly. Dorsal and ventral surfaces regularly rounded, lateral surfaces slightly flattened. Median ventral alveolar groove moderately wide, shallow, broadly V-shaped. In the available specimen it extends down the guard for ~17 mm but is very weakly developed over its terminal 10 mm; it is clearly confined to the anterior one-third of the guard but its exact relationship to post-alveolar length cannot be determined because the protoconch is missing. Lateral lines are not visible, perhaps due to surface damage. Apical line centrally placed at anterior break; a narrow splitting surface extends from apical line to the base of the ventral groove.

Discussion. *Hibolithes* sp. I does not closely resemble any Jurassic or Cretaceous *Hibolithes* known from the southwest Pacific. Its informal designation as *H.* species I continues the nomenclatural practice commenced earlier (Challinor & Skwarko, 1982; Challinor, in press) to record a number of poorly known *Hibolithes* from the southwest Pacific region.

cf. *Hibolithes ingens* Stolley

cf. 1929 *Hibolites ingens* Stolley; Pl. 7, figs 1–5; Pl. 8, figs 1–5.

Locality and material. Parts of ?two poorly preserved specimens from locality 2ONG 2635, sheet SB/55-5, Ramu.

Age and stratigraphic horizon. Cf. *Hibolithes ingens* occurs in the 'Balimbu Greywacke'. This formation was dated by Bain & others

(1975) as Early Jurassic but *Hibolithes ingens* itself is of Callovian–?early Oxfordian age, suggesting the true stratigraphic position of cf. *Hibolithes ingens* is mid-Maril Formation.

Discussion. The material discussed here was received as a number of fragments sectioned by a previous worker and is interpreted as parts of two specimens. The largest appears to have had an original length of about 250 mm and a maximum diameter of about 40 mm. The specimens are strongly recrystallised and were examined in thin section.

The outline and profile are hastate, the point of maximum diameter is posteriorly placed, the cross-section is depressed with regularly rounded dorsal and lateral surfaces and a flattened ventral surface, and the apical line is ventrally placed. No evidence of a ventral or other surface groove is evident: such a groove might have been destroyed during alteration, or confined to part of the guard not preserved.

In gross shape, cross-section and apical line position the large specimens resemble *Hibolithes ingens* Stolley (1929, Pl. 7; Pl. 8, figs 1–5). The latter is the only belemnite known from eastern Indonesia which is of similar large size. The fragment interpreted as a second smaller specimen is similar to *Hibolithes* cf. *ingens* (Challinor, in press, Pl. 15, figs 8–16). It is likely that cf. *H. ingens* is *Hibolithes ingens sensu stricto*, but it is so poorly preserved that firm identification is impossible.

Genus ***Parahibolites*** Stolley 1915

Type species. *Neohibolites duvalaeformis* Stolley 1911

Parahibolites feraminensis n. sp.
Figures 11f–r, 13

1945 *Parahibolites blanfordi* (Spengler) Glaessner, Pl. 6, fig. 10a–c.

Localities and material. Approximately 14 specimens from localities 26 and 29 (sheet 7187/7188) and unlocalised collections (sheet SB/54-7).

Age and stratigraphic horizon. *Parahibolites feraminensis* is of ?Albian age and occurs in the Ieru and Chim Formations.

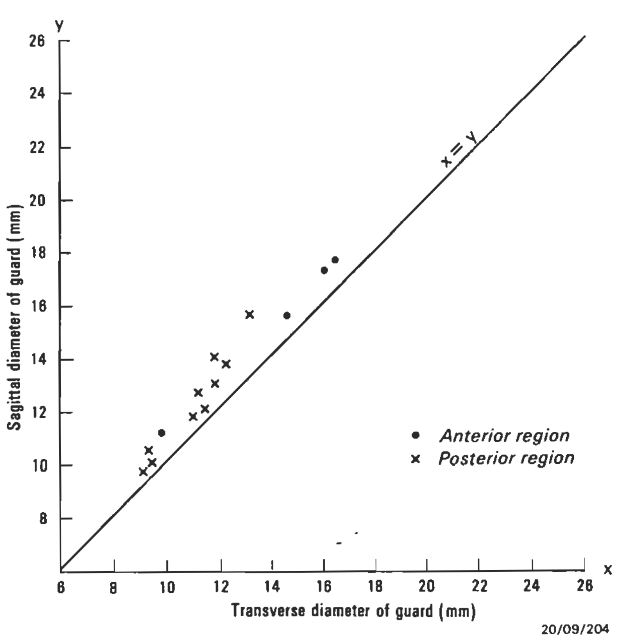

Figure 13. Relationship between guard diameters in *Parahibolites feraminensis* n. sp.

Diagnosis. Guard moderately sized, subconical, laterally compressed, double lateral lines prominent, alveolus long in relation to guard length, ventral alveolar groove very short.

Description. *External features.* Guard subconical and moderately elongate. Total length about 5 times maximum diameter, postalveolar length about 2.5 times maximum diameter in mature specimens. Largest specimen available has a maximum sagittal diameter of 17.8 mm and an estimated reconstructed length of 100 mm.

Outline symmetrical and weakly conical (Fig. 11h,k). Widest point at anterior limit; oral half of guard tapers gradually towards apex; apical half tapers more rapidly, particularly over terminal 20–30 mm; apex acute. Profile conical and asymmetrical (Fig. 11 l,r). Deepest point on guard at anterior limit. Dorsal and ventral surfaces converge steadily towards apex, more rapidly in apical half of guard. Ventral surface begins to converge towards the apex earlier than does the dorsal face, dorsal region near apex slightly inflated; apex slightly dorsally placed and moderately acute.

Cross-sections laterally compressed throughout length of guard (Table 3); slightly more so in apical half and in larger specimens (Figs 11j,o–q, 13); oval, dorsal and ventral faces regularly rounded, lateral faces slightly to markedly flattened (Fig. 11 o–q). Ventral alveolar groove narrow, shallow, V-shaped in section and confined to the anterior alveolar region (Fig. 11f). A splitting surface, best seen in polished transverse sections, is present below the groove (Fig. 11p).

Lateral lines prominent and sharply defined, beginning about 10 mm from apex, at about the midline and extending to or almost to the anterior limit of the guard; double, close together, ventral line better defined than dorsal; they are more prominent in the apical half of the guard although usually clearly visible in the alveolar region.

Internal features. Apical line and protoconch approximately centrally placed; apical line becomes dorsally placed near apex. Dorso-ventral alveolar angle about 20°, alveolus deep, extends about halfway down guard and becomes dorsally eccentric anteriorly. A pseudoalveolus is often present. Growth lines well developed, numerous, close together, clearly visible in polished transverse sections. A well defined embayment present in growth lines at mid-flank marks the position of the lateral lines.

Ontogeny. Early true guard very elongate, hastate. Juvenile and immature guards more elongate and slender than adults, growth in length dominates early ontogeny, growth in diameter late ontogeny. Due to limited material, guard development has not been fully investigated.

Discussion. The specimens conform closely in all characteristics except size to *Parahibolites* Stolley 1915. A single specimen collected earlier from the Feing Group (mid-Bawai unit near localities 129 and 130, Ok Tedi sheet) and described by Glaessner (1945) as *Parahibolites blanfordi* (Spengler) appears identical to this material and is similar in size to Figure 11k,l. However, the taxon is clearly distinct in its large size from *P. blanfordi* (recently redescribed from West Antarctica by Doyle, 1985) and from other *Parahibolites*.

No *in situ* collections of *P. feraminensis* are known but it is associated with *Hibolithes taylori* in float collections (P 5002, P 5009) at localities 26 and 29 (sheet 7187/7188). *H. taylori* also occurs *in situ* at locality 29.

Etymology. *Parahibolites feraminensis* is named from Feramin Village whose people collected most of the specimens.

Table 3. A values for *Parahibolites feraminensis*.

	n	$\bar{x}$	$\theta n\text{-}1$
Anterior half of guard	10	89.0	3.5
Posterior half of guard	4	92.2	2.6

BMR Journal of Australian Geology & Geophysics, 11, 449-472

Mesozoic sedimentary and volcanic rocks dredged from the northern Exmouth Plateau: petrography and microfacies

U. von Rad[1], M. Schott[2], N.F. Exon[3], J. Mutterlose[4], P.G. Quilty[5] & J.W. Thurow[6]

The deeply incised northern margin of the Exmouth Plateau has been dredged extensively along seismic reflection profiles, in water 2000-5600 m deep, by R.V. *Sonne* (Cruise S0-8) and R.V. *Rig Seismic* (BMR Cruise 56). Geological samples obtained have greatly increased our understanding of the Late Triassic-Recent history of the margin. Detailed petrography and microfacies analysis have enabled us to define seven major lithofacies associations. Three Late Triassic to Middle Jurassic associations were laid down roughly coevally on this southeastern margin of Tethys: (1) a Late Triassic-early Liassic volcanic and volcaniclastic association of early rift volcanics, (2) a Late Triassic-Middle Jurassic shallow water carbonate association, and (3) a ?Late Triassic-Middle Jurassic coal measure association. The coal measures were uplifted and weathered to form a ?Jurassic ferruginous sediment and ironstone association. We distinguish 14 Late Triassic-Callovian microfacies types of shallow water carbonates, which can be correlated with the facies of coeval platform carbonates in the Alps and Mediterranean area of the Tethys ocean. During Late Triassic times intertidal to shallow-subtidal carbonates were deposited in the Swan Canyon area close to the palaeo-coastline in the east, and deeper subtidal and shelf lithologies in the Wombat Plateau area in the west. During the latest Triassic and earliest Jurassic, the carbonate platform subsided and was structured into shoals with red biomicrites, and basinal areas with hemipelagic autochthonous micrites and redeposited calcarenitic turbidites. Locally, uplifted blocks, such as the Wombat Plateau horst, were subaerially eroded during Jurassic or earliest Cretaceous times. Carbonate platform deposition continued in places until Middle Jurassic time. Following breakup to form the Argo Abyssal Plain in the earliest Cretaceous, the margin started to subside and a Lower Cretaceous marginal-marine claystone association was deposited, followed by a hemipelagic late Lower Cretaceous radiolarian claystone. As subsidence continued, from Turonian times onwards, there was increasingly pelagic deposition of a Late Cretaceous to Cainozoic association of hemipelagic to eupelagic variably silicified marls and chalks. Complex diagenetic transformations involve silica, silicates, carbonates, and phosphates.

Introduction

Dredging rocks from submarine outcrops of passive continental margins is a very cost-effective and successful method of sampling and dating seismic sequences (von Rad & others, 1979; von Stackelberg & others, 1980). This is especially true for areas where deeply incised submarine canyons and steep escarpments of fault blocks provide exposures of the Mesozoic record. The northern margin of the Exmouth Plateau, with its deeply incised canyons (Fig. 1), has proved to be an ideal dredge area.

During the 1979 *Sonne* 8 cruise we obtained 21 successful dredges from the northern margin of Exmouth Plateau, mainly from Swan Canyon, Cygnet Canyon and Emu Escarpment, as well as from the northern and southern scarps of Wombat Plateau (Figs 1, 2; Tables 1, 2a,b). A wide variety of sedimentary and volcanic facies types could be distinguished (described by von Stackelberg & others, 1980, and von Rad & Exon, 1983). The dredging program during the 1986 *Rig Seismic* cruise (BMR Cruise 56; Exon, Williamson & others, 1988) was equally successful: all 16 dredge hauls contained pre-Quaternary rocks, although dredging at continental margins in water depths of between 2000 m and 5600 m usually has a success rate of 50% or less. Again, a great variety of sedimentary, volcanic, and volcaniclastic rocks was recovered, including Triassic/Jurassic volcanics and volcaniclastics, Upper Triassic to mid-Jurassic shallow water carbonates, coal measures and ferruginised rocks, Lower Cretaceous marginal-marine claystones, mid-Cretaceous radiolarian claystones and hemipelagic marls, and eupelagic Upper Cretaceous to Cainozoic marls and chalks. This paper concentrates largely on the *Rig Seismic* results, but integrates them with the *Sonne* results published earlier.

The combination of detailed seismic-stratigraphic information (Exon & Willcox, 1978, 1980; Exon & others, 1982) with the geological data of the *Sonne* 8 and *Rig Seismic* 56 dredges considerably improves the quality of the seismic interpretations (e.g. dating of reflectors and seismic sequences), and helps us to understand better the Triassic to Cretaceous palaeoenvironments of this passive margin. This was an important prerequisite in the preparation of deep drilling sites for ODP Leg 122 in this area (see von Rad & others, 1988), based on earlier drilling proposals by von Rad, Exon, Williamson and Boyd. Even after the drilling, the data from the adjacent dredge samples remain very important for lateral facies correlations, to extend the facies model from a few vertical sections to a three-dimensional picture valid for the whole northern Exmouth Plateau margin.

This paper was essentially written before ODP Legs 122 and 123. Both legs added significantly to our understanding of the evolution of Exmouth Plateau, but the drilling results await further detailed shore-based study by the shipboard scientific parties. In this paper we will quote a few preliminary Leg 122/123 results, published by the ODP Leg 122 (1988, 1989) and 123 (1989) Shipboard Scientific Parties. For Leg 122, the initial results are detailed in Haq & others (1990). Our studies are complementary to those of Mesozoic rocks drilled by exploration companies on the Exmouth Plateau south of our area of interest (Barber, 1988).

Methods and responsibilities

U. von Rad studied the dredge material on board the *Rig Seismic*, and the preliminary data were reported in the cruise report (Exon & others, 1988). In BGR (Hannover), U. von Rad investigated 65 thin sections from selected rock specimens (Tables 2a,b), covering most of the important facies types. To check the mineralogy of the optical studies, 56 samples were analysed in BGR by the X-ray diffraction method.

M. Schott made a microfacies analysis of 17 thin sections of Upper Triassic-Lower Jurassic shallow water carbonates (Schott, 1988). More detailed microfacies analyses and diagenetic studies of Upper Triassic platform carbonates from the Wombat Plateau Sites 759-761 and 764 (including the dredged rocks) will be published by Rohl & others (in press).

[1] Bundesanstalt für Geowissenschaften und Rohstoffe, Postfach 51 01 53, 3 Hannover 51, Federal Republic of Germany (FRG)
[2] Institut für Paläontologie und Historische Geologie der Universität München, Richard-Wagner-Strasse, 8 München 2, FRG
[3] Marine Geoscience & Petroleum Geology Program, Bureau of Mineral Resources, GPO Box 378, Canberra ACT 2601
[4] Institut für Geologie und Paläontologie, Technische Universität Hannover, Callinstrasse 30, 3 Hannover 1, FRG
[5] Australian Antarctic Division, Channel Highway, Kingston, Tasmania 7050
[6] Geologisch-Paläontologisches Institut der Universität Tübingen, Sigwartstrasse 10, 74 Tübingen, FRG

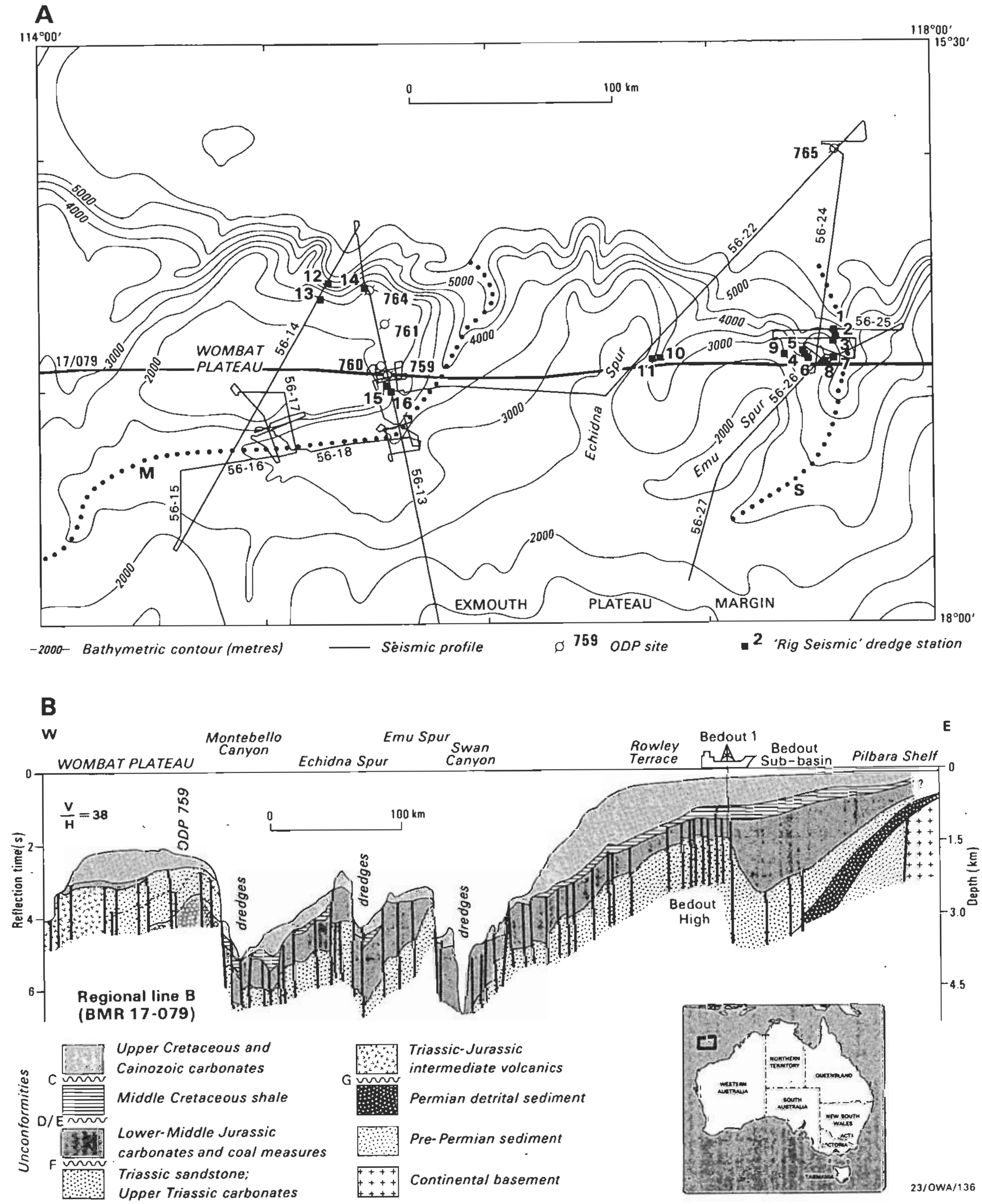

Figure 1. A. Bathymetric map of the northern Exmouth Plateau with regional *Rig Seismic* sample locations, and the location of ODP Leg 122 and 123 drillsites.
M Montebello Canyon, S Swan Canyon, 'Bullant Canyon' between Echidna and Emu Spurs.
B. Geological cross-section interpreted from BMR seismic profile 17-079 and other information, east-west across the northern Exmouth Plateau.

N. Exon, co-chief scientist of the *Rig Seismic* cruise, was responsible for the dredging program and added seismic stratigraphic and regional geological interpretations. P.G. Quilty added foraminiferal age determinations (see also Quilty, in press). J. Mutterlose studied the nannoflora of 18 samples and contributed valuable biostratigraphic age

Table 1. Lithofacies (microfacies = MF) types of pre-Quaternary dredge samples of *Rig Seismic* BMR cruise 56 (and of *Sonne*-8 cruise).
Age: ( ) estimate, * forams (Quilty), ** microfacies (Schott), + rads (Thurow), ++ palynology/dinoflag (Brenner/Burger)

	MF Type	*Colour and generalised lithology*	*Tentative facies interpretation (palaeoenvironment)*	*Age*	*Occurrence in Rig Seismic dredges*
Coal measure association	A1	Black vitreous coal (sub-bituminous)	Paralic (coal swamp)	M.-Lt.Jur++	Only in S0-8 samples
	A2	Grey (brown) carbonaceous (plant-rich) silty clayst)	)		01A & A1, 04C4, 06E, 08E, 08-I, 09E?, 15A
	A3	Grey (brown) carbonac. mica-rich qtz siltst to v.f. sandstone)	Paralic (fluviatile, flood plain, delta . . .))	(?Triassic/?Jurass.)	01C2, 01G, 01H, 03B, 06E, ?08D, 08E, 09A, 15C
	A4	Grey (brown) fine to med. (coarse) qtz sandstone)	)		07A, 15B
	A4a	— ditto, but phosphatised —)	)		16A
	A5	reddish-brown sandy smectite/kaolin shale	Paralic, flood plain?)	(?Triassic/Jurassic)	?09I, 10L, 10-0,
	A5a	— ditto, but phosphatised —	)		4E1, 10D
	A6	Siderite concretions & sideritised clayey qtz siltst etc	Paralic, coal swamps, ?also neritic marls)		01H, 01-I, 07C, 11C
Ferruginous association	B1	reddish-brown clayey ironstone	terrestrial/paralic) later subaerially)		10M
	B2	reddish-brown ferrugin.qtz sdst (sandy ironstone) and ironstone	fluviatile/littoral) exposed to arid conditions)	(?Jurassic)	02G, 04C2, 8E
	B3	brown ferruginous concretions & boxstones & ironstone breccia	terrestrial)		04C4, 06-Ia&b, 16D
Shallow water carbonate association (Lt. Triassic –M. Jurassic)	C1	Algal biosparite/grainstone (calcirudite)	Shallow platform, no terrigen. influx,)	(Lt.Triassic)	16B1, 16B2
	C2	Cream-col. coral biolithite/framestone	algal or other high-energy reef (perireefal)) platform: coral reef, ± sessile foraminif.) Subtidal no terrigen. influx)	(Lt.Triassic)	14B1 cf. Oberhaet-Riffkalk
	C3	yell.-grey qtz-rich, fine-grained biopelspar./grain packstone	well-sorted, near-shore environm.)	Lt/Triassic**/ Callovian*	04I
	C4	lt.-grey, fine-grained, qtz-rich biopelspar./grainstone.	high-energy intertidal flat) intertidal (to shallow-subtidal)	(?Jurassic)	09K
	C4a	sideritised, qtz-& plant-bearing ?pelsparite/grainst.	nearshore, ?deltaic influence)	Callovian*	02H
	C5	bivalve-dasycladacean coquina/bioclastic packst.	Coquina-'tempestites', local deeps)) in platform))	(Lt.Triassic**)	09M2
	C6	oomicrosparite/grain-to packst. w. terrig.qtz	?tidal channels: redeposition of)) ooids in adjacent quiet water))		09M1
	C7	pink oosparite/grainstone	high-energy tidal bars))		04G1
	C8	light-yell.-grey biomicrite/wackestone	adjacent-marine subtidal platform below wave base)		09H
	C8a	red.-brn, ferruginised (+dolomitised) qtz-rich micrite/wackest.	Subtidal w. terrigen. influx)	Lt.Triassic*	11A, ?14C
	C9	yell.-grey encrinite/bioclastic, qtz-rich crin. packst.	foreslope of platform slope or)) outer shelf calcaren. turbidites))	Jurassic*	04K, 04H1

Table 1. Lithofacies (microfacies = MF) types of pre-Quaternary dredge samples of *Rig Seismic* BMR cruise 56 (and of *Sonne*-8 cruise).
Age: ( ) estimate, * forams (Quilty), ** microfacies (Schott), + rads (Thurow), ++ palynology/dinoflag (Brenner/Burger)

	MF Type	*Colour and generalised lithology*	*Tentative facies interpretation (palaeoenvironment)*	*Age*	*Occurrence in Rig Seismic dredges*
	C10	yell.brn biomicrite/wacke-mudstone w.bioclastic horizons and terr.qtz	turbidity currents into deeper- marine platform margin w.pelagic background sed.) resediment carbonate)	(Lt.Triassic)	13M
	C11	chaotic microbreccia w.echinoderm fragments, lithoclasts & terr. qtz	poorly sorted local grain flows(?))	(Lt Cret.)	10E
	C12	echinoderm biomicrite/bioclastic packstone	transition of autochth. C13/14 to C9-11 (local resedimentation of bank sediment))	Lt.Triassic*	14B2
	C13	reddish biomicrite/wackstone	deep bank deposit of fragmented carbonate platform) ± autochthonous)	(Lt.Triassic)	13L cf. Adneth Liassic Red Ls.
	C14	biomicrite/spiculitic wackestone	hemipelagic basin sediment)	Lt.Triassic*	14E, 14A cf. Allgäu Fleckenkalk
	C14a	Lt.-grey dolomitised micrite/wackstone	basin sediment?)	(Lt.Triassic)	09L
Marginal marine to bathyal clayst association	D1	Kaolinitic dark-grey(-brown), qtz & mica-rich, plant mat.-bearing claystone	?prodelta mudst (?Muderong-equivalent) transition — D1 & A5!	?M. Cret. (Apt.++)	07B, 09B, 09E?, 10L?
	D2	green/brown smectite-rich silty claystone, also kaolinite	flood plain or prodelta?	?Jur./?Cret.	11B, ?10-0
	D3	buff/white, qtz-, foram-, nanno-bearing palygorskite claystone	marginal marine (?prodelta)	M.Cret.	06C, 14D
Pelagic marls & chalks (± silicified)	E1	Lt.green-grey hemipelagic, qtz-bear. foram. nanno marl	hemipelagic-bathyal	M-Lt.Cret.	10F, ?14C
	E1a	pelagic foramin. biomicrite/packstone	winnowed foram. sand-bathyal	?Lt.Cret.-Tert.	16C
	E2	lt.-grey qtz-bearing radiolarian-foramin. marl, porcellaneous (opal-CT + clinoptilolite)	hemipelagic-bathyal-high-productivity (? upwelling). ?Windalia Radiol.-equiv.	Albian+ (M.Cret.)	06A, 06D, 06G1 & 2, 10B
	E3	porcellanite = silicified, terrig. qtz-bearing rad.(-for.) marlstone (opal-CT>diag.qtz)	hemipelagic-bathyal, as above	?M.Cret.	06K, 10C2
	E4	qtz-chert = silicified foram. chalk cryptocryst.qtz >opal-CT)	as above, diagenetically more mature	(?M.Cret.)	10H
Volcanic & volcaniclastic rocks	H1	highly altered (?tholeiitic) basalt	?	?	13B, ?13C
	H2a	Lt.-yell-brn aphanitic, felsic volc. rock (potassic rhyolite))	)	Late Triassic to	12A1, ?13C
	H2b	brown (alkali) rhyolite with porphyric texture (large qtz & sanidine phenocr.))	?felsic early rift volcanism dated in S0-8 rhyolites as 213-192 Ma old)	early Liassic (K-Ar)	12A2
	H3	brown altered tuff and tuffaceous sandstone)	)		13G, ?13H, 13I
	H4	epiclastic, volcaniclastic breccia/altered lapilli tuff (± phosphatised))	subaerial (or shallow-submarine?) deposition of volcaniclastics)		12B, 12D, 13F
	H5	bentonitic smectite claystone, buff-grey)	)		13E1 & 2, ?13H, 13K1

Table 2a. Petrography, microfacies and X-ray mineralogy of investigated dredge samples DR 1-9.

Region/seismic profile Water depth of dredge (metres)	1988 Rig Seismic cruise (BMR56) Sample number	Thin-section number 30–	Terrigenous minerals				Matrix/cement				Rock fragment				Second. (diagen.) minerals	XRD mineralogy							Rock name	Age	MF type (see table 1)
			quartz	feldspar	mica-chlorite	heavies	Fe oxides	pyrite	undiff. clay min.	calcite mtx/cement	volcanic	sediment	chert	crystalline		plant fragm.	calcar. bioclasts, other fossils ooids, oncolite, peloid etc.	dominant ca. 50%	abundant ca. 25–50%	common ca. 10–25%	present ca. 2–10%	traces ca. < 2%			
Swan Canyon (W side) (56–24/25B/25C)	DR 01–A																		q	ka, m-il		fs	medium-grey micaceous, quartzose, plant-rich silty claystone		A2
	DR01–A(1)																	ca				(q)	small calcite vein in silty claystone		(A2)
5600	DR 01–C2	787	60	5	2		2	2	25			+				4							grey, well-sorted, mature, clayey quartz siltstone/very fine sandstone		A3
	DR 01–G	788	50	1	10			5	26	3^{v}					59								moderately sorted, massive, mica-rich very fine quartz sandstone	(? Jurassic)	A3
5450	DR 01–H	789	37	4	5		12	1	10	2			8	+	10q, sidl	1		q		sid, ka	fs		light-grey well-sorted, ferruginous, silicified very fine quartz sandstone		A3 (A6)
	DR 01–I	790	12		2			2	12						70 sidl	2		sid		q	ka	m-il	microcrystalline (5–10 μm) siderite concretion		A6
5500	DR 02–G	791	71	1	1		27																red-brown ferruginous quartzose sandy ironstone, well rounded, very mature	(? Jurassic)	B2
4000	DR 02–H	792	6				2	2							83 sidl	3	la, ga	sid				q, ka, m-il, ap	sideritized, quartz and plant-bearing ? pelsparite/grainstone	? Callovian	C 4A
5400 4000	DR 03–B	793	70	1	1	+	5		4						20q	+							light-grey laminated fine quartz sandstone, very poorly sorted, miner-mature		A3
Cygnet Canyon (E side) (S08–04/56–25F)	DR 04–C2	794	68	1			31											q		goe			very poorly sorted (bimodal) ferruginous sandy ironstone (coarse)	(? Jurassic)	B2
	DR 04–C4	795	a 8 b 5		3 1		2 94		+ +						87 col			goe*			ap, q	ka, m-il	a) unferruginized : phophatized (collophane) silty claystone b) ferruginized : clayey ironstone (boxstone)		A2 B3
3970	DR 04–E1	796	29		3		8	+	20						40 col		mol?	a) mtx ap b) vein ba c) undif do	q q		fs	ka,m-il,fs ka, m-il	yellow-brown phosphatized quartzose fine sandy claystone with barite vein, partly dolomitized (yellow)	(? Triassic/ Jurassic)	A 5a
	DR 04–G1	797					+		+	spar +							oo, pel, int, ga la, alg, fb						pink, well cemented, slightly recrystallized oosparite/oolitic grainstone	(?Late Triassic)	C7
3830	DR 04–H1	798	23				6					+					crin, mol, fb						yellow-grey, quartz-rich encrinite/bioclastic crinoidal packstone with reworked A-2 pebbles	E(-M) Jurassic	C9
(3360	DR 04–I	800	18	8			1			40	1		1				ech, mol, fb pel, int, oo						yellow-grey, quartz-rich biopelsparite/grain-packstone (Quilty: ? Callovian)*	Callovian	C3
	DR 04–K	801								+							only crinl						coarse crinoidal limestone-breccia = encrinite bioclastic packstone	E(-M) Jurassic	C9
	DR 06–A	802	+						70						op–CT,cli		30 ra	sm	op–A/CT		cli	q, m-il	slightly silicified (porcellaneous) radiolarian (light olive-grey) mudstone	? Albian	E2
	DR 06–C																		pal	?non		q,ka,fs,ca	very light green-grey nanno-bearing palygorskite claystone	(? Middle-Cretaceous)	
	DR 06–D	803		+	+			+	60						10op–CT		30 ra, tr pi	op–A	sm	op–CT	cli	q, m-il	yellow-grey laminated, semicons., slightly silicified (porcellaneous) radiolarian mudstone	Albian (?)	
3700	DR 06–E	804	a)40 b)70		15 5		10 5		35 20														moderately sorted, cross-laminated clayey quartz siltstone well sorted, ? graded quartz siltstone/silty claystone	(? Jurassic)	A2/3
	DR 06–G1	805							? 10	65^{n}							mol, 3 bry pi 10 fp, 15 ra	ca	op–CT	q			light grey, laminated, slightly silicified, radiolarian-foram.marl	(? Middle-Cretaceous)	E2
3300	DR 06–G2	806	1		1										op–CT,cli		40 ra, pi, fp	op–A,sm		op–CT	cli	q, m-il	slightly silicified radiolarian claystone to porcellanite	(? Middle-Cretaceous)	E2
	DR 06–K	35674	5		+	gc									op – CT> qtz		ra fp mol, bry, fil?						silicified, quartz-bearing, hemipelagic foram-radiolarian nannomicrite (porcellanite)	Albian–Cenom.	E3
	DR 06–Ia																	? goe*?				q,ka,m-il	ferruginous claystone, filling of boxstone	(Triassic/ Jurassic)	B3
	DR 06–Ib																	goe*		ap			ferruginous phosphatized crust of boxstone	(Triassic/ Jurassic)	B3
Swan Canyon (W side) (56–25A) 4470	DR 07–A	807	75	2	10		3		10														olive-green-grey, well-sorted, min. mature, compacted fine to medium quartz sandstone	(Triassic/ Jurassic)	A4
	DR 07–B																	ka		q	m-il	Chl, fs, py	black silty claystone with plant fragments and dinoflagellates	Aptian^{++}	D1
4280	DR 07–C	808													sid		peloids?	sid				(q)	siderite concretion : originally a peloidal micrite?	Jurassic	A6?
4030	DR 08–D	809	84	1	9		1	+	2						2q								moderately sorted, compacted, mineralogically mature, very fine quartz sandstone light-olive green-grey	Jurassic	A3?
	DR 08–E	810	46	2	2		24		26									q		goe*, fs	ka, m-il		brown partly ferruginized, very mature–very fine quartz siltstone/silty claystone	Jurassic	A2/3/B2
4000 (3170)	DR 08–I		15				10		75									sm		q	fs, ka	m-il	yellowish-brown silty, quartz-rich smectite claystone	Middle–Late Jurassic	A2
Cygnet Canyon (E side) (S08–04)	DR 09–A	811	49	2	5	+	2		35				+		5q	2							well sorted, poorly laminated very fine–fine quartz sandstone		A3
	DR 09–B	812	51	+	10		5		33											q,ka, a-c?	m-il, fs	chl	brown-grey, well-sorted, coarse siltstone/very fine quartz sandstone	Aptian ?$^{++}$	D1
	DR 09–E	813	47		6	+	15		32									q		fs, ka	m-il	(chl)	brown-green-grey well sorted, laminated, coarse quartz siltstone	(Triassic/ Jurassic ?)	A2/D1
3850	DR 09–H	814	+				+			mi +							int, pel, mol brach, ost, fp						light-yellow-grey biomicrite/wackestone	(?Late Triassic)	C8
	DR 09–I																			q, ka	m-il, fs, goe		buff silty claystone with ferriginized layers	(? Triassic/ Jurassic)	A6?
	DR 09–K	815	25 to 2							spa +							pel, bivalves, ost, ech, fb						light-grey, partly recrystallized fine-grained, quartz rich pelsparite/grainstone	(?Late Triassic)	C4
2600	DR 09–L	816																do				q, Ca	light-grey, highly consolidated, dolomitized micrite/wackestone	(? Jurassic)	C14A(?)
	DR 09–M1	817	10				+			m spa +							oo, pel, fb						quartz-rich oomicrosparite/grain to packstone with pelmicritic lithoclasts	? Oxfordian	C6
	DR 09–M2	818	10	10	+		8			42							bivalves, alg pel, ga, ost, fb						quartz and K-feldspar-rich bivalve-dasycladacean coquina/bioclastic packstone	(?Late Triassic)	C5
	DR 09–N	819	+	+											q dol		bivalves, alg, ech	do		Ca		q, ka	yellow-brown, recrystallized (dolomitized), ferruginous, quartz-bearing biomicrite/wackestone		C 8A(?)

23/OWA/128

Table 2b. Petrography, microfacies and X-ray mineralogy of investigated dredge samples DR 10–16.

Region/seismic profile; Water depth of dredge (metres)	1986 Rig Seismic cruise (BMR 56) Sample number	Thin-section number	Terrigenous minerals: quartz	feldspar	mica-chlorite	heavies	Matrix/cement: Fe oxides	pyrite	undiff. clay min.	calcite mtx/cement	Rock fragment: volcanic	sediment	chert	crystalline	Second (diagen.) minerals	XRD mineralogy: plant fragm.	calcar. bioclasts other fossils ooids, oncolite, peloid etc.	dominant ca. 50%	abundant ca. 25–50%	common ca. 10–25%	present ca. 2–10%	traces ca. < 2%	Rock name	Age	MF type (see table 1)
Echidna Spur (east side)/Bullant Canyon (56–28A)	DR10–B	820	+		+		5		10	40					45 op–A/CT		(20) ra. + sp	op–A		op–CT, ca, sm		q, m-il	Light-olive-green-grey slightly silicified (porcelan.) semiconsol. calc. rad. claystone	Valang.–E. Turon	E 2
	DR10–C2	821							30	20					50 op–A/CT,10q		(20) ra						olive green-grey silicified calcareous radiol. claystone (= porcelanite)	Berrias.–Campan	E 3
3790	DR10–D	822	5		10		5		70						10 col			sm		ap	q	m-il	ochre, phosphatic, silty smectite claystone	? Aptian	D 2
	DR10–E	823	+				+			mic +		+					ech (crin),mol						chaotic, ferruginous ls-microbreccia w. echinoderm fragments, silty ironstone and goethite oolitic fragment, quartz and mollusks	? Jur	C–11
	DR10–F																	sm	ca	q		m-il	light green-grey, quartz-rich hemipelogic foram marl	E. Cret	E 1
	DR10–H	824								10					q>op-CT		3 fp	q			op-A/CT?		porcelanite/cryptocrystallized quartz chert (origin foram chalk)	(? M. Cret.)	E 4
3710	DR10–L	825	5		5		10		80									ka		q		m-il, fs	reddish-brown (purple), consolidated silty claystone	(? Triass.-Jur.)	A 5
	DR10–M	826	12		+		78		10														reddish-brown clayey ironstone		B 1
	DR10–O	827	28	3	3		26		40									sm		q		fs, m-il	reddish-brown sandy smectite shale		A 5
3230	DR11–A	828	15		1		5		+	79					(do)		? ech ? mol	ca			q, do	ka	reddish-brown, highly consolidated, tectonized and ferruginized quartz-rich micrite/wackestone, ± dolomitized	Triassic?	C 8 A
	DR11–B																		sm, q	ka	fs, m-il		semiconsolidated green silty claystone	(E.–M. Cret.)	D 2
3215 (2840)	DR11–C	829	21		2		13								sidl		mol ?	q		sid	ka	fs,m-il,ca	medium-greyish brown sideritized clayey (kaolinitic) quartz siltstone/very fine sandstone	?	A 6
4800	DR12–A	830	+	san +			+											fs, q					light-yellow-brown, aphanitic (alkali) rhyolite, and porphyritic sanidine quartz phyric rhyolite	(Latest Triassic to E. Liassic?)	H 2a H 2b
	DR12–B	831	+								+				Mn oxide crust		colonial are – nac. foram str						lapilli tuff w.?hyp. dacite and rhyolite fragments, smectitic tuff matrix and colonial arenac. forams		H 4
3500	DR12–D	832									+				coll			ap				q, fs	poorly sorted epiclastic volcaniclastic breccia with collophane matrix and rhyolite/trachytic rock fragments		H 4
North Wombat Plateau (slope) (56–13/14)	DR13–B	833																					highly altered (?tholeiitic) olivine basalt		H 1
	DR13–C	834																					reddish-brown, highly altered microphyric mafic to intermed volcanic rock		H 1/2?
	DR13–E1																	fs		sm	q, do?	m-il, ka	yellowish-white, highly altered laminated tuff (bentonitic)		H 5
	DR13–E2	835																sm		fs	q	ca,ap,do?	brownish, highly altered, ferruginized porphyric intermediate volcanic rock	Middle Jurassic–Cretaceous	H 5
3380	DR13–F	836	+	san +							+				q			q, fs			ka		light grey volcaniclastic conglomerate/lithic crystal lapillituff with trachyte and rhyolite fragments		H 4
	DR13–G	837	5	10	+		25		35		25							fs		sm	q	ka, m-il, do?	mixed, yellowish-grey tuffaceous siltstone to very fine sandstone/altered tuff		H 3
	DR13–H																	sm			magn	fs, (q)	reddish-brown (purple), highly altered tuff		H 3/5
2800	DR13–I	838	35	5	5		35		5		15				goe!		-		goe*	q		q, fs, m-il, ka	brown, ferruginous, clayey, very fine quartz sandstone tuffaceous, with altered volcanic rock and hyaloclastic fragments		H 3
	DR13–K1																	sm			fs	q, ka	medium-grey, ? tuffaceous sandy claystone (? bentonite)		H 5
	DR13–L	839					+			mi +							ech, la, ga, fil, ost, fb						pink well consolidated biomicrite/wackestone	Late Triassic–Liassic	C 13
	DR13–M	840	+	+						mi +	+						ech, mol, ost	ca			q	fs, ka	yellow-brown, ferruginous biomicrite/wacke-mudstone with bioclastic horizons, terrigenous quartz and igneous rock fragments	? Jurassic	C 10
	DR14–A	841	+							mi +							sp, ost, fil ech, fb						yellowish-grey spicule-rich biomicrite/wackestone	? Jur.	C 14
3440	DR14–B1	842	+							+							cor,bivalves,fb						cream-coloured, ± recrystallized coral biolithite/framestone	? Rhaetian	C 2
	DR14–B2	843					+			+							ech, bivalves, brach, ost, fb						recrystallized echinoderm biomicrite (biopelmicrite-biopelsparite)/bioclastic packstone	Late Triassic	C 12
	DR14–C																fp	sm, ca			fs		cream-coloured, semiconsolidated, foram marlstone	Rhaetian	
2690	DR14–D																	pal			q, fs	ca	buff (light yellow) foram-quartz, feldspar-bearing palygorskite claystone	E. Cret.	D 3
	DR14–E	844	+							mi +					dol		sp, ost, fil calc,ech, pel	ca	do		sm	q, fs	yellow-brown, partly recrystallized (dolomitized), ferruginous biomicrite/wackestone	Rhaetian	C 14
(slope) 2720	DR15–A	845	10	+	3		10		72							5			sm	q	ka,m-il,fs		purple-medium-grey quartzose micaceous silty claystone, poorly sorted, laminated	? Late Triassic	A 2
	DR15–B	846	40	5	5				30			10	10										yellow-green, friable, poorly sorted quartz-greywacke (fine-medium sandstone)		A 4
2030	DR15–C	847	56	10	5		5		15				5	35				q		fs	m-il	ka	ochre (buff) densely packed, moderately sorted quartz greywacke (fine sandstone)		A 3
SE Wombat Plateau (5613) (2570) 2480	DR16–A	848	25	10	5		5		+		15		10	5	qtz+coll!			q		ap, fs		m-il, ka	yellow-grey, moderately-well sorted greywacke/medium sandstone		A 4a
	DR16–B1	849					+			spa +							algal fragm. (chlorophycea)						very coarse calcirudite; algal biosparite/grainstone, ± ferruginous	Norian/Rhaetian	C 1
	DR16–B2	850	+							spa +							fb, cor, ga, ech, pel, oo						coralgal calcirudite : ± ferruginous, algal biosparite/grainstone	? Lt. Triassic	C 1
	DR16–C	851	+														fp						pelagic foraminiferal biomicrite/packstone (= winnowed foram.sand)	M. Paleocene	E 1a
2200 (2040)	DR16–D	852	20	3	+		75			mi +			2						goe*	q	fs	ka, m-il	red-brown clayey to very fine sandy ironstone breccia ± quartz	(Triassic/Jurassic)	B 3

23/OWA/129

Abbreviations (1) fossils and carbonate: alg = *calcareous algae*, brach = *brachiopods*, bry = *bryozoans*, calc = *calcispheres*, cor = *corals*, crin = *crinoid fragments*, ech = *echinids*, fil = *filaments*, fb = *benthonic foram.*, fm = *forams (undifferentiated)*, fp = *planktonic foram.*, ga = *gastropods*, la = *lamellibranchs*, mi = *micrite*, m'spa = *microsparite*, mol = *mollusks*, n = *nannos*, ost = *ostracods*, oo = *ooids*, onc = *oncolite*, int = *intraclasts*, pel = *peloids*, pi = *fishdebris*, ra = *radiolarians*, sp = *sponge spicules (± calcitized)*, spa = *sparitic cement*, tr. = *traces of.*

(2) minerals: a-c = *X-ray amorphous matter*, ap = *apatite/collphane*, ba = *barite*, ca = *calcite*, chl = *chorite*, coll = *collophane*, do = *dolomite*, fs = *feldspar*, gc = *glauconite*, goe = *goethite* goe* = *very poorly crystallized goethite*, ka = *kaolinite*, magn = *magnetite*, m-il = *mica-illite*, op–A/CT = *opal-A/CT*, pal = *palygorskite*, py = *prite*, q = *quartz*, san = *sanidine*, sid = *siderite*, sm = *smectite*.

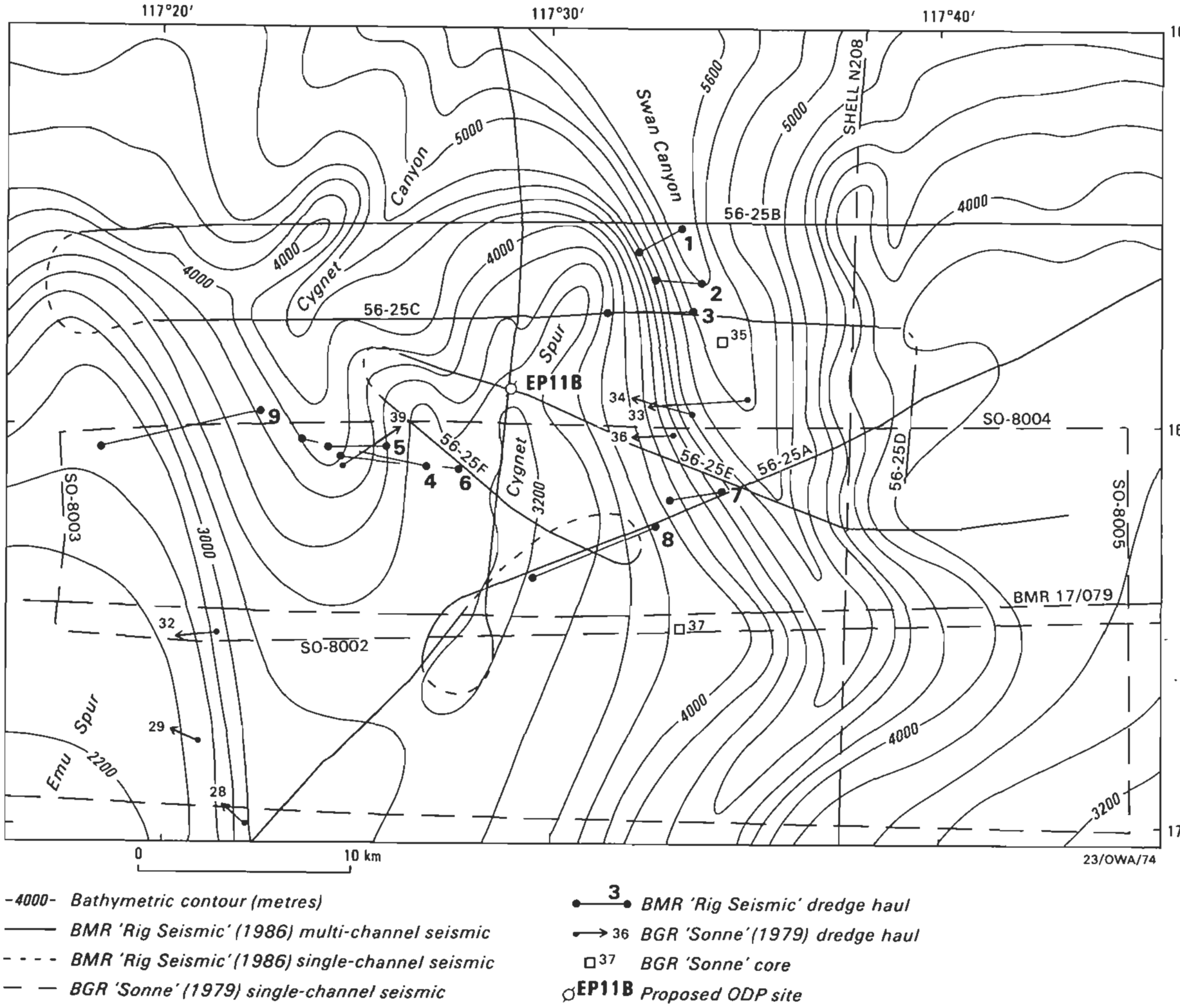

Figure 2. Bathymetric map of the Swan Canyon–Emu Spur area with location of *Rig Seismic* (56-. . .) and *Sonne*-8 (SO-8. . .) seismic lines and location of dredge hauls.

determinations. J. Thurow investigated the microfauna of eight samples, mainly from the radiolarian-rich mid-Cretaceous facies associations D and E (Tables 2a,b). W. Brenner (GEOMAR, Kiel) and M. Muller (BGR Hannover) who determined palynomorphs and dinoflagellates in the samples.

Regional results of the geological sampling program

The study of the northern margin of Exmouth Plateau during the 1986 *Rig Seismic* cruise included eight days of multichannel seismic surveys (long regional survey lines and detailed pre-site surveys for five proposed Leg 122/123 drillsites) and seven days of geological sampling (mainly dredging; see Fig. 1). Dredging was undertaken in five areas: Swan Canyon, Cygnet Canyon, 'Bullant Canyon'/Echidna Spur, northern Wombat Plateau Escarpment, and southeastern Wombat Plateau Escarpment. This section describes the general results of the sampling program in the different regions of the northern Exmouth Plateau. The petrography and microfacies of the Triassic to Cainozoic rock types is dealt with in the following section (see also Tables 1, 2).

Swan Canyon

Dredge hauls in the Swan Canyon all came from the western slope of Emu Spur (Figs 2, 3), mostly well below seismic horizons E and F (?Upper Jurassic). Dredges DR 1, 2, and 3 all came from deep water (5600–4000 m) near the northern (seaward) end of the canyon. The predominant rock types were from the (?Upper Triassic to Jurassic) coal measure association consisting of grey claystone, silty claystone and fine to medium-grained quartz sandstone. The finer sandstones are either massive, or are laminated to cross-laminated and contain abundant plant material and pyrite. The sandstones are lighter grey or buff and vary from laminated to massive. The rocks are well lithified and contain black coal seams and siderite nodules.

Subordinate rock types in dredges DR 1J–L and DR 2B,C (labelled R1 and R2 in Fig. 3A) belong to the shallow-marine detrital association. One is a black, sticky, semiconsolidated clay with bivalve and bone fragments. Another is a soft grey to brown shale containing glauconite, and small plant and mollusc fragments. The age of these rocks may be Early Cretaceous[1]. They were deposited in a marginal-marine environment.

[1] While this paper was in press, new detailed investigations of the *Sonne* and *Rig Seismic* dredge samples by Kristan-Tollmann & Gramann (in press) suggest that the main part of shallow water carbonates from the Wombat Plateau and Cygnet/Swan Canyon area is of Triassic (Norian–Rhaetian) age. Some samples were dated as 'Rhaetian-Liassic', hence it is possible that an early Jurassic age is still represented in the dredged carbonates.

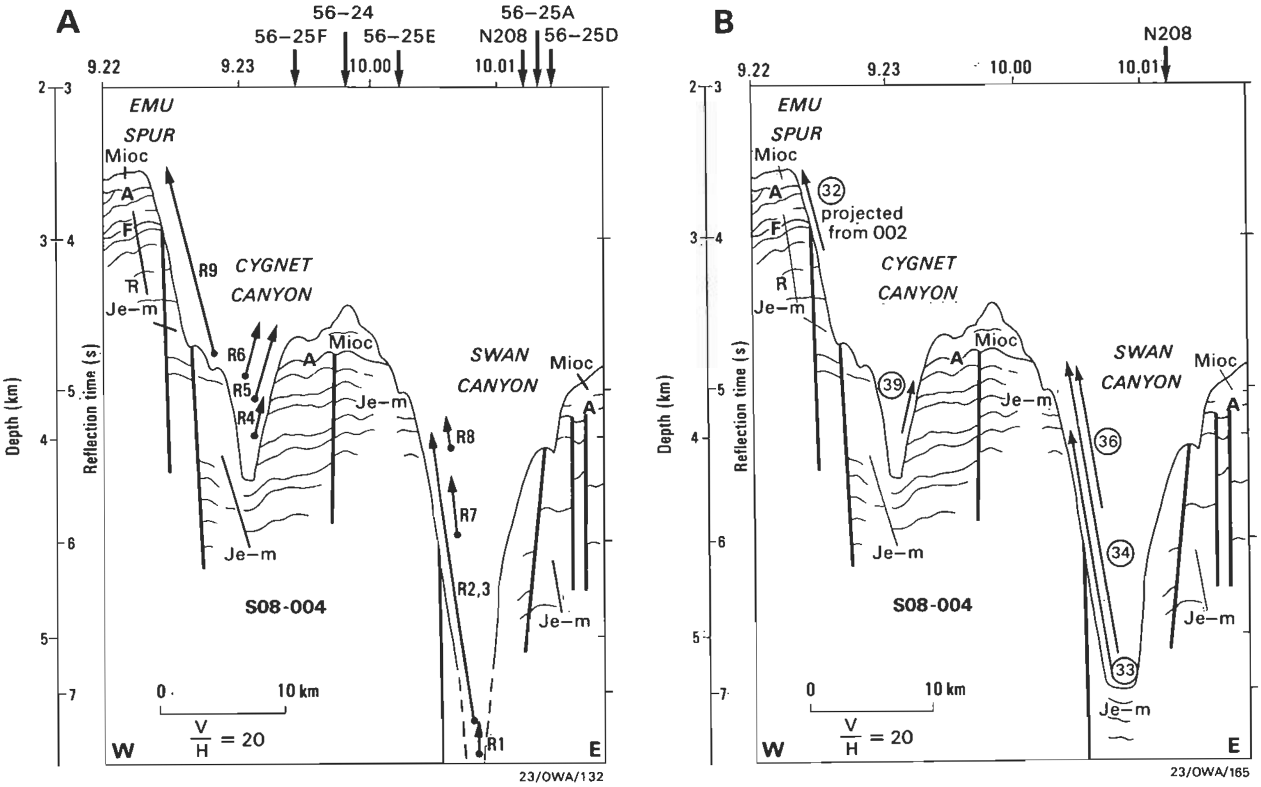

Swan Canyon

R1: ? Jurassic coal measures (A2,3,4); ? Cretaceous marine clay (D3)
R2: Callovian coal measures (A2,3,4); ? Cretaceous marly clay (D2)
R3: ? Jurassic coal measures (A2,3,4)
R7: ? Early Cretaceous marine shale, sandstone (D3,4,6)
R8: ? Jurassic ironstone (B1,2,5); ? Cretaceous marine claystone, sandstone (D3,4,6)

Cygnet Canyon

R4: Callovian shelf carbonates (C2,3,4,8); ? Jurassic coal measures (A2) and ironstone (B1,2,3); ? Cretaceous marine claystone (D5)
R5: ? Jurassic coal measures (A2) and ironstone (B3)
R6: ? Jurassic ironstone (B3); Late Aptian and Cenomanian marine mudstone, sandstone, conglomerate (D2,4,6)
R9: ? Oxfordian shelf carbonates (C1,3,4); ? Cretaceous marine sandstone, mudstone (D2,4,6,7)

32 E1 (Middle Miocene chalk): A2,3 (? Jurassic coal measures); C1,2 (? Jurassic shelf carbonates)
33 E3,4 (Early Aptian chalk); A2,3 (Middle Jurassic coal measures)
34 A1–4 (Middle Jurassic coal measures)
36 E2 (Late Miocene–Early Pliocene chalk); D2 (Late Albian–Early Cenomanian shelf claystone); A1–4 and B1,2 (Middle Jurassic coal measures, some weathered)
39 D1 (? Cretaceous/Tertiary claystone); D2 (Late Albian–Early Cenomanian shelf claystone); B1–4 (? Jurassic terrest/littoral sediments); A4,5 (? Jurassic coal measures); C1,2,4,5 (? Early Jurassic shelf carbonates)

Figure 3. Line drawings of seismic line SO-8-04 with all successful Mesozoic *Rig Seismic* (A) and *Sonne* (B) dredge hauls east of Emu Spur projected onto this line.
A. *Rig Seismic* samples DR1-9 are labelled here R1-9. B. *Sonne* samples are circled.

A crinoidal, quartz-bearing grainstone (DR 2H) contains a Callovian foraminiferal fauna with *Frondicularia franconcica, Pentacrinites*, and *Inoceramus* fragments (Quilty, in press). Overall, dredges DR 1-3 suggest that the lower slope lies between horizons E (Upper Jurassic) and F (Upper Triassic), with some younger material also resting on the slope (Fig. 3).

Dredges DR 7 and 8 came from shallower water, farther south in Swan Canyon (4700-3150 m) (Fig. 2). Rocks belong to the Jurassic coal measure association and the Lower Cretaceous shallow-marine detrital association (grey shale, silty claystone with plant fragments, radiolarians and dinoflagellates). The rocks of finer grain sizes are organic-rich, and some contain nannofossils. DR 7B is of Aptian age and similar to the Muderong Shale. Deposition of these lithologies was probably in marginal-marine, restricted shelf to prodelta environments. Early Cretaceous ages are indicated. The seismic sequence sampled was between horizons C and E. Associated rocks from the ferruginous association (clayey and sandy ironstone) probably represent a period of subaerial weathering.

Cygnet Canyon

Dredges DR 4, 5, and 6 came from the eastern wall of Cygnet Canyon in water 3970-3000 m deep, and DR 9 from its western wall (Figs 2, 3). The eastern dredges contained a wide variety of rocks: ?Jurassic coal measures, Upper Triassic to Jurassic shelf carbonates, and ferruginous claystone, sandstone, boxstone and crusts. Samples DR 4B, DR 6B and DR 6K are possibly equivalents of the Windalia Radiolarite, with an Aptian (-Albian) fauna of radiolarians and foraminifera. DR 6 also contained a single ammonite which will undergo detailed study.

The coal measures, shallow-marine detrital sediments and ferruginous sediments are much like those in Swan Canyon, but the shelf carbonates from dredge DR 4 are a new element. They consist of three lithotypes (C3, C7, C9; see Tables 1 & 2). These rocks also contain echinoid debris, brachiopods, bryozoans and ostracods and, in DR 4I, Callovian foraminiferids. They appear to have been laid down on the shelf or on banks subject to terrigenous influx.

Dredge DR 9 (3650–2600 m) contains ?Upper Triassic to Jurassic shallow marine coquina and calcarenite, chert, and ?Aptian marine mudstone and siltstone. The carbonates contain bivalves, foraminiferids, echinoid spines, ostracods and radiolaria, as well as rounded carbonate pellets. Yellow quartz-rich and oolite-rich grainstone/packstone from sample DR 9M yielded an ?Oxfordian foraminiferid fauna (Quilty, in press).

Echidna Spur/Bullant Canyon

Dredges DR 10 and 11 came from the newly named Bullant Canyon east of Echidna Spur in water 3700–2840 m deep (Fig. 1). The deeper dredge (DR 10) recovered ?Triassic–?Jurassic coal measures, Early Cretaceous marine detrital sediments, and pelagic limestone, chalk, marl, and porcellanite. The coal measure and marine detrital sequences are much like those in Swan and Cygnet Canyons. The marine detrital sequence contains abundant foraminiferids of Aptian age (DR 10B,C,D), along with radiolarians, calcisphaerulids, coccoliths, bivalves, gastropods and brachiopods. More or less silicified varieties of 'Windalia Radiolarite'-type rocks are frequent (DR 10B,C,H).

The pelagic carbonates are varied nanno chalk, foram nanno limestone, and foram nanno marl. Ages determined are late Santonian to early Campanian, and late Paleocene (DR 10Q).

The shallower dredge (DR 11) contained lower to middle Cretaceous marine detrital sediments and pelagic chalks, but no Jurassic coal measures. An additional element was a highly tectonised brown slate with two directions of schistosity, plus a cleavage direction and boudinage structures. This may be a fault-related rock but, if not, it might be of Triassic or even late Palaeozoic or older age. Chalks recovered are late Oligocene and Pliocene.

Dredge DR 10 presumably intersected outcrops of Upper Triassic to Jurassic coal measures (pre-E horizon) and younger debris. Dredge DR 11 was higher on the slope, intersecting the tectonised (?basement) material and material from between the E and C horizons, and above the Oligocene unconformity.

Northern Wombat Plateau

Dredges DR 12, 13 and 14 came from the steep northern escarpment of the Wombat Plateau in water 4600–2690 m deep, close to the later ODP Site 764 (Figs 4, 5). Dredge 12 was a deep dredge aimed at the volcanic sequence of the plateau, some of which had been dated by the K/Ar method as earliest Jurassic (von Stackelberg & others, 1980; von Rad & Exon, 1983). It recovered a large haul of volcanics: brown, very fine-grained, aphanitic rhyolite, trachyte, fine-grained tuff, and volcaniclastic breccia and sandstone.

Dredge DR 13 was aimed at the top of the volcanic sequence and the overlying sedimentary rocks. It recovered a diverse suite of volcanic rocks, and also marine claystone, ferruginous clayey limestone and boxstone. The volcanics include aphanitic basalt, basic or intermediate fine-grained amygdaloidal flows, microporphyritic intermediate flows, various tuffs, and volcaniclastic sandstone and conglomerate. Traces of Upper Triassic (to Jurassic?) fossil-bearing quartz sandstone containing bivalves and foraminiferids were also recovered. DR 13M is a biomicrite containing igneous rock fragments, and should therefore postdate the (?Late Triassic/Liassic) synrift volcanism. DR 13E1 is a Bajocian to Maastrichtian (nannoflora) bentonitic tuff, possibly indicative of post-breakup volcanism.

Dredge 14 was aimed at the sediments above the volcanics of the northern Wombat Plateau. Rocks recovered are largely Late Triassic shallow water carbonates and pelagic limestones and chalks; manganese nodules and crusts are also present. The shallow water carbonates belong to microfacies C12 and C14 (Tables 1, 2). The fauna includes bivalves, corals, gastropods, echinoderms, foraminiferids, ostracods and sponge spicules. The fauna is of Late Triassic age on foraminiferal evidence, and the rocks were laid down in a shelf environment of low energy. Sample DR 14D is a palygorskite claystone of Early Cretaceous age. Pelagic rocks include a foraminiferal limestone and a foram nanno marl of late Miocene age. The manganese crusts have a botryoidal surface and are up to 4 cm thick, the thickness suggesting a long period of non-deposition on the slope where they formed. The manganese nodules have a diameter of 2–5 cm. The dredge results confirm the interpretation of the pre-E sequence and C–E sequence on this margin.

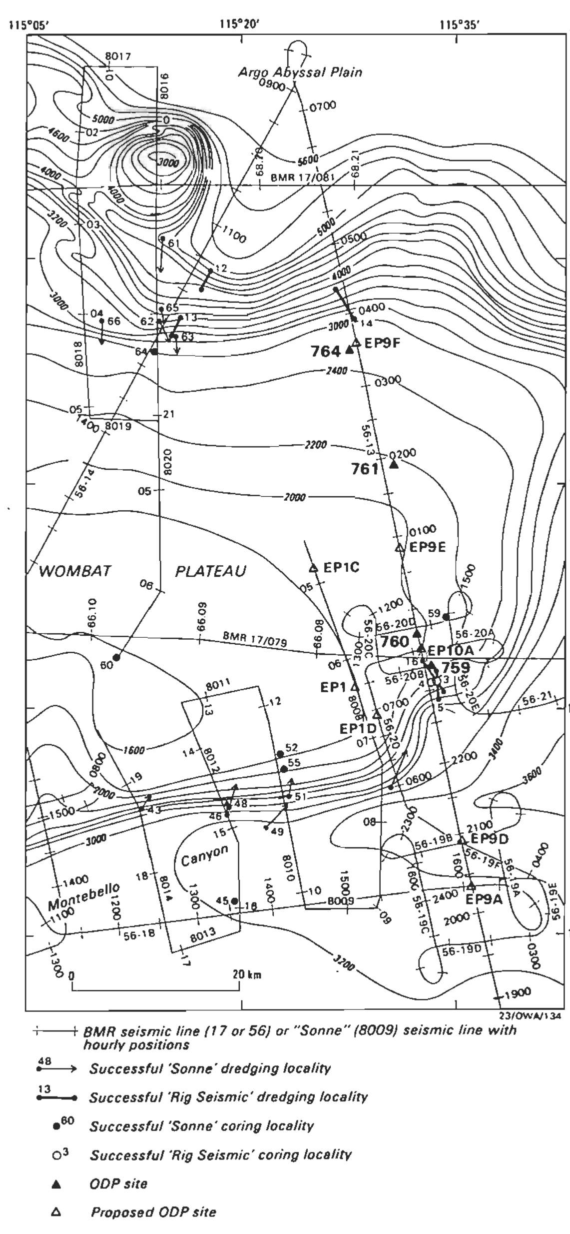

Figure 4. Bathymetric map of the eastern Wombat Plateau area with *Rig Seismic* and *Sonne* seismic lines and dredge/coring localities (for symbols see Fig. 2).

Location of ODP Leg 122 Sites 759–761 and 764 shown.

Southeastern Wombat Plateau

Dredges DR 15 and DR 16 were taken on the southeastern slope of the Wombat Plateau in water 2700–2030 m deep, close to the later drilled ODP Sites 759 and 760 (Figs 4, 5). The dredges recovered Late Triassic shallow water carbonates, red beds, and quartz sandstone. Ferruginous claystone, ironstone crusts, boxstones and breccia, as well as pelagic chalk and silty clay, were also sampled.

Dredge DR 15, the deeper one, contained purplish grey, laminated, quartz-rich carbonate-free, silty claystone which may be Triassic. Other detrital rocks are a silty, fine-grained, calcite-cemented quartz sandstone and a highly porous medium-grained sandstone. Shelf carbonates include grey, highly recrystallised microsparitic limestone, and a less recrystallised former grainstone. Pelagic rocks include a Quaternary semi-consolidated marl, and a foram nanno chalk of late Miocene age.

The shallower Dredge DR 16 contained several types of shelf carbonate, one of which, a very coarse echinoderm–crinoid–mollusc limestone, contains Norian to Rhaetian foraminiferids (Quilty, in press). Other types are very poorly sorted crinoid bryozoan breccia and a finer biocalcarenite which is a packstone. The fauna includes a minute ammonite, bryozoans, gastropods, bivalves, corals, brachiopods, crinoids and foraminiferids. The ammonite (0.2 mm diameter) from sample DR 16B is well preserved, but probably too small to be specifically identifiable. Minor rock types are calcareous, medium-grained quartz sandstone, clayey ironstone/boxstone, mid-Paleocene chalk, and Quaternary silty clay.

The dredges clearly show that the slope is dominantly Upper Triassic (to ?Jurassic) rocks.

Re-interpretation of the seismic stratigraphy of Wombat Plateau after drilling ODP Sites 759–761 and 764 (Leg 122 Shipboard Scientific Party, 1988, 1989) showed that all strata underlying the erosive post-rift unconformity (C/F) on BMR profile 56-13 are Triassic (Fig. 5). Sites 759–761 and 764 were drilled to recover a composite Late Triassic synrift to Cretaceous/Cainozoic post-rift record of sediments. The oldest sediments recovered in Site 759 are of mid-Carnian age (230 Ma). The Wombat Plateau is a horst which was block faulted during various Mesozoic rift phases. During Jurassic (probably Callovian) times, the horst was uplifted to above sea level and subsequently eroded. Non-deposition and/or subaerial erosion during this emergence is the reason for the total lack of Jurassic strata in the Wombat Plateau ODP drill holes. During Tithonian to Berriasian times, after the late Kimmeridgian to Berriasian breakup of the Argo Abyssal Plain (Leg 123 Shipboard Scientific Party, 1989), rapid subsidence of Wombat Plateau below sea level resulted in early Neocomian transgression of the sea. Lower Cretaceous to Cainozoic hemipelagic to eupelagic calcareous sediments formed a thin veneer of post-breakup sediments, as the plateau continued to subside slowly to its present water depth (Fig. 5).

There are K-Ar dated Liassic volcanic rocks (e.g. 190–193.4 Ma, Sonne 8-65 KD) and Liassic (Sinemurian–Pliensbachian) foraminiferal faunas in dredge Sonne 8-61 KD (Zobel, *in* von Stackelberg & others, 1980; Quilty, 1981) along the northern escarpment of Wombat Plateau and very close to ODP Site 764. This is difficult to reconcile with the fact

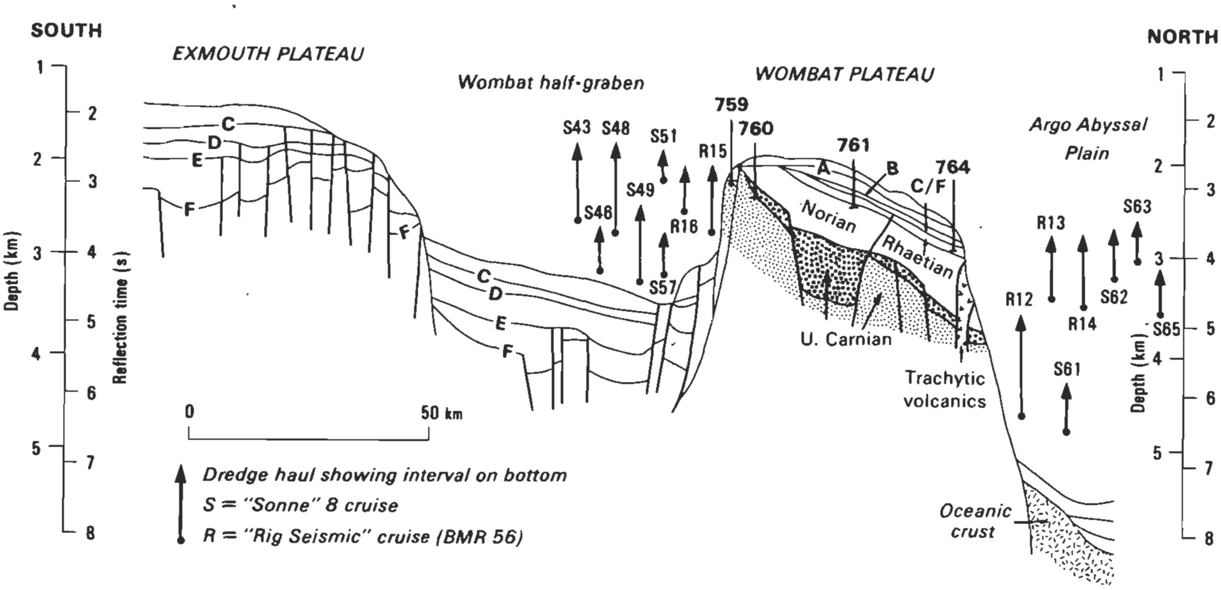

South of Wombat Plateau

S43: Triassic/Jurassic shelf carbonates (C3,4) and claystone (A4)
S46: Triassic brackish sandstone (A3)
S48: L. Triassic paralic siltstone (A2)
S49: Triassic brackish siltstone (A2,3); Triassic/Jurassic shelf carbonates (C5,6) and ironstone (B1)
S51: E. Cretaceous shelf mudstone (D2)
S57: Triassic/Jurassic paralic shale, sandstone (A4,6)
R15: Triassic/Jurassic redbeds (D6), coal measures (D4), carbonates (C6)
R16: E. Cretaceous marine sandstone (D4); L. Triassic shelf carbonates (C2,4); Triassic/Jurassic ironstone (B1,3)

North of Wombat Plateau

S61: L. Triassic/E. Jurassic shelf carbonates and "trachyte" (H4)
S62: E. Jurassic shallow marine carbonates (C2)
S63: Triassic/Jurassic sandstone and mudstone (A2,3,4) and ironstone (B1,2); L. Triassic/E. Jurassic "trachyte" (H4,7)
S65: L. Triassic "trachyte" (H4); ? Cretaceous bryozoan limestone (C7)
R12: Triassic/Jurassic "trachyte" (H4,8)
R13: Triassic/Jurassic "trachyte" (H1,4,7,8), shelf carbonates (C2), ironstone (B2,3); ? E. Cretaceous marine mudstone (D2,6)
R14: L. Triassic shelf carbonates (C2,4,6)

23/OWA/131

Figure 5. Line drawings of *Rig Seismic* multichannel seismic profile BMR 56-13 (Fig. 1).
Interpretation of seismic reflectors of Wombat Plateau after Leg 122 Shipboard Scientific Party (1989). All *Sonne*-8 (S43–S65) and *Rig Seismic* (R12–R16, in text labelled DR12–16) dredge hauls are projected to the northern or southern escarpments of Wombat Plateau.

that neither in Site 761 nor in Site 764 are any post-Rhaetian strata preserved below the post-rift unconformity. Further studies are under way to see whether Liassic rocks escaped erosion and were preserved locally on downfaulted blocks along the steep northern escarpment of Wombat Plateau (see Kristan-Tollmann & Gramann, in press).

Petrography and microfacies

Lithofacies types

In order to describe and interpret the wide variety of lithofacies types of sedimentary, volcaniclastic and volcanic rocks dredged during the 1986 *Rig Seismic* cruise, we adopted the classification used by von Stackelberg & others (1980, table 2) and von Rad & Exon (1983, table 1). The main 'lithofacies associations', which were subdivided into several 'lithotypes' (Table 1), are :

A. coal measure association (mainly Early to Middle Jurassic; some Late Triassic);

B. ferruginous association (?Jurassic);

C. shallow water carbonate association (Late Triassic to Middle Jurassic);

D. marginal-marine claystone association (mid-Cretaceous);

E. hemipelagic to eupelagic more or less silicified marls and chalks (Late Cretaceous–Cainozoic); and

F. volcanic to volcaniclastic rocks (Late Triassic–early Liassic).

The lithofacies found in the *Rig Seismic* samples differ somewhat from those in the *Sonne* 8 samples. The main new discoveries were: sideritised and phosphatised lithologies in the A-association (A4a, A5a, A6); a much greater variety of shallow water carbonate lithologies in the C-association, and of radiolarian mudstones and marls, porcellanites and cherts in the E-association; more types of felsic volcanic rocks and volcaniclastics in the H-association (see Tables 1, 2).

Late Triassic–Jurassic coal measure sequence (lithofacies A1–A6)

Lithofacies A is a heterogeneous group of carbonaceous, clayey to sandy sediments which were dredged between seismic reflectors F and E in the Swan/Cygnet Canyons area (?Early to Middle Jurassic), the eastern Echidna Spur area, and on the southern Wombat Plateau escarpment (?Late Triassic). It is apparently very thick and consists of silty claystones (A2) alternating with parallel-ripple and current-ripple cross-laminated quartz siltstones, very fine sandstones (A3; Plate 1:3,5) and fine to medium quartz sandstones (A4). Vitreous sub-bituminous coal seams (A1; Plate 4:6) were discovered only in the *Sonne* 8 samples. The depositional environment was paralic; the sediments document the mid-Jurassic (Callovian or pre-Callovian) regression with deltaic sedimentation (floodplain claystones, channel sands, delta foresets, coal swamps) alternating with marginal-marine sedimentation.

The terrigenous sediments are carbonate-free and dominated by quartz, muscovite, some biotite, feldspar, pyrite, and traces of heavy minerals. The main clay mineral is normally kaolinite, a typical weathering product of plutonic rocks in the cratonic hinterland. Smectite is sometimes dominant (DR 08I). The fossils in the sediments are plant fragments, palynomorphs, and dinoflagellates, and these provide the only means of dating those rocks (von Stackelberg & others, 1980). The siltstones to very fine sandstones (A3) are tectonically compacted and mineralogically very mature (60–85% quartz), well sorted, and often parallel-laminated to cross-laminated. Pyritised plant material and mica-chlorite are common. Rock fragments include shale clasts and chert, as well as altered volcanics (including palagonitised shards) and metamorphic rock fragments. The moderately to poorly sorted, fine to medium quartz sandstones (A4) are tectonically compacted quartz graywackes, with a ferruginous, clayey matrix which is locally replaced by calcite and/or cryptocrystalline quartz cement. Heavy minerals are dominated by zircon, but include minor epidote and amphibole; the assemblage is thus a mature, highly resistant one.

Secondary minerals, formed during early to intermediate stages of diagenesis, include pyrite (often forming concretions in and around former burrows), calcite (forming secondary cement and veins) and siderite (A6). *Sideritisation* resulted in discrete concretions (with relic-detrital quartz, feldspar, pyrite and clay minerals) and sideritised quartz-rich claystones, siltstones and sandstones (A2, A3, A4). Siderite crystals are cryptocrystalline ($<2\,\mu m$). In general, siderite ($FeCO_3$) is precipitated during early diagenesis at slightly negative Eh and intermediate pH, and in the presence of abundant Fe^{++} and high pCO_2, but with very low S^{--} concentrations in the pore waters. Sideritic ironstones ('blackbands') are typical of coal measure sequences. Sideritisation of shallow water carbonates (DR 02H), that is, the replacement of calcite by siderite, may be influenced by pore solutions from the adjacent rocks of the coal measure sequence (cf. von Rad & Botz, 1987).

Impregnation by *goethite* cement was probably a very late diagenetic process, during exposure to arid desert conditions, which transformed clastic sediments of the A-association into ferruginous rocks of the B-association. The reddish-brown sandy shales (A5) might have been laid down originally in an oxidising floodplain environment.

The early diagenetic *phosphatisation* of some of the A-facies rocks by cryptocrystalline collophane cement (A4a, A5a) is difficult to explain. Phosphatisation also includes volcaniclastic rocks (H4; Plate 2:2), and some of the phosphatised rocks may be replaced shallow water carbonates (DR 7C may originally have been a peloidal limestone). Phosphatised carbonaceous claystones are often associated with diatom-rich and radiolarian-rich sediments (cherts) and typically developed in marginal-marine (estuarine?) environments, influenced by the upwelling of fertile, PO_4-rich deep water along continental margins ('eastern boundary current upwelling', especially off Peru–Chile–Mexico, southwest and northwest Africa, and possibly also off northwest Australia). However, we need more data to substantiate the extent and timing of any northwest Australian upwelling system.

Barite occurs as vein fillings, and *dolomite* apparently replaced original carbonate (DR 4E1). Remobilisation of *silica* produced cryptocrystalline quartz cement.

Ferruginous lithofacies (B1–B3 ?Jurassic)

This association consists of reddish-brown, unfossiliferous, ferruginous sediments, many of which are probably subaerially weathered representatives of the coal measure sequence and hence of Jurassic age (von Stackelberg & others, 1980). The ferruginisation was probably due to a later (?Late Jurassic) emergence of the paralic coal measure sequence, and impregnation by Fe-rich weathering solutions under arid conditions (von Rad & Exon, 1983).

Mineralogically, the reddish-brown iron oxide consists of very poorly crystallised (almost X-ray amorphous) goethite.

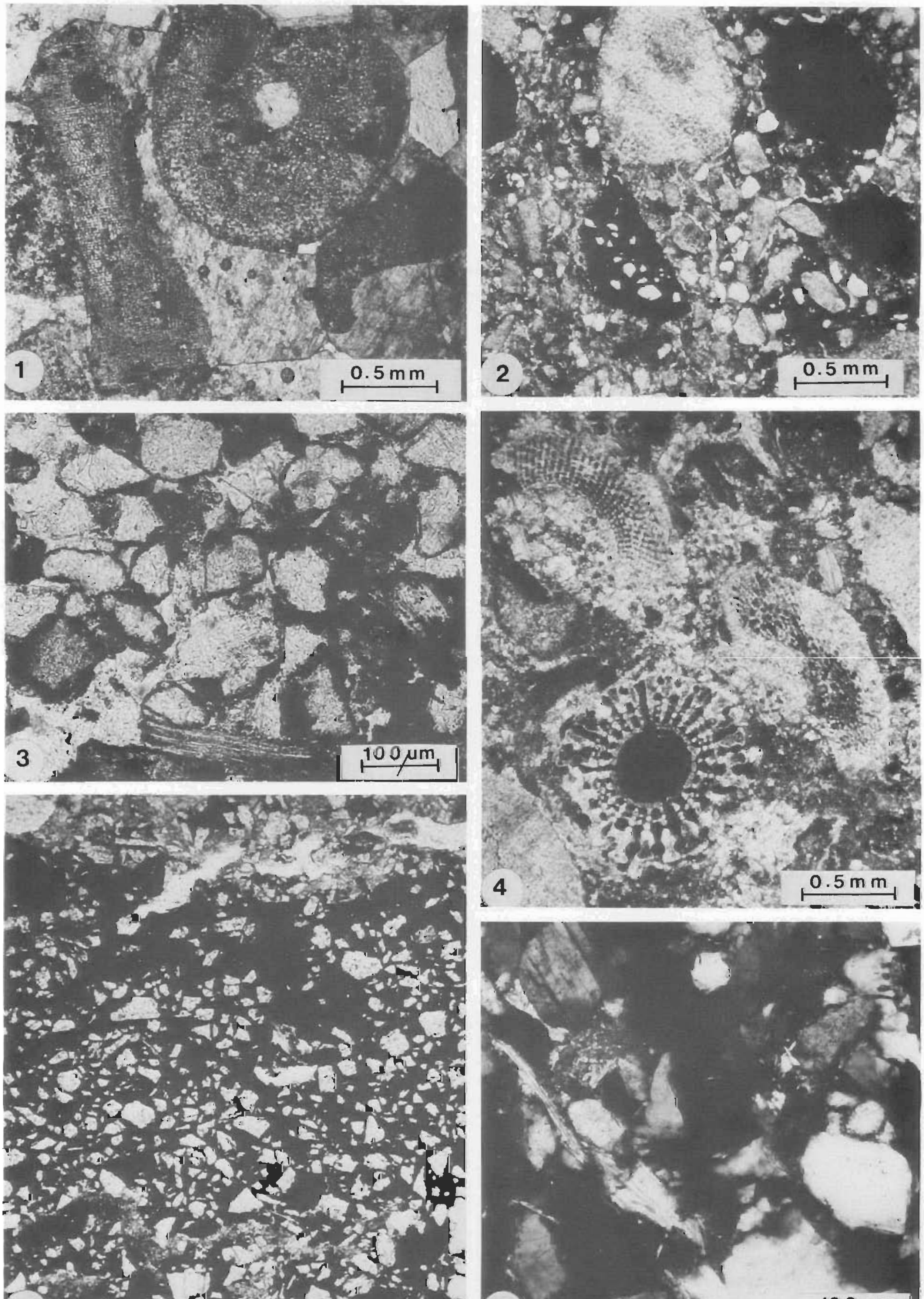
1
0.5mm
2
0.5mm
3
100 µm
4
0.5mm
5
0.5mm
6
100 µm

In particular the semi-consolidated, light-yellowish filling of the 'boxstones' (B3) is almost X-ray amorphous Fe oxide, whereas the hard, dark-brown crust consists of poorly-crystalline goethite. Beautiful goethite 'stalactites' have sometimes grown into the open cavities. The ferruginous concretions contain relict terrigenous material — quartz, feldspar, mica and chert — proving that the original rock was of A 2/3-facies. Sometimes there is diagenetic macrocrystalline ('poikilitic') quartz cement (DR 16D). Apatite (collophane) was also determined, and it may be of late-diagenetic generation, formed during marine conditions (DR 6Ib). The sandy ironstones (B2; Plate 1:5) are extremely mature, and include quartz sandstones with well rounded grains (DR 2G, DR 4C2). In DR 8E we observed a goethitic crust with large, colonial, adhering agglutinated benthonic foraminiferids.

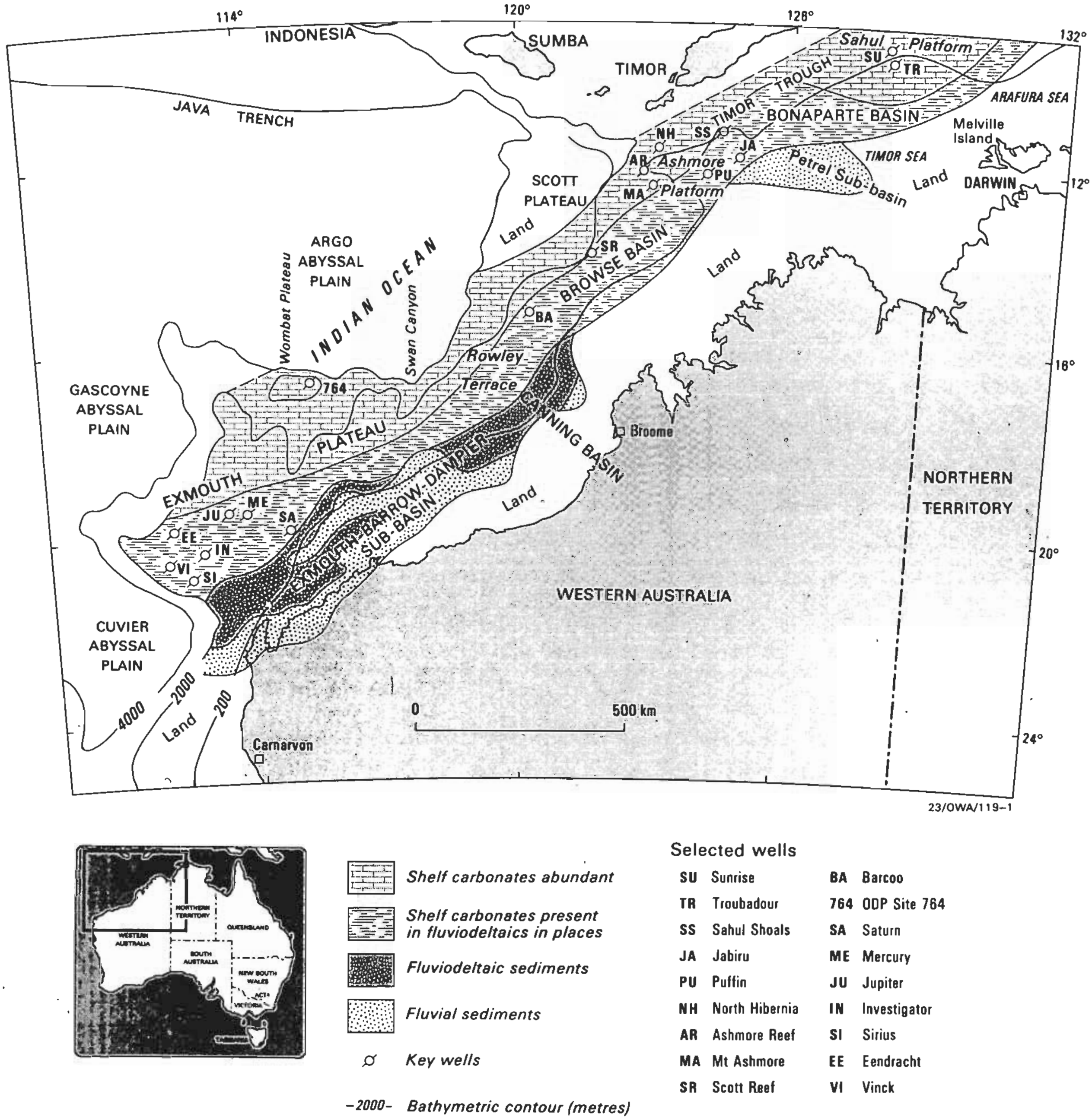

Figure 6. Late Triassic palaeoenvironments on the Northwest Shelf and Exmouth Plateau.
Compiled by N. Exon from various sources (after Williamson & others, 1989).

Plate 1. Triassic (-Liassic) bioclastic and siliciclastic rocks.

1. Crinoidal bioclastic packstone (encrinite, C9) of Early to Middle Jurassic age, explained as turbiditic calcarenite; sample DR 4K (thin section 33801), Cygnet Canyon. Note calcite overgrowth and macro-crystalline calcite cement. **2.** Chaotic limestone microbreccia (C11) of ?Jurassic age; sample DR 10E (thin section 33823), Echidna Spur/Bullant Canyon. Note large crinoid fragments, goethitic oolites, goethitic silty ironstone fragments and a matrix of ferruginous micrite with small (60-100 μm) quartz grains. **3.** Densely packed, moderately sorted quartz graywacke (A3); quartz grains (60-200 μm) surrounded by goethite rims; feldspar and micichlorite also present; ferruginous clay matrix; sample DR 15C (thin section 33847), southern escarpment of Wombat Plateau (?Late Triassic). **4.** Recrystallised echinoderm bioclastic packstone (C12) of Late Triassic age. Echinoderm spines and ?crinoidal fragments with microsparitic matrix; sample DR 14B2 (thin section 33843), northern escarpment of Wombat Plateau. **5.** Goethite-cemented very fine quartz sandstone (sandy ironstone, A2/3, B2); sample DR 8E (thin section 33810), Swan Canyon. Note downward decreasing post-depositional ferruginisation. **6.** Moderately sorted, medium quartz sandstone (A4). Mainly quartz, feldspar, mica, clay matrix; sample DR 7A (thin section 33807), Swan Canyon.

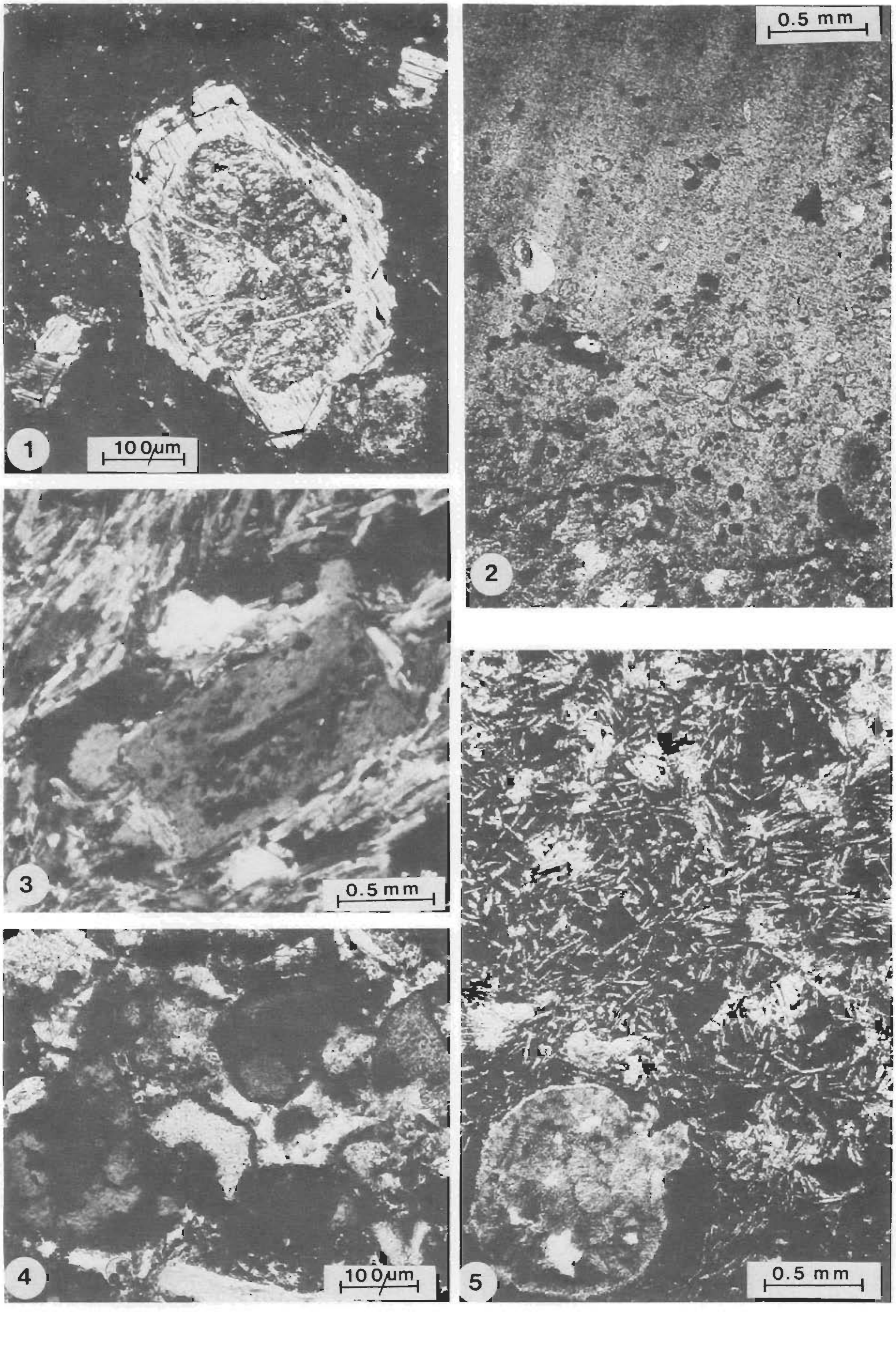
1
100 µm
0.5 mm
2
3
0.5 mm
4
100 µm
5
0.5 mm

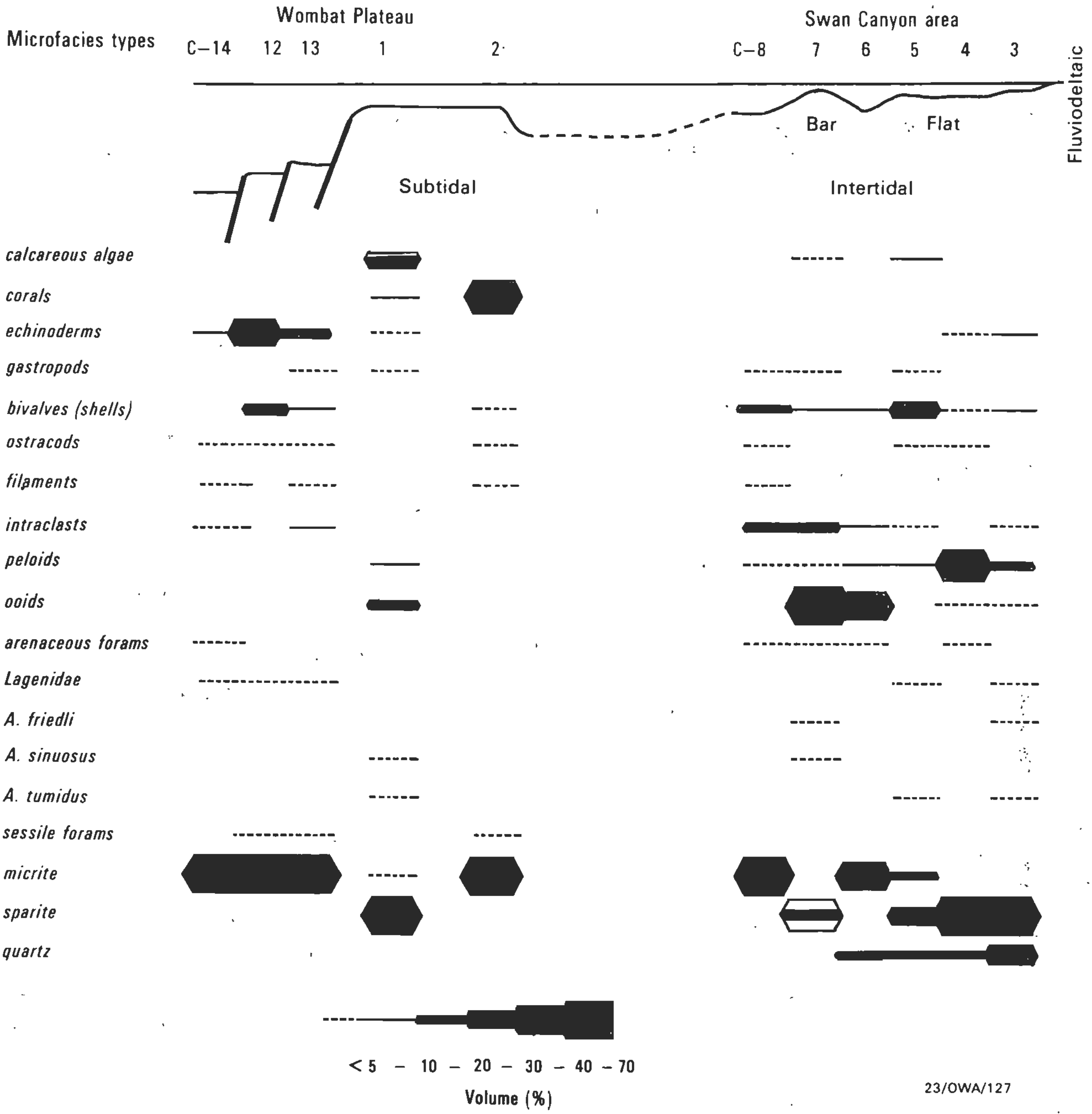

Figure 7. Absolute frequencies of coarse components and groundmass of the Upper Triassic to mid-Jurassic shallow water carbonate microfacies types.
Sketch of the palaeoenvironmental interpretation of microfacies types C1 to C14 on top (compiled by M. Schott).

Shallow water carbonate association (C1-C14a; Late Triassic-Middle Jurassic)

This very heterogeneous group of shallow water marine carbonates is restricted to the northern margin of the Exmouth Plateau and to parts of the Dampier Basin and Beagle Trough. The remainder of the Exmouth Plateau was generally an emergent landmass, being eroded during most of the Jurassic period. Figure 6 shows the distribution of sediment facies during Late Triassic times, after Williamson & others (1989) and Bradshaw & others (1988). A relatively simple pattern of sediment facies existed, with land to the south, and zones parallel to the Gondwanan shoreline: it consisted of fluvial sediments, fluviodeltaic sediments, fluviodeltaic sediments with some shelf carbonates, and finally a zone with abundant shelf carbonates towards the open Tethys sea.

Table 1 and Plates 3-5 show the 17 lithofacies types which can be distinguished by microfacies analysis. The Late Triassic

Plate 2. Volcanic and volcaniclastic rocks (northern escarpment of Wombat Plateau).
1. Olivine (with serpentinised centre) in altered mafic (to intermediate) volcanic rock (H1/2); sample DR 13C (thin section 33834). 2. Volcaniclastic breccia (H4) with collophane (crypto-crystalline apatite) matrix, quartz, feldspar and altered volcanic rock fragments; sample DR 12D (thin section 33832). 3. Silica-rich (71% SiO_2) and alkali-rich (4.3% Na_2O, 5.5% K_2O) altered volcanic rock (?rhyolite) with large feldspar (?K-feldspar) phenocryst, quartz, and feldspar laths (fluidal texture, H2a); original vesicles filled by phyllosilicates; sample DR 12A (thin section 33830). 4. Ferruginous tuffaceous quartz sandstone (hyaloclastite) with dark volcanic glass altered to smectite, quartz, feldspar, clay minerals and Fe oxides (H3); sample DR 13I (thin section 33838). 5. Highly altered olivine-bearing basalt with ophitic texture (H1) and large vesicles, filled by phyllosilicates; sample DR 13B (thin section 33833).

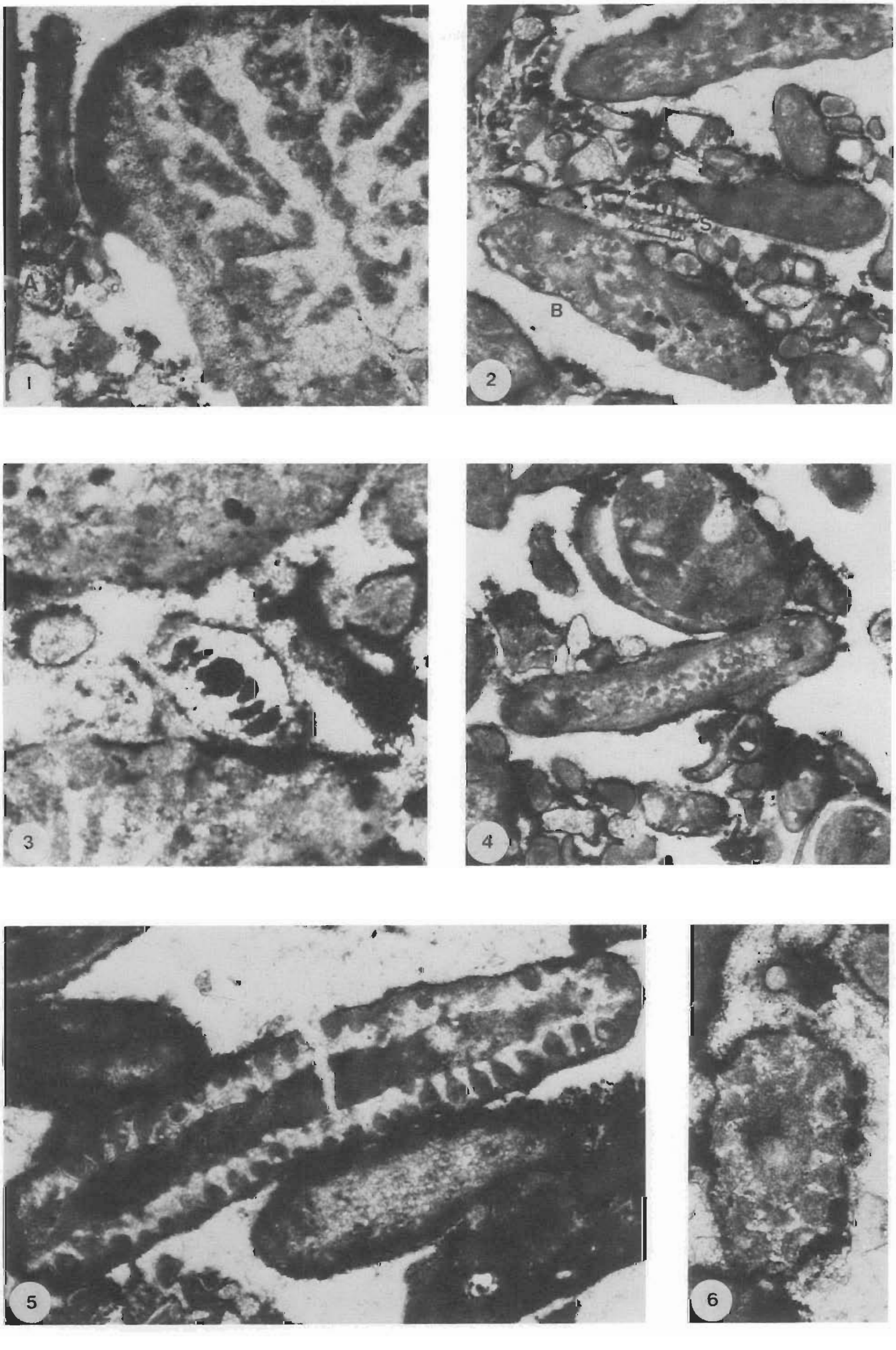
A
1
S
B
2
3
4
5
6

microfacies types C1–C8a and C12–C14 can be differentiated into subtidal types C1–C2 and shelf types C12–14 (both groups without any terrigenous input) in the Wombat Plateau area to the west, and intertidal to shallow-subtidal types C3–C8a in the Swan Canyon area to the east (Fig. 7). Our detailed analysis made it possible to construct a facies model for the Late Triassic (to mid-Jurassic) evolution of the carbonate platform on the northern margin of the Exmouth Plateau.

During Late Triassic times we infer an intertidal to subtidal carbonate platform at an early stage (Fig. 1). Later, the platform was structured into shoals, rises and basinal areas (C12–C14). The intertidal sediments are in the Swan Canyon area to the east, close to the ancient shoreline. They are characterised by fine-grained, quartz-rich biopelsparites and pelsparites (C3, 4, 4a), by coquina tempestites (C5) on tidal flats, by oosparites (C7) on tidal bars, by oomicrites deposited in tidal channels (C6), and by biomicrites redeposited into the adjacent-marine, shallow-subtidal platform areas (C8, ?C8a).

Further west, in the area of the Wombat Plateau, we found some facies types of a subtidal, open-marine platform with algal biosparites (C1; Plate 3) and coral biolithites (C2) — apparently a reef or perireefal facies without any terrigenous influx (Fig. 7). One sample (C5, DR 13M) contains reworked sanidine crystals and igneous rock fragments, clear evidence of erosion of the underlying early-rift volcanics (H1, 2).

Red biomicrites (C13) covered the shoals, and hemipelagic, spiculitic biomicrites (C14) were deposited as more or less autochthonous sediments in the basinal areas. The greater relief of the subsiding carbonate platform is indicated by carbonate redeposition, with echinoderm biosparites (C12) having layers of concentrated, oriented and graded components.

Stratigraphically, these microfacies types could be determined as Late Triassic because of the presence of involutinid foraminiferids which occur in almost all facies zones. In the algal facies of the open-marine subtidal platform a Late Triassic age is based on the foraminiferids *Aulotortus sinuosus* Weynschenk and *Aulotortus tumidus* (Kristan-Tollmann). In the facies of the tidal bars, *Aulotortus friedli* (Kristan-Tollmann) and *Aulotortus sinuosus* Weynschenk are age-diagnostic, as are *Aulotortus friedli* (Kristan-Tollmann) and *A. tumidus* (Kristan-Tollmann) for the tidal flats (see Plate 4).

Within the algal facies we determined the green alga *Boueina hochstetteri* Toula (Family *Udoteaceae*; Late Triassic) and *Boueina hochstetteri* Toula var. *liassica* Le Maitre (late Liassic) (Plate 3:2,4). The dasycladacean *Uragiella liassica* Lebouche & Lemoine (Plate 3:5,6) was until now described only from the Liassic, but we have put a smaller variety of this form into the Late Triassic.

[1] While this paper was in press, new detailed investigations of the *Sonne* and *Rig Seismic* dredge samples by Kristan-Tollmann & Gramann (in press) suggest that the main part of shallow water carbonates from the Wombat Plateau and Cygnet/Swan Canyon area is of Triassic (Norian–Rhaetian) age. Some samples were dated as 'Rhaetian–Liassic', hence it is possible that an early Jurassic age is still represented in the dredged carbonates.

Carbonate sedimentation probably continued into the Jurassic[1], with redeposition common (C9–C12; Plates 1, 5). These carbonates were probably emplaced by small-scale turbidity currents and local grain or debris flows. Quartz-rich, bioclastic crinoidal packstones (Plate 1:1,2, Plate 3:1) are explained as calcarenitic turbidites deposited on the foreslope of the platform, or on the outer shelf close to the shoreline.

Some carbonate lithologies have been partly sideritised (C4a) or dolomitised (C8a, C14a) without completely obliterating information about the original composition.

These Late Triassic and younger microfacies types can be correlated well with the equivalent facies types of the Rhaeto-Liassic carbonate platform in the Alpine and Mediterranean Tethys ocean, which can be studied in the Northern Limestone Alps (Fabricius, 1966; Schott, 1984). Obviously the Exmouth Plateau area was the easternmost part of the giant 'Tethys gulf'.

Marginal-marine claystone association (lithofacies D1–3, ?mid-Cretaceous)

A poorly defined group of probably shallow-marine claystones was subdivided into three lithofacies: a dark-grey, quartz-rich kaolinitic claystone containing mica, pyrite, and plant material (D1) was dated by dinoflagellates as ?Aptian, equivalent to the Muderong Shale overlying the Barrow Group delta in the Central Exmouth Plateau area and on the Northwest Shelf. A green to brown, smectite-rich, kaolinite-bearing silty claystone (D2) is unfossiliferous and similar to the reddish shales of the coal measure sequence (A5). A third variety is a white to buff quartz, foraminiferid and nannofossil bearing, nontronite-rich palygorskite claystone (D3), which probably was laid down in a comparatively deep hemipelagic (?prodelta) environment in front of a major delta system.

Palygorskite is known to form diagenetically under abnormally basic marginal-marine (estuarine), limnic or sabkha conditions, as well as in the deep sea from silica, Mg and Al-rich alkaline solutions. It has been found in many Paleogene sediments off northwest Africa (Riech & von Rad, 1979); there it is debated whether the palygorskite was recycled by wind and current transport from brackish sediments, deposited under subtropical conditions on land or, if it is of authigenic origin, from the diagenetic alteration of pyroclastics or montmorillonite under low temperatures and restricted deep-sea conditions.

Pelagic, more or less silicified marls and chalks (E1–4, Albian to Cainozoic)

This lithofacies association consists of light greenish-grey, hemipelagic, quartz-bearing foraminiferal nanno marls (E1), pelagic foraminiferal packstones (winnowed foraminiferal sands, E1a), and radiolarian-foraminiferal mudstones to marlstones with different degrees of silicification (E2–E4). The radiolarian fauna is rich, moderately preserved, but of low diversity. *Pantanellium lanceola* (early Aptian, but possibly reaching to late Campanian) was found in sample DR 10B (Plate 6:3). Because the radiolarian sediments, which

Plate 3. Upper Triassic subtidal carbonate platform, southeastern escarpment of Wombat Plateau (all figures from dredge sample DR 16B2, thin section 33850).

1. Coral debris biosparite/grainstone (C1) *Thecosmilia* and *Aulotortus* sp. (A). **2.** Algal biosparite/grainstone (C1) with *Boueina hochstetteri* Toula var. *liassica* Le Maitre (B), *Salpingoporella* sp. (S), some small recrystallised peloids, ooids, and a few micritic infillings. Particles and micrite surrounded by fibrous cement, remaining free space filled by granular cement. **3.** *Aulotortus sinuosus* Weynschenk. **4.** Algal biosparite/grainstone (C1) with *Boueina hochstetteri* Toula var. *liassica* Le Maitre, gastropods, peloids, and intraclasts. **5-6** *Uragiella liassica* Lebouche & Lemoine within the algal biosparite facies (C1); a somewhat smaller variety than described for the Liassic; 5, longitudinal; 6, cross-section.
Scale bar 0.5 mm.

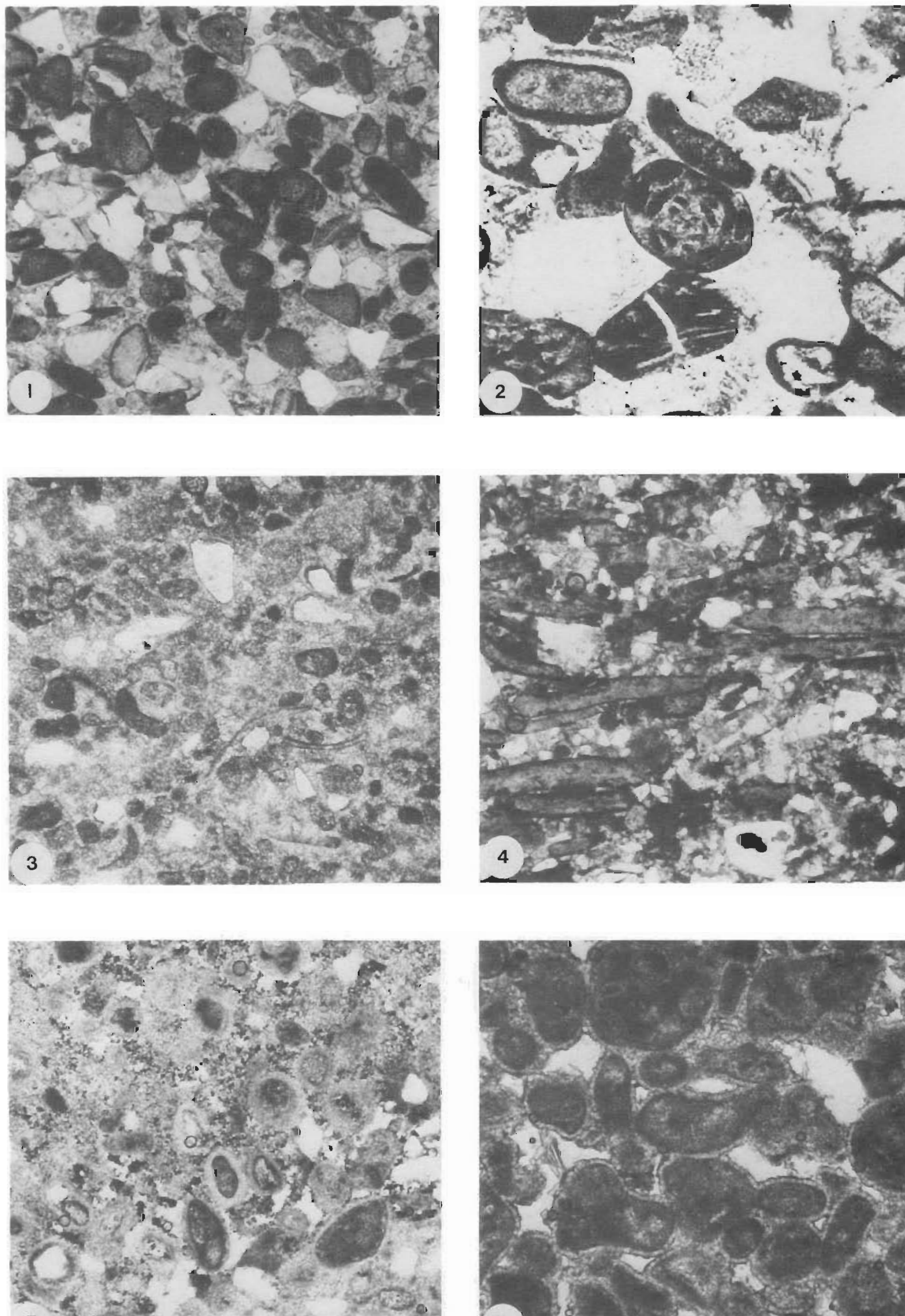
1
2
3
4
5
6

could be determined as Albian in some cases, are very rich in clay, silica diagenesis is retarded (Kastner & others, 1977; Riech & von Rad, 1979). Therefore, in one group of sediments (E2; Plate 6:2,3) the radiolarian skeletons are preserved partly as the original opal-A (proven by X-ray diffraction); mostly, however, the radiolarians are preserved only as outlines of former radiolarians ('ghosts'), and filled with cryptocrystalline opal-CT which also is starting to replace the nannomicritic matrix. Clinoptilolite, a typical authigenic zeolite, also precipitated after the dissolution of opaline silica, is a frequent constituent (Tables 2a,b). These sediments are equivalents to the Windalia Radiolarite of Aptian (-Albian) age.

A more mature stage of silicification is represented by the porcellanites of lithotype E3 (Plate 6:1,4). More than 50% of these sediments consist of diagenetic silica, with opal-CT (filling radiolarian ghosts, replacing radiolarian skeletons, and partly replacing the matrix) being more abundant than cryptocrystalline quartz (mainly filling the chambers of calcite-preserved planktonic foraminiferids). Euhedral calcite cement is an early diagenetic precipitate following the carbonate dissolution in the matrix. Sample DR 06K shows the typical hemipelagic character of these porcellanites very well: before silicification the sediment consisted of about 30% radiolarians, 20% planktonic foraminifera, 5% mollusc and bryozoan fragments, and 5% terrigenous quartz, in a nanno marl matrix. This is a sediment typical of the Upper Cretaceous chert-bearing chalks in northwest Germany, northern France, southern England and Denmark, which were deposited in a shallow (?<200 m) epicontinental sea.

The diagenetically most mature stage of silicification is represented by vitreous quartz chert (E4, sample 10H). In this rock we find about 75% cryptocrystalline quartz, as compared with 10% opal-CT. This means that this rock has almost passed the stage of the opal-CT to quartz conversion.

Volcanic and volcaniclastic rocks (H1-5, Late Triassic to Early Liassic)

A heterogeneous suite of more or less altered volcanic and volcaniclastic rocks was recovered from the northern escarpment of Wombat Plateau (dredge hauls DR 12, 13), an area where similar rocks were discovered during the *Sonne* 8 cruise (von Stackelberg & others, 1980). The rocks crop out below and above the 'early rift unconformity' reflector F (Fig. 5), and document a very interesting stage of early-rift volcanism. Rocks from the *Sonne* cruise could be dated by K-Ar analysis (Kreuzer, *in* von Rad & Exon, 1983, table 3). Hand-picked sanidine phenocrysts from an alkali rhyolite gave the most reliable date: 213.3 Ma (Rhaetian). An undersaturated trachyte was dated as 190-193.4 Ma (Pliensbachian to early Toarcian).

Lithofacies type H1, from the *Rig Seismic* cruise, is a highly altered basalt (DR 13B,C; Plate 2:1,6). X-ray fluorescence (XRF) analysis proved the high degree of alteration (12.7% LOI, 2.8% K_2O, only 42.7% SiO_2). Relatively stable (incompatible) element concentrations are 3.6% TiO_2, 31 ppm Nb, 29 ppm Y and 178 ppm Zr.

Lithofacies type H2a, a light-yellowish brown, aphanitic, potassic rhyolite with a fluidal trachytic texture of alkali-feldspar and ?quartz, is the freshest volcanic rock recovered during the cruise (Plate 2:3). The chemical composition of DR 12A1 (XRF) is 70.96% SiO_2, 0.36% TiO_2, 14.08% Al_2O_3, 1.99% Fe_2O_3 (total Fe), 0.13% MnO, 0.23% MgO, 0.18% CaO, 4.30% Na_2O, 5.53% K_2O, 0.06% P_2O_5 and only 1.59% LOI (probably mainly original volatile content). Rare element concentrations (in ppm) are 59 Cu, 89 Nb, 54 Ni, 11 Pb, 120 Rb, 18 Sr, 14 Ta, 17 Th, 6 U, 11 W, 67 Y, 82 Zn, 727 Zr, 214 Ba, 98 Ce, 9 Co, 5 Cr, 131 La, 5 Sc, 23 V. This rock plots in the rhyolite field of the total alkali vs. silica (TAS) diagram of Le Bas & others (1986). It is a low-Ti, peraluminous, potassic rhyolite with comparatively high Nb, Ta, Y, and especially Zr (727 ppm!) content.

Lithofacies type H2b (DR 12A2) is similar to H2a, except for the presence of abundant large K-feldspar (probably sanidine) and quartz phenocrysts showing a porphyritic texture.

Altered tuffs and tuffaceous sandstones (H3) are mixtures of normal ferruginous muddy quartz sandstones (B3/A4) with volcanic-derived (tuffaceous) components, such as volcanic feldspars, altered volcanic rock fragments, altered (palagonitised) glass and a goethitic matrix (Plate 2:4).

Coarse volcaniclastic sandstones or breccias/conglomerates (H4) are interpreted as lapilli tuffs with a matrix of smectite (DR 12B) or secondary collophane (DR 12D) which has partly replaced the original ashy and marly matrix. Rock fragments include white altered rhyolite, reddish intermediate volcanic rocks (hypersthene porphyric dacite?), trachyte fragments, and altered basalt. DR 13F also contains well preserved sanidine and quartz crystals cemented by cryptocrystalline quartz. A conspicuous Fe-Mn crust with large colonial, adhering agglutinated benthonic foraminiferids was discovered in DR 12B (Plate 6:5,6). This suggests a long period of very slow or non-deposition at the northern Wombat Plateau escarpment, after this fault block had subsided to bathyal water depths.

A number of buff to grey smectite-rich claystones (H5) are interpreted as bentonitic clays derived from the submarine alteration of fine-grained tuffs. Sample DR 17E1 is a bentonitic clay of mid-Jurassic to Maastrichtian age, and hence might be an alteration product of early Cretaceous post-breakup volcanism.

The volcanic and volcaniclastic rocks have not been examined in any detail and deserve further study.

Conclusions

This petrographic study, in conjunction with the earlier ones of von Stackelberg & others (1980) and von Rad & Exon (1983), has revealed a great deal about the geological development of the northern margin of the Exmouth Plateau, as it rifted from Late Permian to Late Jurassic times, broke up in the early Neocomian (Leg 123 Shipboard Scientific Party, 1989) and subsided as the Argo Abyssal Plain formed.

Plate 4. Upper Triassic intertidal carbonate platform, Cygnet Canyon.

1. Small-grained biopelsparite/grain-packstone (C3) with detrital quartz, crinoidal debris, peloids, and *Aulotortus friedli* (Kristan-Tollmann); sample DR 4I (thin section 33800). **2.** *Aulotortus friedli* (Kristan-Tollmann) within the small-grained biopelsparite (C3); thin section 33800. **3.** Small-grained pelsparite/grainstone (C4) with peloids, some detrital quartz, and shell debris; irregular layered fabric; sample DR 9K (thin section 33815). **4.** Coquina/bioclastic packstone (C5) with micritised shells, peloids, and detrital quartz; sample DR 9M2 (thin section 33818). **5.** Oomicrosparite/grain-packstone (C6) with recrystallised ooids, and some detrital quartz; sample DR 9M1 (thin section 33817). **6.** Oosparite/grainstone (C7) with recrystallised ooids, peloids, and grapestones, surrounded by fibrous cement, remaining free space partly filled with granular cement; sample DR4 G1 (thin section 33797).
Scale bar 0.5 mm.

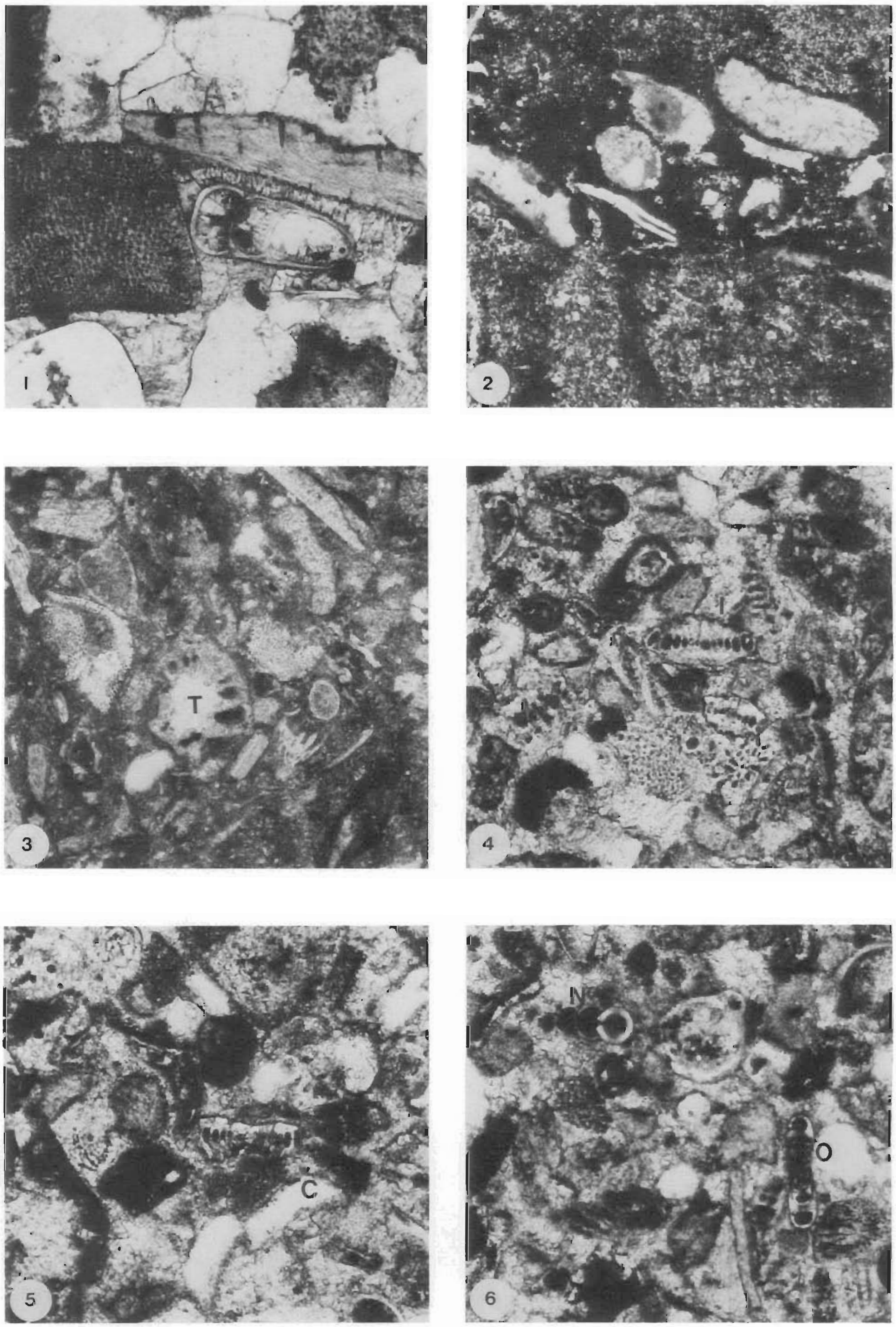
1
2
T
3
I
4
C
5
N
O
6

Late Triassic and Lower Jurassic volcanics and carbonates

At this time the area was part of the southern margin of Tethys. Shallow marine deposits were widespread here, and in the Dampier Basin and Beagle Trough to the southeast and east, but not over most of the Exmouth Plateau in the Late Jurassic. Volcanism and shallow marine carbonate deposition co-existed through Rhaetian and Early Jurassic times (190–213 Ma; von Rad & Exon, 1983).

Highly differentiated alkali-rich silicic volcanic rocks, which were probably deposited under subaerial and shallow marine conditions, have been found only on the northern margin of the Wombat Plateau. Their age straddles that of the post-Rhaetian 'early rift unconformity', and the presence of such volcanics only where breakup of the northern margin of the Exmouth Plateau occurred later, strongly indicates that they are 'early rift volcanics'. They are many hundreds of metres thick.

These volcanic rocks are a heterogeneous mixture of volcanic and volcaniclastic types, for which K-Ar ages of around 213 and 190–193 Ma have been obtained. Most are highly altered. They include basalts, potassic rhyolites, tuffs, tuffaceous sandstones, coarse volcaniclastic sandstones, and lapilli tuffs. Bentonitic clays might have been derived from the submarine alteration of fine-grained ashes, produced during Early Cretaceous post-breakup volcanism.

Shallow marine carbonates are more widespread than the volcanic rocks. They have been dated using foraminiferids (Quilty, 1981; von Stackelberg & others, 1980). They can be separated into subtidal and shelf types in the Wombat Plateau area, and intertidal to shallow-subtidal types in the Swan Canyon area. Some of them have been partly sideritised or dolomitised. We have developed a facies model for the northern Exmouth carbonate platform, summarised as follows:

In the Late Triassic, thick fluviodeltaic detrital sediments of the Mungaroo Formation were laid down to the south and east, but intertidal carbonates were deposited on flats and bars in the Swan Canyon area, and subtidal and shelf carbonates further west in the Wombat Plateau area. The intertidal carbonates of the east include various pelsparites, coquinas, oolitic rock types and micrites. The subtidal carbonates of the west include algal biosparites and coral biolithites. ODP Site 764, on the northern Wombat Plateau, penetrated a 200 m thick Rhaetian reef complex which corresponds to a zone of low reflectivity on seismic profiles (Williamson & others, 1989). Similar reef structures were identified on seismic lines elsewhere on the Wombat Plateau.

Rhaeto(-Liassic)[1] deeper-water wackestones with benthic foraminiferids, and crinoidal and shell fragments have been preserved only at downfaulted blocks along the northern escarpment of Wombat Plateau (DR 13L, SO-8-61KD), whereas the Wombat Plateau was uplifted during Jurassic (?Callovian) times, resulting in the subaerial erosion of all Jurassic rocks down to the uppermost Rhaetian (Leg 122 Shipboard Scientific Party, 1989; von Rad & others, - 1989; Kristan-Tollmann & Gramann, in press). Other Jurassic shallow water carbonates (quartz-rich grainstones of Callovian age, DR 2H, DR 4I) were found in Swan and Cygnet Canyons.

In the latest Triassic and earliest Jurassic, rifting broke the area into swells and basins, and the amount of fluviodeltaic sedimentation to the south and southeast decreased. The swells were covered by biomicrites and the basinal areas were filled with hemipelagic biomicrites. The relief led to reworking, as illustrated by echinoderm biosparites including volcanic fragments, and crinoidal packstones deposited as turbidites. The Upper Triassic to Liassic shallow water limestones were deposited in a shallow embayment of the southern Tethys Sea (cf. Audley-Charles & Hallam, 1988). Their facies can be correlated well with that of the western Tethys, for example, in the Northern Limestone Alps (Schott, 1983, 1984, 1988).

Late Triassic to Jurassic coal measures and ironstones

When the sea receded from the northern margin of the Exmouth Plateau before the Neocomian breakup, coal swamps spread across the coastal plain. Depositional environments represented were lacustrine, deltaic and marginal marine, and up to 1000 m of sediment was laid down. The sediments deposited were very mature quartz sandstones and siltstones, silty kaolinitic claystones and coal. The only fossils are plants, palynomorphs and dinoflagellates. Secondary minerals formed during diagenesis include pyrite, calcite, dolomite, siderite, collophane and silica.

Ferruginous sediments and ironstones appear to represent Late Jurassic and perhaps Early Cretaceous emergence of the paralic coal measure sequence, and impregnation by Fe-rich weathering solutions under arid conditions. Most of the reddish brown iron oxide consists of poorly crystallised goethite. Boxstones and quartz-rich sandy ironstones are characteristic lithologies.

Bentonitic claystones probably record Early Cretaceous post-breakup volcanism (intense ashfalls).

Cretaceous and Cainozoic claystones, marls and chalks

In mid-Cretaceous times a marginal marine to bathyal (<500 m) claystone sequence was laid down on the northern margin of the Exmouth Plateau, much like the Aptian Muderong Shale found elsewhere in the region. The claystones vary from pyritic, carbonaceous and kaolinitic, to unfossiliferous and kaolinitic, to palygorskitic and containing foraminifera and nannofossils.

As the margin sank, deposition of pelagic marls and chalks gradually replaced that of claystones. These Aptian to Recent sediments are more than 500 m thick in places. The more interesting ?mid-Cretaceous types are quartz-bearing foraminiferal nanno marls, foraminiferal packstones, radiolarian-foraminiferal mudstones to marlstones, porcel-

[1] See footnote[1] p. 465

Plate 5. Shallow-water limestones.

1–2. Shallow or allodapic deeper-water limestones with imbrication structures. 1. Quartz-rich, bioclastic crinoidal packstone (C9) with brachiopods, and lagenids; sample DR 4H1 (thin section 33798); Cygnet Canyon. 2. Layer with imbricated shell and crinoidal fragments within a micritic matrix (C10); sample DR 13M (thin section 33840), northern escarpment of Wombat Plateau. **3–6.** ?Liassic deeper-water carbonates. 3. Biomicrite/wackestone (C13) with crinoidal and shell fragments, filaments, ostracods and *Trocholina* cf. *umbo* Frentzen (T); similar to the Liassic Red Limestone (Adnet) facies in the Northern Calcareous Alps; sample DR 13L (thin section 33839), northern escarpment of Wombat Plateau. **4–6.** Biosparite-biomicrite/packstone with crinoidal debris, peloids, and *Involutina* sp. (4 I), *Coronipora* sp. (5 C), *Opthalmidium leischneri* (Kristan-Tollmann) (0), *Opthalmidium* sp., and *Nodosaria* sp. (6 N); similar to the Liassic 'Rotwand' facies in the Northern Calcareous Alps; sample SO-8-61KD/3 (*Sonne* cruise, thin section 25077), northern escarpment of Wombat Plateau.
Scale bar 0.5 mm.

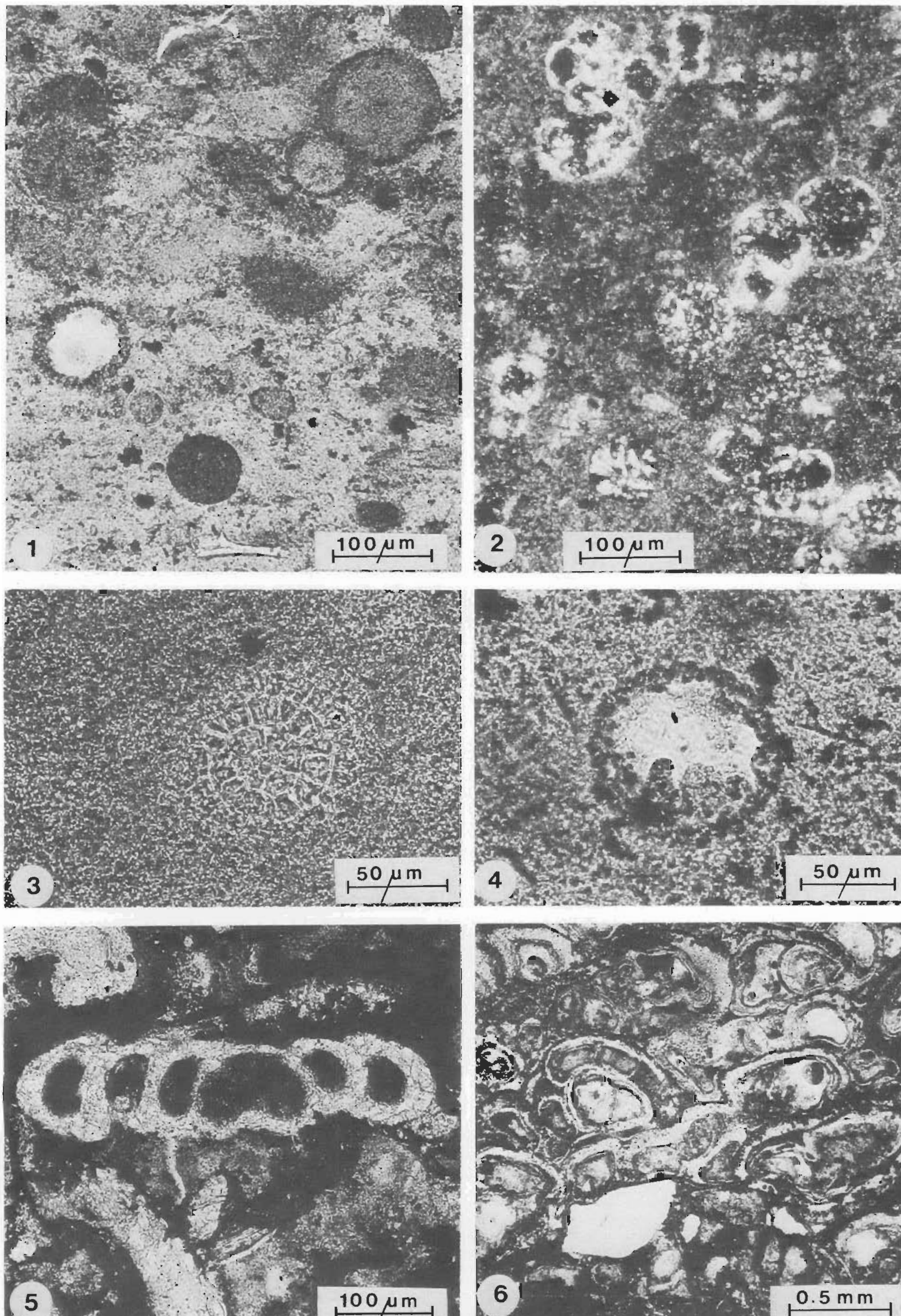
1
100 µm
2
100 µm
3
50 µm
4
50 µm
5
100 µm
6
0.5 mm

lanites and quartz chert. The ?Albian to lower Late Cretaceous radiolarian sediments, equivalent to the Aptian (to Albian) Windalia Radiolarite of the Northwest Shelf, are variably silicified, with both the original opal-A and diagenetic opal-CT present. The porcellanites are more thoroughly silicified radiolarites with opal-CT dominant. The most thoroughly silicified sediments are vitreous quartz cherts with most opal-CT converted to quartz.

Acknowledgements

We are very grateful to Drs H. Rösch and H. Schmitz (BGR) for the X-ray diffraction analyses. X-ray fluorescence analyses were made by Dr Fesser and Mr Requard (BGR), to determine the chemical composition of volcanic and volcaniclastic rocks. We are also grateful to W. Brenner (GEOMAR, Kiel) and H. Müller (BGR, Hannover) who determined dinoflagellates in our samples. We are very grateful for critical comments by Philip O'Brien (BMR) and Dr B Logan (Geology Department, University of Western Australia), which helped to improve our manuscript. All figures were drawn at the Bureau of Mineral Resources drawing office. The paper was reviewed by Ursula Röhl (BGR, Hannover).

References

Audley-Charles, M.G., & Hallam, A., (editors), 1988 — Gondwana and Tethys. *Geological Society Special Publication*, 37, *Oxford University Press, Oxford*, 317 pp.

Barber, P.M., 1988 — The Exmouth Plateau deep water frontier: a case history. *In* Purcell, P.C. & R.R., (editors), The North West Shelf of Australia. *Proceedings of the Petroleum Exploration Society, Australia, Symposium, Perth 1988*, 173-188.

Bradshaw, R.T., Yeates, A.N., Beynon, R.M., Brakel, A.T., Langford, R.P., Totterdell, J.M., & Yeung, M., 1988 — Palaeogeographic evolution of the North West Shelf region. *In* Purcell, P.C. & R.R., (editors), The North West Shelf of Australia. *Proceedings of the Petroleum Exploration Society, Australia, Symposium*, Perth, 1988, 29-54.

Exon, N.F., von Rad, U., & von Stackelberg, U., 1982 — The geological development of the passive margins of the Exmouth Plateau off northwest Australia. *Marine Geology*, 47, 131-152.

Exon, N.F., & Willcox, J.B., 1978 — Geology and petroleum potential of the Exmouth Plateau area off Western Australia. *American Association of Petroleum Geologists, Bulletin* 62(1), 40-72.

Exon, N.F., & Willcox, J.B., 1980 — The Exmouth Plateau: stratigraphy, structure and petroleum geology. *Bureau of Mineral Resources, Australia, Bulletin* 199, 52 pp.

Exon, N.F., Williamson, P.E., & others, 1988 — Rig Seismic Research Cruises 7 & 8 — Sedimentary basin framework of the northern and western Exmouth Plateau. *Bureau of Mineral Resources, Australia, Record* 88/30, 61 pp.

Fabricius, F.H., 1966 — Beckensedimentation und Riffbildung an der Wende Trias/Jura in den Bayerisch-Tiroler Kalkalpen. *In* Cuvillier, J., & Schürmann, H.M.E., (editors), *International Sedimentary Petrography Series*, 9, 1-143, *E.J. Brill, Leiden*, 24 figs, 7 tables, 27 plates.

Gazdzicki, A., 1983 — Foraminifers and biostratigraphy of Upper Triassic and Lower Jurassic of the Slovakian and Polish Carpathians. *Palaeontologica Polonica*, 44, 109-169.

Haq, B.U., von Rad, U., O'Connell, S., & others, 1990 — *Proceedings of the Ocean Drilling Program, Initial Reports*, 122. *College Station, Texas*, 826 pp.

Kastner, M., Keene, J.B., & Gieskes, J.M., 1977 — Diagenesis of siliceous oozes. I. Chemical controls on the rate of opal-A to opal-CT transformation — an experimental study. *Geochimica Cosmochimica Acta*, 41, 1041-1059.

Kristan-Tollmann, E., & Gramann, F., in press — Paleontological evidence for Triassic age of rocks dredged from the northern Exmouth Plateau (Tethyan foraminifers, echinoderms and ostracods). *In* von Rad, U., Haq, B.U., & others, *Proceedings of the Ocean Drilling Program, Scientific Results*, 122. *College Station, Texas.*

Le Bas, M.J., Le Maitre, R.W., Streckeisen, A., & Zanettin, B., 1986 — A chemical classification of volcanic rocks based on the total alkali-silica diagram. *Journal of Petrology*, 27(3), 745-750.

Leg 122 Shipboard Scientific Party (von Rad, U., Haq, B., O'Connell, S., & others), 1988 — Off Northwest Australia — ODP Leg 122 looks at Exmouth Plateau. *Geotimes* 33(12), 10-13.

Leg 122 Shipboard Scientific Party (von Rad, U., Haq, B., O'Connell, S., & others), 1989 — Ocean drilling program — breakup of Gondwanaland. *Nature*, 337, 209-210.

Leg 123 Shipboard Scientific Party (Gradstein, F., Ludden, J., Adamson, A.C., & others), 1989 — The birth of the Indian Ocean. *Nature*, 337, 506-507.

Quilty, P.G., 1981 — Early Jurassic foraminifera from the Exmouth Plateau, western Australia. *Journal of Paleontology*, 55(5), 985-995.

Quilty, P.G., in press — Triassic and Jurassic foraminiferid faunas, northern Exmouth Plateau, eastern Indian Ocean. *Journal of Foraminiferal Research.*

Riech, V., & von Rad, U., 1979 — Silica diagenesis in the Atlantic Ocean: diagenetic potential and transformations. *In* Talwani, M., & others (editors), Deep Drilling Results in the Atlantic Ocean: continental margins and paleoenvironment. *M. Ewing Series* 3, 315-340, *American Geophysical Union, Washington DC.*

Rohl, V., von Rad, U., & Wirsing, G. (in press) — Microfacies, paleoenvironment and facies-dependent carbonate diagenesis in Upper Triassic platform carbonates off Northwest Australia. *In* von Rad, U., Haq, B.U., & others, *Proceedings of the Ocean Drilling Program, Scientific Results*, 122. *College Station, Texas.*

Schott, M., 1983 — Sedimentation und Diagenese einer absinkenden Karbonat-Platform: Rhät und Lias des Brünnstein-Auerbach-Gebietes, Bayerische Kalkalpen. *Facies*, 9, 1-60, 25 figs, 1 table, 8 plates.

Schott, M., 1984 — Mikrofaziell-multivariate Analyse einer rhätoliassischen Karbonatplattform in den Nördlichen Kalkalpen. *Facies*, 11, 229-280, 22 figs, 6 plates.

Schott, M., 1988 — Mikrofazielle Analyse von Karbonaten der Oberen Trias und des Unteren Jura aus dem NW-australischen Kontinentalrand (Wombat-Plateau, Swan-Graben). *Unpublished report, München.*

von Rad, U., & Botz, R., 1987 — Authigenic Fe-Mn carbonates in Cretaceous and Tertiary sediments of the continental rise off North America, Deep sea Drilling Project Site 603. *In* Van Hinte, J.E., Wise, S.W.J.Jr., & others, *Initial Reports of the Deep Sea Drilling Program*, 93, 1061-1077, *US Government Printing Office, Washington DC.*

von Rad, U., Čepek, P., von Stackelberg, U., Wissmann, G., & Zobel, B., 1979 — Cretaceous and Tertiary sediments from the Northwest African slope (dredges and cores supplementing DSDP results). *Marine Geology*, 29, 273-312.

von Rad, U., & Exon, N.F., 1983 — Mesozoic-Cenozoic sediments and volcanics from Exmouth, Scott and Wallaby Plateaus off northwest Australia. *American Association of Petroleum Geologists Geological Memoir* 34, 253-281.

von Rad, U., Haq, B., Gradstein, F., Ludden, J., & O'Connell, S., 1988 — Leg 122/123 Scientific Prospectus. *Ocean Drilling Program, Scientific Prospectus* no. 22/23. *College Station, Texas*, 86 pp.

Plate 6. Pelagic marls and chalks, ferromanganese crust.

1. Silicified radiolarian mudstone (porcellanite, E3) of Albian(?) age; sample DR 6D (thin section 33803), Cygnet Canyon. Note fish fragment (base) and radiolarian 'ghosts', filled with opal-CT (and pyrite) replacing skeletal opal-A and filling voids. **2.** Slightly silicified radiolarian foraminiferal marl (E2) of ?mid-Cretaceous age; planktonic foraminifers still calcitic; radiolarian ghosts and foraminifers mainly filled by (chalcedonic to microcrystalline) quartz; matrix: nannofossil micrite and opal-CT; sample DR 6G1 (thin section 33805, crossed nicols), Cygnet Canyon. **3.** Slightly silicified (porcellaneous) radiolarian marl (E2) of mid-Cretaceous age; opal-CT replaced and filled radiolarian ghost; sample DR 10B (thin section 33820), Echidna Spur/Bullant Canyon. **4.** Detail of radiolarian 'ghost' replaced and filled by opal-CT; sample DR 6D (thin section 33803), Cygnet Canyon. Note opal-CT lepispheres growing into open cavity of radiolarian. **5.** Planispiral arenaceous (benthonic) foraminiferid in ferromanganese crust on volcaniclastic breccia (H2b); sample DR 12B (thin section 33831), northern escarpment of Wombat Plateau. **6.** Arenaceous foraminiferal structures in ferromanganese crust; sample DR 12B (thin section 33831), northern escarpment of Wombat Plateau.

von Rad, U., Thurow, J., Haq, B.U., Gradstein, F., Ludden, J., & the ODP Leg 122/123 Shipboard Scientific Parties (1989) — Triassic to Cenozoic evolution of the NW Australian continental margin and the birth of the Indian Ocean. *Geologisches Rundschau*, 78(3), 1189-1210.

von Stackelberg, U., Exon, N.F., von Rad, U., Quilty, P., Shafik, S., Beiersdorf, H., Seibertz, E., & Veevers, J.J., 1980 — Geology of the Exmouth and Wallaby Plateaus off northwest Australia: sampling of seismic sequences. *BMR Journal of Australian Geology & Geophysics*, 5, 113–140.

Williamson, P.E., Exon, N.F., Haq, B., von Rad, U., & Leg 122 Shipboard Scientific Party, 1989 — A Northwest Shelf Triassic reef play: results from ODP Leg 122. *The APEA Journal*, 29(1), 328–344.

BMR Journal of Australian Geology & Geophysics, 11, 473–497

The Maastrichtian and early Tertiary record of the Great Australian Bight Basin and its onshore equivalents on the Australian southern margin: a nannofossil study

Samir Shafik[1]

Samples dredged during BMR Survey 66 by R.V. *Rig Seismic* in the central Great Australian Bight Basin are examined and their calcareous nannofossils are recorded. The Maastrichtian, Eocene and Oligocene assemblages are compared with those known from the onshore southern Australian sequence, allowing a better understanding of the history of the southern margin of Australia. The Maastrichtian assemblages, the first found in southern Australia, probably represent a marine ingression encompassing three discernible phases. The Eocene record includes assemblages older than any from onshore and is also older than the base of the Eocene section on the Naturaliste Plateau. An offset parallelism with the onshore record is evident: in the offshore (Great Australian Bight) sequence, early Eocene ingressions preceded a middle Eocene transgression, while in the onshore Otway Basin (to the east) middle Eocene ingressions preceded a late Eocene transgression. In both sequences there are earlier Tertiary ingressions which were suited for calcareous foraminiferids but apparently not coccolith-forming nannoplankton. The previously reported excursion of the low-latitude *Sphenolithus ciperoensis* into southern Australia in the Oligocene is confirmed, being a result of a 'short' warm episode. Surface waters along the southern margin of Australia were warmer in the west than in the east during much of the Eocene and Oligocene. This is attributed to a warm intermittent 'proto-Leeuwin Current', beginning in the middle Eocene, which brought warm surface waters from northwestern Australia into southern Australia. Dilution of the current's effects on the surface waters of southern Australia would be expected in an easterly direction. Nannofossil evidence, supported by palynological and lithological data, suggests that the seafloor in the Great Australian Bight Basin has subsided considerably since the Late Cretaceous. The onset of the increase in rate of subsidence in the middle Eocene (as reflected by the nannofossil assemblages) marked the end of a stage of very slow subsidence initiated at about 90 Ma ago. The assemblages provide strong evidence for a marked fall in sea level during the latest late Eocene, at a rate considerably higher than that of subsidence, resulting in shoaling well into the Oligocene.

Introduction

Optical microscopic examination of calcareous nannofossils extracted from samples dredged during BMR Survey 66 by R.V. *Rig Seismic* in the central Great Australian Bight Basin (Fig. 1) was carried out primarily for dating (Shafik, 1988a,b). Only the better preserved and less reworked assemblages are considered here. These are Maastrichtian, Eocene and Oligocene, and include assemblages previously unknown from southern Australia. These assemblages, arranged in a chronological order, together with a hitherto unknown Eocene assemblage from Potoroo No.1 well (Fig. 1), help reveal the history of marine sedimentation during the Eocene in the Great Australian Bight Basin. Previously, the temporal distribution of calcareous nannofossil assemblages in the Eocene of the onshore southern margin (Eucla and Otway Basins) was used by Shafik (1973, 1983, 1985) to indicate patterns of marine sedimentation which could be translated in terms of marine ingressions and transgressions. The term 'ingression' is used to denote a short-lived marine invasion, with either good or restricted access to the open sea. Isolated calcareous microplanktic assemblages (nannofossils and/or foraminiferids) bracketed by barren intervals in the middle Eocene of the Otway Basin are used to indicate such marine ingressions.

The distribution of modern nannoplankton seems to be primarily controlled by temperature (see, for example, McIntyre & Bé, 1967; Okada & Honjo, 1973; Ruddiman & McIntyre, 1976), although the supply of nutrients is an equally important factor. Thus, indications of palaeotemperatures of surface waters during earlier times (e.g. Late Cretaceous and Tertiary) could be based on the presence of certain key taxa whose known geographic distribution suggests narrow latitudinal preference. The presence of a species whose geographic distribution is largely limited to the tropics, for example, would indicate warm surface waters or location within the tropical belt.

Lithologically, the samples studied reflect conditions transitional from non-marine or marginal marine terrigenous sedimentation during most of the Maastrichtian–mid-Eocene interval, to marine carbonate accumulation during the middle Eocene and onward.

During BMR Survey 66, several submarine canyons were identified cutting into the continental slope of the Great Australian Bight. Because most of these have not been named, letters of the alphabet have been used to differentiate them. Sampling sites in the canyons are indicated in Figure 1, which also shows the seafloor morphology of the Great Australian Bight Basin as a wide continental shelf with gently sloping terraces extending from the shelf edge.

Documentation of dredged assemblages

Most of the species identified in this study are illustrated in Figures 2–7. Their negatives are deposited in the Commonwealth Palaeontological Collection (CPC), Bureau of Mineral Resources, Canberra. The Eocene assemblages examined are placed against a set of nannofossil biostratigraphic events (Fig. 8), rather than against a particular formal nannofossil zonal scheme. This permits the use of nannofossil biostratigraphic events not restricted to one zonation. Thus the practice of describing a 'suitable' zonation based on more than one published zonation is not favoured here. Correlation with the low-latitude planktic foraminiferal P zones of Berggren (1969) and Blow (1969, 1979) is attempted wherever possible, in common with established local foraminiferal practice (see, for example, McGowran, 1978, 1988a,b).

Figure 8 also summarises sequences on the Naturaliste Plateau and on the onshore southern margin of Australia (the Eucla and Otway Basins) as based on the work of Shafik (1983, 1985).

Maastrichtian

Siliciclastic sediments of this age were dredged from two stations, 66DR01 and 66DR03, at the northwestern wall of Canyon B which is located at the junction of the Eyre and Ceduna Terraces (Fig. 1). Three assemblages (A, B and C, below) were recognised.

[1] Marine Geoscience & Petroleum Geology Program, Bureau of Mineral Resources, GPO Box 378, Canberra ACT 2601

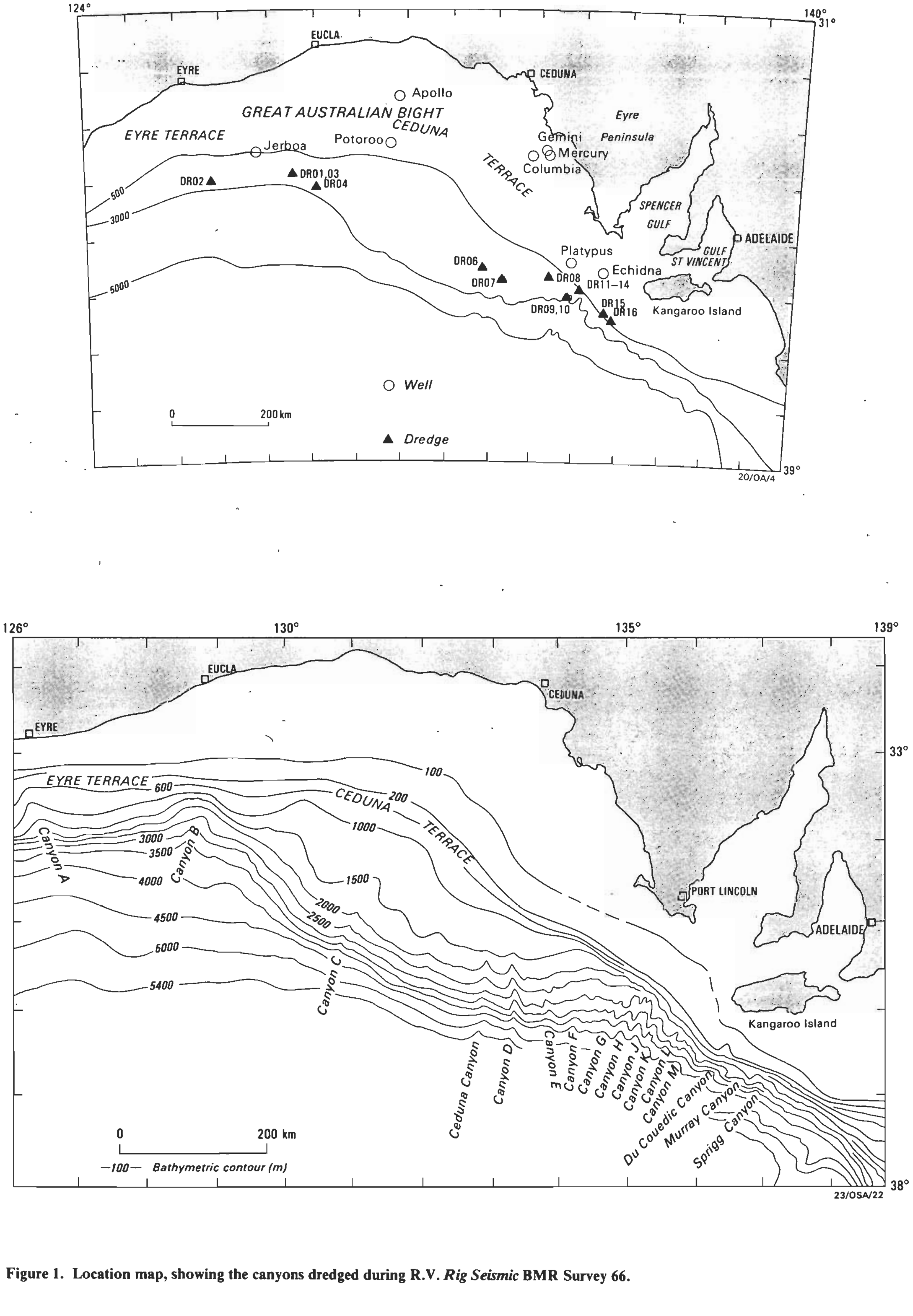

Figure 1. Location map, showing the canyons dredged during R.V. *Rig Seismic* BMR Survey 66.

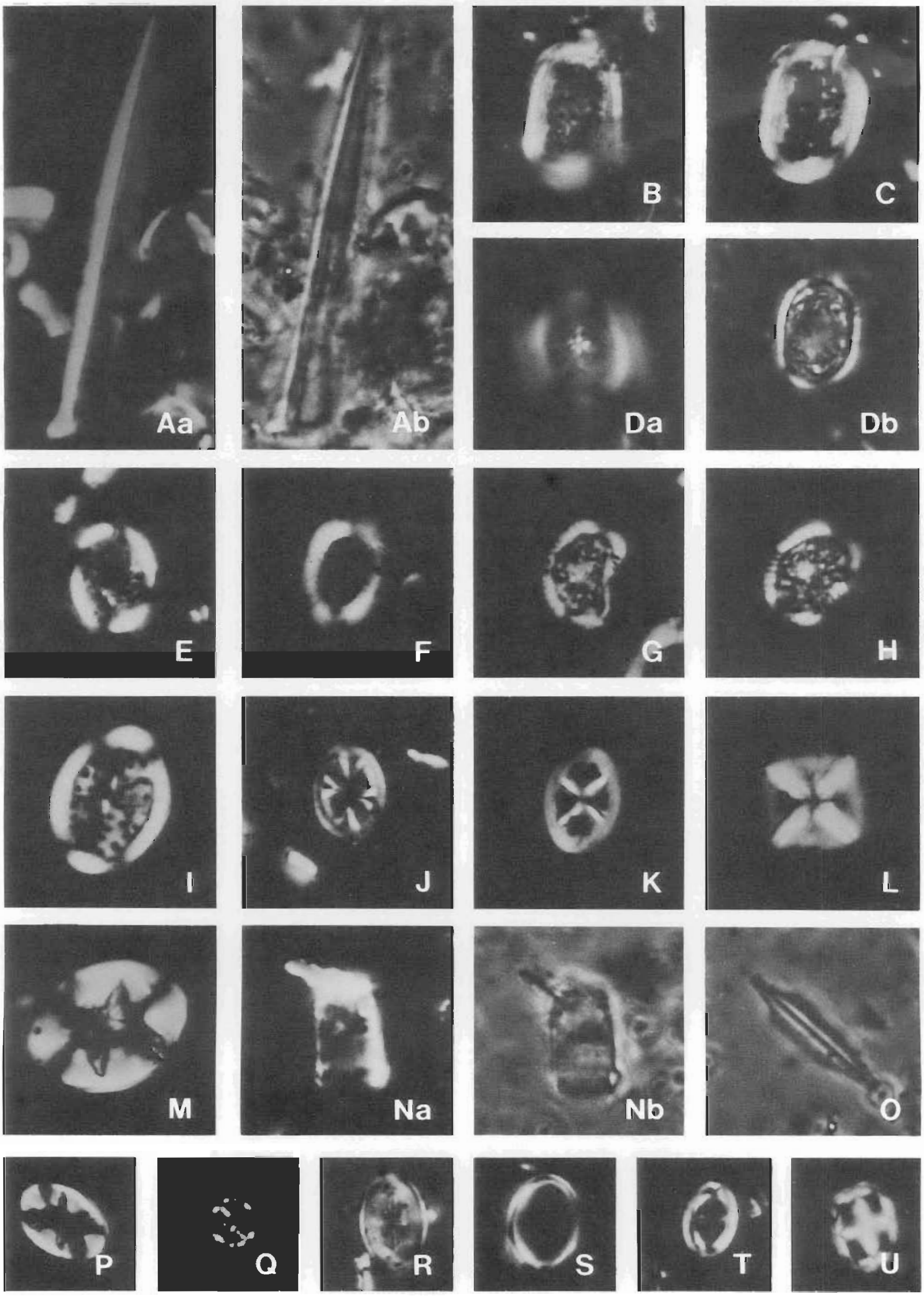

Figure 2. Optical microscopic micrographs of Maastrichtian nannofossils from Canyon B in the central Great Australian Bight Basin. Except for specimen I, which is from 66DR01F, all specimens are from 66DR03A.

Aa, Ab, *Lucianorhabdus* sp. cf. *L. cayeuxii* Deflandre, CPC 28615; **B, C**, *Cribrosphaerella daniae* Perch-Nielsen, B, CPC 28616, C, CPC 28617; **Da, Db**, *Nephrolithus corystus* Wise with two parallel sides, CPC 28618; **E**, *Teichorhabdus ethmos* Wind & Wise, CPC 28619; **F**, *Grantarhabdus camaratus* (Bukry), CPC 28732; **G, H**, *Nephrolithus corystus* Wise (kidney-shaped), G, CPC 28620, H, CPC 28621; **I**, *Arkhangelskiella speciallata* Vekshina, CPC 28634; **J**, *Ahmuellerella octoradiata* (Gorka), CPC 28622; **K**, *Chiastozygus litterarius* (Gorka), CPC 28623; **L**, *Micula staurophora* (Gardet), CPC 28624; **M, P**, *Eiffellithus turriseiffeli* (Deflandre), M, CPC 28625, P, CPC 28626; **Na, Nb**, *Lapideacassis cornuta* (Forchheimer & Stradner), CPC 28627; **O**, *Lithraphidites praequadratus* Roth, CPC 28628; **Q**, *Corollithion exiguum* Stradner, CPC 28629; **R**, *Gartnerago* sp., CPC 28630; **S**, *Kamptnerius magnificus* Deflandre with its asymmetric rim flange preserved but not its central cover, CPC 28631; **T**, *Placozygus fibuliformis* (Reinhardt), CPC 28632; **U**, *Prediscosphaera spinosa* (Bramlette & Martini), CPC 28633. All specimens ×2000.

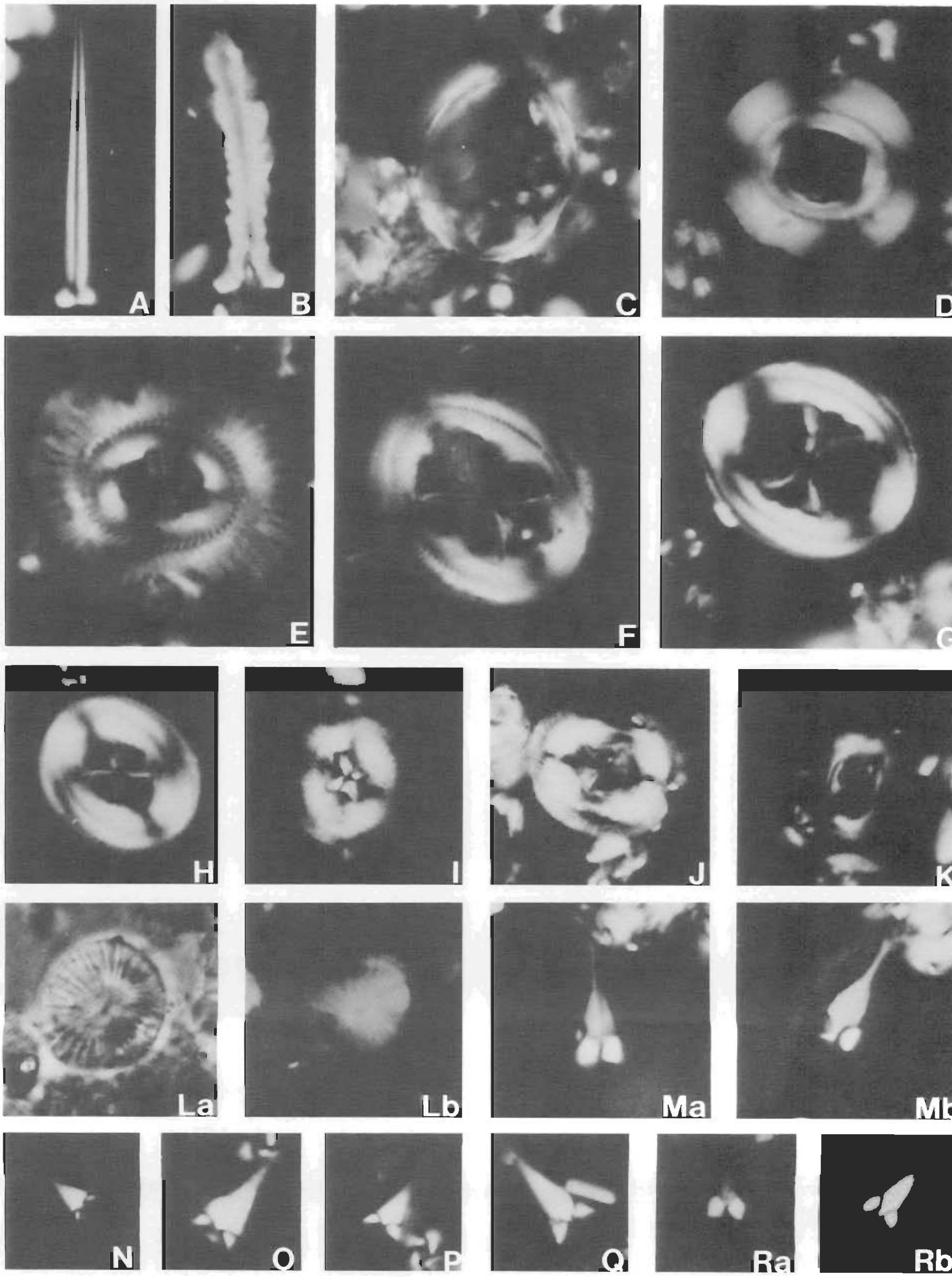

Figure 3. Optical microscopic micrographs of nannofossil taxa from the Eocene of Potoroo No.1 well and Eocene-Oligocene dredges in the central Great Australian Bight Basin.

A, *Blackites tenuis* (Bramlette & Sullivan), CPC 28641 from 66DR14B; **B**, *Zygrhablithus bijugatus bijugatus* (Deflandre), CPC 28642 from 66DR14B; C, *Reticulofenestra oamaruensis* (Deflandre), CPC 28643 from 66DR14B; **D**, *Reticulofenestra umbilica* (Levin), CPC 2864 from 66DR14A(5); **E**, *Chiasmolithus gigas* (Bramlette & Sullivan), CPC 28645 from 66DR01D; **F**, *Chiasmolithus grandis* (Bramlette & Riedel), CPC 28646 from 66DR01D; **G**, *Chiasmolithus oamaruensis* (Deflandre), CPC 28647 from 66DR01A; **H**, *Chiasmolithus altus* Bukry & Percival, CPC 28648 from 66DR06B; **I**, *Chiasmolithus consuetus* (Bramlette & Sullivan), CPC 28649 from 66DR08A; **J**, *Chiasmolithus solitus* (Bramlette & Sullivan), CPC 28650 from 66DR08A; **K**, *Campylosphaera dela* (Bramlette & Sullivan), CPC 28651 from 66DR08A; **La, Lb**, *Striatococcolithus pacificanus* Bukry & Percival, CPC 28652 from Potoroo No.1 at 945.5 m; **Ma, Mb, Ra, Rb**, *Sphenolithus ciperoensis* Bramlette & Wilcoxon, M, CPC 28635, R, CPC 28636, both from 66DR06B; **N, O**, *Sphenolithus predistentus* Bramlette & Wilcoxon, N, CPC 28637, O, CPC 28638, both from 66DR12B; **P, Q**, *Sphenolithus distentus* Bramlette & Wilcoxon, P, CPC 28639, Q, CPC 28640, both from 66DR12B. All specimens ×2000.

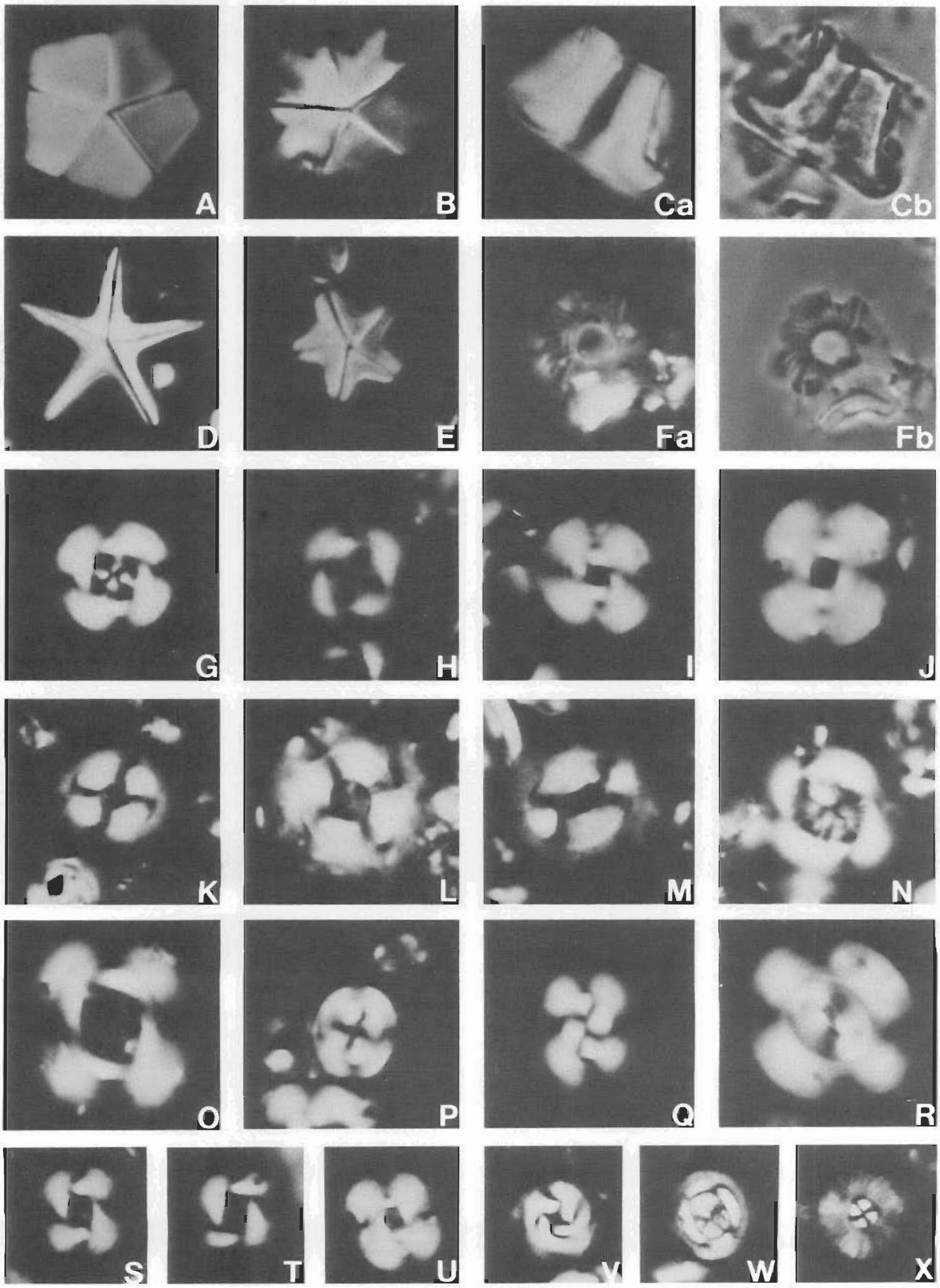

Figure 4. Optical microscopic micrographs of nannofossil taxa from the Eocene of Potoroo No.1 well, and Eocene-Oligocene dredges in the central Great Australian Bight Basin.

A, *Braarudosphaera bigelowii* (Gran & Braarud), CPC 28653 from Potoroo No.1 at 945.5 m; **B**, *Micrantholithus bramlettei* Deflandre, CPC 28654 from Potoroo No.1 at 945.5 m; **Ca, Cb**, *Micrantholithus altus* Bybell & Gartner, CPC 28655 from Potoroo No.1 at 945.5 m; **D**, *Micrantholithus attenuatus* Bramlette & Sullivan, CPC 28656 from Potoroo No.1 at 945.5; **E**, *Micrantholithus pinguis* Bramlette & Sullivan, CPC 28657 from Potoroo No.1 at 945.5 m; **Fa, Fb**, *Pedinocyclus larvalis* (Bukry & Bramlette), CPC 28658 from 66DR14B; **G, H**, *Cyclicargolithus reticulatus* (Gartner & Smith), G, CPC 28659 from 66DR01A, H, CPC 28660 from 66DR14A(5); **I, J**, *Cyclicargolithus abisectus* (Müller), I, CPC 28661, J, CPC 28662, both from 66DR06B; **K, L**, *Coccolithus formosus* (Kamptner), K, CPC 28663, L, CPC 28664, both from 66DR14B; **M**, *Coccolithus eopelagicus* (Bramlette & Riedel), CPC 28665 from 66DR01A; **N**, *Reticulofenestra hampdenensis* Edwards, CPC 28666 from 66DR14D; **O**, *Reticulofenestra umbilica* (Levin), CPC 28667 from 66DR14B; **P**, *Reticulofenestra orangensis* (Bukry) n. comb., CPC 28668 from 66DR01A; **Q**, *Reticulofenestra scrippsae* (Bukry & Percival), CPC 28669 from 66DR01A; **R**, *Reticulofenestra scissura* Hay & others, CPC 28670 from 66DR12B; **S, T**, *Reticulofenestra dictyoda* (Deflandre & Fert), S, CPC 28671, T, CPC 28672, both from Potoroo No.1 at 945.5 m; **U**, *Cyclicargolithus floridanus* (Roth & Hay), CPC 28673 from 66DR06B; **V**, *Cyclicargolithus gammation* (Bramlette & Sullivan), CPC 28675 from 66DR08A; **W**, *Clausicoccus cribellum* (Bramlette & Sullivan), CPC 28674 from 66DR06B; **X**, *Markalius* sp. transitional between *M. astroporus* (Stradner) and *M. inversus* (Deflandre), CPC 28676 from 66DR08A. All specimens ×2000.

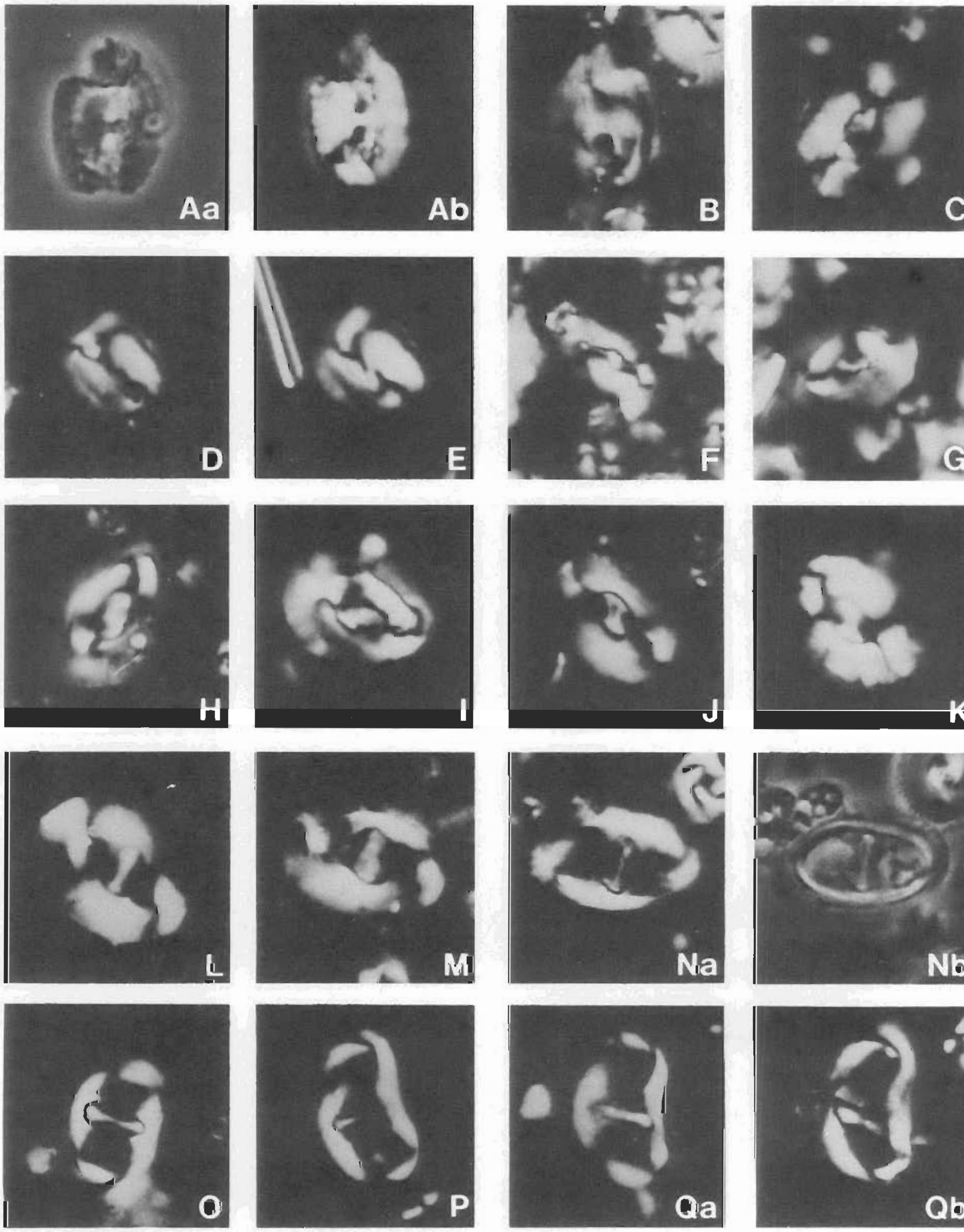

Figure 5. Optical microscopic micrographs of nannofossil taxa from the Eocene of Potoroo No.1 well and Eocene–Oligocene dredges in the central Great Australian Bight Basin.

Aa–B, *Helicosphaera recta* (Haq), A, CPC 28677, B, CPC 28678, both from 66DR06B; **C**, *Helicosphaera euphratis* Haq, CPC 28679 from 66DR06B; **D, E**, *Helicosphaera obliqua* Bramlette & Wilcoxon, D, CPC 28680, E, CPC 28681, both from 66DR12B; **F**, *Helicosphaera* sp., CPC 28682 from 66DR12B; G, *Helicosphaera heezenii* (Bukry), CPC 28683 from 66DR14A(5); **H, I**, *Helicosphaera* sp. aff. *H. reticulata* Bramlette & Wilcoxon, H, CPC 28684, I, CPC 28685, both from 66DR14A(5); **J, K**. *Helicosphaera* sp. cf. *H. bramlettei* (Müller) Jafar & Perch-Nielsen, J, CPC 28686 from 66DR10A, K, CPC 28687 from 66DR14B; **L, M**, *Helicosphaera seminulum* Bramlette & Sullivan, L, CPC 28688, M, CPC 28689, both from Potoroo No.1 at 945.5 m; **Na–O**, *Lophodolithus nascens* Bramlette & Sullivan, N, CPC 28690 from 66DR08A, O, CPC 28691 from Potoroo No.1 at 945.5 m; **P–Qb**, *Lophodolithus mochlophorus* Deflandre, P, CPC 28692 from Potoroo No.1 at 945.5 m, Q, CPC 28693 from 66DR08A. All specimens ×2000.

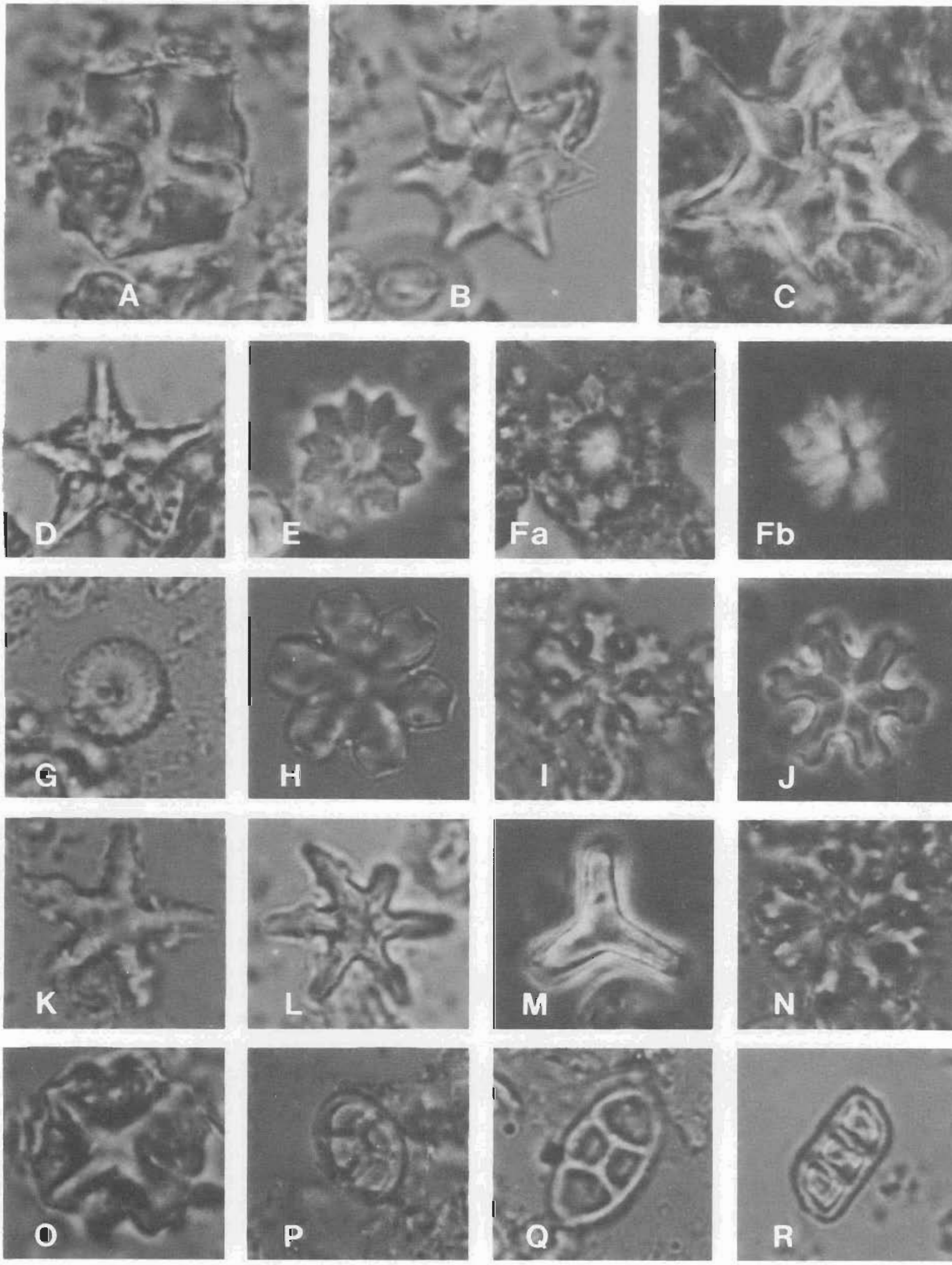

Figure 6. Optical microscopic micrographs of nannofossil taxa from the Eocene of Potoroo No.1 well and Eocene-Oligocene dredges in the central Great Australian Bight Basin.

A, O. *Nannotetrina pappi* (Stradner), A, CPC 28694, O, CPC 28695, both from 66DR01D; **B.** *Discoaster saipanensis* Bramlette & Riedel, CPC 28696 from 66DR01A; **C.** *Discoaster lodoensis* Bramlette & Riedel, CPC 28697 from Potoroo No.1 at 945.5 m; **D.** *Discoaster sublodoensis* Bramlette & Sullivan, CPC 28698 from Potoroo No.1 at 945.5 m; **E.** *Discoaster barbadiensis* Tan Sin Hok, CPC 28699 from 66DR01D; **Fa, Fb.** *Discoasteroides kuepperi* (Stradner), CPC 28700 from Potoroo No.1 at 945.5 m; **G.** *Discoaster delicatus* Bramlette & Sullivan, CPC 28701 from 66DR01D; **H–J.** *Discoaster deflandrei* Bramlette & Riedel 'group', H, CPC 28704 from 66DR06B, I, CPC 28702, J, CPC 28703, both from 66DR01D; **K, L.** *Discoaster tanii nodifer* Bramlette & Riedel, K, CPC 28705, L, CPC 28706, both from 66DR14D; **M.** *Tribrachiatus orthostylus* Shamarai, CPC 28707 from 66DR08A; **N.** *Discoaster gemmifer* Stradner, CPC 28709 from 66DR01D; **P, Q.** *Neococcolithes dubius* (Deflandre), P, CPC 28708 from 66DR08A, Q, CPC 28710 from 66DR01D; **R.** *Isthmolithus recurvus* Deflandre, CPC 28711 from 66DR14D. All specimens ×2000.

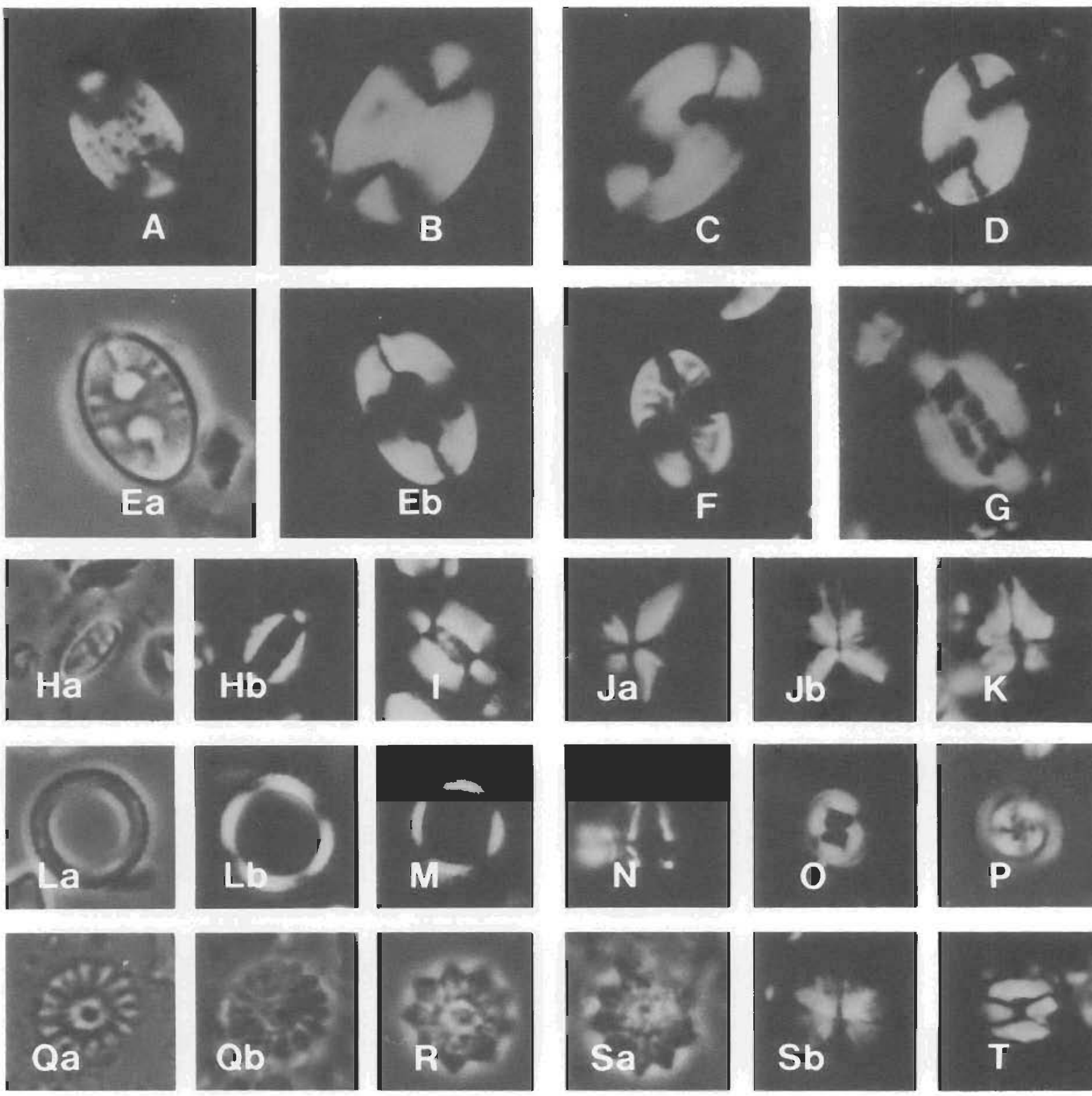

Figure 7. Optical microscopic micrographs of nannofossil taxa from the Eocene of Potoroo No.1 well and Eocene–Oligocene dredges in the central Great Australian Bight Basin.

A, *Pontosphaera multipora* (Kamptner) CPC 28712 from 66DR12B; **B**, *Pontosphaera plana* (Bramlette & Sullivan), CPC 28714 from 66DR08A; **C, D**, *Pontosphaera ocellata* (Bramlette & Sullivan), C, CPC 28713 from Potorooo No.1 at 945.5 m, D, CPC 28715 from 66DR08A; **Ea, Eb**, *Transversopontis pulcher* (Deflandre) CPC 28716 from 66DR08A; **F**, *Pontosphaera pectinata* (Bramlette & Sullivan), CPC 28717 from 66DR08A; **G–Hb**, *Ellipsolithus distichus* Bramlette & Sullivan, G, CPC 28718, H, CPC 28719 from 66DR08A; **I**, *Ellipsolithus lajollaensis* Bukry & Percival, CPC 28720 from 66DR08A; **Ja, Jb**, *Sphenolithus radians* Deflandre, CPC 28721 from Potoroo No.1 at 945.5 m; **K**, *Sphenolithus* sp., CPC 28722 from 66DR12B; **La, Lb**, *Coronocyclus nitescens* (Kamptner), CPC 28723 from 66DR06B; **M**, *Calcidiscus protoannulus* (Gartner), CPC 28724 from Potoroo No.1 at 945.5 m; **N**, *Amitha prolata* Shafik, CPC 28725 from 66DR12B; **O**, *Toweius callosus* Perch-Nielsen, CPC 28726 from Potoroo No.1 at 945.5 m; **P**, *Blackites spinulus* (Levin), CPC 28727 from 66DR12B; **Qa, Qb**, *Discoaster bifax* Bukry, CPC 28728 from 66DR01D; **R–Sb**, *Discoasteroides kuepperi* (Stradner), R, CPC 28729, S, CPC 28730, both from 66DR08A; **T**, *Lanternithus minutus* Stradner, CPC 28731 from 66DR08A. All specimens ×2000.

Assemblage A. Sample 66DR01H, a dark brown-black, highly organic silty mudstone, contained moderately preserved rare nannofossils representing a small number of taxa. This sample was collected from the same station as the highly fossiliferous sample 66DR01F (see below); at this station water depth today is 3280–2950 m. The assemblage is dominated by three species: *Arkhangelskiella speciallata, Micula staurophora* and *M. concava*. Other species represented are *Prediscosphaera cretacea* (frequent), *Markalius astroporus* (rare), *Cribrosphaerella daniae* (extremely rare), and *?Kamtpnerius magnificus* (fragment). The age is considered Maastrichtian on account of the age of the associated, and lithologically similar, sample 66DR01F (discussed below); the presence of *Cribrosphaerella daniae* supports this age assignment. This is confirmed by the co-occurring foraminiferids which are Maastrichtian in age (see McGowran, 1988).

Assemblage B. Sample 66DR03A, a glauconitic, petoidal, dark brown, organic rich silty mudstone, yielded a moderately preserved and highly diversified calcareous nannofossil

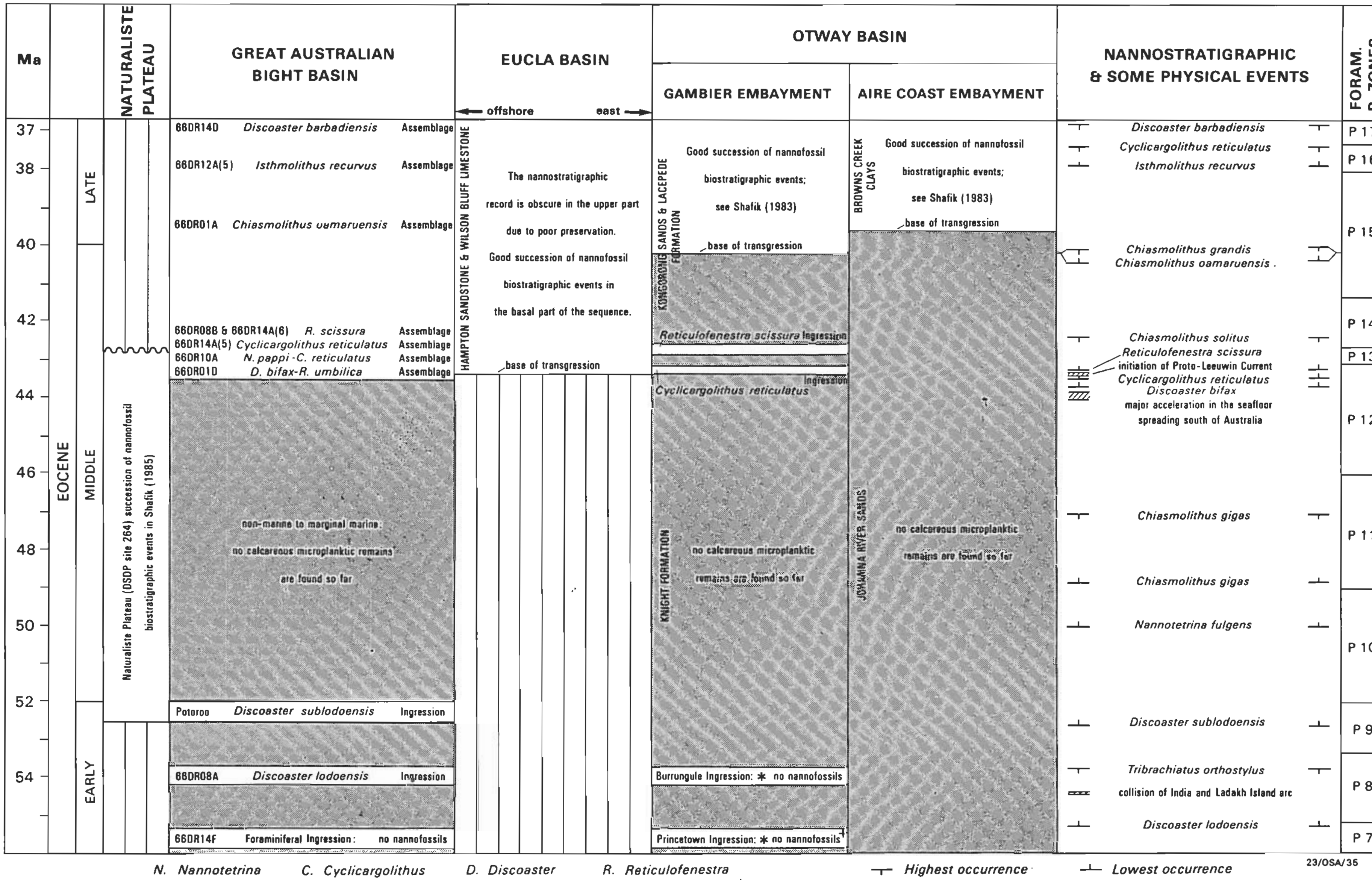

Figure 8. **Eocene calcareous nannofossil biostratigraphic events and some physical events pertinent to the stratigraphic evolution of the southern margin of Australia.**
Correlation of nannofossil events with the foraminiferal P zones and the time scale follows that suggested by Berggren & others (1985) where possible.
* Placement relative to the P zones is based on correlations by McGowran (1988b, in press).

assemblage. This sample was dredged from water depths of 3535–3390 m. The assemblage included:

Acuturris scotus (Risatti) Wind & Wise *in* Wise & Wind, 1977
Ahmuellerella octoradiata (Gorka) Reinhardt, 1967
Arkhangelskiella cymbiformis Vekshina, 1959
Arkhangelskiella speciallata Vekshina, 1959 (rare)
Biscutum notaculum Wind & Wise *in* Wise & Wind, 1977
Boletuvulum sp.
Chiastozygus litterarius (Gorka) Manivit, 1971
Corollithion exiguum Stradner, 1961
Corollithion rhombicum (Stradner & Adamiker) Bukry, 1969
Cretarhabdus conicus Bramlette & Martini, 1964
Cretarhabdus surirellus (Deflandre & Fert) Reinhardt, 1970
Cribrosphaerella daniae Perch-Nielsen, 1973
Cribrosphaerella ehrenbergii (Arkhangelsky) Deflandre, 1952
Eiffellithus turriseiffeli (Deflandre) Reinhardt, 1965
Gartnerago sp.
Grantarhabdus camaratus (Bukry) Wise, 1983
Kamptnerius magnificus Deflandre, 1959
Lapideacassis cornuta (Forchheimer & Stradner) Wind & Wise *in* Wise & Wind, 1977
Lithraphidites carniolensis Deflandre, 1963
Lithraphidites praequadratus Roth, 1978
Lithraphidites quadratus Bramlette & Martini, 1964
Lucianorhabdus sp. cf. *L. cayeuxii* Deflandre, 1959
Markalius astroporus (Stradner) Mohler & Hay *in* Hay & others, 1967
Microrhabdulus belgicus Hay & Towe, 1963
Micula concava (Stradner) Bukry, 1969
Micula staurophora (Gardet) Stradner, 1963
Nephrolithus corystus Wind, 1983
Nephrolithus sp. aff. *N. frequens* Gorka, 1957
Placozygus fibuliformis (Reinhardt) Hoffmann, 1970
Prediscosphaera cretacea (Arkhangelsky) Gartner, 1968
Prediscosphaera grandis Perch-Nielsen, 1979 (very rare)
Prediscosphaera spinosa (Bramlette & Martini) Gartner, 1968
Prediscosphaera stoveri (Perch-Nielsen) Shafik & Stradner, 1971
Rhagodiscus angustus (Stradner) Stradner *in* Stradner, Adamiker & Maresch, 1968
Rhagodiscus reniformis Perch-Nielsen, 1973
Scapholithus fossilis Deflandre *in* Deflandre & Fert, 1954
Stephanolithion laffittie Noel, 1957
Teichorhabdus ethmos Wind & Wise *in* Wise & Wind, 1977
Tetrapodorhabdus decorus Wind & Wise, 1983
Vekshinella elliptica Gartner, 1968
Watznaueria barnesae (Black) Perch-Neilsen, 1968

The key species *Nephrolithus corystus, Cribrosphaerella daniae* and *Arkhangelskiella cymbiformis* are particularly abundant, but *Lithraphidites quadratus* is rare. These species indicate a mid to late Maastrichtian age.

The overall aspect of the assemblage suggests high-latitude position and deposition in a neritic environment: *Watznaueria barnesae* is extremely rare, whereas *Nephrolithus corystus, Cribrosphaerella daniae, Micula concava, Ahmuellerella octoradiata* and *Kamptnerius magnificus* are particularly abundant. The high-latitude position is reinforced by the total lack of distinctly low-latitude species such as *Cribrocorona gallica* (Stradner) Perch-Nielsen, 1973.

Assemblage C. Sample 66DR01F, a pale green-beige silty sandstone including dark brown organic shale, contained another moderately preserved but less diverse nannofossil assemblage. This included:

Arkhangelskiella cymbiformis Vekshina, 1959
Arkhangelskiella speciallata Vekshina, 1959
Biscutum spp.
Chiastozygus litterarius (Gorka) Manivit, 1971
Cretarhabdus conicus Bramlette & Martini, 1971
Cretarhabdus surirellus (Deflandre & Fert) Reinhardt, 1970
Cribrosphaerella daniae Perch-Neilsen, 1973
Cribrosphaerella ehrenbergii (Arkhangelsky) Deflandre, 1952
Cyclogelosphaera reinhardtii (Perch-Nielsen) Roth, 1978
Eiffellithus turriseiffeli (Deflandre) Reinhardt, 1965
Gartnerago sp.
Grantarhabdus camaratus (Bukry) Wise, 1983
Kamptnerius magnificus Deflandre, 1959
Lithraphidites carniolensis Deflandre, 1963
Lithraphidites praequadratus Roth, 1978
Lithraphidites quadratus Bramlette & Martini, 1964
Markalius astroporus (Stradner) Hay & Mohler, 1967
Micula concava (Stradner) Bukry, 1969
Micula staurophora (Gardet) Stradner, 1963
Nephrolithus corystus Wise, 1983 (a single specimen)
Nephrolithus frequens Gorka, 1957
Placozygus fibuliformis (Reinhardt) Hoffmann, 1970
Prediscosphaera cretacea (Arkhangelsky) Gartner, 1968
Prediscosphaera grandis Perch-Nielsen, 1979 (very rare)
Prediscosphaera spinosa (Bramlette & Martini) Gartner, 1968
Prediscosphaera stoveri (Perch-Nielsen) Shafik & Stradner, 1971
Teichorhabdus ethmos Wind & Wise *in* Wise & Wind, 1977
Tetrapodorhabdus decorus (Deflandre) Wind & Wise, 1983
Watznaueria barnesae (Black) Perch-Nielsen, 1968

Like the Maastrichtian assemblage of 66DR03A, this assemblage includes several elements indicative of deposition in a neritic environment at high-latitude location; the sandstone/shale of 66DR01F was collected from water 3280–2950 m deep. The presence of typical *Nephrolithus frequens* suggests that it is late Maastrichtian and may be slightly younger than the assemblage of 66DR03A. Other differences between these two assemblages are worth mentioning: (a) *Arkhangelskiella speciallata*, frequent to common in 66DR03A, is very rare in 66DR01F, (b) *Nephrolithus corystus* is abundant in 66DR03A, but extremely rare in 66DR01F, and (c) *Teichorhabdus ethmos*, represented mainly by large specimens in 66DR03A, is much smaller in 66DR01F.

The assemblages of 66DR03A and 66DR01F compare with similar assemblages from the Perth Basin (Shafik, in press). They differ from the Miria Marl assemblage of the Carnarvon Basin (Shafik, in press) in containing elements which suggest a more southerly location and in lacking low-latitude species such as *Micula murus* (Martini) Bukry, 1973 and *Cribrocorona gallica* (Stradner) Perch-Nielsen, 1973.

Discussion. Deposition of 66DR01F and 66DR03A was in neritic environments (nearshore or shelf), as evidenced by the presence of species such as *Acuturris scotus, Kamptnerius magnificus, Lucianorhabdus* sp., *Ahmuellerella octoradiata* and *Arkhangelskiella cymbiformis*. The lithologies of these samples support deposition in a shallow-water environment. To account for the present water depth of 3535–2950 m in Canyon B (Fig. 1) where 66DR01F and 66DR03A were collected, considerable subsidence of the seafloor since the Late Cretaceous must be presumed. (The term 'subsidence' is used here to denote deepening as a net balance between subsidence of seafloor and eustatic movements, either rises or falls, in sea level). Interpretation of the depositional palaeoenvironment of sample 66DR01C, a dolomitic bioturbated intraclastic silty wackestone collected from the same station as 66DR01F, as possibly paralic (based on Coniacian to Santonian dinoflagellate; Alley, 1988) supports the subsidence viewpoint. Sample 66DR01C lacked calcareous microplanktic (nannofossil and foraminiferid) remains. Indeed, evidence is available from other dredge stations confirming subsidence of the seafloor of the Great Australian Bight Basin since the Late Cretaceous or early Tertiary. For example, sample 66DR12G, a very dark greyish-brown silty mudstone dredged from Canyon H at water depths of 3670–2720 m (Fig. 1) contained Paleocene pollens which suggested non-marine deposition (Alley, 1988); no calcareous microplanktic remains were found in this sample.

Eocene

Eight distinct calcareous nannofossil assemblages are recognised: one early Eocene, four middle Eocene and three late Eocene.

Early Eocene

Sample 66DR08A, a fine-grained yellow brown interbedded mudstone/sandstone from Canyon F on Ceduna Terrace (Fig. 1), contains abundant and moderately preserved calcareous nannofossils. Species identified are:

Blackites creber (Deflandre) Sherwood, 1974
Braarudosphaera bigelowii (Gran & Braarud) Deflandre, 1947 (very rare)
Calcidiscus protoannulus (Gartner) Loeblich & Tappan, 1978
Campylosphaera dela (Bramlette & Sullivan) Hay & Mohler, 1967
Chiasmolithus consuetus (Bramlette & Sullivan) Hay & Mohler, 1967 (very rare)
Chiasmolithus eograndis Perch-Nielsen, 1971 (small, rare)
Chiasmolithus expansus (Bramlette & Sullivan) Gartner, 1970
Chiasmolithus solitus (Bramlette & Sullivan) Locker, 1968
Clausicoccus cribellum (Bramlette & Sullivan) Prins, 1979
Coccolithus eopelagicus (Bramlette & Riedel) Bramlette & Sullivan, 1961
Coccolithus formosus (Kamptner) Wise, 1973
Coccolithus pelagicus (Wallich) Schiller, 1930
Cyclicargolithus gammation (Bramlette & Sullivan) n. comb. (basionym *Coccolithites gammation* Bramlette & Sullivan 1961, p. 152, pl. 7, figs 7a–c, 14a,b) (very rare)
Discoaster binodosus Martini, 1958 (very rare)
Discoaster lodoensis Bramlette & Riedel, 1954 (very rare)
Discoasteroides kuepperi (Stradner) Bramlette & Sullivan, 1961
Ellipsolithus distichus Bramlette & Sullivan, 1961
Ellipsolithus lajollaensis Bukry & Percival, 1971
Holodiscolithus macroporus (Deflandre) Roth, 1970
Lanternithus minutus Stradner, 1962
Lophodolithus mochlophorus Deflandre *in* Deflandre & Fert, 1954
Lophodolithus nascens Bramlette & Sullivan, 1961
Lophodolithus reniformis Bramlette & Sullivan, 1961
A species transitional between *Markalius astroporus* (Stradner) Hay & Mohler, 1967 and *M. inversus* (Deflandre) Bramlette & Martini, 1964
Micrantholithus vesper Deflandre, 1950
Neococcolithes dubius (Deflandre) Black, 1967
Neococcolites minutus (Perch-Nielsen) Perch-Nielsen, 1971
Pontosphaera ocellata (Bramlette & Sullivan) Perch-Nielsen, 1984
Pontosphaera pectinata (Bramlette & Sullivan) Sherwood, 1974
Pontosphaera plana (Bramlette & Sullivan) Haq, 1971
Pontosphaera versa (Bramlette & Sullivan) Sherwood, 1974
Scapholithus fossilis Deflandre *in* Deflandre & Fert, 1954
Sphenolithus moriformis (Brönnimann & Stradner) Bramlette & Wilcoxon, 1967
Sphenolithus primus Perch-Nielsen, 1971
Sphenolithus radians Deflandre *in* Grasse, 1952
Toweius callosus Perch-Nielsen, 1971
Toweius? crassus (Bramlette & Sullivan) Perch-Nielsen, 1984
Toweius? magnicrassus (Bukry) Romein, 1979
Transversopontis pulcher (Deflandre) Perch-Nielsen, 1967
Tribrachiatus orthostylus Shamarai, 1963
Zygodiscus adamas Bramlette & Sullivan, 1961
Zygrhablithus bijugatus bijugatus (Deflandre) Deflandre, 1959

The association of *Tribrachiatus orthostylus, Discoaster lodoensis, Discoasteroides kuepperi, Chiasmolithus solitus, Coccolithus formosus, Lophodolithus reniformis* and *Toweius callosus* indicates an early Eocene age. A correlation is suggested with the foraminiferal zonal interval late P7 to early P9 according to data in Martini (1971), or more precisely to the foraminiferal zone P8 according to data in Berggren & others (1985); the latter is adopted here. In Figure 8, this assemblage is referred to as the 66DR08A *Discoaster lodoensis* ingression.

The occurrence of the hemipelagic species *Zygrhablithus bijugatus bijugatus, Holodiscolithus macroporus, Micrantholithus vesper, Transversopontis pulcher* and several species of the genus *Pontosphaera* suggests deposition in a shallow-water environment (nearshore or shelf, possibly inner to middle neritic). Water depth at Station 66DR08 (in Canyon F, Fig. 1) is now 2826–2244 m. It is worth noting that several sediment samples from this station, 66DR08C, 66DR08D, 66DR08E and 66DR08F, which lack calcareous microplanktic remains, were found by Alley (1988) either to be totally barren or to contain late Paleocene and early Eocene pollens indicative of possible paralic to marginal marine environments. Considerable subsidence must have occurred since the Paleocene for these coastal and non-marine sediments to be now at water depths of more than 2200 m.

Middle Eocene

Assemblage A. Sample 66DR01D, from Canyon B (Fig. 1), contains abundant and well preserved calcareous nannofossils in a pale green-beige poorly sorted sandstone. Species identified are:

Blackites creber (Deflandre) Sherwood, 1974
Blackites tenuis (Bramlette & Sullivan) Sherwood, 1974
Calcidiscus protoannulus (Gartner) Loeblich & Tappan, 1978 (very rare)
Chiasmolithus expansus (Bramlette & Sullivan) Gartner, 1970
Chiasmolithus gigas (Bramlette & Sullivan) Radomski, 1968 (frequent)
Chiasmolithus grandis (Bramlette & Riedel) Radomski, 1968
Chiasmolithus solitus (Bramlette & Sullivan) Locker, 1968
Clausicoccus cribellum (Bramlette & Sullivan) Prins, 1979
Coccolithus eopelagicus (Bramlette & Riedel) Bramlette & Sullivan, 1961

Coccolithus formosus (Kamptner) Wise, 1973
Coccolithus pelagicus (Wallich) Schiller, 1930
Cyclicargolithus floridanus (Roth & Hay) Bukry, 1971
Discoaster barbadiensis Tan Sin Hok, 1927
Discoaster bifax Bukry, 1971
Discoaster deflandrei Bramlette & Riedel, 1954 'group'
Discoaster delicatus Bramlette & Sullivan, 1961
Discoaster gemmifer Stradner, 1961 (very rare)
Discoaster saipanensis Bramlette & Riedel, 1954
Discoaster tanii Bramlette & Riedel, 1954
Gartnerago sp. (rare)
Helicosphaera sp. (rare)
A species transitional between *Markalius astroporus* (Stradner) Hay & Mohler, 1967 and *M. inversus* (Deflandre) Bramlette & Martini, 1964
Nannotetrina pappi (Stradner) Perch-Nielsen, 1971
Neococcolithes dubius (Deflandre) Black, 1967
?*Reinhardtites* sp. (very rare)
Reticulofenestra dictyoda (Deflandre & Fert) Stradner, 1968
Reticulofenestra umbilica (Levin) Martini & Ritzkowski, 1968 (two sizes)
Transversopontis pulcher (Deflandre) Perch-Nielsen, 1967
Zygrhablithus bijugatus bijugatus (Deflandre) Deflandre, 1959

Discoaster barbadiensis is appreciably more common than *Discoaster saipanensis.* A few specimens of *Reticulofenestra scissura* Hay & others, 1967 were encountered, but in the absence of *Cyclicargolithus reticulatus* (Gartner & Smith) and because most other members of the assemblage are typical of a pre-*scissura* assemblage, they are thought to be contaminants. The association of *Reticulofenestra umbilica, Discoaster bifax, Chiasmolithus grandis, C. solitus* and *Discoaster barbadiensis* suggests a middle Eocene age (Gartner, 1971; Bukry, 1973) and a correlation with the foraminiferal mid to late zone P12 of the tropics according to data in Berggren & others (1985). This assemblage, referred to as the 66DR01D *Discoaster bifax-Reticulofenestra umbilica* assemblage in Figure 8, contains the obviously displaced Upper Cretaceous species of *Gartnerago* and ?*Reinhardtites*. Both *Chiasmolithus gigas* and *Nannotetrina pappi* could also be reworked from lower in the middle Eocene.

Deposition in shallow waters (?outer neritic environment) is indicated by the rare occurrence of *Transversopontis pulcher* and *Zygrhablithus bijugatus bijugatus.* Water depth today at Station 66DR01 is 3280–2950 m, and considerable subsidence must have occurred since the middle Eocene. Sample 66DR01I from the same station, which contains no calcareous microplanktic remains, yielded palynomorphs indicative of a late Paleocene marginal marine environment (see Alley, 1988). Upper Cretaceous sediments dredged from the same station include evidence for subsidence since probably the Coniacian (discussed above).

Assemblage B. Sample 66DR10A, a fine-grained limestone from water 3614–2925 m deep in Canyon G on Ceduna Terrace (Fig. 1), contains abundant and moderately preserved calcareous nannofossils. Species identified are:

Blackites creber (Deflandre) Sherwood, 1974
Blackites spinulus (Levin) Roth, 1970
Calcidiscus protoannulus (Gartner) Loeblich & Tappan, 1978
Chiasmolithus eograndis Perch-Nielsen, 1971
Chiasmolithus expansus (Bramlette & Sullivan) Gartner, 1970
Chiasmolithus grandis (Bramlette & Riedel) Radomski, 1968
Chiasmolithus solitus (Bramlette & Sullivan) Locker, 1968
Clausicoccus cribellum (Bramlette & Sullivan) Prins, 1979
Coccolithus eopelagicus (Bramlette & Riedel) Bramlette & Sullivan, 1961
Coccolithus formosus (Kamptner) Wise, 1973
Coccolithus pelagicus (Wallich) Schiller, 1930
Cyclicargolithus floridanus (Roth & Hay) Bukry, 1971
Cyclicargolithus reticulatus (Gartner & Smith) Bukry, 1971 (rare and poorly preserved)
Daktylethra punctulata Gartner *in* Gartner & Bukry, 1969
Discoaster barbadiensis Tan Sin Hok, 1927
Discoaster distinctus Martini, 1958
Discoaster saipanensis Bramlette & Riedel, 1954
Discoaster tanii Bramlette & Riedel, 1954
Helicosphaera seminulum Bramlette & Sullivan, 1961
Helicosphaera sp. cf. *H. bramlettei* (Müller) Jafar & Martini, 1975
A species transitional between *Markalius astroporus* (Stradner) Hay & Mohler, 1967 and *M. inversus* (Deflandre) Bramlette & Martini, 1964
Nannotetrina pappi (Stradner) Perch-Nielsen, 1971
Neococcolithes dubius (Deflandre) Black, 1967
Pontosphaera multipora (Kamptner) Roth, 1970 (very rare)
Reticulofenestra hampdenensis Edwards, 1973 (small)
Reticulofenestra umbilica (Levin) Martini & Ritzkowski, 1968 (two sizes)
Sphenolithus moriformis (Brönnimann & Stradner) Bramlette & Wilcoxon, 1967
Transversopontis pulcher (Deflandre) Perch-Nielsen, 1967
Trochaster simplex Klumpp, 1953
Zygrhablithus bijugatus bijugatus (Deflandre) Deflandre, 1959 (very rare)

The rare occurrence of *Cyclicargolithus reticulatus* in association with *Chiasmolithus solitus* and *C. grandis*, in the absence of *Reticulofenestra scissura*, suggests a mid middle Eocene age and a correlation with the foraminiferal late zone P12 (Shafik, 1978, 1983).

Deposition in shallow waters (?middle neritic environment) was indicated by the presence of *Daktylethra punctulata, Pontosphaera multipora* and *Zygrhablithus bijugatus bijugatus.* It is worth noting that sediments dredged from Canyon G (Fig. 1), at water depths similar to those at which 66DR10A was obtained, contain evidence suggesting subsidence since the Paleocene. A dark brown, pyritic, organic-rich, silty mudstone (66DR09C) contains pollen grains indicative of marginal marine conditions during the Paleocene–early Eocene at the site of Canyon G (Alley, 1988).

Discoasters in 66DR10A are relatively less abundant than in 66DR01D, suggesting slightly cooler surface waters for the assemblage from 66DR10A.

Nannotetrina pappi is probably a displaced species from a lower middle Eocene level. However, the taxa of 66DR10A are referred to in Figure 8 as the 66DR10A *Nannotetrina pappi-Cyclicargolithus reticulatus* assemblage.

Sample 66DR015B, a light greyish-brown calcareous siltstone from water 3394–2494 m deep at Canyon K on Ceduna Terrace, yielded a calcareous nannofossil assemblage similar to that of 66DR10A, except for the lack of *Nannotetrina pappi* and the presence of *Helicosphaera heezenii* (Bukry) Jafar & Martini, *H. compacta* Bramlette & Wilcoxon, *Orthozygus aureus* (Stradner) Bramlette & Wilcoxon, *Syracosphaera labrosa* Bukry & Bramlette, 1969 and more species of *Transversopontis*. Specimens of *Cyclicargolithus* *reticulatus* are small in the assemblage from 66DR015B, but undeniable.

Assemblage C. Sample 66DR14A(5), a light grey argillaceous limestone from Canyon J on Ceduna Terrace (Fig. 1), yielded calcareous nannofossils. These are abundant and moderately preserved, though their debris abounds. Species identified are:

- *Blackites spinulus* (Levin) Roth, 1970 (rare)
- *Calcidiscus protoannulus* (Gartner) Loeblich & Tappan, 1978
- *Chiasmolithus expansus* (Bramlette & Sullivan) Gartner, 1970
- *Chiasmolithus grandis* (Bramlette & Riedel) Radomski, 1968
- *Chiasmolithus solitus* (Bramlette & Sullivan) Locker, 1968
- *Clausicoccus cribellum* (Bramlette & Sullivan) Prins, 1979
- *Coccolithus eopelagicus* (Bramlette & Riedel) Bramlette & Sullivan, 1961
- *Coccolithus formosus* (Kamptner) Wise, 1973
- *Coccolithus pelagicus* (Wallich) Schiller, 1930
- *Cyclicargolithus floridanus* (Roth & Hay) Bukry, 1971
- *Cyclicargolithus reticulatus* (Gartner & Smith) Bukry, 1971
- *Discoaster barbadiensis* Tan Sin Hok, 1927
- *Discoaster saipanensis* Bramlette & Riedel, 1954
- *Discoaster* sp.
- *Discoaster tanii nodifer* Bramlette & Riedel, 1954
- *Helicosphaera heezenii* (Bukry) Jafar & Martini, 1975 (common)
- *Helicosphaera* sp. aff. *H. reticulata* Bramlette & Wilcoxon, 1967
- A species transitional between *Markalius astroporus* (Stradner) Hay & Mohler, 1967 and *M. inversus* (Deflandre) Bramlette & Martini, 1964 (very rare)
- *Neococcolithes dubius* (Deflandre) Black, 1967
- *Pontosphaera multipora* (Kamptner) Roth, 1970 (poorly preserved, very rare)
- *Reticulofenestra hampdenensis* Edwards, 1973
- *Reticulofenestra umbilica* (Levin) Martini & Ritzkowski, 1968
- *Sphenolithus moriformis* (Brönnimann & Stradner) Bramlette & Wilcoxon, 1967
- *Sphenolithus predistentus* Bramlette & Wilcoxon, 1967
- *Zygrhablithus bijugatus crassus* Locker, 1967 (rare)

This assemblage is middle Eocene in age, based on the co-occurrence of *Cyclicargolithus reticulatus* and *Chiasmolithus grandis*, and the absence of *Reticulofenestra scissura* (Shafik, 1978). It correlates with the foraminiferal late zone P12 of the tropics (Shafik, 1978, 1983). Abundant *C. reticulatus* suggests that the assemblage is slightly younger than the assemblages from 66DR10A and 66DR15B; the latter can probably be placed very close to the appearance (lowest occurrence) datum of *Cyclicargolithus reticulatus* (Shafik, 1973), with the 66DR14A(5) assemblage at a slightly higher stratigraphic level. This assemblage is referred to as the 66DR14A(5) *Cyclicargolithus reticulatus* assemblage in Figure 8.

The scarcity of *Pontosphaera multipora* and *Zygrhablithus bijugatus crassus* and the absence of other indicators of shallow-water deposition (neritic environment) — such as *Daktylethra punctulata* and *Transversopontis pulcher*, which are present in the assemblages from 66DR10A and 66DR15B — suggest deposition in deeper waters, probably on the outer shelf or upper continental slope. A comparison of the diversity and abundance of shallow-water indicators in the assemblages from 66DR10A and 66DR15B with those in the slightly younger assemblage from 66DR14A(5) shows noticeable deepening during the middle Eocene biostratigraphic interval bracketed by the lowest occurrences of *Cyclicargolithus reticulatus* and *Reticulofenestra scissura* in the Great Australian Bight Basin. Present water depth at Station 66DR14 is 3064–2627 m.

Assemblage D. Sample 66DR08B, a fine-grained yellow-green carbonate mudstone from Canyon F (Fig. 1), contains abundant and moderately preserved calcareous nannofossils. Taxa identified are:

- *Amitha prolata* Shafik, 1989
- *Blackites tenuis* (Bramlette & Sullivan) Sherwood, 1974
- *Calcidiscus protoannulus* (Gartner) Loeblich & Tappan, 1978
- *Chiasmolithus expansus* (Bramlette & Sullivan) Gartner, 1970
- *Chiasmolithus grandis* (Bramlette & Riedel) Radomski, 1968
- *Chiasmolithus solitus* (Bramlette & Sullivan) Locker, 1968
- *Coccolithus eopelagicus* (Bramlette & Riedel) Bramlette & Sullivan, 1961
- *Coccolithus formosus* (Kamptner) Wise, 1973
- *Coccolithus pelagicus* (Wallich) Schiller, 1930
- *Cyclicargolithus floridanus* (Roth & Hay) Bukry, 1971
- *Cyclicargolithus reticulatus* (Gartner & Smith) Bukry, 1971
- *Discoaster barbadiensis* Tan Sin Hok, 1927
- *Discoaster saipanensis* Bramlette & Riedel, 1954
- *Discoaster tanii* Bramlette & Riedel, 1954
- *Lanternithus minutus* Stradner, 1962 (rare, poorly preserved)
- A species transitional between *Markalius astroporus* (Stradner) Hay & Mohler, 1967 and *M. inversus* (Deflandre) Bramlette & Martini, 1964
- *Neococcolithes dubius* (Deflandre) Black, 1967
- *Reticulofenestra scissura* Hay & others, 1966 (small & rare)
- *Reticulofenestra scrippsae* (Bukry & Percival) Roth, 1973
- *Reticulofenestra umbilica* (Levin) Martini & Ritzkowski, 1968
- *Sphenolithus moriformis* (Brönnimann & Stradner) Bramlette & Wilcoxon, 1967
- *Sphenolithus predistentus* Bramlette & Wilcoxon, 1967
- *Zygrhablithus bijugatus bijugatus* (Deflandre) Deflandre, 1959

The association of *Reticulofenestra scissura, Cyclicargolithus reticulatus* and *Chiasmolithus grandis* suggests a later middle Eocene age and, in the absence of *Daktylethra punctulata*, may correlate with the foraminiferal zone P14 (according to data in Shafik, 1983). The holococcolith *Daktylethra punctulata* is usually absent from oceanic sediments as it is solution-prone, and thus its absence can be biostratigraphically unreliable. However, the presence of other holococcoliths in the assemblage (see below) suggests that the absence of *D. punctulata* may not be due to its dissolution.

Deposition was in outer neritic waters as indicated by the rare occurrence of only two holococcoliths, *Lanternithus minutus* and *Zygrhablithus bijugatus bijugatus*; poor preservation (recrystallisation) of *L. minutus* may account for its scarcity. In comparison with the lower Eocene assemblage from the same dredge haul (66DR08A), the younger (middle Eocene) assemblage from 66DR08B contains fewer species characteristic of neritic water masses. This suggests deposition at greater depth than during the early Eocene. Water depth at Station 66DR08 (in Canyon F on Ceduna Terrace, Fig. 1) is 2826–2244 m. Evidence for subsidence since the Paleocene is given above, based on other samples from the same dredge station at Canyon F.

Sample 66DR14A(6), a light grey argillaceous limestone from water 3064–2627 m deep in Canyon J, yielded a middle Eocene nannofossil assemblage similar to that from 66DR08B: abundant *Cyclicargolithus reticulatus*, common *Helicosphaera reticulata* and rare, small, *Reticulofenestra scissura*. Indicators of shallow-water deposition are rare; the presence of *Zygrhablithus bijugatus* suggests an outer neritic or bathyal environment. The assemblage from 66DR14A(6) differs, however, in containing *Daktylethra* sp. cf. *D. punctulata*. Shafik (1983) used the highest occurrence of typical *D. punctulata* in Otway Basin sections as a biostratigraphic datum high in the foraminiferal zone P13. In Figure 8, the assemblages from 66DR08B and 66DR14A(6) are tentatively considered equivalents, and are placed against the foraminiferal zone P14.

Late Eocene

Assemblage A. Sample 66DR01A, a fine-grained white chalk, dredged from Canyon B between the Eyre and Ceduna Terraces (Fig. 1), yielded a rich nannofossil assemblage. This included:

Blackites spp. (stems)
Bramletteius serraculoides Gartner, 1969 (rare)
Chiasmolithus altus Bukry & Percival, 1971
Chiasmolithus oamaruensis (Deflandre) Hay & others, 1966 (common)
Clausicoccus cribellum (Bramlette & Sullivan) Prins, 1979
Coccolithus eopelagicus (Bramlette & Riedel) Bramlette & Sullivan, 1961
Coccolithus formosus (Kamptner) Wise, 1973
Cyclicargolithus floridanus (Roth & Hay) Bukry, 1971
Cyclicargolithus reticulatus (Gartner & Smith) Bukry, 1971
Discoaster barbadiensis Tan Sin Hok, 1927 (very rare)
Discoaster saipanensis Bramlette & Riedel, 1954 (frequent)
Markalius inversus (Deflandre) Bramlette & Martini, 1964 (very rare)
?*Reticulofenestra hampdenensis* Edwards, 1973
Reticulofenestra orangensis (Bukry) n. comb. (basionym *Coccolithus? orangensis* Bukry, 1971, p. 312, pl. 2, fig. 10; pl. 3, figs 1–3)
Reticulofenestra scissura Hay & others, 1966
Reticulofenestra scrippsae (Bukry & Percival) Roth, 1973
Reticulofenestra umbilica (Levin) Martini & Ritzkowski, 1968
Sphenolithus moriformis (Brönnimann & Stradner) Bramlette & Wilcoxon, 1967

Based on the presence of *Chiasmolithus oamaruensis, Discoaster barbadiensis, D. saipanensis* and *Cyclicargolithus reticulatus* in the absence of *Isthmolithus recurvus*, the age of the assemblage is early late Eocene (Gartner, 1971; Shafik, 1973, 1983). Based on the same evidence, a correlation with a position low within the foraminiferal zone P15 (according to Shafik, 1983) or with the zonal interval P15–early P16 (according to Berggren & others, 1985) can also be made. This assemblage is referred to as the 66DR01A *Chiasmolithus oamaruensis* assemblage in Figure 8, where it is placed against the foraminiferal mid zone P15.

There are appreciably more specimens of the genus *Chiasmolithus* than of the genus *Discoaster*, suggesting cooler surface waters than earlier in the mid middle Eocene.

Deposition in deep waters (probably on the continental slope) is suggested by the rare occurrence of the oceanic *Bramletteius serraculoides* and by the lack of indicators of shallow-water deposition (such as *Lanternithus minutus*). Present water depth at Station 66DR01 (in Canyon B, Fig. 1) is 3280–2950 m. Evidence from the same station (see above) suggests that subsidence must have occurred since the Coniacian, and the assemblages of the upper Eocene (66DR01A) and the middle Eocene (66DR01D) are in harmony with that evidence. Thus, indicators of shallow-water (neritic environment) deposition, although few in number of species, are present in the middle Eocene (66DR01D) but absent from the upper Eocene (66DR01A). Subsidence, being first noticeable in middle Eocene nannofossils, seems to have continued on and, by the late Eocene, Station 66DR01 was on the continental slope (bathyal environment). Table 1 summarises the depositional palaeoenvironments of sediments sampled at this station.

Table 1. Depositional palaeoenvironments of samples from dredge 66DR01, showing deepening with time as an effect of a possible increase in the rate of subsidence of the seafloor of the Great Australian Bight during the middle Eocene.

Age	*Sample*	*Depositional palaeoenvironment*
Late Eocene	66DR01A	bathyal (continental slope)
Middle Eocene	66DR01D	outer neritic (outer shelf)
Early Eocene		not represented
Paleocene	66DR01I	marginal marine
Maastrichtian	66DR01F	(?middle) neritic (marine ingression)
Maastrichtian	66DR01H	(?inner) neritic (marine ingression)
Coniacian–Santonian	66DR01C	possibly paralic

Assemblage B. Sample 66DR12A(5), a fine-grained limestone from Canyon H (Fig. 1), yielded a poorly preserved calcareous nannofossil assemblage which is characterised by the presence of the taxa:

Chiasmolithus altus Bukry & Percival, 1971
Chiasmolithus oamaruensis (Deflandre) Hay & others, 1966
Coccolithus formosus (Kamptner) Wise, 1973
Coccolithus pelagicus (Wallich) Schiller, 1930
?*Cyclicargolithus reticulatus* (Gartner & Smith) Bukry, 1971
Discoaster saipanensis Bramlette & Riedel, 1954
Helicosphaera compacta Bramlette & Wilcoxon, 1967
Isthmolithus recurvus Deflandre *in* Deflandre & Fert, 1954
Markalius inversus (Deflandre) Bramlette & Martini, 1964
Pontosphaera spp.
Reticulofenestra hampdenensis Edwards, 1973
Reticulofenestra orangensis (Bukry) n. comb.
Reticulofenestra scissura Hay & others, 1966
Reticulofenestra umbilica (Levin) Martini & Ritzkowski, 1968
Sphenolithus moriformis (Brönnimann & Stradner) Bramlette & Wilcoxon, 1967
Transversopontis zigzag Roth & Hay *in* Hay & others, 1967
Zygrhablithus bijugatus bijugatus (Deflandre) Deflandre, 1959

The overlap in the ranges of *Discoaster saipanensis* and *Isthmolithus recurvus* indicates a late Eocene age (Martini, 1971; Gartner, 1971; Shafik, 1973). Identification of *Cyclicargolithus reticulatus* is doubtful, and the presence of this species is critical to accurately pointing the age and evaluating correlation with the foraminiferal P zones (Shafik, 1973). *C. reticulatus* would suggest correlation with the foraminiferal zonal interval late P15–early P16 (Shafik, 1983). Its absence may suggest a later Eocene age and correlation near the P16/P17 zonal boundary. This assemblage, being correlated within the foraminiferal P16 zone, is referred to as the 66DR12A(5) *Isthmolithus recurvus* assemblage in Figure 8.

Deposition of 66DR12A(5) was in a neritic environment, as evidenced by the presence of species of the genera *Pontosphaera, Transversopontis* and *Zygrhablithus*. Water depth at Station 66DR12 is now 3670–2720 m. Evidence of non-marine Paleocene sediment from the same dredge station (sample 66DR12G; Alley, 1988) has been cited above to suggest that subsidence/deepening must have occurred since the Paleocene.

Assemblage C. Sample 66DR14D, a light brownish-grey limestone from Canyon J (Fig. 1), yielded moderately preserved nannofossils, including:

- *Blackites tenuis* (Bramlette & Sullivan) Sherwood, 1974
- *Chiasmolithus altus* Bukry & Percival, 1971
- *Chiasmolithus oamaruensis* (Deflandre) Hay & others, 1966
- *Clausicoccus cribellum* (Bramlette & Sullivan) Prins, 1979
- *Coccolithus eopelagicus* (Bramlette & Riedel) Bramlette & Sullivan, 1961
- *Coccolithus formosus* (Kamptner) Wise, 1973
- *Coccolithus pelagicus* (Wallich) Schiller, 1930
- *Discoaster barbadiensis* Tan Sin Hok, 1927
- *Discoaster saipanensis* Bramlette & Riedel, 1954
- *Discoaster tanii* Bramlette & Riedel, 1954
- *Discoaster tanii nodifer* Bramlette & Riedel, 1954 (frequent)
- *Helicosphaera heezenii* (Bukry) Jafar & Martini, 1975
- *Holodiscolithus macroporus* (Deflandre) Roth, 1970 (very rare)
- *Isthmolithus recurvus* Deflandre *in* Deflandre & Fert, 1954
- *Markalius inversus* (Deflandre) Bramlette & Martini, 1964
- *Pedinocyclus larvalis* (Bukry & Bramlette) Loeblich & Tappan, 1973
- *Pontosphaera multipora* (Kamptner) Roth, 1970 (single specimen, corroded)
- *Reticulofenestra hampdenensis* Edwards, 1973
- *Reticulofenestra orangensis* (Bukry) n. comb.
- *Reticulofenestra scissura* Hay & others, 1966
- *Reticulofenestra umbilica* (Levin) Martini & Ritzkowski, 1968
- *Sphenolithus moriformis* (Brönnimann & Stradner) Bramlette & Wilcoxon, 1967
- *Transversopontis zigzag* Roth & Hay *in* Hay & others, 1967
- *Zygrhablithus bijugatus bijugatus* (Deflandre) Deflandre, 1959

Discoaster barbadiensis is more prominent than *D. saipanensis*. The presence of these species with *Isthmolithus recurvus*, in the absence of *Cyclicargolithus reticulatus*, suggests a latest late Eocene age (Shafik, 1973), and probably a correlation with the foraminiferal zone early P17 according to Berggren & others (1985). This assemblage is referred to as the 66DR14D *Discoaster barbadiensis* assemblage in Figure 8.

Deposition was in a shallow water nearshore or shelf environment, based on the presence of hemipelagic species such as *Holodiscolithus macroporus* and *Transversopontis zigzag*. Present water depth at Station 66DR14 (in Canyon J, Fig. 1) is 3064–2627 m.

Discussion. During the middle Eocene, Station 66DR14 was probably on the outer shelf or the upper continental slope, as evidenced by the 66DR14A(5) nannofossil assemblage which contains scarce indicators of neritic water mass. Subsidence must have been occurring since that time. The younger Eocene assemblage from 66DR14D includes more common indicators of shallow-water deposition. This suggests a drastic latest late Eocene fall in sea level, on a presumably subsiding seafloor. Table 2 summarises the depositional palaeoenvironments of sediments sampled at Station 66DR14.

Table 2. Depositional palaeoenvironments of samples from dredge 66DR14, showing effect of a possible increase in the rate of subsidence of the seafloor of the Great Australian Bight during the middle Eocene; a later Eocene fall in sea level reversed this effect.

Age	*Sample*	*Depositional palaeoenvironment*
Early Oligocene	66DR14B	neritic (?middle shelf)
Latest late Eocene	66DR14D	neritic (?middle shelf)
Late Eocene		not represented
Later Middle Eocene	66DR14A(6)	outer neritic or bathyal
Middle Eocene	66DR14A(5)	outer neritic or bathyal
Early Eocene		not represented
Paleocene		not represented
Maastrichtian	66DR14F	(?inner) neritic (marine ingression)

Oligocene

Four distinct Oligocene assemblages are identified.

Early Oligocene

Assemblage A. The assemblage extracted from sample 66DR14B, a white argillaceous limestone in Canyon J on Ceduna Terrace (Fig. 1), included:

- *Blackites spinulus* (Levin) Roth, 1970
- *Blackites tenuis* (Bramlette & Sullivan) Sherwood, 1974
- *Chiasmolithus altus* Bukry & Percival, 1971
- *Chiasmolithus oamaruensis* (Deflandre) Hay & others, 1966 (abundant)
- *Coccolithus formosus* (Kamptner) Wise, 1973
- *Coccolithus pelagicus* (Wallich) Schiller, 1930
- *Discoaster tanii* Bramlette & Riedel, 1954
- *Helicosphaera* sp. cf. *H. bramlettei* (Müller) Jafar & Martini, 1975
- *Isthmolithus recurvus* Deflandre *in* Deflandre & Fert, 1954
- *Lanternithus minutus* Stradner, 1962
- *Pedinocyclus larvalis* (Bukry & Bramlette) Loeblich & Tappan, 1973 (rare)
- *Pontosphaera multipora* (Kamptneri) Roth, 1970
- *Pontosphaera plana* (Bramlette & Sullivan) Haq, 1971 (rare)
- *Reticulofenestra hampdenensis* Edwards, 1973 (frequent to common)
- *Reticulofenestra oamaruensis* (Deflandre) Stradner *in* Stradner & Edwards, 1968 (rare)
- *Reticulofenestra scissura* Hay & others, 1966
- *Reticulofenestra scrippsae* (Bukry & Percival) Roth, 1973
- *Reticulofenestra umbilica* (Levin) Martini & Ritzkowski, 1968
- *Sphenolithus moriformis* (Brönnimann & Stradner) Bramlette & Wilcoxon, 1967
- *Transversopontis pulcher* (Deflandre) Perch-Nielsen, 1967
- *Transversopontis pulcheroides* (Sullivan) Perch-Nielsen, 1971
- *Zygrhablithus bijugatus bijugatus* (Deflandre) Deflandre, 1959.

This assemblage is early Oligocene in age, based on the co-occurrence of *Coccolithus formosus, Isthmolithus recurvus, Lanternithus minutus, Reticulofenestra oamaruensis* and *R. umbilica*, in the absence of the key Eocene species *Cyclicargolithus reticulatus* and *Discoaster saipanensis* (Shafik, 1973; 1983). The same evidence suggests correlation with the foraminiferal zonal interval late P17–early P18 according to Berggren & others (1985).

Deposition was in shallow waters as indicated by the presence of several hemipelagic species such as *Lanternithus minutus, Pontosphaera multipora* and *Zygrhablithus bijugatus bijugatus*. The effect of the latest late Eocene fall in sea level (concluded above) seems to have been maintained during the early Oligocene. In other words, the net effect of this fall in sea level as against a presumed continuing subsidence of the seafloor at Canyon J (probably since the middle Eocene, see Table 2) is a shallow-water environment during the early Oligocene at Station 66DR14. Present water depth at this station is 3064–2627 m.

Assemblage B. The assemblage recovered from sample 66DR06A, a fine-grained white chalk dredged from Ceduna Canyon (Fig. 1), included:

Chiasmolithus altus Bukry & Percival, 1971
Chiasmolithus oamaruensis (Deflandre) Hay & others, 1966
Clausicoccus cribellum (Bramlette & Sullivan) Prins, 1979
Coccolithus pelagicus (Wallich) Schiller, 1930
Pontosphaera plana (Bramlette & Sullivan) Haq, 1971 (corroded)
Reticulofenestra hampdenensis Edwards, 1973
Reticulofenestra oamaruensis (Deflandre) Stradner *in* Stradner & Edwards, 1968
Reticulofenestra scissura Hay & others, 1966
Reticulofenestra umbilica (Levin) Martini & Ritzkowski, 1968
Transversopontis pulcheroides (Sullivan) Perch-Nielsen, 1971
Zygrhablithus bijugatus bijugatus (Deflandre) Deflandre, 1959.

The presence of *Reticulofenestra oamaruensis* and *R. umbilica* in the absence of the key Eocene species *Discoaster saipanensis, D. barbadiensis* and *Cyclicargolithus reticulatus* indicates an early Oligocene age (Martini, 1971; Shafik, 1973) and a correlation with the foraminiferal zone P18 according to Berggren & others (1985). This assemblage is younger than that of 66DR14B because the latter contains *Coccolithus formosus*.

Deposition of 66DR06A was in shallow waters, based on the presence of *Pontosphaera plana, Transversopontis pulcheroides* and *Zygrhablithus bijugatus bijugatus*. The fall in sea level which began during the latest late Eocene (see discussion above) continued to show its effect during the early Oligocene, permitting the presence of hemipelagic species in the 66DR06A assemblage. Deepening of the water (as a net balance between seafloor subsidence and eustatic fluctuation in sea level) above the Ceduna Terrace (Station 66DR06) must later have resumed, to account for the present water depth at Station 66DR06 of 2620–2015 m.

Mid Oligocene

Sample 66DR12B, a soft fine-grained white limestone dredged from Canyon H on Ceduna Terrace (Fig. 1), yielded a well-preserved assemblage. This included:

Blackites spinulus (Levin) Roth, 1970
Blackites tenuis (Bramlette & Sullivan) Sherwood, 1974
Blackites vitreus (Deflandre) Shafik, 1981
Chiasmolithus altus Bukry & Percival, 1971
Coccolithus eopelagicus (Bramlette & Riedel) Bramlette & Sullivan, 1961
Coccolithus pelagicus (Wallich) Schiller, 1930
Coronocyclus nitescens (Kamptner) Bramlette & Wilcoxon, 1967
Cyclicargolithus floridanus (Roth & Hay) Bukry, 1971
Helicosphaera intermedia Martini, 1965
Helicosphaera obliqua Bramlette & Wilcoxon, 1967
Helicosphaera sp. (see Fig. 5)
Lanternithus minutus Stradner, 1962 (one poorly preserved specimen)
Orthozygus aureus (Stradner) Bramlette & Wilcoxon, 1967
Pontosphaera multipora (Kamptner) Roth, 1970
Reticulofenestra scissura Hay & others, 1966
Reticulofenestra scrippsae (Bukry & Percival) Roth, 1973
Reticulofenestra spp.
Sphenolithus distentus (Martini) Bramlette & Wilcoxon, 1967
Sphenolithus moriformis (Brönnimann & Stradner) Bramlette & Wilcoxon, 1967
Sphenolithus predistentus Bramlette & Wilcoxon, 1967
Sphenolithus sp. (see Fig. 7)
Transversopontis zigzag Roth & Hay *in* Hay & others, 1967
Zygrhablithus bijugatus bijugatus (Deflandre) Deflandre, 1959.

Based on the presence of the index species *Sphenolithus distentus*, in the absence of both *Sphenolithus ciperoensis* Bramlette & Wilcoxon, 1967 and *Cyclicargolithus abisectus* (Muller) Wise, the age of the assemblage is mid Oligocene (Martini, 1971; Bukry, 1973). A correlation with the foraminiferal zonal interval late P18–early P21 of the tropics is made, based on Berggren & others (1985).

Deposition was in a neritic (nearshore or shelf) environment, as evidenced by the presence of several hemipelagic species such as *Orthozygus aureus, Transversopontis zigzag* and *Zygrhablithus bijugatus bijugatus*. The non-marine sediments at the same station (sample 66DR12G; Alley, 1988) are considered further indication of the early Tertiary shallowness of the water above Canyon H. Subsidence must have occurred since then, to account for the present water depth of 3670–2720 m at the station in Canyon H (Fig. 1).

Late Oligocene

Sample 66DR06B, a fine-grained pale yellowish-white chalk dredged from Ceduna Canyon (Fig. 1), yielded a late Oligocene assemblage which contained rare displaced Eocene elements:

Chiasmolithus altus Bukry & Percival, 1971
Chiasmolithus oamaruensis (Deflandre) Hay & others, 1966 (probably displaced from older level)
Clausicoccus cribellum (Bramlette & Sullivan) Prins, 1979
Coccolithus eopelagicus (Bramlette & Riedel) Bramlette & Sullivan, 1961
Coccolithus pelagicus (Wallich) Schiller, 1930
Coronocyclus nitescens (Kamptner) Bramlette & Wilcoxon, 1967
Cyclicargolithus abisectus (Müller) Wise, 1973
Cyclicargolithus floridanus (Roth & Hay) Bukry, 1971
Discoaster deflandrei Bramlette & Riedel, 1954 'group'
Discoaster saipanensis Bramlette & Riedel, 1954 (displaced from Eocene)
Discoaster tanii Bramlette & Riedel, 1954
Helicosphaera euphratis Haq, 1966
Helicosphaera recta (Haq) Martini, 1969
Reticulofenestra hampdenensis Edwards, 1973 (displaced from Eocene/lower Oligocene)
Reticulofenestra orangensis (Bukry) n. comb.
Reticulofenestra scissura Hay & others, 1966
Reticulofenestra scrippsae (Bukry & Percival) Roth, 1973
Reticulofenestra spp.
Reticulofenestra umbilica (Levin) Martini & Ritzkowski, 1968 (displaced from Eocene/lower Oligocene)
Sphenolithus ciperoensis Bramlette & Wilcoxon, 1967
Sphenolithus moriformis (Brönnimann & Stradner) Bramlette & Wilcoxon, 1967
Zygrhablithus bijugatus bijugatus (Deflandre) Deflandre, 1959

The co-occurrence of *Helicosphaera recta, Sphenolithus ciperoensis* and *Cyclicargolithus abisectus*, in the absence of *Sphenolithus distentus*, indicates a late Oligocene age (Martini, 1971; Bukry, 1973) and a correlation with the foraminiferal zone P22, based on Berggren & others (1985). The abundant occurrence of *Zygrhablithus bijugatus bijugatus* usually suggests deposition in neritic waters, but the presence of this species in 66R06B may be a result of reworking from older levels. The assemblage contains several displaced species mainly from Eocene levels, and *Z. bijugatus bijugatus* is known to range through the Eocene and Oligocene. Present water depth at Station 66DR06 is 2620–2015 m.

Comparison with onshore and well assemblages

Maastrichtian

Hitherto, *in situ* Cretaceous calcareous nannofossils were unknown from southern Australia. The Maastrichtian assemblages, from Canyon B between the Eyre and Ceduna Terraces in the central Great Australian Bight Basin, are the first found in southern Australia, and are considered to represent a marine ingression. The lithologies of 66DR01H, 66DR03A and 66DR01F, being organic-rich fine-grained and terrigenous, are consistent with this view. The 66DR03A assemblage is probably coeval with the initiation of the high sea-level stand which peaked during the late Maastrichtian on the Australian western margin (Shafik, in press). The slightly younger 66DR01F assemblage probably corresponds with the peak of this sea level.

Shafik (1985) described a significant reworking episode along the Australian western and southern margins, which involved the redeposition of Upper Cretaceous coccoliths in the Eucla and Otway Basins during the middle Eocene. The provenance of these Upper Cretaceous coccoliths was thought to be the Naturaliste Plateau, in the absence of known *in situ* Cretaceous coccoliths in southern Australia. The record herein of what appear to be *in situ* Maastrichtian coccoliths presents an alternative and nearer source for the reworked Cretaceous coccoliths in the Eocene of the Eucla and Otway Basins.

The Cretaceous *Gartnerago* sp. found in the middle Eocene 66DR01D assemblage is seen as a result of localised reworking (both Maastrichtian and middle Eocene strata crop out in Canyon B at Station 66DR01), and therefore may not belong to the same reworking episode described by Shafik (1985). The 66DR01D assemblage is slightly older than the middle Eocene levels with reworked Cretaceous nannofossils in the Eucla and Otway Basins.

Early Eocene

The early Eocene 66DR08A *Discoaster lodoensis* assemblage from Canyon F on Ceduna Terrace (Fig. 1), central Great Australian Bight Basin, is older than any known calcareous nannofossil assemblage in southern Australia. It is also distinctly older than the early Eocene assemblages at the base of the Eocene section on the Naturaliste Plateau (DSDP Site 264). This is based on the presence of the key species *Discoaster sublodoensis* in the Naturaliste Plateau (Shafik, 1985) and not in the 66DR08A assemblage.

In Potoroo No.1 well in the central Great Australian Bight Basin (Fig. 1A), an isolated early Eocene assemblage with *Discoaster sublodoensis* (i.e. correlatable with the Naturaliste Plateau assemblage) is here identified from the 945.5 m level; intervals immediately below and above this level in Potoroo No.1 well are barren of calcareous microplanktic remains. This assemblage included the taxa:

- *Blackites creber* (Deflandre) Sherwood, 1974
- *Braarudosphaera bigelowii* (Gran & Braarud) Deflandre, 1947
- *Braarudosphaera discula* Bramlette & Riedel, 1954
- *Calcidiscus protoannulus* (Gartner) Loeblich & Tappan, 1978
- *Campylosphaera dela* (Bramlette & Sullivan) Hay & Mohler, 1967
- *Clausicoccus cribellum* (Bramlette & Sullivan) Prins, 1979
- A form transitional between *Chiasmolithus bidens* (Bramlette & Sullivan) Hay & Mohler, 1967 and *C. expansus* (Bramlette & Sullivan) Gartner, 1970
- *Chiasmolithus grandis* (Bramlette & Riedel) Radomski, 1968
- *Chiasmolithus solitus* (Bramlette & Sullivan) Locker, 1968
- *Coccolithus eopelagicus* (Bramlette & Riedel) Bramlette & Sullivan, 1961
- *Coccolithus formosus* (Kamptner) Wise, 1973
- *Coccolithus pelagicus* (Wallich) Schiller, 1930
- *Cyclicargolithus gammation* (Bramlette & Sullivan) n. comb.
- *Discoaster barbadiensis* Tan Sin Hok, 1927
- *Discoaster lodoensis* Bramlette & Riedel, 1954
- *Discoaster sublodoensis* Bramlette & Sullivan, 1961
- *Discoasteroides kuepperi* (Stradner) Bramlette & Sullivan, 1961
- *Helicosphaera seminulum* Bramlette & Sullivan, 1961
- *Lophodolithus mochlophorus* Deflandre *in* Deflandre & Fert, 1964
- *Lophodolithus nascens* Bramlette & Sullivan, 1961
- *Lophodolithus reniformis* Bramlette & Sullivan, 1961
- A species transitional between *Markalius astroporus* (Stradner) Hay & Mohler, 1967 and *M. inversus* (Deflandre) Bramlette & Martini, 1964
- *Micrantholithus altus* Bybell & Gartner, 1972
- *Micrantholithus attenuatus* Bramlette & Sullivan, 1961
- *Micrantholithus bramlettei* Deflandre, 1954
- *Micrantholithus pinguis* Bramlette & Sullivan, 1961
- *Neochiastozygus chiastus* (Bramlette & Sullivan) Perch-Nielsen, 1971
- *Neococcolithes dubius* (Deflandre) Black, 1967
- *Pontosphaera ocellata* (Bramlette & Sullivan) Perch-Nielsen, 1984
- *Pontosphaera plana* (Bramlette & Sullivan) Haq, 1971
- *Reticulofenestra dictyoda* (Deflandre & Fert) Stradner, 1968
- *Sphenolithus moriformis* (Brönnimann & Stradner) Bramlette & Wilcoxon, 1967
- *Sphenolithus radians* Deflandre *in* Grasse, 1952
- *Striatococcolithus pacificanus* Bukry & Percival, 1971
- *Toweius callosus* Perch-Nielsen, 1971
- *Toweius? magnicrassus* (Bukry) Romein, 1979
- *Transversopontis pulcher* (Deflandre) Perch-Nielsen, 1967
- *Tribrachiatus orthostylus* Shamarai, 1963
- *Zygodiscus adamas* Bramlette & Sullivan, 1961
- *Zygrhablithus bijugatus bijugatus* (Deflandre) Deflandre, 1959.

The co-occurrence of *Discoaster sublodoensis* and *Discoasteroides kuepperi* suggests a late early Eocene age (Martini, 1971; Bukry, 1973), and a correlation with the foraminiferal late zone P9 according to data in Berggren & others (1985). The presence of *Tribrachiatus orthostylus* in the assemblage is problematic because this species is thought to disappear before the appearance of *D. sublodoensis* (see, for example, Martini, 1971). However, it is possible that *T. orthostylus* may have lasted longer in the Great Australian Bight Basin than elsewhere. The assemblage contains evidence to suggest warmer waters than earlier, during the deposition of the 66DR08A *Discoaster lodoensis* assemblage. Species of *Discoaster* are more frequent in the Potoroo assemblage than in the assemblage from 66DR08A.

Table 3. Depositional palaeoenvironments of samples from dredge 66DR08, showing effect of possible increase in the rate of subsidence of the seafloor of the Great Australian Bight during the middle Eocene.

Age	*Sample*	*Depositional palaeoenvironment*
Later Middle Eocene	66DR08B	outer neritic
Early Eocene	66DR08A	middle neritic (marine ingression)
Paleocene to early Eocene	66DR08E	possibly paralic (pollens)
Late Paleocene	66DR08F	possibly paralic (pollens)

It can be argued that the early Eocene 66DR08A *Discoaster lodoensis* assemblage is an isolated assemblage within the sequence at Canyon F, similar to the *Potoroo* assemblage which is sandwiched between nannofossil-free intervals, and thus representing a marine ingression. The lower Eocene section in the nearby Platypus No.1 well (Fig. 1A) is largely non-marine. McGowran (in press) considered the planktic foraminiferal assemblage of 66DR08A as representing what he termed the Burrungule ingression.

Thus, the 66DR08A *Discoaster lodoensis* assemblage (correlatable with the foraminiferal zone P8) and the Potoroo *Discoaster sublodoensis* assemblage (correlatable with the foraminiferal late zone P9) are considered to represent marine ingressions into the Great Australian Bight Basin. These are referred to in Figure 8 as the 66DR08A *Discoaster lodoensis* and the Potoroo *Discoaster sublodoensis* ingressions. No such ingressions could be detected in the Eucla Basin, and the middle Eocene calcareous nannofossil assemblages recovered from the Hampton Sandstone and the base of the Wilson Bluff Limestone (base of a major transgression) include elements (such as abundant *Cyclicargolithus reticulatus* and *Chiasmolithus grandis*) correlatable with the foraminiferal late zone P12 of the tropics.

Based on a relatively diverse planktic foraminiferal assemblage in 66DR14F — including *Pseudohastigerina wilcoxensis, Planorotalites australiformis, P. pseudoscitula, P.* cf. *imitata, 'Turborotalia'* sp., *Acarinina nitida, A. collactea, Subbotina patagonica, S.* cf. *linaperta* and *Chiloguembelina wilcoxensis* — dredged from Canyon J (Fig. 1), McGowran (1988a,b, in press) was able to recognise an (earlier) early Eocene marine ingression in the Great Australian Bight Basin. Conditions during this ingression were apparently not suited for coccolith-forming nannoplankton (the production of coccoliths and nannoliths was inhibited, and nannoplankton may have survived naked); no calcareous nannofossils could be found in 66DR14F. McGowran correlated the foraminiferal assemblage from 66DR14F with a much less diverse assemblage from the Otway Basin known from the Princetown Member of the Dilwyn Formation; no calcareous nannofossils were ever recovered from this level in the Dilwyn Formation.

Middle Eocene

The middle Eocene assemblages of the Great Australian Bight Basin represent four distinct levels (Fig. 8), the younger two of which can be related to assemblages previously recorded from the Gambier Embayment in the Otway Basin to the east. The older two assemblages can be linked with the Naturaliste Plateau sequence.

The 66DR01D *Discoaster bifax-Reticulofenestra umbilica* and the 66DR10A *Nannotetrina pappi-Cyclicargolithus reticulatus* assemblages are considered to represent the base of the transgression in the Great Australian Bight Basin, but their equivalents on the Naturaliste Plateau, due to erosion, are at the top of the truncated Eocene section at DSDP Site 264.

The assemblage from 66DR14A(5) is correlated with a coeval assemblage recorded previously from the Gambier Embayment, western Otway Basin (referred to as the *Chiasmolithus solitus-Cyclicargolithus reticulatus* association from the 65.2 m level in the Kingston Construction Camp Bore — see Shafik, 1983). However, the Gambier Embayment assemblage is more diverse. It includes several shallow-water indicators such as *Braarudosphaera bigelowii, Daktylethra punctulata, Lanternithus minutus, Pemma basquensis* (Martini) Baldi-Beke, 1967, *Pemma papillatum* Martini, 1959, *Pontosphaera multipora, Transversopontis pulcher, T. zigzag* and *Zygrhablithus bijugatus bijugatus.* Other differences between the two assemblages include (a) the presence of the warmer-water species *Helicosphaera heezenii, H.* sp. aff. *H. reticulata* and *Sphenolithus predistentus* in the 66DR14A(5) assemblage and not in the Gambier Embayment assemblage, (b) most species, and in particular *Reticulofenestra umbilica,* are larger in 66DR14A(5), and (c) the abundance of the species is much greater in 66DR14A(5). These differences would be explained if 66DR14A(5) was deposited at deeper levels (continental slope) beneath warmer surface waters which had much better connection to the open sea, being a part of the middle Eocene transgression. The Gambier Embayment assemblage, representing a marine ingression (discussed in Shafik, 1983), was deposited at shallower (continental shelf) depths; surface waters were evidently cooler than in the Great Australian Bight Basin.

The nearest assemblage in the Gambier Embayment (Otway Basin) to the younger middle Eocene assemblages from 66DR08B and 66DR14A(6) is an assemblage referred to as the *Daktylethra punctulata-Reticulofenestra scissura* association by Shafik (1983, recorded from Kingston Construction Camp Bore and Observation Bore No.1 well). The presence of *Daktylethra punctulata* in the Gambier Embayment assemblage suggests that it is slightly older (correlatable with the foraminiferal zone P13, Shafik, 1983) than these middle Eocene assemblages from the Great Australian Bight Basin (which are correlatable with the foraminiferal zone P14, being above the highest occurrence of *D. punctulata*). The Gambier Embayment assemblage differs also in containing a large number of hemipelagic species (i.e. indicators of deposition in a shallow-water environment), and in lacking the warm-water species *Sphenolithus predistentus* or *Helicosphaera reticulata.* These differences are consistent with the possibility that the Gambier Embayment assemblage represents a marine ingression with cooler surface waters (see Shafik, 1983), whereas the 66DR08B and the 66DR14A(6) assemblages are part of a full transgression with warmer surface waters.

Based on several Eocene nannofossil assemblages from the offshore Otway Basin, Shafik (1987b) suggested a trend of temperature decline begining very late in the middle Eocene, after a peak represented by an assemblage characterised by the presence of the key *Reticulofenestra scissura* and *Daktylethra punctulata* (and thus correlatable with the foraminiferal zone P13). The assemblages from 66DR08B and 66DR14A(6), which include the warm-water species *Sphenolithus predistentus* and/or *Helicosphaera reticulata,* are thought to be slightly younger than this peak.

In the Gambier Embayment (western onshore Otway Basin), the ranges of *Chiasmolithus solitus* and *Reticulofenestra scissura* do not overlap. In the offshore Otway Basin (Shafik, 1987a) and in the Great Australian Bight Basin these taxa co-occur.

Late Eocene-early Oligocene

The rare occurrence of the oceanic species *Bramletteius serraculoides* and the absence of hemipelagic taxa (such as *Lanternithus minutus*) in the late Eocene 66DR01A *Chiasmolithus oamaruensis* assemblage in the Great Australian Bight Basin, distinguish it from coeval assemblages in the onshore Otway Basin; the latter usually include a large number of hemipelagic taxa (Shafik, 1983).

The late Eocene assemblages recovered from 66DR12A(5) and 66DR14D have counterparts in the onshore Otway Basin. The Otway Basin assemblages lack *Discoaster barbadiensis* and *Helicosphaera compacta* which are present in the Great Australian Bight Basin. This suggests that surface waters during the late Eocene were probably warmer in the Great Australian Bight Basin than in the Otway Basin, to the east. *Discoaster barbadiensis* ranges higher in the Great Australian Bight Basin sequence (upper Eocene) than in the equivalent sequence in the Otway Basin, where it disappears high in the middle Eocene (Shafik, 1983). Further to the east in the New Zealand sequence, *D. barbadiensis* disappears at a lower level within the middle Eocene (Edwards, 1971).

The early Oligocene assemblages recovered from 66DR14B and 66DR06A are similar to coeval assemblages in the onshore and offshore parts of the Otway Basin which are recorded by Shafik (1983, 1987a,b).

Mid-late Oligocene

The presence of the low-latitude key species *Sphenolithus distentus* indicates warmer surface waters during the mid Oligocene in the Great Australian Bight Basin (66DR12B) than in the Otway Basin where the species is not known (being either very rare or absent). The late Oligocene 66DR06B assemblage with *Sphenolithus ciperoensis* is correlated with coeval assemblages (also containing *S. ciperoensis*) which were recorded previously from three dredge stations in the offshore Otway Basin and off West Tasmania (Shafik, 1987b) and also noted in the onshore Otway Basin (in the Kingston Construction Camp Bore, location in Shafik, 1983).

Shafik (1987b) concluded that an excursion by *Sphenolithus ciperoensis* into the Otway Basin and West Tasmania occurred as a response to a 'short' warm episode during the late Oligocene. This same warm episode apparently may also be responsible for the presence of *S. ciperoensis* in the Great Australian Bight Basin.

Discussion of results

Maastrichtian-early Eocene marine ingressions

Samples 66DR01G and 66DR01L (from Canyon B between Eyre and Ceduna Terraces, Fig. 1) yielded planktic Maastrichtian foraminiferids (McGowran, 1988a,b), but not calcareous nannofossils. Similarly, sample 66DR14F (from Canyon J on Ceduna Terrace, Fig. 1) yielded early Eocene planktic foraminiferids (McGowran, 1988a,b), but not calcareous nannofossils. Similar situations occur in the onshore lower Tertiary sequence of southern Australia where levels bearing calcareous foraminiferids represent isolated marine ingressions. Several attempts by the writer to extract nannofossils from the Pebble Point Formation, several subunits of the Dilwyn Formation (Rivernook A, Rivernook Member, *Trochocyathus* Bed and Princetown member), and the Burrungule Member of the Knight Formation in the Otway Basin have been unsuccessful. Levels examined from these sediments are known to contain *sparse* calcareous foraminiferids, which include *few* planktic forms, representing early Tertiary marine ingressions (documentation in McGowran, 1965, 1968, 1970; Taylor *in* Singleton, 1967; McGowran & others, 1971; Taylor, 1971). This lack of calcareous nannofossils is probably a consequence of their extreme scarcity in these sediments, which may be initially a result of very shallow-water palaeoenvironments; nannofossil concentration involving very large volumes of samples is needed. However, it could also be the result of a combination of certain other environmental conditions which inhibited the production of coccoliths and nannoliths, while favouring non-coccolith bearing (naked) strains of nannoplankton, and at the same time did not affect the associated planktic foaminiferids. These conditions could have involved some imbalance in the supply of certain nutrients.

Modern nannofloras are generally more tolerant than planktic foraminiferids of marginal marine conditions. They are found in hostile environments such as the low-salinity Black Sea (Bukry, 1974) without the association of planktic foraminiferids, and the highly saline Gulf of Aqaba (Elat), associated with planktic foraminiferids (Winter & others, 1979). However, in a nascent (Cretaceous-Early Tertiary) ocean, the supply of critically limiting nutrients (such as dissolved phosphorus and calcium) and/or an imbalance in other essential components (such as carbon dioxide) may have different effects to those in the open sea, and thus may eventually produce sediments on its floor lacking coccoliths and nannoliths, but containing planktic foraminiferal tests. In addition to a limited planktic foraminiferal fauna, naked nannoflora may have flourished in the top water layers in such an 'ocean'. This scenario is highly likely for the *narrow* Late Cretaceous-early Eocene incipient Southern Ocean which had restricted connection to the world ocean. Changes in the chemistry of surface waters of this Cretaceous-Early Tertiary nascent ocean, which could be brought about temporarily by good connection to the world ocean during times of marine ingressions, may induce its non-coccolith forming nannoplankton to produce plates of calcium carbonate.

It has been shown, in laboratory culture studies of the extant coccolith-bearing *Emiliania huxleyi* (Lohmann) Hay & Mohler *in* Hay & others (1967), that an increase in the phosphate content of the medium in which it was grown may cause its cells to cease secretion of its coccoliths, without affecting the survival of the resultant naked form (Paasche, 1964). Tappan (1980, p. 723) stated that 'cultures can be maintained in a calcium-deficient medium, but although growth is otherwise normal, no coccoliths are produced' (see also Crenshaw, 1964; Paasche, 1964, 1965). Studies by Wilbur & Watabe (1963) and Paasche & Klaveness (1970) have shown that cells of *Emiliania huxleyi* could be decalcified in life by increasing the amount of carbon dioxide in the medium in which they were grown.

Data from southern Australia pertinent to the observations made above are scarce. However, two dredge hauls recovered during BMR Survey 66 by R.V. *Rig Seismic* were found to include phosphatic sediments of the right age, being within the Late Cretaceous and middle Eocene interval. These were sample 66DR01I (from Canyon B, Fig. 1), a laminated micrite and fine sandstone which includes a phosphorite interbed

25 mm thick, dated as late Paleocene by Alley (1988, based on pollen grains) and sample 66DR11F (from Canyon H, Fig. 1), nodules of hard calcareous phosphatic muddy quartz arenite or siltstone, dated as Late Cretaceous to Tertiary by Alley (1988). Sediments with reasonably high calcium carbonate content were not deposited in the Otway Basin before the middle Eocene, when shelf carbonates (Wilson Bluff Limestone) began accumulating in the Eucla Basin. The Paleocene and Lower Eocene sediments of the Otway Basin, which contain planktic foraminiferids, apparently without the association of calcareous nannofossils, are terrigenous, being largely carbonaceous sandy clays or silts, commonly micaceous and pyritic, with minor calcareous sandstones. Evidently, these sediments were deposited in a hostile environment which occasionally permitted planktic foraminiferids, coming from the Indian Ocean in the west, to survive. Coccolith secretion in the associated nannoflora was inhibited, probably due to high dissolved phosphorus and low calcium concentration in the surface waters of the young early Eocene ocean south of Australia.

The occurrence of planktic foraminiferids without the association of nannofossils in the Maastrichtian and early Eocene samples 66DR01G, 66DR01L and 66DR14F from the Great Australian Bight Basin is taken to indicate transient marine conditions, which although not necessarily inhibiting the growth and production of the non-coccolith bearing nannofloral cells, were not favourable for their calcification. Connection to the open sea was probably very restricted and intermittent. On the other hand, the presence of calcareous nannofossils in association with planktic foraminiferids in the Maastrichtian and early Eocene samples 66DR01H, 66DR03A, 66DR01F and 66DR08A, which represent marine ingressions into the Great Australian Bight Basin, is taken to indicate temporary changes to true marine conditions brought about by good connection to the open sea. Such an invasion by the open sea may result, for example, in nitrogen depletion (Tappan, 1986) which in turn may cause non-coccolith forming nannoplankton to produce coccoliths as indicated by studies *in vitro*. (Wilbur & Watabe (1963) showed that secretion of coccoliths occurred in a strain of *Emiliania huxleyi*, which normally lacks coccoliths, when grown in a nitrogen-deficient medium; see also Paasche, 1964.) A good connection with the open sea would also bring a fresh supply of coccolith-bearing nannoplankton and planktic foraminiferids.

Maastrichtian ingression. During the Late Cretaceous, the nascent Southern Ocean was narrow, relatively shallow, and generally unsuitable for coccoliths (Shafik, 1985). However, the data in this study demonstrate that marine conditions were established gradually during the late Maastrichtian in its western part, that is, in the region of the Great Australian Bight Basin. Three phases are probably discernible for the Maastrichtian ingression into the Great Australian Bight Basin, corresponding to a progressive increase in oceanic parameters over time. During the earliest phase, represented by samples 66DR01G and 66DR01L, connection with the open sea was probably restricted and conditions were apparently not favourable for coccolith-forming nannoplankton. Surface-water conditions during the second phase, represented by the 66DR01H assemblage, evidently began to resemble those of the open sea as coccolith-bearing nannoplankton began to flourish in the Great Australian Bight Basin. During the last phase, represented by the 66DR03A and 66DR01F assemblages, open-marine conditions were well established and calcareous nannofossils accumulated between the Eyre and Ceduna Terraces.

Early Eocene ingressions. The 66DR14F foraminiferal assemblage represents an early Eocene marine ingression into the Great Australian Bight Basin (McGowran, 1988a,b, in press) which apparently was incapable of supporting coccolith-forming nannoplankton. Conditions during this early Eocene ingression were less completely marine than during the following early Eocene 66DR08A *Discoaster lodoensis* and Potoroo *Discoaster sublodoensis* nannofossil ingressions. (According to McGowran (1988a,b, in press), the foraminiferids of 66DR14F are older than those of 66DR08A). The 66DR14F foraminiferal ingression (Fig. 8) may be regarded as a prelude to these other early Eocene ingressions. McGowran (in press) correlated the foraminiferids of 66DR14F with zone P7, and pointed out that they are either coeval or very close in age to the early Eocene Princetown marine ingression into the Otway Basin. This correlation is adopted here (see Fig. 8). The 66DR14F ingression (with a relatively diverse planktic foraminiferal fauna in the Great Australian Bight Basin) apparently reached the Otway Basin leaving *rare, sporadic* foraminiferids in the Princetown Member of the Dilywn Formation.

Framework of Eocene marine sedimentation along the Australian southern margin

In the Eocene sequence of the Otway Basin, calcareous nannofossil assemblages sandwiched between barren sediments have been used to define marine ingressions, and their uninterrupted vertical record to define marine transgression (see Shafik, 1983). On this evidence, the base of the Eocene transgression along the Australian southern margin is diachronous (Shafik, 1973, 1983), becoming younger eastward. The sea advanced from the west. The base of the uninterrupted record of nannofossil assemblages is middle Eocene in the Eucla Basin and late Eocene in the Otway Basin, where Eocene marine sedimentation included isolated middle Eocene assemblages representing marine ingressions. In the Eucla Basin no such ingressions (preceding the transgression) were detected. There, the base of the Tertiary (= middle Eocene) calcareous planktic sequence rests directly on Cretaceous or older rocks. The middle Eocene ingressions in the Otway Basin are here considered to represent the distal tongue of the Eucla Basin transgression — the advance of marine influence being from the west.

Like the 66DR14F ingression in the Great Australian Bight Basin, the Burrungule ingression into the Otway Basin, which lacks calcareous nannofossils but not planktic foraminiferids, could be a prelude to other (middle) Eocene marine ingressions (the *Cyclicargolithus reticulatus* and the *Reticulofenestra scissura* ingressions). This is based on an earlier correlation of the foraminiferids of the Burrungule Member with the middle Eocene zone P10 or equivalent (Ludbrook & Lindsay, 1969; McGowran & others, 1971). Recently the Burrungule Member has been correlated with the early Eocene zone P9 (McGowran, 1978) or the early Eocene P8 (McGowran, in press). It may therefore be regarded as representing an extension into the Otway Basin of the Potoroo *Discoaster sublodoensis* (= foraminiferal zone P9) or the 66DR08A *Discoaster lodoensis* (=zone P8) marine ingressions into the Great Australian Bight Basin. In Figure 8, correlation of the Burrungule foraminiferids with zone P8 is adopted, following McGowran (in press).

Data from both the offshore Otway Basin (Shafik, 1987a,b) and the present study suggest that the base of the marine transgression along the Australian southern margin becomes older seawards and in a westward direction, as would be expected. The same data suggest that the marine ingressions with coccolith-bearing nannoplankton, preceding the Eocene transgressions on the same margin, are also diachronous, becoming younger eastward and towards the continent. In the Great Australian Bight Basin, the base of the transgression (taken to be represented by the middle Eocene 66DR01D *Discoaster bifax–Reticulofenestra umbilica* assemblage) is older than the base of the transgression in the Eucla and Otway Basins (Fig. 8). The two early Eocene ingressions with coccolith-bearing nannoplankton (which are indicated by the nannofossil 66DR08A *Discoaster lodoensis* and Potoroo *Discoaster sublodoensis* assemblages) preceding this mid Eocene transgression in the Great Australian Bight Basin are obviously older than the (middle Eocene) *Cyclicargolithus reticulatus* and *Reticulofenestra scissura* ingressions which preceded the (late) Eocene transgression in the western Otway Basin (Gambier Embayment, Fig. 8).

Shafik (1983) suggested that the two middle Eocene ingressions in the Gambier Embayment of the Otway Basin which contained calcareous nannoplankton were related to a major acceleration in the seafloor spreading rate occurring south of Australia at about 44 Ma (Anomaly 20) as documented by Cande & others (1981) and Cande & Mutter (1982); the same is true for the coeval Eucla Basin transgression. This sudden increase in the spreading rate between Australia and Antarctica has been linked with seemingly coeval events in the Indian Ocean: a change in the direction of motion of the Indian Plate and termination of spreading between India and Australia as results of termination of subduction beneath Tibet and crustal shortening/thickening at the time of Anomaly 20, according to Patriat & Achache (1984).

The cause(s) of the (earlier) early Eocene ingressions in the Great Australian Bight Basin may also be related to major tectonic events. For example, the age of the first of these ingressions which contained coccolith-forming nannoplankton (the 66DR08A *Discoaster lodoensis* assemblage) equates with the time, about 54 Ma ago, of a global plate tectonic readjustment initiated by collision of India with the Ladakh island arc (Patriat & Achache, 1984).

Great Australian Bight seafloor subsidence since the Late Cretaceous, and latest Eocene-early Oligocene sea-level fall

Palaeontological data presented above suggest substantial subsidence of the seafloor of the Great Australian Bight Basin since the Late Cretaceous. These data are based on palynological and nannofossil evidence. There is palynological evidence, for example, for a non-marine environment during the Paleocene at a site now at a water depth of 3670–2720 m (in Canyon H, Fig. 1). The nannofossil evidence is based on the presence of certain species (including holococcoliths, braarudosphaerids, pontosphaerids) characteristic of neritic water masses, which I loosely describe as hemipelagic species or indicators of shallow-water deposition. Indeed, some of these species have been used to indicate different *neritic* environments for parts of the middle Eocene Weches Formation of Texas (Sherwood, 1974), deposition in *shallow-water nearshore basins* for Paleocene and Eocene sediments in Western Australia (Shafik, 1978), and to indicate *innner shelf* environments during the late Eocene in Northern Italy (Barbin, 1989) or *shallow-water* conditions for the late Paleocene Patala of Pakistan (Kothe & others, 1989).

Because nannofossils are the remains of mostly planktic algae, it can be argued that they cannot be used directly to indicate shallow-water deposition. However, observations over a number of years and in a number of localities (see, for example, Martini, 1965, 1970; Bukry, 1970; Bukry & others, 1971; Bybell & Gartner, 1972; Roth, 1974; Baldi-Beke, 1984) indicate that certain genera are characteristic of sediments known to have been deposited in shelf environment, and are usually absent from deeper marine sediments. Examples are the Late Cretaceous *Acuturris, Kamptnerius* and *Lucianorhabdus*, and the Tertiary *Daktylethra, Holodiscolithus, Lanthernithus, Micrantholithus, Pontosphaera, Transversopontis* and *Zygrhablithus*.

Thus, based purely on empirical evidence from the observational data record, these genera are putative indicators of a shelf environment. Sediment samples as old as Maastrichtian, in which species of these genera were found, came from sites in the Great Australian Bight Basin (discussed above) where water depth today exceeds 2000–3000 m. The lithologies of the samples which contain nannofossil indicators for deposition in neritic waters, together with the palynological evidence in associated samples, support deposition in a shallow-water environment. Accepting that deposition in the Great Australian Bight Basin occurred on the shelf for most of the Late Cretaceous–mid Eocene interval, it must be concluded, in the absence of any evidence of mass redeposition or slumping, that deepening occurred subsequently.

Details of the deepening/subsidence history of the seafloor of the Great Australian Bight Basin are beyond the scope of this paper. The deepening/subsidence might be due solely to sag as a result of sediment loading (thick sediments resulting from high sedimentation rates during the rifting between Australia and Antarctica) and thermal contraction over time during the drift phase (cooling of the crust being increasingly distant from the mid-ocean ridge over time), periodic sea level rise, or the net balance between such sag of seafloor and eustatic fluctuations in sea level.

The evidence from this study, however, suggests that the effect of deepening on the nannoflora was first noticeable in the middle Eocene (probably during the biostratigraphic interval bracketed by the lowest occurrences of *Cyclicargolithus reticulatus* and *Reticulofenestra scissura*, which equates with a position high in the foraminiferal zone P12). It is thus coincident with the onset of rapid spreading in the Southern Ocean (Cande & Mutter, 1982; Royer & Sandwell, in press). Until that time, the separation of the continental crust of Australia and Antarctica was less than 200 km (see Royer & Sandwell, in press, fig. 13).

Both the Australian and Antarctic margins were under the influence of the thermal anomaly associated with the slow phase of seafloor spreading which lasted to the middle Eocene. Rapid movement of the thermal anomaly, associated with the rapid seafloor spreading phase (middle Eocene onward), caused rapid thermal contraction, and thus faster subsidence of the Australian southern margin since the middle Eocene. Mutter & others (1985) and Hegarty & others (1988) indicated a two-stage subsidence history for the Australian southern margin: an Early Cretaceous very rapid subsidence phase associated with the rifting between Australia and Antarctica (which is indicated as having two stages by Williamson & others, 1990) and a very slow subsidence phase which began about 90 Ma ago, at the onset of seafloor spreading between the two continents. Unlike the initial phase, the slow subsidence phase was thermally-controlled, occurring during a period of a relative tectonic quiescence (Hegarty & others, 1988).

It is this slow subsidence phase (mid Cretaceous onward) which concerns the present study, and it is within this phase that the data presented here suggest an acceleration in the rate of subsidence during the middle Eocene. This change in the subsidence rate seems to represent an inflection point at least in one subsidence curve based on data from Jerboa No.1 well in the Great Australian Bight Basin (see Hegarty & others, 1988; Williamson & others, 1990), and also in the Mussel Platform wells in the Otway Basin (see Williamson & others, 1988).

The depositional palaeoenvironments of all Coniacian–Santonian, Maastrichtian, Paleocene and lower Eocene sediment samples discussed from the Great Australian Bight Basin range between non-marine, marginal marine and neritic (mainly middle shelf), and are incompatible with the present-day water depths from which they were collected. In contrast, some of the younger Eocene sediments, which were collected from similar water depths in the same basin, contain evidence for deeper depositional palaeoenvironments (outer shelf and continental slope) (see, for example, Tables 1–3). It is concluded that during the middle Eocene the rate of subsidence of the seafloor of the Great Australian Bight Basin accelerated, although it was masked during the latest late Eocene by a fall in sea level.

During the latest late Eocene and early Oligocene, the deepening process must have been reversed, with a fall in sea level exceeding the rate of subsidence of the seafloor of the Great Australian Bight Basin. This was indicated above by the presence/absence of indicators of shallow-water deposition in the middle Eocene, latest late Eocene and early Oligocene nannofossil assemblages recovered from dredge haul 66DR14 (see Table 2). This conclusion is consistent with a global fall in sea level which seems to have occurred during the latest late Eocene (see Haq & others, 1988).

Influence of proto-Leeuwin Current

Shafik (1983) suggested that surface-water temperatures decreased progressively in an eastward direction along the southern margin of Australia during the Eocene. The data from the Great Australian Bight Basin support this. The presence of the warmer-water species *Sphenolithus predistentus, Helicosphaera heezenii* and *H.* sp. aff. *H. reticulata* in the 66DR14A(5) assemblage, and not in the coeval Eocene Gambier Embayment assemblage, suggests warmer surface waters in the west (Great Australian Bight Basin) than in the east (Otway Basin). This is supported by the presence of *Sphenolithus predistentus* in the slightly younger 66DR08B assemblage and not in its Gambier Embayment near-equivalent, and by the presence of *Helicosphaera reticulata* in 66DR14A(6). Moreover, other data presented here suggest a similar eastward decrease in surface-water temperatures during the mid to late Oligocene: the low-latitude key species *Sphenolithus distentus* is abundant in the Ceduna Terrace material, whereas it is not known (being either very rare or absent) from the Otway Basin.

Only speculation can be offered on why surface waters were progressively cooler in an eastward direction along the southern margin of Australia during the middle Eocene–late Oligocene. This speculation draws on a modern analogy, although the scenario considered was before the formation of the deep-sea passage south of the South Tasman Rise (Kennett & others, 1975; Kennett, 1977).

Although it is commonly held that currents along the western margins of continents are usually northerly flowing in the southern hemisphere, the Leeuwin Current, off Western Australia, flows in a southerly direction, bringing warm waters from the northwest corner of Australia into its southwest corner and southern Australia (Cresswell & Golding, 1980; Legeckis & Cresswell, 1981; Rochford, 1984, 1986). The Leeuwin Current today contributes to the occurrence of a significant tropical fauna of benthic invertebrates, holothurians and several species of pelagic tuna in the Great Australian Bight (Maxwell & Cresswell, 1981). A similar current, a proto-Leeuwin Current (Fig. 9), seems to have existed during much of the Eocene and Oligocene. It may have begun during the middle Eocene, intermittently bringing warm waters into southern Australia from the Indian Ocean. Dilution of the effect of such current would be expected to occur along the southern margin in an easterly direction, with the result that surface waters in the Otway Basin would be cooler than those in the Great Australian Bight Basin.

The evidence for a proto-Leeuwin Current, presented earlier, suggests that the flow of the current was intermittent, being particularly prominent at times during the middle and late Eocene, and during the mid Oligocene.

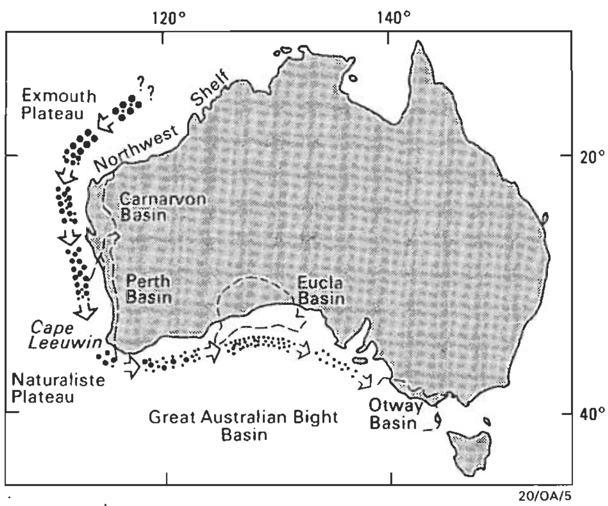

Figure 9. Sketch map of Australia and surroundings, showing the southward flow of a warm proto-Leeuwin Current along the western continental slope and its eastward turning into the southern Australian waters after passing Cape Leeuwin.
This intermittent current was initiated during the middle Eocene. Larger circles correspond to higher surface-water temperatures.

Important Oligocene biostratigraphic datums in the Great Australian Bight Basin sequence

Records of the low-latitude *Sphenolithus distentus* and *S. ciperoensis* in southern Australia (Shafik, 1987b; this study) should in due course provide two important datums for the calcareous microplanktic biostratigraphy of the Oligocene of southern Australia, because they allow a direct link with global time scales. The lowest occurrences of these key nannofossil species have been linked with low-latitude foraminiferal zonations (see, for example, Martini, 1971).

Conclusions

The study documents several new calcareous nannofossil assemblages in southern Australia. These are (a) Maastrichtian assemblages from Canyon B between the Eyre and Ceduna Terraces, which abound with high-latitude elements such as *Nephrolithus corystus, N. frequens, Cribrosphaerella daniae* and *Kamptnerius magnificus*, and (b) Eocene assemblages older than the middle Eocene assemblage known from the base of the Wilson Bluff Limestone (and Hampton Sandstone) in the Eucla Basin. These include two early Eocene (the *Discoaster lodoensis* and *D. sublodoensis*) assemblages and a mid Eocene (*Discoaster bifax–Reticulofenestra umbilica*) assemblage. The *D. lodoensis* assemblage is also older than any known from the Eocene section of the Naturaliste Plateau. The *D. sublodoensis* assemblage is based on material from Potoroo No.1 well, whereas all other assemblages were recovered from dredged samples from the Great Australian Bight Basin. These new Maastrichtian and early Eocene assemblages, apparently individually bracketed by barren intervals, are considered to represent marine ingressions.

Correlation of foraminiferal and nannofossil results on material from the Great Australian Bight and Otway Basins indicates that before the marine ingressions which contained both calcareous nannofossil and foraminiferal assemblages, there are usually other ingressions which apparently were suited for planktic foraminiferids but not coccolith-bearing nannoplankton. Conditions during these early ingressions were not completely marine, probably because of restricted access to the open sea. During later ingressions, better access to the open sea substantially increased the oceanic influence, causing both calcareous foraminiferids and coccolith-forming nannoplankton to flourish.

A comparison of the offshore (Great Australian Bight Basin) and onshore (Otway Basin) sequences reveals an offset parallelism in their history. In the Great Australian Bight Basin, early Eocene ingressions preceded a middle Eocene transgression, while in the onshore Otway Basin, middle Eocene ingressions preceded a late Eocene transgression. The timing of the first early Eocene ingression, which contained coccolith-bearing nannoplankton, into the Great Australian Bight Basin seems to coincide with the timing of a global plate readjustment, initiated by the collision of India with the Ladakh Island Arc at about 54 Ma ago. The first middle Eocene ingression with coccolith-bearing nannoplankton into the Otway Basin was the distal tongue of the Eucla Basin transgression. This ingression has been linked with a major acceleration in the seafloor spreading rate south of Australia at about 44 Ma ago (Shafik, 1983).

Based on interpretations of the depositional palaeoenvironments of sediment samples, using nannofossils and lithological evidence, together with palynological data (Alley, 1988), it is concluded that the seafloor of the Great Australian Bight Basin must have subsided considerably since the Late Cretaceous. The effect of this subsidence on the nannoflora was first noticeable in middle Eocene assemblages, coincident with a major acceleration in the rate of seafloor spreading south of Australia. This middle Eocene increase in the subsidence rate evidently ended a distinctive stage of a very slow subsidence which was initiated at about 90 Ma ago. A latest late Eocene drastic fall in sea level masked the effect of the subsidence well into the Oligocene.

There is evidence to suggest that surface-water temperatures decreased in an eastward direction along the Australian southern margin during much of the Eocene and Oligocene. This was probably caused by an eastward declining effect of a warm current, similar to the present Leeuwin Current, coming from the Indian Ocean since the middle Eocene. The flow of this proto-Leeuwin Current was intermittent, being prominent at times during the middle and late Eocene and during the mid Oligocene.

The excursion of the key low-latitude nannofossil *Sphenolithus ciperoensis* into southern Australia, previously documented in the onshore and offshore areas of the Otway Basin, is demonstrated in the Great Australian Bight Basin.

Acknowledgements

I thank Drs H.L. Davies and P.J. Davies of the Bureau of Mineral Resources, who critically read the manuscript. Their comments were most valuable. The figures were drafted by Mr Larry Hollands and the photographs were printed by Mr P.W. Davis. My thanks to both. The manuscript benefited from criticism by two anonymous reviewers.

References

Alley, N.F., 1988 — Preliminary palynological results. *In Bureau of Mineral Resources, Australia, Record* 1988/16, Appendix 4, 1–2.

Baldi-Beke, M., 1984 — The nannoplankton of the Transdanubian Paleogene formations. *Geologica Hungarica, Series Palaeontologica*, 43, 307 pp.

Barbin, V., 1989 — Calcareous nannofossil assemblages from the Brendola section (Priabonian Stage Stratotype area, Northern Italy). *Marine Micropaleontology*, 14, 327–338.

Berggren, W.A., 1969 — Paleogene biostratigraphy and planktonic foraminifera of northern Europe. *In* Brönnimann, P., & Renz, H. H., (editors), Proceedings of the First International Conference on Planktonic Microfossils, Geneva, 1967. *E.J. Brill, Leiden*, 1, 121–160.

Berggren, W.A., Kent, D.V., & Flynn, J.J., 1985 — Jurassic to Paleogene: Part 2. Paleogene geochronology and chronostratigraphy. *In* Snelling, N.J., (editor), The chronology of the geological record. *The Geological Society, Memoir* 10, 141–195.

Blow, W.H., 1969 — Late middle Eocene to Recent planktonic foraminiferal biostratigraphy. *In* Brönnimann, P., & Renz, H. H., (editors), Proceedings of the First International Conference on Planktonic Microfossils, Geneva, 1967. *E.J. Brill, Leiden*, 1, 199–422.

Blow, W.H., 1979 — The Cainozoic Globigerinida. *E.J. Brill, Leiden*.

Bukry, D., 1970 — Coccolith age determinations, Leg 2, DSDP. Initial Reports of the Deep Sea Drilling Project, 2, *United States Government Printing Office, Washington*, 349–355.

Bukry, D., 1973 — Low-latitude coccolith biostratigraphic zonation. *In* Edgar, N.T., Saunders, J.B., & others, Initial Reports of the Deep Sea Drilling Project, 15, *United States Government Printing Office, Washington*, 685–703.

Bukry, D., 1974 — Coccoliths as paleosalinity indicators — evidence from the Black Sea. *American Association of Petroleum Geologists, Memoir* 20, 353–363.

Bukry, D., Douglas, R.G., Kling, S.A., & Krasheninnikov, V.A., 1971 — Planktonic microfossil biostratigraphy of the northwestern Pacific Ocean. Initial Reports of the Deep Sea Drilling Project, 6, *United States Government Printing Office, Washington*, 1253–1300.

Bybell, L., & Gartner, S., 1972 — Provincialism among mid-Eocene calcareous nannofossils. *Micropaleontology*, 18, 319–336.

Cande, S.C., & Mutter, J.C., 1982 — A revised identification of the oldest seafloor spreading anomaly between Australia and Antarctica. *Earth and Planetary Science Letters*, 58, 151–161.

Cande, S.C., Mutter, J.C., & Weissel, J.F., 1981 — A revised model for the break-up of Australia and Antarctica. *Eos*, 62, 384.

Crenshaw, M.A., 1964 — Coccolith formation by two marine coccolithophorids, *Coccolithus huxleyi* and *Hymenomonas* sp. *Ph.D. thesis, Duke University, Durham, North Carolina*.

Cresswell, G.R., & Golding, T.J., 1980 — Observations of a south-flowing current in the southeastern Indian Ocean. *Deep-Sea Research*, 27A, 449–466.

Davies, H.L., & others, 1988 — Geological results of R/V *Rig Seismic* Cruise 11, Great Australian Bight Basin 1986. *Bureau of Mineral Resources, Australia, Record* 1988/16.

Edwards, A.R., 1971 — A calcareous nannoplankton zonation of the New Zealand Paleogene. *In* Farinacci, A., (editor), Proceedings of the 2nd Planktonic Conference, Roma, 1970. *Edizioni Tecnoscienza, Roma*, 318–336.

Gartner, S., 1971 — Calcareous nannofossils from the JOIDES Blake Plateau cores, and revision of Paleogene nannofossil zonation. *Tulane Studies in Geology and Palaeontology*, 8(3), 101–121.

Haq, B.U., Hardenbol, J., & Vail, P.R., 1988 — Mesozoic and Cenozoic chronostratigraphy and cycles of sea-level change. *In* Sea-level changes — an integrated approach. *Society of Economic Paleontologists and Mineralogists, Special Publication* 42, 71–108.

Hegarty, K.A., Weissel, J.K., & Mutter, J.C., 1988 — Subsidence history of Australia's southern margin: constraints on basin models. *American Association of Petroleum Geologists, Bulletin* 72, 615-633.

Kennett, J.P., 1977 — Cenozoic evolution of the Antarctic glaciation, the circum-Antarctic Ocean and their impact on global paleoceanography. *Journal of Geophysical Research*, 82 (27), 3843-3860.

Kennett, J.P., & others, 1975 — Cenozoic paleoceanography in the southwest Pacific Ocean, Antarctic glaciation, and the development of the circum-Antarctic current. *In* Kennett, J.P., Houtz, R.E., & others, Initial Reports of the Deep Sea Drilling Project, 29, *United States Government Printing Office, Washington*, 1155-1169.

Kothe, A., Khan, A.M., & Ashraf, M., 1989 — Biostratigraphy of the Surghar Range, Salt Range, Sulaiman Range and the Kohat area, Pakistan, according to Jurassic through Paleogene calcareous nannofossils and Paleogene dinoflagellates. *Geologisches Jahrbuch, Reihe B*, 71, 3-87.

Legeckis, R., & Cresswell, G.R., 1981 — Satellite observations of sea-surface temperature fronts off the coast of western and southern Australia. *Deep-Sea Research*, 28A, 297-306.

Ludbrook, N.H., & Lindsay, J.M., 1969 — Tertiary foraminiferal zones in South Australia. *In* Brönnimann, P., & Renz, H.H. (editors), Proceedings of the First International Conference on planktonic microfossils, Geneva 1967. *E.J. Brill, Leiden*, 2, 366-374.

Martini, E., 1965 — Mid-Tertiary calcareous nannoplankton from Pacific deep-sea cores. *In* Whittard, W.F., & Bradshaw, R.B., (editors), Submarine geology and geophysics. Proceedings of the 17th Symposium of the Colston Research Society. *Butterworths, London*, 393-411.

Martini, E., 1970 — The occurrence of pre-Quaternary calcareous nannoplankton in the oceans. *In* Funnell, B., & Riedel, W.R., (editors), The micropaleontology of oceans. *Cambridge University Press, Cambridge*, 535-544.

Martini, E., 1971 — Standard Tertiary and Quaternary calcareous nannoplankton zonation. *In* Farinacci, A., (editor), Proceedings of the 2nd Planktonic Conference, Roma 1970. *Edizioni Tecnoscienza, Roma*, 2, 739-785.

Maxwell, J.G.H., & Cresswell, G.R., 1981 — Dispersal of tropical marine fauna to the Great Australian Bight by the Leeuwin Current. *Australian Journal of Marine and Freshwater Research*, 32, 493-500.

McGowran, B., 1965 — Two Paleocene foraminiferal faunas from Wangerrip Group, Pebble Point coastal section, western Victoria. *Proceedings of the Royal Society of Victoria*, 79, 9-74.

McGowran, B., 1968 — Late Cretaceous and early Tertiary correlations in the Indo-Pacific region. *Memoir of the Geological Society of India*, 2, 335-360.

McGowran, B., 1970 — Late Paleocene in the Otway Basin: biostratigraphy and age of key microfaunas. *Transactions of the Royal Society of South Australia*, 94, 1-14.

McGowran, B., 1978 — Early Tertiary foraminiferal biostratigraphy in southern Australia: a progress report. *In* Belford, D.J., & Scheibnerova, V., (compilers), The Crespin volume: Essays in honour of Irene Crespin. *Bureau of Mineral Resources, Australia, Bulletin* 192, 83-95.

McGowran, B., 1988a — Foraminiferal biostratigraphy of dredged samples. *Bureau of Mineral Resources, Australia, Record* 1988/16, Appendix 2, 1-8.

McGowran, B., 1988b — Foraminiferal biostratigraphy. *In* Davies, H.L., & others, Maastrichtian and younger sediments from the Great Australian Bight. *Bureau of Mineral Resources, Australia, Report* 288, 27-33.

McGowran, B., in press — Maastrichtian and Early Cainozoic, southern Australia: planktonic foraminiferal biostratigraphy. *In* Williams, M.A.J., The Cainozoic of the Australian region. *Geological Society of Australia, Special Publication*.

McGowran, B., Lindsay, J.M., & Harris, W.K., 1971 — Attempted reconciliation of Tertiary biostratigraphic systems. *In* Wopfner, H., & Douglas, J.G., (editors), The Otway Basin of southeastern Australia. *Special Bulletin of the Geological Surveys of South Australia and Victoria*, 273-281.

McIntyre, A., & Bé, A.W.H., 1967 — Modern Coccolithophoridae of the Atlantic Ocean. I. Placoliths and crytoliths. *Deep-Sea Research*, 14, 561-597.

Mutter, J.C., Hegarty, K.A., Cande, S.C., & Weissel, J.K., 1985 — Breakup between Australia and Antarctica: a brief review in the light of new data. *Tectonophysics*, 114, 255-279.

Okada, H., & Honjo, S., 1973 — The distribution of oceanic coccolithophorids in the Pacific. *Deep-Sea Research*, 20, 355-374.

Okada, H., & Honjo, S., 1974 — Community structure of coccolithophores in the photic layer of the mid-Pacific. *Micropaleontology*, 20, 209-230.

Paasche, E., 1964 — A tracer study of the inorganic carbon uptake during coccolith formation and photosynthesis in the coccolithophorid *Coccolithus huxleyi*. *Physiologia Plantarum, Supplementum* 3, 82 pp.

Paasche, E., 1965 — The effect of 3-(p-Chlorophenyl)-1, 1-Dimethylurea (CMU) on photosynthesis and light-dependent coccolith formation in *Coccolithus huxleyi*. *Physiologia Plantarum*, 18, 138-145.

Paasche, E., & Klaveness, D., 1970 — A physiological comparison of coccolith-forming and naked cells of *Coccolithus huxleyi*. *Archiv für Mikrobiologie*, 73, 143-152.

Patriat, P., & Achache, J., 1984 — India-Eurasia collision chronology has implications for crustal shortening and driving mechanism of plates. *Nature*, 5987, 615-621.

Rochford, D.J., 1984 — Effect of the Leeuwin Current upon sea surface temperatures off south-western Australia. *Australian Journal of Marine and Freshwater Research*, 35, 487-489.

Rochford, D.J., 1986 — Seasonal changes in the distribution of the Leeuwin Current waters off southern Australia. *Australian Journal of Marine and Freshwater Research*, 37, 1-10.

Roth, P.H., 1974 — Calcareous nannofossils from the northwestern Indian Ocean, Leg 24, Deep Sea Drilling Project. *In* Fisher, R.L., Brunce, E.T., & others, Initial Reports of the Deep Sea Drilling Project, 24, *United States Government Printing Office, Washington*, 969-994.

Royer, J.-Y., & Sandwell, D.T., in press — Evolution of the Eastern Indian Ocean since the Late Cretaceous: constraints from Geosat altimetry. *Journal of Geophysical Research*.

Ruddiman, W.F., & McIntyre, A., 1976 — Northeast Atlantic paleoclimatic changes over the past 6 000 000 years. *Memoir of the Geological Society of America*, 145, 111-146.

Shafik, S., 1973 — Eocene-Oligocene nannoplankton biostratigraphy in the western and southern margins of Australia. *Australian and New Zealand Association for Advancement of Science, 45th Congress, Abstracts, Section 3*, 101-103.

Shafik, S., 1978 — Paleocene and Eocene nannofossils from the Kings Park Formation, Perth Basin, Western Australia. *In* Belford, D.J., & Scheibnerova, V., (compilers), The Crespin volume: Essays in honour of Irene Crespin. *Bureau of Mineral Resources, Australia, Bulletin* 192, 165-172.

Shafik, S., 1983 — Calcareous nannofossil biostratigraphy: an assessment of foraminiferal and sedimentation events in the Eocene of the Otway Basin, southeastern Australia. *BMR Journal of Australian Geology & Geophysics*, 8, 1-17.

Shafik, S., 1985 — Cretaceous coccoliths in the middle Eocene of the western and southern margins of Australia: evidence of a significant reworking episode. *BMR Journal of Australian Geology & Geophysics*, 9, 353-359.

Shafik, S., 1987a — Coccoliths from the Otway Basin dredge samples. *In* Exon, N.F., Williamson, P.E., & others, *Rig Seismic* research cruise 3; offshore Otway Basin, southeastern Australia. *Bureau of Mineral Resources, Australia, Report* 279, 27-35.

Shafik, S., 1987b — Tertiary nannofossils from offshore Otway Basin and off West Tasmania. *Bureau of Mineral Resources, Australia, Record* 1987/11, 67-96.

Shafik, S., 1988a — Ages of selected samples from calcareous nannofossils. *Bureau of Mineral Resources, Australia, Record* 1988/16, Appendix 3, 1-11.

Shafik, S., 1988b — Calcareous nannofossil biostratigraphy. *In* Davies, H.L., & others, Maastrichtian and younger sediments from the Great Australian Bight. *Bureau of Mineral Resources, Australia, Report* 288, 14-27.

Shafik, S., in press — Late Cretaceous nannofossil biostratigraphy and biogeography of the Australian western margin. *Bureau of Mineral Resources, Australia, Report* 295.

Sherwood, R.W., 1974 — Calcareous nannofossil systematics, paleontology, and biostratigraphy of the middle Eocene Weches Formation of Texas. *Tulane Studies in Geology and Paleontology*, 11, 1-79.

Singleton, O.P., 1967 — Otway Region. *Australian and New Zealand Association for Advancement of Science, 39th Congress, Section C, Excursions Handbook*, 171–181.

Tappan, H., 1980 — The paleobiology of plant protists. *Freeman & Co., San Francisco*.

Tappan, H., 1986 — Phytoplankton: below the salt at the global table. *Journal of Paleontology*, 60, 545-554.

Taylor, D., 1971 — Foraminifera and the Cretaceous and Tertiary depositional history in the Otway Basin in Victoria. *In* Wopfner, H., & Douglas, J.G., (editors), The Otway Basin of southeastern Australia. *Special Bulletin of the Geological Surveys of South Australia and Victoria*, 217–234.

Wilbur, K.M., & Watabe, N., 1963 — Experimental studies on calcification in molluscs and alga *Coccolithus huxleyi. Annals of the New York Academy of Sciences*, 109, 82–112.

Williamson, P.E., Exon, N.F., Swift, M.G., O'Brien, G.W., Heggie, D.T., McKirdy, M., Lee, C.S., & Stephenson, A.E., 1988 — Offshore Otway Basin study. *Continental Margins Folio* 2, *Bureau of Mineral Resources, Canberra*.

Williamson, P.E., Swift, M.G., O'Brien, G.W., & Falvey, D.A., 1990 — Two-stage Early Cretaceous rifting of the Otway Basin margin of southeastern Australia: implications for rifting of the Australian southern margin. *Geology*, 18, 75–78.

Winter, A., Reiss, Z., & Luz, B., 1979 — Distribution of living coccolithophore assemblages in the Gulf of Elat (Aqaba). *Marine Micropaleontology*, 3, 295–298.

BMR Journal of Australian Geology & Geophysics, 11, 499-507

Pattern of slow seafloor spreading (<4 mm/year) from breakup (96 Ma) to A20 (44.5 Ma) off the southern margin of Australia

J.J. Veevers[1], H.M.J. Stagg[2], J.B. Willcox[2] & H.L. Davies[3]

Australia separated from Antarctica by continental extension between the mid-Jurassic (>160 Ma) and mid-Cretaceous (96 Ma), then by slow seafloor spreading (half-rate <4.4 mm/year) on a separation azimuth of 335° until A21 time (49 Ma), at an intermediate half-rate (10 mm/year) until A20 time (44.5 Ma), and then at a fast rate (20 mm/year) on a separation azimuth of 360° to the present. A compilation of seafloor spreading magnetic data for the entire southern margin, including critical data collected during the cruise of the R/V *Rig Seismic* in 1986, confirms the previous work except for the re-interpretation of the oldest anomalies. The phase of slow spreading is characterised by (a) jumps of the spreading ridge to Australia between 131.25°E and Tasmania to accommodate the southeastward offset of the line of separation between Tasmania and Antarctica, and (b) variable azimuths of spreading isochrons within individual spreading segments, as, for example, from 090°±5° between 129° and 130°E (an angle of 65° between separation and spreading azimuths) and 075° and 080° between 130° and 131.75°E (an almost orthogonal 80°). The variable azimuth of the spreading isochrons, oblique to the separation azimuth, is similar to that found in the young (<5 Ma) slow spreading (half-rate 10 mm/year) ocean basin of the Gulf of Aden, and is interpreted as the response of a slow spreading system to confinement between continental margins whose boundaries are oblique to the separation azimuth.

Introduction

Before breakup in the mid-Cretaceous, Antarctica and Australia separated by several hundred kilometres of continental extension that started in the Jurassic. Two models of this extension have been made. The model of Veevers (1987a), Powell & others (1988), and Veevers & Eittreim (1988) postulates extension in the Great Australian Bight on the same SSW azimuth as that in the Bass Strait (Etheridge & others, 1984); the amount of extension along this azimuth was estimated as 360 km from crustal thinning in the zone of extension on the conjugate margins. The model of Etheridge & others (in press) and Willcox & others (1987) involves extension in the Great Australian Bight on a SE azimuth, indicated by transfer faults interpreted from seismic profiles in the Eyre Sub-basin (Bein & Taylor, 1981) and elsewhere; as in the other model, the amount of extension is estimated from crustal thinning. Both models remain tentative in the absence of data on the azimuth of extension on the conjugate Antarctic margin. By contrast, relatively abundant information is available about the subsequent separation of Australia and Antarctica by seafloor spreading of the Southeast Indian Ocean.

Since breakup of Antarctica and Australia 96 Ma ago, the Southeast Indian Ocean has developed in three stages of seafloor spreading (Fig. 1, Table 1), as first shown by Cande & Mutter (1982): stage 1 (96–49 Ma) at a slow half-rate of <4.4 mm/year, stage 2 (49–44.5 Ma) at an intermediate half-rate of 10 mm/year, and stage 3 (44.5 Ma to present) at a fast half-rate of 20 mm/year. Magnetic isochrons and fracture zone trends (Weissel & Hayes, 1972; Vogt & others, 1983) generated in stage 3 are clear (Fig. 1). Isochrons generated in stages 2 and 1 are also clear, despite the poor resolution of some individual anomalies due to slow spreading, but until recently fracture zone trends were unknown. A synthetic separation azimuth was derived by interpolation between the reconstruction at A20 (finite pole c′) and the continent-ocean boundary (COB) (finite pole c) to give a 500 km separation on an azimuth of 155° (Veevers & Eittreim, 1988). This azimuth has been confirmed by the recent mapping by satellite altimetry (Haxby, 1987; Sandwell & McAdoo, 1988) of the trace of the George V Fracture Zone in the zone of slow spreading off Antarctica (Fig. 1) (Veevers, 1988; Veevers, in press).

[1] School of Earth Sciences, Macquarie University, NSW 2109
[2] Marine Geoscience and Petroleum Geology Program, Bureau of Mineral Resources, GPO Box 378, Canberra, ACT 2601
[3] Geology Department, University of Papua New Guinea, Box 320, University PO, Papua New Guinea; formerly Marine Geoscience and Petroleum Geology Program, Bureau of Mineral Resources.

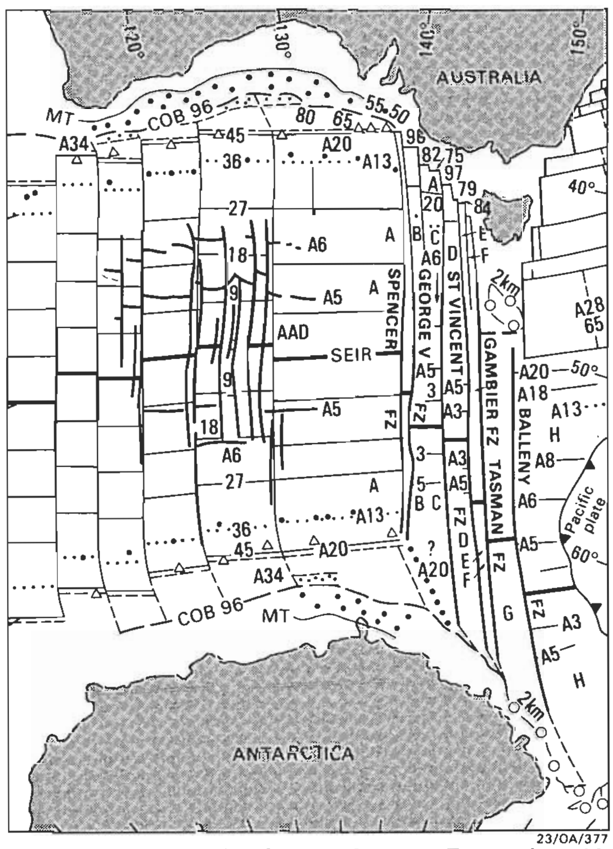

Figure 1. Southeast Indian Ocean and western Tasman Sea with adjacent continents.

Lambert equal-area projection. From Veevers (1988), by permission of the Geological Society of Australia.

SE Indian Ocean and SE Indian Ridge (SEIR): observed magnetic anomalies and fracture zones about the Australian–Antarctic discordance (AAD) (heavy lines) from Vogt & others (1983); observed A13 (dot), A20 (triangle) and magnetic trough (MT) W of Spencer Fracture Zone (FZ) from Konig (1987); A34, and A20 in segment B off Antarctica, from Veevers (1987a); details of fracture zones E of 138° (observed FZs in heavy lines) interpreted from Sandwell & McAdoo (1988); information to the E of the Balleny FZ from Circum-Pacific Map Project (1981); notional A13 (dotted line) and A20 (full line) W of Tasmania from this paper; continent-ocean boundary (COB) and age of oldest oceanic crust (Ma) from Veevers (1987a, 1988); magnetic quiet zones: continental margin (heavy stipple), Cretaceous (fine stipple). Fine lines linking conjugate points on the COBs are synthetic fracture zones for the fast and intermediate spreading phases (0–49 Ma) and short broken lines for the slow spreading phase between A21 (49 Ma) and 96 Ma; A21 is shown by long broken lines; heavy dotted line shows SE continuation of the George V FZ interpreted by Veevers (in press) from SEASAT and GEOSAT altimetry/gravity measurements (Haxby 1987; Sandwell & McAdoo, 1988). Seafloor spreading isochrons: fast spreading modelled by rotation from stage poles 3′ and 3″, intermediate from pole 2, and slow from pole 1.

Tasman Sea, E of Tasmania: A28 (broken line) marks the position of the spreading ridge abandoned at 65 Ma.

Table 1. Poles for reconstructing Antarctica to Australia.
Positive values indicate north latitudes, east longitudes, and anticlockwise rotations when viewed from above the pole.

	Pole	*Age (Ma)*	*Latitude (°)*	*Longitude (°)*	*Angle (°)*		*Notes and references*
Finite poles and angles, relative to Australia							
	a	96	1.5	37.0	27.85		Konig (1987), angle adjusted by Veevers (1987a)
	b	49 (A21y)	13.0	31.5	24.9		Derived from c′ by Powell & others (1988)
	c′	44.5 (A20)	13.0	31.5	24.1		Konig (1987)
	c″	35.5 (A13)	12.0	34.0	20.8		Angle adjusted by Veevers (1987b) from Konig (1987)
Stage poles and angles, relative to Australia							
Spreading rate						*separation (km) azimuth (°)*	
Slow	1 a–b	96–49 COB-A21y	-39.56	80.2	6.49	500 km 155°	Powell & others (1988)
Intermediate	2 b–c′	49–44.5 A21y-A20	13.0	31.5	0.8		Powell & others (1988)
	3′ c′–c″	44.5–35.5 A20-A13	15.23	15.16	3.46		Derived from finite poles
Fast						2600 km 180°	
	3″	35.5–0	12.0	34.0	20.8 c″		Derived from finite poles

Quantities given to 1 or 2 decimals for the sake of repeatibility. Konig (1987) estimates the uncertainty of the finite poles as ±1.5° in latitude and ±1.2° in longitude.

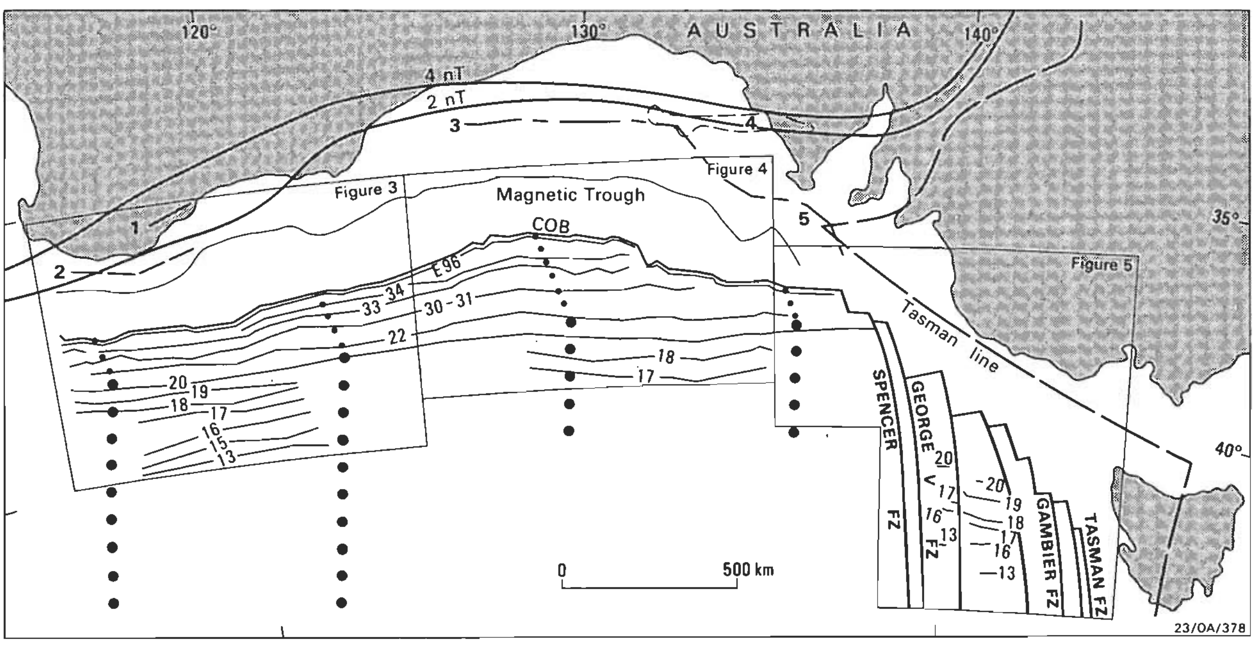

Figure 2. Magnetic trends of the southern margin and adjacent Southeast Indian Ocean.
Lambert equal-area projection. Boxes show the location of Figures 3-5. Magnetic trends are (a) selected MAGSAT anomalies (in nanoTeslas, nT) (Johnson & Mayhew, 1985); (b) magnetic trough; (c) magnetic anomaly (E96) near the 96 Ma continent-ocean boundary (COB); (d) seafloor spreading magnetic anomalies A34, 33, 31/30, 22, and 20, generated during slow and subsequent intermediate spreading; and (e) A19-15, A13, generated during fast spreading. The fine dotted lines are the synthetic fracture-zone azimuths generated during slow spreading (small circles about stage pole 1, Table 1) and the coarse dotted lines the synthetic fracture zones generated during fast spreading (stage 1 pole 3′). Estimated position of fracture zones east of 138°E shown by heavy lines. Other features shown are (1) the Bremer Fault (Geological Society of Australia, 1971) parallel to the Archean/Proterozoic boundary; (2) the basement flexure of the Bremer Basin (Cooney & others, 1975); (3) the west-east-trending northern edge of the Eyre Sub-basin as shown by contours of depth to basement (Bein & Taylor, 1981; Fraser & Tilbury, 1979); (4) the outline of the Polda Trough (Nelson & others, 1986); and (5) the northern edge of the Duntroon Basin (Fraser & Tilbury, 1979).

Before the satellite altimetry data were available, the best estimate by direct evidence of the separation azimuth was from the pattern of the seafloor spreading isochrons. In an attempt at precisely determining this pattern, detailed magnetic mapping in two areas of the Great Australian Bight region was undertaken during the cruise of the *Rig Seismic* in November–December 1986 and was followed by a fresh compilation from primary sources of magnetic data along the entire southern margin, including the hitherto unmapped area off western Tasmania (Veevers, 1988). With the

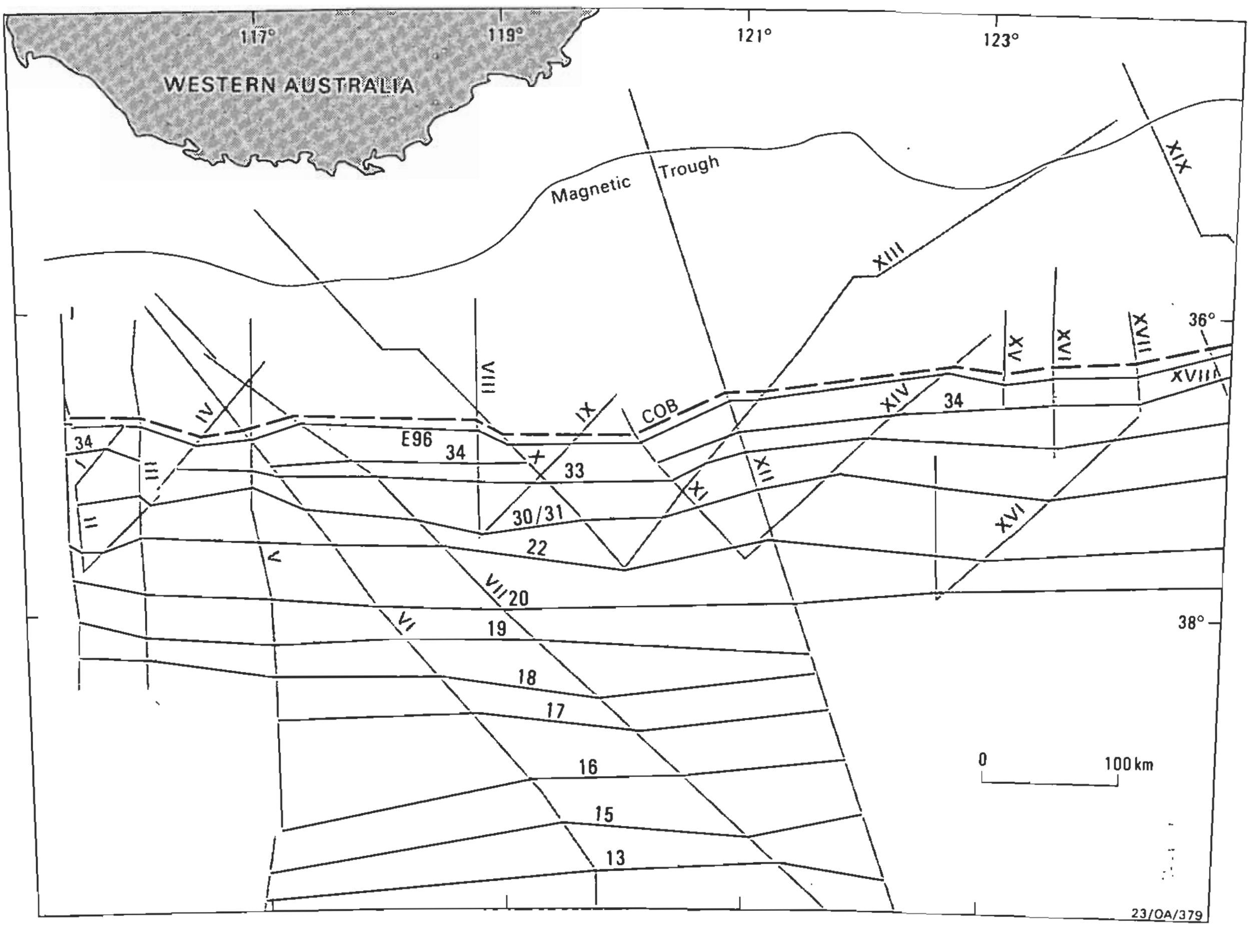

Figure 3. Western area, located in Figure 2, showing magnetic trough, COB, peak of edge anomaly (E96), and seafloor spreading magnetic anomalies A34, 33, 31/30, 22, 20-15, and 13, from ships' tracks I-XIX.
Source of data in this and allied Figures 4–6 given in caption to Figures 7 and 8. Simple conical projection with two standard parallels at 18° and 36°S.

confirmation by satellite-altimetry observations of the synthetic azimuth of the stage of slow separation, the trend of the magnetic isochrons generated during this stage can now be compared with the observed azimuth of separation to see whether they are orthogonal or oblique to the separation azimuth.

Pattern of spreading during slow drift

Magnetic anomaly data are presented for the entire southern margin region (Fig. 2), individually for the western (Fig. 3), central (Fig. 4), and eastern (Fig. 5) sectors, in a detail of the central sector containing the *Rig Seismic* surveys (Fig. 6), and in sets of stacked profiles from all the available ships' tracks (Figs 7, 8). In presenting at common scales all the profiles from the western and central sectors, Figures 7 and 8 are an expansion of the previous work by Talwani & others (1979), Cande & Mutter (1982) and Konig (1980, 1987), who stacked selected profiles only. These figures include the tentatively identified anomalies east of the George V Fracture Zone (Veevers, 1988).

The compilation confirms the position of the previously mapped anomalies except for minor differences in a few areas. We follow Veevers (1986) in re-interpreting the crest of the prominent anomaly near the seismically determined COB as an edge anomaly called E96 (Figs 7, 8) in place of Weissel & Hayes' (1972) A22 and Cande & Mutter's (1982) and Konig's (1987) A34; the first negative anomaly seaward of the Cretaceous normal polarity interval, reflecting the edge of the first reversely polarised block with an age of 84 Ma, is picked as A34.

Sector west of 131.25° E

A full set of A-series anomalies to the Cretaceous quiet zone is found west of the change in trend of the COB at 131.25° E on the southern margin of Australia (Figs 1, 7) and west of 132.5° E on the conjugate Antarctic margin. The westerly convergence of the COB and anomalies A34 to A20 off Australia is indicated by the change in half-rate from 4.4 mm/year east of profile XVII at 124° E to 2.65 mm/year west of it. This contrasts with the parallel COB and A20 off Antarctica and the symmetry of the Australian and Antarctic profiles at 132° E (profiles El 37 and 41 in fig. 9 of Veevers, 1987a), suggesting that spreading in the west was asymmetrical. The slower spreading Australian limb corresponds to the Diamantina Zone, which is prominent west of 125° E (Talwani & others, 1979).

Sector between 131.25° E and the George V Fracture Zone

In this sector, the anomalies maintain an easterly trend that converges with the change in trend of the COB to the ESE, so that A34 and progressively younger anomalies to A20 terminate at the COB, as shown in Figures 4 and 5. In the conjugate part off Antarctica, A20 diverges from the COB in compensation for the convergence off Australia (Fig. 1), and the angular width of the floor of the Southeast Indian Ocean, measured along the separation azimuths, is constant. Modelling of the magnetic anomalies off the conjugate margins (Veevers, 1987a) shows that the segment immediately east of 131.25° E off Australia and of 132.5° E off Antarctica contains seafloor as old as 80 Ma against the COB on the

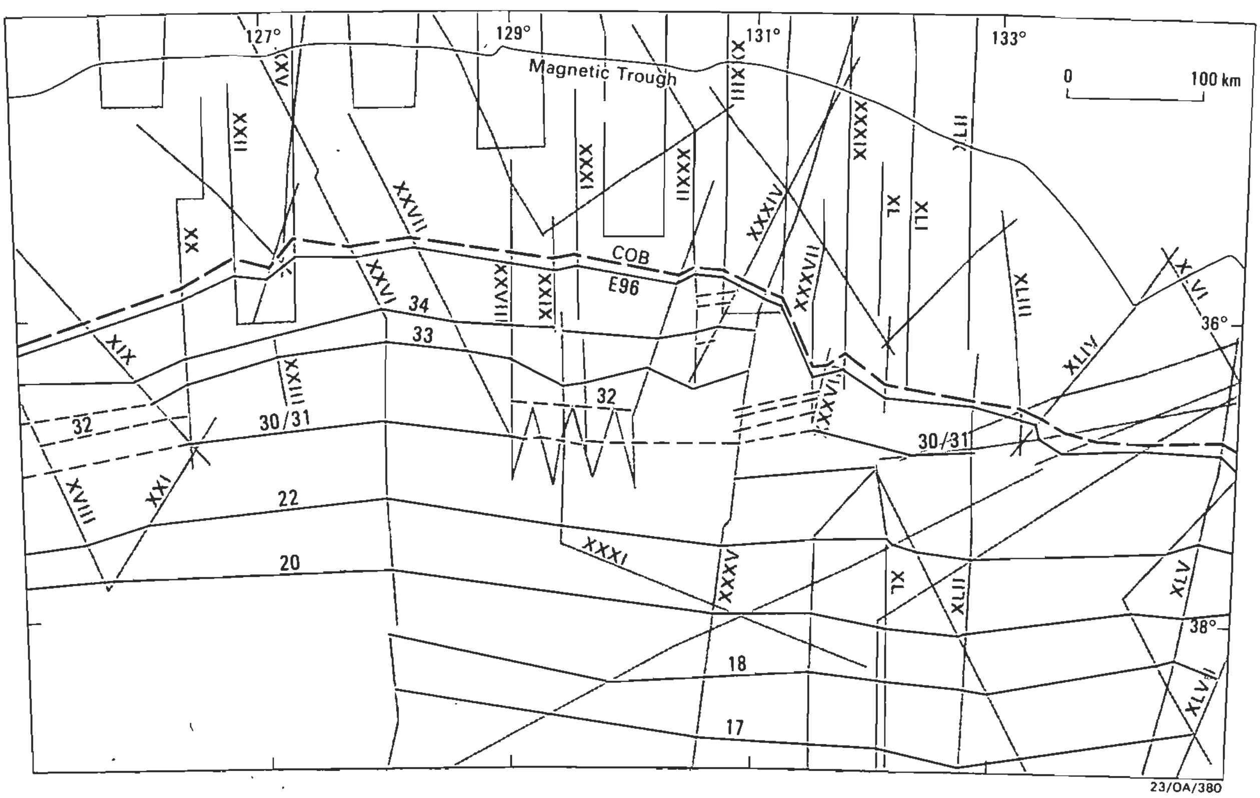

Figure 4. Central area, located in Figure 2, showing magnetic trough, COB, peak of edge anomaly (E96), and seafloor spreading magnetic anomalies A34, 33, 31/30, 22, 20–17, from ships' tracks XVIII–XLVI.

Australian margin, balanced in the eastward widening zone off Antarctica by the length of the missing set from 80 Ma to 96 Ma; this is interpreted as being due to a jump of the spreading ridge to the Australian COB at 80 Ma. The younger ages of truncation of the Australian set of anomalies are interpreted likewise as indicating ridge jumps to the Australian COB at 65, 55, and 50 Ma. In summary, the change in trend of the COB was accommodated in the young Southeast Indian Ocean by transfer of parts of the oceanic plates from Australia to Antarctica by ridge jumps to the Australian COB.

Sector between the George V Fracture Zone and Tasmania

In this sector, the COB has a regional trend of southeast. The tentatively identified A20 in segment B is offset southward across the George V fracture by about 300 km. This is the same distance from the COB as immediately west of 131.25°E, and is consistent with spreading that started at 96 Ma. Slightly shorter distances between A20 and the COB in segments C and D suggest ridge jumps to Australia at about 80 Ma and 75 Ma ago (Veevers, 1988). According to this interpretation, the longer southward offsets in the COB are compensated by equivalent to slightly shorter offsets of the ridge, so that ridge jumps are short compared with those immediately to the west.

Oblique spreading

On the November–December 1986 cruise of the *Rig Seismic*, we made closely spaced traverses of two areas in the central sector (Fig. 4). Eight traverses on track XXVIII no more widely spaced than 15 km show A30/31 to trend 090°±5°. The anomaly thus subtends an angle of 65°±5° with the separation azimuth of 155°, or 25°±5° with the orthogonal. To the northeast, two intersecting traverses (XXXII and XXXIV) of A34 and adjacent anomalies define trends of 075° and 080° that subtend angles of 80° and 75° with the azimuth of separation, or 10° to 15° with the orthogonal. To the southeast, the intersecting tracks of XXXVII and XXXVIII and the parallel XXXV define a trend of 075° in A30/31 and older anomalies. The anomalies subtend an angle of 80° with the azimuth of separation, or 10° with the orthogonal.

The local trend of 075° to 080° between 130°E and 130.75°E is similar to the regional trend west of 128°E (Fig. 2) of the isochrons, the COB, parts of the magnetic trough, a basement flexure, and MAGSAT anomalies (mirrored on the conjugate Antarctic margin; Veevers, 1987b). Between 129°E and 130°E, the local trend of 090°±5° corresponds with the trend of the COB, magnetic trough, a basement flexure, and MAGSAT anomalies to the north. From these geometrical relationships, we infer that west of 128°E, the breakup of Antarctica and Australia at 96 Ma took place along a line, with short north–south offsets, parallel to the ENE-trending magnetic and structural grain. Subsequent seafloor spreading was within 15° of being orthogonal to the separation azimuth. Between 128°E and the George V Fracture Zone, breakup at 96 Ma likewise followed the magnetic and structural grain but here with an easterly trend, as shown by the trend of the MAGSAT anomalies and the axis of the Polda Trough. East° 132.5°E, the trends of the magnetic trough and the basement flexure diverge from that of the MAGSAT anomalies so that two segments of the magnetic trough lie parallel to, and another orthogonal to, the separation azimuth, presumably on lines of incipient shear and extension. Actual shear on a continent–continent transform fault between 131.25°E off Australia and 132.5°E off Antarctica (Figs 1, 2) was along the azimuth of extension.

East of the George V Fracture Zone, individual segments of the COB and corresponding segments of the ridge are

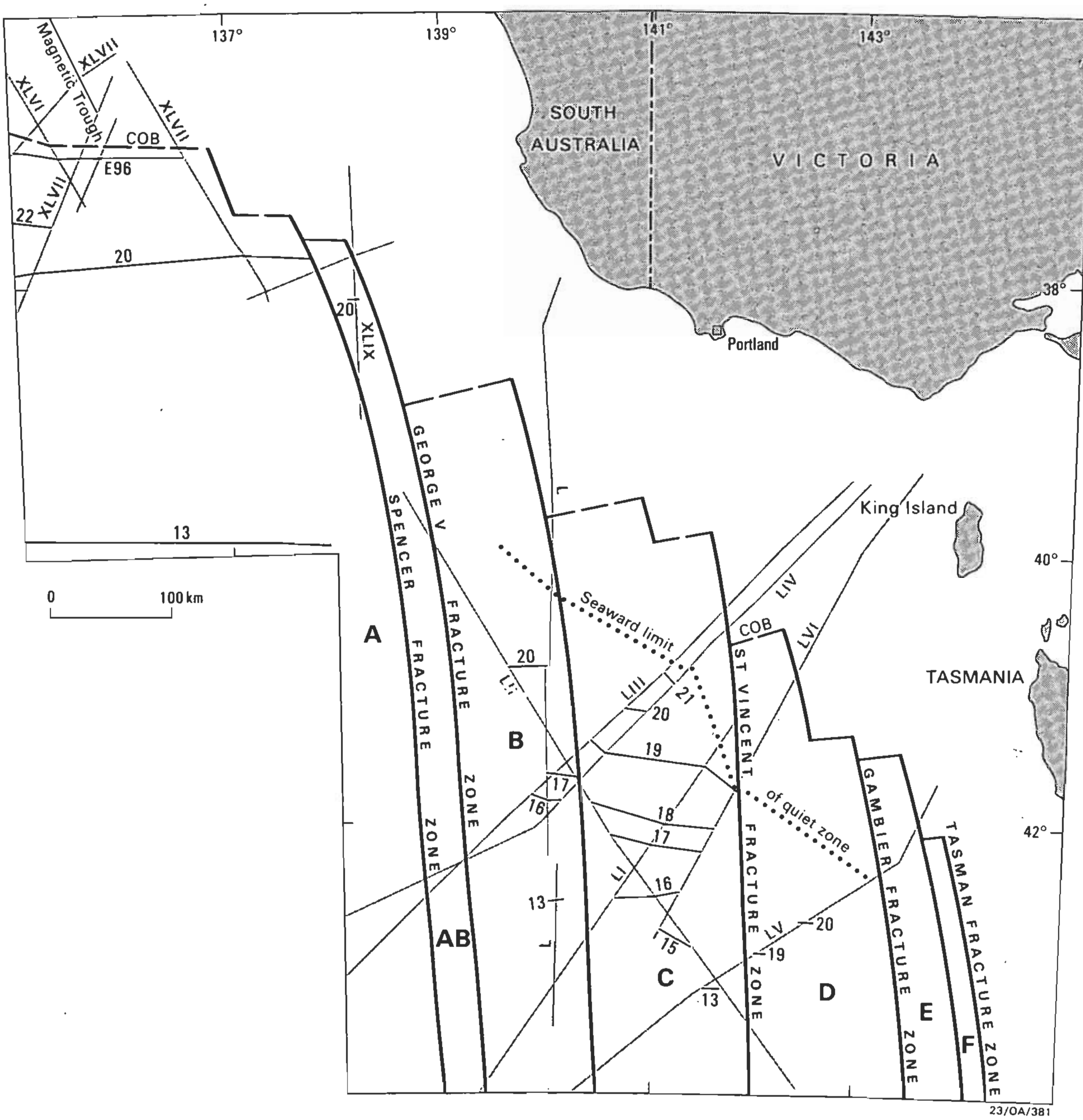

Figure 5. Eastern area, located in Figure 2, showing COB, peak of edge anomaly (E96), and seafloor spreading magnetic anomalies A22, 20–15, 13 from ships' tracks XLVI–LVI.
From Veevers (1988).

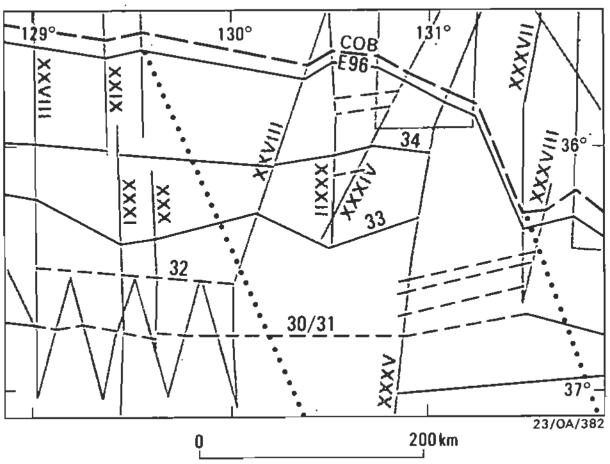

Figure 6. Detail of central area about 36.5° S 130.5° E.
The dotted lines are the synthetic fracture-zone azimuths generated during slow spreading (small circles about stage pole 3, Table 1).

offset southward by as much as 100 km across individual fracture zones, with jumps of the ridge to Australia shorter than those to the west, but no less important in generating structure in the adjacent margin (Veevers, 1988). The trends of the anomalies appear to vary, with a bias towards 105°; this subtends an angle of 50° with the separation azimuth of 155°. The gross southeast trend of the COB between the George V Fracture Zone and 144° E and thence its southerly trend is approximately parallel to the trend between Kangaroo Island and Tasmania (Fig. 2) of the Tasman Line, the boundary between exposed Precambrian terrane and the Phanerozoic Tasman Fold Belt (Veevers, 1984).

Similar relation between spreading and separation azimuths in the Gulf of Aden

Seafloor spreading in the Gulf of Aden between Arabia and Somalia (Fig. 9) started 4.5 Ma ago and followed a stage of continental extension that dates from 30 Ma ago

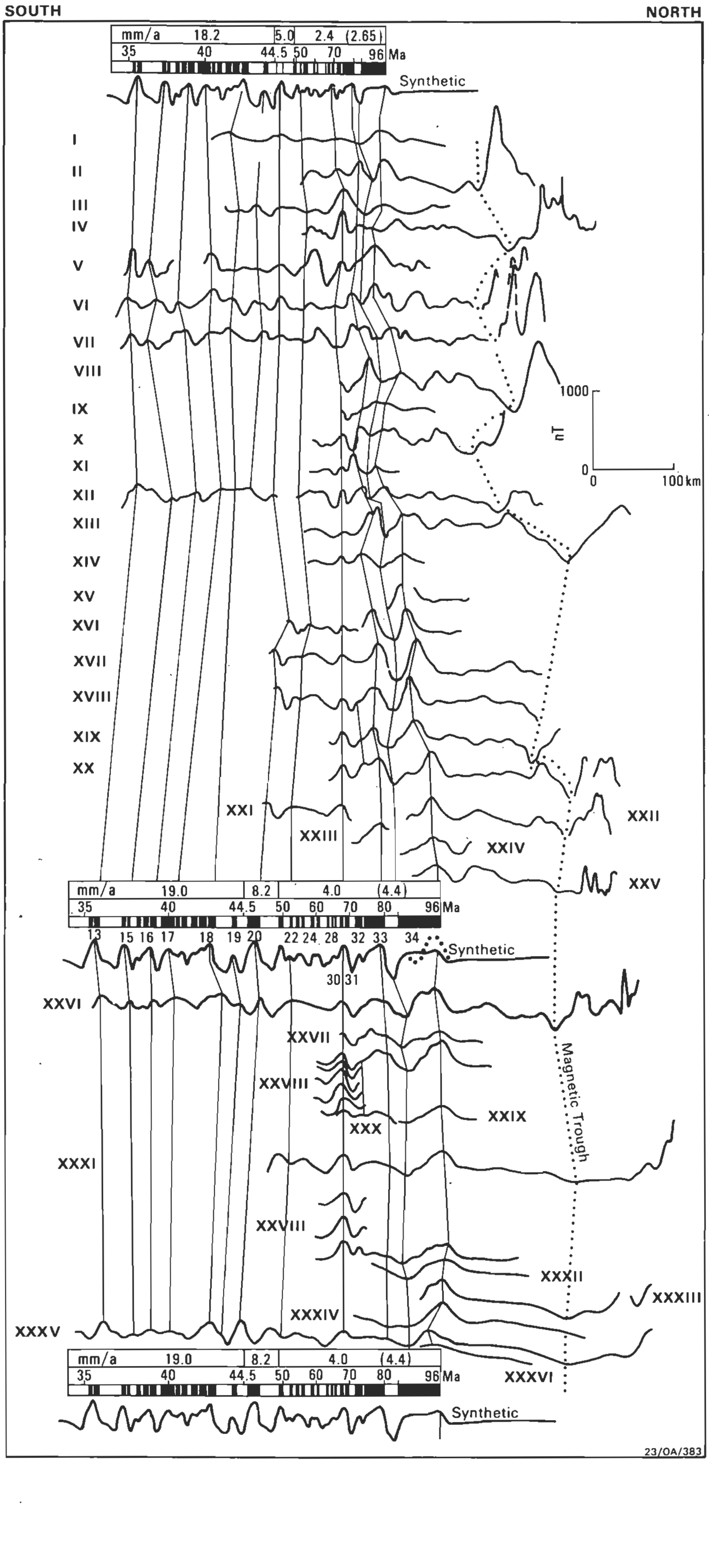

Figure 7. Magnetic anomaly profiles along ships' tracks I-XXXVI for the sector west of 131.25° E.
Projected on an azimuth of 180°, aligned on A20 (I-VII) and then A31 (VIII-XXXVI), and compared with synthetic profiles from Veevers (1986, 1987a) derived from Cande & Mutter (1982), and updated to the time scale of Berggren & others (1985) and Kent & Gradstein (1985). Parameters of block model: source depth 5.5 to 6.0 km, trend 090°, remanent magnetisation 0.007 emu/cm³, I_0 -70°, D_0 10°, I_r -74°, D_r 0°. The higher peak of E96 between XIII and XXXV is modelled (dotted line) by a block between 90 and 96 Ma with magnetisation double that of the other blocks (Veevers, 1986). The spreading half-rates are measured on an azimuth of 180°, and hence correspond to the full rate for the stages of fast and intermediate separation. Slow separation (>A21) had an azimuth of 155°, and the full rates along this azimuth are enclosed in brackets. Information from BMR data file, comprising Lamont-Doherty Geological Observatory data given in Weissel & Hayes (1972), Hayes & others (1975, 1976, 1977, 1978), Konig & Talwani (1977), Talwani & others (1979), Konig (1980, 1987), Cande & Mutter (1982), and BMR data from the early 1970s Marine Geophysical Survey of the Australian Continental margin (Willcox, 1978; Bureau of Mineral Resources, 1979) and the 1986 *Rig Seismic* cruises 10 and 11.

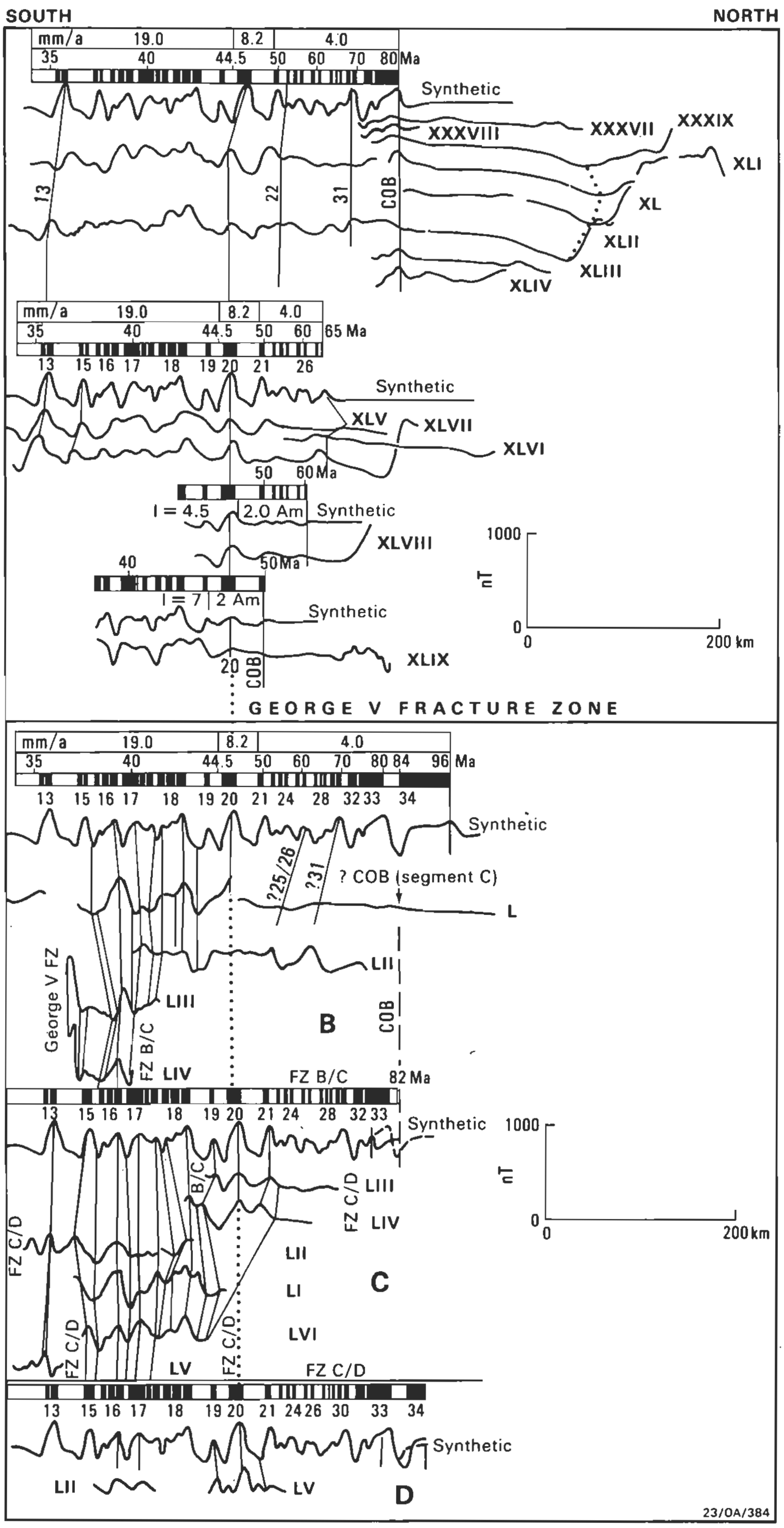

Figure 8. Magnetic anomaly profiles along ships' tracks XXXVII–LVI for the 131.25° E–George V Fracture Zone and George V Fracture Zone–Tasmania sectors.

Projected on an azimuth of 180°, aligned on A20, and compared with synthetic profiles from Veevers (1986, 1987a) east to the George V Fracture Zone, and from Veevers (1988) to the east. Note that the identification of anomalies east of the George V Fracture Zone is tentative. Information from Veevers (1988).

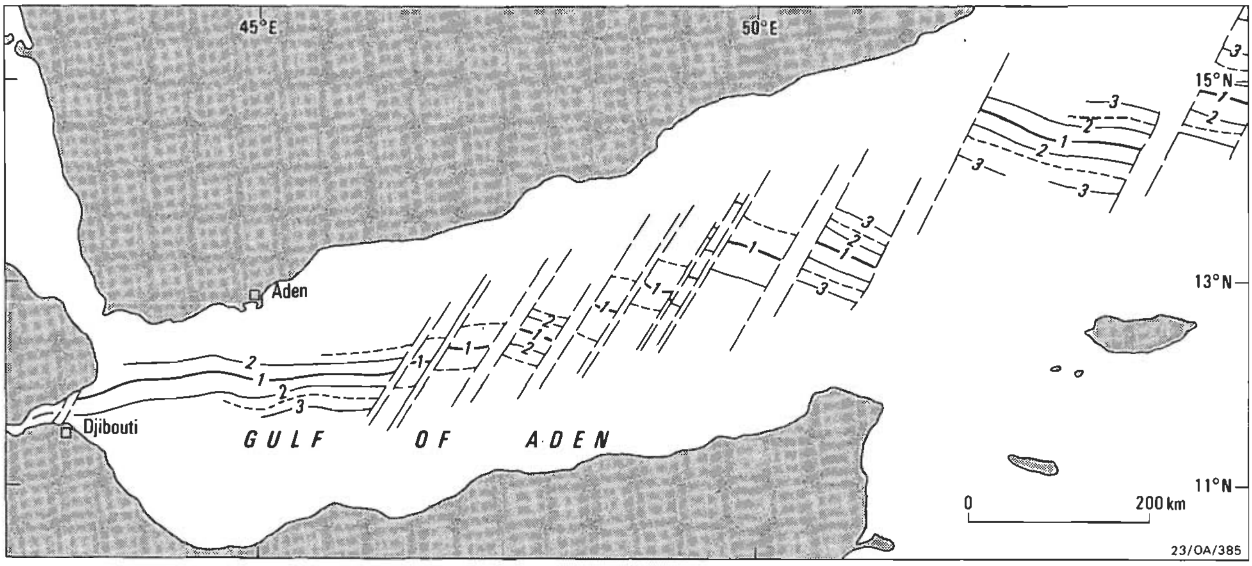

Figure 9. Oblique spreading in the Gulf of Aden.
Isochrons of spreading that started with A3 about 4.5 Ma ago (Hempton, 1987). Azimuth of separation shown by dotted lines. From Laughton and others (1970), by permission of A.S. Laughton and the Royal Society of London.

(Hempton, 1987). The spreading half-rate of 10 mm/year is similar to that of the intermediate stage of spreading between Antarctica and Australia. The separation azimuth, defined by the transform faults, is 210°. It subtends an angle of 77°±5° with the isochron azimuth in the area east of 47.5°E, and 55°±5° to the west. This change of isochron azimuth is sharp, and is interpreted as the response of a slow-intermediate (10 mm/year) spreading system to confinement between continental margins now only 90 km apart, whose boundaries are oblique to the separation azimuth. The variable oblique angles between the azimuths of spreading and separation off the southern margin of Australia are likewise attributable to the narrow space between the continental margins reaching no more than 500 km after 45 Ma of slow spreading (half-rate <4.4 mm/year).

In the stage of fast spreading that followed, the pattern of spreading was apparently unaffected by the now widely separated margins, and ridge jumps were negligible, except in the Australian-Antarctic discordance (AAD) (Weissel & Hayes, 1974; Vogt & others, 1983). Instead, the main irregularity was the asymmetric spreading (Weissel & Hayes, 1972) that brought the Southeast Indian Ridge (SEIR) relatively closer to Antarctica (Fig. 1).

The pattern of slow spreading now detailed in the Great Australian Bight, together with the recognition of ridge jumps to the Australian COB east of 131°E, allows a clearer understanding of the influence of the oceanic crust on the structure and subsidences of the Late Cretaceous and early Cainozoic continental margin.

Postscript. During the 16 months between submission of this paper in May 1988 and its acceptance in September 1989, the following works on the Southeast Indian Ocean and its margins have appeared or been accepted for publication:

1. Veevers (1988), on magnetic anomalies off western Tasmania interpreted as due to jumps of the spreading ridge to Australia;
2. a set of papers that describe and interpret the seafloor trends from satellite altimetry data: Sandwell & McAdoo (1988), Gahagan & others (1988), Lawver & others (in press), Royer & Sandwell (in press), and Veevers (in press).

All confirm the pattern of slow spreading given in this paper and hence the rotation poles given in Table 1, which Royer & Sandwell (in press) subdivide more finely.

Acknowledgements

We thank the ship's crew of the *Rig Seismic* (Captain D. Harvey) and scientific and technical colleagues for their willing cooperation on *Rig Seismic* cruises 10 and 11, B.D. Johnson for the use of his INTERMAP program, M.F. Coffin for supplying a reference, and L.A. Lawver, J.-Y. Royer and D.T. Sandwell for pre-prints. Permission to use previously published figures was granted by the Geological Society of Australia (Fig. 1) and by the Royal Society of London and A.S. Laughton (Fig. 9). The figures were fair-drawn by B. Pashley and D. O'Donoghue. Veevers' work was supported by the Australian Research Grants Scheme.

References

Bein, J., & Taylor, M.L., 1981 — The Eyre Sub-basin: recent exploration results. *The APEA Journal*, 21, 91–98.

Berggren, W.A., Kent, D.V., Flynn, J.J., & van Couvering, J.A., 1985 — Cenozoic geochronology. *Geological Society of America, Bulletin*, 96, 1407–1418.

Bureau of Mineral Resources, 1979 — Australian continental margin survey, scale 1:1 000 000. *Australian Government Publishing Service, Canberra*, 188 sheets.

Cande, S.C., & Mutter, J.C., 1982 — A revised identification of the oldest sea floor spreading anomalies between Australia and Antarctica. *Earth and Planetary Science Letters*, 58, 151–160.

Circum-Pacific Map Project, 1981 — Plate-tectonic map of the Circum-Pacific Region, Southwest Quadrant. 1:10 000 000. *American Association of Petroleum Geologists, Tulsa, Oklahoma.*

Cooney, P.M., Evans, P.R., & Eyles, D., 1975 — Southern Ocean and its margins. *In* Veevers, J.J., (editor), Deep sea drilling in Australasian waters. *Challenger Symposium, Sydney*, 26–28.

Etheridge, M.A., Branson, J.C., Falvey, D.A., Lockwood, K.L., Stuart-Smith, P.G., & Scherl, A.S., 1984 — Basin-forming structures and their relevance to hydrocarbon exploration in Bass Basin, southeastern Australia. *BMR Journal of Australian Geology & Geophysics*, 9, 197–206.

Etheridge, M.A., Symonds, P.A., & Lister, C.R., in press — Application of detachment model to reconstruction of conjugate passive margins. *In* Tankard, A.J., & Balkwill, H.R., (editors), Extensional tectonics and stratigraphy of the North Atlantic margins. *American Association of Petroleum Geologists, Memoir.*

Fraser, A.R., & Tilbury, L.A., 1979 — Structure and stratigraphy of the Ceduna Terrace region, Great Australian Bight Basin. *The APEA Journal*, 19, 53–65.

Gahagan, L.M., Scotese, C.R., Royer, J.-Y., Sandwell, D.T., Winn, J.K., Tomlins, R.L., Ross, M.I., Newman, J.S., Muller, R.D., Mayes, C.L., Lawver, L.A., & Heubeck, C.E., 1988 — Tectonic fabric map of the ocean basins from satellite altimetry data. *Tectonophysics*, 155, 1–26.

Geological Society of Australia, 1971 — Tectonic map of Australia and New Guinea, 1:5 000 000. *Geological Society of Australia, Sydney.*

Haxby, W.F., 1987 — Gravity field of the world's oceans. *National Oceanic and Atmospheric Administration, Boulder, Colorado, Marine Geology & Geophysics Report* 3 (MGG-3).

Hayes, D.E., & others, 1975 — Lamont-Doherty Survey of the World Ocean, Preliminary report of Volume 23, USNS Eltanin, cruises 33–38. *Lamont-Doherty Geological Observatory Technical Report* CU-1-75, 230 pp.

Hayes, D.E., & others, 1976 — Lamont-Doherty Survey of the World Ocean, Preliminary report of Volume 24, USNS Eltanin, cruises 39–45. *Lamont-Doherty Geological Observatory Technical Report* CU-2-76, 220 pp.

Hayes, D.E., & others, 1977 — Lamont-Doherty Survey of the World Ocean, Preliminary report of Volume 25, USNS Eltanin, cruises 46–50. *Lamont-Doherty Geological Observatory Technical Report* CU-1-77, 170 pp.

Hayes, D.E., & others, 1978 — Lamont-Doherty Survey of the World Ocean, Preliminary report of Volume 26, USNS Eltanin, cruises 51–55A. *Lamont-Doherty Geological Observatory Technical Report* CU-1-78, 160 pp.

Hempton, M.R., 1987 — Constraints on Arabian plate motion and extensional history of the Red Sea. *Tectonics*, 6, 687–705.

Johnson, B.D., & Mayhew, M.A., 1985 — Interpretation of satellite magnetometer data. *Exploration Geophysics*, 16 (2/3), 238–240.

Kent, D.V., & Gradstein, F.M., 1985 — A Cretaceous and Jurassic geochronology. *Geological Society of America, Bulletin*, 96, 1419–1427.

Konig, M., 1980 — Geophysical investigations of the southern continental margin of Australia and the conjugate sector of East Antarctica. *Ph.D. thesis, Columbia University, New York*, 311 pp.

Konig, M., 1987 — Geophysical data from the continental margin off Wilkes Land, Antarctica — implications for breakup and dispersal of Australia–Antarctica. *Circum-Pacific Council for Energy and Mineral Resources Earth Sciences Series*, 5A, 117–145.

Konig, M., & Talwani, M., 1977 — A geophysical study of the southern continental margin of Australia: Great Australian Bight and western sections. *Geological Society of America, Bulletin*, 88, 1000–1014.

Laughton, A.S., Whitmarsh, R.B., & Jones, M.T., 1970 — The evolution of the Gulf of Aden. *Philosophical Transactions of the Royal Society of London*, A, 267, 227–266.

Lawver, L.A., Royer, J.-Y., Sandwell, D.T., & Scotese, C.R., in press — Evolution of the Antarctic continental margins. *Proceedings of the Fifth International Symposium on Antarctic Earth Sciences. Cambridge University Press.*

Nelson, R.G., Crabb, T.N., & Gerdes, R.A., 1986 — A review of geological exploration in the Polda Basin, South Australia. *The APEA Journal*, 26, 319–333.

Powell, C.McA., Roots, S.R., & Veevers, J.J., 1988 — Pre-breakup continental extension in East Gondwanaland and the early opening of the eastern Indian Ocean. *Tectonophysics*, 155, 261–283.

Royer, J.-Y., & Sandwell, D.T., 1989 — Evolution of the Eastern Indian Ocean since the Late Cretaceous: constraints from Geosat altimetry. *Journal of Geophysical Research*, 94, B10, 13755–13782.

Sandwell, D.T., & McAdoo, D.C., 1988 — Marine gravity of the Southern Ocean and Antarctic margin from GEOSAT. *Journal of Geophysical Research*, 93, 10389–10396.

Talwani, M., Mutter, J., Houtz, R., & Konig, M., 1979 — The crustal structure and evolution of the area underlying the magnetic zone on the margin south of Australia. *American Association of Petroleum Geologists, Memoir*, 29, 151–175.

Veevers, J.J., (editor), 1984 — Phanerozoic earth history of Australia. *Clarendon Press, Oxford*, 418 pp.

Veevers, J.J., 1986 — Breakup of Australia and Antarctica estimated as mid-Cretaceous (95±5 Ma) from magnetic and seismic data at the continental margin. *Earth and Planetary Science Letters*, 77, 91–99.

Veevers, J.J., 1987a — The conjugate margins of Antarctica (Wilkes Land) and Australia. *Circum-Pacific Council for Energy and Mineral Resources Earth Science Series*, 5A, 45–73.

Veevers, J.J., 1987b — Earth history of the Southeast Indian Ocean and the conjugate margins of Australia and Antarctica. *Journal and Proceedings of the Royal Society of New South Wales*, 120, 57–70.

Veevers, J.J., 1988 — Seafloor magnetic lineation off the Otway/West Tasmania Basins: ridge jumps and the subsidence history of the Southeast Australian margins. *Australian Journal of Earth Sciences*, 35, 451–462.

Veevers, J.J., in press — Antarctica–Australia fit resolved by satellite mapping of oceanic fracture zones. *Australian Journal of Earth Sciences.*

Veevers, J.J., & Eittreim, S.L., 1988 — Reconstruction of Antarctica and Australia at breakup (95±5 Ma) and before rifting (160 Ma). *Australian Journal of Earth Sciences*, 35, 355–362.

Vogt, P.R., Cherkis, N.Z., & Morgan, G.A., 1983 — Project Investigator-1: Evolution of the Australia–Antarctic discordance deduced from a detailed aeromagnetic study. *In* Oliver, R.L., James, P.R., & Jago, J.B., (editors), Antarctic earth science. *Australian Academy of Science, Canberra*, 608–613.

Weissel, J.K., & Hayes, D.E., 1972 — Magnetic anomalies in the Southeast Indian Ocean. *American Geophysical Union, Antarctic Research Series*, 19, 165–196.

Weissel, J.K., & Hayes, D.E., 1974 — The Australian–Antarctic discordance: new results and implications. *Journal of Geophysical Research*, 84, 4572–4582.

Willcox, J.B., 1978 — The Great Australian Bight: a regional interpretation of gravity, magnetic, and seismic data from the Continental Margin Survey. *Bureau of Mineral Resources, Australia, Report* 201, 111 pp.

Willcox, J.B., Symonds, P.A., & Stagg, H.M.J., 1987 — Tectonic evolution of the central Southern Margin of Australia. *Bureau of Mineral Resources, Australia, Record* 1987/51, 150–160.

BMR Journal of Australian Geology & Geophysics, 11, 509–519

Significance of pseudotachylite vein systems, Giles basic/ultrabasic complex, Tomkinson Ranges, western Musgrave Block, central Australia

A.Y. Glikson[1] & T.P. Mernagh[1]

Pseudotachylite vein-breccia networks and pseudotachylites intrafoliated with mylonites occur pervasively in the Tomkinson Ranges, western Musgrave Block, central Australia, about 50 km south and constituting part of the hanging wall of the Woodroffe thrust. The pseudotachylites are almost exclusively confined to gabbro, anorthosite and dolerite, and are rarely seen in basic granulites, felsic granulites and granitic gneiss. Pseudotachylite is ubiquitous in steeply tilted, deformed and mylonite-intersected sectors of the Giles Complex (Hinckley Range, Kalka, Michael Hills) but was not detected in the mildly tilted and little deformed western sectors of the Giles Complex (Blackstone Range, Cavenagh Range, Jameson Range), suggesting that fusion events concentrated in deformed relatively deep crustal levels. Two principal modes of occurrence of pseudotachylite are recognised: 1, vein-breccia networks superimposed on older lithological contacts and associated with brittle fracture systems; 2, penetrative pseudotachylite laminae interleaved with mylonite along shear zones. It is inferred that friction fusion events triggered by seismic faulting have affected intermediate crustal levels where mylonite shears separate brittle fracture domains. Contemporaneous development of pseudotachylite in each domain may be suggested by the lack of observed intersecting relationships between the two types of pseudotachylite vein systems. Alternatively, the mylonite-related pseudotachylites may have formed in quasi-plastic deep crustal zones. Comparisons between the chemistry of pseudotachylites and bulk host rock composition suggest a limited degree of selective fusion, increasing the silica levels and lowering the Mg' values and Cr levels in the melt. Alternatively, these variations may have been brought about by fluid phase activity. Evidence for a high temperature melt origin of the pseudotachylite includes finer-grained margins, resorbed microclasts, micron-scale subhedral crystal texture of the pseudotachylite and distinct chemistry of microphenocrysts compared with host rock mineral composition. Laser-Raman spectroscopy has shown that the material is mostly crystalline but also suggests the occurrence of minor glass components in the pseudotachylite. High-Al and high-K pyroxenes from the pseudotachylite suggest seismic overpressures of the order of 30 kb, or metastable disequilibrium quench crystallisation of the pseudotachylite melt.

Introduction

Occurrences of pseudotachylite as vein material associated with zones of brittle fracture have been documented along the Outer Hebrides thrust fault (Francis & Sibson, 1973), the Alpine fault zone of the South Island, New Zealand (Seward & Sibson, 1985) and the Woodroffe thrust zone of the Musgrave Block, central Australia. Frictional fusion has been demonstrated at the base of a major landslide along the Himalayan thrust zone (Scott & Drever, 1953; Masch & Preuss, 1977). The instantaneous fusion events reflected by pseudotachylite net-vein systems is generally attributed to earthquake-related seismic faulting (Philpotts, 1964; McKenzie & Brune, 1972; Sibson, 1975; Allen, 1979; Grocott, 1981; Maddock, 1983; Sibson, 1986). Although, in principle, friction fusion can occur in any lithology, it is significantly enhanced in super-dry fine-grained rock types such as basic igneous rocks and granulites, due to the paucity of hydrous lubrication effects (Sibson, 1975).

The layered basic/ultrabasic Giles Complex in the Tomkinson Ranges, western Musgrave Block, central Australia (Nesbitt & others, 1970; Daniels, 1974) displays a spectacular development of pseudotachylite vein-breccia networks. Goode (1970) has reported the occurrence of pseudotachylite at Kalka in association with both mylonitic shear zones and brittle fractures and in particular along the contacts of dolerite dykes and gabbroic country rocks. Wenk (1978) studied pseudotachylite in felsic granulites and gneisses from the eastern Musgrave Block by transmission electron microscopy. Wenk & Weiss (1982) reported an Al-rich clinopyroxene from a pseudotachylite vein from the Mt Davies intrusion. Camacho & Vernon (1990) studied the thick pseudotachylite-rich mylonite zone associated with the Woodroffe thrust fault in the eastern part of the Musgrave Block. Webb (1985) measured the Rb and Sr isotopic composition of pseudotachylite from the Woodroffe thrust, central Musgrave Block, yielding an isochron age of 1604±117 Ma. This age is consistent with the ages of host granulites, and suggests that little or no isotopic re-equilibration has occurred during the instantaneous fusion/refreezing event. The pseudotachylite consists mainly of one to ten micron scale clast-rich holocrystalline material, although minor occurrence of glass is indicated by Laser Raman spectroscopy. This paper presents a preliminary account of the field occurrence and petrological/geochemical features of the pseudotachylite vein networks with reference to their structural significance and mode of origin.

[1] Minerals & Land Use Program, Bureau of Mineral Resources, GPO Box 378, Canberra ACT 2601

Regional distribution and field occurrence

Pseudotachylite veins and vein-breccia networks are ubiquitous in the Bell Rock Range, Michael Hills, Hinckley Range, Wingelinna Hills and Kalka layered basic/ultrabasic sequences, and are rare to absent in the Blackstone, Cavenagh, Murray and Jameson Ranges west of the area of Figure 1. Pseudotachylite material is associated with brittle fracture domains and ductile shear zones. The two types of pseudotachylite systems are spatially separate; in no instance have pseudotachylite-bearing mylonite shears been observed to intersect pseudotachylite-bearing brittle breccia-vein systems or vice versa. In brittle strain domains pseudotachylite veins cut through and thus clearly postdate all other lithologies and structures. In ductile strain domains the pseudotachylite material is concentrated along and may be interpreted as controlled by shear zones, whereas cross-cutting pseudotachylite apophyses have not been seen. Far from being uniformly or randomly distributed, pseudotachylite networks are specifically associated with particular rock types. Pseudotachylite veins may pervade anorthosites and basaltic to doleritic dykes and sills, and are common in gabbroic rocks, but are rare to absent in basic granulite, felsic granulite, paragneiss, orthogneiss and granite. Pseudotachylite vein-breccia zones display sharp wall rock boundaries but contain rounded and corroded internal fragments (Figs 2A,B), Typically in brittle domains the veins are parasitically superimposed on older faults, fractures, and dyke–host rock boundaries (Fig. 2E), and apophyses from such veins extensively protrude into the country rocks. In some instances two or more generations of pseudotachylite veins occur and cut through one another (Fig. 2F). Where dense pseudotachylite vein networks occur, the engulfed host rocks form angular to well rounded enclaves within the pseudotachylite network, with very high pseudotachylite/host rock ratios in places, particularly along faults. Along some ductile shears, zones several tens of metres wide have been almost completely transformed into pseudotachylite, for

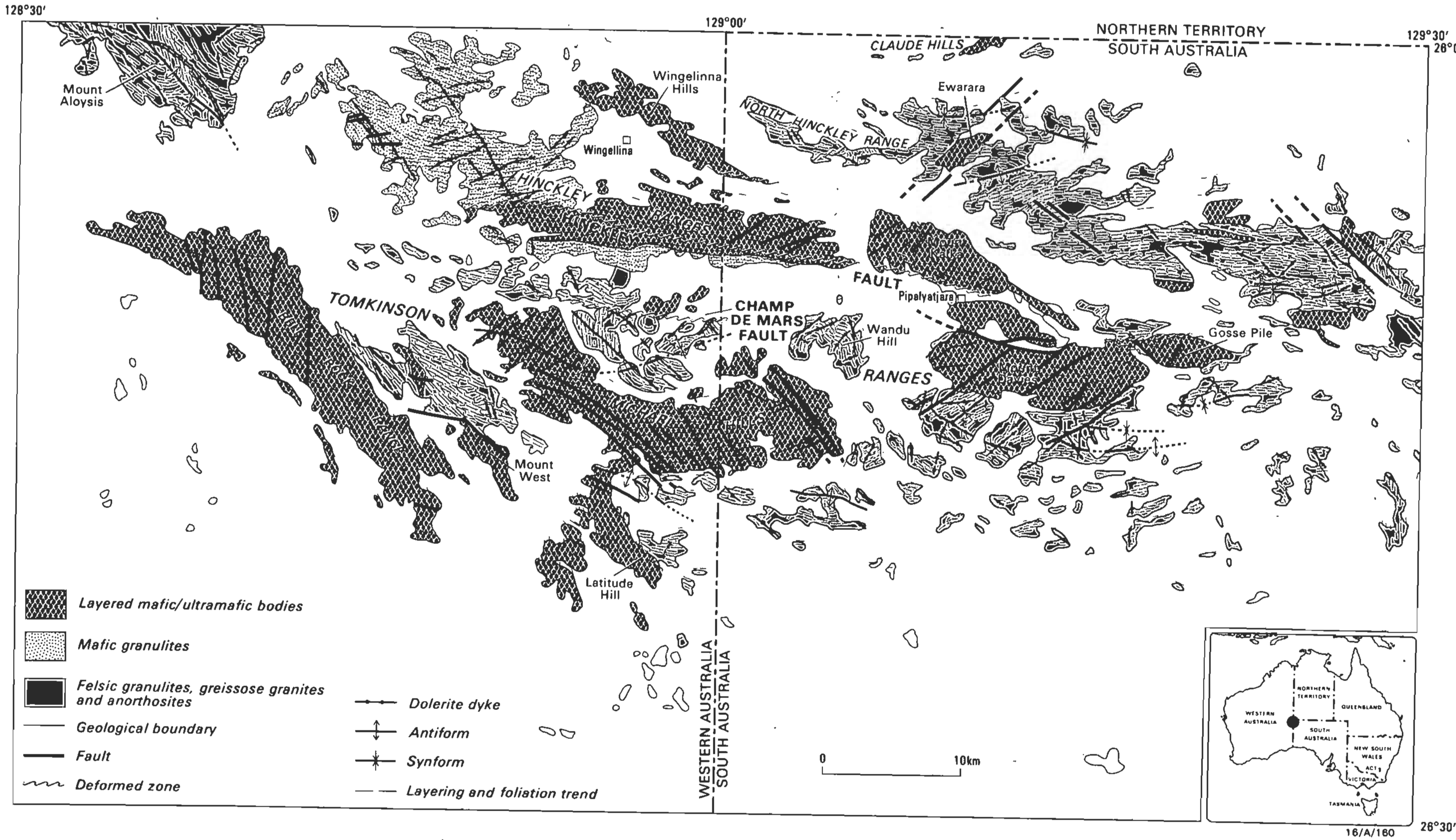

Figure 1. Geological sketch map of the Giles Complex and associated units, Tomkinson Ranges, central Australia, showing the principal outcrops of layered basic/ultrabasic intrusions and structural elements of the terrain.

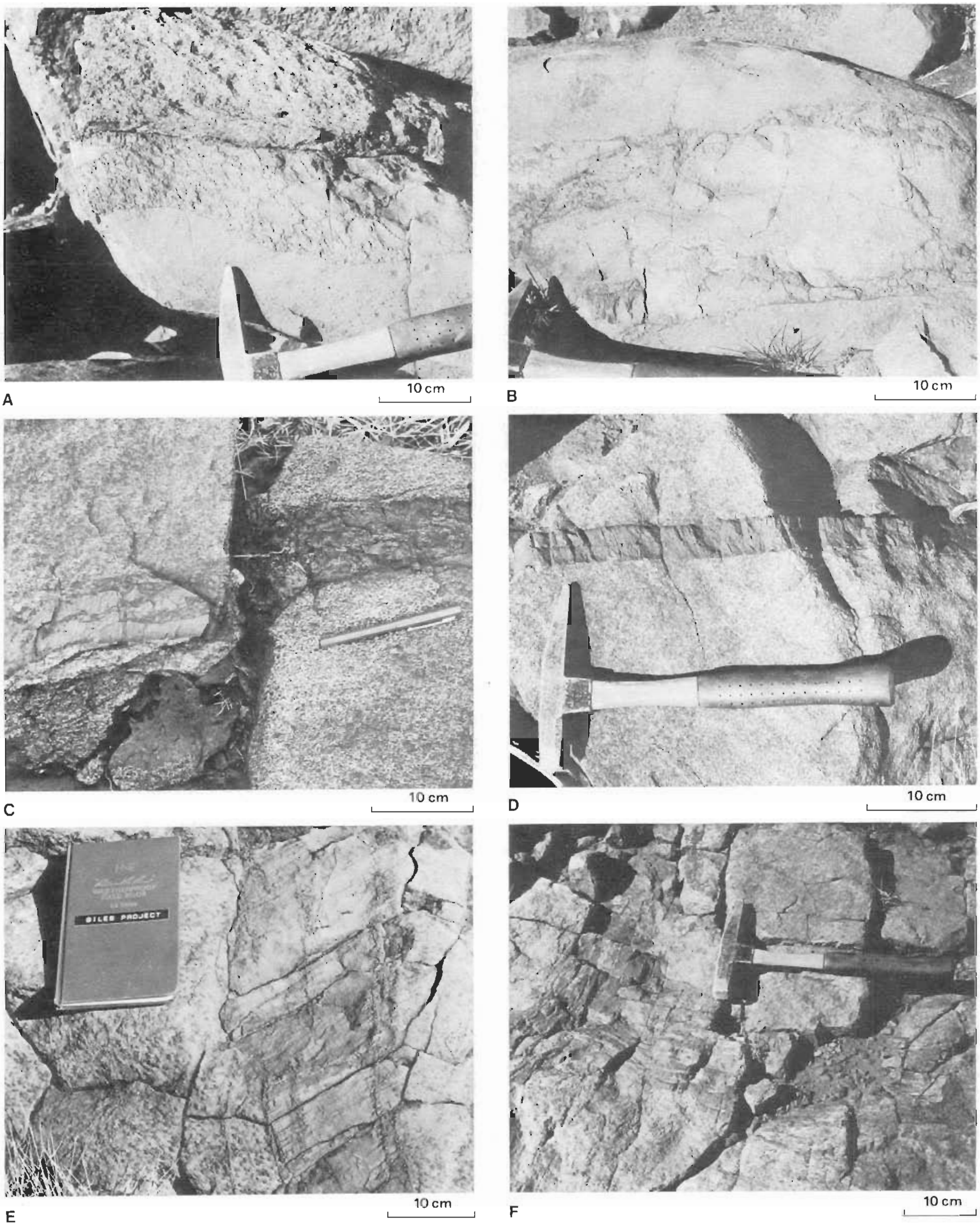

Figure 2. Outcrop-scale features of pseudotachylite vein patterns.
A. Reticulate pseudotachylite-breccia vein located between gabbro (above) and a dolerite dyke (below) and containing rounded enclaves of the dolerite; central Hinckley Range. **B.** Thin veinlets of pseudotachylite emplaced irregularly into fractures and resulting in local angular breccia; central Hinckley Range. **C.** Pseudotachylite breccia vein formed within gabbro and rich in gabbroic enclaves, remnants intermixed with cryptocrystalline pseudotachylite patches; central Hinckley Range. Note the change from solid pseudotachylite to brecciated pseudotachylite/gabbro on various scales. **D.** Pseudotachylite vein intruded into gabbro and showing chilled margins and small fragments of gabbro as enclaves; east Hinckley Range. **E.** Concordant and near-concordant pseudotachylite veinlets emplaced within a dolerite dyke which intrudes gabbro; Wingelinna Hills. **F.** Ductile shear zone formed by interfoliated mylonitised gabbro/pseudotachylite laminae and lenses and intersected (on the left) by another shear zone; east Hinckley Range.

example along major faults in the Hinckley Range and the northern boundary of Michael Hills (Fig. 1).

The thickness of pseudotachylite veins is normally on a millimetre or centimetre scale, but in places they form 10–20 cm thick veins showing chilled margins and features analogous with igneous dykes (Figs 2C,D). However, pseudotachylite veins can be distinguished from igneous dykes by (1) their generally finer grain size and the absence of lath-like plagioclase crystals, (2) the inclusion of rounded enclaves of the host rock (Fig. 2C), (3) the occurrence of apophyses, (4) common superimposition on older structures or contacts, and (5) limited length (in the order of not more than a few metres). Although pseudotachylite veins are commonly superimposed on dyke–host rock boundaries, the pseudotachylite can be distinguished from chilled dyke margins by the stronger relief (Fig. 2E), and by apophyses which protrude into both the igneous dykes and the country rocks. Thick pseudotachylite veins may themselves have chilled margins (Fig. 2D), and in some cases can be distinguished from igneous dykes only in thin section. Pseudotachylite occurrences are not restricted to veins and, in places, this material may form blind patches which may or may not be controlled by older preferred fabric and fracture systems in the host rocks.

Although concordant pseudotachylite veins in brittle zones can be mistaken for ultramylonites, in detail the pseudotachylite veins lack the foliated and lineated strain fabrics of mylonites and contain unstrained xenolithic rock fragments on an outcrop scale to a microscopic scale. Unlike ductile mylonitic shears which form parallel, anastomosing or lenticular patterns, the sub-reticulate geometry of pseudotachylite veins in brittle zones outlines incipient to well advanced brecciation patterns in the host rock, defining pseudotachylite vein breccias which are clearly related to a brittle fracture regime. Such veins are clearly distinguishable from ductile shears where (1) the pseudotachylite material is concordantly superimposed on mylonites, inheriting the fabric of the latter, and (2) pseudotachylite and mylonite are interfoliated and may have formed simultaneously. The pseudotachylite veins are distinguishable from ultraclastics (Sibson, 1977; Wenk, 1978, 1979) by mineralogical features suggestive of fusion (discussed below under 'Mineralogy and chemistry').

Microstructures

Microscopically the pseudotachylite is seen to be markedly porphyroclastic (Fig. 3). There is a tendency for microclasts to concentrate toward veinlet centres and for grain size to decrease toward margins, reflecting the 'Bagnold effect' (Barriere, 1976) and chilled margin effect, respectively. No clear examples of spherulitic or bow-tie type textures have been seen, which places limits on the degree of undercooling of the melt (Macaudier & others, 1985). Samples studied by electron microprobe included a highly deformed gabbro from a shear zone in the central part of the Hinckley Range (sample number S1), a gabbronorite from Wingelinna Hills (S2), an olivine gabbro from Wingelinna Hills (S3), a chromite-rich wehrlite from Wingelinna Hills (S4), and basic granulite samples from the western part of the Hinckley Range (S5, S6) (Fig. 1).

On the whole, the microscopic texture of the pseudotachylite veinlets and their relationships to the host rock and minerals mimic relationships observed on outcrop scale (cf. Figs 2B, and 3A & B). Pseudotachylite veinlets range in thickness from just a few microns to several inches. Where the host rocks of pseudotachylite veins have undergone only brittle deformation and are unfoliated, as is the case in most localities, the pseudotachylite veins normally utilise microfractures and are generally thicker (from about 10–20 microns and upward; Fig. 3B). In contrast, and as observed on outcrop scale (Fig. 2F), pseudotachylite elements associated with mylonitic rocks are concordant to subconcordant (Fig. 3F). The determination of the time relationship between the pseudotachylite and the mylonite fabric is hampered by the difficulty in identifying deformation features within the cryptocrystalline material. The strong mechanical anisotropy of the mylonites explains the lack of discordant pseudotachylite apophyses. A superimposition of mylonite fabrics on existing pseudotachylite concentrations only raises the question as to how such concentrations formed along linear zones in the first place. An interpretation in terms of concordant superimposition of pseudotachylite on discontinuities provided by the mylonite fabric is likely, although there is little evidence for turbulent flow rotation of mylonite fabric elements by the pseudotachylite melt. Nor is there clear evidence for shearing of the pseudotachylite elements. The lack of cross-cutting pseudotachylite veinlets in the mylonite may suggest the absence of cross-fractures at the time of pseudotachylite generation and thereby its development at intermediate rather than shallow crustal levels.

Two distinct types of contact relationship between pseudotachylite and rock or mineral elements are observed:

1. sharp and angular boundaries along fractures where little or no corrosion and/or resorption rounding effects are seen;
2. rounded, resorbed and corroded veinlet boundaries and resorbed grain enclaves within the pseudotachylite vein material, apparently representing melting or resorption along grain boundaries and fractures (Figs 3E,F).

A complete transition exists between these extremes. Clearly the first type of contact represents melt injected from an allochthonous source and rapidly frozen. By contrast the second type of pseudotachylite-rock/mineral relationship must represent *in situ* fusion location and/or sites where the melt was sustained at high temperatures long enough to effect partial fusion. No clear mineralogically preferential fusion is observed, and both ferromagnesian phases and plagioclase grains occur as enclaves in pseudotachylite veinlets.

Scanning electron microscope (SEM) images portray micron-scale subhedral crystallites forming matrices in which relic mineral enclaves on the scale of tens of micron occur. The latter include xenocrysts of plagioclase (Fig. 4A) and orthopyroxene (Fig. 4B). The xenocrysts show serrated margins and are clearly relics of resorbed host rock crystals. Sample S3 contains Fe-rich olivine crystals about 10 microns in diameter, rimmed and replaced by orthopyroxene (Figs 4C,D). As indicated by these textural relationships, as well as by the ferroan composition of the olivine and aluminous composition of the orthopyroxene relative to the host rock phase (see below), these composite grains appear to represent nuclei of crystallisation in the pseudotachylite melt.

Mineralogy and chemistry

Five samples have been studied with the aims of (1) determination of the chemistry of the pseudotachylite, (2) comparison between the latter and bulk rock composition to identify possible preferential fusion, and (3) determination of the composition of quench mineral phases. The samples include a pseudotachylite-rich mylonitic gabbro (S1), a pseudotachylite-injected gabbronorite (S2), a pseudo-

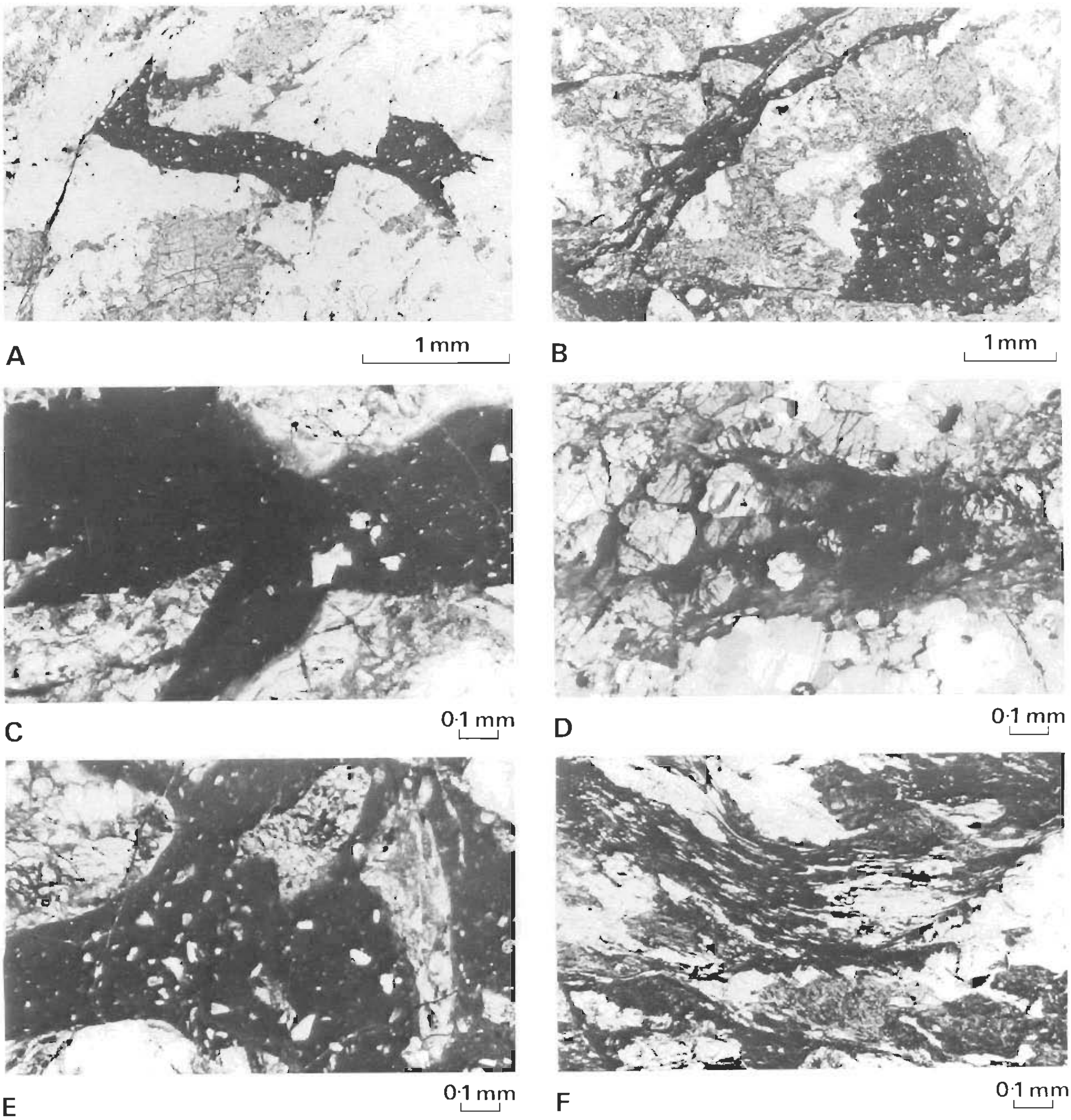

Figure 3. Microscope-scale features of pseudotachylite vein material.
A. Pseudotachylite veinlets and patches in troctolite (sample S3), Wingelinna Hills, showing a vein containing microfragments of the host troctolite within a medium-grained host assemblage of plagioclase (off white), olivine and pyroxene (grey); plane polarised light. **B.** Pseudotachylite vein network intruding a gabbronorite (sample S2), Wingelinna Hills, showing parallel, branching and patchy pseudotachylite intruding a subhedral assemblage of plagioclase and pyroxene; plane polarised light. **C.** Detailed pseudotachylite veinlet-host rock relationships in sample S2, showing the angularity of fragments and paucity of resorption features; plane polarised light. **D.** Detail of pseudotachylite veinlet–host rock relationships in sample 3A, showing well pronounced resorption of deformed and cracked pyroxene grains within pseudotachylite vein and corroded boundaries; cross polars. **E.** Detail of partly resorbed host rock enclaves within pseudotachylite in sample S2, showing rounded and embayed margins of the enclaves interpreted as relics of a partial fusion process; plane polarised light. **F.** Pseudotachylite-rich mylonitic gabbro (sample S1), showing a penetrative alignment of sheared plagioclase and pyroxene foliae and pseudotachylite elements; plane polarised light.

tachylite-injected olivine gabbro (S3), a pseudotachylite-injected chromite-rich wehrlite (S4), and a pseudotachylite-injected basic granulite (S5).

The overall scarcity of primary and secondary hydrosilicates in the layered intrusions of the Giles Complex is reflected by the dry composition of the pseudotachylite, which consists of cryptocrystalline aggregates of subhedral crystals on the scale of a few microns and contains fragments of tens of microns and larger (Fig. 4). The near-absence of water accounts for a remarkably good preservation of the mineralogy and chemistry of the pseudotachylite. The pseudotachylite is rich in partly resorbed to subangular rock fragments and mineral grains identical with those of the host rock (Fig. 3). Table 1 lists bulk rock compositions, host-rock mineral compositions, pseudotachylite compositions and quench phase compositions of the studied samples. The compositions of microporphyritic Fe-rich olivine and orthopyroxene for sample S3 are also listed. Due to the micron-scale dimensions, spot analyses of cryptocrystalline phases in the pseudotachylite groundmass often yield mixed-phase compositions, as well as questions where the distinction

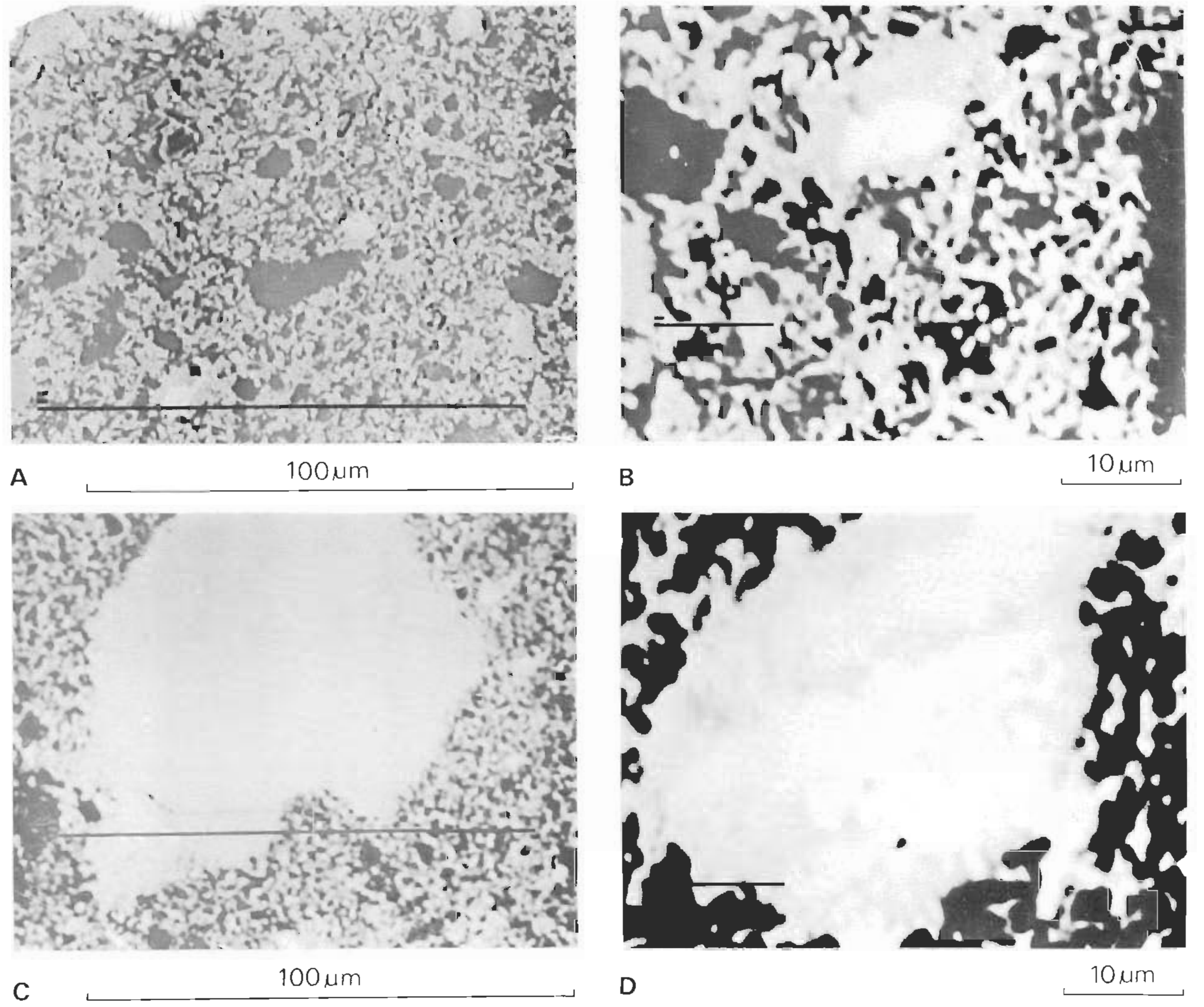

Figure 4. Scanning images of pseudotachylite from sample S3 on the CAMICA electron microprobe.
A. Pseudotachylite showing plagioclase fragments (dark grey) and Fe-rich olivine fragments (white) rimmed by orthopyroxene (grey) in a micron-scale groundmass consisting of subhedral aggregate of feldspar and pyroxene; ×800. **B.** Detail of the pseudotachylite aggregate showing an Fe-rich olivine (white) grain rimmed by orthopyroxene (grey) in a groundmass of feldspar and pyroxene; ×2000. **C.** Composite Fe-rich olivine/orthopyroxene microporphyroblast in pseudotachylite showing replacement of the olivine by orthopyroxene; ×2000. **D.** Relic resorbed grain of orthopyroxene in pseudotachylite; ×800.

between relic host rock phases and quench phases is uncertain. This problem requires resolution by transmission electron microscopy and laser Raman spectroscopy (discussed below). Some of the pseudotachylite-hosted microfragments contain high-Al pyroxenes (Table 1c) similar to those observed by Wenk & Weiss (1982). It is not clear whether these represent high pressure conditions (Goode & Moore, 1975) or disequilibrium quench composition.

Comparisons between bulk rock composition and pseudotachylite composition suggest overall similarities but also local heterogeneity of the pseudotachylite (Table 1), reflecting some selective melting of mineral phases. See, for example, pseudotachylite analysis no. 7 of sample S2 (Table 1b) and pseudotachylite analyses 5 and 6 of sample S5 (Table 1e). In some instances pseudotachylite analyses have higher SiO_2 (S1 and S3), higher FeO (total Fe as FeO) (S1 and S2) and lower Mg′ values (S2 and S3) than the bulk rock analysis. The Cr levels of pseudotachylite in the chromite-rich wehrlite (sample S4) are more than four times lower than the bulk rock composition of 4.65% Cr_2O_3 (Table 1d), indicating low degrees of fusion of chromite. No consistent difference is observed between the An values of the bulk rock and the pseudotachylite. The tendency to more siliceous and ferroan chemistry in the pseudotachylite in some samples may reflect either selective melting and/or secondary enrichment of the glass in silica and iron in connection with fluid phase activity.

Composite micro-porphyritic orthopyroxene-rimmed olivine grains are more ferroan than the host rock olivine (Table 1c). In sample S3 the average Mg′ value of five analysed quench olivine crystals was 46.8, and that of five host rock olivine grains, 61.4. Likewise, the Mg′ value of cryptocrystalline orthopyroxene is lower than that of the host rock Opx grains (Table 1c). This suggests that the olivine and orthopyroxene constitute metastable quench phases such as are commonly obtained in experimental runs. Orthopyroxene rims around the quench olivine yield values with low SiO_2 and high Al_2O_3 (Table 1c), which may either betray submicron-scale spinel inclusion or disequilibrium crystallisation upon rapid quenching. A spinel grain in the pseudotachylite yields an Mg-bearing (MgO 8.30%) hercynite composition (Table 1c). In sample S3 the quench plagioclase is significantly more calcine than the bulk rock plagioclase, suggesting rapid high temperature crystallisation with no subsequent re-equilibration.

Table 1. Whole rock, mineral and pseudotachylite compositions of five samples from the Tomkinson Ranges, Western Australia.

Table 1a. Sample S1: pseudotachylite-rich mylonitic gabbro, Hinckley Range.

Wt %	1 Whole rock	2 Plg	3 Opx	4 Cpx	5 PT1	6 PT2	7 PT3
SiO_2	48.82	53.32	52.60	52.70	50.03	49.69	51.00
TiO_2	0.82		0.26	0.28	0.76	0.99	0.77
Al_2O_3	16.50	29.57	1.04	1.94	14.97	15.60	14.38
Cr_2O_3	0.19				0.17	0.21	0.11
FeO(t)	9.93	0.14	22.30	7.63	11.80	10.06	10.48
MnO	0.17		0.56	0.13	0.13	0.11	
MgO	7.59		22.25	14.12	8.62	8.58	8.88
CaO	11.69	11.95	0.99	22.86	11.29	12.25	12.28
Na_2O	2.33	4.68		0.32	2.14	2.23	1.78
K_2O	0.35	0.34			0.11	0.29	0.32
LOI	0.84						
total	99.23		normalised to 100%				
total cat.		20.04	4.007	4.005			
		p32ox	p6ox	p6ox			
Mg′	57.7		64.1	76.8	56.6	60.4	60.2
An	88.6	79.8			89.1	89.5	91.4

Table 1b. Sample S2: Pseudotachylite-injected gabbronorite, Wingelinna Hills.

Wt %	1 Whole rock	2 Plg	3 Opx	4 PT1	5 PT2	6 PT3	7 PT4	8 PT5	9 PT6
SiO_2	47.28	50.50	51.25	47.82	46.91	48.03	44.47	48.54	48.17
TiO_2	0.29			0.84	0.86	0.86	0.64	0.79	0.81
Al_2O_3	16.55	31.55	0.78	16.15	16.43	14.08	10.92	16.40	16.75
Cr_2O_3	0.11			0.14		0.11	0.14	0.11	0.10
FeO(t)	8.21	0.42	22.00	9.38	10.65	9.60	15.71	9.24	9.45
MnO	0.14		0.18	0.12			0.22	0.13	0.14
MgO	11.66	0.18	25.32	10.41	11.52	11.35	17.37	10.42	10.42
CaO	13.03	13.85	0.46	12.94	11.76	13.87	9.94	11.35	11.87
Na_2	1.56	3.42		2.18	1.87	2.00	0.38	2.36	2.19
K_2O	0.09	0.08				0.09	0.15	0.11	0.11
LOI	0.87								
total	99.82			normalised to 100%					
total cat.		20.02	4.07						
		p32ox	p6ox						
Mg′	71.7		67.3	66.5	65.9	67.9	66.4	66.8	66.3
An	92.8	86.2		90.2	90.7	91.5	97.6	88.1	89.3

Table 1c. Sample S3: Pseudotachylite-injected olivine gabbro, Wingelinna Hills.

Wt %	1 Whole rock	2 Plg	3 Ol	4 Opx	5 Cpx	6 Ph	7 PT1	8 PT2	9 PT3	10 PT av. of 8 scans	11 Plg (PT)	12 Ol(PT)	13 Opx(PT)	14 Sp(PT)
SiO_2	47.68	51.73	36.10	52.70	52.13	37.99	49.72	48.96	49.56	47.96	48.53	34.78	44.55	0.18
TiO_2	0.36				0.43	8.01	0.58	0.68	0.51	0.50			0.43	0.05
Al_2O_3	21.16	30.48		2.33	3.30	15.57	23.10	21.74	21.62	19.22	32.85		8.45	58.26
Cr_2O_3	0.003		0.12											
FeO(t)	8.30		33.88	20.84	7.60	14.29	6.75	7.91	7.63	10.61	0.34	43.33	25.48	32.73
MnO	0.12		0.46		0.12					0.16		0.49	0.47	0.17
MgO	6.96	0.14	29.48	23.31	13.34	13.74	4.85	5.96	5.80	8.71		21.05	20.03	8.38
CaO	10.66	13.66	0.07	0.43	22.66	0.09	11.57	11.62	11.76	10.40	15.74	0.25	0.47	0.22
Na_2O	2.71	3.86			0.42		3.10	2.72	2.87	1.98	2.43		0.11	
K_2O	0.33	0.12					0.34	0.41	0.26	0.46	0.10			
LOI	0.87													
total	99.81			normalised to 100%							total normalised to 100%			
											20.01	2.99	4.097	3.04
											p32ox	p4ox	p6ox	p4ox
total cat.		19.96	3.00	4.00	3.99	15.37								
		p32ox	p4ox	p6ox	p6ox	p22ox								
Mg′	60.0	58.0	66.6	75.8	63.2		56.2	57.4	57.6	59.5		46.5	58.41	31.4
An	85.9	84.6					85.2	86.8	86.4	89.0	90.9			

Table 1d. Sample S4: Pseudotachylite-injected chromite-rich wehrlite, Wingelinna Hills.

Wt %	1 Whole rock	2 Plg	3 Ol	4 Cpx	5 PT1	6 PT2
SiO_2	37.04	52.22	40.82	53.51	43.83	43.33
TiO_2	0.21			0.36	0.17	0.14
Al_2O_3	5.54	31.00		3.35	3.75	3.81
Cr_2O_3	4.65			0.62	1.01	1.03
FeO(t)	14.24	0.05	13.81	3.56	11.59	11.52
MnO	0.24		0.19	0.11	0.18	0.19
MgO	33.19		45.18	14.75	33.82	34.00
CaO	3.55	12.96		22.94	5.15	5.43
Na_2O	0.29	3.72			0.45	0.51
K_2O	0.03	0.05			0.05	0.04
LOI	0.24					
total	99.75		normalised to 100%			
tot. cations		19.90	2.98	3.998		
		p32ox	p4ox	p6ox		
Mg′	80.64		85.4	88.1	83.9	84.1
An	94.98	84.3			94.3	94.3

PT pseudotachylite.

Table 1e. Sample S5: Pseudotachylite-injected basic granulite, western Hinckley Range.

Wt %	1 Whole rock	2 Plg	3 Opx	4 Cpx	5 PT1	6 PT2
SiO_2	51.92	55.89	52.05	50.57	52.99	51.57
TiO_2	1.51			2.59	0.56	1.25
Al_2O_3	15.49	27.83	0.88	1.45	20.61	10.53
FeO(t)	10.24	0.36	26.93	10.98	8.43	16.55
MnO	0.16		0.39			0.19
MgO	6.34		18.82	12.92	4.63	10.68
CaO	8.78	9.91	0.92	21.08	7.85	6.53
Na_2O	2.82	5.76		0.41	3.52	1.65
K_2O	1.20	0.26				1.06
LOI	0.59					
total	99.26	normalised to 100%				
tot. cations		20.014	3.998	4.001		
		p32ox	p6ox	p6ox		
Mg′	52.51		55.5	67.8	49.5	53.6
An	82.0	72.7			77.5	86.0

Analyses a1, b1 and c1 were conducted by J. Pyke at the BMR laboratories, using the Phillips PW1404 X-ray fluorescence spectrometer applying the method of Norrish & Chappell (1967). For discussion of accuracy and precision of this method, refer to Sheraton & Labbone (1978). Analyses a2–7, b2–8, c2–9 and e2–6 were conducted by A.Y. Glikson at the Australian National University using the TPD energy dispersive electron microprobe and software designed by Reed & Ware (1975). Analyses b9–11, c10–14 and d2–6 were conducted by A.Y. Glikson using the CAMICA Camebax-Micro scanning electron X-ray microprobe at the Australian National University, using software written by N. Ware (unpublished). Pseudotachylite analyses were conducted on the TPD probe using a defocused beam and on the CAMICA probe by scanning under magnifications of 2000–20 000 and beam currents in the 20–30 nA range. Good agreements were obtained between point analyses and scanning analyses.

Laser Raman spectroscopy

Sample S3 — a pseudotachylite-bearing troctolite from Wingelinna Hills — was studied by a Microdil 28 laser Raman microprobe (Barbillat & others, 1985) at a lateral resolution of one micron, with the aim of identifying crystalline phases and detecting possible glass. The 514.5 nm laser line from a Spectre Physics 2020 3W Ar+ laser was used as the excitation source. Laser power at the sample was 40 mW and the spectral bandpass was approximately 4 cm^{-1}. All Raman spectra recorded from the pseudotachylite groundmass regions and from white and green crystallites (Fig. 5) contain sharp lines typical of those observed in crystalline materials, but some lines may be broader than those reported in crystalline spectra. The white crystals give a plagioclase spectrum with the dominant features being intense bands in the 500 cm^{-1} region. The Raman spectra recorded from the green crystals have intense bands in the 660 and 1000 cm^{-1} regions which are indicative of pyroxene. Spectrum C (Fig 5.) was recorded from the pseudotachylite groundmass region and contains a combination of plagioclase and pyroxene bands.

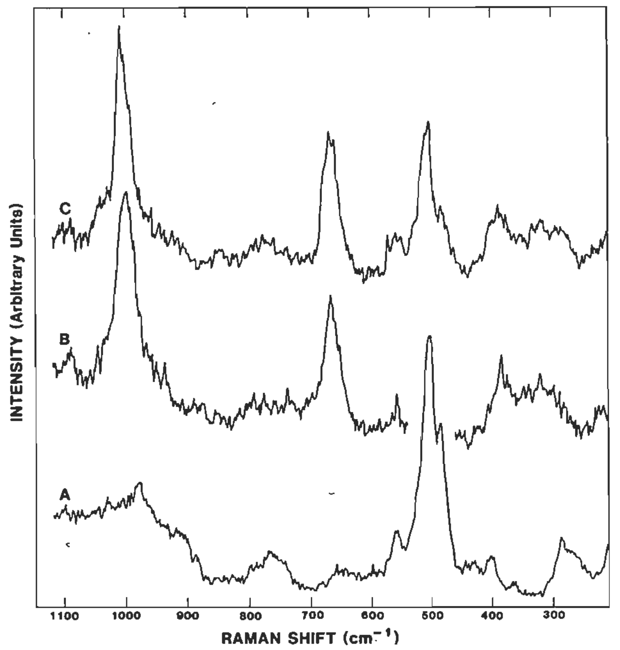

Figure 5. Comparison of Raman spectra obtained from various regions of pseudotachylite vein material in sample S3.
A. Anorthite crystallite. **B.** Diopside xenocryst. **C.** Region with glassy texture including both plagioclase and pyroxene bands.

A list of observed frequencies is given in Table 2. The plagioclase spectrum closely matches that of crystalline anorthite (Matson & others, 1986) while the pyroxene resembles that of diopside (White, 1975). Although Fe-rich olivine also occurs in this rock, the corresponding bands have not been observed in the Raman spectra, probably due to the inherent weakness of Fe-rich olivine spectrum (Sharma & Urmos, 1987).

The Raman spectrum of anorthite (Fig. 5) shows characteristically strong bands at 484 and 504 cm^{-1}. These bands are attributed to dislocated vibrational modes involving stretching of bridging oxygens in T-O-T linkage, where T represents an SiO_4 tetrahedron (Matson & others, 1986). The intense bands observed in the Raman spectra (Fig. 5) at 660 cm^{-1} are attributed to an ether-like symmetric stretch of the bridging oxygens in the pyroxene chains (White, 1975). The intense bands in the 1000 cm^{-1} have been assigned (McMilland, 1984) to vibrations of non-bridging oxygens in silicate tetrahedra.

Table 2. Observed Raman frequencies (cm^{-1}) in spectra recorded from various regions of pseudotachylite veinlets

Apparent glassy region	*Diopside crystallite*	*Anorthite crystallite*
	217	
		270
288		286
317	318	
331		
387	381	
		402
483		484
505		504
550		
559		559
572		
661	665	
668		
		768
		975
1008	997	
	1089	

The Raman spectra of glasses, particularly those of complex composition, exhibit only weak broad bands. In contrast, the bands of well-ordered crystals are intense and sharp (Matson & others, 1986). The broadness of bands in the spectra of glasses results from the elimination of non-bridging oxygens in the glasses and the inherent disorder in the glass network relative to the highly ordered structures of crystalline materials.

The Raman spectra shown in Figure 5 all contain a number of sharp bands which indicate that the material is mostly crystalline. However, several weak and broad bands — some of which underlie sharp bands — can be observed in the spectra and may indicate the presence of some non-crystalline phases. The Raman spectrum from the pseudotachylite groundmass region (Fig. 5, spectrum C) contains a number of intense and sharp pyroxene and feldspar bands and must contain these crystallites on a microscopic scale. There is some evidence from measurements made on lunar glasses (White, 1975) that crystalline particles embedded in glassy fragments would produce sharp Raman spectra indicative of submicroscopic size crystallites. The limit of resolution is controlled by the homogeneity and the degree of crystallinity of the nuclei. The sharpness of the boundary between the crystallites and the surrounding medium is also important. The detection limits are still problematical, but it appears that particles as small as 30 angstroms will produce a distinct Raman spectrum. Interpretations of spectra differences in terms of structural effects using vibrational force field calculations are in progress.

Significance of the pseudotachylites

A derivation of pseudotachylite by friction fusion, forced injection into fractures and supercooling is widely accepted on textural and compositional basis (Sibson, 1975; Grocott, 1981; Maddock, 1983; Macaudiere & others, 1985). In general, rapid slip along discontinuities within brittle strain domains under low fluid pressures is required to give rise to the runaway effect of pseudotachylite generation, whereas dislocations at deeper crustal levels under ductile strain conditions involving continuous flow deformation have been considered previously as unlikely to be associated with the generation of pseudotachylite (see discussion by Shimamoto, 1989). Major fault zones which transect high grade metamorphic terrains are the classic loci for dynamically triggered friction fusion which occurs both along the faults and/or in the footwall or hanging wall, as for example along the Alpine fault (Seward & Sibson, 1985) and the Outer Hebrides thrust fault (Francis & Sibson, 1985). In the Tomkinson Ranges no exclusive association of pseudotachylite with any single structure is evident and, although numerous faults and mylonitic zones occur, no major lineament involving juxtaposition of granulite facies terrains with amphibolite facies terrains such as those observed along major thrust faults in central Australia (Collerson & others, 1972; Glikson, 1986, 1987) is seen. Goode (1978) studied the high strain deformed zone of the Hinckley fault along the southern edge of the Kalka layered basic–ultrabasic body, and similar zones form an anastomosing pattern throughout the Giles Complex and associated gneiss and granulite (Pharoah, 1990). However, the principal western extension of the Woodroffe thrust (Collerson & others, 1972) occurs north of the Mann Range, at least 50 km north of the Tomkinson Ranges (Fig. 1). Thus, the Giles Complex in the region under consideration can be regarded structurally as a part of an extensive hanging wall block in relation to the Woodroffe thrust, though riddled with mylonite zones of probably similar age. A closer definition of the relationships between the hanging wall and the thrust fault must await seismic reflection studies such as those conducted along the Redbank thrust fault, western Arunta Block (Goleby & others, 1989).

The igneous-like subhedral texture of the pseudotachylite matrix (Fig. 4), the iron-rich disequilibrium quench composition of cryptocrystalline olivine and orthopyroxene discussed above, and the occurrence of chilled margins along pseudotachylite veins (Fig. 2D) all suggest high temperature fusion. The overall similarities between pseudotachylite composition and corresponding host rock composition (Table 1), observed also by Wenk & Weiss (1982), suggest mixing of the melt, although notably phases such as chromite have been fused to a lesser extent than silicates.

Wenk (1978, 1979) has suggested a middle to lower crustal origin for pseudotachylite of the eastern Musgrave Block, whereas Goode (1979) and Watt & Williams (1979) argued for an upper crustal origin associated with uplift and transition from ductile to brittle crustal zones. Of central importance in this regard are the temporal relations between mylonitic shear zones and the pseudotachylite vein-breccia networks. The apparent absence of cross-cutting relationships between pseudotachylite veins in ductile and brittle domains alternatively suggests (1) that the shear zones formed later than the brittle zones and smeared the latter out, obliterating original pseudotachylite cross-cutting relationships, (2) a contemporaneous development of the pseudotachylite at the same crustal level and their different manifestation in the ductile shear zones and in the intervening brittle blocks, or (3) formation of pseudotachylite in mylonitic shear zones at a deep crustal ductile regime (Sibson, 1980; Grocott, 1981; Passchier, 1982, 1984; Hobbs & others, 1986; Shimamoto, 1989) followed, after uplift, by formation of pseudotachylite in brittle inter-shear blocks at high crustal levels. Due to their long term ductile behaviour upon uplift to higher crustal levels, these shear zones are unlikely to be overprinted by brittle strain features, thus accounting for the lack of brittle-ductile intersecting relationships noted above. No clear criteria are at hand to distinguish between these models at present.

Although the depth of formation of pseudotachylite veins cannot be defined from the available data, circumstantial evidence suggests their development at intermediate crustal levels of about 10–20 km depth. Thus, the largely holocrystalline texture of the pseudotachylite militates against its formation at very shallow crustal levels, since more extensive formation of glass might be expected to have taken place under these conditions. Such a conclusion is supported by the absence of pseudotachylite vein-breccia networks in the less deformed low-dipping layered intrusions of the Blackstone, Cavenagh and Jameson Ranges. These bodies, interpreted by Daniels (1974) as possible shallower level equivalents of the steeply dipping intrusions of the Hinckley Range, Michael Hills, Kalka and Mount Davies (Fig. 1), may represent upper crustal levels where little or no pseudotachylite formed. It is important to note, however, that the Blackstone intrusion is fringed on the north by basic granulites, indicating marginal recrystallisation associated with the intrusion of proximal rapakivi granites. Typically the shallow-dipping basic bodies, while intersected by faults, are rarely cut by the multiple mylonitic shears common in the Hinckley intrusion. On the other hand, development of pseudotachylite under a high temperature regime at lower crustal levels would have resulted in extensive recrystallisation of the pseudotachylite, contrasted with the pristine textural and compositional features of these rocks (Figs 2, 3; see also 'Mineralogy and chemistry', above). Thus, it follows that the pseudotachylite vein-breccia networks may have been associated with intermediate crustal levels in a strain regime where both quasi-plastic and elastic frictional deformation took place, reflecting different rates and/or timing of seismic movements (Sibson, 1975)

Wenk (1978) suggested a derivation of pseudotachylite by cold working, namely ultra-comminution in the brittle zone, on the basis of transmission electron microscope identification of extreme micro strain features and the scarcity of glass. Wenk & Weiss (1982) considered possible derivation of the pseudotachylite by either ultracomminution or devitrification of glass. On the other hand, the occurrence of re-entrant angles in pseudotachylite-hosted clasts which suggests resorption (Figs 3C,E, 4E), the micron-scale subidiomorphic igneous texture shown on the probe scanner (Fig. 4), and the unique composition of the ferromagnesian phases in the pseudotachylite militate for high temperature crystallisation. Two distinct processes (Figs 2D,F) may have been responsible for the observed pseudotachylite vein patterns: (1) shear and dilatational strains culminating in fusion along brittle fractures and (2) superimposition of pseudotachylite on mechanically weak semiductile shear zones. The interlamination of mylonitised gabbro and pseudotachylite-rich foliae and lenses observed in ductile shear zones (Figs 2F, 3F) may represent strain conditions transitional between those of ductile and brittle failure modes operating at the same crustal level.

Whether the pseudotachylite breccia-vein systems formed simultaneously with the mylonites (Wenk & Weiss, 1982) or have postdated the latter upon uplift (Sibson, 1977; Goode, 1979) is unclear.

The physical conditions and the timing of pseudotachylite vein-breccia networks formation remain the subject of further work. Sibson (1975) suggested that pseudotachylite vein-breccia networks of the Outer Hebrides thrust zone formed in the upper crust under conditions of <10 km depth and $<250°C$. In the Giles Complex, if the Al-rich and K-rich pyroxene in the pseudotachylite constitutes a stable phase, transient dynamic pressures in the order of 30 kb and above are implied by the mineral composition (Wenk & Weiss, 1982). Such pressures, consistent with transient shock pressures of 20–40 kb required for experimentally produced pseudotachylite veins in gabbro, are far in excess of estimates of seismic earthquake pressures and could have resulted from high transient strain rates at the tips of propagating fractures and/or spallation and collapse of unsupported crackwalls, particularly in rocks with the rheological features of gabbro and anorthosite (Weiss & Wenk, 1983). The temperatures at which this process takes place are best gauged from equilibria of crystallising phases in the pseudotachylite, for example the orthopyroxene-rimmed Fe-rich olivine microphenocrysts described above. Likewise, the timing of pseudotachylite formation and the seismic movements they signify remain the subject of fission track and Ar-Ar isotopic work.

Summary

Pseudotachylite vein-breccia networks in the Giles Complex, Tomkinson Ranges, occur ubiquitously in gabbro, anorthosite and doleritic dykes associated with steep dipping deformed units affected by mylonitic shear zones (Hinckley Range). They are absent from little-deformed low-dipping strata (Blackstone, Cavenagh and Jameson Ranges). The pseudotachylite vein-breccia networks are almost exlusively associated with specific lithologies, and tend to be superimposed on older structures and contacts, such as faults and dyke boundaries. Two principal modes of occurrence are seen: (A) pseudotachylite associated with cataclastic deformation in brittle fracture domains, and (B) pseudotachylite associated with mylonites along ductile shears. In the latter, formation of pseudotachylite has occurred either during or later than mylonitisation. The pseudotachylite consists of porphyroclastic cryptocrystalline aggregates which display resorption of clasts, a subidiomorphic igneous texture on the micron scale and microphenocrysts with compositions differing from the host rocks. These characteristics all indicate a high temperature origin. Laser Raman spectroscopy suggests minor occurrence of glass. The microphenocrysts include Al-rich and K-rich orthopyroxene, potentially supporting transient overpressures on the scale of about 20–40 kb, as estimated by Wenk & Weiss (1982). The pseudotachylite is mostly of near-uniform composition, suggesting mixing of the melt, but locally of heterogeneous composition showing SiO_2 and FeO enrichment and Cr_2O_3 depletion relative to the host rock, suggesting selective fusion and possibly secondary alteration. It is suggested that the pseudotachylite vein-breccia networks and pseudotachylite associated with mylonitic shears formed at intermediate crustal levels in conjunction with seismic activity affecting the uniquely dry basic compositions (Sibson, 1975) in a crustal regime in which elastic frictional (brittle) and quasi-plastic (ductile) strain behaviour coexisted. While much of the strain accumulated along shear zones, structural adjustments in intervening blocks may have been largely responsible for their brittle failure. The age/s of pseudotachylite formation and pressure/temperature parameters remain the subject of further studies.

Acknowledgements

We thank R.H. Sibson and H.R. Wenk for correspondence regarding interpretation of the pseudotachylites and C.G. Ballhaus, K. Curry, A.D.T. Goode, T.C. Pharaoh, R.D. Shaw, Toshihiko Shimamoto, M.G. Truscott and P.R. Williams for their comments on the manuscript.

References

Allen, A.R., 1979 — Mechanism of frictional fusion in fault zones. *Journal of Structural Geology*, 1, 231–243.

Barbillat, J., Dhamelincourt, P., Delhayne, M., Da Silva, E., & Roussel, B., 1985 — Nondestructive microprobing by means of a new generation of instruments for Raman and fluorescence spectroscopy. *In* Armstrong, J.T., (editor), Microbeam analysis. *San Francisco Press, San Francisco*, pp. 15–18.

Barriere, M., 1976 — Flowage differentiation: limitation of the 'Bagnol effect' to the Narrow intrusions. *Contributions to Mineralogy and Petrology*, 55, 139–145.

Camacho, A., & Vernon, R.H., 1990 — Pseudotachylite with igneous quench microstructures, eastern Musgrave Ranges, Northern Territory. *Abstract, 10th Australian Geological Convention abstracts, Geological Society of Australia*, 185.

Collerson, K.D., Oliver, R.L., & Rutland, R.W.R., 1972 — An example of structural and metamorphic relationships in the Musgrave Orogenic Belt, central Australia. *Journal of the Geological Society of Australia*, 18, 379–394.

Daniels, J.L., 1974 — The geology of the Blackstone region, Western Australia. *Geological Survey of Western Australia, Bulletin* 123.

Francis, P.W., & Sibson, R.H., 1973 — The Outer Hebrides thrust. *In* Parks, R.G., & others (editors), The early Precambrian of Scotland and related rock of Greenland. *University of Keel, England*, pp. 95–104.

Glikson, A.Y., 1986 — An upthrusted early Proterozoic basic granulite-anorthosite suite and anatectic gneisses, southwestern Arunta Block, central Australia: evidence on the nature of the lower crust. *Transactions of the Geological Society of South Africa*, 89, 263–283.

Glikson, A.Y., 1987 — Regional structure and evolution of the Redbank-Mount Zeil thrust zone: a major lineament in the Arunta inlier, central Australia. *BMR Journal of Australian Geology & Geophysics*, 10, 89–107.

Goleby, B.R., Shaw, R.D., Wright, C., Kennett, B.L.N., & Lambeck, K., 1989 — Geophysical evidence for 'thick-skinned' crustal deformation in central Australia. *Nature*, 337, 325–330.

Goode, A.D.T., 1970 — The petrology and structure of the Kalka and Ewarara layered basic intrusion, Giles Complex, central Australia. *Ph.D. thesis, University of Adelaide*.

Goode, A.D.T., 1978 — High temperature, high strain rate deformation in the lower crustal Kalka intrusion, central Australia. *Contributions to Mineralogy and Petrology*, 66, 137–148.

Goode, A.D.T., 1979 — Comment: are pseudotachylites products of fracture or fusion? *Geology*, 7, 162.

Goode, A.D.T, & Moore, 1975 — High pressure crystallisation of the Ewarara, Kalka and Gosse Pile intrusions, Giles Complex, central Australia. *Contributions to Mineralogy and Petrology*, 51, 77–97.

Grocott, J., 1981 — Fracture geometry of pseudotachylite generation zones: a study of shear fractures formed during seismic events. *Journal of Structural Geology*, 3, 169–178.

Hobbs, B.E., Ord, A., & Teyssier, C., 1986 — Earthquakes in the ductile regime? *Pure and Applied Geophysics*, 124, 309–336.

MacAudiere, J., Brown, W.L., & Ohnenstetter, D., 1985 — Microcrystalline textures resulting from rapid crystallization in a pseudotachylite melt in a meta-anorthosite. *Contributions to Mineralogy and Petrology*, 89, 39–51.

Maddock, R.H., 1983 — Melt origin of fault-generated pseudotachylites demonstrated by textures. *Geology*, 11, 105–108.

Masch, L., & Preuss, E., 1977 — The occurrence of the hydromylonite of Langtang, Himalaya (Nepal). *Neues Jahrbuch für Mineralogie Abhandlungen*, 129, 292–311.

Matson, D.W., Sharma, S.K., & Philpotts, J.A., 1986 — Raman spectra of some tectosilicates and of glasses along the orthoclase-anorthite and nepheline-anorthite joins. *American Mineralogy*, 71, 694–704.

McKenzie, D., & Brune, J.N., 1972 — Melting on fault planes during large earthquakes. *Geophysical Journal of the Royal Astronomical Society*, 29, 65–78.

McMillan, P., 1984 — Structural studies of silicate glasses and melts — applications and limitations of Raman spectroscopy. *American Mineralogist*, 69, 622–644.

Nesbitt, R.W., Goode, A.D.T., Moore, A.C., & Hopwood, T.P., 1970 — The Giles Complex, central Australia: a stratified sequence of mafic and ultramafic intrusions. *Geological Society of South Africa, Special Publication* 1, 547–564.

Norrish, K., & Chappell, B.W., 1967 — X-ray fluorescence spectrography. *In* Zussmann, T., (editor), Physical methods in determinative mineralogy. *Academic Press, London*, pp. 161–214.

Passchier, C.W., 1982 — Pseudotachylite and the development of ultramylonite bands in the Saint Barthelemy Massif, French Pyrenees. *Journal of Structural Geology*, 4, 69–79.

Passchier, C.W., 1984 — The generation of ductile and brittle shear bands in a low angle mylonite zone. *Journal of Structural Geology*, 6, 273–281.

Pharaoh, T.C., 1990 — Aspects of the structural geology of the Giles Complex, central Australia. *Bureau of Mineral Resources, Australia, Record* 1990/5.

Philpotts, A.R., 1964 — Origin of pseudotachylites. *American Journal of Science*, 262, 1008–1035.

Reed, S.J.B., & Ware, N.G., 1975 — Quantitative electron analysis of silicates using energy dispersive X-ray spectrometry. *Journal of Petrology*, 16, 499–519.

Scott, J.S., & Drever, H.I., 1953 — Friction fusion along a Himalayan thrust. *Royal Society of Edinburgh, Proceedings*, 65, 121–140.

Seward, D., & Sibson, R.H., 1985 — Fission track age for a pseudotachylite from the Alpine fault zone, New Zealand. *New Zealand Journal of Geology and Geophysics*, 28, 553–557.

Sharmay, S.K., & Urmos, J.P., 1987 — Micro-Raman spectroscopic studies of materials at ambient and high pressures with CW and pulsed lasers. *In* Geiss, R.H., (editor), Microbeam analysis. *San Francisco Press, San Francisco*, pp. 133–136.

Sheraton, J.W., & Labonne, B., 1978 — Petrology and geochemistry of acid igneous rocks of northeast Queensland. *Bureau of Mineral Resources, Australia, Bulletin* 169.

Shimamoto, T., 1989 — The origin of S-C mylonites and a new fault zone model. *Journal of Structural Geology*, 11, 51–64.

Sibson, R.H., 1975 — Generation of pseudotachylites by ancient seismic faulting. *Geophysical Journal of the Royal Astronomical Society*, 43, 775–794.

Sibson, R.H., 1977 — Fault rocks and fault mechanisms. *Journal of the Geological Society of London*, 133, 191–213.

Sibson, R.H., 1980 — Transient discontinuities in ductile shear zones. *Journal of Structural Geology*, 2, 165–171.

Sibson, R.H., 1986 — Earthquakes and rock deformation in crustal fault zones. *Annual Review of Earth and Planetary Science*, 14, 149–175.

Watts, M.J., & Williams, G.D., 1979 — Comment: are pseudotachylites products of fracture of fusion. *Geology*, 7, 162.

Webb, A.W., 1983 — Geochronology of the Musgrave Block. *Mineral Resources Review, South Australian Department of Mines and Energy*, 155, 23–37.

Weiss, L.E., & Wenk, H.R., 1983 — Experimentally produced pseudotachylite-like veins in gabbro. *Tectonophysics*, 96, 299–310.

Wenk, H.R., 1978 — Are pseudotachylites products of fracture or fusion? *Geology*, 6, 507–511.

Wenk, H.R., 1979 — Reply: are pseudotachylites products of fracture of fusion? *Geology*, 7, 162.

Wenk, H.R., & Weiss, L.E., 1982 — Al-rich calcic pyroxene in pseudotachylite: an indication of high pressure and high temperature? *Tectonophysics*, 84, 329–341.

White, W.B., 1975 — Structural interpretations of lunar and terrestrial minerals by Raman spectroscopy. *In* Karr, C., (editor), Infrared and Raman spectroscopy of lunar and terrestrial minerals. *Academic Press, New York*, pp. 325–358.

BMR Journal of Australian Geology & Geophysics, 11, 521-528

Forearc basin dynamics and sedimentation controls, Tamworth belt, eastern Australia

John F. Lindsay[1]

The eastern margin of the Australian continent was the site of convergent plate interaction for much of the Palaeozoic Era. The Tamworth Terrane, a forearc complex resulting from this interaction, occurs in the northeastern corner of New South Wales. This forearc basin, now preserved as a complex erosional and tectonic remnant in the Tamworth belt and Hastings block, originally formed a relatively linear belt before terrane dispersal resulting from Permian orogenesis. Tectonic-subsidence curves derived from thirteen well-exposed sections show that subsidence began abruptly, continued for approximately 50 Ma, and then ceased just as abruptly. Total tectonic subsidence was 4–6 km at either end of the basin, and 2–3 km in the intervening areas of the southern Tamworth belt. Depositional patterns were controlled largely by sediment supply and subsidence; the preserved sedimentary rocks form a large-scale upward-shallowing succession. In detail, the effects of eustatic sea level change are also apparent, particularly around the basin margins and in the shallower water associations. The continuous interaction among these three major variables produced a basin that changed in morphology both spatially and temporally.

Introduction

Forearc basins are an important element of convergent plate margins and make a major contribution in volume to the accretionary growth of continents. In spite of the fact that these basins contain exceptional thicknesses of sediment (Ingersoll, 1979, 1982; Dickinson & Seely, 1979; Moxon & Graham, 1987) they have not attracted the same attention as divergent-margin basins. Some modern convergent-margin basins, particularly in the Pacific, have been studied in recent years (see, for example, Coulbourn & Moberly, 1977; Dickinson & Seely, 1979; von Huene & Arthur, 1982; Bachman & others, 1983; Dickinson & others, 1987), but basin evolution and controls on sedimentation in these basins are poorly understood. Few ancient basins have been studied in any detail, the one exception being the late Mesozoic–Tertiary Great Valley forearc basin of California, where both the regional stratigraphy and sedimentology (Ingersoll, 1979, 1982) and subsidence history (Moxon & Graham, 1987) have been investigated.

The subsidence history of a Palaeozoic forearc basin, the Tamworth Terrane of eastern Australia (Fig. 1), has been studied regionally in an attempt to understand the broad controls of sedimentation in a convergent-margin setting. This basin provides an ideal opportunity for such a study in that the regional stratigraphy and biostratigraphy are understood, and as a result of later tectonism, well-exposed sections are available for detailed evaluation.

Regional setting

The New England fold belt, which occurs along the eastern margin of the Australian continent (Fig. 1), was the site of convergent plate interaction for much of the Palaeozoic (Leitch, 1975; Cawood, 1976, 1980, 1982a,b; Cawood & Leitch, 1985). During this time, the region consisted of three belts: (1) a magmatic arc, (2) the Tamworth Terrane (Cawood & Leitch, 1985), a forearc-basin complex, and (3) the Tablelands complex, a deep-water accretionary wedge (Leitch, 1974; Day & others, 1978; Cawood, 1982a,b) consisting of a number of terranes (Cawood & Leitch, 1985), all of which are in some part overlain by (4) an overlap sequence (Cawood, 1982a,b; Cawood & Leitch, 1985). The termination of subduction in the late Palaeozoic and subsequent Permian orogenesis resulted in the disruption of the original quasi-linear forearc basin and the dispersal of elements (1) to (3) (Cawood & Leitch, 1985).

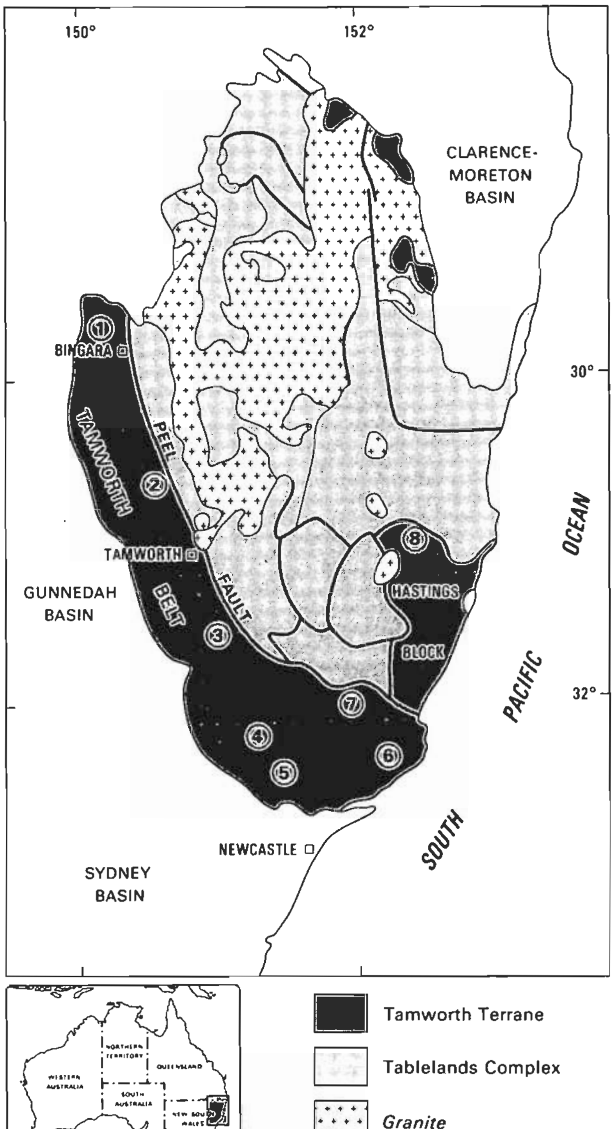

Figure 1. Location map, showing the Tamworth belt and Hastings block, and the location of generalised stratigraphic sections summarised in Figure 2.

1. Magmatic arc. The magmatic arc lies, for the most part, beneath the younger sediments of the Gunnedah, Sydney and Great Artesian Basins. In spite of the poor exposure, the history of volcanic activity is well documented in the

[1] Onshore Sedimentary & Petroleum Geology Program, Bureau of Mineral Resources, GPO Box 378, Canberra ACT 2601

arc-derived sediments of the Tamworth Terrane (e.g. Cawood, 1983; Leitch & Cawood, 1987; McPhie, 1987; Morris, 1988). In early Devonian time eruptions were mainly of andesitic and dacitic composition; later in the Devonian, eruptions reverted to a more mafic composition with the extrusion of basaltic and andesitic rocks. Carboniferous volcanic activity produced rocks of andesitic, dacitic and rhyolitic composition. Plutonic debris in sediments associated with the second cycle appears to be the result of erosion through the volcanic carapace into the roots of the magmatic arc (Lindsay, 1964, 1969; Leitch & Willis, 1982).

2. Tamworth Terrane (forearc basin). The Tamworth Terrane (Cawood & Leitch, 1985) consists of a number of structural blocks, including the Tamworth belt (Harrington, 1974), the associated Hastings block (Fig. 1) (Lindsay, 1969; Scheibner, 1976; Cawood, 1982a,b; Korsch & Harrington, 1987), and the smaller Tabulam and Warwick blocks (Cawood & Leitch, 1985) that formed a single linear structure before dispersal during Permian orogenesis. This terrane, which is interpreted as the forearc basin, consists of a thick Middle Cambrian to Early Permian succession of marine and non-marine sediments (Fig. 2) derived from the magmatic arc.

Whilst basement is not exposed, the island-arc tholeiite affinities of keratophyres preserved in the succession suggest that the forearc basin was underlain by oceanic crust rather than continental crust (Cawood & Flood, 1989). However, as is discussed later, sedimentation in the forearc began in shallow water, which suggests that the nature of the crust underlying the basin is not yet fully understood. The forearc basin, which was well established by the Early Devonian, appears to have filled from the north. During the Carboniferous, the northern Tamworth belt became progressively shallower and was ultimately dominated by paralic and terrestrial sedimentation, whilst in the south and in the Hastings block, marine conditions prevailed into the Early Permian (Leitch, 1974). Limited palaeocurrent data suggest the major direction of transport was transverse to the basin axis with sediment derived from the direction of the magmatic arc (e.g. Crook, 1964; White, 1964a; Russell, 1979), with a general thickening of the succession towards the east. As in other forearc basins (Miall, 1984), smaller volumes of sediment were transported axially (Crook, 1964).

3. Tablelands complex (accretionary wedge). The inferred accretionary wedge is preserved as a series of discontinuous blocks east of the Peel Fault (Fig. 1). The wedge appears to have been formed by the progressive accretion of several terranes, including the Woolomin, Cockburn and Texas Terranes (Cawood & Leitch, 1985; Korsch & Harrington, 1987) which range in age from at least Late Devonian to Late Carboniferous (Korsch & Harrington, 1987; Ishiga & others, 1988; Aitchison, 1988).

4. Overlap sequences. Permian strata occur overlying, or faulted within, the Tamworth belt and the Tablelands complex. They usually occur in sequences 1000 m thick or more and include diamictites, of probable mass-movement origin, and dark micaceous siltstones (Mayer, 1972; Leitch, 1974; Korsch, 1977; Cawood & Leitch, 1985). Cawood & Leitch (1985) have suggested that these sediments are an overlap assemblage deposited in a rapidly subsiding graben flanked by rocks of the older terranes.

Evaluation of forearc basin subsidence

Methods

In the Tamworth belt, middle to upper Palaeozoic sedimentary rocks are exposed in a series of gentle folds, the axes of which generally parallel the long axis of the belt. Sedimentary rocks of similar age are exposed in broad anticlinal structures in the Hastings block. Based on published data and personal experience, thirteen outcrop localities were selected for the construction of a series of subsidence curves (Figs 2, 3). Major published sources used are given in the caption to Figure 2. Tectonic subsidence curves were constructed from basin stratigraphy and on an assessment of facies associations. The method, first proposed by Sleep (1971), has been used and refined by other authors (e.g. Watts & Ryan, 1976; Sclater & Christie, 1980; Bond & Kominz, 1984; Heidlauf & others, 1986; Lindsay & others, 1987; Lindsay & Korsch, 1989). Tectonic subsidence is the subsidence caused entirely by the tectonic forces driving basin formation, and is derived by eliminating the effects of non-tectonic processes. The major non-tectonic processes involve sediment loading and, to a lesser extent, sediment compaction, water-depth changes and sea-level changes.

Several assumptions concerning the physical properties of the sediments filling the basin and sea-level/water-depth histories are made when eliminating the effects of non-tectonic processes. Subsidence curves are then derived by the decompaction or backstripping of the sediment column and correcting for sediment loading. The method used in the present study follows that of Watts & Ryan (1976), Sclater & Christie (1980), and Chadwick (1985, 1986). Since the nature of the crust underlying the basin is poorly understood, a continental average was assumed (see Lindsay & Korsch, 1989).

Backstripping requires some understanding of the compaction of sediments, eustatic sea level, and palaeobathymetry. The stratigraphic sections were delithified using empirical porosity-depth curves (Bond & others, 1983; Bond & Kominz, 1984; Heidlauf & others, 1986) and by assuming that thickness and density changes in the sediments were due entirely to compaction. Backstripping iteratively removes successively younger sedimentary units and decompacts older units as they approach the surface. Porosity is assumed to follow an empirical exponential relationship with depth (Sclater & Christie, 1980). Lithologic variables used in the decompaction of the sedimentary units follow those of Sclater & Christie (1980) and Schmoker & Halley (1982). The general approach to the computational techniques used is based on Sclater & Christie (1980) and is discussed in detail by Heidlauf & others (1986).

The effects of sea-level changes are much more difficult to evaluate. The relative sea-level curves in Figure 2 cannot be tied to absolute sea level. The effects of eustatic sea-level change are almost impossible to separate from basin dynamics and water-depth changes. However, sea-level changes appear to be relatively small in relation to overall subsidence, and can probably be disregarded on the assumption that their effects are minimal and synchronous (i.e. eustatic) throughout the region.

Water-depth changes in the forearc basin are also difficult to evaluate. Estimates of water depth are based largely on facies data with some additional information from contained faunas. Allochthonous limestone blocks in the associated accretionary wedge units (Chappell, 1961; Fitzpatrick, 1975; Cawood, 1976; Hall, 1978; Pickett, 1982; Aitchison, 1988) suggest that before the opening of the forearc basin relatively shallow marine conditions prevailed along the plate margin. Water-depth estimates are relatively reliable in shallow-marine settings but may have errors as large as one kilometre in the deep-water settings. The derived curves (Fig. 2) are thus largely tectonic-subsidence curves but include a small

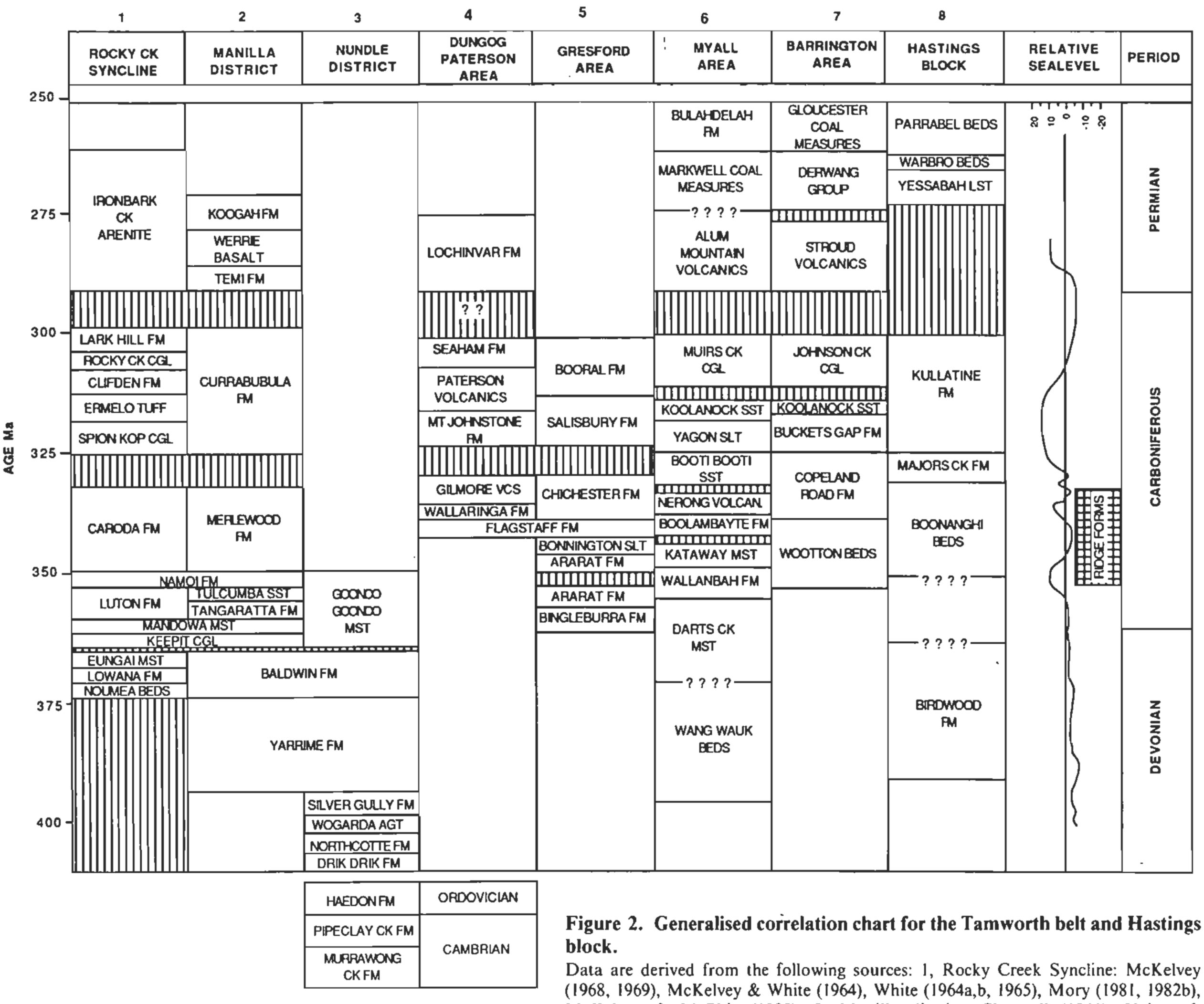

Figure 2. Generalised correlation chart for the Tamworth belt and Hastings block.

Data are derived from the following sources: 1, Rocky Creek Syncline: McKelvey (1968, 1969), McKelvey & White (1964), White (1964a,b, 1965), Mory (1981, 1982b), McKelvey & McPhie (1985); 2, Manilla district: Chappell (1961), Voisey & Williams(1964), Mory (1981, 1982b), McKelvey & McPhie (1985); 3, Nundle district: Crook (1960, 1961a,b, 1964), Ellenor (1975), Cawood (1976, 1983); 4, Dungog-Paterson area: Roberts (1961, 1985); 5, Gresford area: Roberts (1961, 1985), Engel & others, (1969b), Roberts & Oversby (1973, 1974); 6, Myall area: Engel (1962, 1985), Roberts & Oversby (1973), Crane & Hunt (1980); 7, Barrington area: Engel & others (1969a), Campbell & McKelvey (1972), Roberts (1985); 8, Hastings block: Voisey (1936, 1938, 1939a,b), Lindsay (1961, 1969), Brunker & others (1970), Pogson (1972), Northcott, (1973). Sea-level curve is based in part on Talent & Yolkin (1987) and Roberts (1983) and in part on work done in this study. Absolute time scale adapted from Harland & others (1982).

superimposed sea-level component and errors associated with water-depth estimates.

The biostratigraphy of the forearc basin is largely based on conodont zonation (e.g. Jenkins, 1974; Mory, 1982a; Mory & Crane, 1982), brachiopod zonation (e.g. Campbell & McKelvey, 1972; Jones & others, 1973; Roberts, 1985) and palynological assemblages (e.g. Roberts, 1985), such that most units are reasonably well dated. Locally, the biostratigraphy is supported by radiometric dates (e.g. Roberts, 1985) or less widely distributed fossil assemblages such as corals (e.g. Pickett, 1960; Philip & Pedder, 1967; Hall, 1978) and radiolaria (Ishiga & others, 1988; Aitchison, 1988). As might be expected, the dating of these Palaeozoic successions is not as precise as that in younger forearc basin studies (e.g. Ingersoll, 1982; Moxon & Graham, 1987). With the diversity of fossil assemblages needed to develop a regional time framework, it is difficult to estimate errors for the biostratigraphy of the basin. However, the results are consistent in terms of regional correlations and have been refined where possible by using sequence stratigraphy to identify major chronostratigraphic surfaces. Curves should thus be directly comparable on a regional scale.

The curves in Figure 3 show the results of these corrections and give the amount of subsidence that would have occurred if the basin contained only sea water (i.e. if no sedimentation had taken place). Curves for each of the thirteen localities are based upon the best available lithostratigraphic and biostratigraphic information and upon optimal estimates for palaeo-water depth and sea level (Fig. 2).

Results

Overall, in spite of obvious variability, the thirteen curves are similar in that most imply rapid subsidence for 30–50 Ma, beginning at approximately 400 to 350 Ma ago, followed by an abrupt decrease in subsidence rate (Fig. 3). The curves are also similar in form and overall magnitude to those derived for the much younger Great Valley forearc basin of California (Moxon & Graham, 1987). The driving forces were apparently much greater than those involved in thermal subsidence following simple extension; subsidence was more rapid (Fig. 3 inset) and total subsidence was accomplished in less than half the time expected with thermal decay (e.g. Heidlauf & others, 1986; Lindsay & Korsch, 1989).

Variations in the form of the curves show that, on the basis of subsidence history, the basin can be divided into three parts: (1) the northern Tamworth belt, (2) the southern Tamworth belt and (3) the Hastings block. In the northern Tamworth belt, subsidence was both more rapid and of a greater magnitude than to the south. In general, the break between the main early period of rapid subsidence and later slower phase of subsidence is more marked in the north than the south. Typically in the north, total subsidence was 4–5 km, whereas to the south, it reached 5 km but was more typically 2-3 km. Data on the Hastings block are limited to studies in the north. However, at this locality subsidence was rapid, much more so than in the northern Tamworth belt, and to a much greater depth (almost 6 km) (Fig. 3).

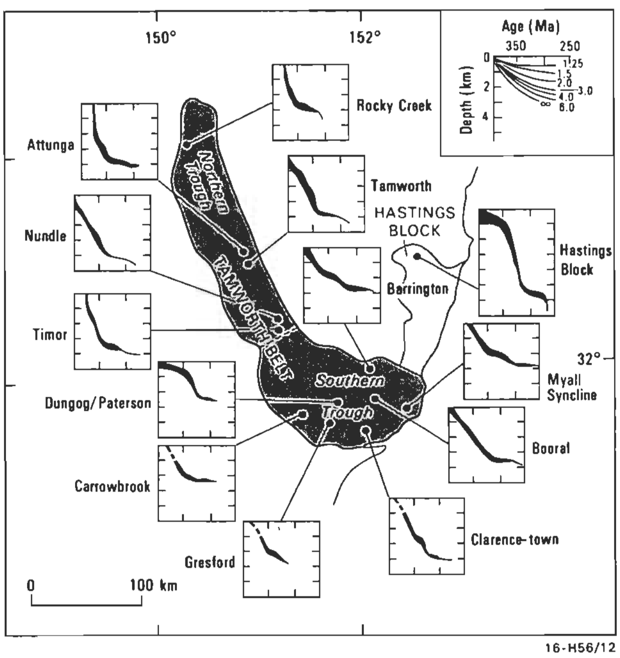

Figure 3. Tectonic subsidence curves for the Tamworth belt and Hastings block.
Vertical thickness of subsidence curves denotes uncertainty in palaeo-water-depth estimates. Stratigraphic data used in the analysis refer to generalised areas in Figure 2. Eustatic sea-level curve is shown in Figure 2. Inset shows thermal-subsidence curves based on the McKenzie (1978) model for simple extension, for comparison. Axial scales for all subsidence curves are the same and are shown on the inset diagram.

The distribution of rock exposures and hence sampling localities (measured sections) is not ideal for information about gradients in subsidence rates across the Tamworth belt. In both north and south, subsidence appears to be somewhat less on the oceanward or trenchward margin of the basin.

Discussion

A major phase in the development of the forearc basin and the associated accretionary wedge began at about 400 Ma ago (Devonian) (Korsch & Harrington, 1981; Aitchison, 1988). Before the initiation of convergent plate interaction, the eastern margin of the Australian plate appears to have been a shallow-marine setting. The onset of subsidence in the forearc basin was abrupt and, once started, was very rapid; most of the depositional space was created within a 50 Ma period (Fig. 3). The subsidence curves suggest, as discussed above, that the forearc basin consisted of three distinct regions: two regions of more rapid subsidence separated by a region of more subdued subsidence.

Forearc basin subsidence appears to have started earliest in the northern Tamworth belt at between 375 and 400 Ma ago (Fig. 3). Almost immediately deeper-water sedimentation, in the form of both pelagic sediments and turbidites, began in the areas of most rapid subsidence. The extreme subsidence in the northern Hastings block is associated with the deposition of a particularly thick massive sequence of turbidites and mass-movement deposits, in what appears to be a very deep-water setting (Lindsay, 1969). Evidence of volcanic activity in the magmatic arc in the form of lavas and volcanoclastics is abundant in these sediments (e.g. Cawood, 1983; Leitch & Cawood, 1987; McPhie, 1987; Morris, 1988). In the central area (the southern Tamworth belt), where subsidence was slower, sedimentation appears to have begun later and in a shallow-marine setting. The area has been described as having a shelf setting as opposed to a basinal setting further north in the Tamworth belt (Engel & others, 1969a; Campbell & McKelvey, 1972; Roberts & Oversby, 1973; Roberts, 1985). The shallow-marine nature of this part of the basin was more influenced by minor fluctuations in sea level and local tectonism, with the result that facies relations are complex.

The width of the Tamworth belt in the south (approximately 100 km) is about twice that in the north and the Hastings block (Fig. 3). Dickinson & Seely (1979) noted that in regions where sedimentation was rapid, forearc terranes broaden, but where sedimentation rates are reduced, the arc trench gap may shorten. Most of the sediments preserved in the southern Tamworth belt were deposited in a shallow-marine setting, which suggests that the sediment supply was greater in this part of the basin. Sedimentation may have been enhanced either by increased volcanic activity along this part of the magmatic arc, or by the entry of a major depositional system (such as a large river delta) into the basin, or both. Such an interpretation is supported by the fact that lavas projected further eastward in the southern Tamworth belt than elsewhere in the basin (Leitch, 1978) (Fig. 3). Conversely, in the Hastings block, where total subsidence was greatest, there is evidence of great water depths and large scale mass movement (Lindsay, 1964, 1969) suggesting that sedimentation was not keeping pace with subsidence. The Tamworth belt is, however, structurally complex, and other mechanisms are possible.

The change in slope of the subsidence curves suggests that rapid subsidence of the forearc basin ceased almost as abruptly as it began. This abrupt change occurred first in the northern Tamworth belt at about 340 to 355 Ma ago, and later in the southern Tamworth belt and the Hastings block at closer to 320 Ma ago (Fig. 3). Fortunately, dating of this part of the section is considerably better than for the onset of basin subsidence, so the timing of changes in subsidence rates and depositional patterns can be more clearly defined. The reduced subsidence rates following the main phase of rapid subsidence are similar to those predicted for thermal subsidence (cf. Fig. 3 inset).

Depositional patterns predictably show evidence of being controlled by basin subsidence. In the northern Tamworth belt, deep-water sedimentation continued to about 345 Ma ago, whereas in the extreme southern Tamworth belt and the Hastings block deep-water sedimentation persisted somewhat longer to perhaps 330 Ma ago (e.g. Lindsay, 1969; Mory, 1981; McKelvey & McPhie, 1985) (Figs 2, 3). Deposition then shifted from deeper-water turbiditic sedimentation to shallow-marine sedimentation and ultimately fluvial or deltaic sedimentation. In the northern Tamworth belt, the shift in depositional patterns began earlier and the interval of shallow-marine sedimentation was brief (less than 5 Ma). In the southern Tamworth belt, shallow-marine conditions developed earlier and persisted longer (approximately 30 Ma) than in the north. In the extreme south of the Tamworth belt and the Hastings block, shallow-marine conditions persisted well into the Carboniferous. In the northern Hastings block, fluvial conditions appeared only briefly at the end of the Carboniferous (Lindsay, 1964, 1966).

As subsidence began to slow in the northern Tamworth belt, older sedimentary rocks of the accretionary wedge were uplifted to form a subaerial ridge between the forearc basin and the trench. Evidence that clastic rocks from the ridge were being shed into the forearc basin is found in sedimentary rocks in both the Tamworth belt and the Hastings block (Lindsay, 1964, 1969; Campbell, 1969; Price, 1973; Leitch & Cawood, 1980; Korsch & Harrington, 1981). Campbell (1969) visualised the ridge as a series of islands rather than a continuously exposed ridge. Evidence from the Carboniferous of the Hastings block suggests that the ridge may have started to rise a little earlier at that end of the forearc basin than in the northern Tamworth belt, and that it continued to shed sediments until at least 320 Ma ago (Lindsay, 1964, 1969).

The presence of plutonic debris, in some cases large boulders, in the Devonian and Carboniferous successions suggests erosion through the volcanic carapace into the roots of the western magmatic arc (Lindsay, 1964, 1969; Leitch & Willis, 1982). Their widespread occurrence suggests that deep erosion of the magmatic arc was occurring regionally throughout this time.

The data suggest that the rise of the ridge and deep erosion of the magmatic arc occurred in the final stages of rapid forearc basin subsidence (Fig. 4). At that time, sediment loading was at a maximum, which suggests a possible connection between these events and the deep erosion of the magmatic arc.

Several unconformities/disconformities have been postulated in the Tamworth belt and Hastings block. As in most basins, there has been a tendency (e.g. Korsch & Harrington, 1981) to associate these surfaces with major tectonic events. However, few of these surfaces are very extensive, and there is evidence that some are basin-edge disconformities (e.g. Russell, 1979). For example, the Keepit Conglomerate can be followed from the basin margin, where it is part of a fan association resting on the Bective unconformity, to canyon fill and finally to a conformable marine mass-movement association towards the basin centre (Crook & Powell, 1976), suggesting that this unit records a major sea-level low (i.e. a Type 1 sequence of van Wagoner & others, 1987). Some surfaces may be associated with superimposed local tectonic events. The subsidence of the forearc basin was, in itself, the product of a major ongoing tectonic event involving converging plate margins. Consequently, a major sea-level fall could have resulted in erosion around the basin margin that caused variations in the nature of the sequence boundary. Once sea level rose again, a conformity would have developed in some areas, whilst in other areas, notably along the basin margin, the succession would be disconformable due to the ongoing subsidence of the basin. This suggestion is supported by the fact that the slope of the subsidence curves is the same either side of the disconformities/unconformities.

In the southern Tamworth belt, where subsidence was slower and water depths minimal, Roberts (1985) has attributed some disconformities to sea-level effects. A relatively widespread erosion surface beneath the Spion Kop Conglomerate and the Currabubula Formation in the northern Tamworth belt may also relate to a major sea-level lowstand identified by Vail & others (1977a,b) at 324 Ma ago. The major disconformity between the Upper Carboniferous and Lower Permian (Fig. 2) is probably due in part to the sudden decrease in basin subsidence rates, and in part to a major sea-level lowstand at about 270 Ma ago (Vail & others, 1977a,b).

Conclusions

The Tamworth belt and Hastings block of northeastern New South Wales are the erosional and structural remnants of a large forearc basin that developed as a result of major convergent plate interaction between approximately 400 and 350 Ma ago (Fig. 4). Data suggest that, in part, the basin was underlain by oceanic crust but that shallow-marine conditions may have prevailed immediately before basin subsidence began. Tectonic-subsidence curves show that the Palaeozoic forearc basin of eastern Australia subsided in a manner similar to that of the Great Valley forearc basin

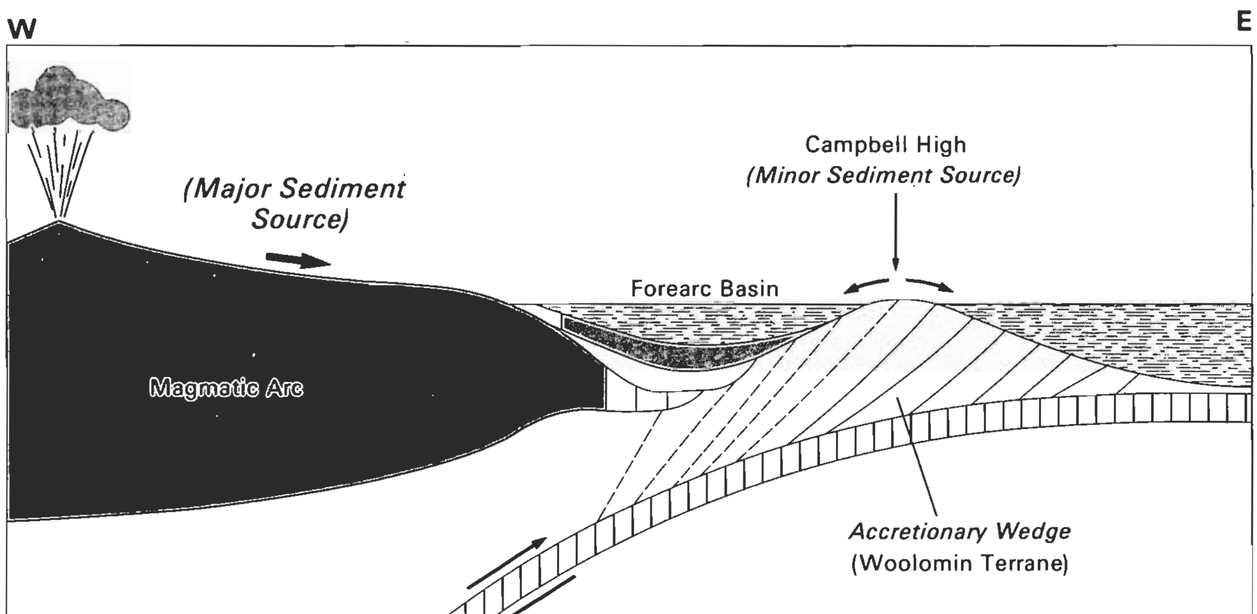

Figure 4. Idealised forearc-basin model (adapted from Ingersoll, 1979, 1982), showing a section across the central Tamworth belt when tectonic subsidence rates were close to their maximum, at approximately 340 Ma ago.

of California. Subsidence began abruptly, continued at a high rate for approximately 50 Ma, and then ceased as abruptly as it began. Subsidence began first in the north and persisted longest at the opposite end of the basin.

The basin evolved as three distinct regions. In the northern Tamworth belt and the Hastings block, subsidence occurred more rapidly and to greater depths than in the southern Tamworth belt. In the northern Tamworth belt and the Hastings block total subsidence was 4-6 km, whereas in the southern Tamworth belt subsidence was typically 2-3 km. Total subsidence appears to have an inverse relationship with basin width so that the cross-sectional area of the basin is conserved. This relationship suggests that basin morphology is modified by sediment supply as suggested by Dickinson & Seely (1979), so that in areas where sediment supply is abundant, the basin width increases but total subsidence is reduced.

In broad terms, sedimentation in the basin was controlled by subsidence and sediment supply. The sedimentary succession begins with deep-water sediments and gradually passes upward to shallow-marine and finally fluvial associations. Sea-level controls interact with the effects of subsidence and sediment supply, and have greatest effect at the basin margin and in the shallow-marine parts of the succession. The effects of sea level are most pronounced in the southern Tamworth belt where subsidence was smaller due to increased sediment supply, and more of the succession was deposited in a shallow-marine setting. As might be expected, sea level, although showing regular patterns, is not necessarily in phase with basin development. The overall result of the interaction of these variables was the production of a basin that constantly changed in morphology both spatially (along its axis) and through time.

Acknowledgements

I wish to thank J. Tipper for assistance with backstripping of the subsidence curves and J. Wilford for considerable assistance in assembling and reducing data. I would also like to thank R. Korsch and H.J. Harrington for discussions about the regional geology of the New England region, and P.A. Cawood, R.A. Chadwick, E.C. Leitch and A. Whittaker for reviewing the manuscript.

References

Aitchison, J.C., 1988 — Late Paleozoic radiolarian ages from the Gwydir Terrane, New England orogen, eastern Australia. *Geology*, 16, 793-795.

Bachman, S.B., Lewis, S.D., & Schweller, W.J., 1983 — Evolution of a forearc basin, Luzon central valley, Philippines. *American Association of Petroleum Geologists, Bulletin*, 67, 1143-1162.

Bond, G.C., & Kominz, M.A., 1984 — Construction of tectonic subsidence curves for the early Paleozoic miogeocline, southern Canadian Rocky Mountains: implications for subsidence mechanisms, age of breakup, and crustal thinning. *Geological Society of America, Bulletin*, 95, 155-173.

Bond, G.C., Kominz, M.A., & Devlin, W.J., 1983 — Thermal subsidence and eustacy in the lower Palaeozoic miogeocline of western North America. *Nature*, 306, 775-779.

Brunker, R.L., Offenberg, A.C., & Cameron, R.G., 1970 — 1:250 000 Geological Sheet SH/56-14 Hastings, New South Wales, Australia. *Geological Survey of New South Wales, Sydney*.

Campbell, K.S.W., 1969 — Carboniferous system. *In* Packham, G.H., (editor), The geology of New South Wales. *Journal of the Geological Society of Australia*, 16, 245-265.

Campbell, K.S.W., & McKelvey, B.C., 1972 — The geology of the Barrington District, N.S.W. *Pacific Geology*, 5, 7-48.

Cawood, P.A., 1976 — Cambro-Ordovician strata, northern New South Wales. *Search*, 7, 317-318.

Cawood, P.A., 1980 — The geological development of the New England Fold belt in the Woolomin-Nemingha and Wisemans Arm regions. The evolution of the Palaeozoic fore-arc terrain. *Ph.D. thesis, University of Sydney*, 429 pp.

Cawood, P.A., 1982a — Tectonic reconstruction of the New England Fold belt in the early Permian: an example of development at an oblique-slip margin. *In* Flood, P.G., & Runnegar, B., (editors) New England geology. *University of New England, Armidale*, 25-34.

Cawood, P.A., 1982b — Structural relations in the subduction complex of the Paleozoic New England Fold belt, eastern Australia. *Journal of Geology*, 90, 381-392.

Cawood, P.A., 1983 — Modal composition and detrital clinopyroxene geochemistry of lithic sandstones from the New England Fold Belt (east Australia): a Paleozoic forearc terrane. *Geological Society of America, Bulletin*, 94, 1199-1214.

Cawood, P.A., & Flood, R.H., 1989 — Geochemical character and tectonic significance of Early Devonian keratophyres in the New England Fold Belt, eastern Australia. *Australian Journal of Earth Sciences*, 36, 68-103.

Cawood, P.A., & Leitch, E.C., 1985 — Accretion and dispersal tectonics of the southern New England Fold belt, eastern Australia. *In* Howell, D.G., (editor), Tectonostratigraphic terranes of the Circum-Pacific region. *Circum-Pacific Council for Energy and Mineral Resources (Houston, Texas), Earth Science Series*, 1, 481-492.

Chadwick, R.A., 1985 — Permian, Mesozoic and Cenozoic structural evolution of England and Wales in relation to the principles of extension and inversion tectonics. *In* Whittaker, A., (editor), Atlas of onshore sedimentary basins in England and Wales: post-Carboniferous tectonics and stratigraphy. *Blackie, London*, 9-68.

Chadwick, R.A., 1986 — Extension tectonics in the Wessex Basin, southern England. *Journal of the Geological Society of London*, 143, 465-488.

Chappell, B.W., 1961 — The stratigraphy and structural geology of the Manilla-Moore Creek district, N.S.W. *Journal and Proceedings of the Royal Society of New South Wales*, 95, 63-75.

Coulbourn, W.T., & Moberly, R., 1977 — Structural evidence of the evolution of forearc basins of South America. *Canadian Journal of Earth Sciences*, 14, 102-116.

Crane, D.T., & Hunt, J.W., 1980 — The Carboniferous sequence in Gloucester-Myall Lakes area. *Journal of the Geological Society of Australia*, 26, 341-352.

Crook, K.A.W., 1960 — Petrology of Tamworth Group, Lower and Middle Devonian, Tamworth-Nundle district, New South Wales. *Journal of Sedimentary Petrology*, 30, 353-369.

Crook, K.A.W., 1961a — Stratigraphy of the Tamworth Group (Lower and Middle Devonian) Tamworth-Nundle district, N.S.W. *Journal and Proceedings of the Royal Society of New South Wales*, 94, 173-188.

Crook, K.A.W., 1961b — Stratigraphy of the Parry Group (Upper Devonian-Lower Carboniferous) Tamworth-Nundle district, N.S.W. *Journal and Proceedings of the Royal Society of New South Wales*, 94, 189-207.

Crook, K.A.W., 1964 — Depositional environments and provenance of Devonian and Carboniferous sediments in the Tamworth trough, N.S.W. *Journal and Proceedings of the Royal Society of New South Wales*, 97, 41-53.

Crook, K.A.W., & Powell, C. McA., 1976 — The evolution of the southeastern part of the Tasman Geosyncline. *25th International Geological Congress Excursion Guide* 17A.

Day, R.W., Murray, C.G., & Whitaker, W.G., 1978 — The eastern part of the Tasman Orogenic Zone. *Tectonophysics*, 48, 327-364.

Dickinson, W.R., & Seely, D.R., 1979 — Structure and stratigraphy of forearc regions. *American Association of Petroleum Geologists, Bulletin*, 63, 2-31.

Dickinson, W.R., Armin, R.A., Beckvar, N., Goodlin, T.C., Janecke, S.U., Mark, R.A., Norris, R.D., Radel, G., & Wortman, A.A., 1987 — Geohistory analysis of rates of sediment accumulation and subsidence for selected California basins. *In* Ingersoll, R.V., & Ernst, W.G., (editors), Cenozoic basin development of coastal California. *Inglewood Cliffs, Prentice-Hall, Rubey*, VI, 1-23.

Ellenor, D.W., 1975 — Sedimentation of the Lower-Middle Devonian Tamworth Group, northeastern New South Wales: a synthesis. *Journal of the Geological Society of Australia*, 22, 311-325.

Engel, B.A., 1962 — Geology of the Bulahdelah-Port Stephens district, N.S.W. *Journal and Proceedings of the Royal Society of New South Wales*, 95, 197-215.

Engel, B.A., 1985 — Tasman Mobile Belt — Myall region. *In* Diaz, C.M., (editor), Carboniferous of the world. *IUGS Publication* No. 20, vol. 2, 33-39.

Engel, B.A., McKelvey, B.C., & Campbell, K.S.W., 1969a — Carboniferous system — Stroud-Gloucester and Myall synclines. *In* Packham, G.H.,(editor), The geology of New South Wales. *Journal of the Geological Society of Australia*, 16, 253-255.

Engel, B.A., Roberts, J., & Campbell, K.S.W., 1969b — The Carboniferous system — lower and middle Hunter Valley. *In* Packham, G.H., (editor), The geology of New South Wales. *Journal of the Geological Society of Australia*, 16, 249-253.

Fitzpatrick, K.R., 1975 — Woolomin-Texas block: Woolomin Beds and associated sediments. *In* Markham, N.L., & Basden, H., (editors), The mineral deposits of New South Wales. *Geological Survey of New South Wales*, Sydney, 338-349.

Hall, R.L., 1978 — A Silurian (Upper Llandovery) coral fauna from the Woolomin Beds near Attunga, New South Wales. *Proceedings of the Linnean Society of New South Wales*, 102, 85-108.

Harland, W.B., Cox, A.V., Llewellyn, P.G., Pickton, C.A.G., Smith, A.G., & Walters, R., 1982 — A geologic time scale. *Cambridge University Press, Cambridge*, 131 pp.

Harrington, H.J. 1974 — The Tasman Geosyncline in Australia. *In* Denmead, A.K., Tweedale, G.W., & Wilson, A.F., (editors), The Tasman Geosyncline. *Geological Society of Australia, Queensland Division, Brisbane*, 383-407.

Heidlauf, D.T., Hsui, A.T., & Klein, G.deV., 1986 — Tectonic subsidence analysis of the Illinois basin. *Journal of Geology*, 94, 779-794.

Ingersoll, R.V., 1979 — Evolution of the Late Cretaceous forearc basin, northern and central California. *Geological Society of America, Bulletin*, 90, 813-826.

Ingersoll, R.V., 1982 — Initiation and evolution of the Great Valley forearc basin of northern and central California, U.S.A. *In* Leggett, J.K., (editor), Trench-forearc geology: sedimentation and tectonics on modern and active plate margins. *Geological Society of London, Special Publication* 10, 459-467.

Ishiga, H., Leitch, E.C., Watanabe, T., Naka, T., & Iwasaki, M., 1988 — Radiolarian and conodont biostratigraphy of siliceous rocks from the New England fold belt. *Australian Journal of Earth Sciences*, 35, 73-80.

Jenkins, T.B.H., 1974 — Lower Carboniferous conodont biostratigraphy of New South Wales. *Palaeontology*, 17, 909-924.

Jones, P.J., Campbell, K.S.W., & Roberts, J., 1973 — Correlation chart for the Carboniferous System of Australia. *Bureau of Mineral Resources, Australia, Bulletin* 156A.

Korsch, R.J., 1977 — A framework for the Palaeozoic geology of the southern part of the New England Geosyncline. *Journal of the Geological Society of Australia*, 25, 339-355.

Korsch, R.J., & Harrington, H.J., 1981 — Stratigraphic and structural synthesis of the New England Orogen. *Journal of the Geological Society of Australia*, 28, 205-226.

Korsch, R.J., & Harrington, H.J., 1987 — Oroclinal bending, fragmentation and deformation of terranes in the New England Orogen, eastern Australia. *American Geophysical Union, Geodynamics Series*, 19, 129-139.

Leitch, E.C., 1974 — The geological development of the southern part of the New England Fold belt. *Journal of the Geological Society of Australia*, 21, 133-156.

Leitch, E.C., 1975 — Plate tectonic history of the Palaeozoic history of the New England Fold belt. *Geological Society of America, Bulletin*, 86, 141-144.

Leitch, E.C., 1978 — Structural succession in a Late Palaeozoic slate belt and its tectonic significance. *Tectonophysics*, 47, 311-323.

Leitch, E.C., & Cawood, P.A., 1980 — Olistoliths and debris flow deposits at ancient consuming plate margins: an eastern Australian example. *Sedimentary Geology*, 25, 5-22.

Leitch, E.C., & Cawood, P.A., 1987 — Provenance determination of volcaniclastic rocks: the nature and tectonic significance of a Cambrian conglomerate from the New England Fold Belt, eastern Australia. *Journal of Sedimentary Petrology*, 57, 630-638.

Leitch, E.C., & Willis, S.G.A., 1982 — Nature and significance of plutonic clasts in Devonian conglomerates of the New England Fold belt. *Journal of the Geological Society of Australia*, 29, 83-89.

Lindsay, J.F., 1961 — The stratigraphy, sedimentation and palaeontology of a Permian and Carboniferous sequence at Willi Willi, near Kempsey, N.S.W. *B.Sc. (Hons) thesis, University of New England, Armidale, Australia*, 100 pp.

Lindsay, J.F., 1964 — Permian and Carboniferous sedimentation of the Macleay district, N.S.W. *M.Sc. thesis, University of New England, Armidale, Australia*, 300 pp.

Lindsay, J.F., 1966 — Carboniferous subaqueous mass-movement in the Manning-Macleay Basin, Kempsey, New South Wales. *Journal of Sedimentary Petrology*, 36, 719-732.

Lindsay, J.F., 1969 — Stratigraphy and structure of the Palaeozoic sediments of the lower Macleay region, northeastern New South Wales. *Journal and Proceedings of the Royal Society of New South Wales*, 102, 41-55.

Lindsay, J.F., & Korsch, R.J., 1989 — Interplay of tectonics and sea-level changes in basin evolution: an example from the intracratonic Amadeus Basin, central Australia. *Basin Research*, 2, 3-25.

Lindsay, J.F., Korsch, R.J., & Wilford, J.R., 1987 — Timing the breakup of a Proterozoic supercontinent: evidence from Australian intracratonic basins. *Geology*, 15, 1061-1064.

Mayer, W., 1972 — Diamictite sedimentation in the Nowendoc-Mt. George area, northeastern New South Wales. *Journal and Proceedings of the Royal Society of New South Wales*, 102, 41-55.

McKelvey, B.C., 1968 — Geological map of New England 1:100 000 Bangheet sheet (No. 280) (with marginal text). *University of New England, Armidale, Australia.*

McKelvey, B.C., 1969 — Carboniferous System — Rocky Creek Syncline. *In* Packham, G.H., (editor), The geology of New South Wales. *Journal of the Geological Society of Australia*, 16, 246-247.

McKelvey, B.C., & McPhie, J., 1985 — Tasman Mobile Belt — Tamworth belt. *In* Diaz, C.M., (editor), Carboniferous of the world. *IUGS Publication*, No. 20, vol. 2, 15-23.

McKelvey, B.C., & White, A.H., 1964 — Geological map of New England 1:100 000 Horton sheet (No. 290) (with marginal text). *University of New England, Armidale, Australia.*

McKenzie, D.P., 1978 — Some remarks on the development of sedimentary basins. *Earth and Planetary Science Letters*, 40, 25-32.

McPhie, J., 1987 — Andean analogue for Late Carboniferous volcanic arc and arc flank environments of the western New England orogen, New South Wales, Australia. *Tectonophysics*, 138, 269-288.

Miall, A.D., 1984 — Principles of sedimentary basin analysis. *Springer-Verlag, New York*, 490 pp.

Morris, P.A., 1988 — Volcanic arc reconstruction using discriminate function analysis of detrital clinopyroxene and amphibole from the New England Fold Belt, eastern Australia. *Journal of Geology*, 96, 299-311.

Mory, A.J., 1981 — The early Carboniferous palaeogeography of the Northern Tamworth belt, New South Wales. *Journal of the Geological Society of Australia*, 29, 357-366.

Mory, A.J., 1982a — A review of early Carboniferous stratigraphy and correlations in the northern Tamworth belt, New South Wales. *Proceeding of the Linnean Society of New South Wales*, 105, 213-236.

Mory, A.J., 1982b — The early Carboniferous palaeogeography of the northern Tamworth belt, New South Wales. *Journal of the Geological Society of Australia*, 29, 357-366.

Mory, A.J., & Crane, D.T., 1982 — Early Carboniferous *Siphonodella* (Conodonta) faunas from east Australia. *Alcheringa*, 6, 275-299.

Moxon, I.W., & Graham, S.A., 1987 — History and controls of subsidence in the late Cretaceous-Tertiary Great Valley forearc basin, California. *Geology*, 15, 626-629.

Northcott, I.W., 1973 — Biostratigraphy of the Carboniferous-Permian succession of the Parrabel Anticline, west of Kempsey, northern New South Wales. *B.Sc. (Hons) thesis, University of New England, Armidale, Australia*, 81 pp.

Philip, G.M., & Pedder, A.E.H., 1967 — A correlation of some Devonian limestones of New South Wales and Victoria. *Geological Magazine*, 104, 232-239.

Pickett, J.W., 1960 — Lower Carboniferous coral faunas from the New England district of New South Wales. *Memoirs of the Geological Survey of New South Wales (Palaeontology)*, No. 15.

Pickett, J.W., 1982 — The Silurian system in New South Wales. *Geological Survey of New South Wales*, 29, 1-264.

Pogson, D.J., 1972 — Geological map of New South Wales. 1:1 1:1 000 000. *Geological Survey of New South Wales, Sydney.*

Price, I., 1973 — A new Permian and Upper Carboniferous(?) succession near Woodsreef N.S.W., and its bearing on the

palaeogeography of western New England. *Proceedings of the Linnean Society of New South Wales*, 91, 202-210.
Roberts, J., 1961 — Geology of the Gresford district, N.S.W. *Journal and Proceedings of the Royal Society of New South Wales*, 95, 77-91.
Roberts, J., 1983 — Carboniferous sea level changes derived from depositional patterns in Australia. *Compte Rendu*, 4, 43-64.
Roberts, J., 1985 — Tasman Mobile Belt — Hunter region. *In* Diaz, C.M.,(editor), Carboniferous of the world. *IUGS Publication*, No. 20, vol. 2, 23-33.
Roberts, J., & Oversby, B., 1973 — The early Carboniferous palaeogeography of the southern New England belt, New South Wales. *Journal of the Geological Society of Australia*, 20, 161-173.
Roberts, J., & Oversby, B., 1974 — The Lower Carboniferous geology of the Rouchel district, New South Wales. *Bureau of Mineral Resources, Australia, Bulletin* 147.
Russell, T.G., 1979 — A reappraisal of the late Devonian Bective Unconformity, Tamworth belt, northeastern New South Wales. *Journal and Proceedings of the Royal Society of New South Wales*, 112, 63-69.
Scheibner, E., 1976 — Explanatory notes on the tectonic map of New South Wales. *Geological Survey of New South Wales, Sydney*.
Schmoker, J.W., & Halley, R.B., 1982 — Carbonate porosity versus water depth: a predictable relation for south Florida. *American Association of Petroleum Geologists, Bulletin* 66, 2562-2570.
Sclater, J.G., & Christie, P.A.F., 1980 — Continental stretching: an explanation of the post-mid-Cretaceous subsidence of the continental North Sea Basin. *Journal of Geophysical Research*, 85, 3711-3739.
Sleep, N.H., 1971 — Thermal effects of the formation of Atlantic continental margins by continental breakup. *Royal Astronomical Society Geophysical Journal*, 24, 325-350.
Talent, J.A., & Yolkin, E.A., 1987 — Transgression-regression patterns for the Devonian of Australia and southern west Siberia. *Courier Forschungsinstitut Senckenberg*, 92, 235-249.
Vail, P.R., Mitchum, R.M., & Thompson, S., 1977a — Seismic stratigraphy and global changes of sea level, part 3: Relative changes of sea level from coastal onlap. *In* Seismic stratigraphy — applications to hydrocarbon exploration. *American Association of Petroleum Geologists, Memoir* 26, 63-81.
Vail, P.R., Mitchum, R.M., & Thompson, S., 1977b — Seismic stratigraphy and global changes of sealevel, part 4: Global cycles of relative changes of sea level. *In* Seismic stratigraphy — applications to hydrocarbon exploration. *American Association of Petroleum Geologists, Memoir* 26, 83-97.
van Wagoner, J.C., Mitchum, R.M., Posamentier, H.W., & Vail, P.R., 1987 — Seismic stratigraphy interpretation using sequence stratigraphy. Part 2: Key definitions of sequence stratigraphy. *In* Bally, A.W., (editor), Atlas of seismic stratigraphy. *American Association of Petroleum Geologists Studies in Geology* 27, vol. 1, 11-14.
Voisey, A.H., 1936 — The Upper Palaeozoic rocks around Yessabah, near Kempsey, New South Wales. *Journal and Proceedings of the Royal Society of New South Wales*, 70, 183-204.
Voisey, A.H., 1938 — The Upper Palaeozoic rocks in the neighbourhood of Taree, New South Wales. *Proceedings of the Linnean Society of New South Wales*, 63, 453-462.
Voisey, A.H., 1939a — The upper Palaeozoic rocks between Mount George and Wingham, N. S. Wales. *Proceedings of the Linnean Society of New South Wales*, 64, 242-254.
Voisey, A.H., 1939b — The geology of the county of Buller. *Proceedings of the Linnean Society of New South Wales*, 64, 385-393.
Voisey, A.H., & Williams, K.L., 1964 — The geology of the Carroll-Keepit-Rangari area of New South Wales. *Journal and Proceedings of the Royal Society of New South Wales*, 97, 65-72.
von Huene, R., & Arthur, M.A., 1982 — Sedimentation across the Japan trench off northern Honshu Island. *Geological Society of London, Special Publication* 10, 27-48.
Watts, A.B., & Ryan, W.B.F., 1976 — Flexure of the lithosphere and continental margin basins. *Tectonophysics*, 36, 25-44.
White, A.H., 1964a — The stratigraphy and structure of the Upper Palaeozoic sediments of the Somerton-Attunga district, N.S.W. *Proceedings of the Linnean Society of New South Wales*, 89, 203-217.
White, A.H., 1964b — Geological map of New England 1:100 000 Tamworth sheet (No. 331) (with marginal text). *University of New England, Armidale, Australia*.
White, A.H., 1965 — Geological map of New England 1:100 000 Tareela sheet (No. 300) (with marginal text). *University of New England, Armidale, Australia*.

The genus *Cordylodus* and a latest Cambrian-earliest Ordovician conodont biostratigraphy

Robert S. Nicoll[1]

The conodont genus *Cordylodus* is interpreted here as a septimembrate apparatus containing M, S and P elements. The individual element morphologies are similar to those found in younger Ordovician apparatuses. Septimembrate apparatus structures are identified in three species studied, *C. proavus, C. lindstromi,* and *C. angulatus.* A partial apparatus structure is recognised for *C. caseyi.* Elements previously identified as *C. intermedius* are now assigned as Sb elements of other species of *Cordylodus.* The *Cordylodus intermedius* Zone, lying above the *Cordylodus proavus* Zone and below the *Cordylodus angulatus* Zone, is here replaced by a lower *Hirsutodontus simplex* Zone and an upper *Clavohamulus hintzei* Zone. Both zones were formerly subzones of the *Cordylodus intermedius* Zone (Miller, 1988) or the upper part of the earlier-used *Cordylodus proavus* Zone (Miller, 1984). The term makellate is introduced to describe an element shape category that includes most M elements, which have previously been included in the dolabrate group of elements.

Introduction

Problems generated by using speciation of the conodont genus *Cordylodus* Pander, 1856, as the major taxon upon which to establish the conodont biostratigraphic subdivisions of the latest Cambrian to earliest Ordovician (see Miller, 1984, 1988; Barnes, 1988) have compounded difficulties in the selection of a biostratigraphically controlled level for the Cambrian-Ordovician boundary. These problems relate to a lack of consensus on the definition of important species of *Cordylodus* and an incomplete understanding of the evolutionary lineage of the genus. The problems have been compounded by lack of recognition of the complete multielement structure of *Cordylodus.* Before this study, no conodont worker has fully described the apparatus structure of any species of *Cordylodus.* Pander (1856) seems to have included a number of different element types in his original illustration of *Cordylodus angulatus* Pander, but no mention is made of these apparent morphological differences in his text. Miller (1980) recognised only two element components in the genus. Viira & others (1987) suggested that *C. proavus* was composed of three element types, and Barnes (1988) has recognised up to four elements.

This study will demonstrate that the apparatus of *Cordylodus* consists of seven element types and that those element types can be recognised in *C. proavus* Müller, *C. lindstromi* Druce & Jones and *C. angulatus.* A partial apparatus is established for *C. caseyi* Druce & Jones. It will also demonstrate that *C. intermedius* Furnish is part of the apparatus of *C. angulatus.* A new species of *Cordylodus, C.* sp. nov. A, is now recognised that will also incorporate some of the elements previously assigned to *C. intermedius.* This species has been illustrated by Druce & Jones (1971, pl. 5) as *C. oklahomensis* Müller.

Cordylodus evolved from a multimembrate coniform lineage containing an M element and, as one of the first (but not the oldest) denticulate conodont genera, might be expected to contain a full set of apparatus element types similar to those found in slightly younger ramiform or ramiform-pectiniform multimembrate apparatuses. Careful examination of two species of *Cordylodus, C. angulatus* and *C. lindstromi,* from the Ninmaroo Formation of the Georgina Basin, northern Australia, indicates that septimembrate apparatuses can be recognised for these species. A partial apparatus of six elements, missing only the Sa element, is also identified for *C. caseyi* in samples from the Ninmaroo Formation. Examination of *C. proavus* material from the same source is hampered by low element abundance, but does indicate that a full complement of seven element types is found in that species. Examination of four samples from the San Saba Limestone Member of the Wilberns Formation and the Threadgill Member of the Tanyard Formation of Texas, provided by James F. Miller (Southwest Missouri State University, USA), helped to document the septimembrate apparatus structure of *C. proavus.* A sample from the Ceratopyge Shale and Limestone exposure in the Änga Quarry at Stora Backor, Sweden (Lindstrom, 1955, Stora Backor locality, sample 5) collected by John Repetski (United States Geological Survey) provided comparative material for determination of the apparatus of *C. angulatus.*

The importance of a full understanding of the apparatus structure of *Cordylodus* becomes apparent when it is realised that the long recognised species *C. intermedius* Furnish, 1938, is in reality the Sb element of *C. angulatus* Pander, 1856. Furnish (1938) established two species of *Cordylodus, C. subangulatus* and *C. intermedius,* based on material obtained from the 'Blue Earth' beds at Mankato, Minnesota, USA. Miller (1980) synonymised *C. subangulatus* with *C. rotundatus* Pander, now considered by most workers to be a part of the apparatus of *C. angulatus.* By inference the original association of *C. intermedius* is thus with *C. angulatus.* The resolution of the problem of the validity of the *C. intermedius* Zone thus lies with the recognition that the element morphology which has been considered to be *C. intermedius* is a slowly evolving Sb element associated with a number of species of the genus *Cordylodus.* One of these is a species that evolved from *C. proavus* and was recognised by Druce & Jones (1971) as *C. oklahomensis* Muller and which later gave rise to *C. angulatus.* It is this as yet undescribed species, *C.* sp. nov. A (see Druce & Jones, 1971, Pl. 5, fig. 7 = a P element) that should be the correct taxonomic assignment of many of the elements previously assigned to *C. intermedius.*

This study is based on relatively limited material and the conclusions are therefore based on limited populations. The recognition of the continuity of morphologic trends (following a single element type from one species to the next), however, offsets the advantage of sheer abundance in the determination of apparatus reconstruction. When this is combined with material of the same species from localities in Australia, North America and Europe, the interpretation is considered by the author to be as valid as (or more valid than) a study based solely on a large population. Ultimately the acceptance, refinement or rejection of the interpretation of *Cordylodus,* and its species, presented in this study will depend on the ability of other workers to recognise the morphologies outlined here in their own collections.

[1] Onshore Sedimentary & Petroleum Geology Program, Bureau of Mineral Resources, GPO Box 378, Canberra ACT 2601

Conodont apparatus structure

If the apparatus structure of the conodont organism evolved into a complex multimembrate form early in the developmental history of the group, probably before the advent of phosphate mineralisation, it is not surprising that most Cambrian conodont taxa, either euconodont or protoconodont, appear to be represented by multielement apparatuses. This is supported by studies such as An & others (1983) and Chen & Gong (1986) using material from China, and by Andres (1988) working with material from Sweden, all of whom recognise multimembrate apparatuses for many Cambrian taxa.

I believe that there are two major groupings of euconodonts, (1) those coniform apparatuses with seximembrate apparatus structures (S and P elements only) and (2) those coniform, ramiform or ramiform–pectiniform apparatuses with septimembrate apparatus structures (M, S and P elements). In conodonts with ramiform or ramiform–pectiniform apparatuses the septimembrate apparatus is considered the optimum apparatus structure. This is based on the studies of clusters, bedding plane assemblages and discrete element reconstructions of Ordovician–Carboniferous faunas (see, for example, Aldridge, 1987 or Nicoll & Rexroad, 1987) that mostly indicate the presence of seven element types in those conodont taxa studied in detail. All ramiform or ramiform–pectiniform apparatuses with fewer than seven element types in the apparatus probably represent secondary loss of element types from an ancestral septimembrate lineage. Most early Ordovician coniform taxa contain six element types in their apparatus structure, and these coniform apparatuses lack a geniculate element that conforms to the makellate (M) element type (see below).

If one accepts this twofold division of euconodont lineages, those with and without an M element, it follows that most post-Cambrian septimembrate taxa are derived from one or two closely related septimembrate Cambrian coniform taxa, because it is unlikely that the geniculate makellate (M) element evolved separately in a number of distantly related seximembrate taxa. *Cordylodus*, with a septimembrate apparatus including an M element, has evolved from *Eoconodontus notchpeakensis* (Miller, 1980), which I believe is part of a probable septimembrate apparatus that includes geniculate elements earlier assigned to the genus *Cambrooistodus* Miller (1980). *Eoconodontus* is in turn derived from *Proconodontus* which may not have a geniculate M element, but is multimembrate.

If many or most Ordovician ramiform and ramiform–pectiniform apparatus structures were probably derived from a lineage that can be traced back to *Cordylodus*, this is both biologically and biostratigraphically significant. Attributes (in addition to denticulation) that we associate with more complex ramiform apparatuses, but which first developed in *Cordylodus*, include lateral processes and expansion of the oral surface of the posterior process to form a 'protoplatform'. The *Cordylodus* ancestor genus, *Eoconodontus*, contains recognisable M, S and P elements. With the development of denticulation in *Cordylodus*, morphologic concepts of these element categories can be developed that are most clearly analogous with morphologies found in younger species. The genus *Cordylodus* is more complex, both in its discrete element morphology and its apparatus structure, than has been previously recognised.

Despite the differences in apparatus element numbers in the seximembrate and septimembrate apparatuses, there is still an ancestral stock common to both groups. Morphologic trends observed in seximembrate and septimembrate apparatuses appear to have many features in common. Some of these features are the direction of the basal cavity opening, the symmetry of the Sa element and the twisted nature of the element in the Sd position.

Interpretation of *Cordylodus*

Beyond the recognition of the septimembrate apparatus structure of *Cordylodus*, there are two other important results of this study. First, *C. lindstromi* is a valid species and has a wide geographic distribution. Second, *C. intermedius* is not a valid species; it is only an element of *C. angulatus*. Documentation of all three of these statements is provided below in the section on systematic palaeontology, but the effects of these observations will be discussed here and in the following section.

Cordylodus primitivus Bagnoli, Barnes & Stevens (1987) is the oldest and most primitive species of the genus. It shows a relatively rapid differentiation into morphologies that are recognisable as distinct species. Thus in *C. proavus* all of the elements are laterally compressed, but in *C. angulatus* the P elements show the development of a lateral expansion of the oral surface — the earliest 'platform' conodont. *C. lindstromi* has an Sa element with the initial stage of development of symmetrical lateral processes; the cusp base is laterally expanded and slightly bifurcated at the anterobasal margin. *C. caseyi* has distinctly recognisable lateral processes on both Sc and Sd elements.

The validity of the species *C. lindstromi* has been questioned by several authors (Landing & others, 1980; Bagnoli & others, 1987). For this study, material from the original collections of Druce & Jones (1971) has been examined and a morphologically distinctive *C. lindstromi* can be identified (see below). The dual tipped basal cavity, in one form or another, can be found in several species of *Cordylodus*. It is not by itself diagnostic of *C. lindstromi*, but is one of the features that define the species.

The validity of *Cordylodus intermedius* Furnish (1938) was questioned by Lindström (1955), but the species has since been accepted as valid and widely used. However, this study suggests that *C. intermedius* is part of the apparatus of *C. angulatus*. Furnish (1938) described two species of *Cordylodus* from the 'Blue Earth' beds of Mankato, Minnesota, USA. Both species, *C. intermedius* and *C. subangulatus*, are similar in size and style of preservation and were probably recovered from a single sample. Miller (1980) placed one of the Furnish species, *C. subangulatus*, in synonymy with *C. rotundatus* but regarded *C. intermedius* as a valid species, a practice that has been followed by most conodont workers. Re-examination of the Furnish type material and comparison with the Sb element material from this study indicate that both *C. subangulatus* and *C. intermedius* are assignable to *C. angulatus*. The holotypes of *C. intermedius*, an Sb element, and of *C. subangulatus*, a Pa element, are both elements belonging to an apparatus of *C. angulatus*.

The recognition that the type of *C. intermedius* is assignable to *C. angulatus* means that much of the material previously assigned to *C. intermedius* should be reassigned to *C. angulatus* Pander. However, not all of the material previously assigned to *C. intermedius* can be reassigned to *C. angulatus*; some of the stratigraphically older specimens should probably be assigned to *C. proavus*. Re-sampling of the Ninmaroo Formation at Black Mountain, western Queensland, in 1988 recovered a partial apparatus of a *Cordylodus* species that does not appear to have been previously described (see below), but has been partially illustrated, as *C. oklahomensis*, by Druce & Jones (1971, Pl. 5, figs 6 & 7). This material is informally referred to below as *Cordylodus* sp. nov. A and is recovered from an interval, with *Hirsutodontus simplex*, that would make it consistent with some of the reported occurrences of *C. intermedius*.

The evolutionary lineage of species of *Cordylodus* cannot be clearly defined at this stage. Bagnoli & others (1987, text-fig. 2) have outlined an evolutionary interpretation of *Cordylodus*. Because some of the Cow Head Group species cannot be recognised in the Black Mountain section, the phylogeny proposed in this study (Fig. 1) differs from the earlier proposal, but with more study of the faunas from the two regions the differences may be minimised. The relationship of *C. caboti* and *C.* sp. nov. A is not yet understood, nor is a possible relationship of *C. caseyi* and *C. deflexus*. Based on morphological considerations, the *C. caseyi*–*C. lindstromi* and the *C.* sp. nov. A–*C. angulatus* lineages are probably not closely related.

Biostratigraphic implications

The recognition that material formerly assigned to *C. intermedius* is, at least in part, assignable to *C. angulatus* and that *C. intermedius* is not a valid species requires re-examination of the significance and name designation of the *Cordylodus intermedius* Zone of either Miller (1988) or Barnes (1988). Conodont faunas recovered by Druce & Jones (1971) from this interval are neither sufficiently abundant nor diverse enough to form the basis for revision of the zonation of this interval. Recent re-collection of the lower part of the Ninmaroo Formation section has recovered many of the zonally important species of the *Cordylodus proavus* Zone, but did not extend up to the level of *Cordylodus lindstromi*. The abundance of *Cordylodus* in the new samples is low and does not significantly modify the information obtained in the original sample set. Thus revision of the zonation must be based on the information in the original sections.

Within the *Cordylodus intermedius* Zone of Miller (1988), the *Hirsutodontus simplex* and *Clavohamulus hintzei* Subzones are sufficiently defined, independent of the existence of *C. intermedius*, to serve as zones. The easiest solution to this nomenclatural problem is to elevate both the *Hirsutodontus simplex* and *Clavohamulus hintzei* Subzones to the rank of Zones and this procedure is followed here. The result (Fig. 1) is thus only a slight nomenclatural change from the zonation proposed by Miller (1988). Ranges of taxa in this interval are provided by Miller (1988), and, with the exception of the elimination of *C. intermedius*, remain substantially unchanged.

Continued use of the *Cordylodus lindstromi* Zone is indicated following substantiation of the validity of the species *C. lindstromi*. However, confusion relating to the various

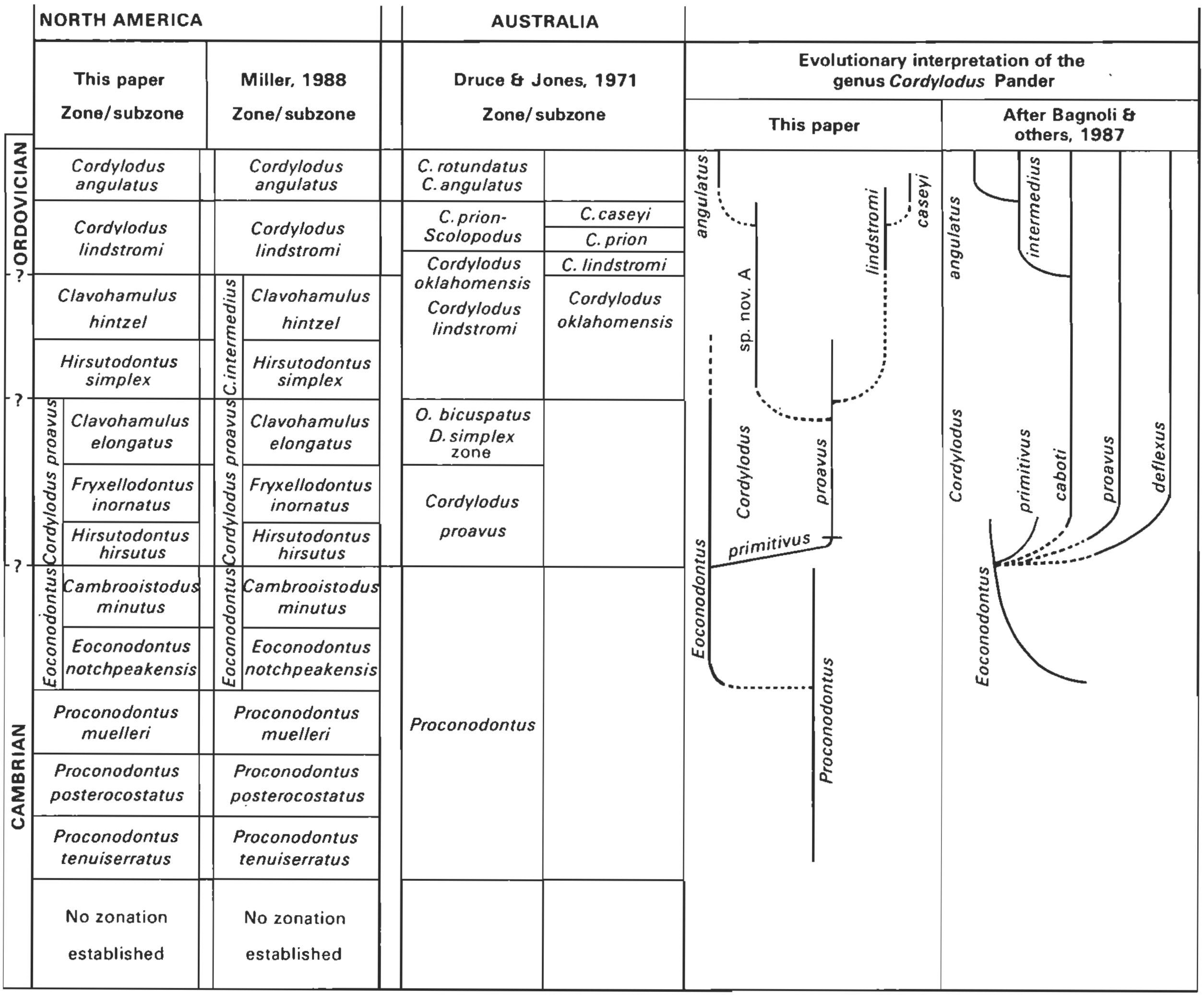

Figure 1. Suggested modification of the Lower Ordovician conodont zonation for North America, and comparison with established and recently modified conodont zonations in North America (Miller, 1988) and the established zonation for Australia (Druce & Jones, 1971).

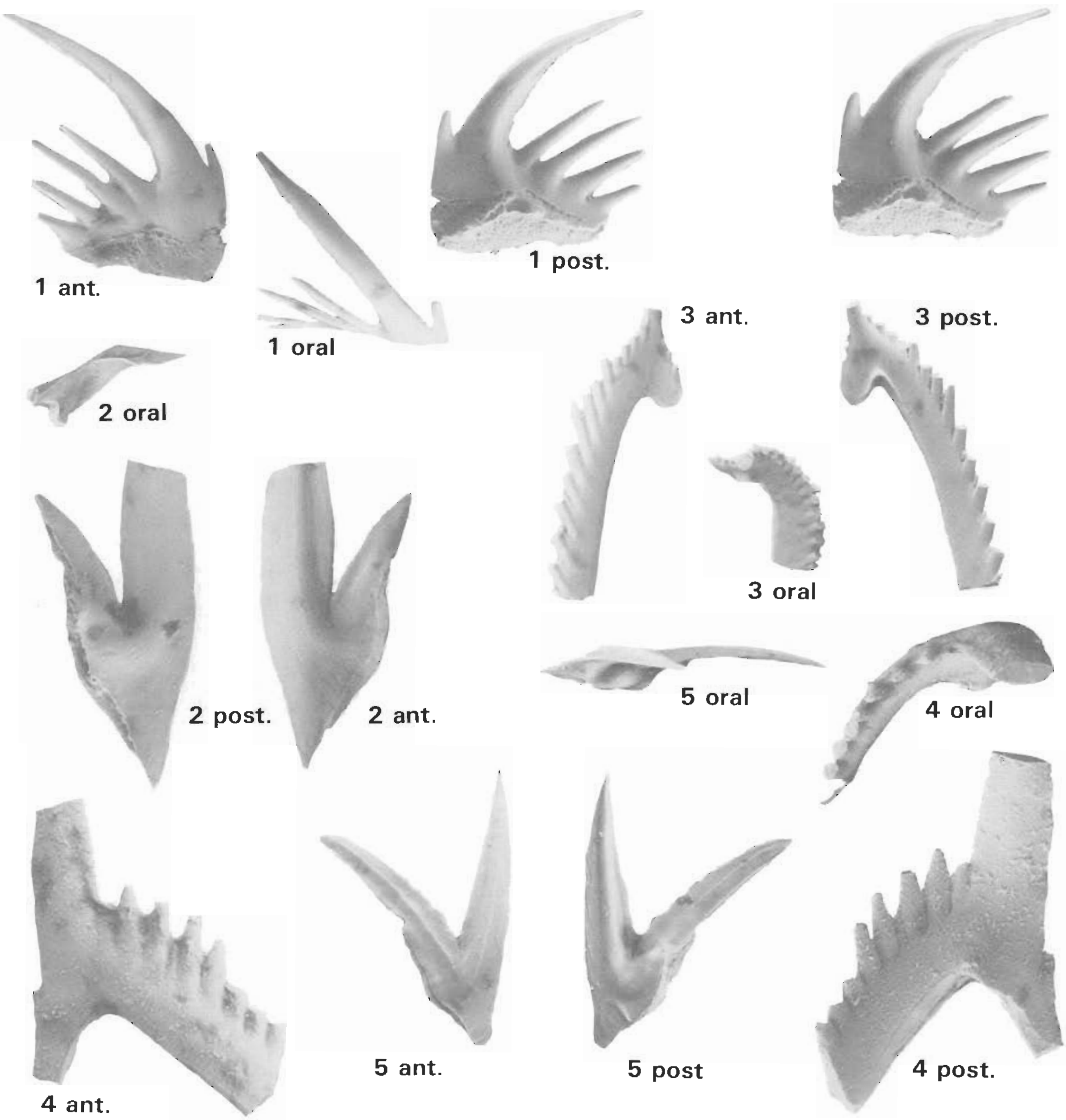

MAKELLATE ELEMENT MORPHOLOGY

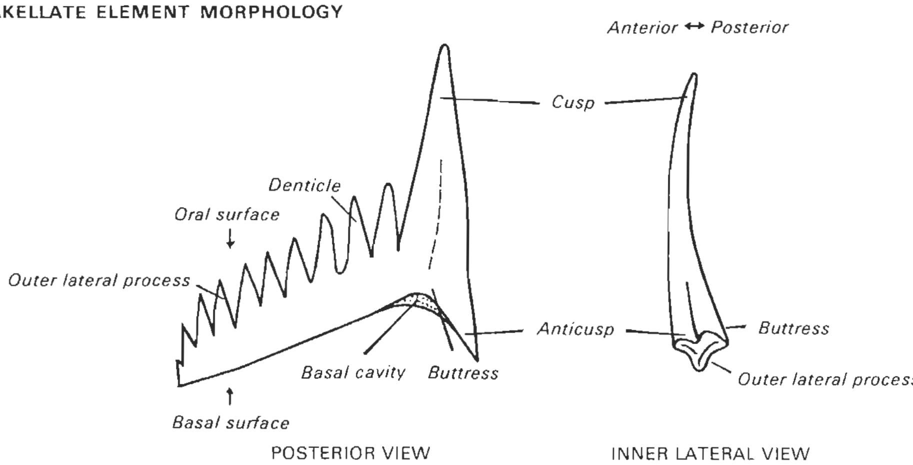

definitions which have been used by conodont workers to define *C. lindstromi* indicates caution in accepting the identification of this zone in the literature. Some workers have applied the name *C. lindstromi* to any species that had a dual tipped basal cavity.

The proposed zonation of Barnes (1988), based on speciation of the genus *Cordylodus*, poses several problems when compared with the Miller (1988) zonation. The first of these problems is the difficulty in determining the end point in the range of one species and the beginning point in its descendant, if there has been gradual evolution of morphological characters from one species to the next.

The second problem is the apparent discrepancy in the range of some species reported by Barnes (1988) compared with the range of those species in other areas. Barnes has equated the base of his *C. lindstromi* Zone with the base of Miller's (1988) *Hirsutodontus simplex* Zone, but this range for *C. lindstromi* is not supported by observations in the Australian sections (Druce & Jones, 1971). Barnes has recorded the base of *C. intermedius* as low as the top of Miller's *Fryxcellodontus inornatus* Zone. This again cannot be substantiated in the Australian sections, even if the species were considered valid. In addition, Barnes (1988) has used *C. lindstromi* in a way that does not correspond with the concept of the species in the type and topotype material of Druce & Jones (1971), nor the revision (this paper) based on that original material. No elements in the Australian section compare with the notched material illustrated by Barnes (1988, figs 13 k, l) or Andres (1988, text-figs 36, 37).

Systematic palaeontology

A new term, **makellate**, is introduced here to describe the shape category of M elements. In the Sweet & Schönlaub (1975) study, three broad groups of element types were introduced as P, S and M. The M notation, an abbreviation of makelliform ('pick-shaped'), was related by Sweet & Schönlaub (1975) to the 'ne' element of Jeppsson (1971) and the 'N' element of Klapper & Philip (1971). In the revised and extended treatment of shape and terminology of elements by Sweet (1981, p. W 12), the shape category dolabrate was proposed to include those ramiform elements which 'have only a posterior process and are commonly pickshaped in lateral aspect'. This category includes two distinctly different shape forms, those referred to as neoprioniodiniform by some authors (Sweet, 1981, fig. 7.1), and those elements in which the cusp is recurved posteriorly over a posterior process (Sweet, 1981, fig. 7.2) and in which the basal cavity is generally parallel with the process.

To reduce confusion and to separate two morphologically and genetically different groups of elements, I propose retention of the term dolabrate to include those elements with only a single posterior process, where the cusp is erect or recurved over the posterior process and the basal cavity lies parallel to, and below, the posterior process.

The new term **makellate** refers to those elements (Fig. 2) which have a cusp that is usually erect but slightly recurved posteriorly over an expanded basal buttress. Most makellate elements have an outer lateral process and an anticusp on the inner lateral margin. In some cases the anticusp may be denticulate. If the outer lateral process is adentate the element is usually geniculate, but if the process is denticulate the element will be nongeniculate. The anterior face is flat, usually without ornamentation, but the posterior face usually has a carina that extends to the basal buttress. The buttress is located on the posterior side of the element and the basal cavity opens either downward or outward, or as some combination of these two directions.

In the apparatus structure the makellate element is transverse to the long axis of the other elements (Nicoll, 1977, 1985), as indicated by the cusp curvature. The outer lateral process may be at a right angle to the long axis of the apparatus, or the process may be bent or angled backward at some angle of less than 90°. The orientation of the process can be determined by an examination of the cusp curvature and buttress position. I know of no case where the morphology of the M element indicates that the long axis of the process lies parallel to the long axis of the apparatus. The element is thus compressed in an antero-posterior direction rather than laterally as in most ramiform elements.

No attempt has been made in this study to produce comprehensive synonymies of species of *Cordylodus* from the literature. In most cases published lateral views of elements do not show the cross-sectional shape and element symmetry that are necessary to determine the element type of the specimen in question. Direct examination of the elements would be required. Only selected papers are discussed here. A re-examination of the identification of all figured and type elements of *Cordylodus* in the Druce & Jones (1971) and Jones (1971) studies is summarised in Appendix 1.

All new material illustrated in this study is deposited in the Commonwealth Palaeontological Collection (CPC) at the Bureau of Mineral Resources, Canberra. I wish to thank the University of Iowa for the loan of the Furnish (1938) type material, examination of which has allowed this interpretation of the status of *Cordylodus intermedius* and *C. subangulatus*.

Genus *Cordylodus* Pander, 1856

Type species. *Cordylodus angulatus* Pander, 1856

Diagnosis. Septimembrate apparatus of ramiform elements with upper portion of cusp composed of white matter and with a denticulate posterior process for the S and P elements, and lateral process for the M element, which may or may not be denticulate. Extent of penetration of the basal cavity into cusp highly variable and species-dependent. Some species may have two tips to the basal cavity with one extending into the cusp and the second into first denticle of the posterior process. Occasional elements may have more than two basal cavity tips, with tips extending into several denticles along the posterior process (Andres, 1988). Element forms M, Sa, Sc, Sb, Sd, Pb and Pa are distinguished. Short adentate

Figure 2. Morphology and orientation of the makellate element.
Illustrated elements range in age from the Ordovician (Arenig) to the Early Carboniferous. Elements show features that differentiate the **makellate** element type from the **dolabrate** type, such as the anticusp, the buttress, cusp curvature and smooth anterior face with no basal expansion. They also indicate part of the range of outer lateral process development and orientation, and show dentate and adentate anticusps. Each specimen is illustrated by posterior, anterior and oral views.
See Appendix 2 for locality and stratigraphic details.

1. ***Erraticodon patu*** (CPC 28051), Lower Ordovician. **2.** ***Triangularis* sp.** (CPC 28052), Lower Ordovician. **3. Unidentified M element** (CPC 28053), Lower Carboniferous. **4. Unidentified M element** (CPC 28054), Lower Carboniferous. **5.** ***Protoprioniodus aranda*** (CPC 28055), Lower Ordovician.
CPC, Commonwealth Palaeontological Collection.

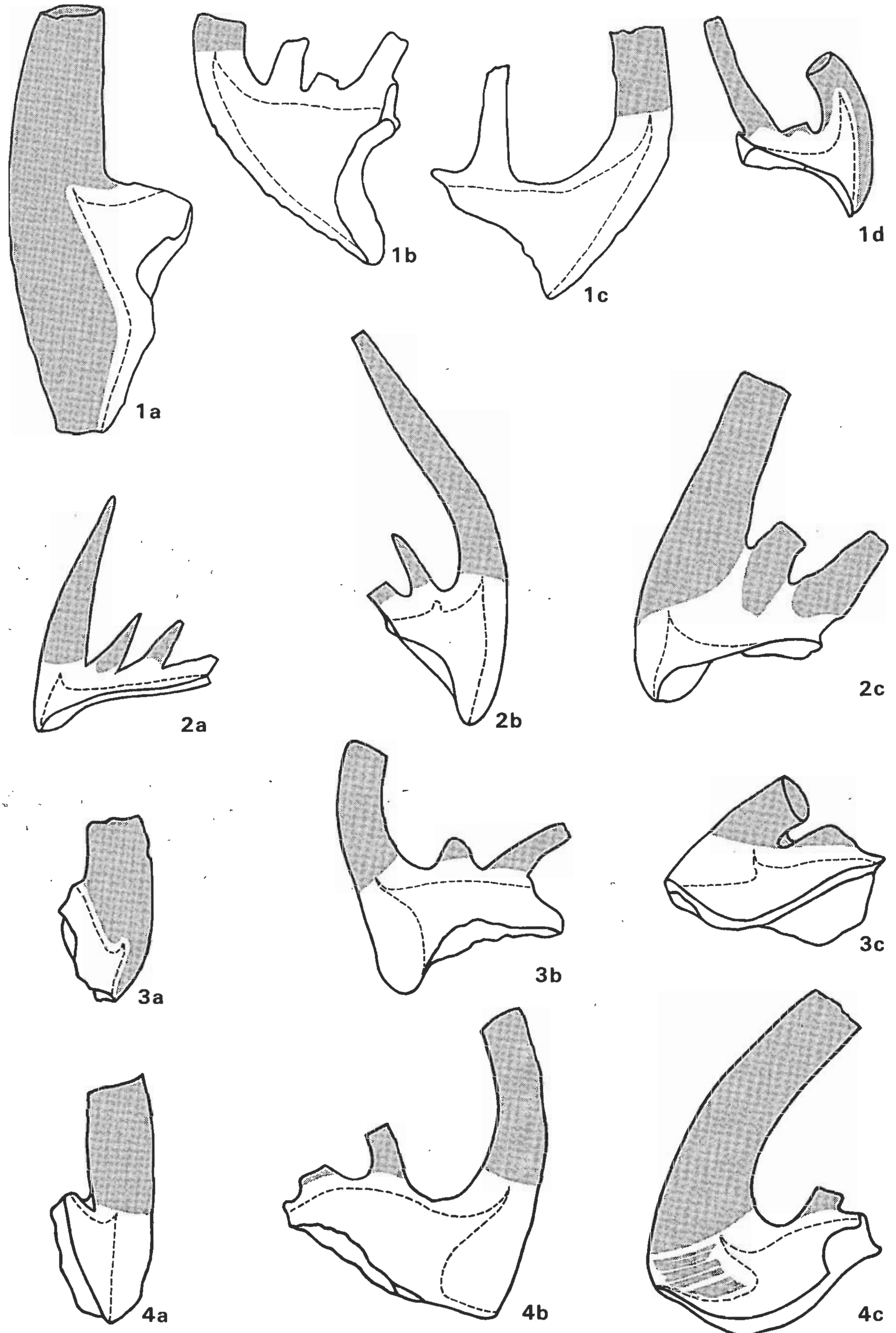

Figure 3. Lateral views of selected specimens of *Cordylodus* showing basal cavity outline (dashed line) and distribution of white matter (shaded area).

1. ***Cordylodus proavus.*** a, M element (CPC 28102) Fig. 15.1; **b,** Sc element (CPC 28113) Fig. 16.2; **c,** Sc element (CPC 28115) Fig. 16.4; **d,** Pa element (CPC 28128) Fig. 18.4. **2.** ***Cordylodus lindstromi.*** **a,** M element (CPC 8732) Fig. 12.5; **b,** Sc element (CPC 28094) Fig. 12.13; **c,** Pa element (CPC 28106) Fig. 14.5. **3.** ***Cordylodus caseyi.*** **a,** M element (CPC 28073) Fig. 9.1; **b,** Sb element (CPC 28078) Fig. 10.1; **c,** Pb element (CPC 28081) Fig. 11.1. **4.** ***Cordylodus angulatus.*** **a,** M element (CPC 28057) Fig. 4.2; **b,** Sa element (CPC 28059) Fig. 4.4; **c,** Pa element (CPC 28071) Fig. 8.2.

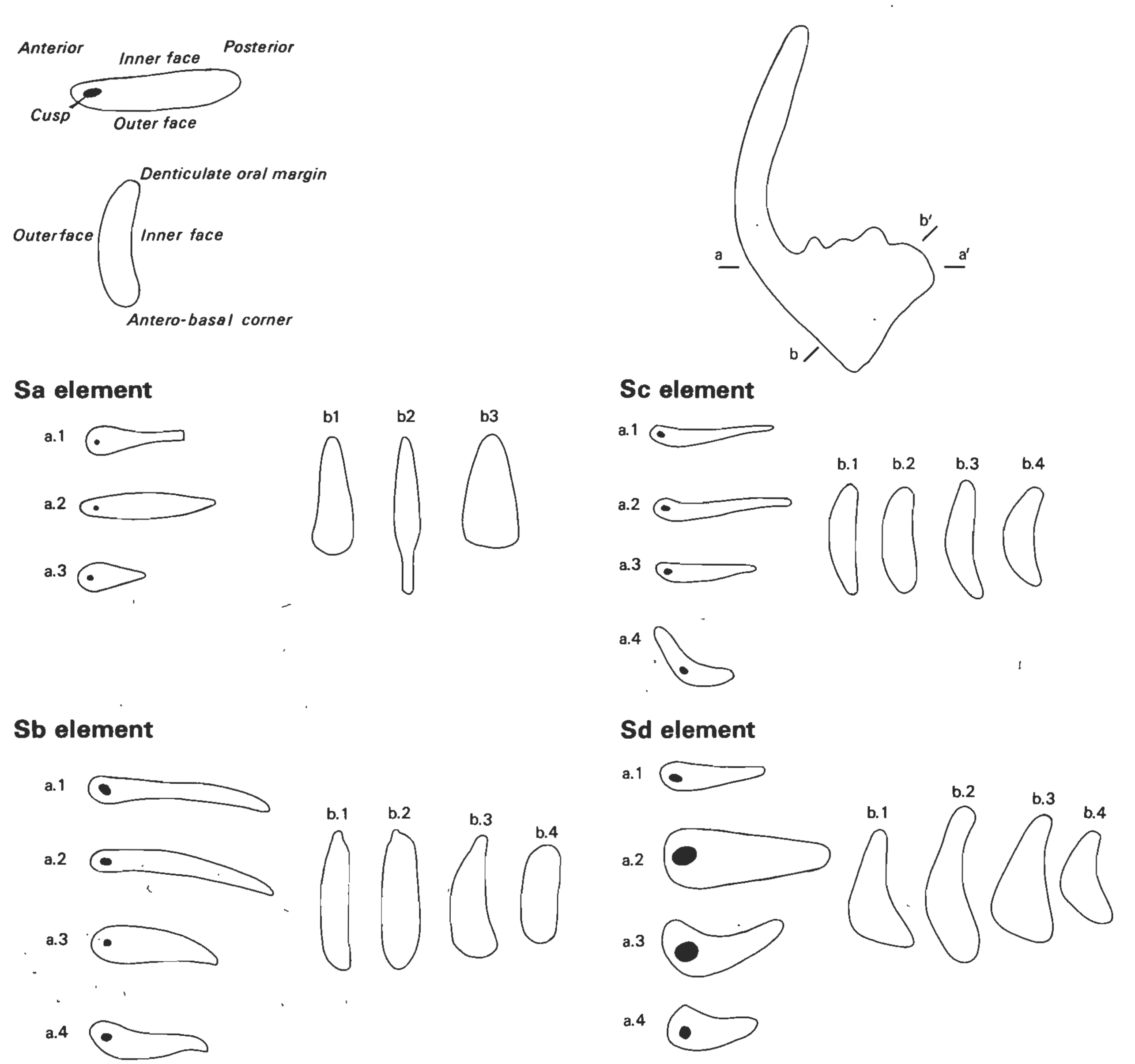

Figure 4. Cross-section shapes of the S elements of *Cordylodus*.
For each species of *Cordylodus* described in this study, a sketch (not to scale) indicates the longitudinal and oblique transverse cross-section. Location of sections is indicated in the sketch of a lateral view of an S element and location of cusp is indicated by the black circle on the longitudinal section. In each case a left element was used as the plan and thus the inner side of the element is to the top of the page (a view) or to the right (b view). Species of each drawing is indicated by number: **1**, *C. proavus;* **2**, *C. angulatus;* **3**, *C. lindstromi;* **4**, *C. caseyi.*

lateral processes may be found on some elements of some species. Element surface smooth, lacking micro-ornamentation, but some elements have carina or keels.

Discussion. Bergström & Sweet (1966) were the first to recognise an apparatus structure for *Cordylodus* when they placed both species described by Pander (1856), *C. angulatus* and *C. rotundatus*, in the multielement *C. rotundatus*. Later Miller (1980) recognised two element types in several species of *Cordylodus*. The compressed elements of Miller (1980) are the P elements of this study, and the rounded elements of Miller correspond to the S elements here. Subsequently, Bagnoli and others (1987) established an apparatus of two morphotypes (*p* and *q*) and indicated that the *p* element morphotype contained a symmetry transition series of three elements. At the same time Viira & others (1987) recognised four element types, following Miller (1980) by using compressed and rounded elements, but with three morphotypes of the rounded elements. These morphotypes were not based on the cross-section of the rounded element, but appear to relate to denticulation on the posterior process. Barnes (1988) recognised four morphotypes: *q*, *p*-1, *p*-2 and *p*-3, with two submorphotypes of the *p*-1 morphotype suggested for one species (*C. hastatus*). Barnes has not adequately defined his *p*-1 element categories so they cannot be easily related to the categories used in this study. However, Bagnoli & others (1987) have a *qa* element that corresponds to the Sa element, a *qb* element corresponding to the Sc element and a *qc* element that may be either the Sb or Sd element, or both.

Distribution of white matter, the shape of the basal cavity and its depth of extension into the cusp are important characteristics used for specific identification of some species of *Cordylodus*. In Figure 3, representative forms of each of the species described in this study are illustrated with photograph-based line drawings to show the basal cavity outline and the distribution of white matter.

Recognition of element type within the S element group is based mainly on the cross-section shape. The generalised shapes of the S elements of each of the species described in this study are shown in Figure 4. In general the Sa elements are symmetrical, and the Sc elements are flattened on the inner face and convex on the outer face. The Sb elements are biconvex, but usually slightly asymmetrical. The Sd elements are irregular in shape but the inner face is usually concave and the outer face is convex.

Cordylodus angulatus Pander, 1856
Figures 3(4a–c), 5–12.

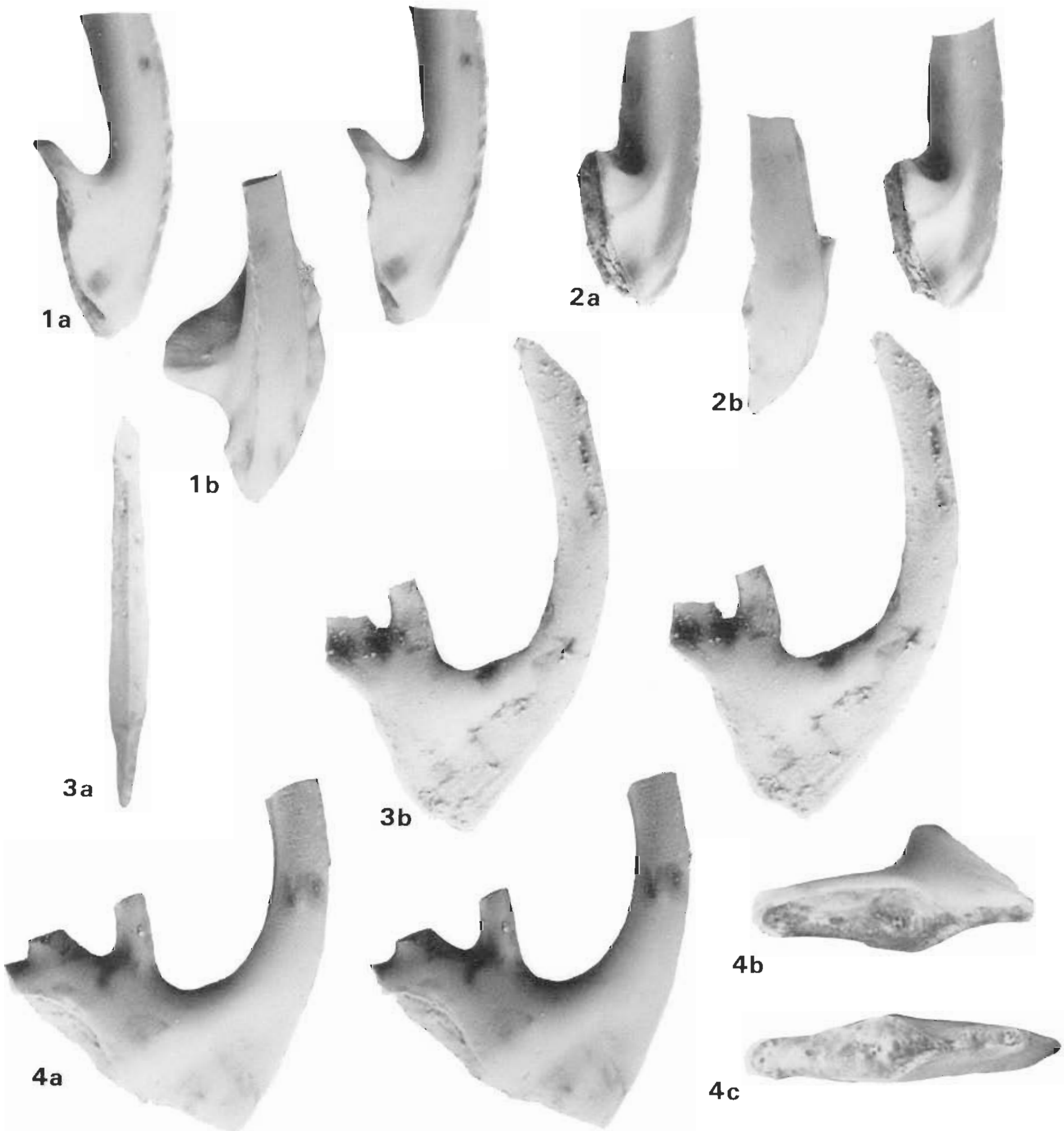

Figure 5. *Cordylodus angulatus*, M and Sa elements.
The number in parentheses is the Commonwealth Palaeontological Collection (CPC) number and the square brackets indicate the sample from which the specimen was obtained. All figures ×92.
1. M element (CPC 28056)[BOU 1/159] left element; **a**, stereo pair, posterior view; **b**, inner lateral view. **2. M element** (CPC 28057)[BOU 1/159] left element; **a**, stereo pair, posterior view; **b**, inner lateral view. **3. Sa element** (CPC 28058)[BOU 1/159]; **a**, anterior view; **b**, stereo pair, lateral view. **4. Sa element** (CPC 28059)[BOU 1/159]; **a**, stereo pair, lateral view; **b**, oblique basal view; **c**, basal view.

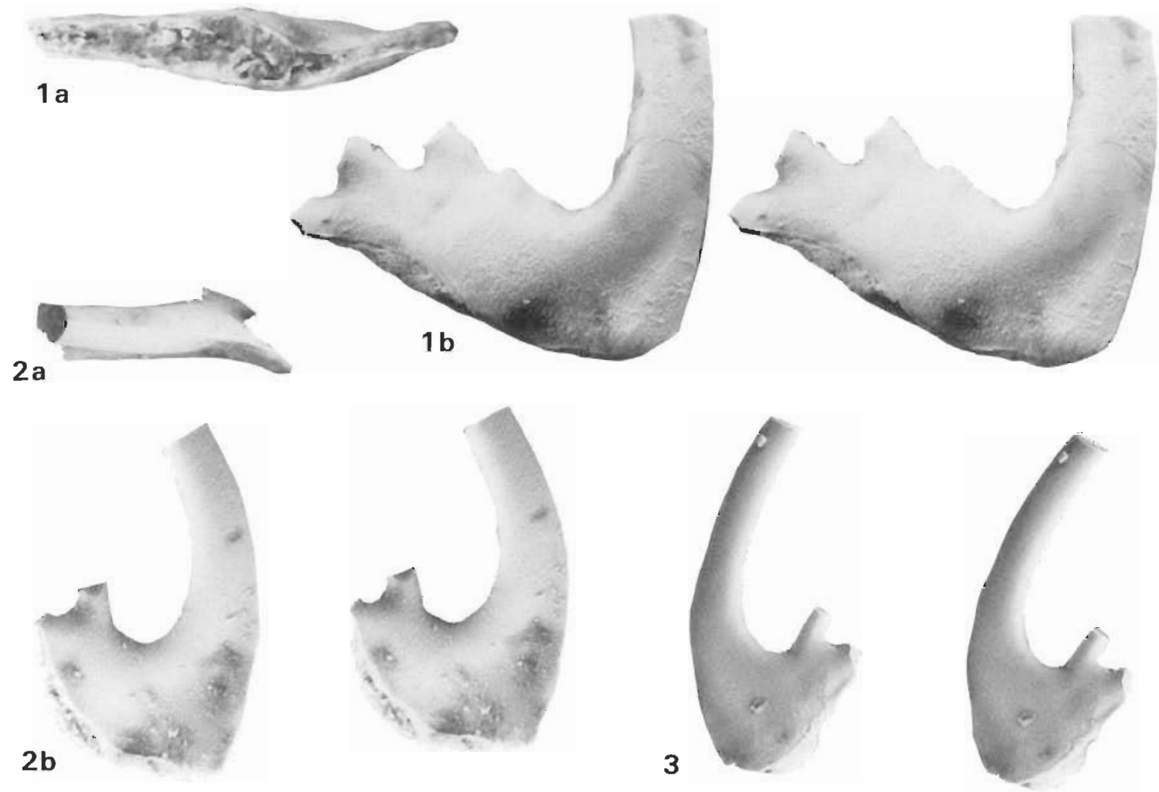

Figure 6. ***Cordylodus angulatus*, Sc element.**
All figures ×92.
1. Left element (CPC 28060)[BOU 1/159]; **a**, basal view; **b**, inner lateral view. **2.** Left element (CPC 28061)[BOU 1/159]; **a**, oral view, **b**, stereo pair, inner lateral view. **3.** Right element (CPC 28062)[BOU 1/159], inner lateral view.

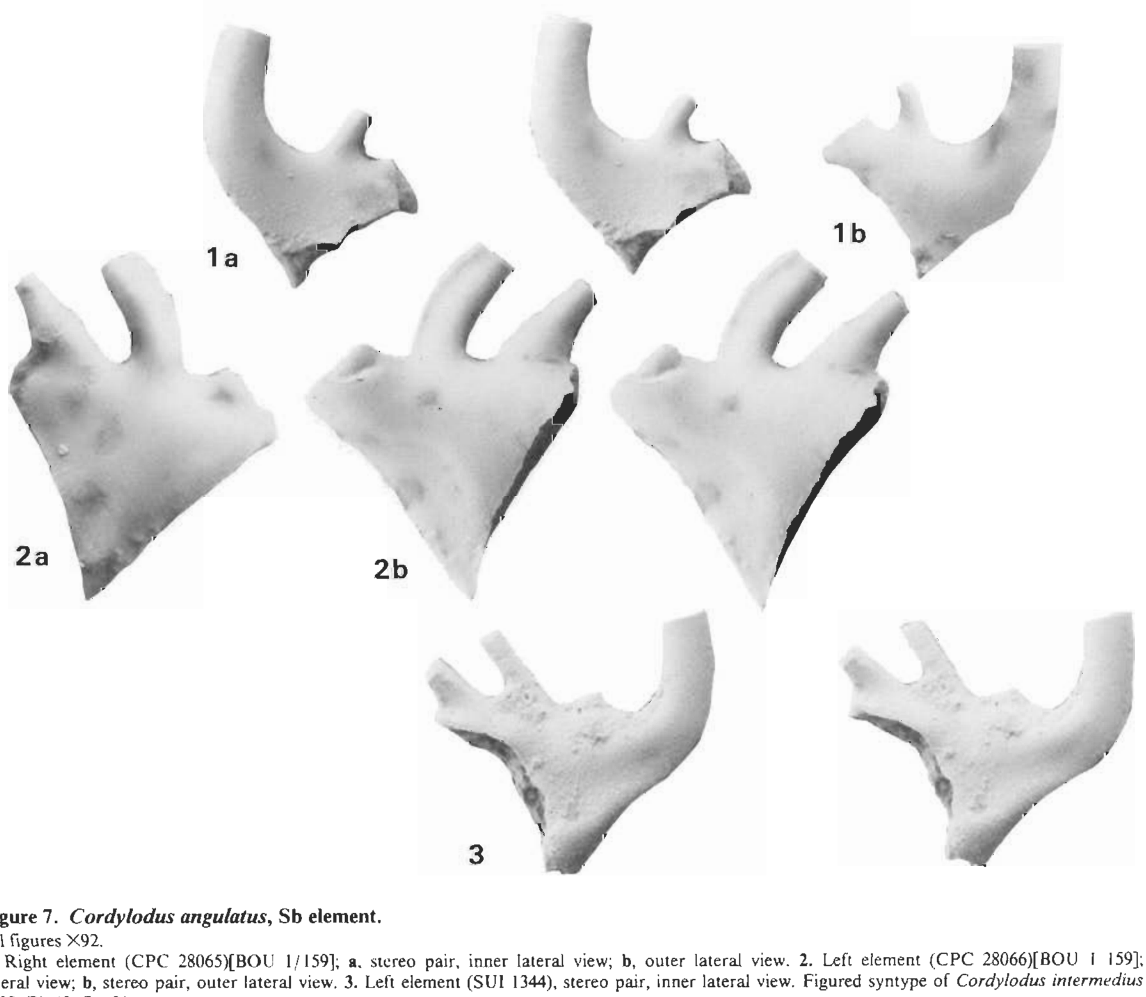

Figure 7. ***Cordylodus angulatus*, Sb element.**
All figures ×92.
1. Right element (CPC 28065)[BOU 1/159]; **a**, stereo pair, inner lateral view; **b**, outer lateral view. **2.** Left element (CPC 28066)[BOU 1/159]; **a**, inner lateral view; **b**, stereo pair, outer lateral view. **3.** Left element (SUI 1344), stereo pair, inner lateral view. Figured syntype of *Cordylodus intermedius* Furnish, 1938, Pl. 42, fig. 31.

Synonymy

1856 *Cordylodus angulatus* n. sp.; Pander, p. 33, Pl. 2, figs 28–31, 34; Pl. 3, fig. 10; Table A, fig. 10, only. (Pl. 2, fig. 28 is a P element, fig. 29 is an Sc element, figs 30, 31 are Sa elements, fig. 34 is an Sb element and Pl. 3, fig. 10 is an Sa element.)

1856 *Cordylodus rotundatus* n. sp.; Pander, p. 33, Pl. 2, figs 32, 33 (fig. 32 is a Pb element and fig. 33 is a P element).

v. 1938 *Cordylodus intermedius* n. sp.; Furnish, p. 338, Pl. 42, fig. 31 (Sb element).

v. 1938 *Cordylodus subangulatus* n. sp.; Furnish, p. 338, Pl. 42, fig. 32 (Pa element).

v. 1971 *Cordylodus angulatus* Pander; Druce & Jones, pp. 66-67, Pl. 3, figs 4–7; text-figs 23a,b (figs 4 & 6 are Sa elements; figs 5 & 7 are Pb elements).

v. 1971 *Cordylodus angulatus* Pander; Jones, pp. 45–46, Pl. 8, fig. 3 (Sa element).

v. 1971 *Cordylodus rotundatus* Pander; Druce & Jones, pp. 71–72, Pl. 3, figs 8–10; text-fig. 23t (figs 8–10 are Pa elements).

v. 1971 *Cordylodus rotundatus* Pander; Jones, p. 49, Pl.

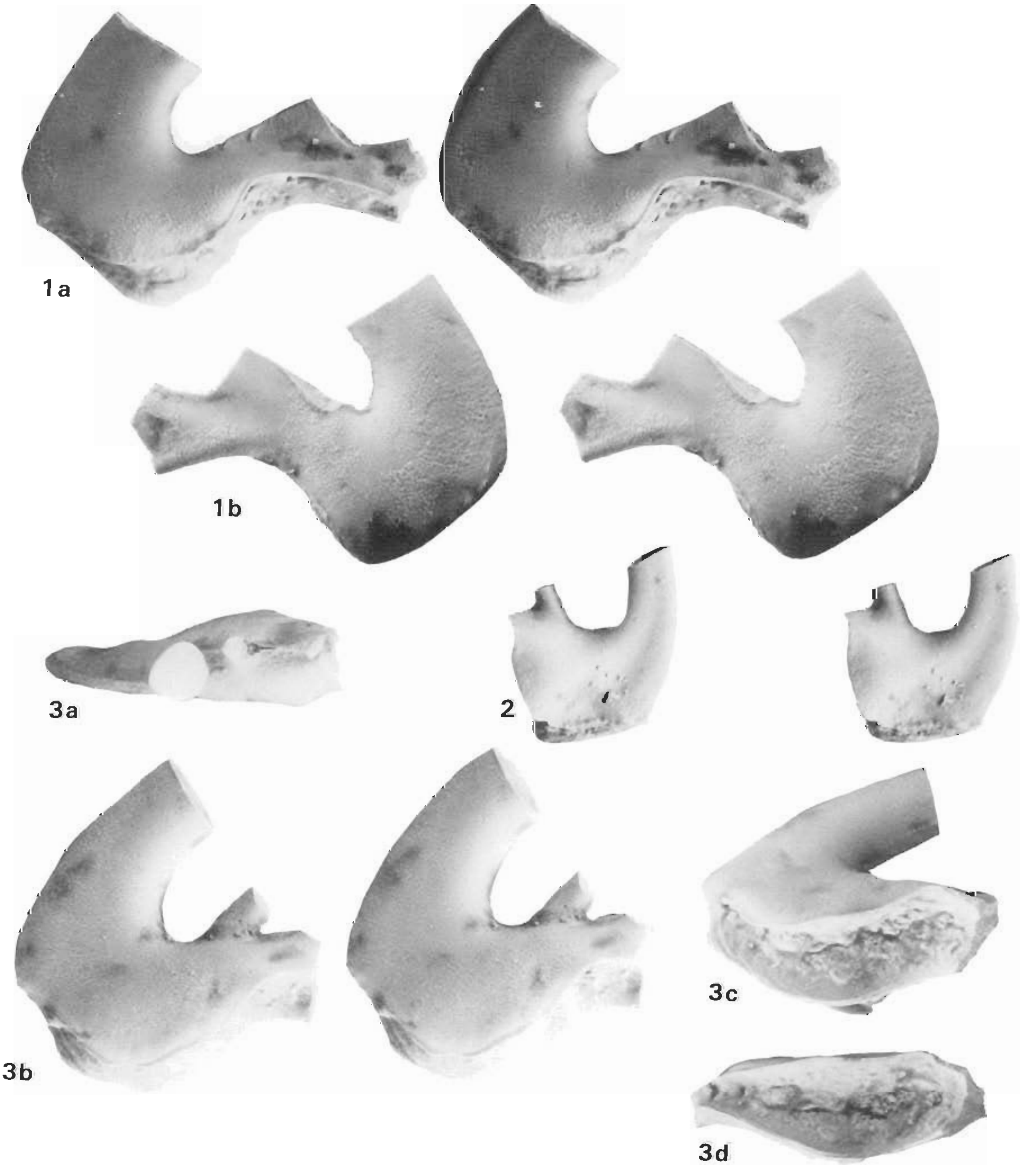

Figure 8. *Cordylodus angulatus*, Pb element.
All figures ×92.
1. Right element (CPC 28067)[BOU 1 159]; **a**, stereo pair, inner lateral view; **b**, stereo pair, outer lateral view. **2.** Left element (CPC 28068)[BOU 1/159], stereo pair, inner lateral view. **3.** Right element (CPC 28069)[BOU 1/159]; **a**, oral view; **b**, stereo pair, inner lateral view; **c**, oblique basal view; **d**, basal view.

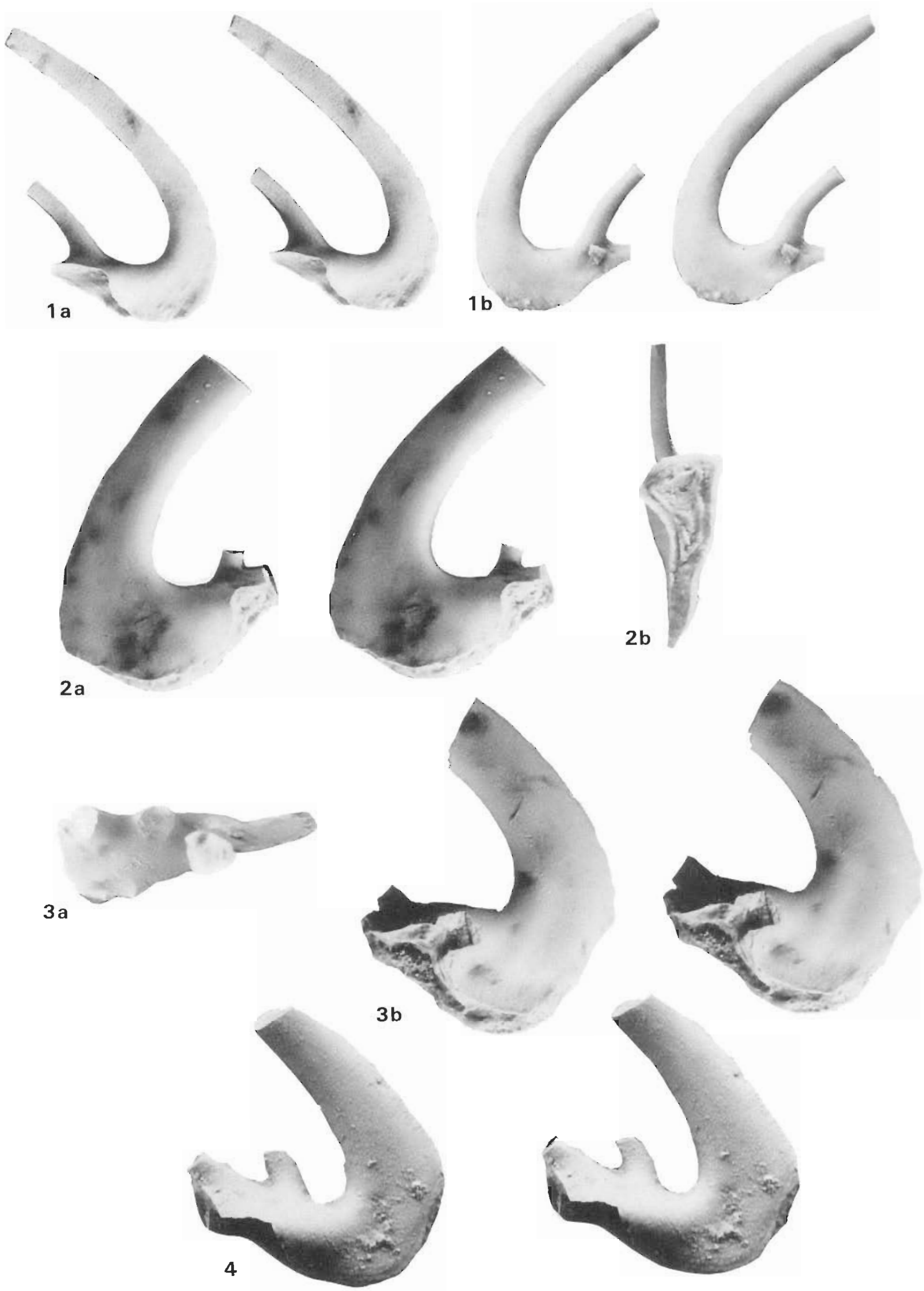

Figure 9. ***Cordylodus angulatus,*** **Pa element.**
All figures ×92.
1. Left element (CPC 28070)[BOU 1/159]; **a**, stereo pair, inner lateral view; **b**, stereo pair, outer lateral view. **2.** Right element (CPC 28071)[BOU 1/159]; **a**, stereo pair, inner lateral view; **b**, basal view into cavity. **3.** Left element (CPC 28072)[BOU 1/159]; **a**, oral view; **b**, stereo pair, inner lateral view. **4.** Left element (SUI 1346), stereo pair, inner lateral view. Figured syntype of *Cordylodus subangulatus* Furnish, 1938, Pl. 42, fig. 32.

2, figs 10, 11 (fig. 10 is a Pa element, fig. 11 is a Pb element).

v. 1971 *Cordylodus intermedius* Furnish; Druce & Jones, p. 68, Pl. 3, fig. 1 only (Sb element).

v. 1971 *Cordylodus* sp. A; Druce & Jones, p. 72, Pl. 8, fig. 10, text-fig. 23u (Sa element).

Material studied. 48 elements from Australia (see Table 1) and over 200 elements from Sweden.

Table 1. Recovery of *Cordylodus angulatus* in a sample from the Ninmaroo Formation, Georgina Basin, Australia.

Element type	*M*	*Sa*	*Sc*	*Sb*	*Sd*	*Pb*	*Pa*
Sample 1/159	2	4	9	5	0	15	13

Diagnosis. Septimembrate apparatus of ramiform elements. The P and S elements are dolabrate and the M element is makellate. Only the Sa element is symmetrical; all other elements are asymmetrical. White matter is generally solid in the cusp, but on the base is usually interlayered with hyaline apatite. Cusps of P and S elements are recurved over the process and denticles are recurved or reclined rather than straight. The upper surface of the posterior process is slightly arched. In lateral view the anterior margin of the basal cavity curves, from the basal cavity tip, posteriorly toward the posterior margin and then recurves anteriorly toward the anterobasal corner.

Description. The Pa and Pb elements have a distinctive lateral profile as the line of the anterior margin of the recurved cusp wraps around the anterobasal corner and curves upward toward the posterior process with only a very slight change in the curvature at the anterobasal corner. The basal cavities of both elements extend toward the white matter of the cusp but only the very finest tip may actually reach the white matter. The anterior margin of the basal cavity curves downward and posteriorly from the cusp tip for a short distance and then abruptly bends to extend to the anterobasal corner. This outline is the 'Phrygian cap' shape of Lindström (1955). The anterior extension of the basal cavity is shallow but wider than similar extensions found in the S elements.

The Pa element (Figs 9, 12) has the denticles of the posterior process located on the outer margin and a narrow platform on the inner side with a rounded inner lateral margin. The width of the platform is greatest next to the first process denticle and from that point it narrows gradually to the posterior and abruptly to the anterior where it joins the posterior margin of the cusp. The cusp of the Pa element curves back over the platform and thus is positioned inside the row of process denticles.

The Pb element (Figs 8, 12) is similar to the Pa element, but lacks the pronounced platform shelf on the inner side of the posterior process and instead has only a slight rounding of the inner margin. The cusp of the Pb element is curved

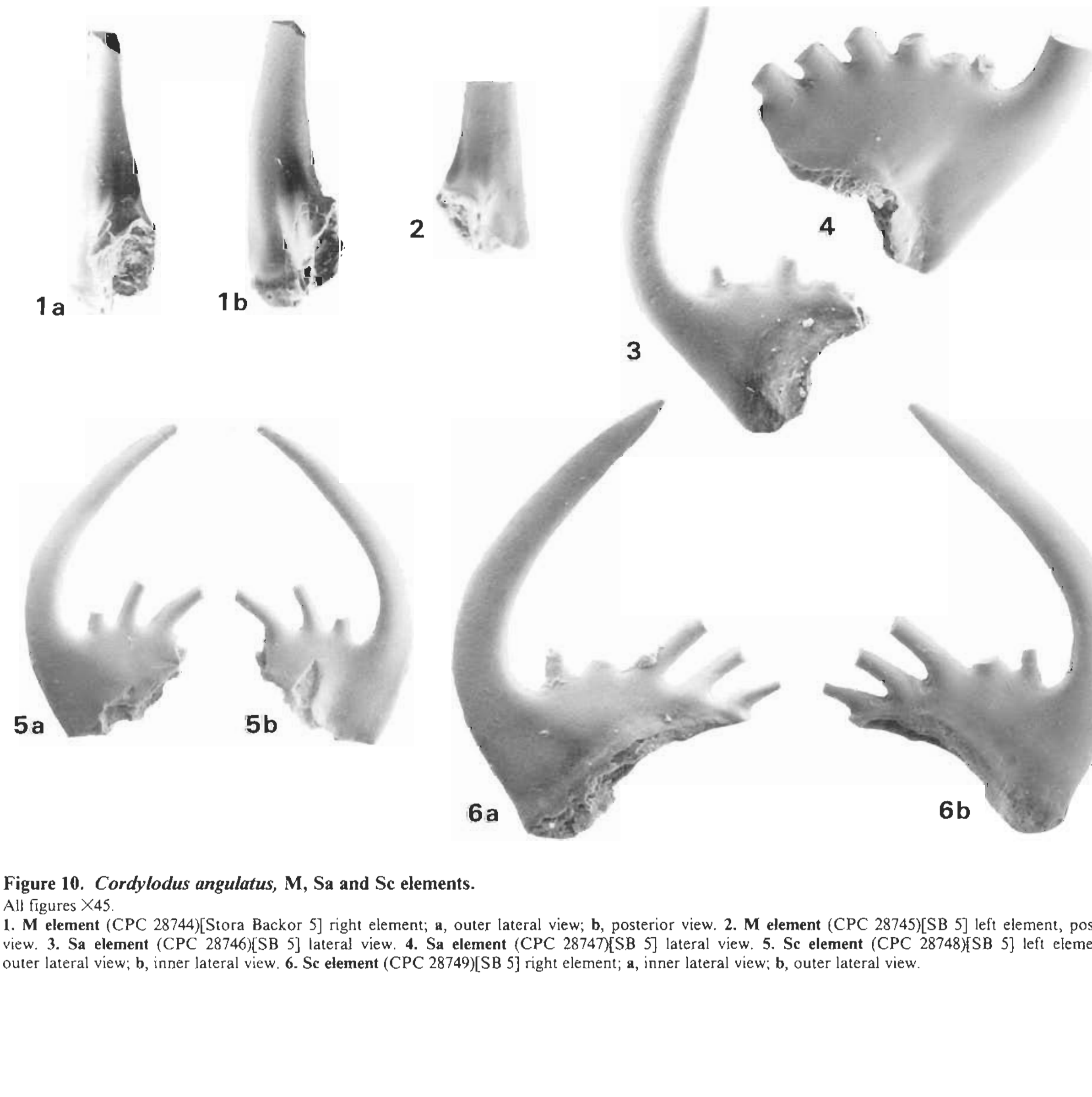

Figure 10. *Cordylodus angulatus,* M, Sa and Sc elements.
All figures ×45.
1. M element (CPC 28744)[Stora Backor 5] right element; **a**, outer lateral view; **b**, posterior view. **2. M element** (CPC 28745)[SB 5] left element, posterior view. **3. Sa element** (CPC 28746)[SB 5] lateral view. **4. Sa element** (CPC 28747)[SB 5] lateral view. **5. Sc element** (CPC 28748)[SB 5] left element; **a**, outer lateral view; **b**, inner lateral view. **6. Sc element** (CPC 28749)[SB 5] right element; **a**, inner lateral view; **b**, outer lateral view.

back and inside the denticle row, but it is much closer to the plane of the denticles than is the case with the Pa element.

The M element (Figs 5, 10) has a lateral process that is broken next to the cusp on the material studied. The process is probably very short and may lack denticles. The specimens examined are large with a very large buttress. The cusp has the inner lateral margin bent posteriorly and the cusp apex is slightly recurved over the buttress.

The S elements, especially the Sa and Sc elements, are laterally compressed and, except for the Sd element, lack the lateral protoprocesses found in some other species of *Cordylodus*. In lateral view the anterior margin of the basal cavity curves downward and posteriorly toward the posterior margin before turning and recurving toward the anterobasal corner. The width of this basal cavity extension is less than the similar extension of the P elements. The posterior process is slightly arched, and the process denticles are curved posteriorly, have rounded edged keels and are laterally compressed.

The Sa element (Figs 5, 10) is symmetrical. The cusp is widest near its posterior margin and narrows toward the anterior margin but has a rounded rather than sharp edged keel on the anterior margin. The posterior side of the cusp is flattened and has a slight groove marking the posterior margin. The basal cavity opening is widest at about midlength of the basal margin and gradually narrows toward the anterior and posterior basal corners. The process supports two to four denticles.

The Sc element (Figs 6, 10) is similar to the Sa element but is asymmetrical because the anterobasal area is laterally compressed and bent slightly outward. The Sc element also

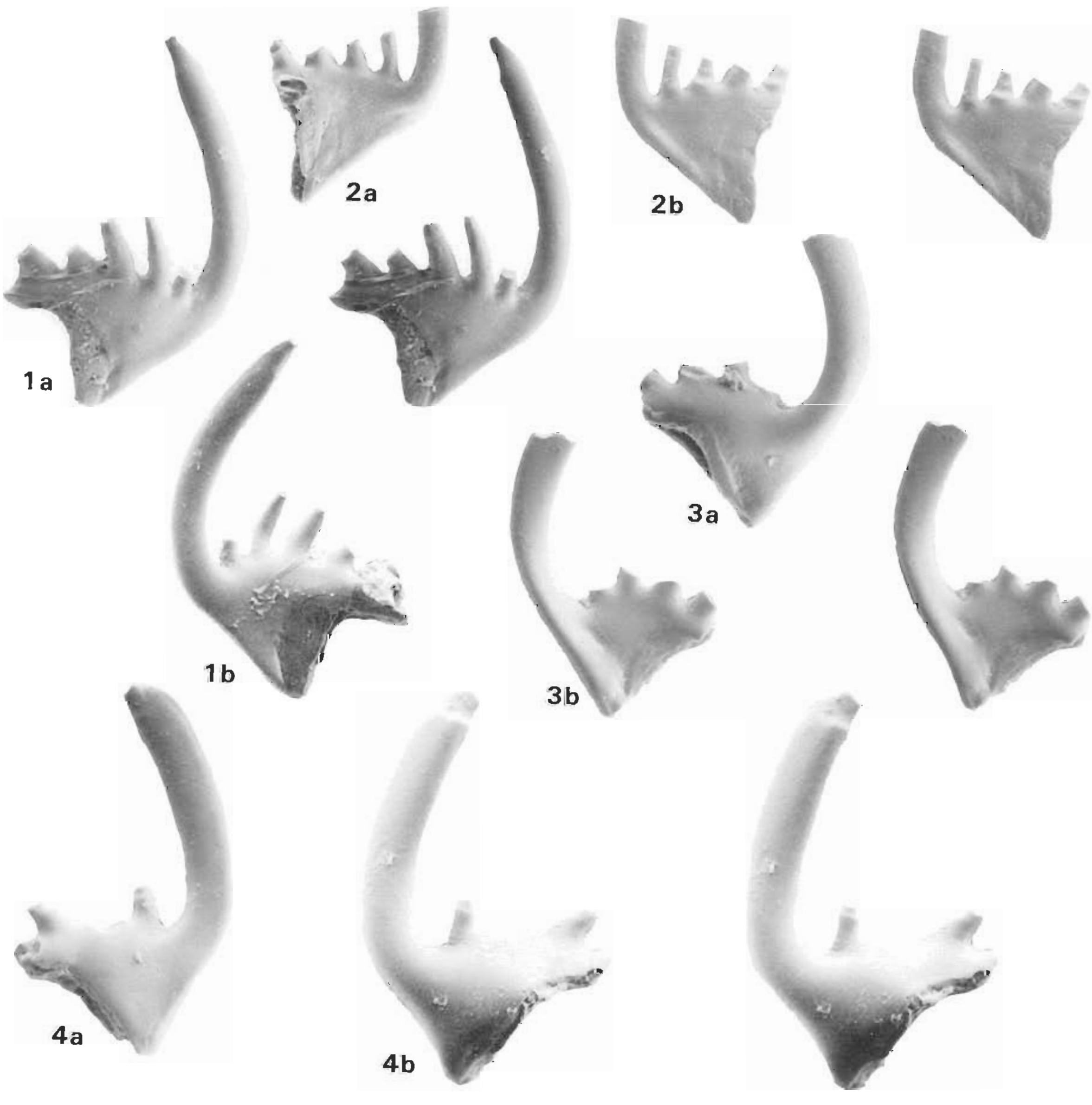

Figure 11. *Cordylodus angulatus,* Sb and Sd elements.
All figures ×45.
1. Sb element (CPC 28750)[SB 5] left element; **a**, stereo pair, inner lateral view; **b**, outer lateral view. **2. Sb element** (CPC 28751)[SB 5] right element; **a**, outer lateral view; **b**, stereo pair, inner lateral view. **3. Sd element** (CPC 28752)[SB 5] right element; **a**, outer lateral view; **b**, stereo pair, inner lateral view. **4. Sd element** (CPC 28753)[SB 5] left element; **a**, inner lateral view; **b**, stereo pair, outer lateral view.

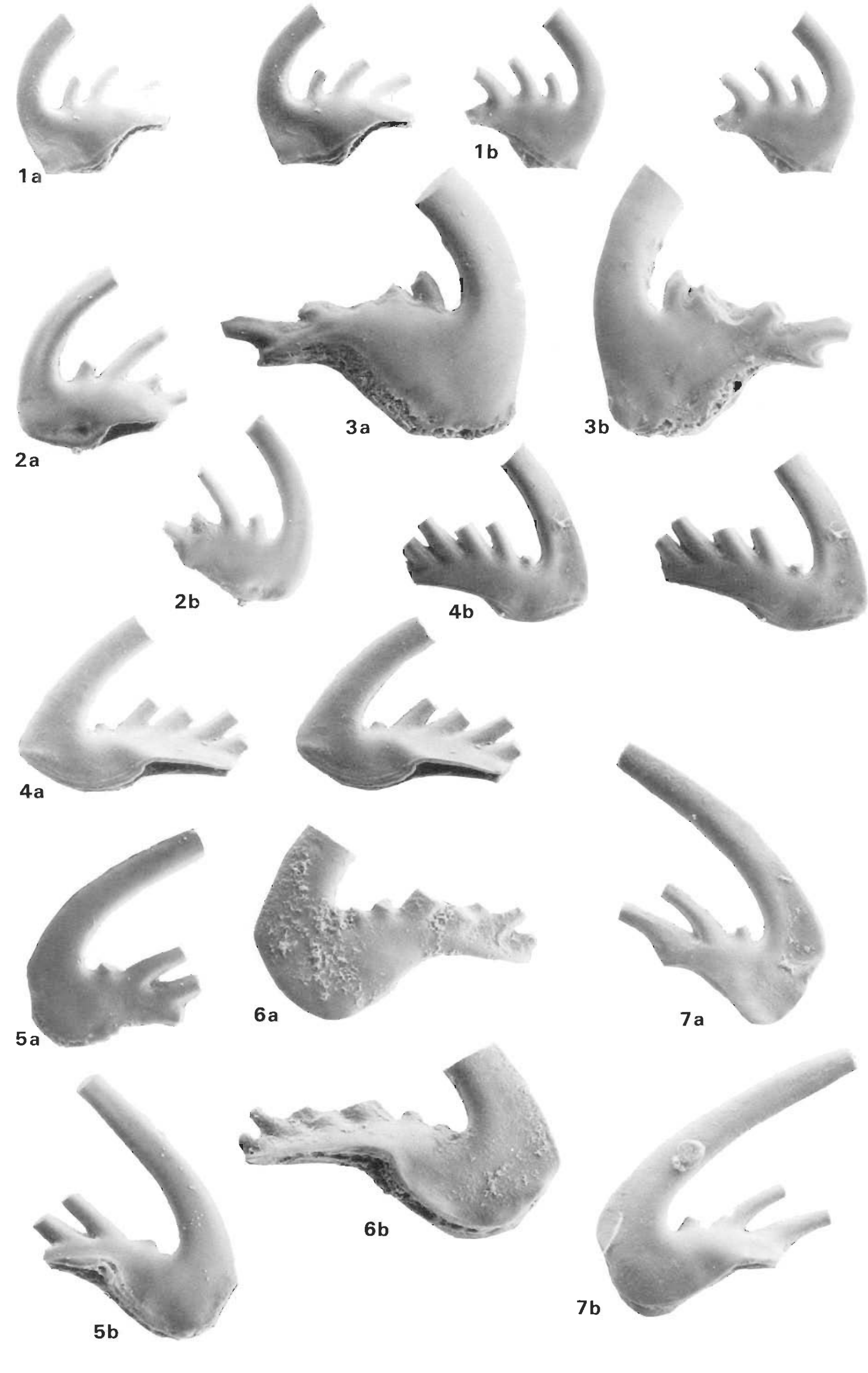
1a
1b
2a
3a
3b
2b
4b
4a
5a
6a
7a
5b
6b
7b

lacks the groove found on the posterior margin of the cusp of the Sa element.

The Sb and Sd elements (Figs 7, 11) have a triangular shape in lateral view. The triangle is formed by the denticulate posterior process, the basal margin and the lower part of the anterior margin. Both elements are oriented with the denticulated posterior process horizontal. The posterior process may be slightly arched; the process denticles are located on the inner margin. The Sb and Sd elements have a neck at the base of the cusp that projects the cusp forward before it curves posteriorly. Due to the neck, the tip of the basal cavity is longer in the Sb and Sd elements than it is in the Sc element.

The Sb and Sd elements are differentiated on the basis of the element cross-section and by the flattened anterior margin of the Sd element. In cross-section the Sb element is asymmetrically biconvex, with the lateral surfaces roughly parallel. The anterior margin is rounded and may have a slight keel on the inner lateral edge. The Sb element has the posterior process bowed laterally outward.

The Sd element is asymmetrical in cross-section with a bulge on the outer lateral face and a moderately developed, rounded keel (a protoprocess) on the anterior inner lateral margin. The anterior margin below the cusp is flattened, especially in large or gerontic elements.

Remarks. Elements assigned to *C. angulatus* in this study show more variation than elements of the other species studied, especially the degree of development of the platform of the Pa element. This may reflect the fact that the material studied was from low in the stratigraphic range of the species. Material from younger samples may have stabilised morphologically. The two specimens illustrated by Furnish (1938) as *C. subangulatus* and *C. intermedius* appear to fit in the mid-range of *C. angulatus* because the Pa element has a moderately developed platform and the Sb element is biconvex and has a rounded anterior margin.

Cordylodus angulatus is distinguished, as has been noted by Lindström (1955), by the distinctive lateral shape of the basal cavity. Other distinctive features are the narrow anterior margin and the lack of lateral process development except in the Sd element.

No Sd elements of *C. angulatus* were identified in the Australian sample BOU 1/159, but the element is abundant in the Swedish Stora Backor sample.

Cordylodus caseyi Druce & Jones, 1971
Figures 3(3a–c), 13–15.

Synonymy.

v. 1971 *Cordylodus caseyi* n. sp.; Druce & Jones, pp. 67–68, Pl. 2, figs 9–12, text-figs 23d,e (figs 10, 12 are Sc elements, fig. 9 is an Sd element and fig. 11 is an Sb element).

1973 *Cordylodus lenzi* n. sp.; Müller, p. 31, Pl. 10, figs 5–9, text-figs 2f, 5a,b (figs 5–8 are Sc elements, fig. 9 is an Sb element).

v. 1971 *Cordylodus caseyi* Druce & Jones; Jones, p. 46, Pl. 2, fig. 1 (Sc element).

Material studied. 38 elements (see Table 2).

Table 2. Distribution of *Cordylodus caseyi* in samples from the Ninmaroo Formation, Georgina Basin, Australia.
Includes CPC material from Druce & Jones (1971) study.

Element type	*M*	*Sa*	*Sc*	*Sb*	*Sd*	*Pb*	*Pa*
Sample							
1/154	—	—	—	—	—	1	—
1/159	3	—	5	1	1	—	2
1/179	—	—	—	1	—	—	—
2/99	—	—	—	—	1	—	—
2/103	—	—	—	—	1	—	—
3/90	—	—	1	—	1	—	—
13/2	—	—	6	2	—	2	2
B456/7	—	—	2	1	2	—	—
B694	—	—	1	1	1	—	—
Total	3	—	15	6	7	3	4

Diagnosis. Probable septimembrate apparatus; six elements (M, Sc, Sb, Sd, Pb and Pa) differentiated in this study. The M element is makellate, the P elements are dolabrate, the Sc and Sd elements are bipennate and the Sb element is dolabrate. The P and S elements have arched posterior processes with two or more denticles. The Sc and Sd elements have short adentate inner lateral processes. All S and P elements have long, ovate to round cusps that usually have a keel or costa on the anterior or lateral margin. The inner and outer lateral margins of the M element are keeled. The basal cavity is broad but shallow with the tip extending to the white matter in the cusp.

Description. The P elements (Fig. 15) have round to subround cusps and a broad opening to the basal cavity. The cavity has an abruptly narrowing tip extending to the white matter in the cusp, and the anterior portion of the basal opening narrows slightly and extends to the anterobasal corner. The posterior portion of the basal opening is very broad and extends posteriorly under the posterior process. The anterior margin of the Pa element is narrow, but rounded, and the cusp is subround. The anterior margin of the Pb element is broad and rounded, and the cusp is round with a keel on the anterior and posterior margins.

The M element (Fig. 13) is antero-posteriorly compressed with a flattened anterior face and moderately developed basal buttress on the posterior face. The cusp recurves slightly over the buttress. The basal cavity tip is near the inner lateral margin and has only a very small cone extending up to the white matter. The inner and outer lateral margins of the cusp are sharp. No denticles are preserved on the material studied.

The S elements (Figs 13, 14) have long rounded to subrounded cusps and round to laterally compressed, moderately long denticles on the posterior process. The basal cavity opening of the Sc and Sd elements extends into the short lateral process. The inner cusp margin of both Sc and Sd elements also has a costa that extends along the upper margin of the inner process. The Sc element has the process angled anteriorly and inward about 45° from the long axis of the element. The Sd element has the process at about a right angle to the axis or slightly to the posterior from that angle.

Figure 12. *Cordylodus angulatus*, Pb and Pa elements.
All figures ×45.
1. Pb element (CPC 28754)[SB 5] right element; **a**, stereo pair, inner lateral view; **b**, stereo pair, outer lateral view. **2. Pb element** (CPC 28755)[SB 5] right element; **a**, inner lateral view; **b**, outer lateral view. **3. Pb element** (CPC 28756)[SB 5] left element; **a**, inner lateral view; **b**, outer lateral view. **4. Pa element** (CPC 28757)[SB 5] right element; **a**, stereo pair, inner lateral view; **b**, stereo pair, outer lateral view. **5. Pa element** (CPC 28758)[SB 5] left element; **a**, outer lateral view; **b**, inner lateral view. **6. Pa element** (CPC 28759)[SB 5] left element; **a**, outer lateral view; **b**, inner lateral view. **7. Pa element** (CPC 28760)[SB 5] right element; **a**, outer lateral view; **b**, inner lateral view.

The Sb element lacks a lateral process and has a rounded anterior margin. The long slender cusp is twisted inside the axial line of the posterior process. The distance from anterobasal corner to the cavity tip of the Sb element is much shorter than in the Sb element of *C. angulatus*.

Several of the S and P elements of *C. caseyi* have a recessive basal margin that is similar to the margin found on some elements of *C. lindstromi*. The limited material available for examination prevents a determination of whether this recessive margin is a feature diagnostic for the species or just an artefact of preservation

Remarks. The lateral processes of the Sc and Sd element of *C. caseyi* are the best developed of any species of *Cordylodus* yet described. When there is the beginning of denticulation on the processes it would probably be best to place the species in another genus, but the degree of process development observed in *C. caseyi* is only a gradual progression from the rounded rib observed on the Sc element of *C. proavus*.

Cordylodus caseyi may have evolved from *C. lindstromi*: both species have developing, but adentate, lateral processes and recessive basal margins of larger elements. However, there is no indication that *C. caseyi* has dual tips of the basal cavity.

The Sa element of *Cordylodus caseyi* was not recovered in the existing collections. I would expect, based on the morphology of the other elements, that the Sa element would be alate, similar to the Sd element but with symmetrical short lateral processes. Druce & Jones (1971) illustrated (see synonymy) the Sc, Sb and Sd elements of the species, but did not define the morphological distinction between the element types. In this revision of the species, six of the expected seven elements have been defined.

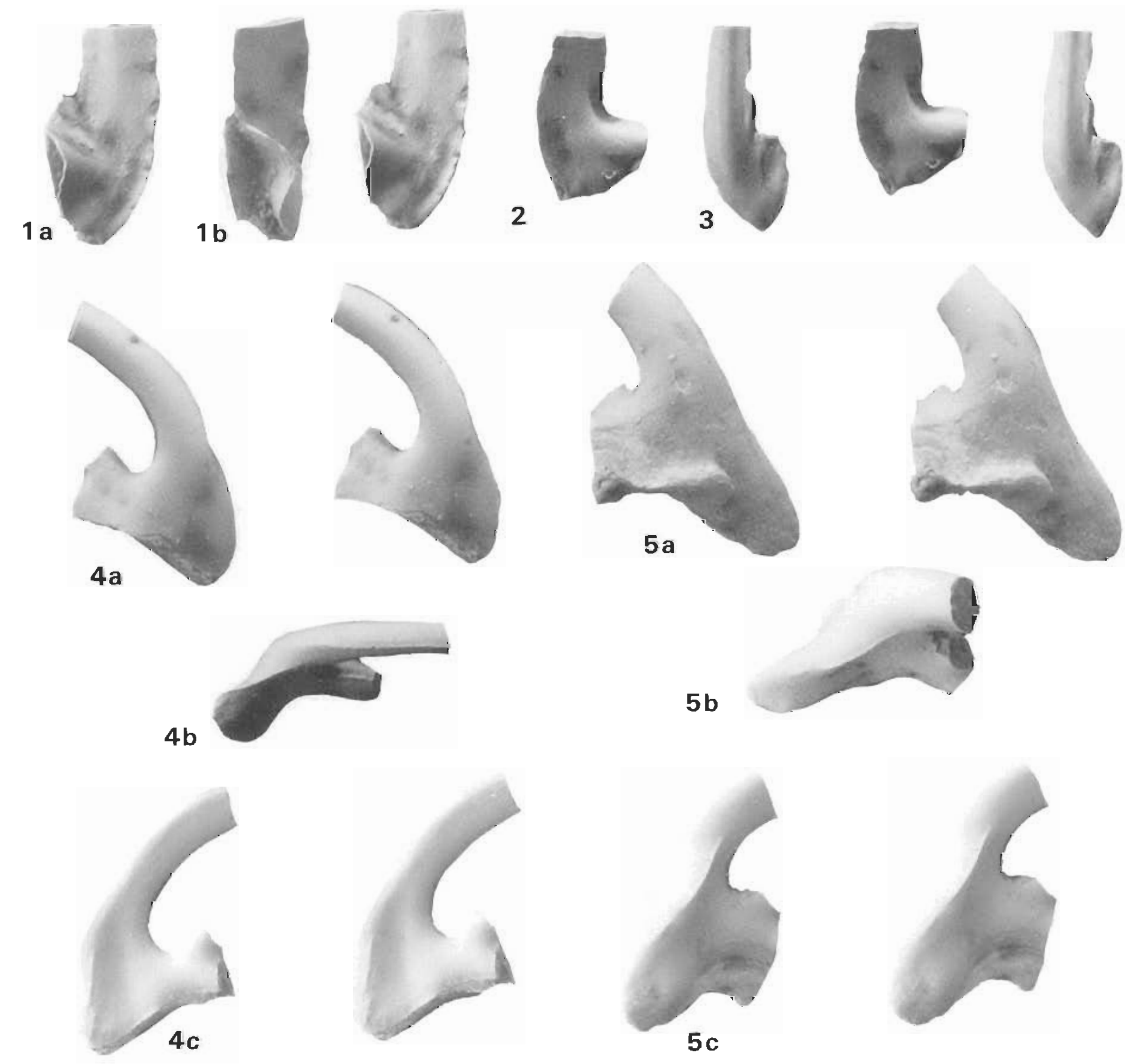

Figure 13. *Cordylodus caseyi*, M and Sc elements.
All figures ×100.
1. M element (CPC 28073)[BOU 1/159] left element; **a**, stereo pair, posterior view; **b**, outer lateral view into basal cavity. **2. M element** (CPC 28074)[BOU 1/159] right element; stereo pair, posterior view. **3. M element** (CPC 28075)[BOU 1/159] left element; stereo pair, anterior view. **4. Sc element** (CPC 28076)[BOU 13/2] right element; **a**, stereo pair, outer lateral view; **b**, oral view; **c**, stereo pair, inner lateral view. **5. Sc element** (CPC 28077)[BOU 13/2] right element; **a**, stereo pair, outer lateral view; **b**, oral view; **c**, stereo pair, inner lateral view.

I agree with Ethington & Clark (1981) that the material described by Müller (1973) as *C. lenzi* should be assigned to *C. caseyi* on the basis of arching of the posterior process, lateral process development, and the thin and rounded cusp. However, the specimen illustrated by Ethington & Clark (1981, Pl. 2, fig. 25) is interpreted here as an Sd element of *C. lindstromi*.

Cordylodus lindstromi Druce & Jones, 1971
Figures 3(2a–c), 16–18.

Synonymy.

v. 1971 *Cordylodus lindstromi* n. sp.; Druce & Jones, pp. 68–69, Pl. 1, figs 7–9, Pl. 2, fig. 8, text-fig. 23h (Pl. 1, fig. 7 is an Sc element, fig. 8 is an Sc element, fig. 9 is a Pb element and Pl. 2, fig. 8 is an Sd element).

v. 1971 *Cordylodus prion* Lindström; Druce & Jones, p. 70, Pl. 2, figs 1–7, text-figs 23i, k–o (fig. 1 is a Pa element, figs 2–7 are M elements).

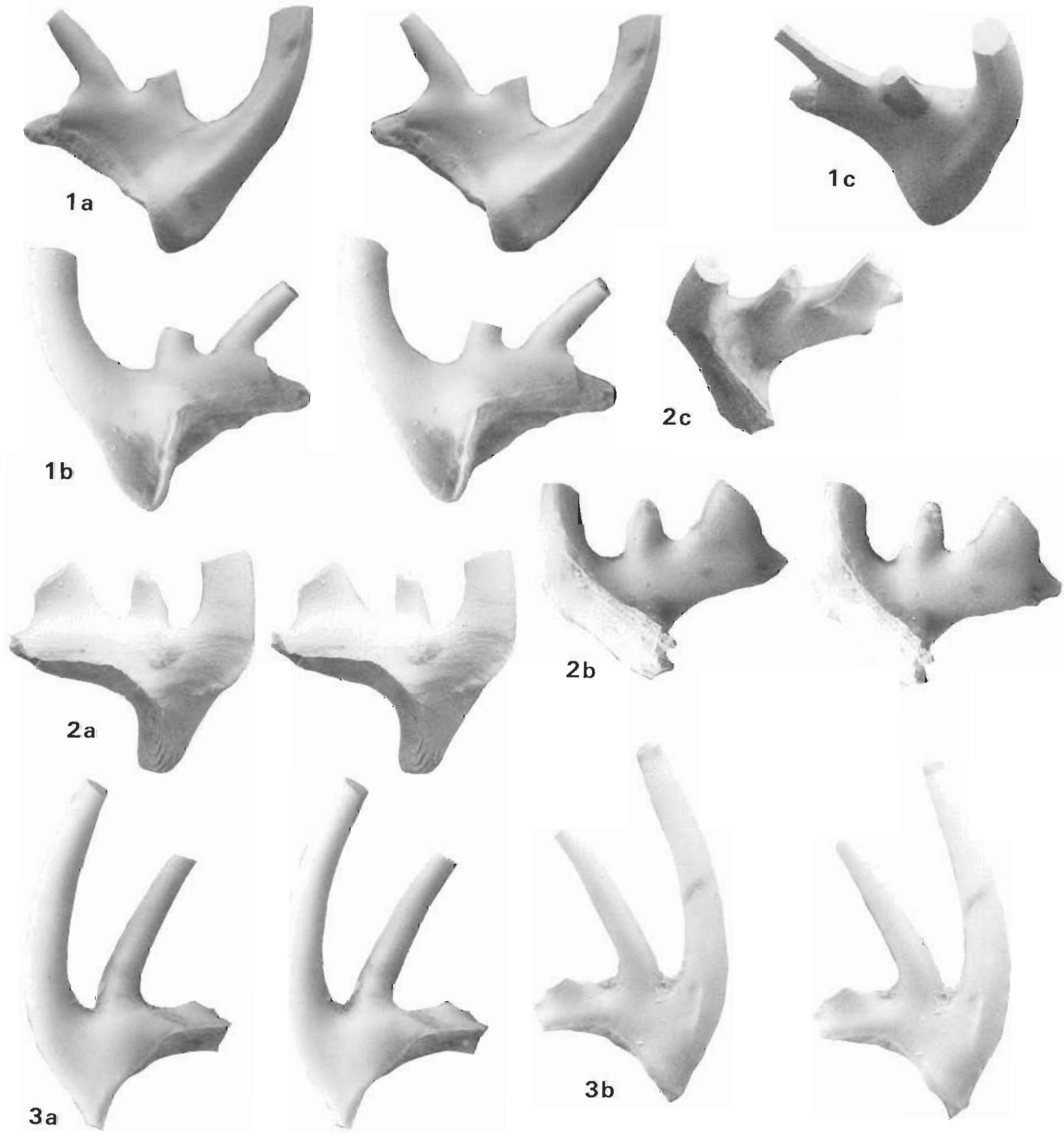

Figure 14. ***Cordylodus caseyi*, Sb and Sd elements.**
All figures ×100.
1. Sd element (CPC 28078)[BOU 13/2] left element; **a**, stereo pair, inner lateral element; **b**, stereo pair, outer lateral view; **c**, oral view. **2. Sd element** (CPC 28079)[BOU 13/2] right element; **a**, stereo pair, outer lateral view; **b**, stereo pair, inner lateral view; **c**, oral view. **3. Sb element** (CPC 28080)[BOU 1/159] right element; **a**, stereo pair, inner lateral view; **b**, stereo pair, outer lateral view.

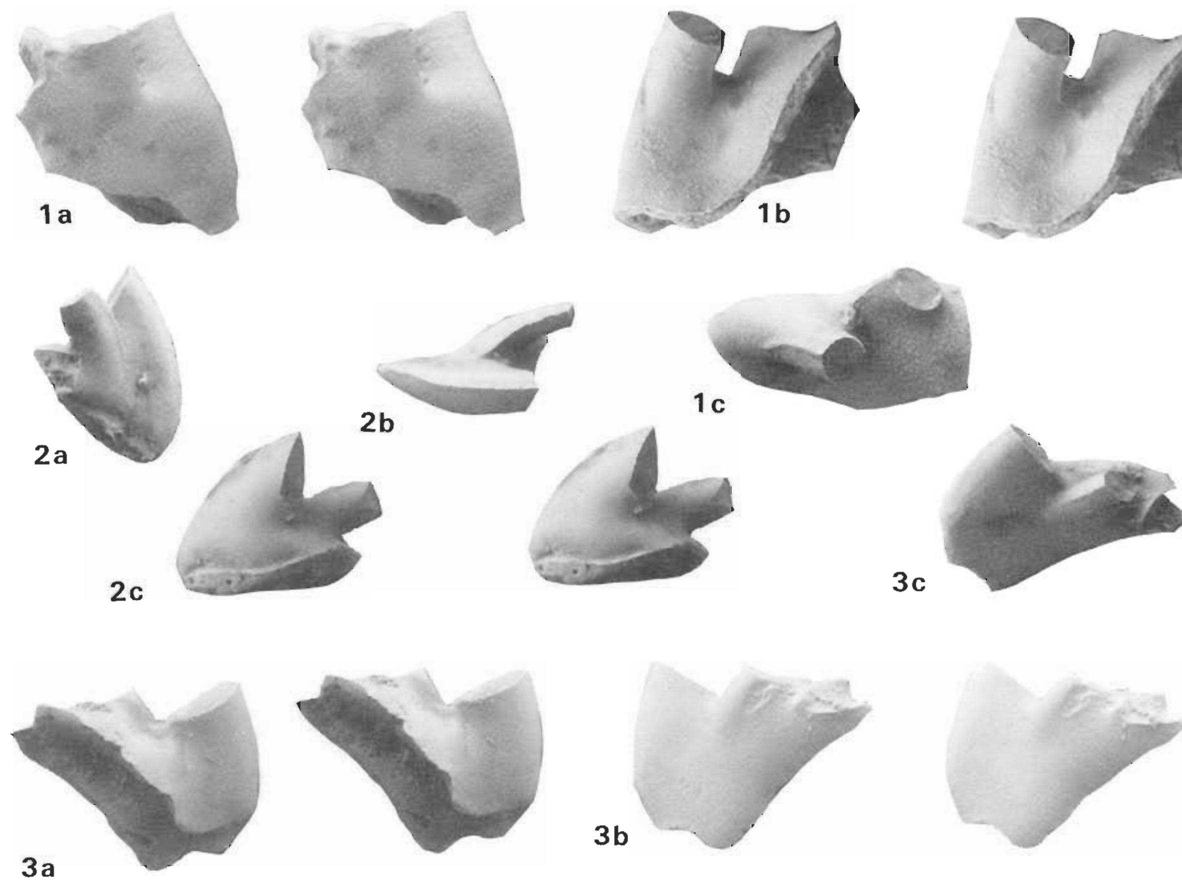

Figure 15. ***Cordylodus caseyi,*** **Pb and Pa elements.**
All figures ×100.
1. Pb element (CPC 28081)[BOU 13/2] right element; **a**, stereo pair, outer lateral view; **b**, stereo pair, inner lateral view; **c**, oral view. **2. Pa element** (CPC 28082)[BOU 1/159] right element; **a**, outer lateral view; **b**, oral view; **c**, stereo pair, inner lateral view. **3. Pa element** (CPC 28083)[BOU 13/2] left element; **a**, stereo pair, inner lateral view; **b**, stereo pair, outer lateral view; **c**, oral view.

1980 *Cordylodus lindstromi* Druce & Jones; Miller, pp. 18–19, Pl. 1, figs 18, 19, text-fig. 4I (fig. 18 is an S element and fig. 19 is a Pa element).

1980 *Cordylodus intermedius* Furnish; Miller, pp. 17–18, Pl. 1, fig. 17 only (P element).

1980 *Cordylodus angulatus* Pander; Miller, pp. 13–16, Pl. 1, fig. 23 only (P element).

1981 *Cordylodus caseyi* Druce & Jones; Ethington & Clark, pp. 31–32, Pl. 2, fig. 25 (Sd element).

Material studied. 186 elements, 162 from Australia and 24 from Texas (see Table 3).

Diagnosis. Septimembrate apparatus of ramiform elements with dual tipped basal cavity found in the S elements and some of the P elements. The M element is makellate, the Sa element is alate and the rest of the elements are dolabrate and asymmetrical. The first denticle of the posterior process is usually very close to the cusp and is frequently touching the posterior cusp margin. Larger elements frequently have a recessive basal margin.

Description. The P elements (Fig. 18) are laterally compressed with rounded anterobasal margin and nearly straight posterior process. The cusp of both Pa and Pb elements is straight rather than recurved as in the S elements. In the Pa element the cusp is twisted slightly inward from the plane of the denticles of the posterior process, but in the Pb element the cusp is not inwardly twisted. The anterior and posterior margins of the cusp are keeled. The basal cavity is shallow, opens downward, and extends posteriorly under the posterior process. The second tip of the basal cavity is generally less prominent on the P elements than it is on the S elements and may be absent entirely, especially if the element is large and has a recessive margin.

Figure 16. ***Cordylodus lindstromi,*** **M, Sa and Sc elements.**
All figures ×100.
1. M element (CPC 28084)[BOU 3/90] right element; **a**, stereo pair, anterior view; **b**, outer lateral view into basal cavity. **2. M element** (CPC 28085)[BOU 2/86] left element; stereo pair, posterior view. **3. M element** (CPC 28086)[BOU 2/86] right element; stereo pair, posterior view. **4. M element** (CPC 28087)[BOU 2/86] left element; stereo pair, posterior view. **5. M element** (CPC 8732)[BOU 2/86] right element; inner lateral view. *'Cordylodus prion'* of Druce & Jones, 1971, Pl. 2, fig. 2. **6. M element** (CPC 8730)[BOU 1/153] left element; inner lateral view. *'Cordylodus prion'* of Druce & Jones, 1971, Pl. 2, fig. 4. **7. Sa element** (CPC 28088)[BOU 2/86] lateral view, base broken, but cusp complete. **8. Sa element** (CPC 28089)[BOU 2/86] posterior view. **9. Sa element** (CPC 28090)[BOU 2/86] antero-lateral view. **10. Sa element** (CPC 28091)[BOU 2/81] **a**, lateral view; **b**, posterior view. **11. Sc element** (CPC 28092)[BOU 2/86] right element; stereo pair, inner lateral view. **12. Sc element** (CPC 28093)[BOU 2/86] left element; posterior view into basal cavity. **13. Sc element** (CPC 28094)[BOU 2/86] left element; stereo pair, inner lateral view. **14. Sc element** (CPC 28095)[BOU 2/86] left element; **a**, stereo pair, outer lateral view; **b**, stereo pair, inner lateral view.

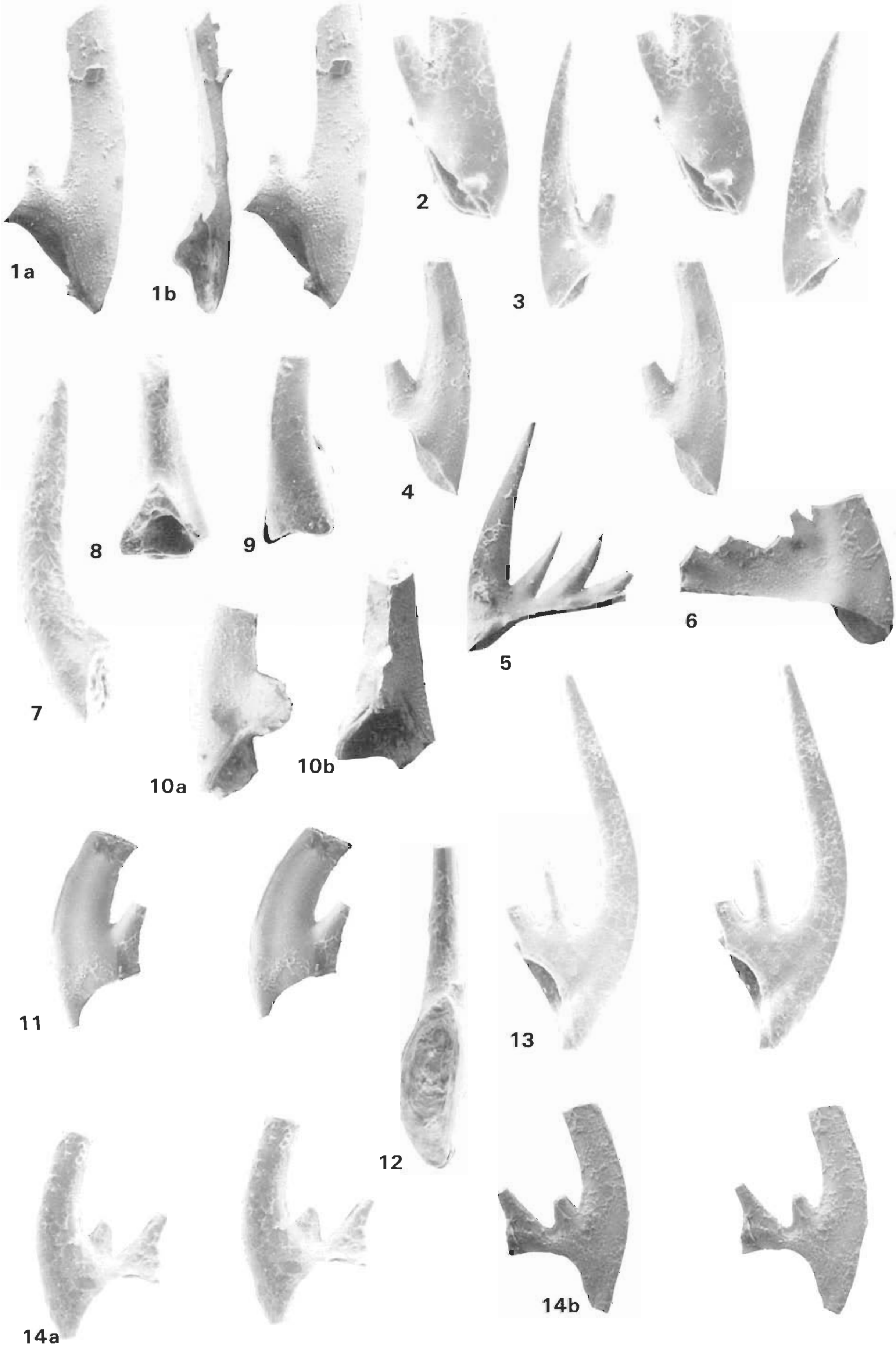
1a
1b
2
3
4
5
6
7
8
9
10a
10b
11
12
13
14a
14b

Table 3. Distribution of *Cordylodus lindstromi* in the Ninmaroo Formation, Georgina Basin, Australia and from a sample of the Tanyard Formation, Texas.

Element type	*M*	*Sa*	*Sc*	*Sb*	*Sd*	*Pb*	*Pa*
Section/sample							
1/132	3	—	2	1	—	—	—
1/142	1	—	—	—	—	—	1
1/149	—	—	1	—	—	—	—
1/150	1	—	—	—	2	1	—
1/152	—	1	1	—	—	—	—
1/153	4	—	3	1	1	—	—
1/154	—	—	2	1	1	1	—
1/159	1	—	1	2	—	—	—
2/65 (TF)	—	—	2	1	1	—	—
2/73 (TF)	—	—	—	1	—	—	—
2/75	1	—	—	1	—	—	—
2/81	5	1	6	5	4	—	—
2/82	1	—	3	1	1	2	—
2/84	2	—	1	1	—	1	—
2/85	1	—	—	—	1	—	—
2/86	15	4	17	14	7	5	4
3/75 (TF)	—	—	—	2	1	—	—
3/80	—	—	—	—	—	—	1
3/82	1	—	—	—	1	—	—
3/90	1	1	1	1	3	2	1
Total	37	7	40	32	23	12	7
TC 1465	8	—	4	7	5	—	—

Sections 1, 2 and 3 are from the Ninmaroo Formation, Georgina Basin, Australia and refer to the original sample collections studied by Druce & Jones (1971; see this for stratigraphic information). The table includes figured material illustrated by Druce & Jones as either *Cordylodus lindstromi* or *C. prion* (CPC 8729–8733, 8747, 8754–8755, 8767).

Section TC is the Threadgill Creek section of Texas; sample provided by J. F. Miller.

(TF) indicates specimens with a flat, rather than pointed, tip on the secondary basal cavity tip. These specimens are regarded as probably transitional from *Cordylodus proavus* to *C. lindstromi.*

The M element (Fig. 16) has an erect, antero-posteriorly compressed cusp with a buttress on the posterior face, and a denticulate outer lateral process. The process supports up to six triangular denticles that are appressed at the base. The cusp is slightly recurved posteriorly over the buttress. The M element has only a single basal cavity tip.

The S elements have erect to recurved cusps of white matter extending down to just above the level of the posterior process. The tip of the main basal cavity is close to the anterior margin and extends up to the base of the white matter. The secondary basal cavity is under the first denticle of the posterior process. The basal cavity opens posteriorly and downward with a groove extending under the posterior process. The cusp is laterally compressed with a sharp margin or keel on both anterior and posterior margins where the cusp is composed of white matter. Process denticles are laterally compressed with sharp margins in small or juvenile specimens, but become fatter or more rounded on larger specimens.

The Sa element (Fig. 16) is bilaterally symmetrical with a short denticulate posterior process and laterally compressed cusp that has keels on both the anterior and posterior margins. About half way down the cusp the anterior margin flattens and the keel ends. At the same point the lateral carinae begin to expanded and there may be a slight bifurcation of the basal margin. This gives the element the appearance of having downwardly directed, adentate lateral processes.

The Sc element (Fig. 16) is asymmetrical with the inner side flattened and the outer side convex. The inner anterior margin has a slightly thickened rim which forms an inner lateral protoprocess.

The Sb element (Fig. 17) is similar to the Sc element but is biconvex with a rounded lower anterior margin. The posterior process is bent slightly inward behind the first process denticle. The first process denticle is tilted outward.

The Sd element (Fig. 17) is highly asymmetrical with a convex outer margin and a strong inner lateral rim (protoprocess) near the anterior margin. The posterior process is bent sharply inward after the first process denticle.

Remarks. There has been some suggestion (Landing & others, 1980; Bagnoli & others, 1986) that *C. lindstromi* is not a valid species and that the basis of its recognition, a dual-tipped basal cavity, is an intraspecific variant. To some degree this is true. The original description of *C. lindstromi* (Druce & Jones, 1971) only says that the new species is similar to *C. angulatus* and *C. prion* and that it has a dual tip on the basal cavity. The description was thus not adequate to distinguish the new species from other species of *Cordylodus* which might also have a dual tip on the basal cavity. This case highlights the inadequacy of many older conodont species descriptions that are not able to be used to distinguish closely related species, nor to accommodate multielement taxonomy. The solution is to re-examine the type specimens and topotype material and to adequately redescribe and redefine the species.

We now recognise that not every *Cordylodus* element with a dual-tipped basal cavity should be assigned to *C. lindstromi*. Several species of *Cordylodus*, all undescribed except for *C. lindstromi*, have dual tips on the basal cavity. For example, the notched material illustrated by Barnes (1988, Figs 13 k,l) or Andres (1988) as *C. lindstromi* is not conspecific with the Australian material. Examination of Stora Backor material indicates that this notched species of *Cordylodus* has a morphologically discrete septimembrate apparatus. I suggest it should be assigned to a new species. There appear to be other species of dual-tipped cordylodids that will be differentiated when enough material is studied.

Examination of the type specimens and material from the original collections demonstrates that *C. lindstromi* can be established as a valid species using a number of characteristics including the dual-tipped basal cavity. Other characters of *C. lindstromi* are the proximity of the first process denticle, the one located over the second cavity tip, to the cusp; the recessive basal margin, and the distorted posterior process of the Sd element. The notched *Cordylodus* species has a marked separation of the posterior process from the cusp and all elements have straight posterior processes. Other species of dual-tipped cordylodids do not have the recessive basal margin of *C. lindstromi.*

Cordylodus lindstromi may have evolved directly from *C. proavus*, but there is some indication of an intermediate form that is morphologically similar to *C. proavus* but has a dual-tipped basal cavity. The two species are similar morphologically, except for the further development of features such

Figure 17. *Cordylodus lindstromi*, Sb and Sd elements.
All figures ×100.
1. Sb element (CPC 28096)[BOU 2/86] left element; **a**, stereo pair, outer lateral view; **b**, stereo pair, inner lateral view. **2. Sb element** (CPC 28097)[BOU 2/81] left element; inner lateral view. **3. Sb element** (CPC 28098)[BOU 2/86] right element; **a**, stereo pair, outer lateral view; **b**, posterior view into basal cavity. **4. Sd element** (CPC 28099)[BOU 2/81] right element; **a**, posterior inner lateral view; **b**, posterior view. **5. Sd element** (CPC 28100)[BOU 3/90] left element; **a**, stereo pair, inner lateral view; **b**, anterior view. **6. Sd element** (CPC 28101)[BOU 2/81] right element; **a**, stereo pair, outer lateral view; **b**, stereo pair, inner lateral view.

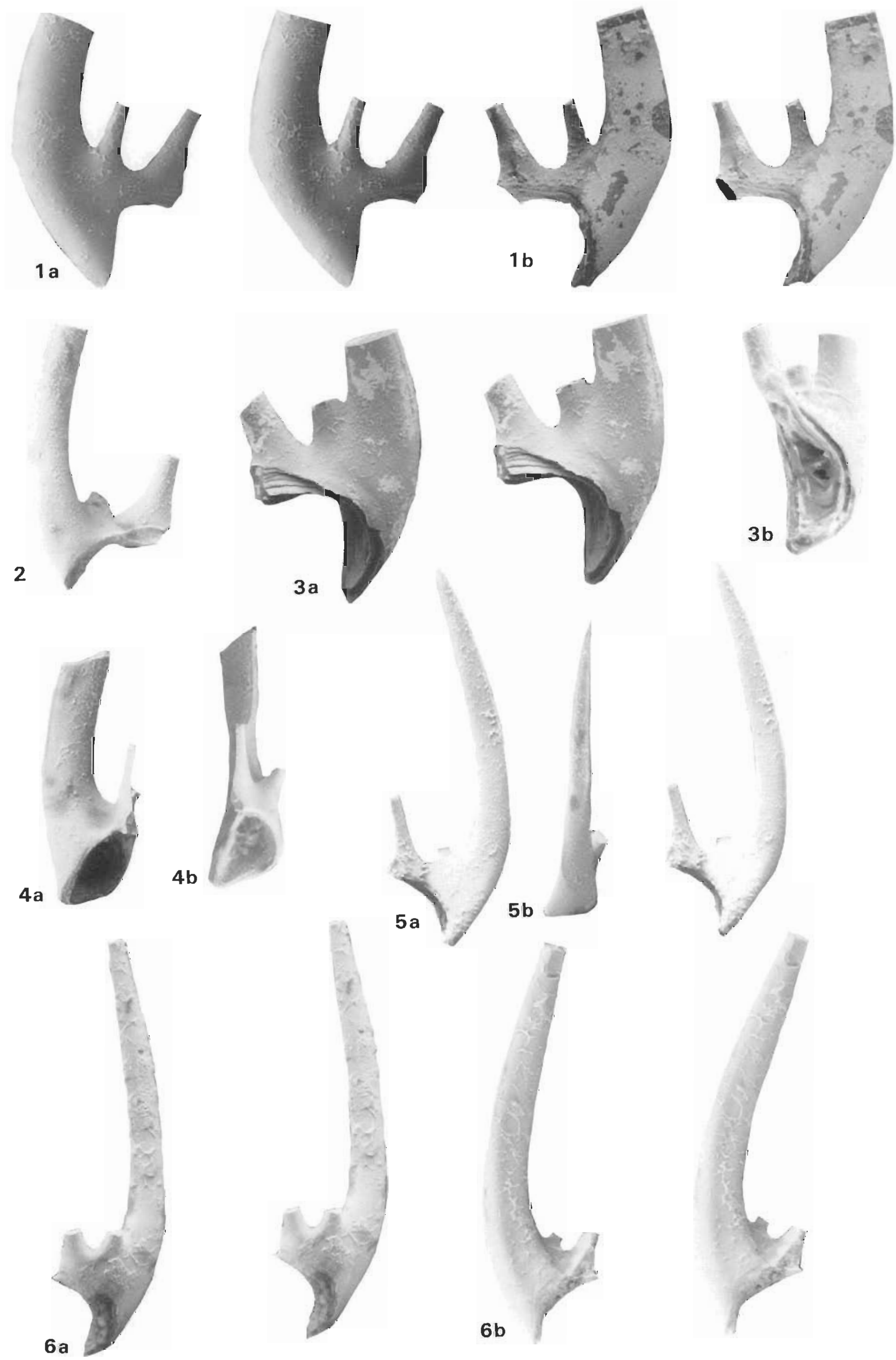
1a
1b
2
3a
3b
4a
4b
5a
5b
6a
6b

as lateral processes and the recessive basal margin in *C. lindstromi*. The earliest specimens assigned to *C. lindstromi* (Table 3) have a modified dual-tipped basal cavity where the second tip of the cavity that extends into the first process denticle has a flattened, rather than pointed, tip.

Cordylodus proavus Müller, 1959
Figures 3(1a–d), 19–22.

Synonymy.

1959 *Cordylodus proavus* n. sp. Müller, pp. 448–449, Pl. 15, figs 11, 12, 18; text-fig. 3B (figs 11 & 18 are probably Sa elements and fig. 12 is probably an Sc element).

v. 1971 *Cordylodus proavus* Müller; Druce & Jones, pp. 70–71, Pl. 1, figs 1–6, text-figs 23p,q,r. (Figs 1 and 4 are Sc elements, fig. 2 is an Sa element, and figs 2, 5 and 6 are Sb elements).

v. 1971 *Cordylodus proavus* Müller; Jones, p. 48, Pl. 2, fig. 9 (Sb element).

1980 *Cordylodus proavus* Müller; Miller, pp. 19–20, Pl. 1, figs 14, 15; text figs 4G,H (fig. 14 is an S element and fig. 15 is a Pb element).

Material studied. 112 elements (see Table 4).

Table 4. Recovery of *Cordylodus proavus* in three samples from the San Saba Member of the Wilburns Formation, Threadgill Creek Section, Texas.

Element type	*M*	*Sa*	*Sc*	*Sb*	*Sd*	*Pb*	*Pa*
Sample							
TC 1429	1	4	16	8	4	13	1
TC 1440	—	7	20	3	2	8	3
TC 1460	—	2	12	4	1	2	1
Total	1	13	48	15	7	23	5

Diagnosis. Septimembrate apparatus of ramiform elements. All elements have a single process; M element makellate, Sa element dolabrate and symmetrical, other elements dolabrate and asymmetrical. In P and M elements, white matter wraps around basal cavity tip and extends along anterior margin to base and along posterior margin to the denticles. In S elements the upper part of cusp, usually about half or two-thirds, is composed of white matter and the basal cavity tip extends up the cusp to the level of the white matter. In all S elements the process denticles are usually few in number and widely spaced.

Description. The P elements (Fig. 22) are similar, with some lateral compression of both cusp and denticles. The basal cavity opens downward and posteriorly and has a groove that extends posteriorly under the process. The anterior margin of lower part of the basal cavity is straight (vertical) in lateral view, unlike the shape in the M element. Denticles of the process frequently touch adjacent denticles basally, unlike the process denticles of S elements, which are discrete. The Pa element has the cusp twisted inward so that the upper part is recurved in a plane inside that of the posterior process. The Pb element also has a slight twist of the cusp, especially the upper part, but it does not turn as much as does that of the Pa element.

The M element (Fig. 19) has an erect cusp, a well developed anticusp, and an outer lateral process of indeterminate length. The cusp is ovate, compressed anteroposteriorly and has sharp margins. The anterior margin extends downward as a wide anticusp. The anterior face is flat and the anterior cavity margin is straight. The posterior face has a large buttress which bends the posterior cavity margin. In a posterior view the inner margin of the basal cavity curves from the cavity tip to near the outer lateral margin and then bends at nearly a right angle to extend as a groove down the outer margin of the anticusp.

The S elements have curved to reclined cusps and a posterior process that supports three to four denticles. The process denticles closest to the cusp are round and erect, but the posterior denticles are laterally compressed and reclined. White matter is restricted to the upper half to two-thirds of the cusp and the basal cavity extends up the cusp to the sharp line separating white matter and hyaline apatite. The basal cavity opens posteriorly.

The Sa element (Fig. 19) is bilaterally symmetrical with a rounded anterior margin. In stratigraphically younger material the lower part of the anterior margin becomes flattened.

The Sc element (Fig. 20) is asymmetrical, the posterior process bows outward, and the anterior margin is rounded. In section view the inner face is flat and the outer face is convex. On the inner face at the anterior margin there is a raised rounded lip extending from the base of the cusp to the basal margin.

The Sb element (Fig. 21) is asymmetrical and similar to the Sc element except for the sectional shape, where both inner and outer faces are convex and the lip on the inner anterior margin is not present.

The Sd element (Fig. 21) is asymmetrical and similar to the Sc and Sb elements except for the sectional shape where the inner face is concave and the outer face is convex. The element has the anterior margin twisted inward out of the plane of the denticles forming an adentate inner lateral protoprocess.

Remarks. The seven elements recognised in *C. proavus* have similar morphologies to the elements of *Eoconodontus*, from which they are distinguished by the presence of denticles. The elements also are generally similar to the elements of both *C. lindstromi* and *C. angulatus*. *Cordylodus proavus* is distinguished from other species of *Cordylodus* by the distribution of white matter, the spacing and shape of the denticles and the shape of the processes.

Separation of *C. primitivus* from *C. proavus* is not considered in this study because adequate material from an appropriate stratigraphic interval is not available. Differences, especially in the Sa and Sc elements, of morphologies among samples TC 1429, TC 1440 and TC 1460 indicate that an examination of all the apparatus elements would differentiate *C. primitivus* from *C. proavus* on characters such as the depth of the basal cavity extension into the cusp, denticle spacing, and development of features related to element symmetry.

Figure 18. *Cordylodus lindstromi*, Pb and Pa elements.
All figures ×100.
1. Pb element (CPC 28102)[BOU 2/86] right element; stereo pair, inner lateral view. **2. Pb element** (CPC 28103)[BOU 2/86] left element; **a**, stereo pair, outer lateral view; **b**, stereo pair, inner lateral view. **3. Pb element** (CPC 28104)[BOU 3/90] left element; **a**, stereo pair, inner lateral view; **b**, stereo pair, outer lateral view. **4. Pa element** (CPC 28105)[BOU 2/86] right element; stereo pair, inner lateral view. **5. Pa element** (CPC 28106)[BOU 2/86] right element; **a**, stereo pair, inner lateral view; **b**, stereo pair, outer lateral view. **6. Pa element** (CPC 28107)[BOU 3/80] right element; stereo pair inner lateral view.

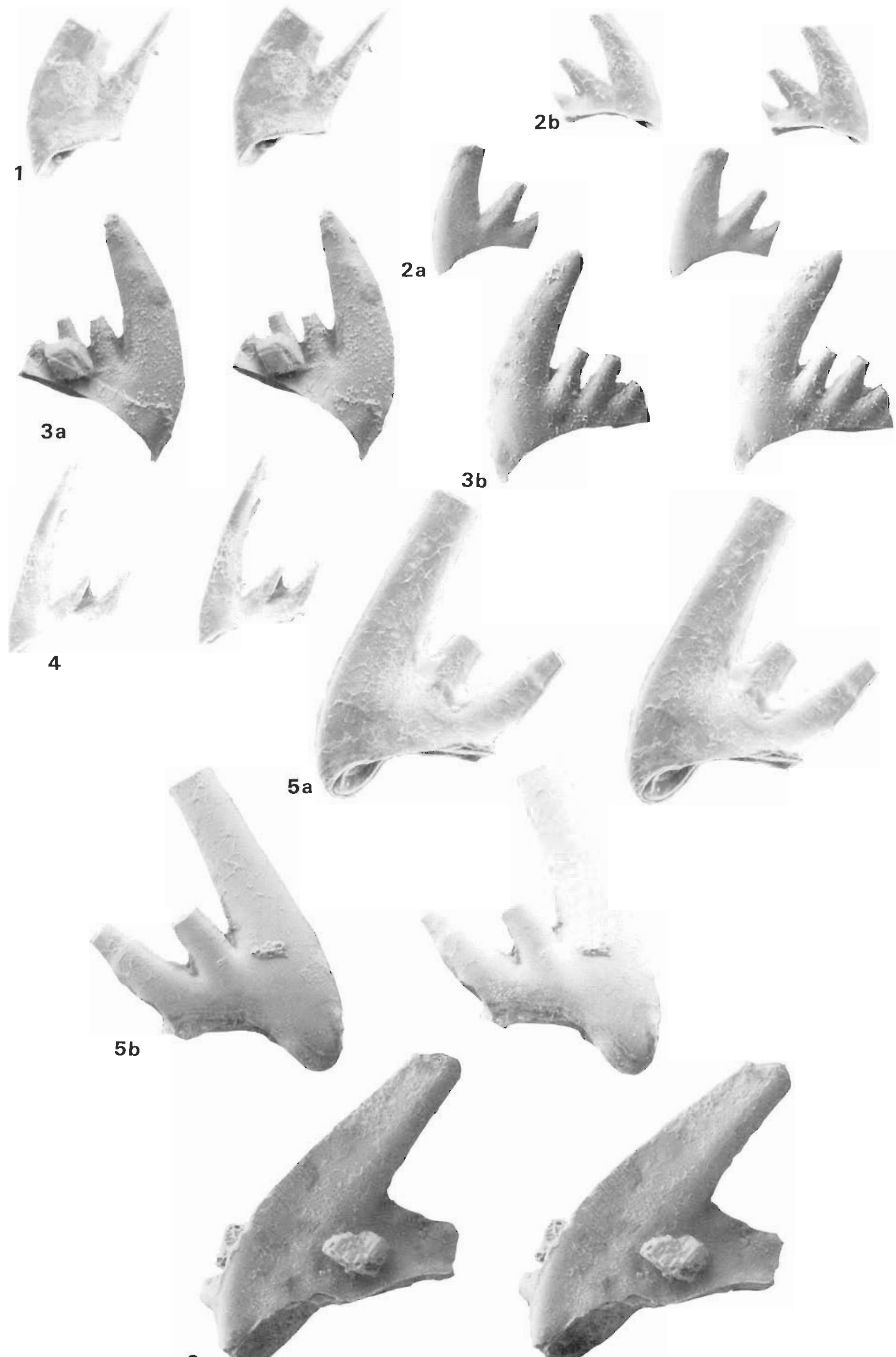
1
2b
2a
3a
3b
4
5a
5b
6

Cordylodus sp. nov. A
Figure 23.

Synonymy.

v. 1971 *Cordylodus oklahomensis* Müller; Druce & Jones, p. 69, Pl. 5, figs 6,7, text-fig. 23j.

Material studied. 16 elements (Pa 8, Sa 2, Sc 3, Sb 3). From a sample collected 276 m above the base of the Ninmaroo Formation at Black Mountain, western Queensland, on the line of the section 1 of Druce & Jones (1971).

Diagnosis. Partial apparatus consisting of Pa, Sa, Sc, and Sb elements. Robust apparatus elements with large erect to recurved cusps on the S elements and erect to slightly recurved cusp on the Pa element. The relatively shallow basal cavity extends posteriorly under the posterior process. Process denticles of the S elements are recurved, or reclined, rather then erect.

Description. The Pa element has a large cusp that is laterally compressed with narrow, but rounded, anterior and posterior margins. The cusp has the anterior margin twisted inward. The posterior process is straight, tapers posteriorly and supports up to four reclined, laterally compressed, denticles. In lateral view the anterior margin is curved. The outer lateral margin is flat and there is a prominent carina on the base of the inner lateral side. The white matter is solid in the cusp from slightly above the level of the posterior process and there is also white matter along the anterior margin. The basal cavity opens downward and is large, extending under the posterior process, into the posterior part of the cusp and curving from the cusp tip down to the anterobasal corner.

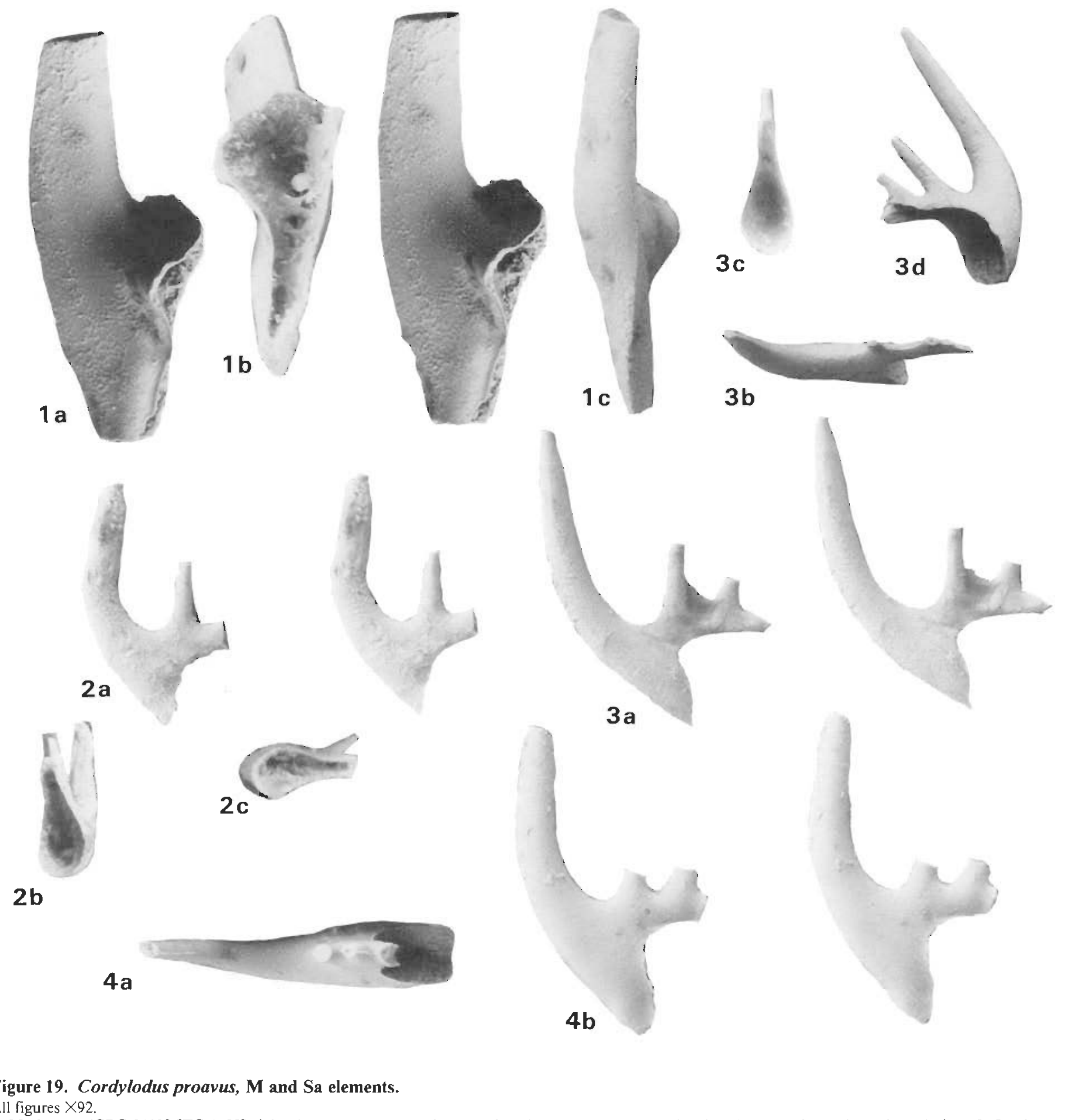

Figure 19. *Cordylodus proavus,* M and Sa elements.
All figures ×92.
1. M element (CPC 28108)[TC 1429] right element; **a**, stereo pair, posterior view; **b**, outer lateral view into basal cavity; **c**, inner lateral view. **2. Sa element** (CPC 28109)[TC 1440] **a**, stereo pair, lateral view; **b**, oblique basal view; **c**, basal view. **3. Sa element** (CPC 28110)[TC 1440] **a**, stereo pair, lateral view; **b**, oral view; **c**, basal view; **d**, oblique lateral view. **4. Sa element** (CPC 28111)[TC 1440] **a**, oral view; **b**, stereo pair, lateral view.

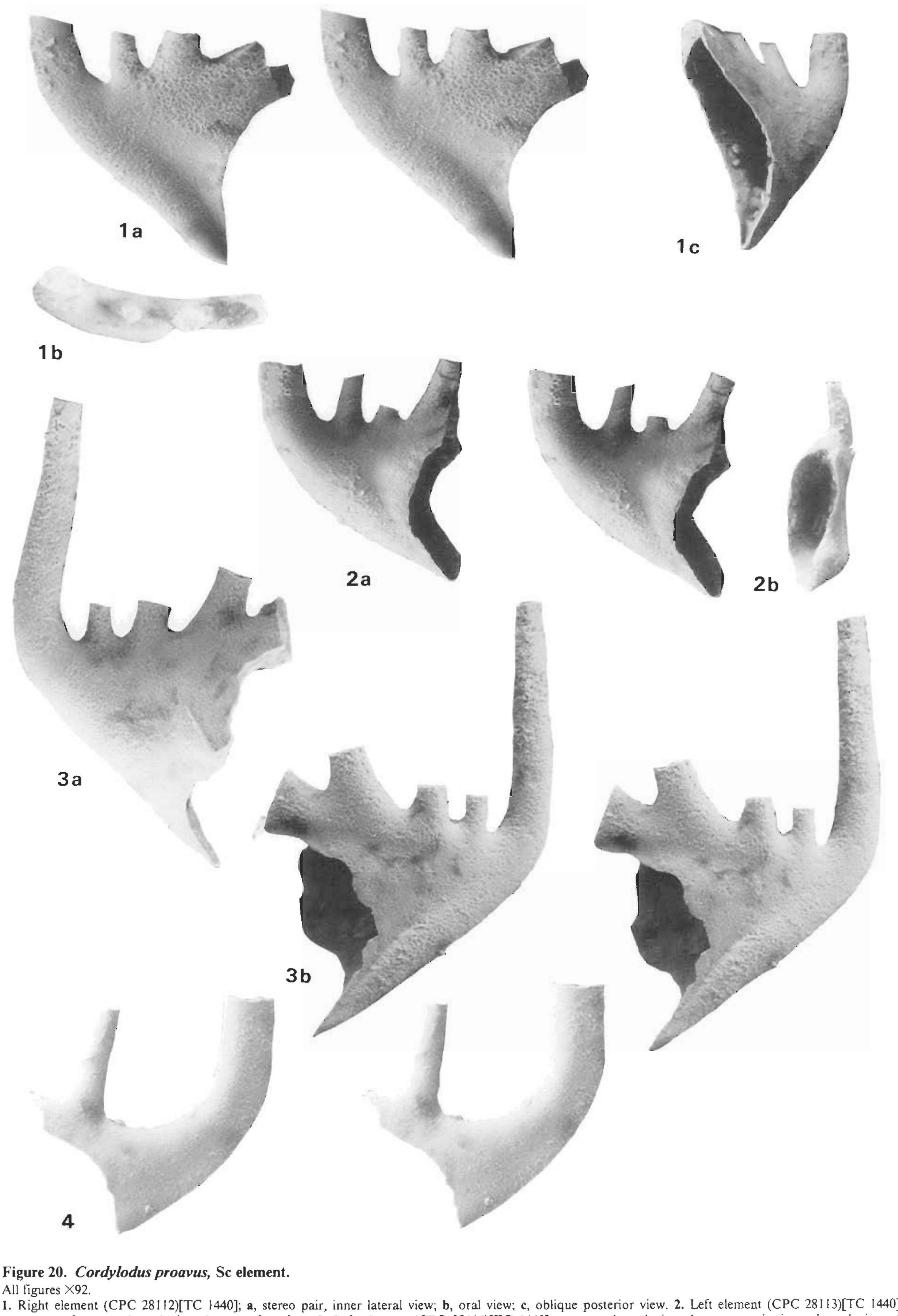

Figure 20. *Cordylodus proavus,* Sc element.

All figures ×92.

1. Right element (CPC 28112)[TC 1440]; **a**, stereo pair, inner lateral view; **b**, oral view; **c**, oblique posterior view. **2.** Left element (CPC 28113)[TC 1440]; **a**, stereo pair, outer lateral view; **b**, posterior view. **3.** Left element (CPC 28114)[TC 1440]; **a**, outer lateral view; **b**, stereo pair, inner lateral view. **4.** Left element (CPC 28115)[TC 1429]; stereo pair, inner lateral view.

The Sa element is bilaterally symmetrical and has a rounded recurved cusp and a rounded anterior margin; the basal cavity opens posteriorly. Posterior process denticles are round in section and recurved to reclined. The Sc and Sb elements are bilaterally asymmetrical and similar to the Sa element except for features related to element symmetry. The cross-section of the base of the Sc element has a flat inner side and a convex outer side. The cross-section of the base of the Sb is biconvex with a rounded anterior margin. On both Sc and Sb elements the posterior process denticles are along the inner lateral margin.

Remarks. Elements assigned to *C.* sp. nov. A are somewhat similar to elements of *C. caboti* Bagnoli & others, 1987, and may be assigned to that species when adequate material is available for study. Both species are considered transitional from *C. proavus* to *C. angulatus*, but they may represent different levels in that transition. The P elements from this study and from Druce & Jones (1971) are robust and do not narrow toward the anterior margin as do the elements of *C. angulatus*. The P element also lacks any development of a platform on the inner side of the posterior process. The Pb, Sd and M elements were not recovered in the limited fauna obtained from the single sample studied.

Locality information

The material examined in this study is from three sources. Most of the material is from the collections reported by Druce & Jones (1971) from the Ninmaroo Formation of the Burke River Structural Belt in Queensland. Samples listed in the tables and locality registrar come from the following sections: Section 1 was a measured section at Black Mountain (Mt Unbunmaroo) (Druce & Jones, 1971, fig. 2A, chart 2), Section 2 was measured at Mt Ninmaroo (Druce & Jones, 1971, fig. 3, chart 3), Section 3 was measured at Mt Datson (Druce & Jones, 1971, fig. 4, chart 4) and locality 13 is a spot sample collected west of Digby Peaks (Druce & Jones, 1971, fig. 8).

The material from Texas was collected and provided by James F. Miller (Southwest Missouri State University), from the Threadgill Creek Section in the Llano Uplift of Texas. See Miller & others (1982) and Miller (1987) for details of the locality. Samples TC 1429, 1440 and 1460 are from the San Saba Member of the Wilberns Formation and sample 1465 is from slightly above the base of the Threadgill Member of the Tanyard Formation.

The material from the Stora Backor section in Sweden was provided by John E. Repetski (US Geological Survey) from a sample he collected from the locality in 1982. The sample is from bed 5 of the Lindström (1955) section and is sample JR8-26-82E of Repetski.

Acknowledgements

The paper has been critically reviewed by Jim Miller (Southwest Missouri State University, USA), John Repetski (US Geological Survey) and John Shergold (BMR). Each has made significant suggestions toward the improvement of the manuscript. None is necessarily convinced of the correctness of the interpreted structure of the apparatus of *Cordylodus*. Photography was the work of Arthur T. Wilson.

References

Aldridge, R.J., 1987 — Conodont palaeobiology: a historical review. *In* Aldridge, R.J., (editor), Palaeobiology of conodonts. *British Micropalaeontological Society/Ellis Horwood Limited, Chichester*, 11-34.

Andres, D., 1988 — Strukturen, apparate und phylogenie primitiver conodonten. *Palaeontographica Abteilung A*, 200, 105-152.

An Taixiang, Zhang Fang, Xiang Weida, Zhang Youqui, Xu Wenhao, Zhang Huijuan, Jiang Debiao, Yang Changsheng, Lin Liandi, Cui Zhangtang, & Yang Xinchan, 1983 — The conodonts of northern China and the adjacent regions. *Science Press, Beijing*, 223 pp.

Bagnoli, G., Barnes, C.R., & Stevens, R.K., 1987 — Lower Ordovician (Tremadocian) conodonts from Broom Point and Green Point, western Newfoundland. *Bollettino della Societa Paleontologica Italiana*, 25, 145-158.

Barnes, C.R., 1988 — The proposed Cambrian-Ordovician global Boundary stratotype and point (GSSP) in Western Newfoundland, Canada. *Geological Magazine*, 125, 381-414.

Bergström, S.M., & Sweet, W.C., 1966 — Conodonts from the Lexington Limestone (Middle Ordovician) of Kentucky. *Bulletins of American Palaeontology*, 50, 271-424.

Chen, Jun-yuan, & Gong, Wei-li, 1986 — Conodonts. *In* Chen, Jun-yuan, (editor), Aspects of Cambrian-Ordovician boundary in Dayangcha, China. *China Prospect Publishing House, Beijing.*

Druce, E.C., & Jones, P.J., 1971 — Cambro-Ordovician conodonts from the Burke River Structural Belt, Queensland. *Bureau of Mineral Resources, Australia, Bulletin*, 110, 1-159.

Ethington, R.L., & Clark, D.L., 1981 — Lower and Middle Ordovician conodonts from the Ibex area western Millard County, Utah. *Brigham Young University Geology Studies*, 28, 1-155.

Furnish, W.M., 1938 — Conodonts from the Prairie du Chien (Lower Ordovician) Beds of the upper Mississippi Valley. *Journal of Palaeontology*, 12, 318-340.

Jeppsson, L., 1971 — Element arrangement in conodont apparatuses of *Hindeodella* type and in similar forms. *Lethaia*, 4, 101-123.

Jones, P.J., 1971 — Lower Ordovician conodonts from the Bonapart Gulf Basin and the Daly River Basin, northwestern Australia. *Bureau of Mineral Resources, Australia, Bulletin*, 117, 1-80.

Klapper, G., & Philip, G.M., 1971 — Devonian conodont apparatuses and their vicarious skeletal elements. *Lethaia*, 4, 429-452.

Landing, E., Ludvigsen, R., & von Bitter, P.H., 1980 — Upper Cambrian to Lower Ordovician conodont biostratigraphy and biofacies, Rabbitkettle Formation, District of Mackenzie. *Life Sciences Contributions Royal Ontario Museum*, 126, 1-42.

Lindström, M., 1955 — Conodonts from the lowermost Ordovician strata of south-central Sweden. *Geologiska Föreningens i Stockholm Förhandlingar*, 76, 517-614.

Miller, J. M., 1980 — Taxonomic revisions of some Upper Cambrian and Lower Ordovician conodonts with comments on their evolution. *University of Kansas Paleontological Contributions*, 99, 1-44.

Miller, J.M., 1984 — Cambrian and earliest Ordovician conodont evolution, biofacies, and provincialism. *Geological Society of America, Special Paper* 196, 43-68.

Miller, J.M., 1987 — Upper Cambrian and basal Ordovician conodont faunas of the southwest flank of the Llano Uplift, Texas. *In* Grayson, R.C., Merrill, G.K., & Miller, J.F., Early and Late Paleozoic conodont faunas of the Llano Uplift region, central Texas — biostratigraphy, systemic boundary relationships, and stratigraphic importance. *The Geological Society of America, 21st Annual Meeting South-Central Section Field Trip Guidebook*, 1-22.

Figure 21. *Cordylodus proavus,* Sb and Sd elements.
All figures ×92.
1. Sb element (CPC 28116)[TC 1440] left element; **a**, stereo pair, outer lateral view; **b**, basal view; **c**, oral view. **2. Sb element** (CPC 28117)[TC 1429] left element; stereo pair, outer lateral view. **3. Sb element** (CPC 28118)[TC 1429] right element; **a**, inner lateral view; **b**, oblique posterior view. **4. Sb element** (CPC 28119)[TC 1429] right element; **a**, stereo pair, outer lateral view; **b**, posterior view. **5. Sb element** (CPC 28120)[TC 1429] right element; stereo pair, inner lateral view. **6. Sb element** (CPC 28121)[TC 1440] right element; **a**, stereo pair, outer lateral view; **b**, oral view; **c**, anterior view. **7. Sd element** (CPC 28122)[TC 1429] right element; **a**, oblique posterior view; **b**, posterior view; **c**, stereo pair, inner lateral view. **8. Sd element** (CPC 28123)[TC 1440] left element; stereo pair, inner lateral view. **9. Sd element** (CPC 28124)[TC 1429] right element; **a**, stereo pair, inner lateral view; **b**, posterior view.

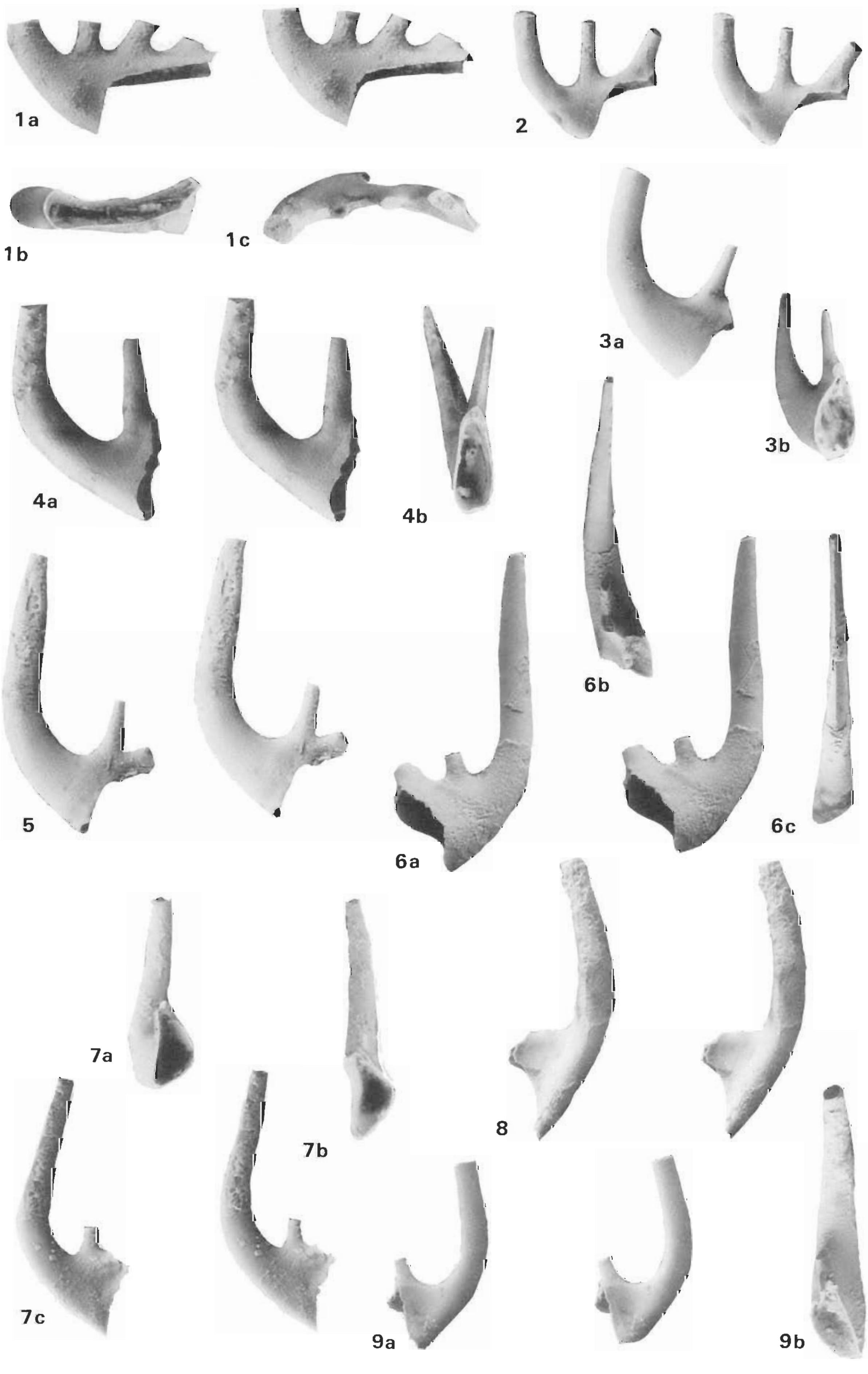
1a
2
1b
1c
3a
4a
4b
3b
6b
5
6a
6c
7a
7b
8
7c
9a
9b

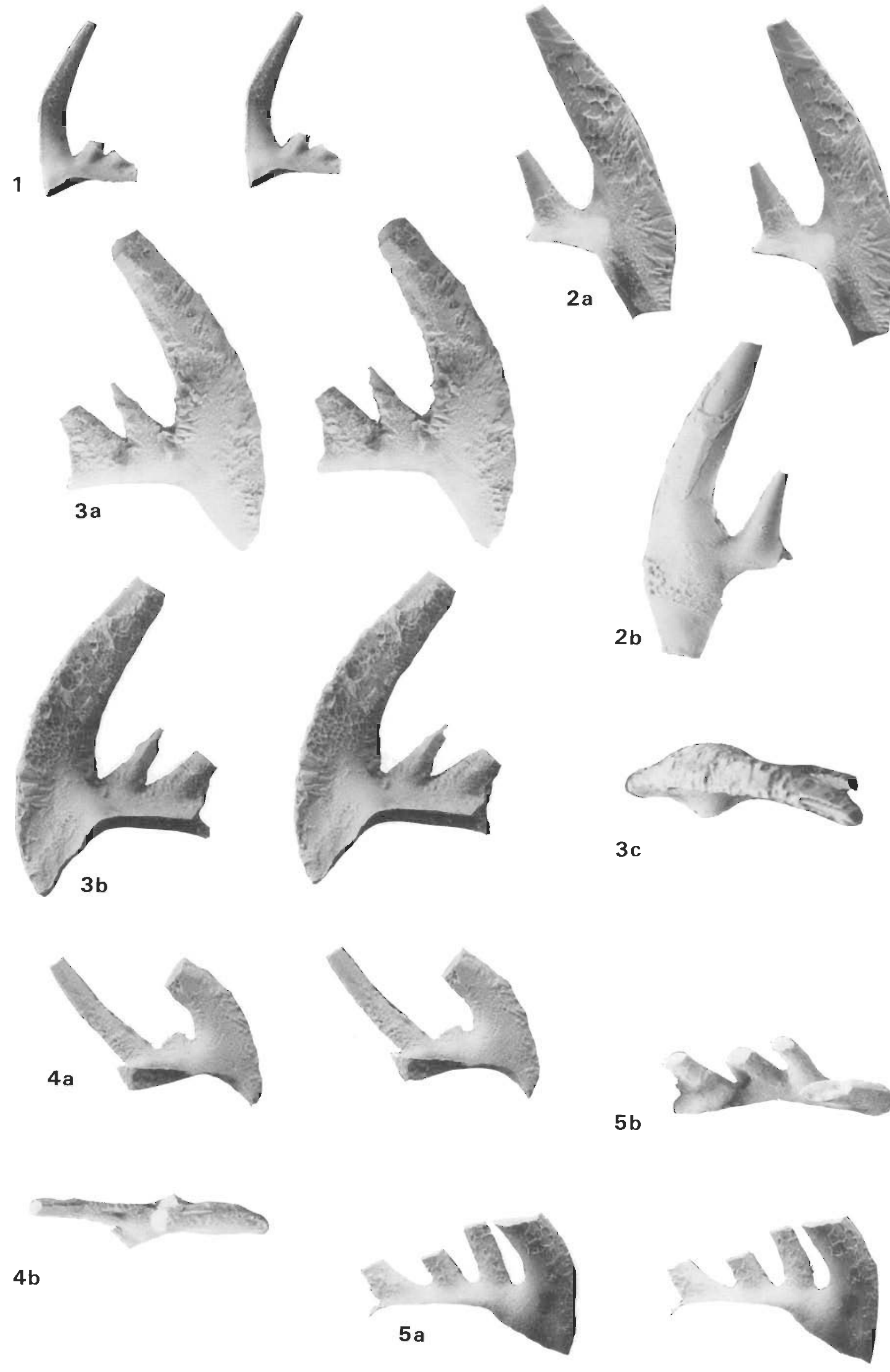
1
2a
3a
2b
3b
3c
4a
5b
4b
5a

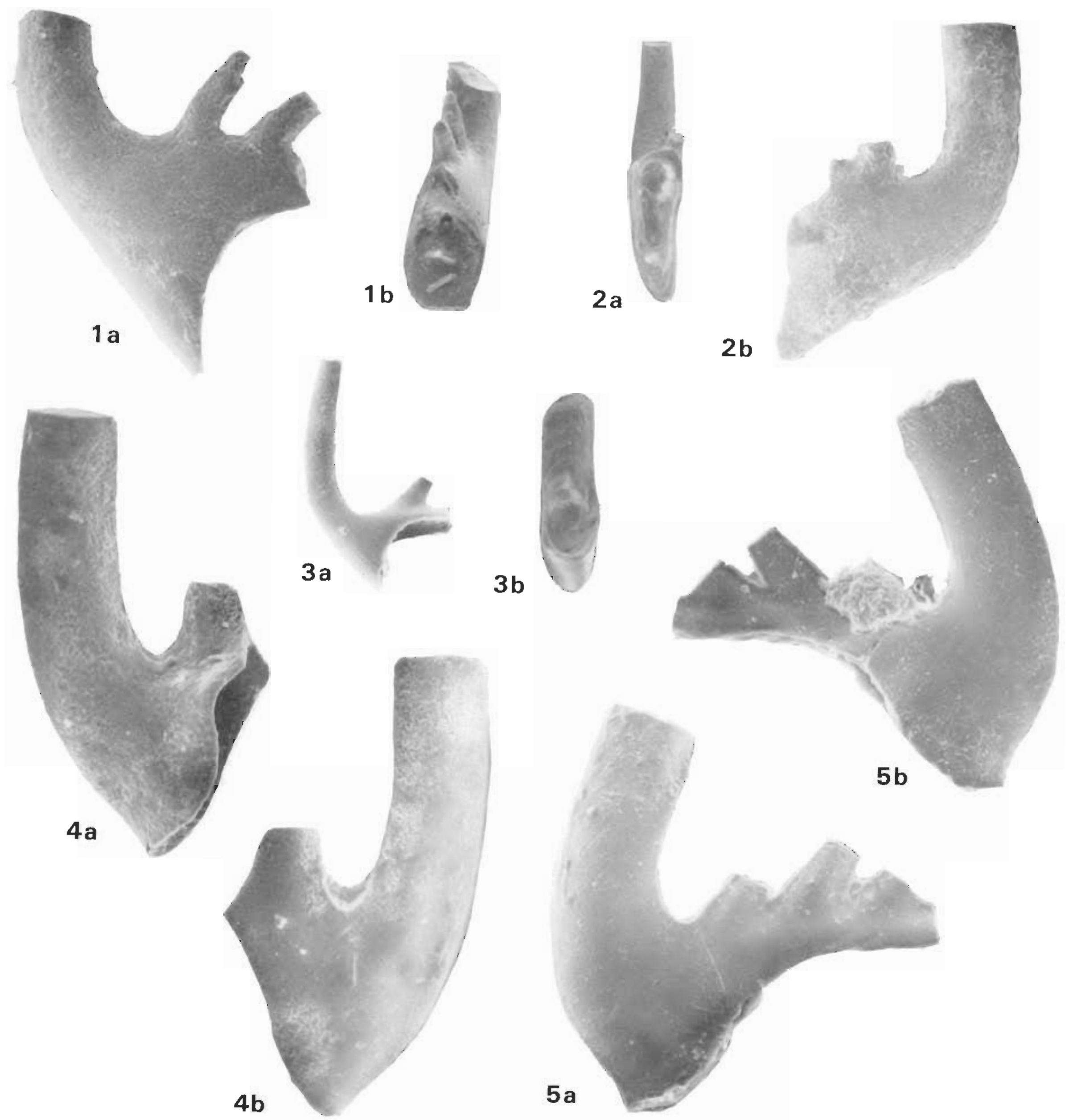

Figure 23. ***Cordylodus*** **sp. nov. A.**
All figures ×100 except as noted.
1. Sa element (CPC 28733)[JHS-BM 276m] **a**, lateral view; **b**, posterior view. **2. Sc element** (CPC 28734)[JHS-BM 276m] left element; **a**, posterior view; **b**, inner lateral view. **3. Sb element** (CPC 28735)[JHS-BM 276m] left element; **a**, outer lateral view; **b**, basal view (×140). **4. Pa element** (CPC 28736)[JHS-BM 276m] right element; **a**, inner lateral view; **b**, outer lateral view. **5. Pa element** (CPC 28737)[JHS-BM 276m] left element; **a**, outer lateral view; **b**, inner lateral view.

Miller, J.M., 1988 — Conodonts as biostratigraphic tools for redefinition and correlation of the Cambrian–Ordovician Boundary. *Geological Magazine*, 125, 349–362.

Miller, J.F., Taylor, M.E., Stitt, J.H., Ethington, R.L., Hintze, L.F., & Taylor, J.F., 1982 — Potential Cambrian–Ordovician boundary stratotype sections in the western United States. *In* Bassett, M.G., & Dean, W. T., (editors), The Cambrian-Ordovician boundary: sections, fossils distributions and correlations. *National Museum of Wales, Geological Series No. 3, Cardiff*, 155–180.

Müller, K.J., 1973 — Late Cambrian and Early Ordovician conodonts from Northern Iran. *Geological Survey of Iran, Report*, 30, 1–77.

Nicoll, R.S., 1977 — Conodont apparatuses in an Upper Devonian palaeoniscoid fish from the Canning Basin, Western Australia. *BMR Journal of Australian Geology & Geophysics*, 2, 217–228.

Nicoll, R.S., 1985 — Multielement composition of the conodont species *Polygnathus xylus xylus* Stauffer, 1940 and *Ozarkodina brevis* (Bischoff & Ziegler, 1957) from the Upper Devonian of

Figure 22. ***Cordylodus proavus,*** **Pb and Pa elements.**
All figures ×92.
1. Pb element (CPC 28125)[TC 1429] right element; stereo pair, inner lateral view. **2. Pb element** (CPC 28126)[TC 1440] left element; **a**, stereo pair, inner lateral view; **b**, outer lateral view. **3. Pb element** (CPC 28127)[TC 1440] right element; **a**, stereo pair, outer lateral view; **b**, stereo pair, inner lateral view; **c**, oral view. **4. Pa element** (CPC 28128)[TC 1440] left element; **a**, stereo pair, inner lateral view; **b**, oral view. **5. Pa element** (CPC 28129)[TC 1429] left element; **a**, stereo pair, inner lateral view; **b**, oral view.

the Canning Basin, Western Australia. *BMR Journal of Australian Geology & Geophysics*, 9, 133–147.

Nicoll, R.S., & Rexroad, C.B., 1987 — Re-examination of Silurian conodont clusters from northern Indiana. *In* Aldridge, R.J., (editor), Palaeobiology of conodonts. *British Micropalaeontology Society/Ellis Horwood Limited, Chichester*, 49–62.

Pander, C.H., 1856 — Monographie der fossilen fische des Silurischen systems der Russich-Baltischen gouvernements. *Akademie der Wissenschaften, St. Petersburg*, 91 pp.

Sweet, W.C., 1981 — Morphology and composition of elements. *In* Clark, D.L.,(editor), Treatise on invertebrate palaeontology — Part W, Miscellanea, Supplement 2, Conodonta, W5–W20.

Sweet, W.C., & Schönlaub, H.P., 1975 — Conodonts of the genus *Oulodus* Branson & Mehl, 1933. *Geologica et Palaeontologica*, 9, 41–59.

Viira, V., Sergeyeva, S. & Popov, L., 1987 — Earliest representatives of the genus *Cordylodus* (Conodonta) from Cambro-Ordovician boundary beds of north Estonia and Leningrad region. *Proceedings of the Academy of the Estonian SSR. Geology*, 36, 145–154.

Appendix 1.

Revised identification of type and illustrated conodonts of the genus *Cordylodus* in the Druce & Jones (1971) and Jones (1971) conodont studies of the Georgina, Bonaparte and Daly River Basins of northern Australia.

Druce, E.C., & Jones, P.J., 1971	**Revised identification**
C. angulatus	*C. angulatus*
CPC 8736 Pl. 3, fig. 5	Pb element
CPC 8737 Pl. 3, fig. 6	Sa element
CPC 8739 Pl. 3, fig. 4	Sa element
CPC 8740 Pl. 3, fig. 7	Pb element
CPC 8757 not figured	? Sc element
C. sp. cf. *C. angulatus*	*C. angulatus*
CPC 8746 text-fig. 23c	Sb element
CPC 8741 not figured	Sb element
C. caseyi	*C. caseyi*
CPC 8748 Pl. 2, fig. 12	Sc element
CPC 8749 Pl. 2, fig. 1i	Sd element
CPC 8750 Pl. 2, fig. 10	Sc element
CPC 8751 Pl. 2, fig. 9	Sb element
C. intermedius	
CPC 8742 Pl. 3, fig. 1	*C. angulatus* Sb element
CPC 8743 Pl. 3, fig. 2	Transition *C. proavus* *C. angulatus*, Sc element
CPC 8744 not figured	*C. angulatus* Sd element
CPC 8745 Pl. 3, fig. 3	Transition *C. proavus* *C. angulatus*, Sc element
C. lindstromi	*C. lindstromi*
CPC 8753 Pl. 1, fig. 8	Sc element
CPC 8754 Pl. 1, fig. 7	Sc element
CPC 8747 Pl. 2, fig. 8	Sd element
CPC 8767 Pl. 1, fig. 9	Pb element
C. oklahomensis	*C.* sp. nov. A
CPC 8727 Pl. 5, fig. 7	Pb element
CPC 8726 Pl. 5, fig. 6	Pb element
C. prion	*C. lindstromi*
CPC 8729 Pl. 2, fig. 1	Pa element
CPC 8730 Pl. 2, fig. 4	M element
CPC 8731 Pl. 2, fig. 5	M element
CPC 8732 Pl. 2, fig. 2	M element
CPC 8733 Pl. 2, fig. 7	M element
CPC 8734 Pl. 2, fig. 6	M element
CPC 8735 Pl. 2, fig. 3	M element
C. proavus	*C. proavus*
CPC 8718 Pl. 1, fig. 1	Sc element
CPC 8719 Pl. 1, fig. 3	Sb element
CPC 8720 Pl. 1, fig. 6	Sb element
CPC 8721 Pl. 1, fig. 4	Sc element
CPC 8722 Pl. 1, fig. 2	Sa element
CPC 8723 Pl. 1, fig. 5	Sb element
C. sp. cf. *C. proavus*	
CPC 8724 Pl. 1, fig. 12	? *C. proavus*, Sc element
CPC 8728 Pl. 1, fig. 10	Indt. Pa element possibly transitional to C. lindstromi
CPC 8725 Pl. 1, fig. 11	? *C. proavus*, Pb element
C. rotundatus	*C. angulatus*
CPC 8752 Pl. 3, fig. 10	Pa element
CPC 8755 Pl. 3, fig. 8	Pa element
CPC 8756 Pl. 3, fig. 9	Pa element
CPC 8757 not figured	? Sc element
C. sp. A	*C. angulatus*
CPC 8738 Pl. 8, fig. 10	Sa element

Jones, P.J., 1971	**Revised identification**
C. angulatus	*C. angulatus*
CPC 9391 Pl. 8, fig. 3	Sa element
C. caseyi	*C. caseyi*
CPC 9392 Pl. 2, fig. 1	Sc element
C. intermedius	? advanced *C. proavus* or sp. nov.
CPC 9393 Pl. 2, fig. 2	Sc element
CPC 9394 Pl. 2, fig. 3	Sb element
C. lindstromi	? advanced *C. proavus* or sp. nov.
CPC 9395 Pl. 2, fig. 4	Sd element
C. oklahomensis	? advanced *C. proavus* or sp. nov.
CPC 9396 Pl. 2, fig. 5	M element
CPC 9397 Pl. 2, fig. 6	Indt. P or S element
CPC 9398 Pl. 2, fig. 7	Sc element
CPC 9399 Pl. 2, fig. 8	Indt S element
C. proavus	*C. proavus*
CPC 9400 Pl. 2, fig. 9	Sb element
C. rotundatus	*C. angulatus*
CPC 9401 Pl. 2, fig. 10	Pa element
CPC 9402 Pl. 2, fig. 11	Pb element

Appendix 2.

Locality and stratigraphic information of the M elements illustrated on figure 2.

Fig. 2/1 *Erraticodon patu* (CPC 28051) Ordovician, Horn Valley Siltstone, Amadeus Basin, Northern Territory, sample 84-2003/14.

Fig. 2/2 *Triangularis* sp. (CPC 28052) Ordovician, Horn Valley Siltstone, Amadeus Basin, Northern Territory, sample 84-2004/13c.

Fig. 2/3 Unidentified M element (CPC 28053) Mississippian, Hannibal Shale, locality unknown, probably from Illinois, sample USA 21 of E.C. Druce.

Fig. 2/4 Unidentified M element (CPC 28054) Lower Carboniferous, Moogooree Formation, Carnarvon Basin, Western Australia, sample CB 83/122R.

Fig. 2/5 *Protoprioniodus aranda* (CPC 28055) Ordovician, Horn Valley Siltstone, Amadeus Basin, Northern Territory, sample 86-2031A.

BMR Journal of Australian Geology & Geophysics, 11, 559-567

The Newcastle, New South Wales, earthquake of 28 December 1989

Kevin McCue[1], Vaughan Wesson[2] & Gary Gibson[2]

An earthquake occurred without warning at 10 27 am on 28 December 1989 (local time) causing loss of life in the city of Newcastle, New South Wales, Australia, the first earthquake to cause fatalities in Australia since European settlement. The magnitude is estimated to have been 5.6 on the Richter scale. Earthquakes of this size occur on average about once every eighteen months in Australia. A single aftershock was recorded on a network of ten seismographs installed on 29 December in and around Newcastle; it had a magnitude of 2.1. The focal depth of the mainshock was 11.5±0.5 km and of the aftershock 13.5±0.8 km, which is beneath the Permian sediments of the Sydney Basin. The epicentres of both earthquakes are coincident within the error bounds and are some 15 km from the centre of damage in the City. The damage in Newcastle was made worse by an underlying thin layer of alluvium which magnified the ground motion substantially. A fault-plane solution indicates that the earthquake had a thrust mechanism with nodal planes striking in a NW-SE direction, parallel to the mapped surface faults in the region. Limited strong motion data were recorded, but not close to the epicentre.

Introduction

The Newcastle earthquake on Thursday 28 December 1989 resulted in 12 deaths, hundreds of injuries, and serious damage to, or destruction of, thousands of homes and buildings. This was the first time in written history that lives have been lost as the result of an earthquake in Australia. The damage was estimated at $400 million to $500 million insured loss, with similar losses both for government and for those under-insured or not insured. (In dollar terms, this was the worst natural disaster in Australian history).

Australia occupies a relatively low risk position in the middle of one of the world's larger tectonic plates, yet there have been many earthquakes larger than the one reported here (Everingham & others, 1987).

A plot of epicentres in Australia from 1873 to 1988 (Fig. 1) shows Newcastle on the edge of a 300–500 km wide seismic

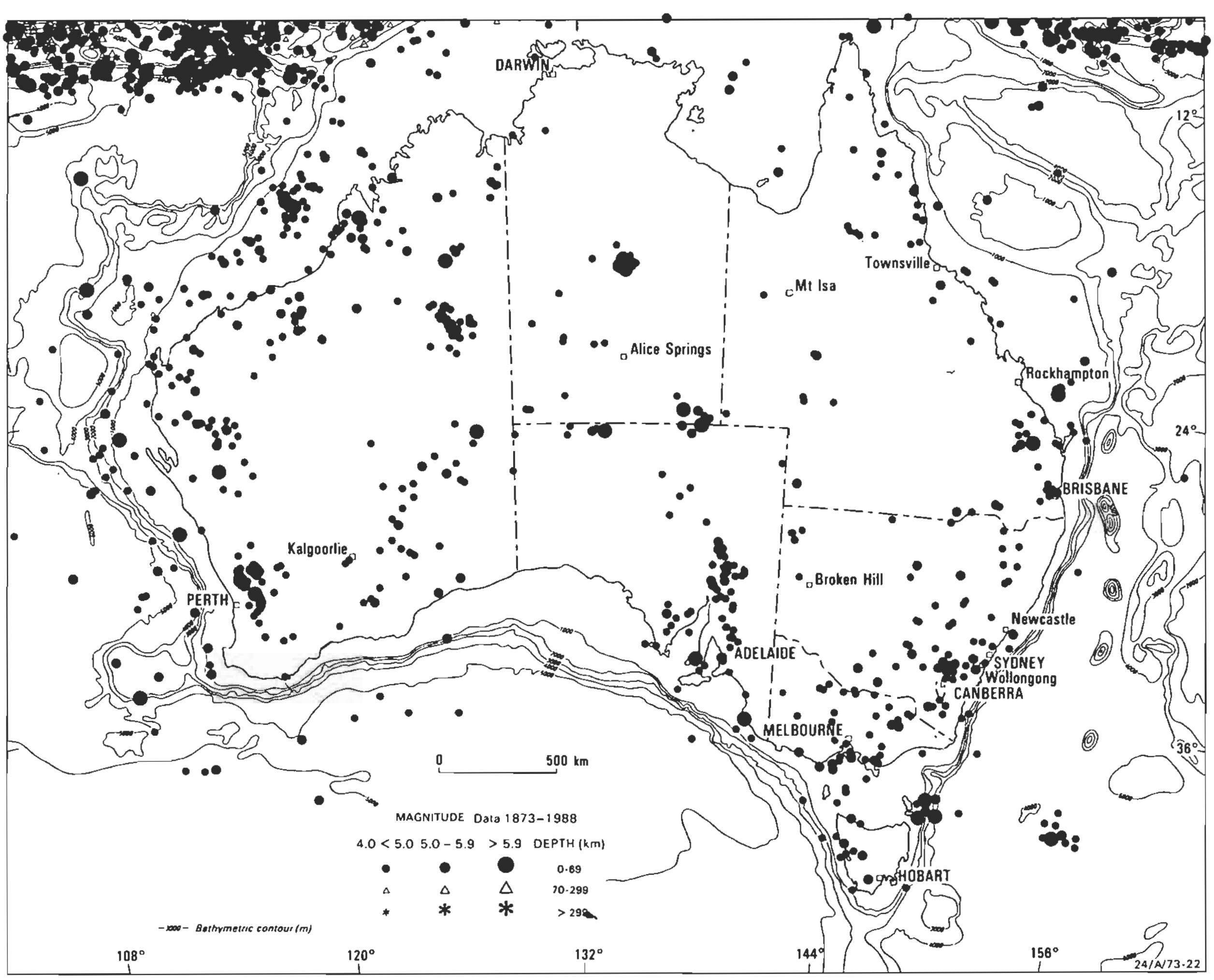

Figure 1. Australian earthquake epicentres (magnitude 4 or greater), 1873-1988.

1 Australian Seismological Centre, Bureau of Mineral Resources, GPO Box 378, Canberra ACT 2601
2 Seismology Research Centre, Phillip Institute of Technology, Bundoora, Victoria 3083

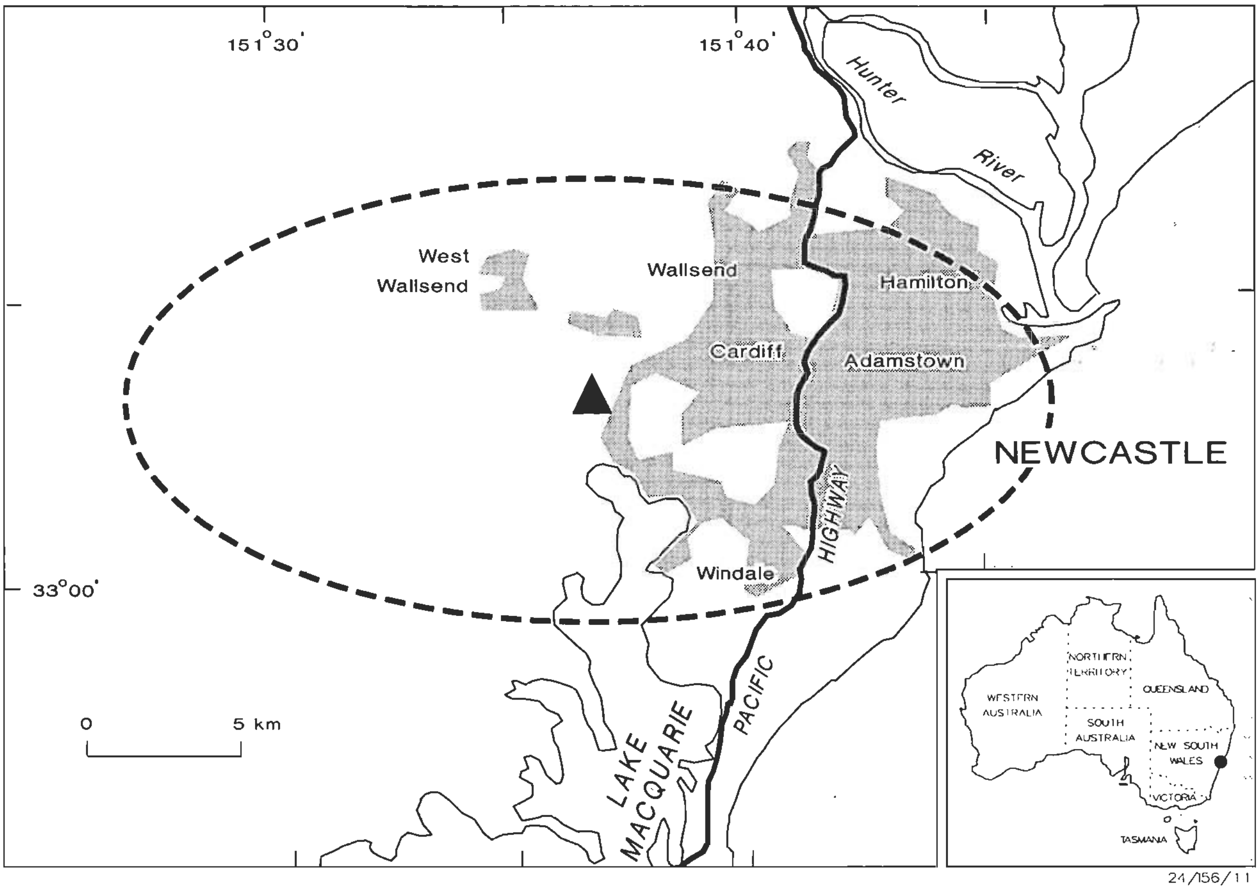

Figure 2. Epicentre and error ellipse of the mainshock, Newcastle, New South Wales, earthquake of 28 December 1989.

zone stretching along the east coast of Australia. Within this zone in the last two hundred years, large (ML>5.9) earthquakes have occurred off northeast Tasmania between 1883 and 1894 (Michael-Leiba, 1989) and in Queensland in 1883 and 1918 (Rynn & others, 1987). Prehistoric earthquake scarps in the zone have been identified near Echuca in the New South Wales–Victorian border region and in Tasmania (McCue, in press).

The earthquake's proximity to the City of Newcastle, its mechanism and the nature of the near-surface foundation conditions all contributed to the ensuing damage.

Focal parameters

The epicentre was near Newcastle but insufficient seismographs were in place at the time to determine the focal coordinates with a precision of better than 12 km. The nearest seismograph was at St Ignatius College, Riverview, 105 km south, and there are no seismographs east of Newcastle for two thousand kilometres. Seismograms recorded at stations of the Lownet array (EAU, EBL, ESY, EAB, ABH, EDU) in Scotland at a distance of 152° provided one vital parameter, the focal depth of the mainshock, through phases identified as pPKIKP and pPKP (these are P waves reflected from the earth's surface at the epicentre which travel through the inner and outer core respectively, arriving at the recording station after the direct PKIKP and PKP waves). In each case the polarity of the supposed reflection was opposite that of the direct phase, which helped in our interpretation of the seismograms (Muirhead, ASC, personal communication, Jan. 1990). The time difference of 4.0±0.1 s between each set of waves is twice the wave's travel time from the focus to the surface, which is equivalent to a focal depth of 11.5±0.5 km using the crustal velocities of Finlayson & McCracken (1981). With the focal depth constrained at 11.5 km, the computed origin time and focal coordinates were:

Origin time:	23 26 58±1.5 s UTC
Location:	32.95±0.06° S
	151.61±0.16° E
Focal depth:	11.5±0.5 km

This epicentre is close to Boolaroo (Fig. 2), about 15 km west-southwest of the Central Business District of Newcastle. The magnitude of the earthquake could not be quickly or precisely computed. Most of the recorders in the national seismographic network have a limited dynamic range; all those within 1600 km were overloaded by the large amplitude of the seismic waves. Beyond that distance the Richter magnitude scale ML is not properly defined. Ultimately its magnitude was computed from a variety of scales: body wave (mb) and surface wave (Ms), duration magnitude (MD) and the felt area ML(I) (Greenhalgh & others, 1989). These and their equivalent Richter magnitudes (ML) are listed in Table 1.

An average magnitude of ML 5.6 has been adopted in this paper. The single Ms reading was excluded because Ms is a poor measure of the size of earthquakes below magnitude 6.

Table 1. Magnitude of mainshock, Newcastle earthquake.

Computed magnitude		*Equivalent Richter magnitude (ML)*
ML (QIS)	5.5	5.5
MD (PIT)	5.7	5.7
Mb (USGS)	5.7	5.4
Ms (NWAO)	4.6	5.0
ML (I)	5.6	5.6

Tectonic framework

The nearest plate boundary to Newcastle is some 2000 km east, where the Australian and Pacific plates collide through New Zealand, the Kermadec Islands, Tonga and Vanuatu. Continental Australia is completely within the Australian plate, and is therefore subject to relatively low earthquake activity.

The foci of Australia's intraplate earthquakes are usually within the upper crust, perhaps no deeper than 15 km. Most of the well constrained larger earthquakes are even shallower (Fredrich & others, 1988).

Newcastle is close to the northern margin of the Sydney Basin (Scheibner, 1987) which extends south to Batemans Bay. The northeast corner of the basin near Newcastle is a structural subdivision known as the Hunter Valley Dome Belt. This belt is bounded by thrust faults, the Hunter thrust to the northeast and a basement fault to the southwest which projected to the surface, forms the southern margin of the Hunter Valley (Herbert & Melby, 1980). Estimates of the depth of the basin in the vicinity of Newcastle vary from about four to eight kilometres, and the nature of the underlying basement is unknown.

Historical seismicity

The first seismograph in New South Wales was installed at Sydney Observatory in 1906 (Doyle & Underwood, 1965), and the 18 December 1925 Newcastle, or Boolaroo, earthquake was recorded on the seismograph at Riverview Observatory. The earthquake was felt widely and reported extensively in the press at the time. Estimates of the magnitude

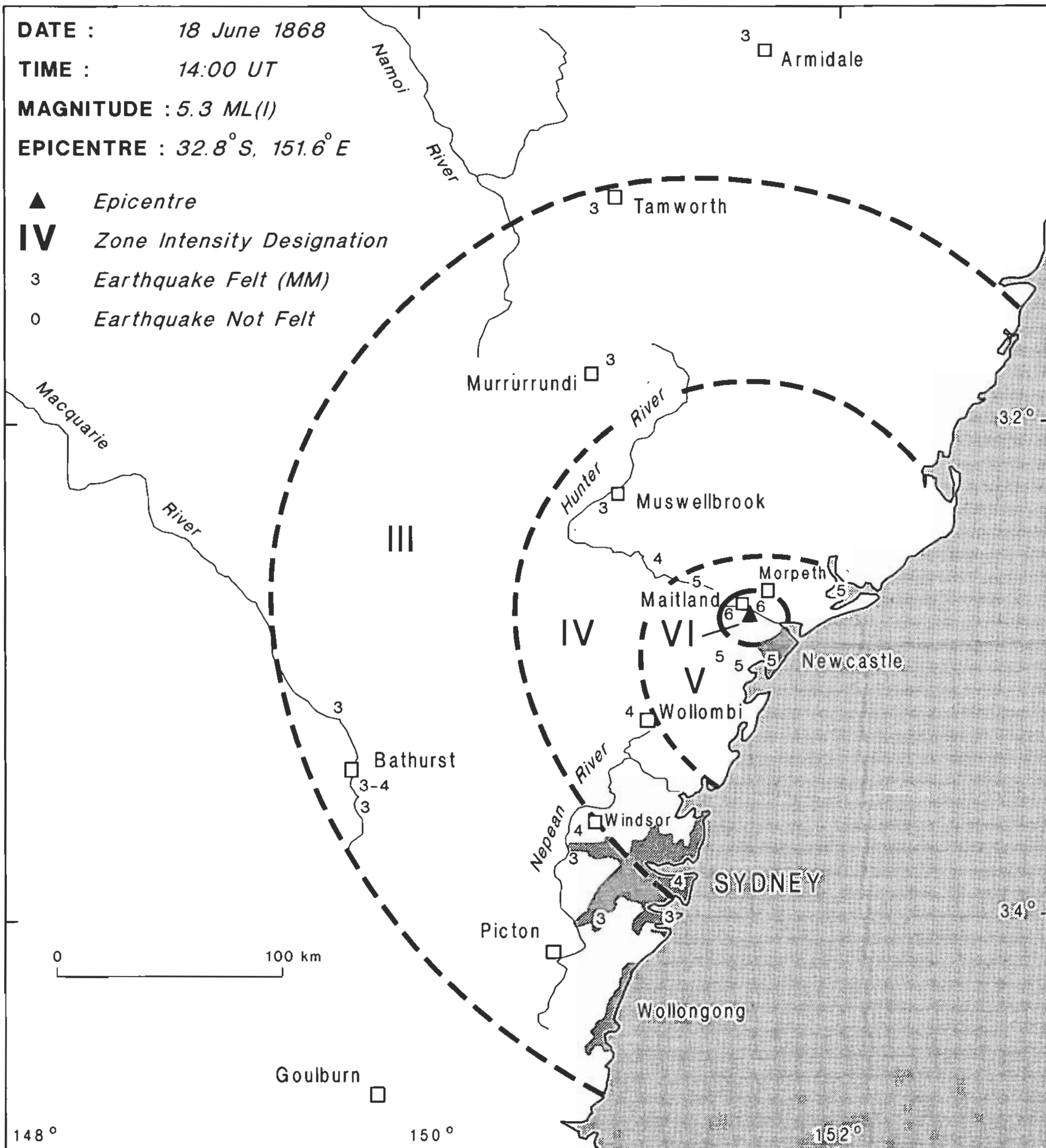

Figure 3. Isoseismal map of the 18 June 1868 Maitland, New South Wales, earthquake.

of this earthquake were ML5.2 from the Riverview seismogram (Drake, 1974) and ML(I)5.3 from its felt area or radius of perceptibility (McCue, 1980). The isoseismal map was not published until recently (Rynn & others, 1987), so this information has not been widely available. Some of the brick buildings repaired after the 1925 earthquake were damaged again in 1989.

The occurrence of the 1925 earthquake has long since passed out of the oral history of the region. There was an even earlier earthquake on 18 June 1868, which one sexagenarian remembers his grandmother describing to him as a small boy. This too is reported in the press of the time and more eloquently by Clarke (1869) but the isoseismal map (Fig. 3) was completed only last year. From this map, a magnitude of ML(I)5.3 is tentatively assigned. The epicentre was in the Newcastle/Maitland area. No real damage was reported after either earthquake although Catherine Foggo (in a letter to Russell Blong, provided to one of the authors, KMcC) referred to the booklet *Back to Singleton September 15 1926* in which the following account was published: 'an important event in our history was . . . the earthquake about 1868 when crockery in most houses was broken and a few chimneys came down'.

Earlier earthquakes on 2 August 1837, 28 January 1841 and 28 October 1842 probably had epicentres in the same region but the felt reports are even more scarce than those of 1868. Their epicentres and magnitudes are still unknown.

Earthquakes of more recent times are listed on the Bureau of Mineral Resources' Australian earthquake datafile. Since 1960, 55 events with magnitude exceeding 2.5 have occurred within 100 km of Newcastle, but none was as close to Newcastle as the 28 December 1989 earthquake, and none exceeded magnitude ML4.1.

Focal mechanism of the 1989 Newcastle earthquake

On a lower hemisphere projection of the focal sphere, Australian seismographic stations plot only in the western hemisphere, and most of them are in the southwest quadrant relative to the earthquake focus. Fortunately a triaxial vibration recorder near Ellalong, about 40 km west of Newcastle, triggered on the P wave (a first motion dilatation) and provided data in the eastern hemisphere (the complementary azimuth was plotted since the ray emerges through the upper hemisphere). The Riverview seismogram has a small short-period compression and a long-period dilatation, indicating that it was near-nodal, which provided strong constraint on the dip of the southwest dipping nodal plane shown in Figure 4. The PKP compressions on the British Geological Survey's (BGS) seismograms in Scotland helped us eliminate an alternative solution with a 'normal' mechanism.

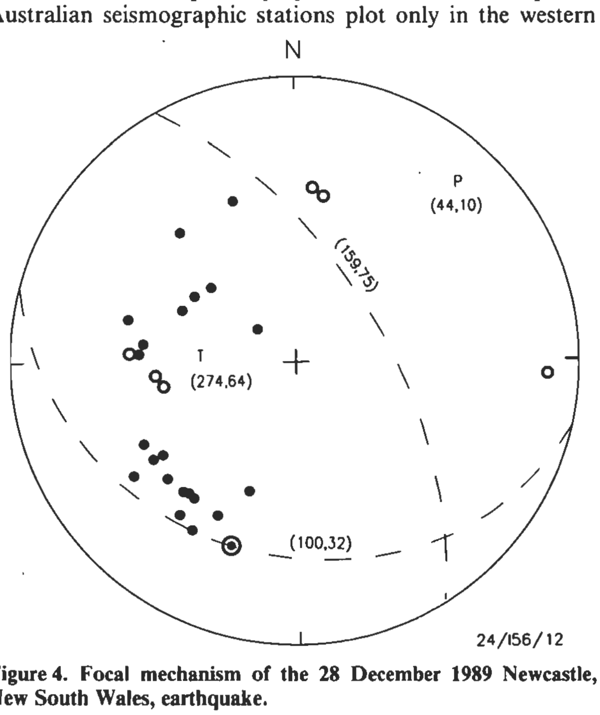

Figure 4. Focal mechanism of the 28 December 1989 Newcastle, New South Wales, earthquake.
P, T & B are the principal stress axes, the solid dots are compressions and the open dots dilatations at short period seismograph stations. Projection is onto the lower hemisphere.

The final solution is that of a thrust mechanism with a near-horizontal principal stress direction striking N44° E (Table 2). First motions from the aftershock recorded on the digital network stations also fitted this solution. Without surface faulting or a well defined aftershock sequence it is not possible to distinguish which of the two planes is the fault plane.

Table 2. Fault-plane parameters of the Newcastle earthquake.

Axis	*Strike*	*Dip*
P	044	10
T	274	64
B	140	12
Plane		
1	150	75
2	110	32

P, maximum stress axis; T, minimum stress axis; B, intermediate stress axis. Planes 1 and 2 are the nodal planes.

Aftershocks

Within twelve hours of the mainshock, a single, vertical component, analogue seismograph was operational at Newcastle. In the following twelve hours another analogue and eight triaxial digital recorders had been installed within a 10 km radius of the City (Fig. 5). Two of these recorders were accelerographs, insensitive seismographs with a wide dynamic range to record the strong near-field ground motion.

Only one aftershock large enough to be located was detected by this network in the subsequent week, and it had well constrained focal coordinates (Table 3).

Table 3. Focal coordinates of aftershock, Newcastle earthquake 28 December 1990.

Date	29 December 1989
Origin time	09 08 9.6±0.2 UTC
Location	32.95±0.024°S
	151.62±0.032°E
Focal depth	13.6±0.8 km

This aftershock was recorded on the Armidale seismograph (COO) from which its magnitude was measured as ML2.1. The focal depth of the aftershock was computed as 13.6±0.8 km, based on arrival times of P and S phases at seismographs of the temporary network.

The lack of aftershocks is remarkable; a similar sized earthquake in the Sydney Basin near Picton, New South Wales, on 21 May 1961 was followed by 60 aftershocks of up to magnitude 3.5 in the first 24 hours (Cleary & Doyle, 1962). Their absence makes it difficult to determine the mainshock fault dimensions. Errors in the computed spatial

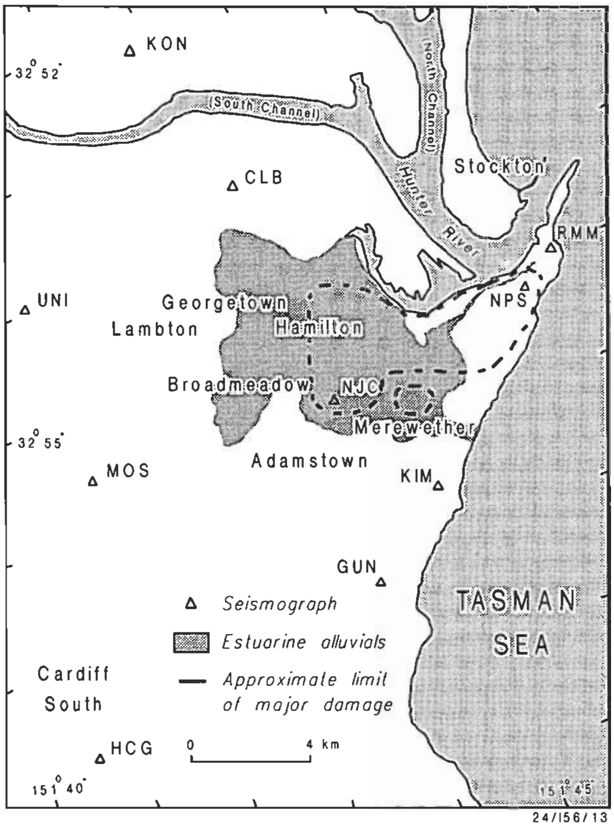

Figure 5. Location of the ten seismographs of the joint Bureau of Mineral Resources (BMR) and Phillip Institute of Technology (PIT) portable array deployed in the Newcastle area during the week following the 28 December 1989 earthquake, and the three that were left for the following month.
The dotted line outlines the approximate edge of estuarine alluvials, the dashed line the area of greatest damage.

coordinates of the aftershock are small but it was close to the poorly located mainshock.

That they are indeed close is corroborated by the fact that the aftershock too was felt most strongly at Hamilton where some of the worst damage occurred during the mainshock.

The coincidence of the computed focal coordinates, and the facts that both foci are at mid-crustal depth and that the felt patterns are similar, convince us that the epicentre of the mainshock was indeed near Boolaroo and about 15 km from the centre of damage. As a corollary, much of the damage in Newcastle may be attributed to amplification of the ground motion in the near-surface foundation materials, the several metres of estuarine alluvial silt and sand that cover a former course of the Hunter River and a swamp.

It is also possible that the earthquake mechanism contributed to the focusing of strong ground motion in Newcastle. Shear wave energy would have been preferentially radiated towards the Central Business District regardless of which nodal plane was the fault plane. However had this been a dominant effect, a similar high intensity should have been observed in areas such as Belmont and Toronto where the complementary shear wave lobe surfaced. No such effect was observed there.

Isoseismal map

Questionnaires designed to assess the felt intensity were distributed by J. Vahala (BMR) and the returned forms were used to compile an isoseismal map (Fig. 6). Other supplementary data were obtained by personal and radio and telephone interviews. The maximum intensity is assessed at MMVIII and the radius of perceptibility as 310 km, corresponding to a magnitude of ML(I)5.6. The shape of the contours is similar to those in Figure 3 and Rynn & others (1987, fig. 6), but the recent earthquake is obviously the largest of the three since it was felt over a wider area.

In the meizoseismal region, the rapid attenuation of intensity would normally indicate that the focus was very shallow, but in this case the focal depth is well constrained at 11.5 km. The difference of two intensity units between the epicentral region and the city amounts to at least a fourfold magnification of peak ground velocity, v (from the relation of Newmark & Rosenblueth, 1971: I = log 14v/log 2) due to the alluvial fill.

Secondary effects

One of the more surprising aspects of this earthquake, given the foundation materials, is the almost complete lack of ground deformation. There was no obvious subsidence or extensive ground cracks, despite the added instability from shallow mining, and no liquefaction (sand boils or mud volcanoes). In fact the only documented coseismic subsidence was on the southern abutment of the Stockton Bridge, 10 km north of Newcastle. Numerous homeowners have reported that slow structural deformation has continued in the Newcastle area in the month following the earthquake, but the few measurements of the width of structural cracks that have been made do not support these reports. The measured movements were diurnal, alternately increasing then decreasing with day and night temperature variation. Unusually high rainfall fell in the Hunter region in the week following the earthquake, but only further geotechnical research to determine the extent of known highly reactive clays will determine whether this combination, and not the earthquake, can be blamed for any continuing deformation.

There was no seismic sea wave recorded on the Newcastle tide gauge (operated by the New South Wales Marine and Harbours Board), though press reports referred to sightings of anomalous waves offshore.

The lack of surface faulting is not surprising for an earthquake of this size and focal depth. In Australia during the last twenty years, five faults have ruptured the surface following large, very shallow earthquakes in Western Australia, South Australia and the Northern Territory. In eastern Australia there are at least two Recent earthquake scarps, in Victoria and Tasmania, but each predates written history.

Strong motion data

Most observers in Newcastle described the event as more like an explosion than an earthquake and agreed that it was very short, lasting no more than 2 or 3 s. Others near Hamilton reported having difficulty in standing and some observed waves travelling down the road or pavement.

There were no strong motion recorders in the Newcastle area at the time of the earthquake. The nearest was a triaxial vibration recorder at Ellalong near Cessnock, New South Wales, which recorded the first 3.6 s of shaking but missed the strongest ground motion in the later S phase and surface waves. The peak resultant ground velocity of the P wave was 7.4 $mm.s^{-1}$ at a frequency of 6.8 Hz, but the actual maximum velocity was probably several times this value (Frank Rice, Resource Planning Pty Ltd, & Russell Rigby, Newcastle Wallsend Coal Co., personal communications, Jan. 1990).

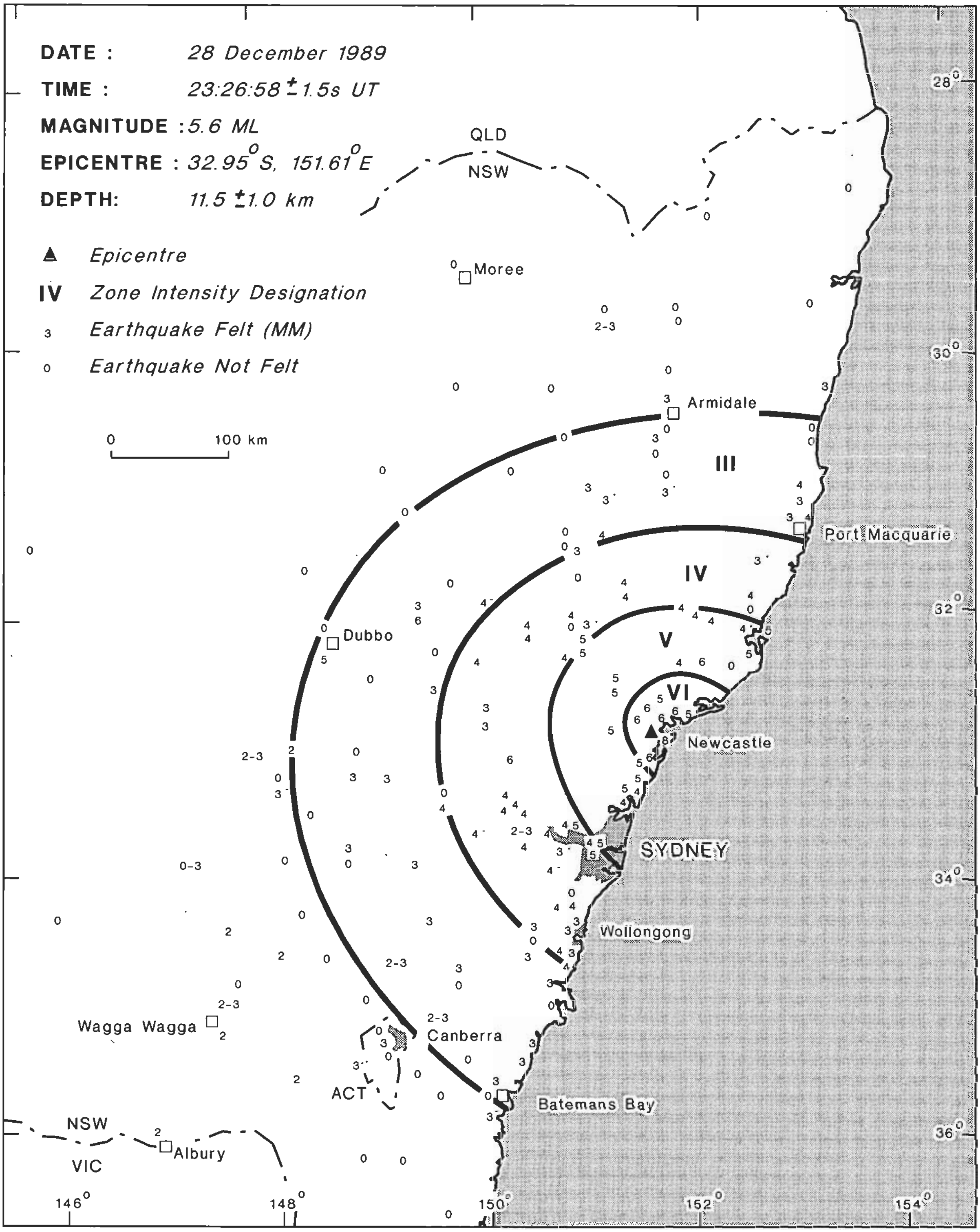

Figure 6. Isoseismal map of the 28 December 1989 Newcastle, New South Wales, earthquake.

Another two vibration recorders south of Muswellbrook were triggered; the peak velocities in the complete wavetrain were 1.5 $mm.s^{-1}$ horizontally and 1.26 $mm.s^{-1}$ vertically (Pam Simpson, Dreighton Coal Mine, personal communication, Jan. 1990), corresponding to accelerations estimated to be 130 $mm.s^{-2}$. The nearest accelerograph to trigger was located at Lucas Heights south of Sydney, New South Wales. Two of those installed near Canberra also triggered on the surface waves, where the recorded peak ground acceleration was about 10 $mm.s^{-2}$.

Discussion and ramifications for Australian building codes

This earthquake has highlighted several deficiencies in the monitoring of earthquakes in Australia. No large metropolitan area in Australia is adequately covered. The current network operated by the Bureau of Mineral Resources is designed for Australia-wide coverage and local networks have been installed to monitor seismicity near large dams or in

Figure 7. The Newcastle Workers Club, where 9 people died when an addition built in the mid 1970s collapsed.
Photo: M. Maloy.

Figure 9. Final stages of clean-up at the Newcastle Workers Club site.
Photo: M. Michael-Leiba.

Figure 8. Rescue workers in front of the Newcastle Workers Club.
Photo: M. Maloy.

Figure 10. Butcher's shop in Hamilton. The parapet collapsed onto the awning, which fell to the street, showering bricks and rubble over the window display.
Photo: M. Maloy.

areas of known higher than average activity, but not in the cities.

The lack of near-field strong motion recordings makes it difficult for the engineering community to analyse specific failures, such as the Workers Club building (Figs 7–9), and to compute the effects of the underlying alluvium in magnifying the ground motion. Each city in Australia should have a network of at least four seismographs to monitor nearby seismicity, and a number of accelerographs to measure both the ground motion on a range of appropriate foundation materials and the response of important structures.

At the time of writing this report, a Standards Australia subcommittee is engaged in reviewing the Building Code, AS2121-1979, which includes an earthquake risk map of Australia. Since the introduction of the code, Newcastle has had Zone 0 status, that is, no seismic lateral forces had to be considered in the design of normal buildings. Most, if not all, of the damage was to buildings constructed before the publication of the code in 1979 (Figs 10–15), so a higher zone status would have made no difference to the damage pattern in the recent earthquake.

Figure 11. Typical damage in masonry walls, where cracks have formed at stress concentrations at the corners of windows and doors.
Photo: M. Maloy.

Figure 12. Part of the brick wall in Figure 11 was considered unsafe. It was demolished, and the rest of the wall propped up before repair.
Photo: M. Michael-Leiba.

Figure 13. Two storey commercial building, Beaumont St, Hamilton, showing failure of both inner and outer brick walls of top storey and gable.
Photo: M. Maloy.

Figure 14. Falling masonry is a hazard to people and property, as this car shows.
Photo: M. Maloy.

Two problems face legislators in the wake of the earthquake: to ensure that the old and decaying buildings and their attachments are continually renovated to current code practice, and to ensure that domestic dwellings, currently excluded in the building code because they are not generally designed by an engineer, are constructed with adequate earthquake resistance.

Although the level of seismicity appears to have remained stable at least this century, both in Australia and worldwide, the risk of another disaster such as that of 28 December 1989 in Newcastle occurring in Australia has increased with the growth and ageing of urban areas in Australia. Recognition of this fact alone will surely lead to changes in our building codes and construction practices, and in our use of building materials. It could also limit the effects of soft foundation materials on the level of ground shaking during earthquakes.

Acknowledgements

Tony Corke from the Seismology Research Centre (PIT) and Bill Greenwood (BMR) were instrumental in establishing the joint BMR/PIT field seismograph network. Maureen

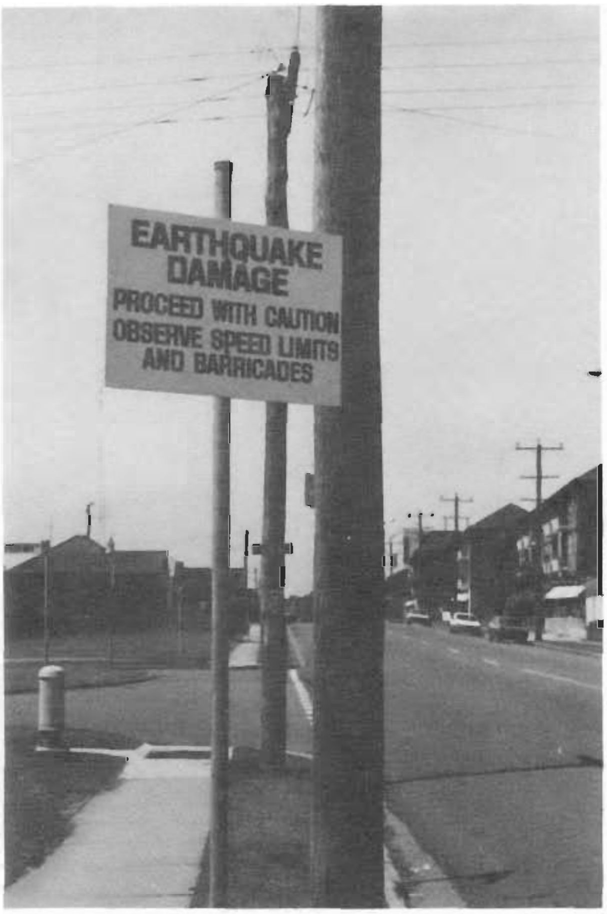

Figure 15. An unexpected signpost in an Australian city.
Photo: K. McCue.

Maloy gave us two days as photographer. Richard and Kim Hughes provided the perfect operations centre at Hillcrest, and Tonee Holley assisted with logistics. Jerry Vahala distributed the isoseismal questionnaires and Marion Leiba (BMR) and Tony Preston (Sydney Water Board) provided additional data. The British Geological Survey kindly provided data from the Lownet array to Ian Hodgson, BMR. Marion Leiba, Ken Muirhead and David Denham reviewed the draft manuscript. We thank Gunther Bock (University of New England) and Bruce Boreham (University College of Central Queensland), who refereed the paper and suggested improvements. Figures 2–6 were produced by BMR's Cartographic Services Unit using computer-aided drafting.

References

Clarke, W.B., 1869 — On the causes and phenomena of earthquakes, especially in relation to shocks felt in New South Wales, and in other provinces of Australasia. *Transactions of the Royal Society of New South Wales*, 2, 51–86.

Cleary, J., & Doyle, H., 1962 — Application of a seismograph network and electronic computer in near earthquake studies. *Seismological Society of America, Bulletin*, 52(3), 673–682.

Doyle, H., & Underwood, R., 1965 — Seismological stations in Australia. *Australian Journal of Science*, 28, 40–43.

Drake, L., 1974 — The seismicity of New South Wales. *Journal and Proceedings of the Royal Society of New South Wales*, 107, 35–40.

Everingham, I.B., Denham, D., & Greenhalgh, S.A., 1987 — Surface-wave magnitudes of some early Australian earthquakes. *BMR Journal of Australian Geology & Geophysics*, 10, 253–259.

Finlayson, D.M., & McCracken, H.M., 1981 — Crustal structure under the Sydney Basin and Lachlan fold belt, determined from explosion seismic studies. *Journal of the Geological Society of Australia*, 28, 177–190.

Fredrich, J., McCaffrey, R., & Denham, D., 1988 — Source parameters of large Australian earthquakes from body waveform inversion. *Geophysical Journal*, 95, 1–13.

Greenhalgh, S.A., Denham, D., McDougall, R., & Rynn, J.M., 1989 — Intensity relations for Australian earthquakes. *Tectonophysics*, 166, 255–267.

Herbert, C., & Melby, R., 1980 — A guide to the Sydney Basin. *Geological Survey of New South Wales, Bulletin*, 26.

McCue, K.F., 1980 — Magnitudes of some early earthquakes in south-eastern Australia. *Search*, 11(3), 78–80.

McCue, K.F., in press — Australia's large earthquakes and Recent fault scarps. *Journal of Structural Geology (special issue on Australian tectonics).*

Michael-Leiba, M.O., 1989 — Macroseismic effects, locations and magnitudes of some early Tasmanian earthquakes. *BMR Journal of Australian Geology & Geophysics*, 11, 89–99.

Newmark, N.M., & Rosenblueth, E., 1971 — Fundamentals of earthquake engineering. *Prentice-Hall, Englewood Cliffs, New Jersey.*

Rynn, J., Denham, D., Greenhalgh, S., Jones, T., Gregson, P.J., McCue, K.F., & Smith, R.S., 1987 — Atlas of isoseismal maps of Australian earthquakes. *Bureau of Mineral Resources, Australia, Bulletin* 222.

Scheibner, E., 1987 — Paleozoic development of eastern Australia in relation to the Pacific region. *In* Monger, J.W.H., & Franchetau, J., (editors), Circum-Pacific orogenic belts and evolution of the Pacific Ocean basin. *American Geophysical Union Geodynamics Series*, 18, 133–165.

CORRECTION

G. Taylor & others — Discussion: Major geomorphic features of the Kosciusko-Bega region
Volume 11, number 1, 123-124

The authors for this paper should be:
Graham Taylor, K.G. McQueen & M.C. Brown.

VOLUME 11

CONTENTS

VOLUME 11

CONTENTS

VOLUME 11 NUMBER 1

VOLUME 11 NUMBER 2/3

VOLUME 11 NUMBER 4

CONTENTS

9 780644 125727

B90/21001 Cat. No. 90 1112 2